UNIVERSIDADE FEDERAL DE MINAS GERAIS
Instituto de Geociências
Programa de Pós-Graduação em Geologia

Pedro Leonardo Nicolau do Carmo Rossi Vieira

HIGH- TO ULTRAHIGH TEMPERATURE METAMORPHISM IN THE SOUTHERN BRASÍLIA AND ARAÇUAÍ OROGENS: implications to U-Pb zircon geochronology

Belo Horizonte
2023

Pedro Leonardo Nicolau do Carmo Rossi Vieira

HIGH- TO ULTRAHIGH TEMPERATURE METAMORPHISM IN THE SOUTHERN BRASÍLIA AND ARAÇUAÍ OROGENS: implications to U-Pb zircon geochronology

Tese de doutorado apresentada ao Programa de Pós-Graduação em Geologia da Universidade Federal de Minas Gerais como requisito parcial para obtenção do título de Doutor em Geologia.

Orientadora: Prof. PhD Mahyra Tedeschi
Coorientadores: Prof. PhD Brenda Chung da Rocha, Prof. PhD Tiago Amâncio Novo

Belo Horizonte
2023

F658h
2023

Vieira, Pedro Leonardo Nicolau do Carmo Rossi.
High- to ultrahigh temperature metamorphism in the Southern Brasília and Araçuaí Orogens [manuscrito] : implications to U-Pb zircon geochronology / Pedro Leonardo Nicolau do Carmo Rossi Vieira. – 2023.
360 f., enc. il. (principalmente color.)

Orientadora: Mahyra Tedeschi.
Coorientadores: Brenda Chung da Rocha.
Coorientador: Tiago Amâncio Novo.
Tese (doutorado) – Universidade Federal de Minas Gerais, Instituto de Geociências, 2023.
Área de concentração: Geologia Regional.
Inclui bibliografia.
Inclui apêndices.

1. Tempo geológico – Teses. 2. Metamorfismo (Geologia) – Teses. I. Tedeschi, Mahyra. II. Rocha, Brenda Chung da. III. Novo, Tiago Amâncio. IV. Universidade Federal de Minas Gerais. Instituto de Geociências. V. Título.

CDU: 550.93(815.1)

Ficha catalográfica elaborada por Graciane Aparecida de Paula – CRB6 3404
Biblioteca "Vitória Pedersoli", Instituto de Geociências da UFMG

UNIVERSIDADE FEDERAL DE MINAS GERAIS

PROGRAMA DE PÓS-GRADUAÇÃO EM GEOLOGIA DO IGC-UFMG

FOLHA DE APROVAÇÃO

HIGH- TO ULTRAHIGH TEMPERATURE METAMORPHISM IN THE SOUTHERN BRASÍLIA AND ARAÇUAÍ OROGENS: IMPLICATIONS TO U-PB ZIRCON GEOCHRONOLOGY

PEDRO LEONARDO NICOLAU DO CARMO ROSSI VIEIRA

Tese submetida à Banca Examinadora designada pelo Colegiado do Programa de Pós-Graduação em GEOLOGIA do IGC-UFMG, como requisito para obtenção do grau de Doutor(a) em GEOLOGIA, área de concentração GEOLOGIA REGIONAL, pelo Programa de Pós-graduação em Geologia do Instituto de Geociências da Universidade Federal de Minas Gerais.

Aprovada em 30 de outubro de 2023, pela banca constituída pelos membros:

Profa. Dra. Mahyra Ferreira Tedeschi – Orientadora
UFMG

Prof. Dr. Henrique Bruno
UERJ

Profa. Dra. Eliza Inez Nunes Peixoto
UnB

Prof. Dr. Rafael Gonçalves da Motta
UFRN

Dra. Alice Westin Teixeira
USP

Belo Horizonte, 30 de outubro de 2023.

À minha família, aos amigos e aos companheiros de jornada.

À minha avó Yolanda (in memoriam). A defesa do doutorado chegou enfim, vó!

AGRADECIMENTOS

Aos meus pais, Pedro e Guiomar, por pavimentarem os caminhos que me trouxeram até aqui. À minha mãe, Guiomar, por prover todo o apoio, suporte, aconselhamento e amparo que permitiram que esta jornada prosseguisse. À minha irmã, Amana, pelos momentos de descontração, pelo apoio (especialmente com o inglês das “cover letters”) e pelo suporte.

Às tias e tios que sempre estiveram na torcida, sobretudo à minha madrinha Marília. Aos meus avós, Guiomar, José, Yolanda e Pedro (in memoriam), por estabelecerem as bases de tudo. À Ártemis, Loki, Hilda, Bast, Tupã e Bob, por toda amizade, por alegrarem meus dias e por iluminarem minha vida.

À minha orientadora, Mahyra, e aos meus co-orientadores, Brenda e Tiago, por todo apoio fornecido, pelas discussões científicas, pelo companheirismo, e sobretudo pela compreensão e paciência.

Aos companheiros e companheiras da geologia pela amizade, apoio e pelas discussões frutíferas. Em especial à equipe do Petrochronics, por tantas trocas de idéias, e ao Ramon, pela parceria na reta final do doutorado.

Às amigas e amigos de outros círculos, pelos momentos de descontração, pelas conversas, pelos bons momentos juntos, pelas viagens, pelos puxões de orelha e por todo o amparo ao longo dessa trajetória.

Aos meus calouros e calouras da UFMG, que me fizeram querer ser professor, e aos meus alunos e alunas do UniBH, que me fizeram ter certeza da minha paixão pelo ensino e me deram forças para seguir até o fim com este objetivo.

À Pró-reitoria de Pós-graduação da UFMG e ao Programa de Pós-Graduação em Geologia do Instituto de Geociências da Universidade Federal de Minas Gerais pelo financiamento e pela infraestrutura cedida. Ao Centro de Pesquisas Professor Manoel Teixeira da Costa (CPMTC) pela infraestrutura cedida.

Ao CNPq e ao projeto “Metamorfismo de temperatura ultra-alta em gnaisses paraderivados no Orógeno Brasília Meridional: estudos de proveniência e reconstrução de trajetórias Pressão-Temperatura-tempo (P-T-t)” da agência UFMG Edital PRPq 03/2019 pelo financiamento do projeto.

Ao projeto de pesquisa “O significado do metamorfismo de ultra-alta pressão e temperatura para a evolução do Orógeno Brasília Meridional: insights a partir de estudos de proveniência e reconstrução de trajetórias pressão-temperatura-tempo (P-T-t)”, do qual esta tese faz parte.

“When you open your eyes
When you gaze at the sky
When you look to the stars
As they shut down the night
You feel this story ain't over”
- Avantasia, Story Ain’t Over

RESUMO

As regiões compreendidas pelo Complexo Caparaó e pela Nappe Socorro-Guaxupé, pertencentes respectivamente ao sul dos orógenos Araçuaí e Brasília Meridional, foram afetadas por metamorfismo de temperatura alta (≥850 °C) a ultra-alta (≥900 °C) ((U)HT) durante o ciclo Brasiliano. Rochas paraderivadas destas regiões podem ou não apresentar paragêneses minerais típicas (como safirina+quartzo e hercinita+quartzo) e exibem típico espalhamento concordante a sub-concordante nas idades U-Pb em zircão (em intervalos de até ca. 260 Ma), representando desafios tanto para a determinação das condições de temperatura e pressão do pico metamórfico quanto para a interpretação das idades metamórficas e de proveniência. O Complexo Caparaó situa-se nos domínios do Arco Magmático Rio Doce (Orógeno Araçuaí), e representa uma lasca tectônica onde rochas do embasamento e supracrustais se encontram justapostas. Foram identificados dois tipos de migmatitos paraderivados que registram metamorfismo UHT: hercinita-silimanita-granada migmatitos (1020-1035 °C, 7,0-7,1 kbar), contendo típicas paragêneses hercinita+quartzo; e ortopiroxênio-granada migmatitos (962-978 °C, 9,5-9,6 kbar), exibindo ortopiroxênio rico em Al. Análises U-Pb em zircão revelam idades metamórficas entre *ca.* 635-610 Ma, mais antigas que o pico metamórfico regional colisional (*ca*. 563 Ma), correspondendo ao período pré-colisional do orógeno e à formação do Arco Magmático Rio Doce. Interpreta-se que as fontes de calor responsáveis pelo metamorfismo UHT estão relacionadas tanto a um mecanismo de "janela de placa", provocado pela subducção da dorsal oceânica, quanto a magma underplating e espessamento crustal durante a edificação do arco. A Nappe Socorro-Guaxupé (Orógeno Brasília Meridional) representa as raízes do arco magmático formado às margens do paleocontinente Paranapanema, exibindo rochas orto e paraderivadas afetadas por metamorfismo (U)HT. Análises U-Pb e Lu-Hf em zircão foram realizadas em seis amostras pertencentes ao Complexo São João da Mata (orto e paraderivadas), a fim de resgatar informações sobre os protólitos, sua história deposicional e desvendar os impactos do metamorfismo (U)HT no registro geocronológico. Foi identificada forte contribuição de protofontes relacionadas ao período de desenvolvimento do arco magmático (entre *ca*. 816-776 Ma), que exibem tanto assinaturas crustais ($\varepsilon Hf_{(804-776)}$ = -16 a -2) quanto moderadamente juvenis ($\varepsilon Hf_{(816)}$ = +3 a +9) - estas possivelmente relacionadas a um arco de ilhas de idade mínima Toniana (*ca*. 816 Ma). A partir de idades mínimas de cristalização de um

leucossoma e um granito intrusivo foram interpretadas idades entre ca. 690-660 Ma para o início do metamorfismo UHT. A partir dos dados obtidos e de uma compilação de dados do metamorfismo UHT no Brasil, observa-se uma aparente correlação entre as ocorrências de metamorfismo UHT e o contexto de transição subducção-colisão no Sul dos orógenos Araçuaí e Brasília Meridional, embora ambos tenham evoluído diacronicamente.

Palavras-chave: metamorfismo HT; metamorfismo UHT; geocronologia U-Pb; geocronologia Lu-Hf; janela de placa; subducção; zircão detrítico; fontes sedimentares; pseudoseções

ABSTRACT

The regions comprised by the Caparaó complex and the Socorro-Guaxupé Nappe, from the southern Araçuaí and Southern Brasília orogens respectively, were affected by high (≥850 °C) to ultra-high (≥900 °C) temperature ((U)HT) metamorphism during the Brasiliano cycle. Paraderived rocks from both regions may or may not exhibit characteristic mineral assemblages (such as sapphirine+quartz and hercynite+quartz) and exhibit a typical spreading of concordant to sub-concordant U-Pb zircon dates (up to ca. 260 Ma). Thus, interpreting these datasets if challenging regarding sedimentation and metamorphic events. The Caparaó complex lies on the Rio Doce Magmatic Arc domain (Araçuaí Orogen). It represents a tectonic sliver in which basement and supracrustal rocks are juxtaposed. Two types of paraderived migmatites affected by UHT metamorphism are identified: hercynite-sillimanite-garnet migmatites (1020-1035 °C, 7.0-7.1 kbar), exhibiting typical hercynite+quartz assemblages; and orthopyroxene-garnet migmatites (968-975 °C, 9.5-9.6 kbar), exhibiting high-Al orthopyroxene. U-Pb in zircon dating revealed a range of metamorphic ages between ca. 635-610 Ma, constrained to the pre-collisional stage and the formation of the Rio Doce Magmatic Arc. Those ages are older than the collisional metamorphic peak (ca. 563 Ma). Heat sources responsible for the UHT metamorphism are interpreted to be related to a “slab window” mechanism triggered by the subduction of an ocean ridge, as well as arc-related magma underplating and crustal thickening. The Socorro-Guaxupé Nappe (Southern Brasília Orogen) represents the roots of a magmatic arc formed at the margins of the Paranapanema paleocontinent. It exhibits ortho- and paraderived rocks affected by (U)HT metamorphism. Zircon crystals from six samples from the São João da Mata Complex were analyzed for U-Pb and Lu-Hf isotopes in order to retrieve information about their protoliths, depositional history and impacts of the (U)HT metamorphism on their ages register. A main contribution of arc-derived sources (ages between ca. 804-776 Ma) was identified, exhibiting both crustal ($\varepsilon Hf_{(804-776)}$ = -16 to -2) and moderately juvenile ($\varepsilon Hf_{(816)}$ = +3 a +9) signatures. The latter are interpreted to be related to a Tonian (ca. 816 Ma) island arc. Ages between ca. 690-660 Ma obtained for the crystallization of a leucosome and an intrusive granite were interpreted as the onset of the UHT metamorphism. Based on the data obtained and a compilation of UHT metamorphism occurrences in Brazil, a possible correlation between UHT metamorphism and the subduction-collision transition is observed on

the Southern Araçuaí and Southern Brasília orogens, regardless of their diachronic evolution.

Keywords: HT metamorphism; UHT metamorphism; U-Pb geochronology; Lu-Hf geochronology; slab window; subduction; detrital zircon; sedimentary sources; pseudosections

SUMMARY

1 INTRODUCTION 13

1.1 Scope of this thesis 13

1.2 Organization of the thesis 14

1.3 References 15

2 (U)HT METAMORPHISM AND THE U-PB AND LU-HF SYSTEMS 18

2.1 (U)HT metamorphism and its effects on U-Pb zircon geochronology – a synthesis 18

2.2 References 21

3 GEOLOGICAL CONTEXT AND SCIENTIFIC QUESTIONS 25

3.1 UHT metamorphism on the Southern Brasília and Araçuaí orogens .. 25

3.1.1 South of the Southern Brasília Orogen 25

3.1.2 Araçuaí Orogen 27

3.2 Justificative and scientific questions 30

3.3 References 32

4 UNVEILING THE P-T EVOLUTION OF ULTRAHIGH TEMPERATURE METAMORPHISM FROM HERCYNITE-BEARING AND ORTHOPYROXENE-GARNET MIGMATITES – TECTONIC IMPLICATIONS FOR THE EDIACARAN EVOLUTION OF THE ARAÇUAÍ OROGEN (SE BRAZIL) 40

5 DETRITAL ZIRCON U-PB-HF ISOTOPES-BASED RECONSTRUCTION OF THE DEPOSITIONAL HISTORY OF (ULTRA)HIGH-TEMPERATURE METAMORPHIC ROCKS FROM THE SOCORRO-GUAXUPÉ NAPPE (SOUTHERN BRASÍLIA OROGEN, BRAZIL) 114

6 COMPLEMENTARY LU-HF DATA 173

6.1 Layered orthopyroxene-garnet diatexite (P013) – Caparaó complex, Araçuai orogen 173

6.2 References 175

7 DISCUSSIONS 176

7.1 Data compilation: known occurrences of ultrahigh temperature metamorphic rocks in Brazil 178

7.1.1 Paleoproterozoic UHT metamorphism – the São Francisco Craton and Borborema Province 178

7.1.2 UHT metamorphism in the Brasília Orogen 179

7.1.3 UHT metamorphism in the Araçuaí Orogen 181

7.2 UHT metamorphism in the Brasiliano cycle – a link between the Southern Brasília and Araçuaí orogens 184

7.3 References 190

8 CONCLUSION 199

9 APPENDICES 201

9.1 **APPENDIX A – Supplementary file 1 (Chapter 4): Standards for EMPA and WRG preparation** 202

9.1.1 Analytical standards for electron microprobe analysis (EMPA) 202

9.1.2 Analytical procedures for whole-rock geochemical analysis 202

9.2 APPENDIX B – Supplementary file 2 (Chapter 4): Representative mineral compositions 204

9.3 APPENDIX C – Supplementary file 3 (Chapter 4): Al-in-orthopyroxene thermobarometry for analyzed samples 226

9.4 APPENDIX D – Supplementary file 4 (Chapter 4): Bulk-rock compositions of analyzed samples 228

9.5 APPENDIX E – Supplementary file 5 (Chapter 4): U-Pb LA-ICP-MS analyses 229

9.6 APPENDIX F – Supplementary file 6 (Chapter 4): Compilation of ages from the Araçuaí orogen 240

9.7 APPENDIX G – Supplementary figure 1 (Chapter 4) 244

9.8 APPENDIX H – Supplementary figure 2 (Chapter 4) 244

9.9 APPENDIX I – Supplementary figure 3 (Chapter 4) 245

9.10 APPENDIX J – Supplementary figure 4 (Chapter 4) 245

9.11 APPENDIX K – Supplementary data 1 (Chapter 5): Zircon LA-MC-ICP-MS results 246

9.12 APPENDIX L – Supplementary data 2 (Chapter 5): Interference of Yb on Hf 307

9.13 APPENDIX M – Supplementary data 3 (Chapter 5): Petrography 308

9.13.1 Amphibolite enclave (PC12.1) 308

9.13.2 Hornblende-biotite stromatic metatexite (PC12.2) 308

9.13.3 Biotite-bearing pink leucosome (PC12.3) 308

9.13.4 Garnet-biotite stromatic metatexite (PC12.4) 309

9.13.5 Garnet-bearing white leucosome (PC12.5) 309

9.13.6 (Hornblende-)biotite-stromatic metatexite (C1071A) 310

9.14 APPENDIX N – Supplementary data 4 (Chapter 5): U-Pb and Lu-Hf compilation from the Brasília and Ribeira orogens 311

9.15 APPENDIX O – Lu-Hf and U-Pb data from sample P013 (Chapter 6) 343

9.16 APPENDIX P – Compilation of UHT metamorphism occurrences in Brazil (Chapter 6) 358

1 INTRODUCTION

1.1 Scope of this thesis

This doctoral thesis addresses the impact of high- (≥850 °C) to ultrahigh (≥900 °C) ((U)HT) metamorphism on the geochronological record, focusing on paraderived rocks (paragneisses and migmatites) from the Socorro-Guaxupé Nappe (Southern Brasília Orogen) and Caparaó complex (Araçuaí Orogen). It represents the continuity of the works developed by its author during the geological mapping of the Caldas and Poços de Caldas 1:100,000 sheet (Tedeschi et al., 2015) and during its master's degree on the Caparaó complex (Vieira, 2018). Both orogens present UHT metamorphism occurrences (Moreira, 1997; Costa, 1998; Campos Neto and Caby, 1999, 2000; Del Lama et al., 2000; Belém, 2006; Gradim, 2013; Gradim et al., 2014; Rocha et al., 2017, 2018; Tedeschi et al., 2018; Wisniowski et al., 2021; Motta et al., 2021) although they evolved differently and diachronically (Campos Neto and Caby, 1999, 2000; Pedrosa-Soares et al., 2001, 2008), and were selected as case studies for this thesis in order to comprehend the similarities and differences between the tectonic settings, time intervals and geological processes involved in those occurrences, as well as to establish their possible correlations.

The first part of this thesis focused on the metamorphic conditions attained by migmatites from the Caparaó Complex were investigated, comprising the scope of this thesis first paper submitted to Gondwana Research (Rossi-Vieira et al., submitted; Chapter 4). Previous studies reported the existence of ultrahigh temperature orthoderived rocks on the Manhuaçu region (Moreira, 1997; Costa, 1998) and on the Caparaó Suite (Da Silva et al., 2002), however a detailed characterization of the peak P-T conditions and metamorphic paths on paraderived rocks was absent.

The second part of this thesis focused on a U-Pb and Lu-Hf in zircon study on paraderived rocks from the Socorro-Guaxupé Nappe (SGN), representing the scope of the second paper which is published in the Journal of South American Earth Sciences (Rossi-Vieira et al., 2023; Chapter 5). Minimum crystallization ages were determined for the possible protosources (i.e., igneous or metamorphic rocks in which a zircon population originally crystallized, Pell et al. 1997) and their geotectonic context was discussed. Part of the data analyzed in this work was also studied by the author on a paper published in Geoscience Frontiers (Tedeschi et al. 2023), which established the theoretical parameters employed on the second paper. During this stage the author also worked on another paper published in the Journal of South American Earth

Sciences (Costa et al., 2022), reporting the first known occurrence of moderately juvenile rocks in the Socorro-Guaxupé Nappe, probably related to an island arc.

The third part of this thesis integrates the results from the papers mentioned above with a compilation of data from UHT metamorphism occurrences in Brazil and new Lu-Hf and U-Pb data for one of the Caparaó Complex samples. It presents a discussion on the similarities, differences and possible correlations between the UHT metamorphic events on the South of the Southern Brasília Orogen and Araçuaí Orogen, as well as a conclusion to this thesis.

1.2 Organization of the thesis

This thesis is organized as it follows:

Chapter 1 – Introduction represents the initial presentation and overall structure of this thesis.

Chapter 2 – (U)HT metamorphism and the U-Pb and Lu-Hf systems presents a synthesis of the theoretical aspects involved in this research.

Chapter 3 – Geological context and scientific questions presents a synthesis of the geological context, the theoretical aspects involved in this research and the scientific questions this thesis tries to answer.

Chapter 4 – "Unveiling the P-T evolution of ultrahigh temperature metamorphism from sapphirine-bearing and orthopyroxene-garnet migmatites - Tectonic implications for the Ediacaran evolution of the Araçuaí orogen (SE Brazil)" represents the first article from this thesis, submitted to Gondwana Research.

Chapter 5 – "Detrital zircon U-Pb-Hf isotopes-based reconstruction of the depositional history of (ultra)high-temperature metamorphic rocks from the Socorro-Guaxupé Nappe (Southern Brasília orogen, Brazil)" represents the second article from this thesis, published in the Journal of South American Earth Sciences.

Chapter 6 – Complementary Lu-Hf data and possible correlations presents the complementary Lu-Hf and U-Pb data obtained for the layered orthopyroxene-garnet diatexite, as well as a brief discussion on the correlations between this sample and possible sources on the Araçuaí Orogen (sample P013 from Chapter 4).

Chapter 7 – Discussions around the similarities, differences and possible correlations between the UHT metamorphism occurrences in the Southern Araçuaí and Southern Brasília orogens. It provides a compilation of UHT metamorphism

occurrences in Brazil and insights about the role of UHT metamorphism on the evolution of the Brasiliano orogens.

Chapter 8 – Conclusion presents the closing remarks and conclusion of this thesis.

Appendix A to J are the Supplementary data from this thesis' first paper (Chapter 3). Appendix K to N are the Supplementary data from this thesis' second paper (Chapter 4). Appendix O and P are the Lu-Hf and U-Pb data presented in Chapter 6 and the compilation of UHT occurrences in Brazil presented in Chapter 7 (respectively).

1.3 References

Belém, J. 2006. **Caracterização Mineralógica, Física e Termobarométrica de Minérios de Grafita da Província Grafítica Bahia-Minas**. (Dissertação de Mestrado). Universidade Federal de Minas Gerais, Belo Horizonte, Brasil. 180 pp;

Campos-Neto, M. C. and Caby, R. 1999. **Neoproterozoic high-pressure metamorphism and tectonic constraint from the nappe system south of the Sao Francisco Craton, southeast Brazil.** Precambrian Research 97 (1–2): 3–26.

Campos-Neto, M. C. and Caby, R. 2000. **Terrane accretion and upward extrusion of high-pressure granulites in the Neoproterozoic nappes of southeast Brazil: Petrologic and structural constraints**. Tectonics 19(4): 669–687.

Costa, A. G., 1998. **The Granulite-Facies Rocks of the Northern Segment of the Ribeira Belt, Eastern Minas Gerais, SE Brazil**. Gondwana Research, 1(3-4), 367-372.

Costa, F. M., Penna, J. L. A., Martins, L. C. D., Tedeschi, M., Novo, T. A., Araujo, C. S., Vieira Rossi, P. L., Lana, C., Pedrosa-Soares, A. C. 2022. **Zircon petrochronology reveals the moderately juvenile signature of a diatexite from the boundary zone between the Brasília and Ribeira orogens (SE Brazil): Relict of a Tonian arc?** Journal of South American Earth Sciences, 116, 103767. https://doi.org/10.1016/j.jsames.2022.103767.

Da Silva, L. C., Armstrong, R., Noce, C. M., Carneiro, M. A., Pimentel, M., Pedrosa-Soares, A. C., Leite, C. A., Vieira, V. S., Silva, M. A., Paes, V. J. C., Cardoso Filho, J. M. 2002. **Reavaliação da evolução geológica em terrenos Pré-Cambrianos brasileiros com base em novos dados U-Pb SHRIMP, parte II: Orógeno Araçuaí, Cinturão Mineiro e Cráton São Francisco Meridional**. Revista Brasileira de Geociências, 32(4), 513-528.

Del Lama, E. A., Zanardo, A., Oliveira, M. A. F., Moralles, N. 2000. **Exhumation of high-pressure granulites of the Guaxupé Complex, Southeastern Brazil.** Geological Journal 35: 231-249.

Gradim, C. 2013. **Complexo Nova Venécia e magmatismo associado, Orógeno Araçuaí, Estado do Espírito Santo** (Dissertação de Mestrado). Universidade Federal de Minas Gerais, Belo Horizonte, Brasil. 123 pp.

Gradim, C., Roncato, J., Pedrosa-Soares, A.C., Cordani, U., Dussin, I., Alkmim, F.F., Babinski, M. 2014. **The hot back-arc zone of the Araçuaí orogen, Eastern Brazil: from sedimentation to granite generation**. Brazilian Journal of Geology, 44, 155-180. DOI: http://dx.doi.org/10.5327/Z2317-4889201400010012.

Moreira, L. M. 1997. **Evolução crustal do Leste de Minas Gerais: uma contribuição a partir do estudo geotermobarométrico de metamorfitos da região Simonésia-Manhuaçu (MG).** (Tese de Doutorado). Universidade Federal de Minas Gerais, Belo Horizonte, Brasil. 116 pp.

Motta, R. G., Fitzsimons, I. C. W., Moraes, R., Johnson, T. E., Schuindt, S., Benetti, B. Y. 2021. **Recovering P-T-t paths from ultra-high temperature (UHT) felsic orthogneiss: An example from the Southern Brasília Orogen, Brazil**. Precambrian Research, 359, p. 106222

Pedrosa-Soares, A. C., Alkmim, F. F., Tack, L., Noce, C. M., Babinski, M. Da Silva, L. C., Martins-Neto, M. A. 2008. **Similarities and differences between the Brazilian and African counterparts of the Neoproterozoic Araçuaí-West-Congo orogen**. Geological Society, London, Special Publications, 294, 153-172.

Pedrosa-Soares, A. C., Noce, C. M., Wiedemann, C. M., Pinto, C. P. 2001. **The Araçuaí-West-Congo Orogen in Brazil: an overview of a confined orogen formed during Gondwanaland assembly**. Precambrian Research, 110, 307-323.

Pell, S. D., Williams, I. S., Chivas, A. R. 1997. **The use of protolith zircon-age fingerprints in determining the protosource areas for some Australian dune sands**. Sedimentary Geology, 109, 233-260.

Rocha, B. C., Moraes, R., Möller, A., Cioffi, C. R. 2018. **Magmatic inheritance vs. UHT metamorphism: Zircon petrochronology of granulites and petrogenesis of charnockitic leucosomes of the Socorro–Guaxupé nappe, SE Brazil**. Lithos 314-315: 16-39.

Rocha, B. C., Moraes, R., Möller, A., Cioffi, C. R., Jercinovic, M. J. 2017. **Timing of anatexis and melt crystallization in the Socorro–Guaxupé Nappe, SE Brazil: Insights from trace element composition of zircon, monazite and garnet coupled to U-Pb geochronology**. Lithos 277: 337-355.

Rossi-Vieira, P. L. N. C., Tedeschi, M., Rocha, B. C., Lana, C. C., Barrote, V., Pedrosa-Soares, A. C., Dussin, I. A. and Alkmim, A. 2023. **Detrital zircon U-Pb-Hf isotopes-based reconstruction of the depositional history of (ultra)high-temperature metamorphic rocks from the Socorro-Guaxupé Nappe (Southern Brasília orogen, Brazil).** Journal of South American Earth Sciences, 128, 104469. https://doi.org/10.1016/j.jsames.2023.104469

Tedeschi, M., Vieira, P. L. N. C. R., Novo, T. A. 2015. **Geologia e recursos minerais das Folhas Caldas (SF.23-V-D-IV) e Poços de Caldas (SF.23-V-C-VI) 1:100.000.** Projeto Fronteiras de Minas, CODEMIG-UFMG, Belo Horizonte, Brasil.

Tedeschi, M., Pedrosa-Soares, A.; Dussin, I., Lanari, P., Novo, T., Pinheiro, M. A. P., Lana, C., Peters, D. 2018. **Protracted zircon geochronological record of UHT garnet-free granulites in the Southern Brasília orogen (SE Brazil): Petrochronological constraints on magmatism and metamorphism**. Precambrian Research 316: 103-126.

Tedeschi, M., Rossi Vieira, P. L., Kuchenbecker, M., Ribeiro, B. V., Barrote, V., Reis, H., Stutenbecker, L., Lana, C., Pedrosa-Soares, A., Dussin, I. 2023. **Unravelling and overcoming potential biases in U-Pb detrital zircon records induced by high to ultra-high temperature metamorphism (> 850 ºC).** Geoscience Frontiers, 14, 101515. https://doi.org/10.1016/j.gsf.2022.101515

Vieira, P. L. N. C. R. 2018. **Caracterização, condições de metamorfismo e implicações geotectônicas dos migmatitos granatíferos da Serra do Caparaó (MG).** (Dissertação de Mestrado). Universidade Federal de Minas Gerais, Belo Horizonte, Brasil. 124 pp.

Wisniowski, L, Pedrosa-Soares, A, Medeiros-Junior, E, Belém, J, Dussin, I, Queiroga, G., 2021. **Ultra-high temperature, mid-crustal level, contact metamorphism imprinted on granulite facies paragneisses by a norite intrusion (São Gabriel da Baunilha, Araçuaí orogen, southeast Brazil).** Journal of Metamorphic Geology, 39, 867– 895. Doi.org/10.1111/jmg.12594

2 (U)HT METAMORPHISM AND THE U-PB AND LU-HF SYSTEMS

2.1 (U)HT metamorphism and its effects on U-Pb zircon geochronology – a synthesis

U-Pb zircon geochronology is an important tool for the investigation of igneous, metamorphic and sedimentary terrains (Fedo et al., 2003; Corfu et a., 2003; Rubatto, 2017) owing to some of zircon characteristics: i) high closure temperatures (> 850 °C or even >1000 °C; Cherniak, 2010); ii) resistance to weathering (Hoskin and Schaltegger, 2003); iii) stability over a wide range of pressure-temperature conditions (Cherniak and Watson, 2001; Finch and Hanchar, 2003). In addition, its ability to preserve records of multiple thermal events has contributed significantly in the last decades to improve the understanding around Earth's crust generation and recycling, the dynamics behind sedimentary basins and the evolution of orogenic belts throughout the geological history (Hastie et al., 2016; Johnson et al., 2017).

Detrital zircon analysis (on both sedimentary and metasedimentary rocks) might reveal information about the formation and distribution of multiple sedimentary sources that, in many cases, are not exposed or no longer preserved (Cawood et al., 2012; Andersen et al., 2019). Maximum depositional ages can also be obtained for (meta)sedimentary sequences in which dating syn-sedimentary igneous rocks is not possible (Nelson, 2001; Coutts et al., 2019). Through U-Pb age patterns in zircon cores it is possible to infer the type of sedimentary basin in which those rocks (or their protoliths) were deposited and to stablish correlations with possible source areas (Cawood et al., 2012). In that sense, detrital zircon ages provide crucial information about the conditions and rates involved in the evolution of Earth crust throughout the geological history (Cawood et al., 2013; Andersen et al., 2019; Barham et al., 2019), while also playing a fundamental role in paleogeographic reconstructions and geotectonic models (Fedo et al., 2003; Hoskin and Schaltegger, 2003 ; Murphy et al., 2004; Cawood et al., 2012).

However, several challenges are faced when detrital zircon ages are investigated in rocks affected by high- (≥850 °C) to ultrahigh (≥900 °C) temperature ((U)HT) metamorphism. UHT metamorphic terrains represent one of the extreme end-members of the spectrum of pressure-temperature conditions to which the crust might be submitted during tectonic cycles (Harley, 1998; Kelsey, 2008). First studied cases were interpreted as rare occurrences, mostly related to specific geological contexts (Harley, 1998, 2016; Kelsey, 2008; Kelsey and Hand, 2015), partially because UHT

metamorphism was identified through very specific mineral assemblages such as sapphirine+quartz, orthopyroxene+sillimanite+quartz or hercynite+quartz (Harley, 1998, 2016; Kelsey, 2008) that can only be formed in specific protolith (or microdomainial) compositions. Also, empirical geothermometer and geobarometer calibrations based on cation exchange (e.g. Fe-Mg-based conventional or classical thermobarometry) tend to fail to retrieve the prograde metamorphic history in rocks past 900 °C due to thermal re-equilibration, providing data without a geological meaning or simply the cooling metamorphic path (e.g. e.g., Frost and Chacko, 1989; Harley, 1989; Pattinson and Bégin, 1994). However, in the last decades there was a significant advance on thermobarometry methods (Powell and Holland, 2008; Lanari and Duesterhoeft, 2019), as: trace elements-based techniques applied to accessory phases (as Ti-in-zircon, Watson et al., 2006); garnet-orthopyroxene thermobarometry corrected for Al contents in orthopyroxene (Pattison et al., 2003); advances in reverse (as Average P-T, Powell and Holland, 1994, and TWEEQU, Berman, 1991) and forward (THERMOCALC, Powell and Holland, 1988; PERPLE_X, Conolly and Kerrick, 1987; Theriak-Domino, De Capitani and Petrakakis, 2010) thermodynamic modeling techniques; and iterative phase equilibria modeling techniques, as Bingo-Antidote (Lanari et al., 2017; Duesterhoeft and Lanari, 2020). A growing number of UHT metamorphism occurrences have been identified through the application of those methods (Kelsey, 2008), although UHT metamorphic terranes are still relatively uncommon in a global perspective (Kelsey and Hand, 2015).

This kind of extreme metamorphism is related to different tectonic settings, as the closure of back-arc basins, the hot and deep roots of orogens, subduction zones, thick nappe stacks and others (Harley, 1998, 2016; Santosh and Kusky, 2010; Kelsey, 2008; Kelsey and Hand, 2015). Inferences about the tectonic context related to a UHT metamorphic occurrence can be made based on metamorphic paths (P-T, P-T-t or T-t), the age and duration of UHT metamorphism, and in the time window between metamorphism, magmatism and sedimentation in a regional geological context (Harley, 1998, 2016; Kelsey and Hand, 2015). However, geochronological investigations in UHT metamorphic rocks require attention on possible sources of systematic bias, especially concerning provenance studies.

Rocks submitted to (U)HT metamorphic conditions tend to exhibit a continuous record of concordant to slightly discordant U-Pb ages (a protracted zircon record) which might be related to several processes: masked Pb loss; partial opening or

dissolution; crystallization from melt; recrystallization; intracrystalline Pb diffusion (with or without the formation of clusters), plastic deformation and/or incorporation of Pb (Friend and Kinny, 1995; Lee et al., 1997; Wan et al., 2011; Bindeman and Melnik, 2016; Taylor et al., 2016; Vervoort and Kemp, 2016; Rubatto, 2017; Laurent et al., 2018; Kunz et al., 2018; Andersen et al., 2019). This kind of register commonly generates “age groups” which might not represent geological events but variable degrees of disturbance in the U-Pb system that create “age” intervals between actual geological processes (Tedeschi et al., 2023) or even thermal events (protracted or not; Rocha et al., 2018; Tedeschi et al., 2018).

Detrital zircon provides some of the few registers of protosources involved in the formation of paraderived rocks. As it is expected that core dates (individual U-Pb time values from spot data, e.g. Kunz et al., 2018) reflect the crystallization age of their respective protosources they are used in maximum depositional age estimates (Andersen et al., 2019). However, the spreading of U-Pb dates caused by (U)HT metamorphism might completely erase information about the crystallization age of protosources creating a record of dates without geological meaning, thus extreme caution is required in this type of study. Additionally, although modern dating routines include detailed backscattered electron (BSE) and/or cathodoluminescence (CL) imaging (Hoskin and Schaltegger, 2003), (U)HT metamorphism might cause the decoupling between internal zircon textures and the isotopic register (Kunz et al., 2018). As such, complementary techniques are needed in order to retrieve geological meaning from U-Pb dating and allow (minimum) age estimates for sources and also for the processes that caused those disturbances, as Lu-Hf isotopic analyses (Whitehouse and Kemp, 2010; Taylor et al., 2016; Tedeschi et al., 2018, 2023; Andersen et al., 2019), trace elements (Kunz et al., 2018) and oxygen isotopes (Laurent et al., 2018).

Combined Lu-Hf and U-Pb in zircon analyses present an especially useful approach to unravel the isotopic disturbance history on the U-Pb system (Whitehouse and Kemp, 2010; Taylor et al., 2016; Andersen et al., 2019; Tedeschi et al., 2023). Original $^{176}Hf/^{177}Hf_{(t)}$ ratios of an igneous rock tend to be preserved in zircon throughout geological time as radiogenic Hf variations are lower than those of observed on the whole rock by of several orders of magnitude due to its low incorporation of Lu (Andersen et al., 2019). For that reason, zircon populations affected by (U)HT metamorphism might be identified through sub-horizontal linear trends in $^{176}Hf/^{177}Hf_{(t)}$

x apparent U-Pb age plots, representing Pb loss lines from the crystallization age of a protosource (Whitehouse and Kemp, 2010; Vervoort and Kemp, 2016; Andersen et al., 2019). That way, the oldest zircon grains in a population can be used to define its minimum crystallization age (Whitehouse and Kemp, 2010; Tedeschi et al., 2023).

2.2 References

Andersen, T., Elburg, M., Magwaza, B., 2019. **Sources of bias in detrital zircon geochronology: Discordance, concealed lead loss and common lead correction**. Earth-Science Reviews 197, 102899. Doi: 10.1016/j.earscirev.2019.102899

Barham, M., Kirkland, C., Hollis, J., 2019. **Spot the difference: zircon disparity tracks crustal evolution.** Geology, 47(5), 435–439. Doi:10.1130/G45840.1.

Berman, R.G. 1991. **Thermobarometry using multi-equilibrium calculations: a new technique, with petrological applications**. In**:** Gordon, T M; Martin, R F. (Eds). **Quantitative methods in petrology: an issue in honor of Hugh J. Greenwood.** Canadian Mineralogist v. 29, 833-855.

Bindeman, I.N. and Melnik, O.E., 2016. **Zircon Survival, Rebirth and Recycling during Crustal Melting, Magma Crystallization, and Mixing Based on Numerical Modelling**. Journal of Petrology, 57(3), 437–460. https://doi.org/10.1093/petrology/egw013.

Cawood, P.A., Hawkesworth, C.J., Dhuime, B., 2012. **Detrital zircon record and tectonic setting**. Geology 40, 875–878. Doi:10.1130/G32945.1

Cawood, P.A., Hawkesworth, C.J., Dhuime, B., 2013. **The continental record and the generation of continental crust**. Geological Society of America Bulletin, 125, 14–32.

Cherniak, D.J., 2010. **Diffusion in accessory minerals: zircon, titanite, apatite, monazite and xenotime**. Reviews in Mineralogy and Geochemistry, 72, 827–869. https://doi.org/10.2138/rmg.2010.72.18;

Cherniak, D.J. and Watson, E.B., 2001. **Pb diffusion in zircon**. Chemical Geology172 (1 – 2), 5 – 24.

Connolly J. A. D. and Kerrick D.M. 1987. **An algorithm and computer program for calculating composition phase diagrams**. CALPHAD, 11, 1-55.

Corfu, F., Hanchar, J.M., Hoskin, P.W.O., Kinny, P., 2003. **Atlas of zircon textures**. In: Hanchar, J.M., Hoskin, P.W.O. (Eds.). **Zircon**. Reviews in Mineralogy and Geochemistry 53, Washington, pp. 469–500.

Coutts, D.S., Matthews, W.A., Hubbard. S.M. 2019. **Assessment of widely used methods to derive depositional ages from detrital zircon populations**. Geoscience Frontiers, 10 (4), 1421-1435.

De Capitani, C. and Petrakakis, K. 2010. **The computation of equilibrium assemblage diagrams with Theriak/Domino software.** American Mineralogist, 95, 1006-1016. DOI: http://dx.doi.org/10.2138/am.2010.3354.

Duesterhoeft, E. and Lanari, P. 2020. **Iterative thermodynamic modelling – Part 1: A theoretical scoring technique and a computer program (BINGO-ANTIDOTE).** Journal of Metamorphic Geology, 38, 527-551.

Fedo, C. M., Sircombe, K. N., Rainbird, R. H. 2003. **Detrital zircon analysis of the sedimentary record**. Reviews in Mineralogy and Geochemistry 53(1), 278-303.

Finch, R. J. and Hanchar, J. M. 2003. **Structure and chemistry of zircon and zircon-group minerals.** Reviews in Mineralogy and Geochemistry 53(1), 1-25.

Friend, C. R. L. and Kinny, P. D., 1995. **New evidence for the protolith ages of Lewisian granulites, northwest Scotland**. Geology, 23, 1027–1030.

Frost, B. R. and Chacko, T. 1989. **The granulite uncertainty principle: limitations on thermobarometry in granulites**. Journal of Geology, 97, 435-450.

Harley, S. L. 1989. **The origins of granulites: a metamorphic perspective**. Geological Magazine, 126, 215-247.

Harley, S. L. 1998. **Ultrahigh temperature granulite metamorphism (1050 °C, 12 kbar) and decompression in garnet (Mg70)–orthopyroxene–sillimanite gneisses from the Rauer Group, East Antarctica**. Journal of Metamorphic Geology, 16 (4), 541-562 doi:10.1111/j.1525-1314.1998.00155.x

Harley, S. L. 2016. **A matter of time: the importance of the duration of UHT metamorphism**. Journal of Mineralogical and Petrological Sciences, 111, 50-72.

Hastie, A.R., Fitton, J.G., Bromiley, G.D., Butler, I.B., Odling, N.W.A. 2016. **The origin of Earth's first continents and the onset of plate tectonics**. Geology 44, 855– 957 Doi: 10.1130/G38226.1.

Hoskin, P. W. O. and Schaltegger, U. 2003. **The Composition of Zircon and Igneous and Metamorphic Petrogenesis**. Reviews in Mineralogy and Geochemistry (2003) 53 (1): 27–62.

Johnson, T.E., Brown, M., Gardiner, N.J., Kirkland, C.L., Smithies, R.H. 2017. **Earth's first stable continents did not form by subduction**. Nature 543, 239–24, doi: 976 10.1038/nature21383.

Kelsey, D. E. 2008. **On ultrahigh-temperature crustal metamorphism**. Gondwana Research, 13, 1-29.

Kelsey, D. E. and Hand, M. 2015. **On ultrahigh temperature crustal metamorphism: Phase equilibria, trace element thermometry, bulk composition, heat sources, timescales and tectonic settings.** Geoscience Frontiers, 6, 311-356.

Kunz, B.E., Regis, D., Engi, M., 2018. **Zircon ages in granulite facies rocks: decoupling from geochemistry above 850 °C?** Contributions to Mineralogy and Petrology 173, 26. Doi: 10.1007/s00410-018-1454-5.

Lanari, P. and Duesterhoeft, E. 2019. **Modelling metamorphic rocks using equilibrium thermodynamics and internally consistent databases: past achievements, problems and perspectives**. Journal of Petrology, 60, 19-56.

Lanari, P., Giuntoli, F., Loury, C., Burn, M., Engi, M. 2017**. An inverse modeling approach to obtain P-T conditions of metamorphic stages involving garnet growth and resorption.** European Journal of Mineralogy, 29, 181-199.

Laurent, A., Bingen, B., Duchene, S., Whitehouse, M.J., Seydoux-Guillaume, A.-M., Bosse, V., 2018. **Decoding a protracted zircon geochronological record in ultrahigh temperature granulite, and persistence of partial melting in the crust, Rogaland, Norway.** Contributions to Mineralogy and Petrology 173, 29. https://doi.org/10.1007/s00410-018-1455-4.

Lee, J., Williams, I., Ellis, D., 1997. **Pb, U and Th diffusion in natural zircon**. Nature, 390, 159–162. https://doi.org/10.1038/36554.

Murphy, J.B., Pisarevsky, S.A., Nance, R.D., Keppie, J.D. 2004. **Neoproterozoic–early Paleozoic evolution of peri-Gondwanan terranes implications for Laurentia–Gondwana connections in The Avalonian–Cadomian belt and related peri-Gondwanan terranes.** International Journal of Earth Sciences 93, 659–682. https://doi.org/10.1007/s00531-004-0412-9

Nelson, D.R., 2001. **An assessment of the determination of depositional ages for Gondwana clastic sedimentary rocks by U–Pb dating of detrital zircons**. Sedimentary Geology, 141–142, 37–60.

Pattison, D. M. and Begin, N. J. 1994. **Hierarchy of closure temperatures in granulites and the importance of an intergranular exchange medium (melt?) in controlling maximum Fe-Mg exchange temperatures**. Mineralogical Magazine, 58ª, 694-695.

Pattison, D. M., Chacko, T., Farquhar, J., McFarlane, C. R. M. 2003. **Temperatures of granulite-facies metamorphism: constraints from experimental phase equilibria and thermobarometry corrected for retrograde exchange.** Journal of Petrology, 44(5), 867-900. https://rclc.facsci.ualberta.ca/

Powell, R. and Holland, T. J. B. 1988. **An internally consistent thermodynamic dataset with uncertainties and correlations: 3: application methods, worked examples and a computer program.** Journal of Metamorphic Geology, 6, 173-204.

Powell, R. and Holland, T. J. B. 1994. **Optimal geothermometry and geobarometry**. American Mineralogist, 79, 120-133.

Powell, R., and Holland, T. J. B. 2008. **On Thermobarometry**. Journal of Metamorphic Geology, 26, 155-179.

Rocha, B. C., Moraes, R., Möller, A., Cioffi, C. R. 2018. **Magmatic inheritance vs. UHT metamorphism: Zircon petrochronology of granulites and petrogenesis of charnockitic leucosomes of the Socorro–Guaxupé nappe, SE Brazil**. Lithos 314-315: 16-39.

Rubatto, D. 2017. **Zircon: the metamorphic mineral**. Reviews in Mineralogy and Geochemistry, 83, 261-295.

Santosh, M. and Kusky, T. 2010. **Origin of paired high pressure–ultrahigh-temperature orogens: a ridge subduction and slab window model.** Terra Nova, 22, 35-42.

Taylor, R.J.M., Kirkland, C.L., Clark, C., 2016. **Accessories after the facts: Constraining the timing, duration and conditions of high-temperature metamorphic processes.** Lithos 264, 239–257.

Tedeschi, M., Pedrosa-Soares, A.; Dussin, I., Lanari, P., Novo, T., Pinheiro, M. A. P., Lana, C., Peters, D. 2018**. Protracted zircon geochronological record of UHT garnet-free granulites in the Southern Brasília orogen (SE Brazil): Petrochronological constraints on magmatism and metamorphism**. Precambrian Research 316: 103-126.

Tedeschi, M., Rossi Vieira, P. L., Kuchenbecker, M., Ribeiro, B. V., Barrote, V., Reis, H., Stutenbecker, L., Lana, C., Pedrosa-Soares, A., Dussin, I. 2023**. Unravelling and overcoming potential biases in U-Pb detrital zircon records induced by high to ultra-high temperature metamorphism (> 850 ºC)**. Geoscience Frontiers, 14, 101515. https://doi.org/10.1016/j.gsf.2022.101515

Vervoort, J. D. and Kemp, A. I. S. 2016. **Clarifying the zircon Hf isotope record of crust–mantle evolution.** Geochemical Geology, 425, 65-75.

Wan, Y., Liu, D., Dong, C., Liu, S., Wang, S., Yang, E. 2011**. U–Th–Pb behavior of zircons under high-grade metamorphic conditions: A case study of zircon dating of meta-diorite near Qixia, eastern Shandong**. Geoscience Frontiers, 2(2), 137–146. https://doi.org/10.1016/j.gsf.2011.02.004.

Watson, E.B., Wark, D.A., and Thomas, J.B., 2006, **Crystallization thermometers for zircon and rutile.** Contributions to Mineralogy and Petrology, 151, 413–433. Doi: 10.1007/s00410–006–0068–5.

Whitehouse, M. J. and Kemp, A. I. S. 2010. **On the difficulty of assigning crustal residence, magmatic protolith and metamorphic ages to Lewisian granulites: constraints from combined in situ U–Pb and Lu–Hf isotopes**. Geological Society, London, Special Publication, 335, 81-101.

3 GEOLOGICAL CONTEXT AND SCIENTIFIC QUESTIONS

3.1 UHT metamorphism on the Southern Brasília and Araçuaí orogens

The Brasília and Araçuaí orogens are part of the Brasiliano – Pan African orogenic systems developed at the margins of the São Francisco paleocontinent during the amalgamation of the Gondwana supercontinent between ca. 640 – 500 Ma, although both orogens evolved diachronically (Campos Neto and Caby., 2000; Almeida et al., 2000; Heilbron et al., 2017).

The Brasília Orogen was developed as the result of the accretion of several exotic terranes onto the western and southwestern margins of the São Francisco paleocontinent during the Neoproterozoic, such as: the Goiás paleocontinent, Goiás and Mara Rosa magmatic arcs on its northern sector; and the Paranapanema paleocontinent and Guaxupé magmatic arc on its southern sector (Pimentel and Fuck, 1992; Pimentel et al., 2003; Jost et al., 2005, 2013; Mantovani et al., 2005; Laux et al., 2005; Valeriano, 2017; Campos Neto et al., 2020). The Araçuaí Orogen resulted from the convergence between the Congo and Sâo Francisco paleocontinents, two continental blocks that remained connected by a crustal bridge from the Rhyacian until the Lower Cretaceous (Porada, 1989; Ledru et al., 1994; Da Silva et al., 2002; Pedrosa-Soares et al., 2001, 2008; Alkmim et al., 2006, 2017).

A synthesis of the regional geological context for the works carried out during the development of this thesis is presented below.

3.1.1 South of the Southern Brasília Orogen

The Brasília Orogen exhibits preserved petrotectonic associations corresponding to the rift stage, passive margin, continental and island magmatic arc, and syn-collisional magmatism and sedimentary basins accreted during its evolution (Fuck et al., 1994; Campos Neto and Caby, 2000). In the South of the Southern Brasília Orogen, those different crustal sections are exposed as a stack of nappes (Figure 1): i) the Socorro-Guaxupé Nappe corresponds to the deep roots of the Guaxupé magmatic arc, developed at the active margin of the Paranapanema paleocontinent between ca. 790 – 640 Ma; ii) the Andrelândia Nappe System (composed of the upper Três Pontas-Varginha Nappe, the intermediate Liberdade Nappe and the lower Andrelândia Nappe) represents the accretionary prism and foreland; and iii) the passive margin of the São Francisco paleocontinent, represented by the Lima Duarte and Carrancas Nappes, the São Vicente Complex and by basement orthogneisses. (Campos-Neto and Caby, 1999, 2000; Trouw et al., 2000, 2013; Fetter et al., 2001;

Campos Neto et al., 2004, 2010, 2020; Reno et al., 2009, 2012; Cioffi et al., 2016a,b, 2019; Westin et al., 2016, 2019; Coelho et al., 2017; Rocha et al., 2017, 2018; Frugis et al., 2018; Tedeschi et al., 2018; Kuster et al., 2020; Motta et al., 2021).

Those nappes record different stages of the Southern Brasília Orogen metamorphic history. The UHT metamorphic stage is mainly represented on the northern domain (Guaxupé Lobe) of the Socorro-Guaxupé Nappe (Campo Neto and Caby, 2000; Del Lama et al., 2000; Campos Neto et al., 2004; Rocha et al., 2017; Rocha et al., 2018; Tedeschi et al., 2018; Motta et al., 2021). The Andrelândia Nappe System records an inverted metamorphic pattern, in which the high-pressure (HP) granulites observed in the uppermost allochton (Três Pontas-Varginha Nappe) overlie lower pressure rocks found in the intermediate and lower members of the stack (Liberdade and Andrelândia nappes, respectively) (Campos Neto and Caby, 1999, 2000; Campos Neto et al., 2010, 2020; Reno et al., 2009, 2012; Cioffi et al., 2012; Motta and Moraes, 2017).

Arc-related rocks in the Socorro-Guaxupé Nappe are represented by plutonic (meta)igneous rocks of granitic to tonalitic composition and their granulitic counterparts (including charnockitic rocks), exhibiting magmatic ages between ca. 790 – 640 Ma and crustal isotopic signatures which points out to a continental arc affinity (Basei et al., 1995; Ebert et al., 1996; Janasi, 1999; Hackspacher et al., 2003; Reno et al., 2009; Mora et a., 2014; Vinagre et al., 2014; Rocha et al., 2017, 2018; Tedeschi et al., 2018). Moderately juvenile rocks with island arc to continental arc affinity were only recently found in the nappe (Costa et al., 2022; Rossi-Vieira et al., 2023).

UHT metamorphic conditions between 900 – 1040 °C, 12 – 15 kbar were estimated in the northern lobe of the Socorro-Guaxupé Nappe (Guaxupé domain) by the works of Campos Neto and Caby (1999, 2000), Del Lama et al. (2000), Reno et al. (2009), Rocha et al. (2017, 2018), Tedeschi et al. (2018) and Motta et al. (2021). Different tectonic settings were proposed for the UHT metamorphic event: i) Campos Neto and Caby (1999, 2000) and Campos-Neto et al. (2004) propose that UHT metamorphic conditions were achieved at the roots of the magmatic arc during the subduction to collision transition between ca. 630 – 625 Ma; ii) Del Lama et al. (2000) proposed a collisional setting for the UHT metamorphic event, with a duration between ca. 660 – 630 Ma; iii) Reno et al. (2009) proposes a subduction-related metamorphic peak, with near-peak ages of ca. 680 Ma and a high density of post-peak zircon formation and melt crystallization ages at ca. 648 Ma and ca. 622 Ma; iv) Rocha et al

(2017, 2018) propose a long-lived (~30 Myr) metamorphic event, with an UHT metamorphic peak between ca. 630 – 625 Ma related to crustal thickening and the accumulation of radiogenic elements during the collisional stage, followed by melt crystallization between ca. 625 – 600 Ma; v) Tedeschi et al. (2018) proposes a two-stage arc-related metamorphic event, the first related to the development of the magmatic arc between ca. 680 – 640 Ma, with the onset of the UHT metamorphism at ca. 660 Ma, and the second related to collision and posterior decompression between ca. 640 – 600 Ma.

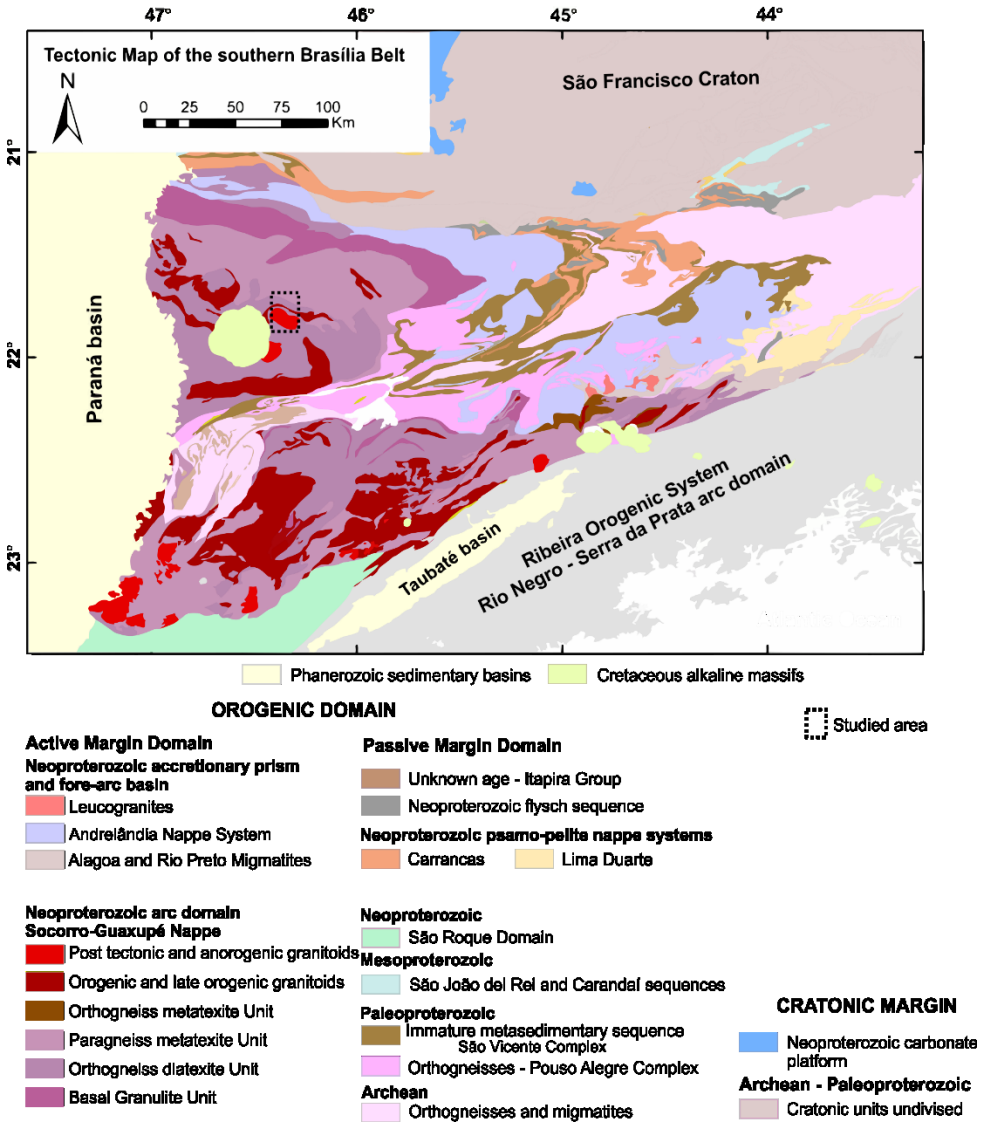

Figure 3-1 - Sketch map of the Southern Brasília Orogen (modified from Cioffi et al., 2016a).

3.1.2 Araçuaí Orogen

The Araçuaí Orogen and its African counterpart, the West-Congo Orogen, define a typical confined orogenic system developed inside an embayment on the São Francisco-Congo paleocontinent (Pedrosa-Soares et al., 2001; Rogers and Santosh,

2004; Alkmim et al., 2006; Pedrosa-Soares et al, 2008). It exhibits geotectonic components from the rift to ocean stage precursor basins, pre-collisional Rio Doce Magmatic arc, pre- to syn-orogenic basins and a large volume of collisional to post collisional magmatic rocks (Pedrosa-Soares et al., 1998; Pedrosa-Soares et al., 2011; Gradim et al., 2014; Kuchenbecker et al., 2015; Tedeschi et al., 2016; Richter et al., 2016; De Campos et al. 2016; Melo et al., 2017; Degler et al., 2017; Serrano et al., 2018; Deluca et al., 2019; Castro et al., 2019, 2020; Amaral et al., 2020; Araujo et al., 2020) (Figure 2).

The precursor basins are represented by: the Macaúbas Group, representative of the rift (Lower and Middle Macaúbas Group) to passive margin (Upper Macaúbas Group, including the ophiolite-related Ribeirão da Folha Formation) sequences (Pedrosa-Soares et al., 2011a, 2020; Pedrosa-Soares and Alkmim, 2011; Kuchenbecker et al., 2015; Amaral et al., 2020); the Jequitinhonha Complex, correlated to the passive margin units of the Macaúbas Group (Gonçalves-Dias et al., 2011; Alkmim et al., 2017); the Dom Silvério Group (Gradim, 2012) and Santo Antônio do Grama Unit (Queiroga, 2010), both representative of ophiolite sequences (Pedrosa-Soares et al., 2007, 2020; Amaral et al., 2020); and partially by the Andrelândia Unit, which represents passive margin, forearc and intra-arc sedimentary sequences (Degler et al., 2017; Pedrosa-Soares et al., 2020). The arc-related and orogenic basins are represented by: the metavolcanic and metasedimentary rocks from the Rio Doce Group (Vieira et al., 2004, 2006; Novo et al., 2018); the Andrelândia Unit (Degler et al., 2017; Pedrosa-Soares et al., 2020); the back-arc-related Nova Venécia Complex (Gradim et al., 2014; Richter et al., 2016; Araújo et al., 2020); and the Salinas Formation, representative of arc-related and orogenic deposits (Lima et al., 2002; Peixoto et al., 2015; Deluca et al., 2019; Pedrosa-Soares et al., 2020).

The evolution of the Araçuaí orogen can be synthetized in three main stages with their characteristic igneous supersuites: i) the pre-collisional stage (ca. 630 – 585 Ma), corresponding to the generation of the Rio Doce Magmatic arc; ii) the collisional stage (ca. 585 – 540 Ma), corresponding to the regional metamorphic peak associated with a large volume of granites; and iii) the post-collisional stage (ca. 530 – 480 Ma), corresponding to the orogenic collapse. Those stages are associated with characteristic plutonism grouped in five igneous supersuites: the I-type G1 Supersuite, composed by igneous and metaigneous rocks of tonalitic to granodioritic affinity generated in the pre-collisional to early-collisional stage; the S-type G2 Supersuite,

encompassing garnet-, cordierite- and sillimanite-bearing (meta)granites from the late pre-collisional to tardi-collisional stages; the S-type G3 Supersuite, composed of (cordierite-)garnet leucogranites (and metagranites) formed by anatexis of the G2 metagranites during the late-collisional to post-collisional stages; and the G4 (mostly S-type) and G5 (mostly A- to I-type) Supersuites, with a variety of granitic-charnockitic and gabbronoritic post-collisional intrusions (Pedrosa-Soares et al., 2011, 2020; Gradim et al., 2014; De Campos et al., 2016; Gonçalves et al., 2016, 2018; Tedeschi et al., 2016; Melo et al., 2017, 2020; Deluca, 2018; Serrano et al., 2018; Aranda et al., 2020; Araújo et al., 2020, 2023; Soares et al., 2020).

Ultrahigh temperature metamorphic rocks are scarce along the Araçuaí Orogen. Known reports are: i) in the Nova Venécia Complex (990 °C, ~6 kbar; Gradim, 2013; Gradim et al., 2014; Wisniowski et al., 2021), interpreted as a result of high thermal gradients in a back-arc context (Gradim, 2013; Gradim et al., 2014) or a metamorphic halo around mafic post-collisional intrusions (ca. 520 Ma; Wisniowski et al., 2021); ii) in graphite-bearing paragneisses (kinzingites) and granulites from the Jequitinhonha Complex (930 °C, 7 kbar; Belém, 2006); iii) in granulitic orthogneisses from the Juiz de Fora Complex in the Manhuaçu region, part of the orogen basement (~990 °C; Moreira, 1997; Costa, 1998); iv) in paraderived rocks of uncertain affiliation found along the Caparaó Range (965 – 1030 °C, 7.0 – 9.6 kbar; Vieira, 2018; Rossi-Vieira et al., submitted). High pressure granulites were first described by Degler et al. (2019) at the Manhuaçu region, 35 km to the northwest of the Caparaó Range (Ky-Grt-Kfs granulites, ~800 °C, 17 kbar).

Due to their spatial proximity with high pressure granulites, the Caparaó Range occurrences might be indicative of a subduction-related context for the UHT metamorphism. Minimum ages obtained for this metamorphic event (ca. 635 – 610 Ma; Vieira, 2018; Rossi-Vieira et al., submitted) are inside the range of the pre-collisional stage, corresponding to the development of the Rio Doce Magmatic Arc (ca. 635 – 585 Ma; Novo et al., 2010; Pedrosa-Soares et al., 2011; Bento dos Santos et al., 2015; Tedeschi et al., 2016).

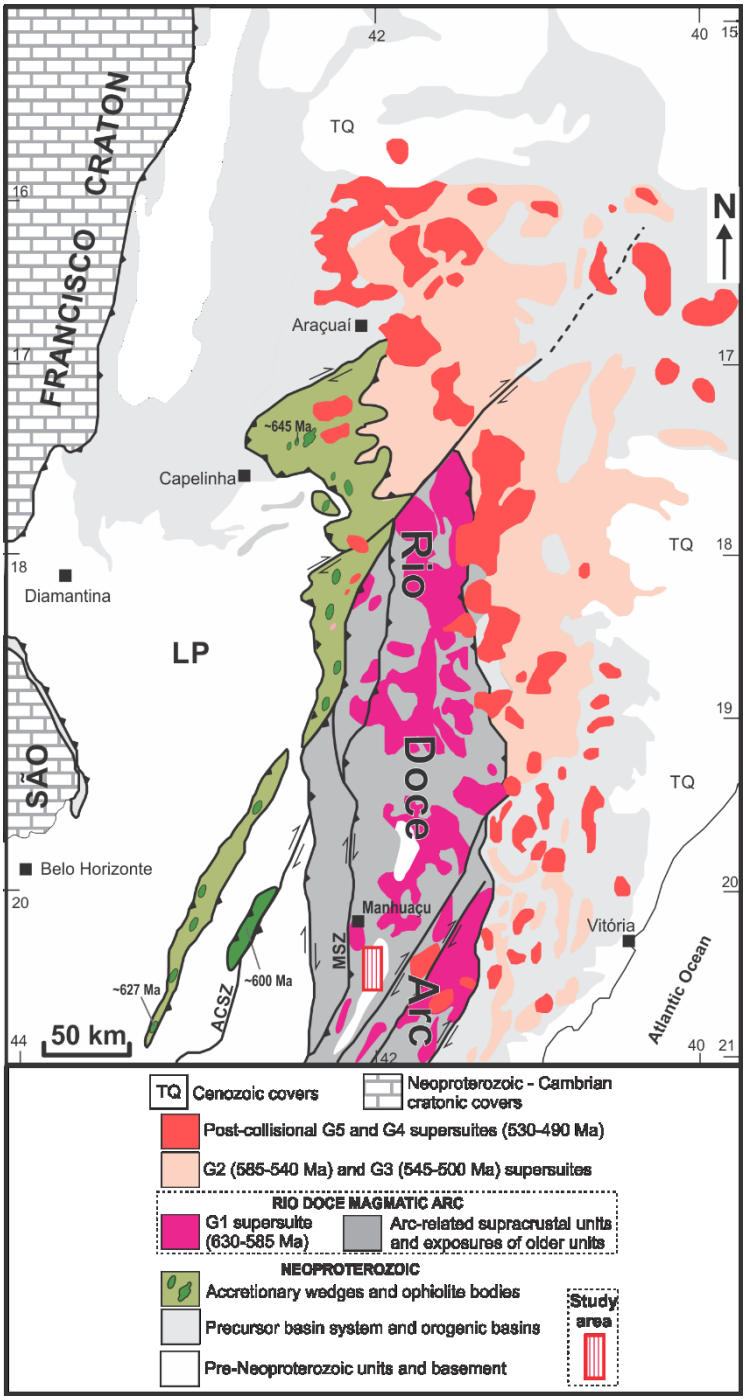

Figure 3-2 - Sketch geological map of the Araçuaí orogen (modified from Pedrosa-Soares et al., 2011, and Amaral et al., 2020).

3.2 Justificative and scientific questions

In the light of the geological context, the main motivations behind the development of this thesis are:

- Although there are previous studies about the UHT metamorphism in the Araçuaí Orogen (Moreira, 1997; Costa, 1998; Belém, 2006; Gradim, 2013; Gradim et al., 2014; Vieira, 2018; Wisniowski et al., 2021), there was a

need for detailed metamorphic modelling and a better comprehension of the age of the UHT metamorphic event(s);

- As previous works about UHT metamorphism on the Socorro-Guaxupé Nappe were mostly based on orthoderived metamorphic rocks (e.g., Campos Neto and Caby, 2000; Del Lama et al., 2000; Trouw et al., 2013; Rocha et al., 2018; Tedeschi et al., 2018; Motta et al., 2021), a deeper investigation about the provenance and possible sedimentary sources for paraderived metamorphic rocks (e.g., Rocha et al., 2017) was needed, as well as the effects of (U)HT metamorphism on them in order to better comprehend the temporal link between sedimentation and metamorphism;
- Although it is commonly observed on dating routines for (U)HT metamorphic rocks, the effects of U-Pb dates spreading on sedimentary provenance studies and possible strategies to retrieve their geological meaning were focused by relatively few studies in the literature (e.g., Tedeschi et al., 2023);
- The time window for the UHT metamorphic events on the Socorro-Guaxupé Nappe (between ca. 630 – 625 Ma, Campos Neto and Caby, 2000, Campos-Neto et al., 2004, Rocha et al., 2017, 2018; between ca. 660 – 630 Ma, Del Lama et al., 2000; between ca. 680 – 640 Ma, Tedeschi et al., 2018; between ca. 625 – 595 Ma, Motta et al., 2021; at ca. 680 Ma, Reno et al., 2009) and on the Caparaó Complex (ca. 635 – 610 Ma; Vieira, 2018, Rossi Vieira et al., submitted) appear to be similar, as well as their tectonic contexts;

The driving questions that motivated these investigations are:

- What are the pressure-temperature metamorphic conditions achieved during the UHT metamorphic event at the Southern Araçuaí Orogen? What is the tectonic setting related to the UHT metamorphism?
- Is it possible to retrieve information about protosources that contributed to the deposition of paraderived rocks affected by (U)HT metamorphism?
- What are the geological and tectonic settings in which the sedimentary protoliths of paraderived rocks from the Socorro-Guaxupé Nappe were deposited, based on U-Pb geochronology and Lu-Hf isotopes?

- What are the geological and tectonic settings in which the sedimentary protoliths of paraderived rocks from the Caparaó Complex were deposited, based on U-Pb geochronology and Lu-Hf isotopes?
- What are the possible correlations and similarities between the UHT metamorphism occurrences on the Southern Brasília and Araçuaí orogens?

Based on those questions, the driving hypothesis for the development of this research are:

- UHT metamorphism occurrences on the Caparaó Complex and Manhuaçu region are inside the Rio Doce magmatic arc domain, which is indicative of a correlation between both and processes involved in the development of the Rio Doce magmatic arc;
- The spatial proximity between the Caparaó Complex and Manhuaçu region UHT and HP granulite metamorphism occurrences and the seemingly absence of similar occurrences in farther areas inside the Rio Doce magmatic arc domain might be indicative of a paired UHT-HP belt;
- The occurrence of UHT paraderived rocks inside the magmatic arc domains both on the South of the Araçuaí and Southern Brasília orogens is indicative that sedimentary sources are probably mainly arc-related, possibly with varied contributions from basement and other sources;
- Since the UHT metamorphism occurences on the South of the Araçuaí and Southern Brasília Orogen exhibit a spatial correlation with arc-related rocks, the processes involving subduction probably had a main role in the development of extreme metamorphic temperatures in the context of the West Gondwana amalgamation.

3.3 References

Alkmim, F. F., Kuchenbecker, M., Reis, H. L. S., Pedrosa-Soares, A. C. 2017. **The Araçuaí Belt. In: Heilbron, M., Cordani, H. G., and Alkmim, F. F. (eds.). São Francisco Craton, Eastern Brazil – Tectonic Genealogy of a Miniature Continent.** Regional Geology Reviews. Springer. P. 255-276. https://doi.org/10.1007/978-3-319-01715-0_14

Alkmim, F. F., Marshak, S., Pedrosa-Soares, A. C., Peres, G. G., Cruz, S. C. P., Whittington, A. 2006. **Kinematic evolution of the Araçuaí-West Congo orogen in Brazil and Africa: nutcracker tectonics during the Neoproterozoic assembly of Gondwana**. Precambian Research, 149, 43-63.

Almeida, F.F.M., Brito Neves, B.B., Carneiro, C.D.R., 2000. **Origin and evolution of the South American Platform.** Earth-Science Reviews, 50, 77 – 111.

Amaral, L., Caxito, F. A., Pedrosa-Soares, A. C., Queiroga, G., Babinski, M., Trindade, R., Lana. C., Chemale, F. 2020. **The Ribeirão da Folha ophiolite-bearing accretionary wedge (Araçuaí orogen, SE Brazil): New data for Cryogenian plagiogranite and metasedimentary rocks**. Precambrian Research, 336, DOI: https://doi.org/10.1016/j.precamres.2019.105522

Araujo, C., Pedrosa-Soares, A., Lana, C., Dussin, I., Queiroga, G., Serrano, P., Medeiros-Junior, E. 2020. **Zircon in emplacement borders of post-collisional plutons compared to country rocks: A study on morphology, internal texture, U-Th-Pb geochronology and Hf isotopes (Araçuaí orogen, SE Brazil).** Lithos, 352-353, 105252.

Belém, J. 2006. **Caracterização Mineralógica, Física e Termobarométrica de Minérios de Grafita da Província Grafítica Bahia-Minas**. (Dissertação de Mestrado). Universidade Federal de Minas Gerais, Belo Horizonte, Brasil. 180 pp.

Bento dos Santos, T.M., Tassinari, C.C.G., Fonseca, P.E. 2015. **Diachronic collision,slab break-off and long-term high thermal flux l Brasiliano-Pan-Africanorogeny: implications for the geodynamicevolution of the Mantiqueira Province.** Precambrian Research, 260, 1-22. DOI: http://dx.doi.org/10.1016/j.precamres.2014.12.018

Campos-Neto, M.C., Basei, M.A.S., Vlach, S.R.F., Caby, R., Szabó, G.A.J., Vasconcelos, P.,2004. **Migração de orógenos e superposição de orogêneses: um esboço da colagem Brasíliana no sul do Cráton do São Francisco, SE e Brasil**. Revista do Instituto de Geociências e USP. Geologia USP Série Científica 4 (1): 13-40.

Campos-Neto, M. C. and Caby, R. 1999. **Neoproterozoic high-pressure metamorphism and tectonic constraint from the nappe system south of the Sao Francisco Craton, southeast Brazil**. Precambrian Research 97 (1–2): 3–26.

Campos-Neto, M. C. and Caby, R. 2000. **Terrane accretion and upward extrusion of high-pressure granulites in the Neoproterozoic nappes of southeast Brazil: Petrologic and structural constraints.** Tectonics 19(4): 669–687.

Campos Neto, M. C., Cioffi, C. R., Moraes, R., Motta, R. G., Siga Jr., O., Basei, M. A. S., 2010. **Structural and metamorphic control on the exhumation of high-P granulites: the Carvalhos Klippe example, from the oriental Andrelândia Nappe system, southern portion of the Brasília Orogen, Brazil**. Precambrian Research 180, 125 – 142.

Campos Neto, M. C., Cioffi, C. R., Westin, A., Rocha, B. C., Frugis, G. L., Tedeschi, M., Pinheiro, M. A. P. 2020. O Orógeno Brasília Meridional. In: Bartorelli, A., Teixeira, W., Brito Neves, B. B. (eds). 2020. **Geocronologia e Evolução Tectônica do Continente Sul-Americano: a contribuição de Umberto Giuseppe Cordani**. Solaris. P. 146-180.

Campos-Neto, M. C. and Figueiredo, M. C. H. 1995. **The Rio Doce orogeny, southeastem Brazil**. Journal of South American Earth Sciences 8(2): 143–162.

Castro, M. P., Queiroga, G., Martins, M., Pedrosa-Soares, A., Dias, L., Lana, C., Silva, M. A. 2020. **Provenance shift through time in superposed basins: From Early Cryogenian glaciomarine to Late Ediacaran orogenic sedimentations (Araçuaí Orogen, SE Brazil).** Gondwana Research, 87, 41-66.

Castro, M. P., Queiroga, G., Martins, M., Alkmim, F., Pedrosa-Soares, A., Dussin, I., Souza, M. E. 2019. **An Early Tonian rifting event affecting the São Francisco-Congo paleocontinent recorded by the Lower Macaúbas Group, Araçuaí Orogen, SE Brazil**. Precambrian Research, 331, 105351.

Cioffi, C. R., Campos Neto, M. C., Möeller, A., Rocha, B. C. 2016a. **Paleoproterozoic continental crust generation events at 2.15 and 2.08 Ga in the basement of the southern Brasília Orogen, SE Brazil.** Precambrian Research, 275, 176-196.

Cioffi, C. R., Campos Neto, M. C., Möller, A., Rocha, B. C. 2016b. **Tectonic significance of the Meso- to Neoarchean complexes in the basement of the southern Brasília Orogen**. Precambrian Research, 287, 91-107.

Cioffi, C. R., Campos Neto, M. C., Moller, A., Rocha, B. C. 2019. **Titanite petrochronology of the southern Brasília Orogen basement: effects of retrograde net-transfer reactions on titanite trace element compositions.** Lithos, 344 – 345, 393 – 408.

Cioffi, C. R., Campos Neto, M. C., Rocha, B. C., Moraes, R., Henrique-Pinto, R. 2012. **Geochemical signatures of metasedimentary rocks of high-pressure granulite facies and their relation with partial melting: Carvalhos Klippe, Southern Brasília Belt, Brazil.** Journal of South American Earth Sciences, 40, 63 – 76.

Coelho, M. B., Trouw, R. A. J., Ganade, C. E., Vinagre, R., Mendes, J. C., Sato, K. 2017. **Constraining timing and P-T conditions of continental collision and late overprinting in the Southern Brasília Orogen (SE-Brazil): U-Pb zircon ages and geothermobarometry of the Andrelândia Nappe System.** Precambrian Research, 292, 194 – 215

Costa, A. G., 1998. **The Granulite-Facies Rocks of the Northern Segment of the Ribeira Belt, Eastern Minas Gerais**, SE Brazil. Gondwana Research, 1(3-4), 367-372.

Da Silva, L. C., Pedrosa-Soares, A. C., Armstrong, R., Noce, C. M. 2011. **Determinando a duração do período colisional do Orógeno Araçuaí com base em geocronologia U-Pb de alta resolução em zircão: uma contribuição para a história da amalgamação do Gondwana Ocidental**. Geonomos, 19(2), 180-197.

De Campos, C. P., De Medeiros, S. R., Mendes, J. C., Pedrosa-Soares, A. C., Dussin, I., Ludka, I. P., Dantas, E.L., 2016. **Cambro-Ordovician magmatism in the Araçuaí Belt (SE Brazil): snapshot from a post-collisional event**. Journal of South American Earth Sciences, 68, 248–268.

Degler, R., Costa, A. G., Pedrosa-Soares, A. C., Queiroga, G. N. 2019. **High pressure metamorphism related to suture zone in the Araçuaí orogen (SE Brazil): further evidence against ensialic models**. XVII Simpósio Nacional de Estudos Tectônicos (SNET), Annals, p. 124. Sociedade Brasileira de Geologia, SBG

Degler, R., Pedrosa-Soares, A. C., Dussin, I., Queiroga, G., Schulz, B. 2017. **Contrasting provenance and timing of metamorphism from paragneisses of the Araçuaí-Ribeira orogenic system, Brazil: Hints for Western Gondwana assembly.** Gondwana Research, 51, 30-50

Del Lama, E. A., Zanardo, A., Oliveira, M. A. F., Moralles, N. 2000. **Exhumation of high-pressure granulites of the Guaxupé Complex, Southeastern Brazil.** Geological Journal 35: 231-249.

Deluca, C., Pedrosa-Soares, A., Lima, S., Cordani, U., Sato, K. 2019. **Provenance of the Ediacaran Salinas Formation (Araçuaí Orogen, Brazil): Clues from lithochemical data and zircon U-Pb (SHRIMP) ages of volcanic clasts**. Brazilian Journal of Geology, 49, 1-19.

Fetter, A. H., Hackspacher, P. C., Ebert, H. D., Dantas, E. L., Costa, A. C. D. 2001. **New Sm-Nd and U-Pb Geochronological Constraints on the Archean to Paleoproterozoic Evolution of the Amparo Basement Complex of the Central Ribeira Belt, South-eastern Brazil.** 3rd South American Symposium on Isotope Geology (Extended Abstracts, CD-ROM).

Frugis, G. L., Campos Neto, M. C., Lima, R. B. 2018. **Eastern Paranapanema and southern São Francisco orogenic margins: records of enduring Neoproterozoic oceanic convergence and collision in southern Brasília Orogen**. Precambrian Research, 308, 35 – 57.

Fuck, R. A., Pimentel, M. M., D'el-Rey Silva, L. J. 1994. **Compartimentação Tectônica na Porção Oriental da Província Tocantins**. In XXXVIII Congresso Brasileiro de Geologia, Camboriú, SBG. Boletim Resumos Expandidos SBG. 1. 215-217.

Gradim, C. 2013. **Complexo Nova Venécia e magmatismo associado, Orógeno Araçuaí, Estado do Espírito Santo** (Dissertação de Mestrado). Universidade Federal de Minas Gerais, Belo Horizonte, Brasil. 123 pp.

Gradim, C., Roncato, J., Pedrosa-Soares, A.C., Cordani, U., Dussin, I., Alkmim, F.F., Babinski, M. 2014. **The hot back-arc zone of the Araçuaí orogen, Eastern Brazil: from sedimentation to granite generation**. Brazilian Journal of Geology, 44, 155-180. DOI: http://dx.doi.org/10.5327/Z2317-4889201400010012.

Heilbron, M., Cordani, U. G., Alkmim, F. F. 2017. **The São Francisco Craton and its margins.** In: Heilbron, M., Cordani, U. G., Alkmim, F. F. (eds). 2017. **The São Francisco Craton, Eastern Brazil – Tectonic Genealogy of a Miniature Continent.** Regional Geology Reviews, Springer. P. 3-14.

Jost, H., Chemale Jr., F., Fuck, R. A., Dussin, L. A. 2013. **Uvá complex, the oldest orthogneisses of the Archean-Paleoproterozoic terrane of Central Brazil**. Journal of South American Earth Sciences, 47, 201-212.

Jost, H., Fuck, R. A., Dantas, E. L., Rancan, C. C., Rezende, D. B., Santos, E., Portela, J. F., Mattos, L., Chiarini, M. F. N., Oliveira, R. C., Silva, S. E. 2005. **Geologia e geocronologia do Complexo Uvá, Bloco Arqueano de Goiás**. Revista Brasileira de Geociências, 35, 559 – 572.

Kuchenbecker M., Pedrosa-Soares A.C., Babinski M., Fanning M. 2015. **Detrital zircon age patterns and provenance assessment for pre-glacial to post-glacial successions of the Neoproterozoic Macaúbas Group, Araçuaí Orogen, Brazil.** Precambrian Research, 266, 12-26.

Kuster, K., Ribeiro, A., Trouw, R. A. J., Dussin, I., Marimon, R. S. 2020. **The Neoproterozoic Andrelândia group: Evolution from an intraplate continental margin to an early collisional basin south of the São Francisco craton, Brazil.** Journal of South American Earth Sciences, 102, 102666

Laux, J. H., Pimentel, M. M., Dantas, E. L., Armstrong, R. A., Junges, S. L. 2005. **Two Neoproterozoic crustal accretion events in the Brasília belt, central Brazil.** Journal of South American Earth Sciences, 18, 183 – 198.

Ledru, P. J., Johan, V., Milési, J. P., Tegycy, M. 1994. **Markers of the last stage of the Paleoproterozoic collision: Evidence for a 2 Ga continent involving circum-South Atlantic provinces.** Precambrian Research, 69, 169-191.

Mantovani, M. S. M., Quintas, M. C. L., Shukowsky. W., Brito Neves. B. B. 2005. **Delimitation of the Paranapanema Proterozoic block: a geophysical contribution.** Episodes, 28, 18 – 22.

Melo, M. G., Lana, C., Stevens, G., Pedrosa-Soares, A. C., Gerdes, A., Alkmin, L. A., Alkmim, F. F., 2017. **Assessing the isotopic evolution of S-type granites of the Carlos Chagas batholith, SE Brazil: clues from U-Pb, Hf isotopes, Ti geothermometry and trace element composition of zircon**. Lithos, 284-285, 730-750

Mora, C.A.S., Campos Neto, M.C., Basei, M.A.S., 2014. **Syn-collisional lower continental crust anataxis in the Neoproterozoic Socorro-Guaxupé Nappe System, southern Brasília Orogen, Brazil: constraints from zircon U-Pb dating, Sr-Nd-Hf signatures and whole-rock geochemistry**. Precambrian Research, 255, 847–864.

Moreira, L. M. 1997. **Evolução crustal do Leste de Minas Gerais: uma contribuição a partir do estudo geotermobarométrico de metamorfitos da região Simonésia-Manhuaçu (MG).** (Tese de Doutorado). Universidade Federal de Minas Gerais, Belo Horizonte, Brasil. 116 pp.

Motta, R. G., Fitzsimons, I. C. W., Moraes, R., Johnson, T. E., Schuindt, S., Benetti, B. Y. 2021. **Recovering P-T-t paths from ultra-high temperature (UHT) felsic orthogneiss: An example from the Southern Brasília Orogen, Brazil**. Precambrian Research, 359, p. 106222.

Motta, R. G. and Moraes, R. 2017. **Pseudo- and real-inverted metamorphism caused by the superposition and extrusion of a stack of nappes: a case study**

of the Southern Brasília Orogen, Brazil. International Journal of Earth Sciences, 106, 2407 – 2427.

Novo, T. A., Pedrosa-Soares, A. C., Noce, C. M., Alkmim, F. F., Dussin, I. A. 2010. **Rochas charnockíticas do sudeste de Minas Gerais: a raiz granulítica do arco magmático do Orógeno Araçuaí**. Revista Brasileira de Geociências, 40(4), 573-592.

Pedrosa-Soares, A. C., Alkmim, F. F., Tack, L., Noce, C. M., Babinski, M. Da Silva, L. C., Martins-Neto, M. A. 2008. **Similarities and differences between the Brazilian and African counterparts of the Neoproterozoic Araçuaí-West-Congo orogen.** Geological Society, London, Special Publications, 294, 153-172.

Pedrosa-Soares, A. C., Campos, C. P., Noce, C., Da Silva, L. C., Novo, T. A., Roncato, J., Medeiros, S., Castañeda, C., Queiroga, G., Dantas, E., Dussin, I., Alkmim, F. F. 2011. **Late Neoproterozoic–Cambrian granitic magmatism in the Araçuaí orogen (Brazil), the Eastern Brazilian Pegmatite Province and related mineral resources.** Geological Society, London, Special Publications, 350, 25-51.

Pedrosa-Soares, A. C., Noce, C. M., Wiedemann, C. M., Pinto, C. P. 2001. **The Araçuaí-West-Congo Orogen in Brazil: an overview of a confined orogen formed during Gondwanaland assembly**. Precambrian Research, 110, 307-323

Pedrosa-Soares, A.C., Vidal, P., Leonardos, O.H., Brito-Neves, B.B., 1998. **Neoproterozoic oceanic remnants in eastern Brazil: Further evidence and refutation of an exclusively ensialic evolution for the Araçuaí-West Congo Orogen**. Geology, 26, 519–522.

Pimentel M. M. and Fuck R. A., 1992**. Neoproterozoic crustal accretion in central Brazil**. Geology, 20, 375 – 379.

Pimentel, M. M., Jost, H., Fuck, R. A., Armstrong, R. A., Dantas, E. L., Potrel, A. 2003. **Neoproterozoic anatexis of 2.9 old granitoids in the Goiás-Crixás block, Central Brazil: Evidence from new SHRIMP U-Pb data and Sm-Nd Isotopes.** Geologia USP. Série Científica, 3, 1-12.

Porada, H. 1989. **Pan-African rifting and orogenesis in southern to equatorial Africa and Eastern Brazil**. Precambrian Research, 44,103-136.

Reno, B.L., Brown, M., Kobayashi, K., Nakamura, E., Piccoli, P.M., Trouw, R.A.J., 2009. **Eclogite–high-pressure granulite metamorphism records early collision in West Gondwana: new data from the Southern Brasília Belt, Brazil**. Journal of the Geological Society, London, 166, 1013–1032.

Reno, B. L., Piccoli, P. M., Brown, M., Trouw, R. A. 2012. **In situ monazite (U-Th)-Pb ages from the Southern Brasília Belt, Brazil: constraints on the high-temperature retrograde evolution of HP granulites**. Journal of Metamorphic Geology, 30, 81 – 112.

Richter, F., Lana, C., Stevens, G., Buick, I., Pedrosa-Soares, A. C., Alkmim, F. F., Cutts, K. 2016. **Sedimentation, metamorphism and granite generation in a back-**

arc region: Records from the Ediacaran Nova Venécia Complex (Araçuaí orogen, Southeastern Brazil). Precambrian Research, 272, 78-100.

Rocha, B. C. 2016. **Idade, duração e condições P-T do metamorfismo de temperatura ultra-alta, anatexia e cristalização de fundido na Nappe Socorro-Guaxupé**. (Tese de Doutorado). Universidade de São Paulo, São Paulo, Brasil. 229 pp.

Rocha, B. C., Moraes, R., Möller, A., Cioffi, C. R. 2018. **Magmatic inheritance vs. UHT metamorphism: Zircon petrochronology of granulites and petrogenesis of charnockitic leucosomes of the Socorro–Guaxupé nappe, SE Brazil**. Lithos 314-315: 16-39.

Rocha, B. C., Moraes, R., Möller, A., Cioffi, C. R., Jercinovic, M. J. 2017. **Timing of anatexis and melt crystallization in the Socorro–Guaxupé Nappe, SE Brazil: Insights from trace element composition of zircon, monazite and garnet coupled to U-Pb geochronology**. Lithos 277: 337-355.

Rogers, J. W. and Santosh, M. 2004**. Continents and Supercontinents**. Oxford, Oxford University Press, 289 p.

Rossi-Vieira, P. L. N. C., Tedeschi, M., Queiroga, G. N., Novo, T., Pedrosa-Soares, A., Lana, C. submitted. **Unveiling the P-T evolution of ultrahigh temperature metamorphism from sapphirine-bearing and orthopyroxene-garnet migmatites – Tectonic implications for the Ediacaran evolution of the Araçuaí orogen (SE Brazil).** Gondwana Research.

Serrano, P., Pedrosa-Soares, A., Medeiros-Junior, E., Fonte-Boa, T., Araujo, C., Dussin, I., Queiroga, G., Lana, C., 2018. **A-type Medina batholith and post-collisional anatexis in the Araçuaí orogen (SE Brazil)**. Lithos, 320-321, 515-536.

Tedeschi, M., Novo, T., Pedrosa-Soares, A.C., Dussin, I., Tassinari, T., Silva, L.C., Gonçalves, L., Alkmim, F.F., Lana, C., Figueiredo, C., Dantas, E., Medeiros, S., De Campos, C., Corrales, F., Heilbron, M., 2016. **The Ediacaran Rio Doce magmatic arc revisited (Araçuaí- Ribeira orogenic system, SE Brazil).** Jounal of South American Earth Sciences, 68, 167–186.

Tedeschi, M., Pedrosa-Soares, A.; Dussin, I., Lanari, P., Novo, T., Pinheiro, M. A. P., Lana, C., Peters, D. 2018. **Protracted zircon geochronological record of UHT garnet-free granulites in the Southern Brasília orogen (SE Brazil): Petrochronological constraints on magmatism and metamorphism.** Precambrian Research 316: 103-126.

Tedeschi, M., Rossi Vieira, P. L., Kuchenbecker, M., Ribeiro, B. V., Barrote, V., Reis, H., Stutenbecker, L., Lana, C., Pedrosa-Soares, A., Dussin, I. 2023. **Unravelling and overcoming potential biases in U-Pb detrital zircon records induced by high to ultra-high temperature metamorphism (> 850 ºC).** Geoscience Frontiers, 14, 101515. https://doi.org/10.1016/j.gsf.2022.101515

Trouw, R. A. J., Heilbron, M., Ribeiro, A., Paciullo, F., Valeriano, C. M., Almeida, J. C. H., Tupinambá, M., Andreis, R. R. 2000. **The central segment of Ribeira Belt**. In: Cordani, U.G., Milani, E.J., Thomaz-Filho, A., Campos, D.A. (Eds.). **Tectonic**

Evolution of South America. 31th International Geological Congress. Rio de Janeiro, Brasil. P. 287 – 310

Trouw, R.A., Peternel, R., Ribeiro, A., Heilbron, M., Vinagre, R., Paciullo, F.V.P., Duffles P., Trouw, C.C., Fontainha, M., Kussama, H.H. 2013. **A new interpretation for the interference zone between the Southern Brasília belt and the central Ribeira belt, SE Brazil.** Journal of South American Earth Sciences, 48: 43-57.

Valeriano, C. M. 2017. **The Southern Brasília Belt**. In: Heilbron, M., Cordani, U. G., Alkmim, F. F. (eds). 2017. **The São Francisco Craton, Eastern Brazil – Tectonic Genealogy of a Miniature Continent**. Regional Geology Reviews, Springer. P. 189-203.

Vieira, P. L. N. C. R. 2018. **Caracterização, condições de metamorfismo e implicações geotectônicas dos migmatitos granatíferos da Serra do Caparaó (MG).** (Dissertação de Mestrado). Universidade Federal de Minas Gerais, Belo Horizonte, Brasil. 124 pp.

Westin, A., Campos Neto, M. C., Cawood, P. A., Hawkesworth, C. J., Dhuime, B., Delavault, H. 2019. **The Neoproterozoic southern passive margin of the São Francisco craton: Insights on the pre-amalgamation of West Gondwana from U-Pb and Hf-Nd isotopes**. Precambrian Research, 320, 454 – 471. https://doi.org/10.1016/j.precamres.2018.11.018

Westin, A., Campos Neto, M. C., Hawkesworth, C. J., Cawood, P. A., Dhuime, B., Delavault, H. 2016. **A Paleoproterozoic intra-arc basin associated with a juvenile source in the Southern Brasília Orogen: Application of U-Pb and Hf–Nd isotopic analyses to provenance studies of complex areas**. Precambrian Research, 276, 178 – 193.

Wisniowski, L, Pedrosa-Soares, A, Medeiros-Junior, E, Belém, J, Dussin, I, Queiroga, G., 2021. **Ultra-high temperature, mid-crustal level, contact metamorphism imprinted on granulite facies paragneisses by a norite intrusion (São Gabriel da Baunilha, Araçuaí orogen, southeast Brazil).** Journal of Metamorphic Geology, 39, 867– 895. Doi.org/10.1111/jmg.12594

4 UNVEILING THE P-T EVOLUTION OF ULTRAHIGH TEMPERATURE METAMORPHISM FROM HERCYNITE-BEARING AND ORTHOPYROXENE-GARNET MIGMATITES – TECTONIC IMPLICATIONS FOR THE EDIACARAN EVOLUTION OF THE ARAÇUAÍ OROGEN (SE BRAZIL)

Rossi Vieira, Pedro L. N. C.[1], Tedeschi, Mahyra[1], Queiroga, Gláucia N.[2], Novo, Tiago A.[1], Pedrosa-Soares, Antonio[1], Lana, Cristiano[2]

1 Universidade Federal de Minas Gerais, Programa de Pós-Graduação em Geologia, CPMTC-IGC-UFMG, Av. Antônio Carlos 6627, Pampulha, 31270-901 Belo Horizonte, MG, Brazil; E-mail: pedro.leonardo@gmail.com*, mtedeschi@ufmg.br, tiagoanovo@gmail.com, pedrosasoares@gmail.com

2 Departamento de Geologia, Escola de Minas, Universidade Federal de Ouro, Morro do Cruzeiro, 35400-000 Ouro Preto, MG, Brazil; E-mail: glauciaqueiroga@ufop.edu.br, cristianodeclana@gmail.com

Submitted to Gondwana Research

Abstract

Ultrahigh temperature (UHT) metamorphic rocks are unusual in orogenic belts around the world, because they require abnormally high heat flows for their genesis and special exhumation processes to preserve their UHT mineral assemblages. They are also useful pathfinders for tracing geotectonic settings and processes. In the Araçuaí orogen, a confined orogenic system developed during the closure of the terminal branch of the Adamastor ocean between the São Francisco and Congo paleocontinents, UHT metamorphic rocks are found in the Caparaó complex (southeastern Brazil) as tectonic slices of metasedimentary garnet-bearing migmatites interleaved with orthoderived granulites and migmatites from basement units. These garnet-bearing migmatites can be subdivided into hercynite-sillimanite-garnet migmatites and orthopyroxene-garnet migmatites. Field-based observation combined with petrography, thermobarometry, thermodynamic modelling has been applied to determine the metamorphic conditions attained in one of the lowermost sections exposed within the southern Araçuaí orogen. Hercynite-sillimanite-garnet migmatites show preserved metamorphic peak assemblages containing hercynite + quartz, while orthopyroxene-garnet migmatites exhibit high-Al orthopyroxene crystals, both characteristic of rocks submitted to UHT conditions. Combined Al-in-orthopyroxene thermobarometry and phase-equilibria modelling revealed the highest metamorphic peak conditions ever disclosed for rocks in the Araçuaí orogen, including 1020 – 1035

°C, 7.0 – 7.1 kbar for hercynite-sillimanite-garnet migmatites, and 962 – 975 °C, 9.5 – 9.6 for orthopyroxene-garnet migmatites. U-Pb (LA-ICP-MS) data for zircon crystals from both migmatite types provided metamorphic ages between ca. 635 Ma to ca. 610 Ma. This time interval corresponds to the pre-collisional stage (630 – 585 Ma) of the Araçuaí orogen, when the Rio Doce magmatic arc was formed, and are considerably older than the collisional metamorphic peak (ca. 563 Ma) obtained from other granulite-facies rocks found in the orogen hot core. The studied rocks are found within the Rio Doce Arc domain, favouring possible sources of heat for achieving UHT metamorphism related to the upwelling of the asthenosphere through a “slab-window” during the subduction of oceanic lithosphere associated with magma underplating and crustal thickening during arc-related magmatism.

Keywords: hercynite, granulite, UHT, magmatic arc, Araçuaí – West Congo orogen

1 Introduction

Ultrahigh temperature (UHT) granulite-facies metamorphic conditions might be achieved in a variety of tectonic settings through different mechanisms: i) the intrusion of large volumes of magma in the lower crust due to magma underplating processes (Harley, 1989; Kelsey, 2008; Harley, 2016); ii) lithospheric thinning associated with asthenospheric ascension (Harley, 1989; Kelsey, 2008; Harley, 2016); iii) accumulation of radiogenic elements due to crustal thickening in orogens (Clark et al., 2011; Harley, 2016); iv) astenospheric ascension due to the presence of a “slab window” during subduction (Brown, 1998a; Santosh and Kusky, 2010). Sections of the crust that underwent large-scale partial melting in past tectonic cycles (e.g. pre-conditioning, Clark et al., 2011; Kelsey and Hand, 2015) seems to be more susceptible to the development of UHT conditions. In order to determine the tectonic setting and mechanism in which UHT metamorphic conditions were attained, a link between the timespan of the metamorphic event, P-T paths and peak metamorphic conditions must be stablished (Harley, 2016).

As several tectonic settings and mechanisms must be taken into account while interpreting UHT metamorphism occurrences, understanding their metamorphic evolution presents several challenges to petrologists. As temperatures (≥900 °C) surpass most closure boundaries for cation-exchange reactions and partial melting takes place, the record of mineral assemblages and their compositions at the metamorphic peak can be completely replaced by those generated during cooling

(Frost and Chacko, 1989; Harley, 1989; Fitzsimons and Harley, 1994; White and Powell, 2002; Powel and Holland, 2008; Moraes et al., 2015). This makes it difficult to determine accurate conditions reached at the metamorphic peak based on classic geothermobarometers. Furthermore, finding the classical “UHT assemblages” (e.g. sapphirine+quartz, hercynite+quartz, orthopyroxene+sillimanite±quartz and osumillite+quartz for metapelitic compositions or garnet+orthopyroxene for metapsammitic compositions) does not necessarily mean that UHT conditions were attained as elements like Fe^{3+} and Zn can substantially change the stability field for those minerals (Waters, 1991; Harley, 1998a; Kelsey, 2008; Taylor-Jones and Powell, 2010). Therefore, thermodynamic calculations involving these rocks might be evaluated with caution. Despite difficulties, retrieving the pressure (P) and temperature (T) trajectories attained by these rocks are of critical importance to understand the origin and tectonic setting in which UHT metamorphism takes place within orogenies.

Special attention might be paid for geochronological studies on UHT rocks as well, as temperatures above 900 °C may partially or fully reset the zircon U-Pb system (Cherniak and Watson, 2003; Wang et al, 2017). Consequently, U-Pb zircon dating in UHT metamorphism can be difficult to interpret due to the data spreading along the Concordia diagram, a common place owing to UHT conditions in long-lived metamorphic history (Whitehouse and Kemp, 2010; Vervoort and Kemp, 2016; Tedeschi et al., 2018, 2023). The understanding of these data, however, is crucial as the timespan between metamorphism and magmatism and the sedimentation history provides insights about the geotectonic settings where ultrahigh temperature conditions take place (Kelsey and Hand, 2015; Harley, 2016).

Our work focuses on high-grade metamorphic rocks of the southern Araçuaí orogen (Brazil) (Figure 1). This orogen is an Ediacaran-Cambrian segment of the Brasiliano/Pan-African orogenic system connected, to the south, with the Ribeira orogen, and correlated with the West Congo belt of central-southwestern Africa (cf. Pedrosa-Soares et al., 2001, 2008; Alkmim et al., 2006). While evidence of ultrahigh temperature (UHT) metamorphic rocks have been documented in the literature for the Araçuaí orogen, there is scarce information regarding the pressure-temperature-time trajectories described by these rocks, especially concerning its southern sector, hampering solid geotectonic interpretations. Here, we present a detailed geothermobarometric investigation on garnet-bearing rocks from the Caparaó Complex (Faria et al., 2022), providing robust data for UHT metamorphic rocks in the

southern sector of the Araçuaí orogen. We employed phase-equilibria modelling and Al-in-orthopyroxene thermobarometry to reconstruct the metamorphic P-T trajectory, as well as U-Pb in zircon geochronology to provide new insights on the evolution of the southern Araçuaí orogen.

2 Geological setting

2.1 The Araçuaí-West Congo orogen

The Ediacaran-Cambrian Araçuaí orogen of southeastern Brazil and its counterpart located in Africa, the West Congo belt (Figure 1A), characterizes a confined orogenic system developed within a large embayment carved into the Congo – São Francisco paleocontinent (Pedrosa-Soares et al., 2001, 2008; Alkmim et al., 2006). Archaean blocks and Rhyacian-Orosirian orogenic systems formed the basement of the Congo – São Francisco palaeocontinent, including its extensions reworked within the Araçuaí – West Congo orogenic system (Cutts et al., 2018; Degler et al., 2018). The Araçuaí orogen (Figure 1B) comprises a complete precursor basin system, evolved from continental rifting to ocean-floor spreading (Pedrosa-Soares et al., 1998; Kuchenbecker et al., 2015; Castro et al., 2019, 2020; Amaral et al., 2020), a pre-collisional magmatic arc (the Rio Doce arc; e.g., Tedeschi et al., 2016) and related orogenic basins (Gradim et al., 2014; Richter et al., 2016; Degler et al., 2017; Novo et al., 2018; Deluca et al., 2019), as well as voluminous collisional to post-collisional granitic and related rocks (Pedrosa-Soares et al., 2011; Melo et al., 2017; Serrano et al., 2018; Araujo et al., 2020).

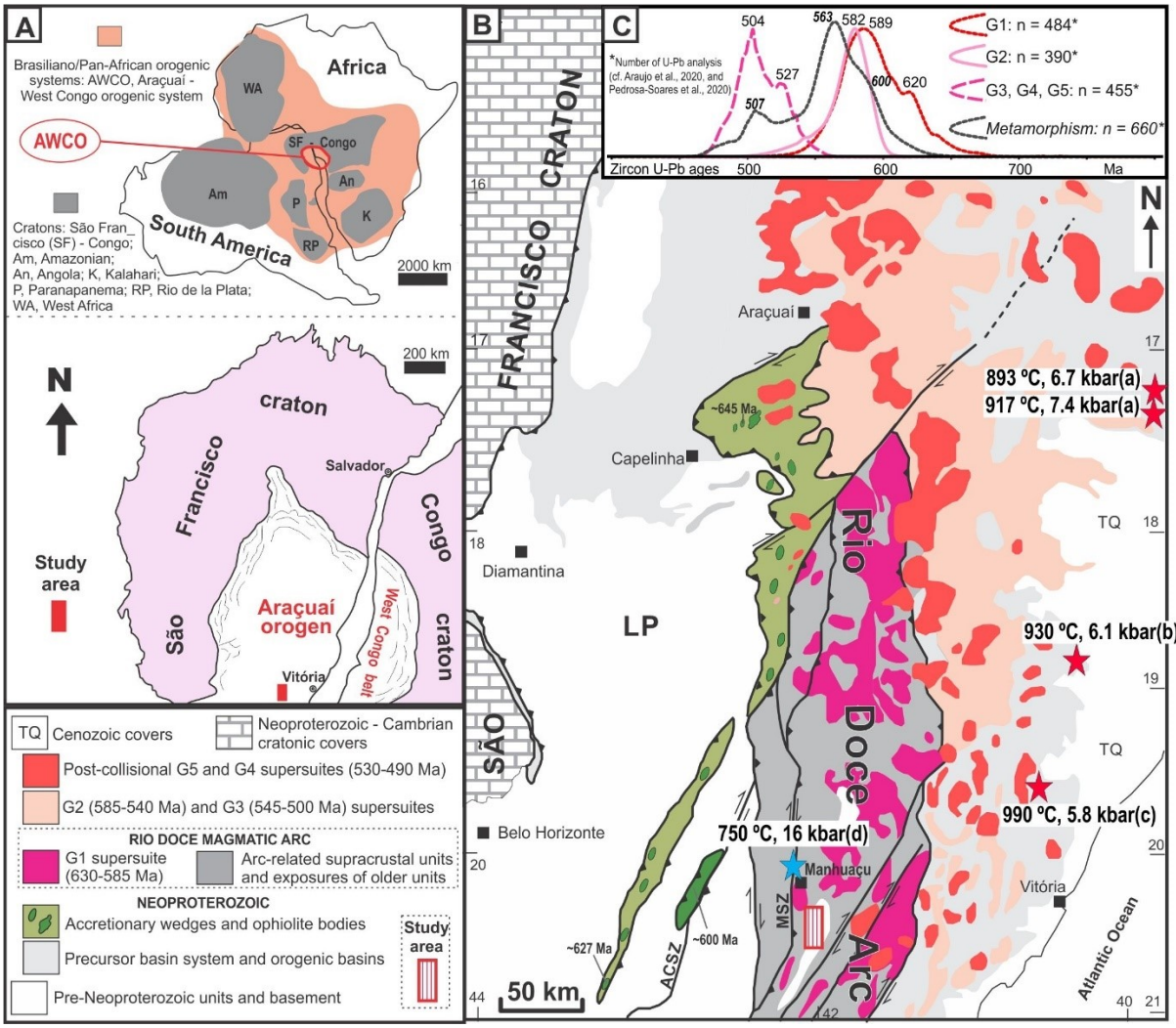

Figure 4-1 - A) Geotectonic setting of the Araçuaí – West Congo orogenic system (AWCO) in West Gondwana and its relation to the São Francisco – Congo craton. B) Sketch geological map of the Araçuaí orogen (modified from Pedrosa-Soares et al., 2011, and Amaral et al., 2020). Red stars: UHT metamorphism data from: (a) Belém (2006); (b) Gradim (2013) and Gradim et al. (2014); (c) Wisniowski et al., 2021. Blue star: HP metamorphism data from (d) Degler et al. (2019). ACSZ, Abre Campo shear zone; MSZ, Manhuaçu shear zone. LP, lower plate basement. C) Zircon U-Pb age distributions for the G1 to G5 plutonic supersuites and metamorphic events (cf. Araujo et al., 2020; Pedrosa-Soares et al., 2020).

The precursor basin system is represented by: i) the Macaúbas group, contraining rift (Lower and Middle sections) to passive margin (Upper section, including the ophiolite-associated Ribeirão da Folha formation) sequences (Pedrosa-Soares et al., 2011a, 2020; Pedrosa-Soares and Alkmim, 2011; Kuchenbecker et al., 2015; Amaral et al., 2020); ii) the Jequitinhonha complex, analogue to the Upper Macaúbas group (Gonçalves-Dias et al., 2011; Alkmim et al., 2017); iii) the Dom Silvério group (Gradim, 2012) and Santo Antônio do Grama unit (Queiroga, 2010), which represents sections of ophiolite sequences (Amaral et al., 2020; Pedrosa-Soares et al., 2020); and iv) the Andrelândia unit, which encompasses passive margin, forearc and intra-arc

sedimentary sequences (Degler et al., 2017; Pedrosa-Soares et al., 2020). Arc-related and orogenic basin systems are constrained by: i) the Rio Doce group, represented by both metasedimentary and metavolcanic rocks (Novo et al., 2018); ii) the Andrelândia unit (Degler et al., 2017; Pedrosa-Soares et al., 2020); iii) the Nova Venécia complex, represented by back-arc sequences (Gradim et al., 2014; Richter et al., 2016; Araújo et al., 2020); and iv) the Salinas formation, represented by orogenic sequences (Peixoto et al., 2015; Deluca et al., 2019; Pedrosa-Soares et al., 2020).

Besides tectonic and metamorphic features, each orogenic stage is marked by at least one characteristic assemblage of metamagmatic and/or igneous rocks regionally recognized in the Araçuaí orogen, which have been grouped into five plutonic supersuites (cf. Pedrosa-Soares et al., 2011; updated by Serrano et al., 2018) summarized ahead (Figure 1B and 1C):

i) the pre-collisional G1 supersuite (630 – 585 Ma) mostly comprises tonalitic to granodioritic (meta)igneous rocks with calc-alkaline-magnesian, metaluminous to slightly peraluminous, I-type signature, representing the plutonic part of the Rio Doce magmatic arc (Gonçalves et al., 2016, 2018; Tedeschi et al., 2016; Novo et al., 2018);

ii) the collisional G2 supersuite (585 – 540 Ma) mostly comprising garnet-rich and two-mica granites (and their metamorphosed to migmatized equivalents) with peraluminous S-type signature (Gradim et al., 2014; Richter et al., 2016; Melo et al., 2017; Serrano et al., 2018);

iii) the late collisional to post-collisional G3 supersuite (545 – 500 Ma) that consists of garnet-cordierite leucogranites with peraluminous S-type signature, free of the regional ductile foliation, forming leucosomes and small plutons hosted by G2 metagranites (Pedrosa-Soares et al., 2011; Gradim et al., 2014; Serrano et al., 2018);

iv) the post-collisional stage comprises: a) the G4 supersuite (530 – 490 Mye), represented by subalkaline to alkaline, peraluminous, garnet-bearing two-mica and pegmathoid granites (Pedrosa-Soares et al., 2011); and b) the G5 supersuite (525 – 480 Ma), represented by A-type and I-type granitic plutons and mafic intrusions which crosscuts the regional ductile structures (De Campos et al., 2016; Serrano et al., 2018; Araujo et al., 2020);

Based on a large dataset (cf. Araujo et al., 2020; and Pedrosa-Soares et al., 2020), the distributions of zircon U-Pb ages show the main peaks related to the orogenic plutonic (G1 to G5) supersuites, as well as a curve obtained from overgrowth rims and neoformed crystals with metamorphic characteristics (Figure 1C). This

metamorphism age distribution unravels two main age peaks: i) the ca. 563 Ma peak corresponds to the regional metamorphism and partial melting associated with the collisional deformation; and ii) the ca. 507 Ma peak for the thermal metamorphism related to the climax of post-collisional magmatism and hydrothermal alteration along shear zones (Degler et al., 2017; Serrano et al., 2018; Gonçalves et al., 2019; Araujo et al., 2020; Pedrosa-Soares et al., 2020). A signal of the existence of pre-collisional metamorphism is given by a discrete peak around ca. 600 Ma in the probability density distribution (Figure 1C), and it has been only recently unravelled by monazite and zircon U-Pb data (Degler et al., 2017; Cutts et al., 2018; Schannor et al., 2019).

Ultra-high temperature conditions in the Araçuaí orogen are mainly reported in its northern sector. Ediacaran hercynite-sillimanite-cordierite granulite from the Nova Venécia complex records metamorphic UHT conditions up to ~930 – 990 °C, 6 – 6.1 kbar (Gradim, 2013; Wisniowski et al., 2021), interpreted as the result of: i) anomalous heat influx under the back-arc due to the subduction of an ocean ridge (“slab window” mechanism) between ca. 590 – 580 Ma (Gradim, 2013); and ii) as product of contact metamorphism around post-collisional mafic magmatism emplacement at ca. 520 Ma (Wisniowski et al., 2021). The Neoproterozoic migmatitic Al-rich graphite-bearing paragneiss and granulite from the Jequitinhonha complex reached conditions up to 930°C, 7 kbar (Belém, 2006). In its southern sector, orthoderived granulites of the Rhyacian basement (Juiz de Fora complex) located northwest of the studied area records temperature of ~990 °C (Moreira, 1997, and Costa, 1998). Nearby this occurrence, located between the area with accretionary wedges and ophiolite slivers and the Rio Doce arc, the Abre-Campo and Manhuaçu shear zones outline the suture zone boundaries from the central to southern Araçuaí orogen (Peres et al., 2004; Alkmim et al., 2006; Peixoto et al., 2015; Degler et al., 2019; Amaral et al., 2020). The first known occurrence of high-pressure granulites (~800 °C, 17 kbar) in the Araçuaí orogen, a K-feldspar-garnet-kyanite paragneiss crops out on the Manhuaçu shear zone (Degler et al., 2019), located 35 km NW of the studied area (Figure 1B).

2.2 The Caparaó Complex

A variety of granulite-facies rocks and migmatites outcrop in the Caparaó complex, located along the Caparaó Range. It includes orthopyroxene-clinopyroxene-bearing orthogneisses and migmatites of dioritic to gabbroic composition, locally with granitic, granodioritic and noritic terms, which have been correlated to the Rhyacian Juiz de Fora complex (Campos-Neto and Figueiredo, 1990; Da Silva et al., 2002; Noce

et al., 2007; Da Silva et al., 2011; Novo et al., 2011). The gneissic banding outlines a N-S-trending, large-scale antiformal structure along the Caparaó Complex, which is thrusted over the Neoproterozoic metasedimentary gneisses and migmatites of the Andrelândia unit through large-scale (about 6 km wide) mylonitic to ultramylonitic zones (Cunningham et al., 1998; Novo et al. 2011; Novo, 2013; Vieira et al., 2019) (Figure 2).

In the study area, the orthoderived migmatites of the Caparaó complex (Caparaó suite, Novo et al., 2011) are divided in two units (metatexite and diatexite) according to their most representative rock type (Figure 2). The metatexite unit is composed of orthopyroxene-clinopyroxene-bearing orthogranulites and patch to stromatic metatexites, with variable contents of orthoclase, hornblende and biotite, ranging in composition from diorite to gabbro. The diatexite unit comprises nebulitic, schöllen and schlieren orthopyroxene-clinopyroxene diatexites and granulites. They are similar in composition to those of the metatexite unit, although rocks free of hornblende and biotite are more common. Garnet is rarely found in both units, and usually forms in reaction rims between orthopyroxene and plagioclase.

Metasedimentary garnet-bearing migmatites, gneisses and granulites are also found in the studied area, forming tectonic slivers interleaved with the orthoderived migmatites. They were subdivided, based on their mineral assemblage relations (see section 4.1), into two major divisions (Figure 2): orthopyroxene-garnet migmatites and hercynite-sillimanite-garnet migmatites. Metasedimentary rocks found near the Caparaó Range have been correlated to the Neoproterozoic Andrelândia unit, including high-pressure granulites with calcsilicate lenses and minor quartzite (Noce et al., 2006; Novo et al., 2012, 2014; Degler et al., 2017; Schannor et al., 2019).

Pre- (G1) to syncollisional (G2) granitoid plutons also outcrop in the surroundings of the Caparao Range, crosscutting both the Caparao complex and the Andrelândia unit rocks. However, no crosscutting relations have been observed between those granitoids and the garnet-bearing migmatites found along the range (Noce et al., 2006; Novo et al., 2012, 2014).

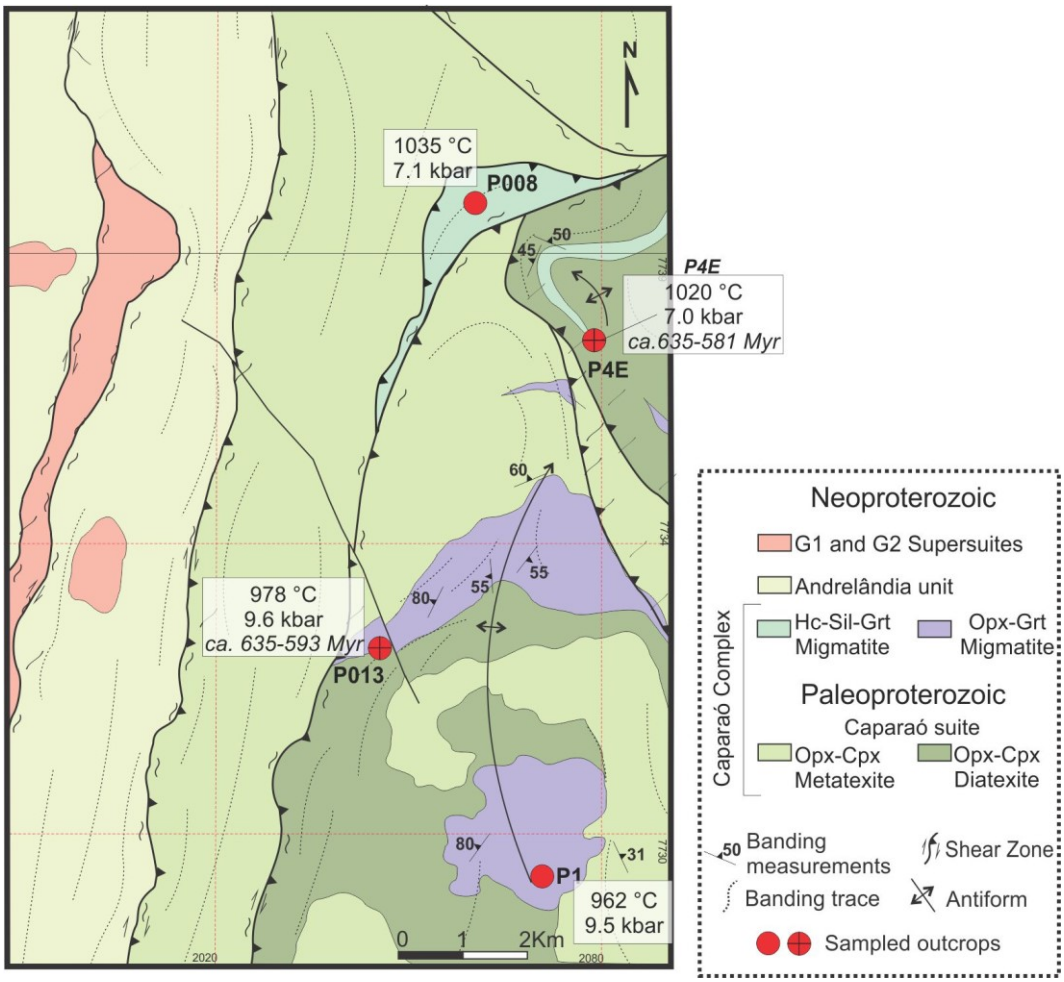

Figure 4-2 - Geological map of the studied area modified after Amaral et al. (2016) and Vieira et al. (2017), emphasizing the locations of the selected outcrops, metamorphic peak pressure-temperature values and metamorphic age ranges obtained in this work. Orthopyroxene-garnet migmatites and hercynite-sillimanite-garnet migmatites are informal units/sequences focused and characterized in this work (see text). Red dots represent outcrops sampled for petrography, electron microprobe analysis and whole-rock geochemistry. Outcrops also sampled for LA-ICP-MS U-Pb geochronology are marked with a cross. Names of samples correspond to the names of the respective outcrops (see Table 1). P1 – schlieren orthopyroxene-garnet diatexite. P013 – layered orthopyroxene-garnet diatexite. P4E – schlieren/schöllen hercynite-sillimanite-garnet diatexite. P008 – sapphirine-bearing schlieren hercynite-sillimanite-garnet diatexite.

3 Materials and Methods

Four outcrops of garnet-bearing migmatites (Figures 2, 3A-D) were selected for detailed characterization. Five samples were collected, prepared and analyzed for petrography (P), electron microprobe analysis (EMPA), laser ablation inductively coupled plasma mass spectrometry (LA-ICP-MS) U-Pb geochronology and whole-rock geochemistry (in order to obtain their bulk-rock composition for phase-equilibria modeling, PEM) as indicated on Table 1. Mineral abbreviations follow the recommendations of Whitney and Evans (2010). Proportions (%) between phases in

petrographic descriptions are reported in vol%, proportions of components in solid solutions are reported in molecular %, and X_{Mg} ($Mg/(Mg+Fe^{2+})$) is reported as a ratio. The nomenclature of migmatites is after Sawyer (2008).

3.1 Mineral chemistry

Mineral chemistry data was obtained from six polished thin sections (Table 1) using a JEOL JXA-8230 electron microprobe at the Microscopy and Microanalysis Laboratory of the Universidade Federal de Ouro Preto (LMIc-UFOP). The electron beam was set at 15 kV, 20 ηA acceleration current, 5-10μm spot size. The raw data was processed with common ZAF matrix corrections. Counting times on the peaks/background were 10/5s for all elements (Si, Al, Ti, Fe, Mn, Mg, Ca, Na, K, Zn, F) except for Cr and Cl (30/15 s). Analytical errors are within 0.2% and 1.1%. Minerals were characterized by analyses from cores and rims when applicable. Analytical standards are presented in Supplementary file 1. A total of 1160 spots of the following minerals were carried out: biotite (Bt), cordierite (Crd), garnet (Grt), hercynite (Hc), ilmenite (Ilm), orthoclase (Or), orthopyroxene (Opx), plagioclase (Pl), sapphirine (Spr) and sillimanite (Sil). As the electron-microprobe analyses accounted all Fe as FeO_T, Fe^{3+} contents (when applicable) were recalculated by charge-balance and stoichiometric equations, along with structural formulae, based on the following authors: Tindle and Webb (1990) for biotite; Deer et al. (1992) for cordierite and sillimanite; Perkins (2007) for garnet, pyroxene and feldspars; Droop (1987) for ilmenite; Higgins et al. (1979), Grew et al., (2008) and Taylor-Jones and Powell (2010) for sapphirine; and using the Spinel End-Member Generator software by Ferracutti et al., (2015) for hercynite and magnetite. Some representative mineral compositions are presented in Supplementary file 2. Mineral phases were divided into different generations based on textural and chemical criteria when applicable, and a summary of the chemical composition of analyzed phases is presented on Tables 2 and 3. Mineral compositions were graphically represented using the TriQuick software, version 1.0.0.23 (Dolivo-Dobrovolsky, 2012), and are presented on Supplementary Figures 1 – 4.

3.2 Temperature and pressure estimates

Temperature and pressure conditions were calculated using garnet-orthopyroxene thermobarometry calibration corrected for Al contents in orthopyroxene (Al-in-orthopyroxene thermobarometry, c.f. Fitzsimons and Harley, 1994; Pattison and Begin, 1994; Pattison et al., 2003; Supplementary file 3) for the layered orthopyroxene-

garnet diatexite (P013) and the schlieren orthopyroxene-garnet diatexite (P1), using the web-based version of the RCLC software (Pattison et al., 2003). Analysis of rims, cores and xenomorphic crystals were selected in order to identify possible metamorphic stages, and metamorphic paths were interpreted accordingly.

Phase-equilibria modelling was applied for the sapphirine-bearing schlieren hercynite-sillimanite-garnet diatexite (P008), schlieren/schöllen hercynite-sillimanite-garnet diatexite (P4E) and layered orthopyroxene-garnet diatexite (P013) in order to plot isochemical diagrams using the Theriak-Domino software (De Capitani and Brown, 1987; De Capitani and Petrakakis, 2010), with a THERMOCALC-translated database 6.2 (Ague, 2023). Bulk-rock compositions correspond to the same rock blocks from which thin sections were made, and calculations were done in the MnNCKFMASHTO system. Isopleths and isolines were combined to the diagrams in order to determine the (near) metamorphic peak, retrograde conditions and metamorphic paths. Activated mineral solution models for phases in the phase equilibria models include: garnet, biotite, orthopyroxene, cordierite and ilmenite from White et al. (2014a, 2014b); feldspar from Holland and Powell (2003); clinoamphibole from Green et al. (2016); sapphirine from Wheeler and Powell (2014); spinel and melt from White et al. (2002, 2007).

The bulk-rock composition of each analyzed sample was obtained through whole-rock geochemistry analysis at the GEOX Laboratory (UFOP) and the SGS GEOSOL Labs. Analytical procedures for each are listed on Supplementary file 1. Three samples were analyzed for major elements; their compositions are presented at Supplementary file 4. As all Fe was accounted as $Fe_2O_3^T$ on the analyses, the total iron was converted to FeO^T through the formula $FeO^T = Fe_2O_3^T*0{,}8998$, and actual Fe^{3+} contents of the samples were determined as described below.

Both H_2O and Fe^{3+} were determined using binary diagrams following an approach similar to that described on Kelsey and Hand (2015) (and references therein), as the values obtained by geochemical analyses usually do not represent the actual contents of analyzed samples and as Fe^{3+} plays an important role on the stability of both spinel (Waters, 1991; Das et al., 2001; White et al. 2002; Kelsey, 2008) and sapphirine (Taylor-Jones and Powell, 2010).

H_2O contents were determined using binary T-X diagrams, initially setting H_2O from 0 to 10% at constant pressures and then refining the analysis for best fitting the observed mineral assemblages by changing the pressure if needed. Fe^{3+} contents

were determined using binary T-X diagrams at constant pressure using the following procedures: 1) set the Fe_2O_3 content of each sample from 0 to 10% of the FeO_T; 2) calculate phase diagrams; 3) calculate isopleths for Fe^{2+} and Fe^{3+}-bearing phases, such as ilmenite (Xhem), garnet (Xalm) and hercynite (XHc); 4) analyze if the intercept is coherent with the observed assemblage, and then identify the corresponding X value; 5) evaluate if the resulting phase equilibria diagrams are representative of the rock assemblages, and change the pressure conditions and repeat steps 1 to 4 if needed.

3.3 LA-ICP-MS U-Pb geochronology

Two samples, the schlieren/schöllen hercynite-sillimanite-garnet diatexite (P4E) and layered orthopyroxene-garnet diatexite (P013) were selected for LA-ICP-MS U-Pb zircon geochronology (Table 1). About 10-15 kg of rock for each sample were prepared for analyses in the Isotopic Geochemistry Laboratory of the Universidade Federal de Ouro Preto (UFOP, Brazil). Zircon separation was performed using conventional methods (crushing, grinding, gravimetric, and magnetic-Frantz isodynamic separator). For geochronological analyses, we selected zircon crystals from the least magnetic fractions, aiming to determine metamorphic ages and possible inherited or igneous zircon populations. A final concentration of zircon crystals was obtained by density separation using bromoform. As this separate consisted of almost only zircon grains (>99%), the grains were randomized in an ethanol solution and then pipetted over epoxy mounts, guaranteeing minimum bias on the selection of zircon crystals for analysis. The mounts were submitted to polishing for exposing grain centers, and backscattered electron (BSE) and cathodoluminescence (CL) images were obtained on a JEOL JSM-6510 Scanning Electron Microscope, equipped with a Centaurus CL detector, at the Microscopy and Microanalysis Laboratory of the Universidade Federal de Ouro Preto (LMIc-UFOP), for revealing morphological features and internal structures of zircon grains.

Analytical spots were performed avoiding grain areas with inclusions, fractures, and metamict features. U-Pb isotopic analyses were performed in the Laboratory of Isotope Geochemistry and Geochronology of the Universidade Federal de Ouro Preto, using a Laser Ablation Multi-Collector Inductively Coupled Plasma Mass Spectrometry (LA-MC-ICP-MS), Neptune Plus model, with a coupled Laser system by Photo Machines. BB (Santos et al., 2017), Gj-1 (Jackson et al., 2004; Morel et al., 2008) and Plešovice (Sláma et al. 2008) standard zircons were used in LA-MC-ICP-MS analytical

routines as reference materials (BB primary, GJ-1 and Plešovice secondary) in order to verify accuracy and reproducibility of the data. Weighted average $^{206}Pb/^{238}U$ ages calculated for the analyzed standards were: 564±3 (P4E routine) and 564±4 (P013 routine) Ma for BB zircon (Santos et al., 2017); 603±2 (P4E routine) and 603±2 (P013 routine) Ma for GJ-1 zircon (Jackson et al., 2004); 339±2 (P4E routine) and 338±2 (P013 routine) Ma for Plešovice zircon (Sláma et al., 2008). The spot diameter size was 25 µm. Data reduction used the Glitter software (Van Achterbergh et al., 2001), and the Excel sheet developed by Ludwig (2003). Data evaluation for each spot considered the common Pb contents, errors of isotopic ratios, the position of each analyzed spot, and the existence of inherited grains and percentage of discordance.

Initial Pb corrections were done after removing the ^{202}Hg interference on the ^{204}Pb signal (e.g., Lana et al 2017, Frei and Gerdes, 2009; Schneider et al., 2015). The ^{204}Pb was calculated by subtracting the average mass 204 signal of the background, which is largely caused by ^{204}Hg in the carrier gas (300–700 cps), from the mass 204 signal during sample ablation whenever possible. However, due to the substantial Hg background, this approach may have unsatisfactory findings for lower radiogenic Pb analyses (e.g., ^{206}Pb 2-104 cps). For low ^{206}Pb, very low $^{206}Pb/^{204}Pb$, and Th/U < 0.6, we use we used the ^{208}Pb signal to determine the ^{204}Pb content by subtracting the radiogenic ^{208}Pb, estimated from the Th signal, and the $^{206}Pb/^{238}U$ age of the analysis. The two-stage evolution model of terrestrial Pb composition (Stacey and Kramers, 1975) was used to do the common-Pb correction based on the interference and background-corrected ^{204}Pb signal. From the selected spots, only those with discordance less than 5% were used for age calculations and plotted in Concordia diagrams. Ages are reported as $^{206}Pb/U^{238}$ ages with 2σ uncertainties. The Concordia diagrams were obtained with the software Isoplot 4.15 (Ludwig, 2008). The U-Pb analytical results are available on Supplementary file 5.

Sample	Lithotype	Coordinates	Mineral Assemblage	P	EMPA	PEM	LA-ICP-MS
P1	Schlieren Opx-Grt diatexite	X: 207104 Y: 7729088 Z: 1347	Ilm+Opx+Grt+Or+Pl+Qz; **A.P.:** Rt, Zr, Mnz, Ap, Py, Cpy, Po	X	X		
P1D		X: 207175 Y: 7729248 Z: 1352	Grt+Bt+Or+Pl+Qz; **A.P.:** Ilm, Rt, Zr, Mnz, Ap, Py, Cpy	X	X		
P4E	Schlieren/ schöllen Hc-Sil-Grt diatexite	X: 207977 Y: 7737495 Z: 2839	Ilm+Hc+Sil+Grt+Pl+Or+Qz; **A.P.:** Ap, Zr, Mnz, Mag	X	X	X	X
P008	Spr-bearing schlieren Hc-Sil-Grt diatexite	X: 206475 Y: 7739546 Z: 2321	Ilm+Hc+Sil+Grt+Pl+Or+Qz; **A.P.:** Spr, Crn, Ap, Zr, Mnz, Mag	X	X	X	
P013	Layered Opx-Grt diatexite	X: 204722 Y: 7732591 Z: 1847	Ilm+Opx+Grt+Or+Pl+Qz **A.P.:** Ap, Zr, Mnz, Py	X	X	X	X

Table 4-1 - Characteristics of outcrops and samples collected for this work. A.P. – accessory phases. X, Y and Z – UTM northing, easting and elevation respectively (Datum SIRGAS 2000, UTM zone 23S). P – Petrography. EMPA – Electron Microprobe Analysis. PEM – Phase-equilibria modeling. LA-ICP-MS – Laser Ablation Inductively Coupled Plasma Mass Spectrometry.

4 Results

4.1 Field relationship and sampling

4.1.1 Orthopyroxene-garnet migmatites

Orthopyroxene-garnet migmatites comprise schlieren to schöllen diatexites (Figure 3A) and subordinate layered diatexites, which outcrop preferably associated with shear zones and the regional fold hinge zone. They are mainly leucosome-rich migmatite bodies, with granitic to dioritic composition, consisting of tectonic slivers of schlieren orthopyroxene-garnet diatexites (P1 and P1D, Figure 2; Table 1) interleaved with orthopyroxene-clinopyroxene diatexites of the Caparaó Suite through ductile shear zones (as evidenced by the presence of mylonites along contact zones). Minor occurrences of layered orthopyroxene-garnet diatexites are observed along shear zones in the central-western part of the Caparaó Range (P013, Figure 2; Table 1).

4.1.2 Hercynite-sillimanite-garnet migmatites

The hercynite-sillimanite-garnet migmatites are schöllen to schlieren diatexites (Figure 3B-D), often exhibiting a flow-banded structure. They exhibit granitic leucosomes and a granulite residue composed of hercynite, sillimanite, garnet and/or cordierite.

Hercynite-sillimanite-garnet diatexites (outcrop P4, Figure 2; sample P4E, Figure 3B) are observed southwest to the highest peak of the Caparao Range (Bandeira Peak), outcropping as tectonic slivers interleaved with orthopyroxene-clinopyroxene diatexites. They consist of schlieren to schöllen diatexites, often presenting similar proportions of residue and leucosome. In parts where schöllen structures are predominant, leucosome “pools” with very coarse garnet crystals (up to 4 cm in diameter) are commonly observed.

Sapphirine-bearing hercynite-sillimanite-garnet diatexites (outcrop P008, Figure 2; sample P008, Figure 3C-D) are schlieren diatexites, exhibiting diffuse to moderately oriented granulite residue schlieren interleaved with leucosome. In weathering-free exposures, the residue exhibits a bluish hue (Figure 3D). They outcrop as a tectonic sliver thrusted over orthopyroxene-clinopyroxene diatexites, as evidenced by contact zones through ductile shear zones. Next to the shear zones, sapphirine is absent.

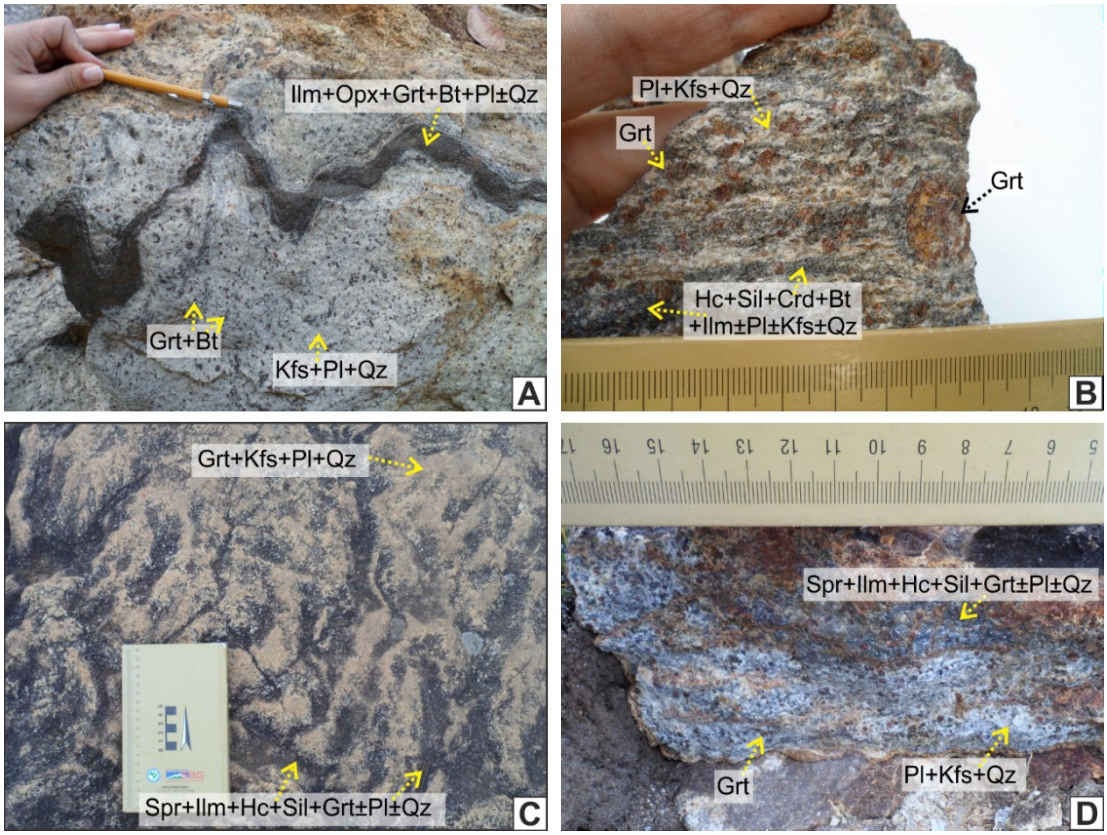

Figure 4-3 - Outcrop- and hand sample-scale features of orthopyroxene-garnet migmatites and hercynite-sillimanite-garnet migmatites. A) Schlieren orthopyoxene-garnet diatexite (P1); B) Schlieren/schöllen hercynite-sillimanite-garnet diatexite (P4E), exhibiting flow banding and cm-scale garnet crystals; C-D) Sapphirine-bearing schlieren hercynite-sillimanite-garnet diatexite (outcrop P008).

4.2 Petrography and Mineral Chemistry

Based on petrography, the migmatites from the four selected outcrops were divided into two groups: hercynite-sillimanite-garnet migmatites, corresponding to the schlieren/schöllen hercynite-sillimanite-garnet diatexite (sample P4E) and the schlieren sapphirine-bearing hercynite-sillimanite-garnet diatexite (sample P008), and the orthopyroxene-garnet migmatites, corresponding to the schlieren orthopyroxene-garnet diatexite (samples P1, P1D) and the layered orthopyroxene-garnet diatexite (sample P013).

4.2.1 Sapphirine-bearing schlieren hercynite-sillimanite-garnet diatexite (sample P008)

The residue of the sapphirine-bearing schlieren hercynite-sillimanite-garnet diatexites consists of a granoblastic granulite composed of hercynite (5%), sillimanite (9%), garnet (14%), plagioclase (16%), orthoclase (23%) and quartz (29%), with ilmenite as a main accessory phase (4%) and minor contents of sapphirine (up to 1%), corundum, apatite, zircon, biotite and magnetite.

Sapphirine is mostly observed as minute crystals at the borders of hercynite crystals (Figure 4A), commonly exhibiting straight contacts. It is also associated, in direct contact or in local domains with garnet, quartz, ilmenite or corundum (+ minor feldspars) (Figure 4B). Sapphirine crystals have compositions close to the 7:9:3 end-member (Table 2, Supplementary figure 1), with considerable Fe^{2+} substitution for Mg (X_{Mg} = 0.78–0.80) and estimated Fe^{3+} contents between 0.10–0.22 apfu (Table 2, Supplementary file 1). Hercynite crystals (mean XHc_{53}) are fine- to medium-grained, often exhibit magnetite exsolution lamellae, present low Zn and low Fe^{3+} contents (Table 2, Supplementary file 2). Straight contacts between hercynite and garnet, quartz, sillimanite, orthoclase and plagioclase dominate (Figure 4A-C), although sillimanite or garnet moats around hercynite may also be observed (Figure 4D). Contacts between hercynite and corundum or sapphirine, when observed, are straight to lobate. Garnet crystals are predominantly medium-grained (Figure 4C), have a homogeneous composition (mean $Xalm_{48}$, $Xpyr_{46}$, $XSps_{02}$, $XGrs_{03}$; Table 2) and frequently exhibit inclusions of biotite, plagioclase, orthoclase, sillimanite, quartz, and less commonly, hercynite and ilmenite. No compositional zoning has been observed for garnet (Supplementary figure 1). Plagioclase in the matrix is homogeneous with andesine composition, while inclusions in garnet show slightly higher anorthite contents (Table 2). Orthoclase crystals are predominantly perthitic with the feldspar matrix exhibiting a homogeneous composition (Table 2). Ilmenite is observed as a

heterogeneous phase, showing hematite-rich lamellae in an ilmenite-rich matrix and low Mn contents (Table 2). It exhibits straight contacts with sapphirine, garnet, hercynite, sillimanite, and felsic minerals. However, interlobate contacts with hercynite are seldom observed.

Corundum is rarely observed, occurring as fine-grained colorless rounded to prismatic crystals in local domains with garnet, hercynite, quartz, ilmenite and sapphirine. In those local domains, corundum is usually found between hercynite and garnet crystals (Figure 4B). It is observed in straight contacts with quartz and ilmenite and in straight to lobate contacts with garnet, sapphirine and hercynite (Figure 4B). Garnet overgrowths around seemingly relict corundum crystals have also been observed (Figure 4B).

Outside the local domains with sapphirine, prismatic sillimanite occurs in straight to lobate contacts with garnet, plagioclase, hercynite, orthoclase and quartz (Figure 4C). Locally, sillimanite forms moats surrounding hercynite crystals (Figure 4D). The crystals are fine- to medium- grained and contain up to 1.2 wt.% FeO_T (Supplementary file 2). Biotite (< 1 vol.%) seldom occurs as inclusions in garnet (Bt_1), showing lower Mg^{2+} contents and TiO_2 (Table 2), or as a phase crystallized along borders and/or fractures on garnet, sillimanite and ilmenite (Bt_2), with higher Mg^{2+} and TiO_2 (Table 2). Cordierite is seldom observed as pinitized moats around sapphirine or hercynite.

The mineral assemblage from the leucosome is similar to the residue but lacks sapphirine and corundum and exhibits higher amounts of biotite, quartz and feldspar. It contains up to 75% of orthoclase+plagioclase+quartz, 15% garnet and ca. of 10% of biotite, ilmenite, hercynite and sillimanite. Fine-grained orthoclase, plagioclase and quartz crystals often form fine-grained intergrowths between larger crystals, showing acute or cuspate terminations.

Metamorphic peak assemblage is interpreted to be Ilm+Hc+Sil+Grt+Pl+Or+Qz (+melt) based on the observed contacts between these minerals suggesting equilibrium conditions. As sapphirine and corundum are seemingly restricted to specific compositional domains they are not considered part of the peak assemblage for the whole rock. Disequilibrium textures, such as coronas of prismatic sillimanite around hercynite, cordierite around hercynite or sapphirine and biotite formed along the borders of garnet, hercynite or sillimanite are rarely observed (Figure 4D).

Sample	Plagioclase	Orthoclase	Garnet	Biotite	Ilmenite	Hercynite	Sillimanite	Cordierite	Sapphirine
P008	i, m: $Com_{37(35-40)}$, $Ab_{61(57-64)}$	m: $Or_{87(85-88)}$, $Ab_{12(11-14)}$	c: $Alm_{48(47-50)}$, $Prp_{46(45-47)}$, $Sps_{02(02-03)}$, $Grs_{03(03-04)}$ r: $Alm_{49(48-50)}$, $Prp_{46(45-47)}$, $Sps_{02(02-03)}$, $Grs_{03(03-04)}$	1(i): Ti = 0.16_{apfu} (0.15-0.17); X_{Mg} = 0.87 (0.86-0.87) 2(i): Ti = 0.67_{apfu}; X_{Mg} = 0.81 (0.80-0.82)	Ilm-l: $Ilm_{81(78-83)}$, $Hem_{13(11-15)}$, $Gk_{06(05-07)}$ Hem-l: $Ilm_{32(30-35)}$, $Hem_{66(64-67)}$, $Gk_{02(01-02)}$	1(m): $Sp_{44(41-46)}$, $Hc_{52(49-58)}$, Ghn_{01}, $Mag+Mfr_{03(00-07)}$	Fe = 0.03 apfu (0.02-0.03)	–	Al = 8.72_{apfu} (8.67 – 8.75); Si = 1.56_{apfu} (1.55-1.59); X_{Mg} = $0.78_{(0.78-0.80)}$
P4EL	i, m: $Com_{38(32-41)}$, $Ab_{61(58-67)}$	m: $Or_{81(70-88)}$, $Ab_{19(11-29)}$	c: $Alm_{50(47-57)}$, $Prp_{43(37-46)}$, $Sps_{03(02-03)}$, $Grs_{04(03-05)}$ r: $Alm_{53(49-59)}$, $Prp_{41(36-44)}$, $Sps_{03(02-03)}$, $Grs_{03(03-05)}$	1(i,m): Ti = 0.45_{apfu} (0.35-0.55); X_{Mg} = 0.80 (0.73-0.84) 2(m): Ti = 0.57_{apfu} (0.49-0.66); X_{Mg} = 0.69 (0.64-0.73)	Ilm-l: $Ilm_{81(49-88)}$, $Hem_{15(7-48)}$, $Gk_{04(02-05)}$ Hem-l: $Ilm_{34(26-47)}$, $Hem_{65(51-73)}$, $Gk_{01(01-02)}$	1(i): $Sp_{45(43-50)}$, $Hc_{50(45-52)}$, $Ghn_{00(00-01)}$, $Mag+Mfr_{05(04-06)}$ 2(m): $Sp_{38(35-41)}$, $Hc_{57(56-61)}$, $Ghn_{01(00-01)}$, $Mag+Mfr_{04(03-06)}$	Fe = 0.02 apfu (0.02-0.03)	1: X_{Mg} = $0.85_{(0.84-0.86)}$; Mn = 0.00 apfu (0.00-0.01) 2: X_{Mg} = $0.86_{(0.86-0.87)}$; Mn = 0.00 apfu (0.00-0.01)	–
P4ER			mo: $Alm_{58(57-60)}$, $Prp_{36(34-38)}$, $Sps_{03(02-03)}$, Grs_{03}	3(mo): Ti = 0.24_{apfu} (0.13-0.33); X_{Mg} = 0.75 (0.72-0.78)		2(I,m): $Sp_{41(39-45)}$, $Hc_{56(52-58)}$, Ghn_{00}, $Mag+Mfr_{03(02-04)}$		3: X_{Mg} = $0.84_{(0.83-0.84)}$; Mn = 0.00 apfu (0.00-0.01)	

Table 4-2 - Chemical composition of mineral phases from the hercynite-sillimanite-garnet diatexites. Compositions are presented as mean values of compositional end-members followed by compositional ranges between brackets (when applicable). Numbers before brackets or colon represent different mineral generations. R = residue; L = leucosome; I = inclusions; m = matrix; mo = moats; c = cores; r = rims; Ilm-l = ilmenite lamellae; Hem-l = hematite lamellae; apfu = atoms per formula unit.

Sample	Plagioclase	Orthoclase	Garnet	Biotite	Ilmenite	Orthopyroxene
P013Rr	i: $An_{69(59-76)}$, $Ab_{30(23-39)}$ m: $An_{44(42-46)}$, $Ab_{55(53-57)}$	m: $Or_{90(89-91)}$, $Ab_{09(09-11)}$	c: $Alm_{58(57-60)}$, $Prp_{32(31-32)}$, Sps_{02}, $Grs_{08(06-09)}$ r: $Alm_{61(59-63)}$, $Prp_{31(30-33)}$, Sps_{02}, $Grs_{06(05-06)}$	1(i): Ti = $0.22_{apfu\ (0.21-0.22)}$; X_{Mg} = 0.77 (0.76-0.77) 2(m,mo): Ti = $0.58_{apfu\ (0.55-0.62)}$; X_{Mg} = 0.68 (0.65-0.72)	$Ilm_{85(85-87)}$, $Hem_{12(11-13)}$, Gk_{02}	1(c,r,x): $Com_{57(56-58)}$, Al = $0.21_{apfu\ (0.19-0.23)}$
P013Lr	i, m: $Com_{44(43-45)}$, $Ab_{55(54-56)}$	m: $Or_{90(87-91)}$, $Ab_{10(08-12)}$	c: $Alm_{60(58-62)}$, $Prp_{33(31-35)}$, Sps_{02}, $Grs_{06(05-07)}$ r: $Alm_{62(60-64)}$, $Prp_{31(28-33)}$, Sps_{02}, $Grs_{05(05-06)}$ x: $Alm_{63(62-64)}$, $Prp_{27(26-29)}$, Sps_{02}, $Grs_{08(07-09)}$	1(i): Ti = $0.24_{apfu\ (0.21-0.25)}$; X_{Mg} = 0.81 (0.78-0.83) 2(m): Ti = $0.56_{apfu\ (0.52-0.64)}$; X_{Mg} = 0.67 (0.64-0.70) 3(i): Ti = $0.70_{apfu\ (0.70-0.71)}$; X_{Mg} = 0.72 (0.71-0.73)		
P1R	i, m: $Com_{49(46-51)}$, $Ab_{50(48-53)}$	m: Or_{94}, Ab_{06}	c: $Alm_{62(60-63)}$, $Prp_{29(28-31)}$, $Sps_{02(02-03)}$, $Grs_{07(06-08)}$ r: $Alm_{62(60-64)}$, $Prp_{28(26-30)}$, Sps_{02}, $Grs_{07(07-09)}$	1(i): Ti = $0.70_{apfu\ (0.69-0.71)}$; X_{Mg} = 0.70 (0.69-0.70) 2(m,mo): Ti = $0.54_{apfu\ (0.41-0.62)}$; X_{Mg} = 0.68 (0.64-0.75)	$Ilm_{89(87-90)}$, $Hem_{10(08-10)}$, $Gk_{01(01-02)}$	1(c,r): $Com_{59(57-60)}$, Al = $0.17_{apfu\ (0.14-0.20)}$ 2(c,r): $Com_{59(55-62)}$, Al = $0.12_{apfu\ (0.09-0.14)}$
P1L	i, m: $Com_{47(44-49)}$, $Ab_{52(50-54)}$	i, m: $Or_{88(86-90)}$, $Ab_{11(10-13)}$	c: $Alm_{61(60-63)}$, $Prp_{30(28-31)}$, Sps_{02}, $Grs_{07(06-08)}$ r: $Alm_{62(61-63)}$, $Prp_{29(28-30)}$, Sps_{02}, $Grs_{07(06-08)}$	1(i): Ti = $0.67_{apfu\ (0.66-0.67)}$; X_{Mg} = 0.71 2(m,mo): Ti = $0.52_{apfu\ (0.25-0.62)}$; X_{Mg} = 0.70 (0.65-0.78)		–
P1D	i, m: $Com_{38(32-40)}$, $Ab_{61(59-68)}$	i, m: $Or_{90(88-93)}$, $Ab_{10(07-12)}$	c: $Alm_{61(57-66)}$, $Prp_{32(27-36)}$, $Sps_{02(01-02)}$, $Grs_{05(05-06)}$	1(i,m): Ti = $0.52_{apfu\ (0.45-0.59)}$; X_{Mg} = 0.69 (0.64-0.74)	–	–

			r: $Alm_{63(58-65)}$, $Prp_{31(28-36)}$, Sps_{02}, Grs_{05}			

Table 4-3 - Chemical compositions of mineral phases from the orthopyroxene-garnet migmatites. Compositions are presented as mean values of compositional end-members followed by compositional ranges between brackets (when applicable). Numbers before brackets or colon represent different mineral generations. Rr = residuum-rich bands; Lr = leucosome-rich bands; R = residue; L = leucosome; I = inclusions; m = matrix; mo = moats; c = cores; r = rims; x = xenomorphic; apfu = atoms per formula unit.

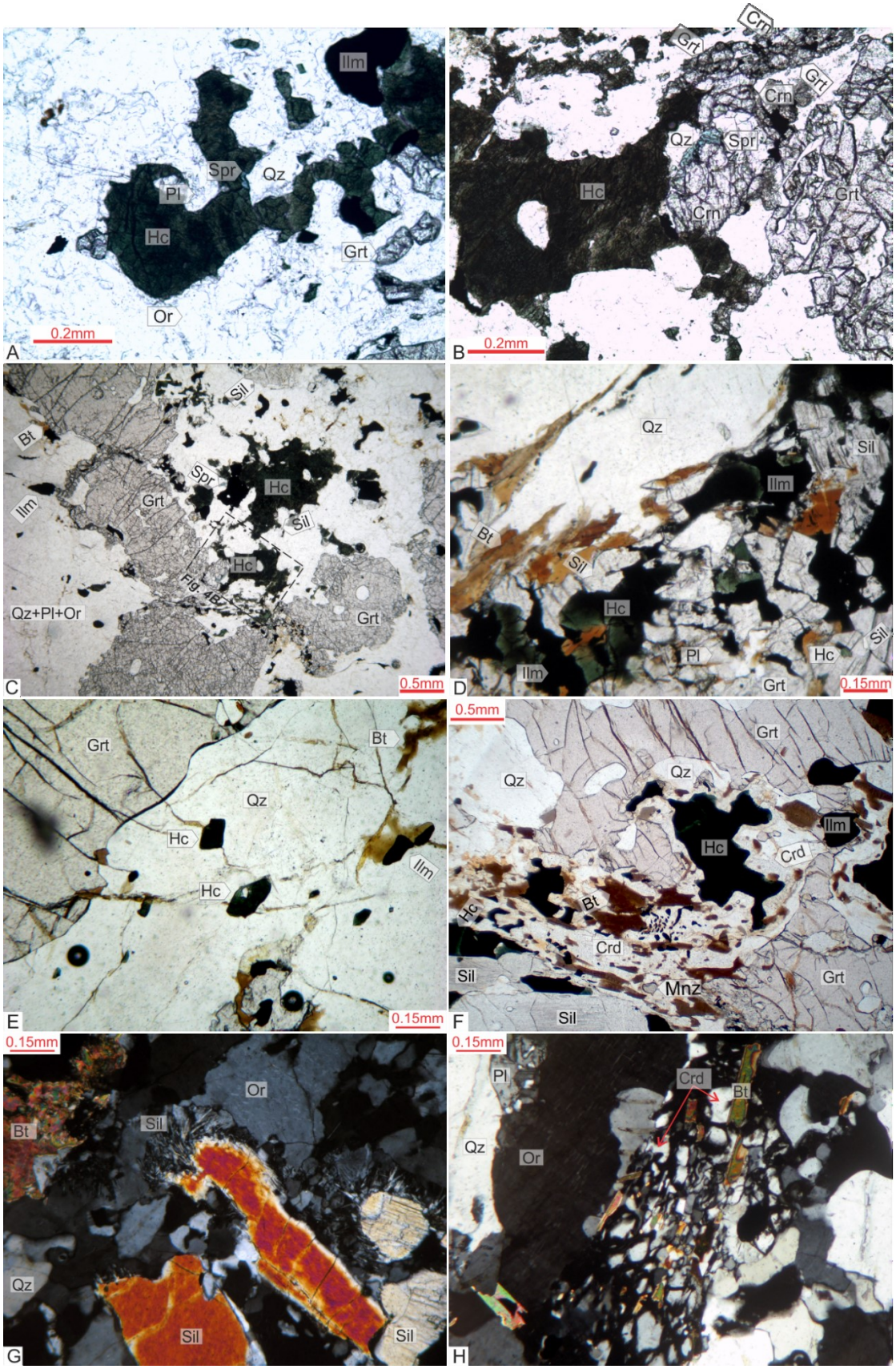

Figure 4-4 - Microtextures of the sapphirine-bearing schlieren hercynite-sillimanite-garnet diatexite (sample P008, A-D) and the schlieren/schöllen hercynite-sillimanite-garnet diatexite (sample P4E, E-H). A) Sapphirine crystal along the borders of hercynite; B) Local domains exhibiting garnet, hercynite, sapphirine

and corundum in straight contacts with quartz; C) Overview of the mineral assemblage Ilm+Hc+Sil+Grt+Or+Pl+Qz; D) Sillimanite mantles formed after hercynite, as well as biotite overgrowths over Al-rich phases; E) Hercynite, ilmenite, quartz and biotite inclusions in very coarse (>1 cm) garnet (outside microphotograph scale), with straight contacts between hercynite and quartz; F) Biotite, cordierite and sillimanite at the borders of cm-scale garnet crystal, which contains sillimanite, ilmenite, quartz, hercynite (exhibiting a cordierite moat), orthoclase and biotite inclusions; G) fibrous sillimanite (Sil) formed around prismatic sillimanite crystals; H) Cordierite crystal partially altered to pinite (pseudo-isotropic mass around cordierite relicts) and biotite.

4.2.2 Schlieren/schollen hercynite-sillimanite-garnet diatexites (sample P4E)

The residue of schlieren/schöllen hercynite-sillimanite-garnet diatexites is composed of ilmenite (5%), hercynite (6%), cordierite (8%), biotite (9%), sillimanite (11%), garnet (20%) and quartz (23%), with fine-grained orthoclase and plagioclase (18%). Sillimanite, biotite and ilmenite are strongly oriented parallel to the banding, defining a main foliation. The leucosome is composed of medium- to very coarse-grained biotite (7%), garnet (9%), fine- to coarse-grained plagioclase (15%) and perthitic orthoclase (30%), fine- to medium-grained quartz (35%) and up to 4% hercynite, cordierite and sillimanite. Zircon, monazite, apatite and magnetite are present as accessory phases on both domains.

Hercynite crystals are fine- to medium-grained, occurring as inclusions in garnet or as a free phase in matrix, rarely showing stable contacts with quartz and feldspars (Figure 4E, F). Inclusions in garnet are locally surrounded by sillimanite or cordierite coronas. Straight contacts between hercynite and ilmenite, sillimanite or garnet are observed, although most hercynite crystals are separated from quartz and feldspars by a sillimanite or (pinitized) cordierite moat (Figure 4F) or, when in contact with garnet, by a thin layer of surrounding garnet. Hercynite compositions contain low Zn contents (XGhn ≤ 02), and can be divided into three generations: inclusions in garnet from the leucosome (Hc_1; Table 2, Supplementary figure 2) are more magnesian (mean XHc_{50}) than those observed in the matrix (Hc_2, mean XHc_{57}; Table 2), while in the residue both hercynite inclusions and free crystals show similar compositions (Hc_2, mean XHc_{56}). Exsolution lamellae composed of a Fe^{3+}-rich phase (Xmag+Mfr up to 49) are more prominent on matrix crystals and inclusions on garnet rims, while inclusions closer to the cores of coarse to very coarse garnet crystals exhibit a lower exsolution lamellae volume.

Garnet crystals are very coarse- (diameter up to 4 cm) to medium-grained, predominantly occurring as poikiloblastic porphyroblasts exhibiting inclusions of

hercynite, sillimanite, quartz, plagioclase, orthoclase, ilmenite and accessory phases. Most crystals do not exhibit oriented inclusions, excepting acicular sillimanite which occasionally define a pre- to syn-kinematic internal foliation (Figure 5A). Garnet grains with diameter > 1 cm (coarse to very coarse crystals) exhibit the lowest Alm contents and record a discrete compositional zoning between cores and rims (mean cores: $Xalm_{48}$, $XPrp_{45}$, $XGrs_{04}$, $XSps_{03}$; mean rims: $Xalm_{51}$, $XPrp_{42}$, $XGrs_{04}$, $XSps_{03}$). Coarse- to medium-grained crystals exhibit more homogeneous compositional profiles and higher Alm contents (mean cores: $Xalm_{51-55}$, $XPrp_{40-42}$, $XGrs_{03-04}$, $XSps_{02-03}$; mean rims: $Xalm_{53-56}$, $XPrp_{38-41}$, $XGrs_{03-04}$, $XSps_{02-03}$). Thin garnet overgrowths (moats) around biotite or ilmenite at the borders of crystals exhibit the highest Alm contents (Table 2). Domains composed of cordierite, biotite and sillimanite (±ilmenite) are often observed at the borders of coarse to very coarse garnet crystals (Figure 4F). Embayments at the borders of garnet crystals are often observed, filled with plagioclase, orthoclase, cordierite, quartz and biotite. Ilmenite crystals are predominantly fine-grained, commonly in direct (straight to lobate) contact with hercynite and garnet and often with sillimanite. Straight contacts between ilmenite and quartz or feldspars are observed locally, as ilmenite is more often separated from both minerals by a sillimanite or cordierite moat. Crystals show low Mn (XPph ≤ 1; Table 2, Supplementary file 2) and most are heterogeneous, both in leucosome and residue, showing Ilm-rich lamellae (mean $Xilm_{81}$) interleaved with Hem-rich ones (mean $Xhem_{65}$). Reintegrated ilmenite composition provided $Xilm_{67}$, $Xhem_{29}$, XGk_{03} and $XPph_{01}$. Plagioclase and orthoclase crystals are fine- to coarse-grained on the leucosome, often showing inclusions of ilmenite or hercynite, and fine grained on the residue, often developing fine-grained intergrowths and filling interstitial sites between crystals. Small variations in compositions are observed in both cases (Table 2)

Cordierite is observed as: i) a free phase (Crd_1), commonly with poikiloblastic texture (Figure 5B, C) and a range of compositions between X_{Mg} = 0.84 – 0.86 (Table 2), exhibiting straight to lobate contacts with sillimanite, garnet, quartz or feldspars; ii) as moats around ilmenite or hercynite (Crd_2), showing slightly higher X_{Mg} (0.86 – 0.87). Cordierite partially altered to pinite and biotite (Crd_3, Figure 4H), exhibit the lowest X_{Mg} (0.83 – 0.84). Sillimanite crystals show prismatic habits (Figure 4G), are fine- to medium-grained and have high FeO_T contents (up to ca. 1.2 wt.%; Table 2, Supplementary file 2). Straight contacts are frequently observed between prismatic sillimanite and quartz, feldspars and cordierite, and less often between prismatic

sillimanite and hercynite, garnet or ilmenite. Fibrous sillimanite is observed locally at the borders of the prismatic crystals (Figure 4G). Biotite is observed as three distinct generations (Supplementary figure 2): Bt_1 is found as inclusions in garnet crystals at the leucosome or as a free phase in the residue matrix, showing moderate to high TiO_2 and X_{Mg} (Table 2); Bt_2 occurs as free lamellae in the matrix, showing high TiO_2 and low to moderate X_{Mg} (Table 2); and Bt_3 is crystallized as partial moats after garnet or cordierite rims (rarely at hercynite rims), showing low TiO_2 and moderate X_{Mg} values (Table 2).

The metamorphic peak assemblage is interpreted as Ilm+Hc+Sil+Grt+Pl+Or+Qz(+melt) based on the coexistence in local domains and contact relations between phases suggesting equilibrium conditions (Figure 4E, G; Figure 5 B, C). Poikiloblastic cordierite (Crd_1) could possibly be interpreted as a near peak phase due to its occurrence as a free phase not associated with disequilibrium textures around other phases (like moats) which exhibits straight contacts with sillimanite, garnet, quartz and feldspars. However, most cordierite observed in this sample occur as moats around hercynite or ilmenite, or in local domains composed by cordierite+biotite+sillimanite observed at the borders of garnet crystals, and thus belong to the retrograde path of the metamorphic history. Other disequilibrium textures that provide evidence for retrograde conditions include sillimanite moats around hercynite and partial biotite moats formed around garnet or cordierite.

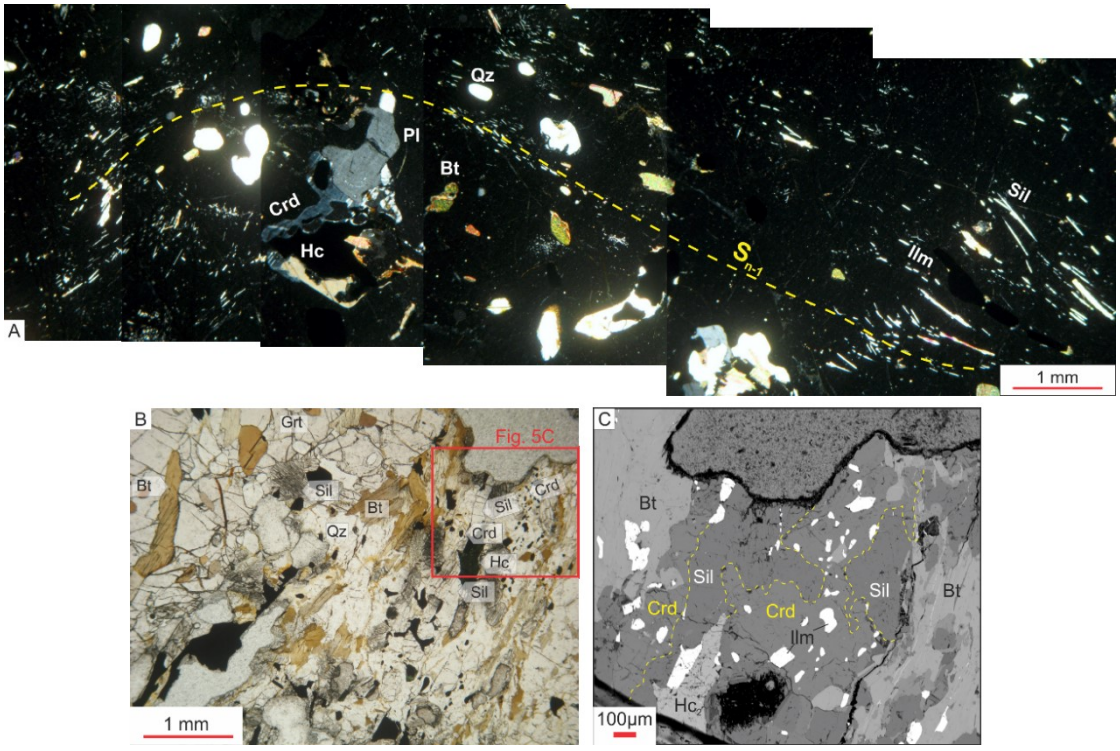

Figure 4-5 - A) Mosaic exhibiting oriented inclusions of sillimanite, ilmenite and biotite on very coarse (>1 cm) garnet crystal, defining an internal foliation (referred as Sn-1 for graphical purposes only). Cordierite, hercynite, quartz and plagioclase inclusions are also observed. B) Residue assemblage (sillimanite, cordierite, ilmenite, garnet, hercynite, quartz) and late biotite at the vicinity of the garnet crystal of Fig. 5A. Poikiloblastic cordierite crystals are observed in interlobate contacts with sillimanite and biotite. C) Backscattered electron image of the area inside the red rectangle of Fig. 5B, highlighting the poikiloblastic cordierite crystals.

4.2.3 Layered orthopyroxene-garnet diatexite (sample P013)

Residue-rich bands of the layered orthopyroxene-garnet diatexites consists of fine-grained plagioclase (20%), orthoclase (20%), quartz (24%), orthopyroxene (1%) and biotite (11%) domains surrounding medium- to coarse-grained garnet (22%), with ilmenite, zircon, apatite and monazite as accessory minerals (Figure 6A, B). Orthopyroxene is mostly observed as fine-grained relicts surrounded by biotite mantles. Straight contacts with feldspars and quartz are rarely observed. Garnet crystals are predominantly poikiloblastic hosting inclusions of biotite, plagioclase, quartz, ilmenite, zircon, and monazite without internal orientation. Garnet compositions show overall flat patterns between its components on chemical sections, with a slight zoning between cores and rims (mean cores: $Xalm_{58}$, $Xpyr_{32}$, $XGrs_{08}$, $XSps_{02}$; mean rims: $Xalm_{61}$, $Xpyr_{31}$, $XGrs_{06}$, $XSps_{02}$; Table 2, Supplementary Figure 3). Matrix is composed of biotite, plagioclase, orthoclase and quartz, and exhibits a foliation defined by oriented biotite and opaque minerals as well as preferentially elongated felsic

minerals. Plagioclase observed as inclusions in garnet (Pl_i) has compositions between labradorite and bytownite (Table 2, Supplementary figure 3), while matrix plagioclase (Pl_m) is strictly andesine. Orthoclase has a homogeneous composition (Table 2) being only present in the matrix.

Biotite in residue-rich bands belongs to two distinct chemical generations (Table 2): (i) inclusions in garnet (Bt_1), showing the highest X_{Mg} values and the lowest TiO_2 contents (Table 2); (ii) free crystals in the matrix, mantles formed around garnet or orthopyroxene, and biotite filling embayments in garnet crystals (Bt_2), showing lower X_{Mg} and the highest observed TiO_2 (Table 2).

Leucosome-rich bands consists of fine- to medium-grained quartz-feldspathic domains, composed of orthoclase (19%), quartz (20%) and plagioclase (29%), interlayered with thin residue domains composed of ilmenite (3%), orthopyroxene (6%), biotite (6%) and garnet (17%) (Figure 6-D). Foliation is less developed and, when observed, is parallel to the banding. Magnetite, apatite, zircon and rare pyrite and chalcopyrite occur as minor components. Garnet crystals are observed as two morphological types: i) crystals chemically similar to the type found in the residue-rich bands (mean cores: $Xalm_{60}$, $Xpyr_{33}$, $XGrs_{06}$, $XSps_{02}$; mean rims: $Xalm_{62}$, $Xpyr_{31}$, $XGrs_{05}$, $XSps_{02}$; Table 2, Supplementary Figure 3), also showing general flat patterns, occurring both as medium- to coarse-grained inclusion-rich crystals (Figure 6C), containing biotite, opaque, plagioclase, orthoclase, quartz, zircon, apatite and orthopyroxene inclusions, and as fine- to medium grained crystals with few inclusions; and ii) xenomorphic crystals, showing slightly higher Ca^{2+} (mean $XGrs_{08}$) and Fe^{2+} ($Xalm_{63}$) and the lowest Mg^{2+} ($XPrp_{27}$), often being associated with xenomorphic orthopyroxene (Figure 6D). Orthopyroxene occurs both, as prismatic (Figure 6C) and xenomorphic (Figure 6D) crystals. No significant chemical differences are observed between the two types, defining a single generation with hypersthene composition (mean Xen_{57}) and high Al contents (mean Al_{apfu} = 0.21, Table 2), showing little differences from core to rim compositions (Supplementary file 2) Contacts between garnet and orthopyroxene are predominantly straight to lobate, and both minerals are often found in straight contacts with quartz, plagioclase, orthoclase and ilmenite. Biotite overgrowths or mantles are also often observed around garnet and orthopyroxene. Plagioclase, orthoclase and quartz occur both as inclusions in garnet, as in the matrix, with increasing grain size from residue to leucosome bands. Plagioclase inclusions in garnet and in the matrix are homogeneous andesine (Table 2). Orthoclase inclusions

and matrix crystals are also homogeneous (Table 2, Supplementary file 2). Ilmenite found on both the residue and leucosome are fine-grained and homogeneous crystals (Table 2). Ilmenite exhibits predominantly straight to lobate contacts with orthopyroxene, garnet, quartz and feldspars. Biotite overgrowths are occasionally observed around ilmenite. Biotite crystals observed as inclusions in garnet are chemically divided into two generations: Bt_1 is associated with larger garnet crystals and show compositions similar to those observed in the residue-rich bands (Table 2); Bt_3 is found as inclusions in fine- to medium-grained crystals and show lower X_{Mg} and higher TiO_2 (Table 2) than Bt_1. Free biotite in the matrix belongs to a single generation (Bt_2) similar to that observed on residue-rich bands, exhibiting lower X_{Mg} values and intermediate TiO_2 (Table 2).

The metamorphic peak assemblage is interpreted to be Opx+Grt+Pl+Or+Qz(+melt)±Ilm based on their coexistence and contact relations suggesting equilibrium conditions. Local domains exhibiting xenomorphic garnet and orthopyroxene are interpreted as disequilibrium textures, and higher Alm contents observed in garnet are suggestive of retrograde conditions. Other disequilibrium textures include biotite moats around garnet or orthopyroxene.

4.2.4 Schlieren orthopyroxene-garnet diatexite (samples P1 and P1D)

The schlieren orthopyroxene-garnet diatexite exhibits moderate to nearly complete segregation between leucosome (proximal leucosome, $P1_L$) and residue ($P1_R$). Leucocratic veins (distal leucosome, P1D) crosscutting other rocks (usually orthopyroxene-clinopyroxene orthogneisses) are often observed with almost no residue.

Residue schliere may show random orientation or be parallel to leucosome foliation. The residue is fine- to medium-grained, composed of plagioclase (30%), biotite (20%), garnet (20%), orthopyroxene (15%), quartz (10%) and ilmenite (5%), and lesser amounts of orthoclase and magnetite. The accessory assemblage is composed of apatite, zircon, rutile and sulphides (pyrite, chalcopyrite and pyrrhotite). Secondary sulphides (pyrite and chalcopyrite) are also observed associated with chlorite and carbonate pseudomorphs after orthopyroxene, garnet or biotite along veins. Orthoclase is rarely observed on the residue, commonly exhibiting corroded rims in contact with myrmekitic plagioclase. Orthopyroxene crystals occur both as: (i) prismatic, fine- to medium-grained crystals (Opx_1), with exhibiting moderate to high Al contents (0.14 – 0.20 apfu, Table 2), often exhibiting straight contacts with plagioclase,

quartz and garnet (Figure 6E); and (ii) irregular, fractured, fine-grained crystals which are usually affected by chlorite-carbonate alteration (Opx_2), showing low Al contents (0.09 – 0.14 apfu) (Figure 6G). Compositions correspond to hypersthene (mean Xen_{59}; Table 2, Supplementary figure 4). Garnet crystals are fine- to coarse-grained, contain inclusions of ilmenite, orthopyroxene, biotite, plagioclase, quartz, apatite, zircon and rutile, usually with no internal orientation (Figure 6E). Garnet compositions are homogeneous (Table 2, Supplementary figure 4), defining a single generation (mean cores: $Xalm_{62}$, $XPrp_{29}$, $XGrs_{07}$, $XSps_{02}$; mean rims: $Xalm_{62}$, $XPrp_{28}$, $XGrs_{07}$, $XSps_{02}$), defining flat chemical profiles. Straight contacts are commonly observed between garnet and quartz or plagioclase and between garnet and orthopyroxene, ilmenite or rutile. Some garnet crystals exhibit sulphide inclusions in circular patterns marking growth zones (Figure 6E). Plagioclase and quartz are observed as fine-grained granoblastic crystals or as veinlets of very fine-grained intergrowths that fill intergranular sites (white arrows on Figure 6G). Plagioclase inclusions in garnet show no chemical differences from matrix plagioclase, both exhibiting andesine to labradorite composition (Table 2, Supplementary Figure 4). Ilmenite crystals are homogeneous, with high Ilm contents and low Mn (Table 2), exhibiting straight to lobate contacts with quartz, feldspars, garnet and orthopyroxene, and lobate to indented contacts with biotite and rutile. Rutile is seldom observed and usually as minor contents, occurring as fine-grained aggregates with ilmenite and biotite or as prismatic crystals, exhibiting straight contacts with quartz, plagioclase or garnet (Figure 6E), and may seldom occur as inclusions in garnet (Figure 6H). Biotite crystals are predominantly fine-grained and are divided into two generations: Bt_1 occurs as inclusions in garnet crystals, showing the highest TiO_2 (and high X_{Mg} (Table 2); Bt_2 occurs as a free phase in the biotite-dominated matrix, as overgrowths/mantles around orthopyroxene and garnet crystals or as inclusions affected by fractures on these, next to alteration fronts, showing intermediate TiO_2 and a wider range of X_{Mg} (Table 2).

The peak metamorphic assemblage from the residue is interpreted to be represented by Rt+Ilm+Grt+Opx+Pl+Qz+melt±Or based on their coexistence on the residue and contact relations suggesting equilibrium conditions. As orthoclase crystals are observed in the residue just as corroded relicts it is interpreted that most orthoclase was consumed due to partial melting, although it was probably part of the metamorphic peak assemblage for this rock. Disequilibrium textures include biotite mantles around

garnet and orthopyroxene and partial to total substitution of orthopyroxene or garnet crystals by carbonate+chlorite(±pyrite±chalcopyrite) pseudomorphs.

Leucosome is fine- to coarse-grained, foliated, with modal composition between granitic and granodioritic. It is composed of plagioclase (15-35%), orthoclase (15-20%), quartz (20-40%), garnet (10-15%), biotite (10-15%), rutile (<1-5%) and rare orthopyroxene (<5% when present). The accessory mineral assemblage is composed of pyrite, chalcopyrite, ilmenite, zircon and monazite. When observed, alteration processes are more intense on the leucosome, with replacement of all the orthopyroxene for pseudomorphs composed of pyrite/chalcopyrite+chlorite+carbonate with few orthopyroxene relicts preserved.

Rutile is often found with biotite overgrowths in the matrix, though it may occur as inclusions in garnet or quartz, as a free phase in the matrix, exhibiting straight contacts with garnet, plagioclase, orthoclase or quartz, or in pressure shadows around garnet crystals, exhibiting prismatic to granular habit. Garnet crystals range from fine- to very coarse-grained, containing inclusions of biotite, feldspars, quartz, ilmenite, apatite, rutile and, rarely, even phases absent from the matrix (like hercynite, Figure 6F), which may form an internal foliation. Orthoclase and plagioclase may form subhedral crystals, fine- to coarse-grained and commonly perthitic/anti-perthitic or occur as intergrowths with quartz on very fine-grained veinlets fulfilling interstitial grain sites. Quartz may also occur as fine- to coarse-grained crystals and show chessboard extinction patterns. Biotite occurrence is similar to that observed on the residue, and in the leucosome it is preferably oriented defining a foliation.

Separate mineral chemistry analyses were made for the proximal ($P1_L$) and distal (P1D) leucosome. The summary of the results is presented on Table 2, and representative mineral analysis on Supplementary file 2. Garnet compositions are similar to those of the residue, with a slight increase in XAlm and decrease in XGrs (Table 2); on both cases a single generation of garnet crystals is identified. Orthoclase crystals on both $P1_L$ and P1D have similar composition (mean Xor_{88} and Xor_{90}, respectively), while plagioclase from $P1_L$ is remarkably more calcic (Xan_{47}) than P1D (An_{38}).

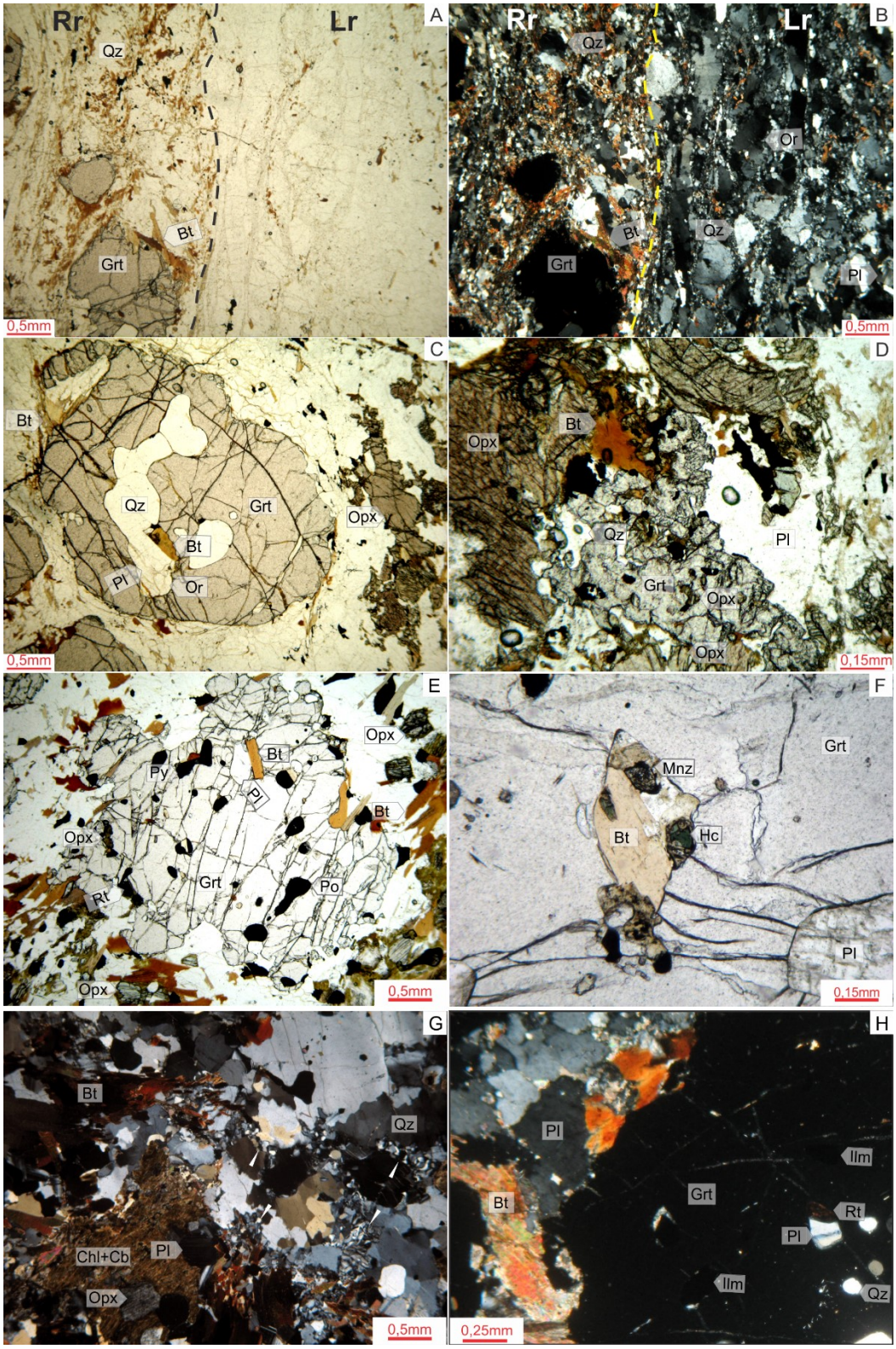

Figure 4-6 - Microtextures of the layered orthopyroxene-garnet diatexite (sample P013, A-D) and the schlieren orthopyroxene-garnet diatexite (samples P1 and P1D, E-H). A-B) Typical aspects of residue-rich (Rr) and leucosome-rich (Lr) bands; C) Biotite, quartz, plagioclase and orthoclase inclusions in garnet crystal, as well as prismatic orthopyroxene in straight contacts with plagioclase and quartz; D) Xenomorphic garnet, showing quartz, biotite and orthopyroxene inclusions, and xenomorphic orthopyroxene; E) Residue (P1) garnet, containing inclusions of plagioclase, biotite, pyrite (Py) and

pyrrhotite (Po), as well as orthopyroxene crystals in straight contacts with plagioclase and quartz; F) Garnet crystal exhibiting biotite, hercynite and monazite inclusions; G) Orthopyroxene crystals partially replaced by chlorite + carbonate; H) Garnet crystal exhibiting rutile, plagioclase, quartz and ilmenite inclusions.

4.3 Pressure-temperature estimates

4.3.1 Phase equilibria modeling

4.3.1.1 Schlieren/schöllen hercynite-sillimanite-garnet diatexite (sample P4E)

The calculated stability fields from the phase equilibrium diagram (Figure 7A) which best corresponds to the interpreted peak metamorphic assemblage are the narrow field identified as “18”, constrained between ~970 °C, ~6.2 kbar and ~1020 °C, ~7 kbar in which the assemblage Ilm+Sp+Grt+Sil+Pl+Or+Qz+melt is stable, and the field identified as “06”, constrained between ~990 °C, ~6.6 kbar and ~1100 °C, ~8.7 kbar in which the assemblage Ilm+Sp+Grt+Sil+Fsp+Qz+melt is stable.

Minimum *P-T* estimates for the metamorphic peak were obtained combining garnet cores XAlm and XGrs isopleths with spinel XHc isopleths. XAlm = 0.48 isopleth corresponds to the mean core composition of coarse to very coarse garnet crystals (Figure 7B; see section 3.1 and Supplementary file 2). XHc = 0.51 isopleth was selected considering a slight (+1%) correction for the magnetite lamellae on the mean composition of hercynite inclusions in coarse to very coarse garnet crystals (XHc = 0.50). Metamorphic conditions of 1020 °C, 7.0 kbar (Figure 7A, B) were obtained through the intercept between both isopleths. Both intersections lie inside field “06” (Ilm+Sp+Grt+Sil+Fsp+Qz+melt).

An estimate for the retrograde *P-T* conditions was obtained combining garnet (XAlm) and cordierite (X_{Mg}) moats isopleths/isolines. XAlm = 0.58 isopleth corresponds to the mean composition of garnet moats around ilmenite and biotite (Figure 7B). X_{Mg} = 0.84 corresponds to the mean composition of cordierite moats around hercynite (Figure 7B). Metamorphic conditions of 745 °C, 5.3 kbar were obtained through the intercept between both isolines. The intersection lies inside the field where the assemblage Ilm+Grt+Sil+Crd+Bt+Or+Pl+Qz (“40”) is stable, which is representative of the observed retrograde assemblage.

An approximation of the cooling path is marked as a yellow dashed arrow in the diagram (Figure 7A), comprising both *T* and *P* estimates and the following sequence of microstructures observed in thin section: I) cordierite and sillimanite moats around hercynite (Figure 4F, H); II) biotite formation after garnet and cordierite.

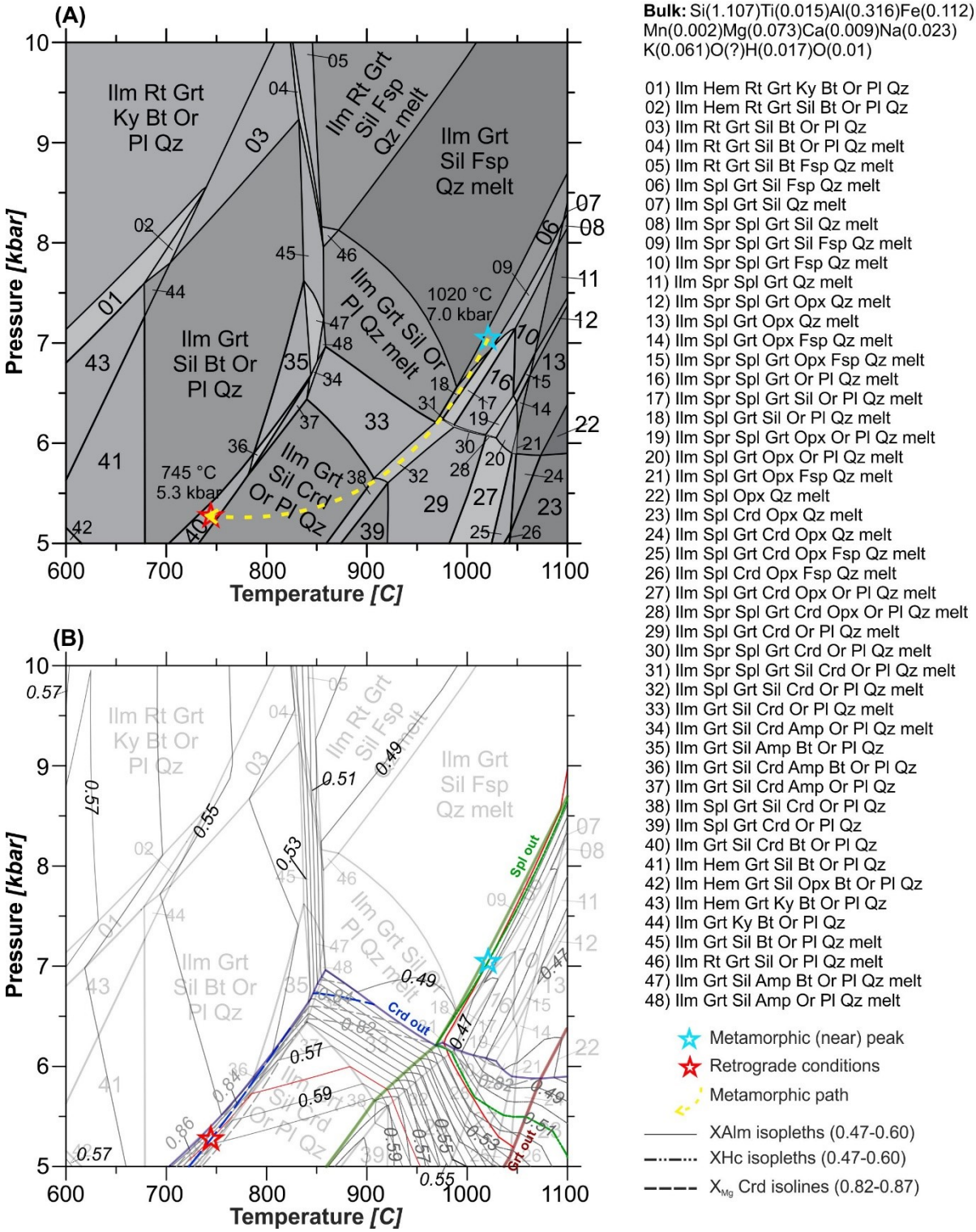

Figure 4-7 - Phase-equilibria modeling for the schlieren/schöllen hercynite-sillimanite-garnet diatexite (sample P4E). A) Stable assemblages on P-T interval between 600-1100 °C, 5.0-10.0 kbar. Metamorphic assemblage corresponds to the field labeled as "18". The dashed arrows represent a possible metamorphic trajectory (see text); B) Xalm and XHc isopleths, as well as X_{Mg} cordierite isolines, projected on the stability fields. The intersection between Hc_{51} and Alm_{48} isopleths (blue star) marks a minimum estimate for the metamorphic peak (T = 1020 °C, P = 7.0 kbar). The red star marks an estimate for retrograde conditions based on garnet moats (Alm_{58}) and X_{Mg} cordierite (0.84) compositions (T = 745 °C, P = 5.3 kbar).

4.3.1.2 Sapphirine-bearing schlieren hercynite-sillimanite-garnet diatexite (Sample P008)

The calculated stability field which best corresponds to the interpreted peak metamorphic assemblage is the narrow field constrained between ~930 °C, ~6 kbar and 1100 °C, ~9 kbar in which the assemblage Ilm+Sp+Grt+Sil+Pl+Or+Qz+melt is stable (Figure 8A). Corundum and sapphirine could not be predicted by the database used for calculations for the bulk composition of this sample.

A minimum *P-T* estimate for the metamorphic peak was obtained combining garnet cores XAlm and XGrs isopleths and spinel cores XHc isopleths. XAlm = 0.48 and XGrs = 0.03 isopleths corresponds to the mean composition of garnet crystal cores (Figure 8B; Table 2). XHc = 0.52 and XHc = 0.53 isopleths corresponds to the mean composition of hercynite cores. A *P-T* estimate of 1035 °C, 7.1 kbar was obtained through the intercept between XAlm and XHc isolines, while an estimate of 1075 °C, 8 kbar was obtained through the intercept of XGrs and XHc isolines. Both estimates lie inside the calculated stability field (Figure 8A, B).

An approximation of the cooling path is marked as a yellow dashed arrow in the diagram (Figure 8A), considering the following sequence of microstructures observed in thin section: I) sillimanite (and cordierite) moats around hercynite; II) biotite formation after garnet.

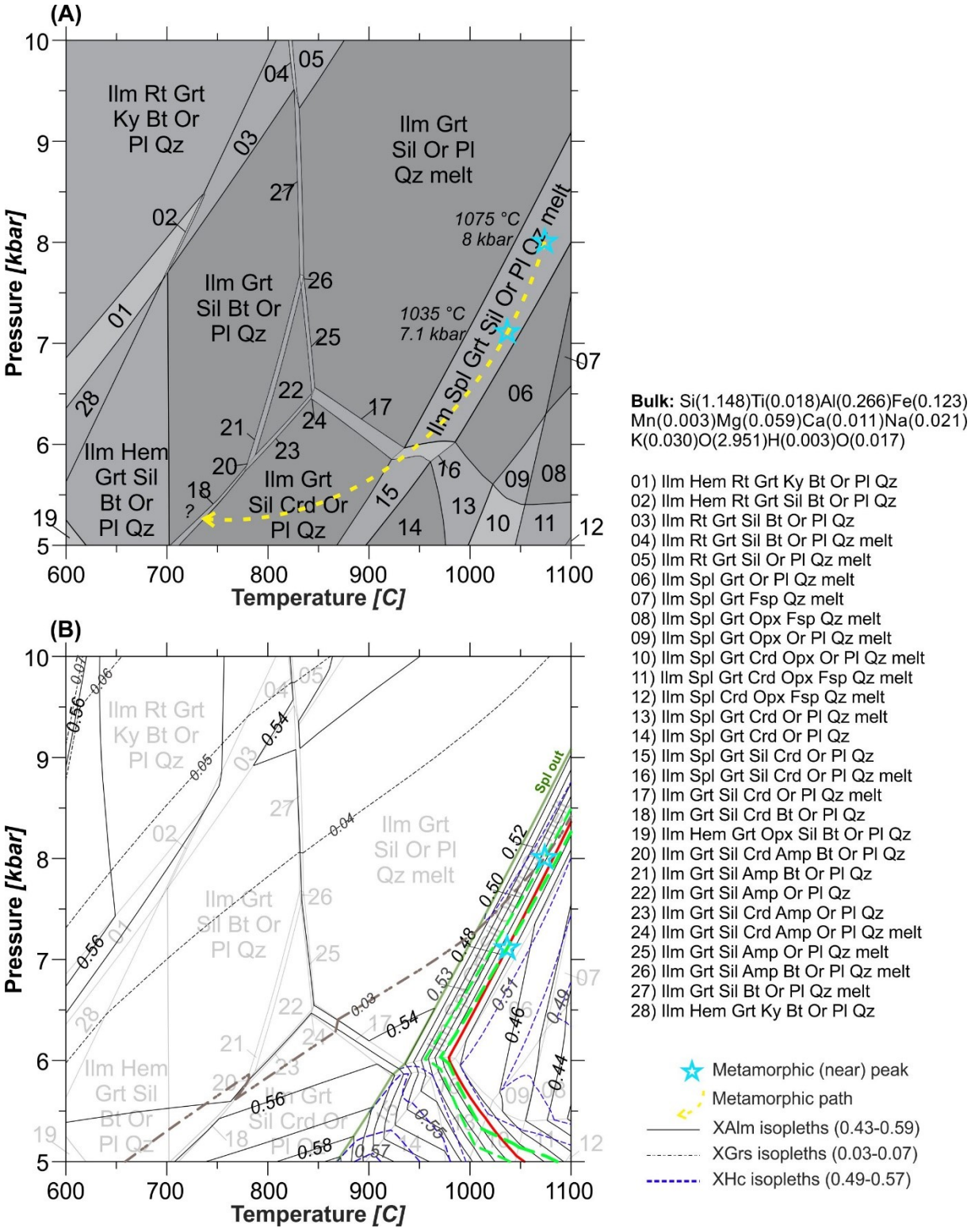

Figure 4-8 - Phase-equilibria modeling for the sapphirine-bearing schlieren hercynite-sillimanite-garnet diatexite (sample P008). A) Stable assemblages on P-T interval between 600-1100 °C, 5.0-10.0 kbar. Metamorphic assemblage corresponds to the field in which the blue star lies. The dashed arrow represent a possible metamorphic trajectory (see text); B) XAlm, XGrs and XHc isopleths projected on the stability fields. The intersection between Hc_{52} and Alm_{48} isopleths and between Hc_{53} and Grs_{03} isopleths (blue stars) marks minimum estimates for the metamorphic peak (respectively T = 1035 °C, P = 7.1 kbar and T = 1075 °C, P = 8 kbar).

4.3.1.3 Layered orthopyroxene-garnet diatexite (sample P013)

Wide stability fields were calculated for this sample (Figure 9). The field constrained between ~840 °C, 5 kbar and 1100 °C, 10 kbar, presenting the assemblage Ilm+Opx+Grt+Or+Pl+Qz+melt corresponds to P013 interpreted peak metamorphic assemblage (Figure 9A).

A minimum *P-T* estimate for the metamorphic peak was obtained combining garnet (XAlm) cores isopleths and Al in orthopyroxene isolines (Figure 9B). XAlm = 0.58 isopleth corresponds to the mean core composition of garnet crystals from the residue rich bands. $Al_{[apfu]}$ = 0.22 is representative of the composition of orthopyroxene crystals with Al-richer cores. Metamorphic conditions of 925 °C, 7.8 kbar were obtained through the intercept between both isopleths.

An estimate for the retrograde *P-T* conditions was obtained combining garnet (XAlm) and biotite (X_{Mg}) moats isopleths/isolines. XAlm = 0.62 isopleth corresponds to the mean composition of garnet rims (Figure 9B). X_{Mg} = 0.67 corresponds to the mean composition of biotite moats around garnet (Figure 9B). Metamorphic conditions of 670 °C, 5 kbar. Were obtained through the intercept between both isolines. The intersection lies inside the field where the assemblage Ilm+Opx+Grt+Bt+Or+Pl+Qz is stable, which is representative of the observed retrograde assemblage.

An approximation of the cooling path is marked as a black dashed arrow in the diagram (Figure 9A), considering the formation of biotite moats after garnet and orthopyroxene.

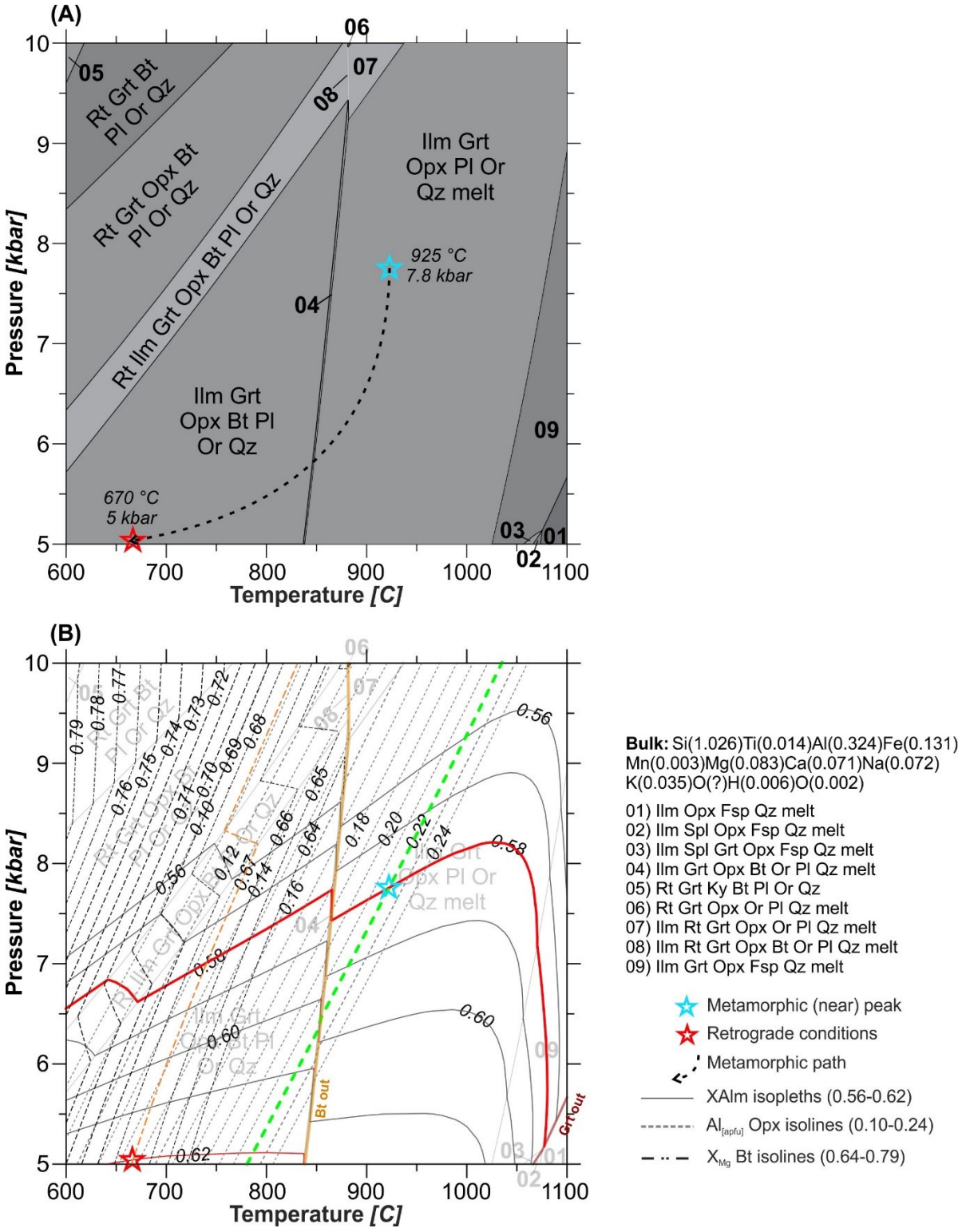

Figure 4-9 - Phase-equilibria modeling for the layered orthopyroxene-garnet diatexite (sample P013). A) Stable assemblages on P-T interval between 600-1100 °C, 5.0-10.0 kbar. Metamorphic assemblage corresponds to the field in which the blue star lies. The dashed arrows represent a possible metamorphic trajectory (see text); B) Xalm isopleths and $Al_{[apfu]}$ in orthopyroxene isolines, as well as X_{Mg} biotite isolines, projected on the stability fields. The intersection between Alm_{58} isopleth and $Al_{[apfu]}$ = 0.21 isoline (blue star) marks a minimum estimate for the metamorphic peak (T = 925 °C, P = 7.8 kbar). The red star marks an estimate for retrograde conditions based on garnet rims (Alm_{62}) and X_{Mg} biotite (0.67) compositions (T = 670 °C, P = 5.0 kbar).

4.3.2 Al-in-orthopyroxene thermobarometry

The full set of Al-in-orthopyroxene thermobarometry calculations are presented on Supplementary file 3.

4.3.2.1 Layered orthopyroxene-garnet diatexite (sample P013)

Mean compositions for garnet cores and high-Al orthopyroxene core compositions provided temperatures between 948 – 1021 °C and pressures between 8.8 – 10.8 kbar (mean 978 ± 24 °C, 9.6 ± 0.7 kbar). Garnet cores with higher XGrs (and lower XAlm) and orthopyroxene with the highest Al_{apfu} cores (Figure 10) provided temperatures between 1040-1054 °C and pressures between 11.5 and 11.9 kbar (mean 1043 ± 4 °C, 11.7 ± 0.1 kbar).

Calculations involving xenomorphic garnet and orthopyroxene crystals yielded two different sets of *T* and *P.* Higher XGrs (and lower XAlm) garnet and higher Al_{apfu} orthopyroxene yielded temperatures between 1018 – 1066 °C and pressures between 10.0 – 11.3 kbar (mean 1042 ± 22 °C, 10.7 ± 0.7 kbar). Lower XGrs garnet and lower Al_{apfu} orthopyroxene values provided temperatures between 940 – 970 °C and pressures between 9.0 – 9.4 kbar (mean 955 ± 17 °C, 9.2 ± 0.2 kbar).

Garnet and orthopyroxene (low-Al) rim compositions provided temperatures between 912 – 975 °C and pressures between 7.5 – 8.4 kbar (mean 936 ± 28 °C, 8.0 ± 0.4 kbar) (Figure 10).

4.3.2.2 Schlieren orthopyroxene-garnet diatexite (sample P1)

Garnet cores and high-Al orthopyroxene crystals from the residue (Figure 10) yielded temperatures between 932 – 983 °C and pressures between 8.6 – 10.2 kbar (mean 962 ± 19 °C, 9.5 ± 0.6 kbar). Pressure-temperature values for calculations involving garnet rims and low-Al orthopyroxene provided temperatures between 782 – 839 °C and pressures between 7.2 – 8.2 kbar (mean 808 ± 14 °C, 7.5 ± 0.3 kbar) (Figure 10).

4.3.3 Integrated metamorphic paths

Data obtained from phase-equilibria modeling and Al-in-orthopyroxene thermobarometry are presented on Figure 10.

As Al-corrected Grt-Opx thermometers provide reliable near peak *T* and *P* conditions for UHT metamorphic rocks (Fitzsimons and Harley, 1994; Pattison and Begin, 1994; Pattison et al., 2003), Al-in-orthopyroxene results reported here are considered as the best approach for such conditions for the orthopyroxene-garnet migmatites. Retrograde metamorphic conditions for this group were interpreted to be

better represented by the retrograde coditions obtained from phase-equilibria modelling of the layered orthopyroxene-garnet diatexite (sample P013) as they combine biotite and garnet rim compositions.

As phase-equilibria modeling from the hercynite-sillimanite-garnet migmatites provided similar peak conditions and both samples present similar mineral assemblages, retrograde conditions calculated for the schilieren/schollen hercynite-sillimanite-garnet diatexite (sample P4E) were interpreted as representative of the retrograde path for this group.

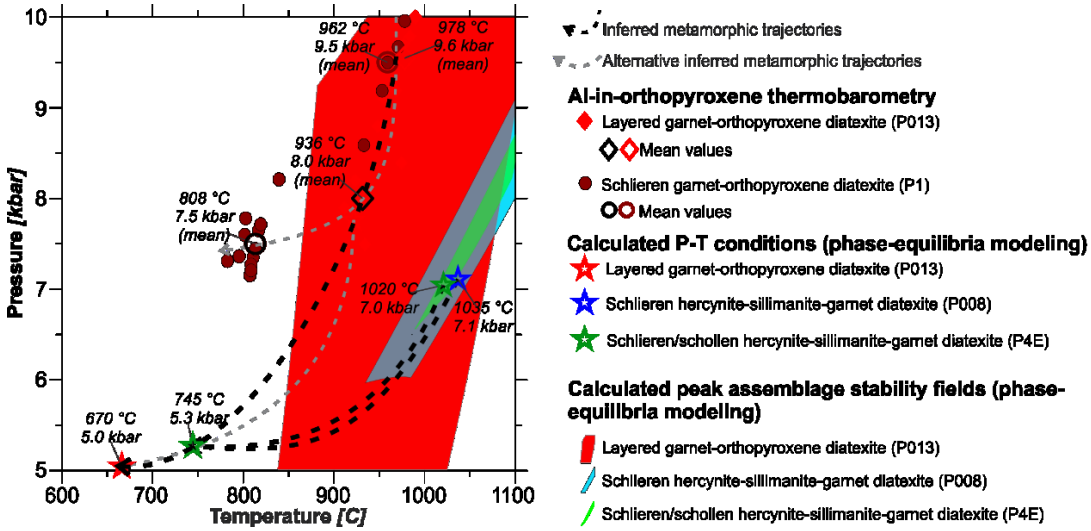

Figure 4-10 - Comparison between stability fields, calculated P-T conditions and inferred metamorphic paths for the samples analyzed in this work through both methods. All samples define clockwise trajectories.

4.4 U-Pb Geochronology

U-Pb (LA-ICP-MS) zircon geochronology was carried out on samples of the layered orthopyroxene-garnet diatexite (P013) and schlieren-schöllen hercynite-sillimanite-garnet diatexite, mainly comprising its residue (P4E). The assumptions for the best metamorphic age for rocks submitted to ultrahigh temperature metamorphism require a careful evaluation of the isotopic data. Therefore, we applied a similar approach to those described by Whitehouse and Kemp (2010) and Taylor et al. (2016) for high-grade metamorphic zones and proceeded with careful investigation of the internal structure of the zircons through cathodoluminescence (CL) imaging, allowing the identification of domains presenting same CL-response (cores, rims and single grains/entire grains). In the present work, the term ‘date’ refers to individual time values from $^{206}Pb/^{238}U$ spot data, while the term ‘age’ is used for groups of $^{206}Pb/^{238}U$ dates with geological significance, as employed by Kunz et al. (2018). Both samples have

showed a variety of zircon morphologies and textures including (Supplementary file 5): 1) convoluted zoning crystals; 2) fir-tree zoning crystals; 3) high luminescence crystals; 4) homogeneous crystals; 5) oscillatory zoned crystals; 6) sector zoning crystals; 7) “soccer ball” crystals; 8) xenocrystic core crystals. Figures 11A and 12A shows examples of zircon textural types observed on both samples, analytical spot sites and related $^{206}Pb/^{238}U$ dates. Crystals exhibiting an inverse age pattern (i.e., rims older than cores) are observed rarely on both samples.

4.4.1 Schlieren/schollen hercynite-sillimanite-garnet diatexite (Sample P4E)

Cathodoluminescence images (Figure 11) exhibit slightly rounded to short-prismatic zircon grains with approximate 1:1 length:width ratio, and subordinate ratios from 2:1 to 3:1, for a maximum length of 150 μm. Grains with high to intermediate luminescence, homogeneous to sub-homogeneous internal aspect and “soccer ball” grains with sector zoning (Figure 11) compose ca. 22% of the analyzed grains. A high proportion of grains (ca. 47%) presents xenocrystal cores displaying a variety of internal structures (Figure 11). Apparently preserved original igneous features (i.e., oscillatory and sector zoning crystals in Figure 11) occur in ca. 26% of the crystals. Crystals exhibiting fir-tree and convolute zoning represent the less frequent type (ca. 5%) and the smallest grains (<90 μm). Luminescent overgrowths up to 60 μm-wide are broadly observed in all the aforementioned varieties.

Hundred six U-Pb dates obtained from seventy-seven zircon crystals do not form an unique coherent statistical population. Instead, a portrayal of dates in the Concordia diagram is observed. The dates cluster in the range from ca. 617 Ma to ca. 585 Ma (ca. 86% of dates, Figure 12A-C). No relationship is observed between textural types and age distributions, with both, cores and rims, exhibiting a superposition of dates.

Zircon cores dates spread continuously over the Concordia diagram (Figure 12A) from 635 ± 10 Ma to 581 ± 10 Ma, exhibiting four older outlier dates (646 ± 10 Ma, 662 ± 15 Ma, 693 ± 11 Ma and 1190 ± 18 Ma). A single statistical peak is defined at ca. 600 Ma (Figure 12B). Similarly, zircon rim dates spread continuously over the Concordia diagram from 615 ± 11 Ma to 581±11 Ma, with a single statistical peak defined at ca. 595 Ma (Figure 12C). For the rims, two older outlier spots are observed, one inside the range of dates observed for zircon cores (633 ± 11 Ma) and one registering an older date (715 ± 12 Ma). Th/U ratios higher than 1 (up to 2.05) are observed on ca. 13% of the analyzed core and rim spots of xenocrystic core crystals,

high luminescence crystals and “soccer ball” crystals within a range of ages between ca. 615 – 581 Ma, as well as two older outliers (715 ± 11 Ma and 1190 ± 18 Ma).

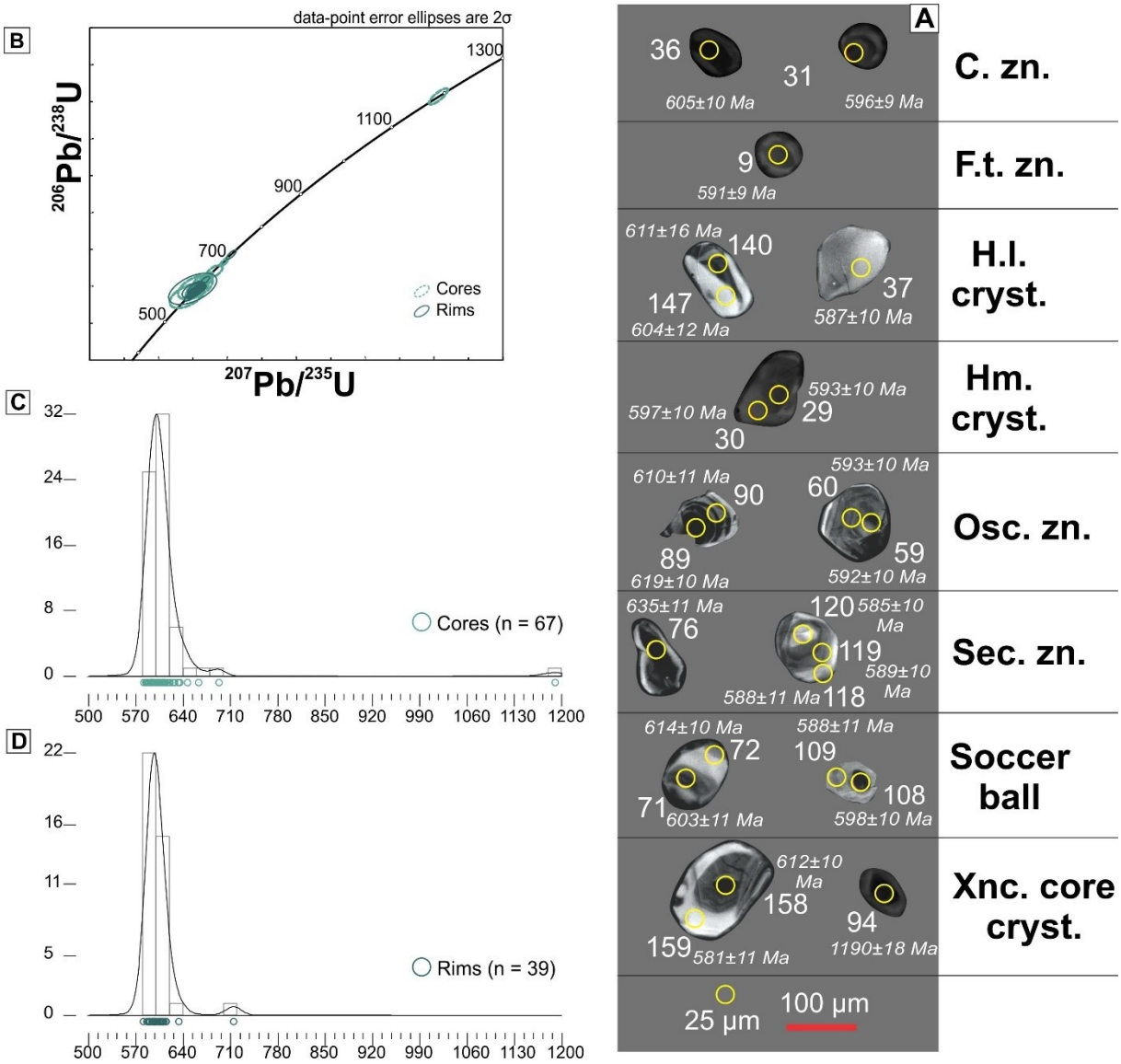

Figure 4-11 – Zircon textures and U-Pb dates plots for the schilieren/schöllen hercynite-sillimanite-garnet diatexite (sample P4E). A) Cathodoluminescence images of zircon grains, exhibiting external shapes, internal morphologies, spot sites and $^{206}Pb/^{238}U$ dates. C. zn. – convolute zoning crystals; F.t. zn. – fir-tree zoning crystals; H.l. cryst. – high luminescence crystals; Hm. cryst. – homogeneous crystals; Osc. zn. – oscillatory zoning crystals; Sec. zn. – sector zoning crystals; Soccer ball – ‘‘soccer ball’’ crystals; Xnc. core cryst. – xenocrystic core crystals. B) Concordia diagram for zircon cores and rims. C and D) $^{206}Pb/^{238}U$ dates probability density diagrams for zircon cores and rims, respectively.

4.4.2 Layered orthopyroxene-garnet diatexite (Sample P013)

Cathodoluminescence images reveal a great variability in the morphology of grains of this sample. The majority of crystals are prismatic to gently round with an approximate 2:1 length:width ratio and a maximum length of 200 µm. Approximately ca. 10% of the analyzed grains show a homogeneous to sector zoned internal structure

and a high luminescence internal aspect in CL-response, including “soccer ball” crystals (Figure 11). Most “soccer ball” crystals display a diameter smaller than 75 μm. Grains with preserved igneous oscillatory or sector zoning constitute ca. 20% of the zircon population and are frequently surrounded by metamorphic rims of high luminescence (Figure 11). Convolute and fir-tree zoned crystals correspond to ca. 12% of grains. Ca. 58% of grains correspond to xenocrystic core grains, exhibiting irregular-shaped cores with luminescent rims or cores with preserved oscillatory zoning and extremely thin to absent luminescent rims (Figure 11).

The eight-five zircon U-Pb spots for sixty-four grains exhibit a spread over the Concordia curve (Figure 12D) from 993 ± 15 Ma to 593 ± 10 Ma. No correlation between textural types, morphologies and the distribution of the dates is observed. U-Pb dates corresponding to analyses in cores and rims largely overlap. High Th/U ratios (>1, up to 8.7) are observed on both, cores and rims analysis of crystals of almost all types (except homogeneous crystals) and are concentrated (ca. 79%) in a range of ages between 635 ± 10 Ma and 593 ± 10 Ma. Most analyses (66%) exhibit Th/U < 1. U-Pb dates in the range of ca. 635 – 593 Ma are observed on 19.6% of those spots.

Zircon core dates are distributed among six main statistical peaks at ca. 600 Ma, ca. 630 Ma, ca. 665 Ma, ca. 720 Ma, ca. 750 Ma and ca. 785 Ma (Figure 12E). Zircon rim dates are distributed among three main statistical peaks at ca. 610 Ma, ca. 655 Ma, and ca. 705 Ma (Figure 12F). Older grain cores are identified in two lesser significant peaks at ca. 838 and ca. 983 Ma, as well as two older outlier grains (1135 ± 17 Ma and 1704 ± 25 Ma). Two date ranges constitute the most statistically significant for zircon cores and rims: ca. 635 – 593 Ma (36% of cores, 48% of rims) and ca. 796 – 714 Ma (32% of cores, 23% of rims).

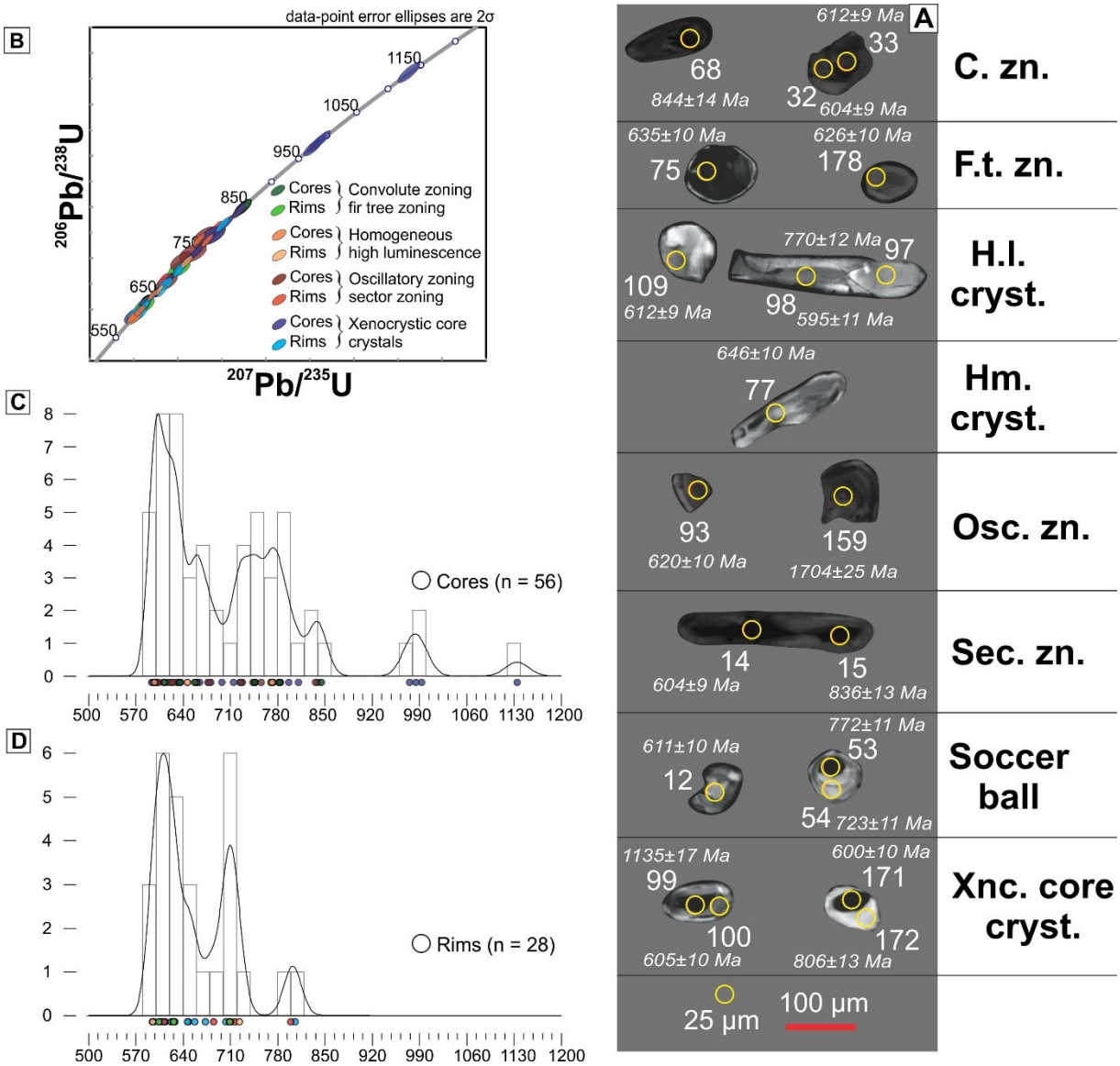

Figure 4-12 - Zircon textures and U-Pb dates plots for the layered orthopyroxene-garnet diatexite (sample P013). A) Cathodoluminescence images of zircon grains, exhibiting external shapes, internal morphologies, spot sites and $^{206}Pb/^{238}U$ dates. C. zn. – convolute zoning crystals; F.t. zn. – fir-tree zoning crystals; H.l. cryst. – high luminescence crystals; Hm. cryst. – homogeneous crystals; Osc. zn. – oscillatory zoning crystals; Sec. zn. – sector zoning crystals; Soccer ball – ''soccer ball'' crystals; Xnc. core cryst. – xenocrystic core crystals. B) Concordia diagram for zircon cores and rims. C and D) $^{206}Pb/^{238}U$ dates probability density diagrams for zircon cores and rims, respectively.

5 Discussions

5.1 Metamorphic record of the Caparaó Complex migmatites

The thermodynamic data obtained from all analyzed samples unravel a metamorphic record that ranges from ultrahigh temperature granulite metamorphism to retrograde metamorphism under amphibolite conditions (Table 5; Figure 10). Characteristic UHT assemblages consist of hercynite+quartz, on both hercynite-sillimanite-garnet migmatite samples, and high-Al orthopyroxene+garnet, on both

orthopyroxene-garnet migmatites. However, different metamorphic peak conditions were obtained for each of the studied migmatite groups. Hercynite-sillimanite-garnet migmatites register higher temperatures (1020 – 1035 °C), while orthopyroxene-garnet migmatites record higher pressures (7.8 kbar or higher, see below).

5.1.1 UHT metamorphic peak

5.1.1.1 Evidences from hercynite-sillimanite-garnet migmatites

Results from petrography and mineral chemistry showed many similarities between the sapphirine-bearing schlieren hercynite-sillimanite-garnet diatexites (sample P008) and the schlieren/schöllen hercynite-sillimanite-garnet diatexites (sample P4E), including the same metamorphic peak assemblage for both rocks (Ilm+Hc+Sil+Grt+Pl+Or+Qz+melt, see section 4.2). Whole-rock geochemistry (Supplementary file 4) and phase-equilibria modeling suggests that their compositions are correlated by a probable melt loss as: i) P008 composition shows lower K_2O+Na_2O contents than P4E; ii) H_2O contents calculated for both samples through T-X_{H2O} modelling is considerably different, with higher contents observed on sample P4E; iii) phase-equilibria modelling for both samples provided similar models, and the main difference between them lie on the stability fields for higher temperatures (including their similar metamorphic peak assemblage fields).

It is noteworthy that although sapphirine and corundum are observed as accessory phases in the sapphirine-bearing schlieren hercynite-sillimanite-garnet diatexite, those phases are absent from the phase equilibria model for this sample. Both are mostly found in local domains with garnet, hercynite and/or corundum (plus ilmenite and quartz) in the absence of sillimanite, and thus were not interpreted as part of the metamorphic peak assemblage for this rock even though sapphirine+quartz assemblages are characteristic of high-Mg UHT metamorphic rocks (Harley, 1989, 1998a; Kelsey, 2008; Taylor-Jones and Powell, 2010). Corundum+quartz assemblages have been reported in high to ultrahigh temperature, moderate to high pressure metamorphic terrains around the world, commonly in Fe-rich, Si-poor or Mg-rich metasedimentary granulites in which magnetite+ilmenite+hercynite, spinel+quartz or sapphirine+quartz assemblages are also present (Mouri et al., 2004). Discussions about whether corundum+quartz could consist of a stable assemblage (Anovitz et al., 1993; Guiraud et al., 1996; Shaw and Arima, 1998) or be metastable (Clark et al., 1957; Powers and Bohlen, 1985; Motoyoshi et al., 1990; Harlov and Newton, 1993; Harlov and Milke, 2002) under lower crustal or upper mantle conditions are extensive in the

literature. The occurrence of both phases on very specific domains is suggestive that sapphirine and corundum consist of products of domanial reactions on this sample, such as

$$Sp+Sil(+Ilm) \rightarrow Grt+Crn(+Mag/Ilm')$$
$$Sp+Sil(+Ilm) \rightarrow Spr+Crn(+Mag/Ilm')$$

Hercynite crystals are widespread along the sapphirine-bearing schlieren hercynite-sillimanite-garnet diatexite, and usually exhibits straight contacts with quartz, feldspars, garnet and sillimanite (Figure 4A-D). Garnet or sillimanite moats around hercynite are seldom observed, thus it is interpreted that hercynite+quartz in equilibrium was mostly preserved. Both garnet and hercynite compositions are considerably uniform (Table 2, Supplementary Figure 1), and metamorphic peak conditions of 1035 °C and 7.1 kbar were retrieved through the intercept of isopleths corresponding to their respective mean compositions ($Xalm_{48}$ and XHc_{52}).

Coarse- to very coarse (>1 cm) garnet crystals from the schlieren/schöllen hercynite-sillimanite-garnet diatexite (P4E) present the lowest almandine and higher pyrope contents observed in this sample (Supplementary Figure 2; Supplementary file 2), and an increase in XPrp contents is observed towards higher temperatures according to its phase equilibria model (Figure 7B). It is possible that smaller garnet crystals also had similar compositions but affected by diffusion and homogenization during UHT metamorphism. Those crystals also host inclusions of other metamorphic peak phases, including hercynite crystals with the lowest Fe^{2+} contents and with few magnetite exsolution lamellae. It is interpreted that both compositions belong to the (near) metamorphic peak assemblage, and thus *P-T* conditions of 1020 °C, 7.0 kbar were retrieved from the intersection of their respective isopleths ($Xalm_{48}$ and XHc_{51}). This intersection lies inside the Ilm+Sp+Sil+Grt+Fsp+Qz+melt assemblage field, which is indicative that closer to the peak a single feldspar phase could be stable instead of two (plagioclase and orthoclase). Matrix hercynite crystals are usually surrounded by cordierite coronae and exhibit a higher volume of magnetite exsolution lamellae, which is indicative that their original composition is not preserved.

5.1.1.2 Evidences from orthopyroxene-garnet migmatites

Orthopyroxene-garnet migmatites show a variety of migmatitic structures along the Caparaó Range. They exhibit similarities in terms of mineral assemblages and bulk-rock compositions, as well as differences in terms of macroscopic structure and proportions between migmatite parts (leucosome x residue). The banded structure of

layered orthopyroxene-garnet diatexites (sample P013) is probably related to their spatial association with ductile shear zones (see Figure 1B) rather than their degree of partial melting as it was submitted to UHT metamorphic conditions. Schlieren orthopyroxene-garnet diatexites (samples P1 and P1D) seems to occur preferably along the regional hinge zone. Schlieren orthopyroxene-garnet diatexites exhibit higher leucosome proportions than layered orthopyroxene-garnet diatexites, which is suggestive of differences between the composition of the protoliths as both rocks were submitted to similar *P-T* conditions.

The characteristic peak metamorphic assemblage observed in those migmatites consists of high-Al orthopyroxene+garnet (+plagioclase+quartz±orthoclase), with rutile also being present on sample P1. Although the association of garnet and high-Al orthopyroxene in straight contacts with quartz is not self-sufficient to attest UHT-metamorphic conditions (Harley, 1998a; Kelsey, 2008), that assemblage is found in many UHT terrains worldwide. Indeed, Grt-Opx pairs (c.f. Harley and Green, 1982; Harley, 1984a, 1984c) have been successfully used for Al-in-orthopyroxene corrected thermobarometry to constrain peak metamorphic conditions (cf. Harley, 1984b; Fitzsimons and Harley, 1994; Pattison and Begin, 1994; Pattison et al., 2003; Kelsey, 2008; Kelsey and Hand, 2015; Rocha et al, 2017, 2018; Motta et al., 2021; Wisniowski et al., 2021). Orthopyroxene crystals with preserved metamorphic peak compositions exhibit a range of $Al_{[apfu]}$ values between 0.14-0.23 in analysed samples, similarly to many granulite to UHT-granulite terrains around the world (Pattison et al., 2003).

Little compositional variations are observed between garnet crystals found on residue-rich and leucosome-rich bands from the layered orthopyroxene-garnet diatexite (P013). Nonetheless, the former exhibit cores with lower mean Xalm which are characteristic of higher temperatures and pressures according to the phase equilibria model, while xenomorphic crystals exhibit the highest mean Xalm contents (Figure 9, Table 3). Orthopyroxene crystals exhibit similar compositional ranges regardless of their textural type (prismatic or xenomorphic crystals) or crystal zone (core or rim). Metamorphic peak conditions of 925 °C and 7.8 kbar were obtained combining the isopleths for interpreted (near) peak compositions of garnet and orthopyroxene ($Xalm_{58}$ and $Al_{[apfu]}$ = 0.22, respectively).

When compared, Al-in-orthopyroxene thermobarometry for the same mean mineral compositions from sample P013 provided considerably different *P-T* conditions, with an estimated metamorphic peak of 978±24 °C and 9.6±0.7 kbar.

Similar conditions were obtained combining the compositions of xenomorphic garnet with lower XGrs and xenomorphic orthopyroxene with lower Al_{apfu} (955±17 °C and 9.2±0.2 kbar). Considering a hypothesis where the association of xenomorphic garnet and orthopyroxene represent a breakdown feature during retrograde metamorphism, the higher *P-T* values (1043±4 °C, 11.7±0.1 kbar) obtained through the combination of higher XGrs (and lower Xalm) garnet with higher Al_{apfu} orthopyroxene could represent the actual metamorphic peak for the layered orthopyroxene-garnet diatexite. Al-in-orthopyroxene thermobarometry for the schlieren orthopyroxene-garnet diatexite (sample P1) provided similar *P-T* conditions to those obtained for the mean compositions of sample P013. Garnet cores and high-Al orthopyroxene crystals provided a metamorphic peak of 962±19 °C and 9.5±0.6 kbar.

A possible explanation for the differences observed between both methods, specially concerning pressure estimates, might be related to the bulk composition chosen for modeling the layered orthopyroxene-garnet diatexite (P013), which might not have been able to predict the actual behavior of Al in orthopyroxene and garnet compositions due to the mixing of domains (residue-rich and leucosome-rich bands). Although the presence of rutile in the assemblage of the schlieren orthopyroxene-garnet diatexites (P1 and P1D) could favor *P-T* calculations involving higher pressures, a (near) metamorphic peak of 962 – 978 °C and 9.5 – 9.6 kbar is considered a better estimate as the analysed rocks (seemingly) lack additional evidence for justifying pressures > 10 kbar.

5.1.2 Retrograde conditions and metamorphic paths

Similar metamorphic paths can be inferred for the sapphirine-bearing schlieren hercynite-sillimanite-garnet diatexite (P008) and the schlieren/schöllen hercynite-sillimanite-garnet diatexite (P4E) based on calculated *P-T* conditions (Figures 7, 8 and 10). As sample P4E exhibit better evidence of retrograde metamorphism, the following reactions are predicted by its respective phase equilibria model compared to textural observations.

Starting at the metamorphic peak at 1020 – 1035 °C and 7.0 – 7.1 kbar, the rock underwent cooling associated with decompression reaching estimated *P-T* conditions of ~900 – 925 °C and ~5.5 – 5.7 kbar, which resulted in the formation of cordierite and sillimanite moats around hercynite through the following retrograde reactions:

$$Sp+Pl+Qz+liq \rightarrow Crd+Grt+Or$$

$$Crd+Sp+Ilm+liq \rightarrow Grt+Or+Ilm/Hem+Sil+liq'$$

The rock then underwent near isobaric cooling until it reached final estimated *P-T* conditions of 745 °C and 5.3 kbar, marked by the formation of biotite at the expense of garnet and cordierite through the following reactions:

$$Grt+Or+liq \rightarrow Bt+Pl+Sil+Qz$$

$$Crd+Grt+Or+liq \rightarrow Bt+Sil+Qz$$

An integrated metamorphic path can be inferred for the layered orthopyroxene-garnet diatexite (P013) and the schlieren orthopyroxene-garnet diatexite (P1) combining data from phase equilibria modelling, Al-in-orthopyroxene thermobarometry and textural observations (Figures 9, 10).

Starting at the metamorphic peak at 962 – 978 °C and 9.5 – 9.6 kbar, both rocks underwent continuous cooling associated with decompression until crossing the biotite-in field at ~850 °C and ~6.4 kbar, in which biotite formed at the expense of peak garnet and orthopyroxene in the presence of melt through the reaction:

$$Opx+Grt+Or+Ilm+melt = Grt'+Pl+Bt+Qz$$

Additional cooling associated with decompression probably increased biotite production until the rock reached final *P-T* conditions of 670 °C and 5.0 kbar.

Both migmatite types exhibit clockwise metamorphic trajectories and reached final *P-T* conditions in the amphibolite field (670 – 745 °C, 5.0 – 5.3 kbar). However, peak pressure conditions differ by the order of 2.5 kbar, implying that both rocks underwent UHT metamorphism at different crustal depths (~24 km for the hercynite-sillimanite-garnet migmatites and ~33 km for the orthopyroxene-garnet migmatites, considering a pressure gradient of 0.29 kbar/km).

Rock type	Sample	Al-in-Opx		Phase-equilibria modelling		LA-ICP-MS U-Pb dating
		T (°C)	P (kbar)	T (°C)	P (kbar)	Main age ranges (Ma)
Spr-bearing schlieren Hc-Hc-Grt diatexite	P008	-	-	1035	7.1	-
Schlieren/schöllen Hc-Sil-Grtdiatexite	P4E	-	-	1020	7.0	635±10 – 581±10
Layered Opx-Grt diatexite	P013	978	9.6	925	7.8	635±10 – 593±10
Schlieren Opx-Grt diatexite	P1	962	9.5	-	-	-

Table 4-4 - Summary of metamorphic peak conditions obtained from Al-in-orthopyroxene thermobarometry and Theriak-Domino phase-equilibria modelling for each rock type.

5.2 Constraints on the origin of the protolith and correlation with other units from the Araçuaí orogen

A thorough compilation of U-Pb zircon and monazite ages from the literature, presented on Supplementary file 6, addresses the following discussions and correlations.

No correlation was observed between the morphological and textural features from the zircon domains, identified through the CL images (Figure 11), and the distribution of U-Pb dates obtained from the layered orthopyroxene-garnet diatexite (P013) and the schlieren-schöllen hercynite-sillimanite-garnet diatexite (P4E). U-Pb dates largely overlap within the eight morphological and textural domains identified in both samples. Decoupling between CL textures and U-Pb isotopic data in zircon is a feature well known in high- to ultrahigh temperature metamorphic terrains (e.g., Whitehouse et al., 2014; Kunz et al., 2018).

As a noteworthy characteristic of the analyzed samples, the zircon U-Pb data spread concordantly along the Concordia curve (Figure 11A, D). The layered orthopyroxene-garnet diatexite (P013) exhibits a larger spreading than the schlieren-schöllen hercynite-sillimanite-cordierite-garnet diatexite (P4E). Zircon grains subjected to temperatures over 900 °C may exhibit a downline spreading range along the Concordia curve, owing to partial isotopic system opening, resorption or dissolution and recrystallization caused by metamorphic reactions, partial melting and/or protracted zircon growth through the metamorphic evolution (Corfu et al., 1994; Ashwal et al., 1999; Shaltegger et al., 1999; Hoskin and Black, 2000; Kelly and Harley, 2005; Harley et al., 2007; Gerdes and Zeh, 2009; Rubatto, 2017; Vervoort and Kemp, 2016; Tedeschi et al., 2023). Inverse age zoning (rims older than cores), observed on scarce zircon crystals in both samples (see Figure 10), might be related to recrystallization of metamict domains under dry ultrahigh temperature conditions as discussed by Laurent et al. (2018). Because this type of protracted record has been attributed to Pb-loss (Ashwal et al., 1999; Harley et al., 2007; Gerdes and Zeh, 2009; Whitehouse and Kemp, 2010), the interpretation of the obtained U-Pb dates for both samples are based on the distribution patterns of the dates for the cores and rims and their comparison with the literature, rather than the distribution of each statistical population.

U-Pb dates obtained for the schlieren-schöllen hercynite-sillimanite-garnet diatexite (P4E) spread continuously over the Concordia diagram in a range between ca. 635 Ma to 581 Ma. The mineral assemblage of the schlieren/schöllen hercynite-sillimanite-garnet diatexite (P4E) points to a sedimentary protolith (possibly a metapelite). The high concentration of dates in such intervals, the scarcity of older

grains and the decoupling between zircon textures might be indicative that: i) most U-Pb dates obtained for the hercynite-sillimanite-garnet diatexite (P4E) suffered isotopic disturbance; ii) the protolith had few detrital zircon grains (e.g. a clay-rich pelite in which few to no heavy minerals were originally deposited), and most grains were produced by protracted zircon growth during the metamorphic event; iii) the sedimentary sources for the protolith were crystallized inside a similar time span than that of the metamorphic event. Considering the latter scenario, U-Pb data suggest that the sediments are likely to have been formed mainly by Late-Neoproterozoic sources, while it is not possible to precisely retrieve an age through U-Pb data nor address the source(s) involved.

U-Pb dates obtained for the layered orthopyroxene-garnet diatexite (P013) range between ca. 1704 Ma to ca. 593 Ma and are mainly concentrated in two date ranges: i) between ca. 635 Ma to 593 Ma; and ii) between ca. 796 Ma and ca. 714 Ma. While the mineral assemblage of the layered orthopyroxene-garnet diatexite (Sample P013) is not sufficiently diagnostic of an igneous or sedimentary protolith (e.g. Kelsey and Hand, 2015), the zircon U-Pb record points out to a sedimentary protolith for this sample (possibly a metagraywacke). An (meta)igneous protolith cannot be completely ruled out, however, as UHT metamorphism can possibly generate a similar U-Pb date distribution in metaigneous rocks (e.g., Whitehouse and Kemp, 2010; Tedeschi et al., 2018; Tedeschi et al., 2023). The differences in U-Pb date distribution when compared to the schlieren/schöllen hercynite-sillimanite-garnet diatexite (P4E) are suggestive that distinct sedimentary sources contributed to the zircon record of each rock and/or the isotopic disturbance was probably less pervasive on sample P013, not sufficiently to rehomogenize the U-Pb isotopic ratio to the same extent observed on sample P4E.

Older dates obtained in both samples are related to possible protosources (i.e. Pell et al., 1997) or detrital zircons, though these relations must be taken carefully as the dates ranges obtained in zircon cores from rocks submitted to UHT metamorphic conditions are likely to record younger dates than that of the crystallization of their protoliths (Kelsey, 2008; Gerdes and Zeh, 2009; Vervoort and Kemp, 2016; Tedeschi et al., 2018). Thus, even though some similarities may be pointed out between the U-Pb dates obtained in this work with other units from the Araçuaí-Ribeira orogen, São Francisco Craton, Kaoko belt and West Congo belt, the metasedimentary units found in the Caparaó complex were not associated to any specific unit on the Araçuaí-Ribeira orogen.

The ranges and peaks observed in the zircon records of both analysed samples can be correlated to other units from the Araçuai-Ribeira orogen and the São Francisco craton. Dates between 664 ± 10 Ma and 646 ± 10 Ma found in both samples are also found on ophiolite bodies along the suture zone of the Araçuaí orogen (ca. 660 – 600 Ma; Pedrosa-Soares et al., 1998; Queiroga et al., 2007, 2010; Amaral et al., 2020), as well as on the Rio Negro-Serra da Prata magmatic arc system in the Ribeira orogen (ca. 860 – 600 Ma; Tupinambá et al., 2012; Peixoto et al., 2017; Santiago et al., 2020, 2022). Dates between 844 ± 14 Ma and 673 ± 12 Ma, found mainly in the layered orthopyroxene-garnet diatexite (P013), are also found on the Rio Negro-Serra da Prata arc (op. cit.), in the Southern Bahia alkaline province (ca. 734 – 676 Ma; Rosa et al., 2007) and in the Kaoko belt (ca. 1800 – 660 Ma; Konopásek et a., 2014; Luft et al., 2011). Scarce dates ranging from 993 ± 15 Ma to 975 ± 15 Ma can be correlated to the timespan of rift-related magmatic suites found along the Araçuaí orogen and São Francisco Craton (e.g., Formiga dyke swarm: ca. 984 – 906 Ma; Chaves and Neves, 2005) or the West Congo Belt (ca. 1000 – 910 Ma; Tack et al., 2001). Older zircon dates ranging from ca. 1704 – 1135 Ma are also found in the Kaoko Belt (Konopásek et al., 2014; Luft et al., 2011), in the Espinhaço supergroup (Machado et al. 1989; Dussin and Dussin, 1995; Chemale et al., 2012) and in alkaline granulites intruded in the Juiz de Fora and Mantiqueira complexes (ca. 1765 – 1656 Ma, Heilbron et al., 2010).

5.3 Constraints on the timing of metamorphism and correlations within the evolution context of of the Araçuaí orogen

Though Th/U ratios < 0.1 have been commonly considered in the identification of metamorphic domains in zircon crystals (Rubatto and Gebauer, 2000; Rubatto, 2002), those ratios can vary largely depending on which minerals are competing with zircon for the available Th in a given equilibrium volume (Yakymchuk et al., 2018) or the rock composition (Rubatto, 2017). In HT/UHT rocks zircon can exhibit a wide range of Th/U ratios, often > 0.1 (Kelly and Harley, 2005; Harley et al., 2007; Yakymchuk et al., 2018) and lack any correlation with specific CL domains (Kunz et al., 2018; Rubatto, 2017).

On the hercynite-sillimanite-garnet diatexite sample (P4E), Th/U ratios higher than 1.0 are observed mainly on younger zircons (ca. 604 – 581 Ma), while lower ratios are also observed throughout the full range of ages, thus no specific relation can be pointed out. On the layered orthopyroxene-garnet diatexite sample (P013), spots with

high Th/U (>1.0) ratios are mostly concentrated in the U-Pb date interval between ca. 635 – 593 Ma (in which most analysed dates are constrained), though no correlation with specific domains or zircon types/textures can be pointed out.

One of the challenges in obtaining ages for UHT metamorphic events consists in the fact that U-Pb ages commonly reflect not the age of the metamorphic peak but the timing of the cooling path, as several processes (see section 5.2 and references therein) contribute to form a protracted zircon record and/or generate a high volume of zircon crystals crystallized from the melt (Corfu et al., 2003; Harley et al., 2007; Taylor et al., 2016; Rubatto, 2017; Chen and Zheng, 2017; Tedeschi et al., 2023). Therefore, the obtained ages must be taken as a minimum estimate for the thermal peak. In the analyzed samples, the continuous spread and the high concentration of dates in the ca. 635 – 581 Ma range in both samples points out to a probable minimum age of ca. 635 Ma for the UHT metamorphic event. Inside this range, observed peaks and a higher concentration of ages between ca. 610 – 590 Ma on both samples is probably related to the post-peak closure of zircon and melt crystallization, as discussed by Kelsey (2008) and Kelsey and Hand (2015). Therefore, an estimate for the lifespan of the HT-UHT metamorphism is possibly related to the age range between ca. 635 – 610 Ma.

It is possible, however, that the differences between the main statistical peaks for the U-Pb dates obtained from both samples reflect differences in the onset of UHT metamorphism on each one. In this case, both samples would have been submitted to UHT conditions under different tectonic contexts or on different stages of the evolution of the Araçuaí orogen. Although this hypothesis would agree with the possibility that the analyzed hercynite-sillimanite-garnet migmatites and orthopyroxene-garnet diatexites were submitted to UHT conditions on different tectonic levels (as discussed on section 5.1), it is not possible to precise if the apparent age differences between those statistical peaks have an actual geological meaning based on U-Pb dates alone.

The range between ca. 635 – 580 Ma is in agreement with metamorphic ages obtained for Caparaó Suite and Juiz de Fora ortho-granulites and migmatites by Söllner et al. (1991; ca. 586 Ma), Da Silva et al. (2002; ca. 587 Ma), Noce et al. (2007; ca. 594 Ma), Heilbron et al. (2010; ca. 654 – 584 Ma), Faria et al. (2022; ca. 633 – 584 Ma), and with metamorphic ages obtained for Andrelândia unit and other Neoproterozoic metasedimentary units located nearby by Degler et al. (2017; ca. 618 – 573 Ma). This range spans the age interval given by the pre-collisional igneous rocks

of the Rio Doce magmatic arc (Figure 1B, Figure 13), encompassing plutonic bodies of the G1 Supersuite and related volcanic rocks (ca. 630 – 585 Ma) (Novo et al., 2010; Pedrosa-Soares et al., 2011; Bento dos Santos et al., 2015; Tedeschi et al., 2016; Novo et al., 2018). Local occurrences of early S-type igneous intrusions, possibly related to collisional igneous activity, have been reported in the literature on the Araçuaí orogen, such as a garnet-bearing charnockite intrusion of the Manhuaçu region (ca. 584 Ma: Da Silva et al., 2002), and a few garnet-rich granites of the G2 supersuite located in the back-arc region (ca. 590 – 580 Ma; Gradim et al., 2014; Richter et al., 2016; Melo et al., 2017).

Figure 13 exhibits a comparison between the distribution of zircon U-Pb dates on both analyzed samples and the observed distribution of U-Pb ages corresponding to the five orogenic suites and the metamorphism on the Araçuaí orogen (Araújo et al., 2020; Pedrosa-Soares et al., 2020). Most of the data obtained for the schlieren/schöllen hercynite-sillimanite-garnet diatexite (sample P4E) is constrained between the two age peaks of the Rio Doce magmatic arc (pre-collisional G1 Supersuite). The statistical peak for both cores and rims in this sample corresponds to the discrete ca. 600 Ma peak observed for metamorphic ages on the orogen. U-Pb dates from the layered orthopyroxene-garnet diatexite (sample P013) are older than the main age peak (ca. 589 Ma) for the G1 Supersuite, and the older peak (ca. 620 Ma) for this suite falls between the ca. 610 Ma and ca. 630 Ma date peaks for rims and cores (respectively) of sample P013. The ca. 600 Ma peak for metamorphic ages is also observed on zircon cores of this sample. Only the youngest U-Pb dates obtained in this work (2 spots in sample P4E, 581±10 Ma) correlate to the age peak for the collisional G2 suite. Therefore, a correlation between the UHT metamorphic event and the pre-collisional stage of the Araçuaí orogen can be pointed out.

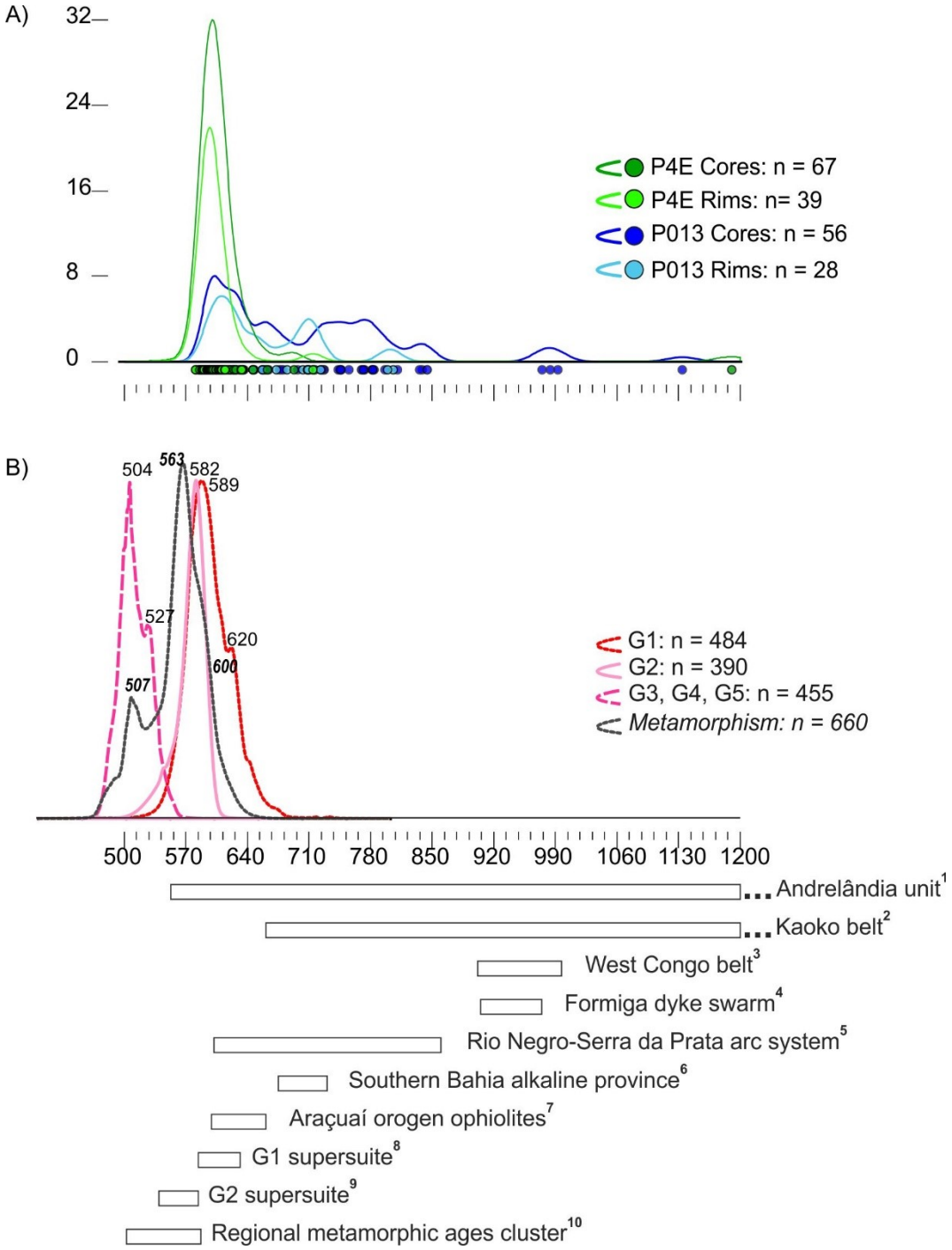

Figure 4-13 - Comparison between the distribution of zircon $^{206}Pb/^{238}U$ dates on the A) layered orthopyroxene-garnet diatexite (sample P013) and schlieren/schöllen hercynite-sillimanite-garnet diatexite (P4E) and B) U-Pb age patterns on the Araçuaí orogen (cf. Araújo et al., 2020, and Pedrosa-Soares et al., 2020). Both datasets are compared with the distribution of ages from geological units, magmatic arcs and orogenic belts from the regional context. N = number of U-Pb analysis. 1 – Degler et al. (2017); 2 – Luft et al. (2011), Konopásek et al. (2014); 3 – Tack et al. (2001); 4 – Chaves and Neves (2005); 5 – Tupinambá et al. (2012), Peixoto et al. (2017), Santiago et al. (2020, 2022, 2023); 6 – Rosa et al. (2007); 7 – Pedrosa-Soares et al. (1998), Queiroga et al. (2007), Queiroga (2010), Amaral et al. (2020); 8 – Novo et al. (2010, 2018), Pedrosa-Soares et al. (2011), Bento dos Santos et al. (2015), Tedeschi et al. (2016), Gonçalves-Dias et al. (2016, 2018), Araújo et al. (2020, 2023); 9 and 10 – De Campos et al. (2004), Bento dos Santos et al. (2011, 2015), Gradim et al. (2014), Gonçalves-Dias et al. (2016), Richter et al. (2016), Melo et al. (2017), Serrano et al. (2018).

5.4 Tectonic setting for UHT metamorphism in the Araçuaí orogen

The age range obtained for the HT-UHT event (ca. 635 – 610 Ma) is considerably older than ages related to the collisional metamorphic peak (ca. 575 – 560 Ma) recorded by high-grade paragneiss complexes of the Araçuaí orogen and northern Ribeira belt (De Campos et al., 2004; Bento dos Santos et al., 2011; Gradim et al., 2014; Bento dos Santos et al., 2015; Dias et al., 2016; Richter et al., 2016; Degler et al., 2017), suggesting a correlation between ultrahigh temperature metamorphic event and the pre-collisional to early collisional stages of the Araçuaí orogen.

Processes capable of attaining UHT conditions in Earth's crust have been widely debated in the literature (e.g. Harley, 1898, 1998a, 2008, 2016; Harley et al., 2007; Kelsey, 2008; Santosh and Kusky, 2010; Korhonen et al., 2013; Kelsey and Hand, 2015). Comparing the results obtained in this work to the tectonic evolution of the Araçuaí orogen, some hypothesis to explain the context in which UHT conditions were attained can be proposed:

1) As the presented ages range for the UHT metamorphic event are cronocorrelated with the magmatic development of Rio Doce arc, a process of magma underplating could be responsible for attaining UHT metamorphism in the studied region, as previously suggested by Costa (1998). UHT conditions would have taken place at middle to lower crust by combining large-scale emplacement of uprising arc magmas with increasing radiogenic heat production due to crustal thickening (cf. Ducea, 2001; Clark et al., 2011; Tedeschi et al., 2018). Expressive thickening of arc crust due to the combination of compressive tectonic stresses and the accumulation of magmas at the neutral buoyancy level might be related to a magmatic flare-up process (cf. Cao et al., 2016; Ganade et al., 2021). This proposition is corroborated by the presence of pre-collisional to early collisional charnockitic plutons (Amaral et al., 2016; Vieira et al., 2017).
2) The metamorphic peak pressure estimates for the orthopyroxene-garnet migmatites (9.5 – 9.6 kbar) and hercynite-sillimanite-garnet migmatites (7.0 – 7.1 kbar) imply that rocks from different crustal depths (~33 km and ~24 km respectively) were affected by the UHT metamorphic event and juxtaposed through shear zones along the crustal block that became the Caparaó complex. Thus, a tectonic context related to astenospheric ascension in a back-arc zone, typically involving lower pressures, may be ruled out. High-pressure granulites

(Ky-Gr-Kfs gneisses) have been identified in the Manhuaçu shear zone (Figure 1B), ~35 km northwest of the studied area, with pressure estimates up to 16 kbar (Degler et al., 2019). The spatial association of high-pressure and ultrahigh temperature rocks in a restricted area might be indicative of a slab-window setting during subduction (e.g. Santosh and Kusky, 2010; Santosh et al., 2011). Subduction of the oceanic ridge creates a “window” for the ascension of hot, dry asthenosphere providing enough heat to attain ultrahigh temperature conditions at the deep levels of the arc and forearc (Santosh et al., 2011). This process seems to be related to a temporary interruption in the generation of wet arc magmas during the descent of the slab window (cf. Bradley et al., 2003) and thus favors the preservation of UHT mineral assemblages (cf. Santosh and Kusky, 2010; Santosh et al., 2011);

3) High concentration of radiogenic elements owing to lithospheric overthickening during continental collision tectonics may also provide heat for achieving UHT metamorphic conditions. Del Lama et al. (2000), Campos Neto and Caby (2000) and Rocha et al. (2018) suggested the radiogenic heat as the main cause for the ultrahigh temperature metamorphism recorded in the Socorro-Guaxupé Nappe (Southern Brasília Orogen). Ultrahigh temperature conditions assisted by crustal overthickened related to nappe tectonics have been related to long-lived (30 – 100 Ma) UHT metamorphic events (cf. Harley, 2016). However, evidence of collisional-related nappe tectonics seems to be absent of the Araçuaí orogen (Alkmim et al., 2006, 2017) and the UHT metamorphic age range for the studied rocks falls within the pre-collisional stage. Therefore, such a mechanism seems to be less plausible to explain the studied UHT rocks and the high-pressure granulite rocks observed in the Manhuaçu shear zone near the study area.

Therefore, we suggest two possible mechanisms responsible for reaching UHT metamorphic conditions in the studied region: i) heat increasing caused by a slab-window effect related to subduction of an ocean ridge segment, due to the ascension of the asthenosphere through this “window” (cf. Santosh and Kusky, 2010; Santosh et al., 2011); or ii) heat increasing due to the emplacement of a large volume of arc-related magmas following the descent of the slab during subduction, increased radiogenic heating due to crustal thickening caused by the arc growth and transition to an early-collisional tectonic setting (cf. Ducea, 2001; Clark et al., 2011; Cao et al.,

2016; Tedeschi et al., 2018; Ganade et al., 2021). It is also possible that both mechanisms were involved to a certain extent during the evolution of the Rio Doce magmatic arc. Figure 14 presents a tectonic model for the slab-window mechanism proposed for achieving UHT metamorphic conditions in the Caparaó complex in the light of the pre-collisional evolution of the Araçuaí orogen (cf. Tedeschi et al., 2016).

This conclusion is mainly based on: i) the minimum ages associated with the UHT metamorphic event, which point out to a correlation between the onset of UHT conditions and the evolution of the Rio Doce magmatic arc; ii) the spread of U-Pb ages along the Concordia line, a characteristic of long-lasting UHT events; iii) the existence of high pressure granulites in a short distance from the Caparaó Range; and iv) the abundance of charnockitic rocks in the region between the Caparaó range and Manhuaçu shear zone that might be related to a dry heating process beneath the Rio Doce arc, a process typically associated with slab window phenomenon (cf. Bradley et al., 2003; Santosh and Kusky, 2010). Examples of UHT granulites possibly related to a “slab-window” mechanism include the metamorphic belt in the Palghat-Cauvery Suture Zone (Santosh and Kusky, 2010) and the granulites belonging to the Khondalite Belt in the Northern China Craton (Santosh et al., 2012). An example of an arc-related ultrahigh metamorphic event with no correlation to a back-arc setting is discussed by Tedeschi et al. (2018) for the UHT metamorphic rocks observed on the Socorro-Guaxupé Nappe. In their work, crustal thickening by magmatic addition, increased radiogenic heat and the emplacement of basic magmas are pointed out as possible heat sources for a relatively long-lived (~40 Ma) ultrahigh temperature metamorphic event.

Gradim et al. (2014) previously suggested a similar (slab-window) mechanism in order to explain the oldest S-type granites (ca. 590 – 580 Ma) found in the back-arc region, and Tedeschi et al. (2016) discussed that oceanic ridge subduction in-between 605 – 585 Ma might have promoted abnormal increase of magma production along the Rio Doce arc. Such a mechanism would also explain the relative scarcity of ultrahigh temperature rocks in the Araçuaí orogen, even considering the deep crustal levels exposed by erosion in the orogen hot core, because UHT rocks in this setting are restricted to the extensional site related to the slab window phenomenon (cf. Santosh and Kusky, 2010).

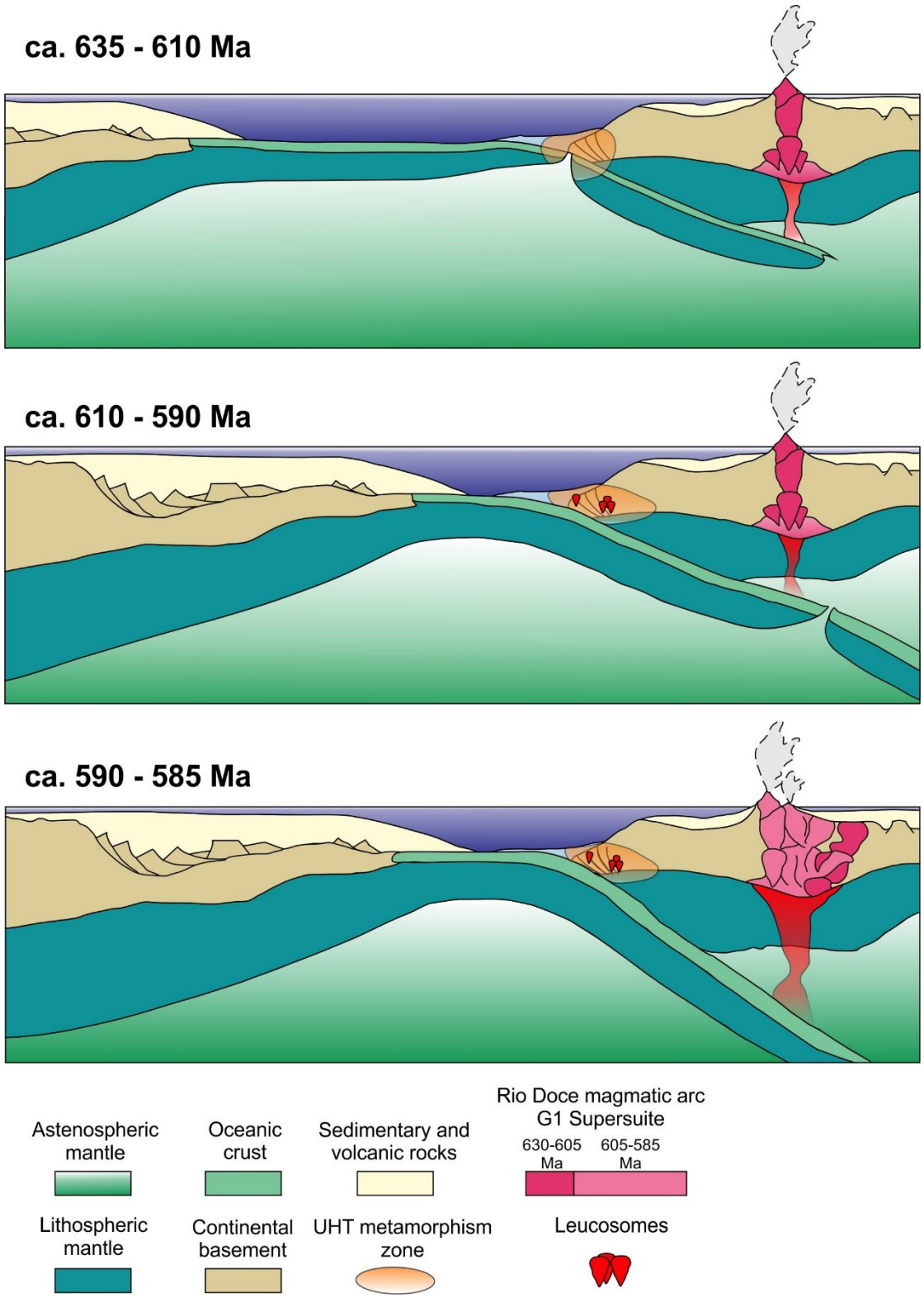

Figure 4-14 – Tectonic model illustrating the mechanism proposed for achieving UHT metamorphic conditions in the Caparaó complex (modified from the Rio Doce magmatic arc tectonic model from Tedeschi et al., 2016). Increased heat due to the subduction of an ocean ridge (slab-window mechanism) triggers the onset of UHT metamorphic conditions between ca. 635-610 Ma, followed by a large-scale crystallization of melts produced by anatexis of crustal rocks between ca. 610 – 590 Ma.

6 Conclusions

Within the Caparaó complex, migmatites derived from metasedimentary protoliths are juxtaposed to the orthogneisses and associated migmatites of the Caparaó Suite/Juiz de Fora Complex by shear zones. These rocks have been divided into two types: orthopyroxene-garnet migmatites and hercynite-sillimanite-garnet migmatites. Both are likely to have derived from sedimentary protoliths. The orthopyroxene-garnet migmatites record metamorphic peak assemblages composed of orthopyroxene, garnet, plagioclase, orthoclase, quartz (plus accessory ilmenite and rutile), for which *P-T* conditions between 962 – 975 °C and 9.5 – 9.6 kbar were calculated. Hercynite-sillimanite-garnet migmatites register peak metamorphism at 1020 – 1035 °C, 7.0 – 7.1 kbar, preserving a peak metamorphic assemblage composed of ilmenite, hercynite, sillimanite, garnet, plagioclase, orthoclase and quartz. The textural and thermodynamic data presented in this work highlights a new ultrahigh temperature (UHT) metamorphism occurrence for the Araçuaí orogen. U-Pb zircon data obtained for both migmatite groups exhibit a protracted record along the Concordia curve owing to isotopic disturbance during the UHT metamorphic event, thus a precise correlation to sedimentary sources and other metasedimentary units along the Araçuaí orogen was not possible. However, data obtained from zircon cores is similar to those found in other units along the Araçuaí orogen, Ribeira belt, Kaoko belt, West Congo belt and São Francisco Craton. Minimum metamorphic ages between ca. 635 – 610 Ma were determined for the UHT event, which are coeval with arc-related magmatism observed on the Araçuaí orogen. Thus, the UHT metamorphic conditions recorded by the Caparaó complex rocks are interpreted to have been attained during the subduction stage, driven by heating derived from a slab-window mechanism and/or by continuous arc magmatism related to arc growth and crustal thickening.

7 Acknowledgements

The first author would like to thank Centro de Pesquisa Professor Manoel Teixeira da Costa (CPMTC-UFMG), under the coordination of A. Pedrosa-Soares and F. Caxito, and Conselho Nacional de Desenvolvimento Tecnológico (CNPq) for the financial support provided (grant number: 447654/2014-4); Geotectonics Laboratory (CPMTC-UFMG) and the staff of CPMTC-UFMG (Johnny, Carlos, Denise, Helvio and Leonardo) for the technical support; Coordenação de Aperfeiçoamento de Pessoal de Nível Superior (CAPES) for the MSc scholarship received by P. L. N. C. R. Vieira;

Microscopy and Microanalyses Laboratory (LMIc), member of the Microscopy and Microanalysis Network of Minas Gerais State (FAPEMIG, Brazil), GEOX Laboratory and the Isotopic Geochemistry Laboratory, all three from the Universidade Federal de Ouro Preto (UFOP), for EMPA, WRG and LA-IPC-MS analytical data. Special thanks to professors Ph.D. Pattison, Chacko, Rocha, Moraes, Heilbron and Da Silva for the attention, discussions and help with various technical questions, and to the Parque Nacional do Caparaó for allowing the research to be conducted inside the national park area. G. Queiroga, T. Novo, A. Pedrosa-Soares and C. Lana are grateful to the Brazilian Research Council – CNPq for their productivity grants.

8 References

Ague, J. 2023. **Jay Ague – Software and Pseudosections** – Yale University Website. Retrieved from https://people.earth.yale.edu/software-and-pseudosections/jay-ague

Alkmim, F. F., Marshak, S., Pedrosa-Soares, A. C., Peres, G. G., Cruz, S. C. P., Whittington, A. 2006. **Kinematic evolution of the Araçuaí-West Congo orogen in Brazil and Africa: nutcracker tectonics during the Neoproterozoic assembly of Gondwana**. Precambian Research, 149, 43-63.

Alkmim, F. F., Kuchenbecker, M., Reis, H. L. S., Pedrosa-Soares, A. C. 2017. **The Araçuaí Belt**. In: Heilbron, M., Cordani, H. G., and Alkmim, F. F. (eds.). **São Francisco Craton, Eastern Brazil – Tectonic Genealogy of a Miniature Continent**. Regional Geology Reviews. Springer. P. 255-276. https://doi.org/10.1007/978-3-319-01715-0_14

Amaral, L., Caxito, F. A., Pedrosa-Soares, A. C., Queiroga, G., Babinski, M., Trindade, R., Lana. C., Chemale, F. 2020. **The Ribeirão da Folha ophiolite-bearing accretionary wedge (Araçuaí orogen, SE Brazil): New data for Cryogenian plagiogranite and metasedimentary rocks.** Precambrian Research, 336, DOI: https://doi.org/10.1016/j.precamres.2019.105522.

Amaral, L. S. S., Vieira, P. L. N. C. R., Barroso, P. D., Carvalho, J. S., Figueiredo, V. D., Hoerlle, F. O., Laranjeira, J. O., Machado, R. D. M., Rosa, E. S., Novo, T. A. 2016. **Migmatitos da Serra do Caparaó: petrografia e metamorfismo**. 48º Congresso Brasileiro de Geologia, Annals, 785. Sociedade Brasileira de Geologia, SBG. ISBN: 978-85-99198-13-1.

Anovitz, L. M., Essene, E. J., Metz, G. W., Bohlen, S. R., Westrum, E. F. and Hemingway, B. M. 1993. **Heat capacity and phase equilibria in almandine, [$Fe_3Al_2Si_3O_{12}$].** Geochimica et Cosmochimica Acta, 57, 4191-4204.

Araujo, C., Pedrosa-Soares, A., Lana, C., Dussin, I., Queiroga, G., Serrano, P., Medeiros-Junior, E. 2020. **Zircon in emplacement borders of post-collisional plutons compared to country rocks: A study on morphology, internal texture, U-Th-Pb geochronology and Hf isotopes (Araçuaí orogen, SE Brazil).** Lithos, 352-353, 105252.

Ashwal, L. D, Tucker, R. D., Zinner, E. K. 1999. **Slow cooling of deep crustal granulites and Pb-loss in zircon**. Geochimica et Cosmochimica Acta 63: 2839-2851

Barbero, L. and Villaseca, C. 1992. **The Layos granite, Hercynian complex of Toledo (Spain): an example of parautochthonous restite-rich granite in a granulitic area.** Second Hutton Symposium: The Origin of Granites and Related Rocks, 83 (1-2), 127-138.

Barbosa, J. S. F., Leal, A. B. M., Fuck, R. A., Oliveira, J. S. S., Gonçalves, P., Leite, C. M. M. 2017. **Ultrahigh-temperature metamorphism of 2.0 Ga-Old sapphirine-bearing granulite from the Itabuna-Salvador-Curaçá Block, Bahia, Brazil**. Geologia USP, Série científica, 17(1), 89-108. DOI: 10.11606/issn.2316-9095.v17-287.

Belém, J. 2006. **Caracterização Mineralógica, Física e Termobarométrica de Minérios de Grafita da Província Grafítica Bahia-Minas**. (Unpublished master's thesis). Universidade Federal de Minas Gerais, Belo Horizonte, Brazil.

Bento dos Santos, T., Munhá, J., Tassinari, C., Fonseca, P., and Dias Neto, C. 2011. **Metamorphic P-T evolution of granulites in central Ribeira Fold Belt, SE Brazil**. Geosciences Journal, 15(1), 27-51.

Bento dos Santos, T.M., Tassinari, C.C.G., and Fonseca, P.E. 2015. **Diachronic collision,slab break-off and long-term high thermal flux in the Brasiliano-Pan-Africanorogeny: implications for the geodynamicevolution of the Mantiqueira Province**. Precambrian Research, 260, 1-22. DOI: http://dx.doi.org/10.1016/j.precamres.2014.12.018.

Bradley, D.C., Kusky, T.M., Haeussler, P., Rowley, D.C., Goldfarb, R., Nelson, S. 2003. **Geologic signature of early ridge subduction in the accretionary wedge, forearc basin, and magmatic arc of south-central Alaska**. In: Sisson, V.B., Roeske, S., and Pavlis, T.L. (Eds.). **Geology of a transpressional orogen developed during a ridge – trench interaction along the North Pacific Margin**. Geological Society of America Special Paper 371, p. 19–50.

Brown, M., 1998a. **Ridge-trench interactions and high-T e low-P metamorphism, with particular reference to the Cretaceous evolution of the Japanese Islands**. In: Treloar, P.J., O'Brien, P.J. (Eds.), **What Drives Metamorphism and Metamorphic Reactions?** Geological Society, London, Special Publication, 138, 131 – 163.

Campos Neto, M. C. and Caby, R. 2000. **Lower crust extrusion and terrane accretion in the Neoproterozoic nappes of southeast Brasil.** Tectonics, 19, 669-687.

Campos Neto, M. C. and Figueiredo, M. C. H. 1990. **Evolução geológica dos terrenos Costeiro, Paraíba do Sul e Juiz de Fora (RJ-MG-ES).** XXXVI Congresso Brasileiro de Geologia, Annals, 6, 2631-2648. Sociedade Brasileira de Geologia, SBG.

Cao, W., Paterson, S., Saleeby, J., Zalunardo, S. 2016. **Bulk arc strain, crustal thickening, magma emplacement, and mass balances in the Mesozoic Sierra Nevada arc**. Journal of Structural Geology, 84, 14–30.

Castro, M. P., Queiroga, G., Martins, M., Alkmim, F., Pedrosa-Soares, A., Dussin, I., Souza, M. E. 2019. **An Early Tonian rifting event affecting the São Francisco-Congo paleocontinent recorded by the Lower Macaúbas Group, Araçuaí Orogen, SE Brazil**. Precambrian Research, 331, 105351.

Castro, M. P., Queiroga, G., Martins, M., Pedrosa-Soares, A., Dias, L., Lana, C., Babinski, M., Alkmim, A. R., Silva, M. A. 2020. **Provenance shift through time in superposed basins: From Early Cryogenian glaciomarine to Late Ediacaran orogenic sedimentations (Araçuaí Orogen, SE Brazil).** Gondwana Research, 87, 41-66.

Chaves, A. O. and Neves, J. M. N. 2005. **Radiometric ages, aeromagnetic expression, and general geology of mafic dykes from southeastern Brazil and implications for African–South American correlations**. Journal of South American Earth Sciences, 19, 387-397.

Chemale, F., Dussin, I. A., Alkmim, F. F., Martins, M. S., Queiroga, G., Armstrong, R., Santos, M. N. 2012. **Unravelling a Proterozoic basin history through detrital zircon geochronology: The case of the Espinhaço Supergroup, Minas Gerais, Brazil.** Gondwana Research, 22, 200-206.

Chen, R. X., Zheng, Y. F 2017. **Metamorphic zirconology of continental subduction zone.** Journal of Asian Earth Sciences, 145, 149 – 176

Cherniak, D. J. and Watson, E. B. 2003. **Diffusion in Zircon**. Reviews in Mineralogy and Geochemistry, 53, 113-143. DOI: 10.2113/0530113.

Clark, C., Fitzsimons, L.C.W., Healy, D. and Harley, S.L., 2011**. How does the continental crust get really hot?** Elements, 7, 235–240.

Clark, S. P., Robertson, E. C., and Birch, F. 1957. **Experimental determination of kyanite-sillimanite equilibrium relations at high temperatures and pressures.** American Journal of Science, 255, 628-640.

Corfu, F., Hanchar, J. M., Hoskin, P. W. O., Kinny, P. 2003. **Atlas of zircon textures**. In: Hanchar, J. M., Hoskin, P. W. O. (Eds.). **Zircon.** Reviews in Mineralogy and Geochemistry, 53, 469 – 500

Corfu, F., Heaman, L. M., Rogers G. 1994. **Polymetamorphic evolution of the Lewisian complex, NW Scotland, as recorded by U- Pb isotopic compositions of zircon, titanite and rutile.** Contributions to Mineralogy and Petrology, 117, 215-228.

Costa, A. G., 1998**. The Granulite-Facies Rocks of the Northern Segment of the Ribeira Belt, Eastern Minas Gerais, SE Brazil**. Gondwana Research, 1(3-4), 367-372.

Cunningham, D., Alkmim, F. F., and Marshak, S. 1998. **A structural transect across the coastal mobile belt in the Brazilian Highlands (latitude 20 °S): the roots of a Precambrian transpressional orogen**. Precambrian Research 92, 251-275.

Cutts, K., Lana, C., Alkmim, F., Peres, G. G. 2018. **Metamorphic imprints on units of the southern Araçuaí belt, SE Brazil: The history of superimposed Transamazonian and Brasiliano orogenesis**. Gondwana Research 58, 211-234.

Da Silva, L. C., Armstrong, R., Noce, C. M., Carneiro, M. A., Pimentel, M., Pedrosa-Soares, A. C., Leite. C. A., Vieira, V. S., Silva, M. A., Paes, V. J. C., Cardoso Filho, J. M. 2002. **Reavaliação da evolução geológica em terrenos Pré-Cambrianos brasileiros com base em novos dados U-Pb SHRIMP, parte II: Orógeno Araçuaí, Cinturão Mineiro e Cráton São Francisco Meridional**. Revista Brasileira de Geociências, 32(4), 513-528.

Da Silva, L. C., Pedrosa-Soares, A. C., Armstrong, R., and Noce, C. M. 2011. **Determinando a duração do período colisional do Orógeno Araçuaí com base em geocronologia U-Pb de alta resolução em zircão: uma contribuição para a história da amalgamação do Gondwana Ocidental**. Geonomos, 19(2), 180-197.

Das, K., Dasgupta, S., and Miura, H. 2001. **Stability of osumilite coexisting with spinel solid solution in metapelitic granulites at high oxygen fugacity.** American Mineralogist, 86, 1423-1434.

De Campos, C.P., Mendes, J.C., Ludka, I.P., de Medeiros, S.R., de Moura, J.C., and Wallfass,C. 2004. **A review of the Brasiliano magmatism in southern Espírito Santo, Brazil,with emphasis on post-collisional magmatism.** In: Weinberg, R., Trouw, R., Fuck, R., and Hackspacher, P. (Eds). **The 750-550 Ma Brasiliano Event of South America.** Journal of the Virtual Explorer, Electronic Edition, 17(1). ISSN 1441-8142. DOI: http://dx.doi.org/10.3809/jvirtex.2004.00106.

De Campos, C. P., De Medeiros, S. R., Mendes, J. C., Pedrosa-Soares, A. C., Dussin, I., Ludka, I. P., Dantas, E.L., 2016. **Cambro-Ordovician magmatism in the Araçuaí Belt (SE Brazil): snapshot from a post-collisional event**. Journal of South American Earth Sciences, 68, 248–268.

De Capitani, C. and Brown, T. H. 1987. **The computation of chemical equilibrium in complex systems containing non-ideal solutions**. Geochimica et Cosmochimica Acta, 51, 2639–2652.

De Capitani, C. and Petrakakis, K. 2010. **The computation of equilibrium assemblage diagrams with Theriak/Domino software**. American Mineralogist, 95, 1006-1016. DOI: http://dx.doi.org/10.2138/am.2010.3354.

Deer, W. A., Howie, R. A. and Zussman, J. 1992. **An introduction to the rock-forming minerals.** 2nd edition. Burnt Mill, Harlow: Longman Scientific and Technical.

Degler, R., Costa, A. G., Pedrosa-Soares, A. C., Queiroga, G. N. 2019. **High pressure metamorphism related to suture zone in the Araçuaí orogen (SE Brazil): further evidence against ensialic models**. XVII Simpósio Nacional de Estudos Tectônicos (SNET), Annals, p. 124. Sociedade Brasileira de Geologia, SBG.

Degler, R., Pedrosa-Soares, A. C., Dussin, I., Queiroga, G., and Schulz, B. 2017. **Contrasting provenance and timing of metamorphism from paragneisses of the Araçuaí-Ribeira orogenic system, Brazil: Hints for Western Gondwana assembly.** Gondwana Research, 51, 30-50.

Degler, R., Pedrosa-Soares, A. C., Novo, T. A., Tedeschi, M., Da Silva, L. C., Dussin, I. A., Lana, C. 2018. **Rhyacian-Orosirian isotopic records from the basement of the Araçuaí-Ribeira orogenic system (SE Brazil): Links in the Congo-São Francisco palaeocontinent.** Precambrian Research, 317, 179-195.

Del Lama, E. A., Zanardo, A., Oliveira, M. A. F., and Morales, N. 2000. **Exhumation of high-pressure granulites from the Guaxupé complex, southeastern Brazil.** Geological Journal, 35, 231-249.

Deluca, C., Pedrosa-Soares, A., Lima, S., Cordani, U., Sato, K. 2019. **Provenance of the Ediacaran Salinas Formation (Araçuaí Orogen, Brazil): Clues from lithochemical data and zircon U-Pb (SHRIMP) ages of volcanic clasts**. Brazilian Journal of Geology, 49, 1-19.

Dias, T. G., Caxito, F. A., Pedrosa-Soares, A. C., Stevenson, R., Dussin, I., Da Silva, L. C., Alkmim, F., Pimentel, M. 2016. **Age, provenance and tectonic setting of the high-grade Jequitinhonha Complex, Araçuaí orogen, eastern Brazil**. Brazilian Journal of Geology, 46(2), 199-219. DOI: 10.1590/2317-4889201620160012.

Dolivo-Dobrovolsky, D. V. 2012. **TriQuick software, version 1.0.0.23.** Retrieved from http://www.dimadd.ru/en/Programs/triquick

Droop, G. T. R. 1987. **A general equation for estimating Fe^{3+} concentrations in ferromagnesian silicates and oxides from microprobe analyses, using stoichiometric criteria**. Mineralogical Magazine, 51, 431-435.

Ducea, M. N. 2001. **The California arc: thick granitic batholiths, eclogitic residues, lithospheric-scale thrusting, and magmatic flare-ups**. GSA Today, 11, 4–10.

Dussin, I.A., Dussin, T.M., 1995. **Supergrupo Espinhaço: Modelo de Evolução Geodinâmica**. Geonomos 1, 19–26.

Faria, T. G., Alves, M. I., Potratz, G. L., Silva, L. F. R., Rodrigues, S. W. O., Martins, M. V. A., Geraldes, M. C. 2022. **The Serra do Caparaó Complex, Mantiqueira Province, Brazil, revisited: metamorphic age constraints by U-Pb and Lu-Hf method in zircon by LA-ICP-MS.** Journal of the Geological Survey of Brazil, 5(1), 49-80.

Ferracuti, G. R., Gargiulo, M. F., Ganuza, M. L., Bjerg, E. A., and Castro, S. M. 2015. **Determination of the spinel group end-members based on electron microprobe analyses**. Mineralogy and Petrology, 109, 153-160. DOI: 10.1007/s00710-014-0363-1.

Fitzimons, I. C. W. and Harley, S. L. 1994. **The influence of retrograde cation exchange on granulite P-T estimates and a convergence technique for the recovery of peak metamorphic conditions**. Journal of Petrology, 35(2), 543-576

Frei, D. and Gerdes, A. 2009. **Precise and accurate in situ U-Pb dating of zircon with high sample throughput by automated LA-SF-ICP-MS**. Chemical Geology 261, 3-4, 261-270. Doi: 10.1016/j.chemgeo.2008.07.025.

Frost, B. R. and Chacko, T. 1989. **The granulite uncertainty principle: limitations on thermobarometry in granulites.** Journal of Geology, 97, 435-450.

Ganade, C. E., Lanari, P., Rubatto, D., Hermann, J., Weinberg, R. F., Basei, M. A. S., Tesser, L. R., Caby, R., Agbossoumondé, Y., Ribeiro, C. M. 2021. **Magmatic fl are-up causes crustal thickening at the transition from subduction to continental collision**. Comunications Earth and Environment, 2, 41.

Gerdes, A. and Zeh, A. 2009. **Zircon formation versus zircon alteration – New insights from combined U-Pb and Lu-Hf in-situ La-ICP-MS analyses of Archean zircons from the Limpopo Belt**. Chemical Geology, 261(3-4), 230-243.

Gonçalves, L., Alkmim, F. F., Pedrosa-Soares, A. C., Dussin, I. A., Valeriano, C. M., Lana, C., Tedeschi, M. 2016. **Granites of the intracontinental termination of a magmatic arc: an example from the Ediacaran Araçuaí orogen, southeastern Brazil.** Gondwana Research, 36, 439-458.

Gonçalves, L., Alkmim, F. F., Pedrosa-Soares, A. C., Gonçalves, C. C., Vieira, V. 2018. **From the plutonic root to the volcanic roof of a continental magmatic arc: a review of the Neoproterozoic Araçuaí orogen, southeastern Brazil**. International Journal of Earth Science (Geologische Rundschau), 107, 337-358.

Gonçalves, G., Lana, C., Buick, I., Alkmim, F., Scholz, R., Queiroga, G. 2019. **Twenty million years of post-orogenic fluid production and hydrothermal mineralization across the external Araçuaí orogen and adjacent São Francisco craton, SE Brazil.** Lithos, 342-343, 557-572.

Gradim, C. 2013. **Complexo Nova Venécia e magmatismo associado, Orógeno Araçuaí, Estado do Espírito Santo** (Unpublished master's thesis). Universidade Federal de Minas Gerais, Belo Horizonte, Brazil.

Gradim, C., Roncato, J., Pedrosa-Soares, A.C., Cordani, U., Dussin, I., Alkmim, F.F., Queiroga, G., Jacobsohn, T., Silva, L. C., Babinski, M. 2014. **The hot back-arc zone of the Araçuaí orogen, Eastern Brazil: from sedimentation to granite generation.** Brazilian Journal of Geology, 44, 155-180. DOI: http://dx.doi.org/10.5327/Z2317-4889201400010012.

Green, E. C. R., White, R. W., Diener, J. F. A., Powell, R., Holland, T. J. B., Palin, R. M. 2016. **Activity-composition relations for the calculation of partial melting equilibria in metabasic rocks**. Journal of Metamorphic Geology, 34, 845-869.

Grew, E. S., Halenius, U., Pasero, M. and Barbier, J. 2008. **Recommended nomenclature for the sapphirine and surinamite groups (sapphirine supergroup).** Mineralogical Magazine, 72(4), 839-876.

Guiraud, M., Kienast, J. R., and Ouzegane, K. 1996. **Corundum-quartz-bearing assemblages in the Ihouhaouene area (In Ouzzal, Algeria).** Journal of Metamorphic Geology, 14, 755-762.

Harley, S. L. 1984a. **An experimental study of the partitioning of Fe and Mg between garnet and orthopyroxene.** Contributions to Mineralogy and Petrology, 86, 359-373.

Harley, S. L. 1984b. **The solubility of Alumina in orthopyroxene coexisting with garnet in FeO-MgO-Al_2O_3-SiO_2 and CaO-FeO-MgO-Al_2O_3-SiO_2.** Journal of Petrology, 25, 665-696.

Harley, S. L. 1984c. **Comparison of the garnet-orthopyroxene geobarometer with recent experimental studies, and applications to natural assemblages.** Journal of Petrology, 25, 697-712.

Harley, S. L. 1989. **The origins of granulites: a metamorphic perspective**. Geological Magazine, 126, 215-247.

Harley, S. L. 1998a. **On the occurrence and characterization of ultrahigh-temperature crustal metamorphism**. In: Treloar, P. J. & O'Brien, P. J. (eds) **What drives metamorphism and metamorphic reactions?** Geological Society, London, Special Publications, 138, 81-107.

Harley, S. L. 2016. **A matter of time: the importance of the duration of UHT metamorphism.** Journal of Mineralogical and Petrological Sciences, 111, 50-72.

Harley, S.L. and Green, D.H. 1982. **Garnet-Orthopyroxene barometry for granulites and garnet peridotites**. Nature, 200, 697-700.

Harley, S. L., Kelly, N. M. and Moller, A. 2007**. Zircon Behaviour and the Thermal Histories of Mountain Chains**. Elements, 3, 25-30.

Harlov, D. E. and Milke, R. 2002. **Stability of corundum+quartz relative to kyanite and sillimanite at high temperature and pressure**. American Mineralogist, 87, 424-432.

Harlov, D.E. and Newton, R.C. 1993. **Reversal of the metastable kyanite + corundum + quartz and andalusite + corundum + quartz equilibria and the enthalpy of the formation of kyanite and andalusite.** American Mineralogist, 78, 594–600.

Heilbron, M., Duarte, B. P., Valeriano, C. M., Simonetti, A., Machado, N., and Nogueira, J. R. 2010. **Evolution of reworked Paleoproterozoic basement rocks within the Ribeira belt (Neoproterozoic), SE-Brazil, based on U–Pb geochronology: Implications for paleogeographic reconstructions of the São Francisco-Congo paleocontinent.** Precambrian Research, 178, 136-148.

Higgins, J. B., Ribbe, P. H., and Herd R. K. 1979. **Sapphirine I: Crystal chemical contributions**. Contributions to Mineralogy and Petrology, 68, 349-356.

Holland. T. J. B. and Powell, R. 2003. **Activity-composition relations for phases in petrological calculations: an asymmetric multicomponent formulation**. Contributions to Mineralogy and Petrology, 145, 492-501.

Hoskin, P. W. O and Black, L. P. 2000. **Metamorphic zircon formation by solid state recrystallization of protolith igneous zircon**. Journal of Metamorphic Geology, 18, 423-439

Jackson, S. E., Pearson, N. J., Griffin, W. L., and Belousova, E. A. 2004. **The application of laser ablation-inductively coupled plasma-mass spectrometry to in situ U-Pb zircon geochronology**. Chemical Geology, 211, 47-69.

Laurent, A., Bingen, B., Duchene, S., Whitehouse, M. J., Seydoux-Guillaume, A. M., Bosse, V. 2018. **Decoding a protracted zircon geochronological record in ultrahigh temperature granulite, and persistence of partial melting in the crust, Rogaland, Norway**. Contributions to Mineralogy and Petrology, 173, 29. https://doi.org/10.1007/s00410-018-1455-4

Luft, J. L., Chemale, F., and Armstrong, R. 2011. **Evidence of 1.7- to 1.8-Ga collisional arc in the Kaoko Belt, NW Namibia**. International Journal of Earth Sciences 100, 305–321.

Kelly, N. M. and Harley, S. L. 2005. **An integrated microtextural and chemical approach to zircon geochronology: refining the Archaean history of the Napier Complex, east Antarctica.** Contributions to Mineralogy and Petrology, 149, 57-84

Kelsey, D. E. 2008. **On ultrahigh-temperature crustal metamorphism**. Gondwana Research, 13, 1-29.

Kelsey, D. E. and Hand, M. 2015. **On ultrahigh temperature crustal metamorphism: Phase equilibria, trace element thermometry, bulk composition, heat sources, timescales and tectonic settings**. Geoscience Frontiers, 6, 311-356.

Konopásek, J., Kosler, J., Sláma, J., Janousek, V. 2014. **Timing and sources of pre-collisional Neoproterozoic sedimentation along the SW margin of the Congo Craton (Kaoko Belt, NW Namibia).** Gondwana Research, 26, 386-401.

Korhonen, F. J., Clark, C., Brown, M., Bhattacharya, S., Taylor, R. 2013. **How long-lived is ultrahigh temperature (UHT) metamorphism? Constraints from zircon and monazite geochronology in the Eastern Ghats orogenic belt, India**. Precambrian Research, 234, 322-350. DOI: http://dx.doi.org/10.1016/j.precamres.2012.12.001.

Kuchenbecker M., Pedrosa-Soares A.C., Babinski M., Fanning M. 2015. **Detrital zircon age patterns and provenance assessment for pre-glacial to post-glacial successions of the Neoproterozoic Macaúbas Group, Araçuaí Orogen, Brazil**. Precambrian Research, 266, 12-26.

Kunz, B. E., Regis, D., Engi, M., 2018. **Zircon ages in granulite facies rocks: decoupling from geochemistry above 850 °C?** Contributions to Mineralogy and Petrology 173, 26. Doi: 10.1007/s00410-018-1454-5.

Lana, C., Farina, F., Gerdes, A., Alkmim, A., Gonçalves, G. O., Jardim, A. C. **2017. Characterization of zircon reference materials via high precision U–Pb LA-MC-**

ICP-MS. Journal of Analytical Atomic Spectrometry 32, 2011-2032. Doi: https://doi.org/10.1039/C7JA00167C .

Ludwig, K. 2003. **Isoplot/Ex, version 3: A geochronological toolkit for Microsoft Excel**. Berkeley, California: Geochronology Center.

Ludwig, K. 2008. **Isoplot, version 4.15**. Retrieved from: http://www.bgc.org/isoplot_etc/isoplot.html.

Luft Jr., J. L., Chemale Jr., F., Armstrong, R. 2011. **Evidence of 1.7- to 1.8-Ga collisional arc I Kaoko Belt, NW Namibia.** International Journal of Earth Sciences, 100, 305–321.

Machado, N., Schrank, A., Abreu, F.R., Knauer, L.G., Almeida-Abreu, P.A. 1989. **Resultados preliminares da geocronologia U–Pb na Serra do Espinhaço Meridional.** Boletim do Núcleo Minas Gerais. Sociedade Brasileira de Geologia 10, 171–174.

Melo, M. G., Lana, C., Stevens, G., Pedrosa-Soares, A. C., Gerdes, A., Alkmin, L. A., Nalini Jr. H. A., Alkmim, F. F. 2017. **Assessing the isotopic evolution of S-type granites of the Carlos Chagas batholith, SE Brazil: clues from U-Pb, Hf isotopes, Ti geothermometry and trace element composition of zircon.** Lithos, 284-285, 730-750.

Moraes, R., Nicollet, C., Barbosa, J. S. F., Fuck, R. A., and Sampaio, A. R. 2015. **Applications and limitations of thermobarometry in migmatites and granulites using as an example rocks of the Araçuaí orogen in southern Bahia, including a discussion on the tectonic meaning of the current results**. Brazilian Journal of Geology, 45(4)**,** 517-539. DOI: 10.1590/2317-4889201520150026.

Moreira, L. M. 1997. **Evolução crustal do Leste de Minas Gerais: uma contribuição a partir do estudo geotermobarométrico de metamorfitos da região Simonésia-Manhuaçu (MG).** (Unpublished doctoral thesis). Universidade Federal de Minas Gerais, Belo Horizonte, Brazil.

Morel M.L.A., Nebel O., Nebel-Jacobsen Y.J., Miller J.S., and Vroon P.Z. 2008. **Hafnium isotope characterization of the GJ-1 zircon reference material by solution and laser-ablation MC-ICP-MS.** Chemical Geology, 255, 231-235.

Motoyoshi, Y., Hensen, B.J., and Matsueda, H. 1990. **Metastable growth of corundum adjacent to quartz in a spinel-bearing quartzite from the Archaean Napier Complex, Antarctica.** Journal of Metamorphic Geology, 8, 125–130.

Motta, R. G., Fitzsimons, I. C. W., Moraes, R., Johnson, T. E., Schuindt, S., Benetti, B. Y. 2021. **Recovering P-T-t paths from ultra-high temperature (UHT) felsic orthogneiss: An example from the Southern Brasília Orogen, Brazil**. Precambrian Research, 359, p. 106222.

Mouri, H., Guiraud, M. and Osanai, Y. 2004. **Review on "corundum+quartz" assemblage in nature: possible indicator of ultra-high temperature conditions?** Journal of Mineralogical and Petrological Sciences, 99, 159-163.

Noce, C. M., Costa, A. G., Piuzana, D., Vieira, V., Carvalho, C. M. 2006. **Folha Manhuaçu SF-23-X-B-III (1:100.000).** Programa Geologia do Brasil. Levantamentos Geológicos Básicos. CPRM.

Noce, C.M., Pedrosa-Soares, A.C., Silva, C.C., Armstrong, R., and Piuzana, D., 2007. **Evolution of polycyclic basement complexes in the Araçuaí orogen, based on U–Pb SHRIMP data: implications for Brazil–Africa links in Paleoproterozoic time.** Precambrian Research, 159 (2), 60–78.

Novo, T. A. 2013. **Caracterização do Complexo Pocrane, magmatismo básico mesoproterozóico e unidades neoproterozóicas do sistema Araçuaí-Ribeira, com ênfase em geocronologia U-Pb (SHRIMP e LA-ICP-MS).** (Unpublished doctoral thesis). Universidade Federal de Minas Gerais, Belo Horizonte, Brazil.

Novo, T. A., Noce, C. M., Pedrosa-Soares, A. C., Batista, G. A. P. 2011. **Rochas granulíticas da Suíte Caparaó na região do Pico da Bandeira: embasamento oriental do Orógeno Araçuaí.** Geonomos, 19(2), 70-77.

Novo, T. A., Noce, C. M., Figueiredo, C. M., Pedrosa-Soares, A. 2012. **Folha Carangola SF.23-X-B-VI (1:100.000).** Programa Geologia do Brasil. Levantamentos Geológicos Básicos. CPRM.

Novo, T. A., Noce, C. M., Batista, G. A., Quéméneur, J. J., Martins, B. S., Santos, S. W., Carneiro, G. A., Horn, A. H. 2014. **Folha Manhumirim SF.24-V-A-I (1:100.000).** Programa Geologia do Brasil. Levantamentos Geológicos Básicos. CPRM.

Novo, T. A., Pedrosa-Soares, A. C., Noce, C. M., Alkmim, F. F., and Dussin, I. A. 2010. **Rochas charnockíticas do sudeste de Minas Gerais: a raiz granulítica do arco magmático do Orógeno Araçuaí.** Revista Brasileira de Geociências, 40(4), 573-592.

Novo, T. A., Pedrosa-Soares, A. C., Vieira, V. S., Dussin, I., Da Silva, L. C. 2018. **The Rio Doce Group revisited: An Ediacaran arc-related volcanosedimentary basin, Araçuaí orogen (SE Brazil).** Journal of South American Earth Sciences, 85, 345-361.

Pattison, D. M., Chacko, T., Farquhar, J., McFarlane, C. R. M. 2003. **Temperatures of granulite-facies metamorphism: constraints from experimental phase equilibria and thermobarometry corrected for retrograde exchange.** Journal of Petrology, 44(5), 867-900. https://rclc.facsci.ualberta.ca/

Pattison, D. M. and Begin, N. J. 1994. **Hierarchy of closure temperatures in granulites and the importance of an intergranular exchange medium (melt?) in controlling maximum Fe-Mg exchange temperatures**. Mineralogical Magazine, 58ª, 694-695.

Pedrosa-Soares, A.C., Vidal, P., Leonardos, O.H., Brito-Neves, B.B., 1998. **Neoproterozoic oceanic remnants in eastern Brazil: Further evidence and refutation of an exclusively ensialic evolution for the Araçuaí-West Congo Orogen.** Geology, 26, 519–522.

Pedrosa-Soares, A. C., Noce, C. M., Wiedemann, C. M., Pinto, C. P. 2001**. The Araçuaí-West-Congo Orogen in Brazil: an overview of a confined orogen formed during Gondwanaland assembly**. Precambrian Research, 110, 307-323.

Pedrosa-Soares, A. C., Alkmim, F. F., Tack, L., Noce, C. M., Babinski, M. Da Silva, L. C., Martins-Neto, M. A. 2008. **Similarities and differences between the Brazilian and African counterparts of the Neoproterozoic Araçuaí-West-Congo orogen**. Geological Society, London, Special Publications, 294, 153-172.

Pedrosa-Soares, A. C., Campos, C. P., Noce, C., Da Silva, L. C., Novo, T. A., Roncato, J., Medeiros, S., Castañeda, C., Queiroga, G., Dantas, E., Dussin, I., Alkmim, F. F. 2011. **Late Neoproterozoic–Cambrian granitic magmatism in the Araçuaí orogen (Brazil), the Eastern Brazilian Pegmatite Province and related mineral resources.** Geological Society, London, Special Publications, 350, 25-51.

Pedrosa-Soares, A., Deluca, C., Araujo, C. S., Gradim, C., Lana, C. C., Dussin, I., Da Silva, L. C., Babinski, M. 2020. **O Orógeno Araçuaí à luz da Geocronologia: um tributo a Umberto Cordani.** In: Bartorelli, A., Teixeira, W. and Brito-Neves, B. B. (Eds.). **Geocronologia e evolução tectônica do Continente Sul-Americano: a contribuição de Umberto Cordani.** Sâo Paulo, SP, Brazil: Solaris Edições Culturais. p. 252-271.

Peixoto, E., Pedrosa-Soares, A. C., Alkmim, F. F., Dussin, I. A. 2015. **A suture–related accretionary wedge formed in the Neoproterozoic Araçuaí orogen (SE Brazil) during Western Gondwanaland assembly.** Gondwana Research, 27(2), 878-896.

Peixoto, C. A., Heilbron, M., Ragatky, D., Armstrong, R., Dantas, E., Valeriano, C.M., Simonetti, A., 2017. **Tectonic evolution of the juvenile tonian serra da prata magmatic arc in the ribeira belt, se Brazil: implications for early west gondwana amalgamation.** Precambrian Research, 302, 221 – 254.

Pell, S. D., Williams, I. S. and Chivas, A. R. 1997. **The use of protolith zircon-age fingerprints in determining the protosource areas for some Australian dune sands.** Sedimentary Geology, 109, 233 – 260

Peres, G.G., Alkmim, F.F., Jordt-Evangelista, H., 2004. **The southern Araçuaí belt and the Dom Silvério Group: geologic architecture and tectonic significance**. Annals of the Brazillian Academy of Sciences, 76, 771–790.

Perkins, D. 2007. **Olivine, Pyroxene, Garnet, Spinel and Feldspar Spreadsheets.** Retrieved from: https://serc.carleton.edu/research_education/equilibria/mineralformulaerecalculation.html.

Powell, R. and Holland, T. J. B. 2008. **On Thermobarometry**. Journal of Metamorphic Geology, 26, 155-179.

Powers, R. E. and Bohlen, S. R. 1985. **The role of synmetamorphic igneous rocks in the metamorphism and partial melting of metasediments, Northwest Adirondacks**. Contributions to Mineralogy and Petrology, 90, 401–409.

Queiroga, G. N., 2010. **Caracterização de restos de litosfera oceânica do Orógeno Araçuaí entre os paralelos 17° e 21° S**. (Unpublished doctoral thesis). Universidade Federal de Minas Gerais, Belo Horizonte, Brazil.

Queiroga, G. N., Pedrosa-Soares, A. C., Noce, C. M., Alkmim, F. F., Pimentel, M. M., Dantas, E., Martins, M., Castañeda, C., Suita, M. T. F., Prichard, F. 2007. **Age of the Ribeirão da Folha ophiolite, Araçuaí Orogen: the U–Pb zircon dating of a plagiogranite**. Geonomos, 15, 61–65.

Richter, F., Lana, C., Stevens, G., Buick, I., Pedrosa-Soares, A. C., Alkmim, F. F., Cutts, K. 2016. **Sedimentation, metamorphism and granite generation in a back-arc region: Records from the Ediacaran Nova Venécia Complex (Araçuaí orogen, Southeastern Brazil).** Precambrian Research, 272, 78-100.

Rocha, B. C., Moraes, R., Möller, A., Cioffi, C. R. 2018. **Magmatic inheritance vs. UHT metamorphism: Zircon petrochronology of granulites and petrogenesis of charnockitic leucosomes of the Socorro–Guaxupé nappe, SE Brazil**. Lithos, 314-315, 16-39.

Rocha, B. C., Moraes, R., Möller, A., Cioffi, C. R., Jercinovic, M. J. 2017. **Timing of anatexis and melt crystallization in the Socorro–Guaxupé Nappe, SE Brazil: Insights from trace element composition of zircon, monazite and garnet coupled to U-Pb geochronology.** Lithos, 277, 337-355.

Rosa, M. L. S., Conceição, H., Macambira, M., Galarza, M. C., Cunha, M., Menezes, R., Marinho, M. M., Filho, B. E. C., Rios, D. C. 2007. **Neoproterozoic anorogenic magmatism in the Southern Bahia Alkaline Province of NE Brazil: U-Pb and Pb-Pb ages of the blue sodalite syenites**. Lithos, 97, 88-97.

Rubatto, D. 2002. **Zircon trace element geochemistry: partitioning with garnet and the link between U-Pb ages and metamorphism.** Chemical Geology, 184, 123-138.

Rubatto, D. 2017. **Zircon: the metamorphic mineral**. Reviews in Mineralogy and Geochemistry, 83, 261-295.

Rubatto, D. and Gebauer, D., 2000. **Use of Cathodoluminescence for U–Pb Zircon Dating by Ion Microprobe: Some Examples From the Western Alps**. Cathodoluminescence in Geosciences. Springer, pp. 373–400.

Santiago, R., Caxito, F. A., Pedrosa-Soares, A., Neves, M. A., Dantas, E. L. 2020. **Tonian island arc remnants in the northern Ribeira orogen of Western Gondwana: The Caxixe batholith (Espírito Santo, SE Brazil).** Precambrian Research, 351, 105944

Santiago, R., Caxito, F. A., Pedrosa-Soares, A., Neves, M. A., Calegari, S. S., Lana, C. 2022. **Detrital zircon U – Pb and Lu – Hf constraints on the age, provenance and tectonic setting of arc-related high-grade units of the transition zone of the Araçuaí and Ribeira orogens (SE Brazil).** Journal of South American Earth Sciences, 116, 103861

Santos, M. M., Lana, C., Scholz, R., Buick, I., Schmitz, M. D., Kamo, S. L., Gerdes, A., Corfu, F., Tapster, S., Lancaster, P., Storey, C. D., Basei, M. A. S., Tohver, E., Alkmim, A., Nalini, H., Krambrock, K., Fantini, C., Wiedenbeck, M. 2017. **A new appraisal of Sri Lankan BB Zircon as a reference material for LA-ICP-MS U-Pb geochronology and Lu-Hf isotope tracing.** Geostandards and Geoanalytical Research, 41(3), 335-358.

Santosh, M., Liu, S.J., Tsunogae, T., Li, J.H., 2012. **Paleoproterozoic ultrahigh-temperature granulites in the North China Craton: implications for tectonic models on extreme crustal metamorphism.** Precambrian Research, 222-223, 77-106.

Santosh, M. and Kusky, T. 2010. **Origin of paired high pressure–ultrahigh-temperature orogens: a ridge subduction and slab window model**. Terra Nova, 22, 35-42.

Santosh, M., Kusky, T., and Wang, L. 2011. **Supercontinent cycles, extreme metamorphic processes, and changing fluid regimes**. International Geology Review, 53(11-12), 1403-1423.

Sawyer, E. W. 2008. **Atlas of Migmatites**. Ottawa, Ontario, Canada: NRC Research Press.

Schaltegger, U., Fanning, C. M., Günther, D., Maurin, J. C., Schulmann, K., Gebauer, D. 1999. **Growth, annealing and recrystallization of zircon and preservation of monazite in high-grade metamorphism: conventional and in-situ U-Pb isotope, cathodoluminescence and microchemical evidence**. Contributions to Mineralogy and Petrology, 134, 186-201

Schannor, M., Lana, C. and Fonseca, M. 2019. **São Francisco-Congo Craton break-up delimited by U-Pb-Hf isotopes and trace-elements of zircon from metasediments of the Araçuaí Belt.** Geoscience Frontiers, 10, 611-628.

Schneider,S., Hammerschmidt, K., Rosenberg, C. L., Gerdes, A., Frei, D., Bertrand, A. 2015. **U-Pb ages of apatite in the western Tauern Window (Eastern Alps): Tracing the onset of collision-related exhumation in the European plate.** Earth and Planetary Science Letters, 418, 53-65. Doi: 10.1016/j.epsl.2015.02.020

Serrano, P., Pedrosa-Soares, A., Medeiros-Junior, E., Fonte-Boa, T., Araujo, C., Dussin, I., Queiroga, G., Lana, C., 2018. **A-type Medina batholith and post-collisional anatexis in the Araçuaí orogen (SE Brazil).** Lithos, 320-321, 515-536.

Shaw, R. K. and Arima, M. **A corundum-quartz assemblage from the Eastern Ghats Granulite Belt, India: evidence for high P-T metamorphism?** Journal of Metamorphic Geology, 16, 189-196.

Sláma, J., Kosler, J., Condon, D.J., Crowley, J.L., Gerdes, A., Hanchar, J.M., Horstwood, M. S. A., Morris, G. A., Nasdala, L., Norberg, N., Schaltegger, U., Schoene, B., Tubrett, M. N., Whitehouse, M.J. 2008. **Plesovice zircon—a new natural reference material for U-Pb and Hf isotopic micro-analysis**. Chemical Geology, 249, 1-35;

Söllner, F., Weber-Diefenbach, K., and Lammerer, B. 1991. **Die Krustenentwicklung in der Küstenregion nördlich von Rio de Janeiro: altersbestimmungen (U-Pb an Zirkonen und Rb-Sr an Gesteinen) an hochdruck- und -temperaturfaziellen Gesteinen des Ribeira Mobile Belt und des Sao Francisco Kratons (Espirito Santo/Minas Gerais).** Müncher Geologische Hefte, 4, 100.

Stacey, J. S. S. and Kramers, J. D. D. 1975. **Approximation of terrestrial lead isotope evolution by a two-stage model**. Earth and Planetary Science Letters 26, 207-221. Doi: 10.1016/0012-821X(75)90088-6

Tack, L., Wingate, M. T. D., Liégeois, J. P., Fernandez-Alonso, M., Deblond, A. 2001. **Early Neoproterozoic magmatism (1000–910 Ma) of the Zadinian and Mayumbian Groups (Bas-Congo): onset of Rodinia rifting at the western edge of the Congo craton**. Precambrian Research, 110, 277-306.

Taylor, J., Zeh, A., and Gerdes, A. 2016. **U-Pb-Hf isotope systematics of detrital zircons in high-grade paragneisses of the Ancient Gneiss Complez, Swaziland: Evidence for two periods of juvenile crust formation, Paleo- and Mesoarchean sediment deposition, and 3.23 terrane accretion**. Precambrian Research, 280, 205-220.

Taylor-Jones, K. and Powell, R. 2010. **The stability of sapphirine+quartz: calculated phase equilibria in FeO–MgO–Al2O3–SiO2–TiO2–O.** Journal of Metamorphic Geology, 28, 615-633.

Tedeschi, M., Novo, T., Pedrosa-Soares, A.C., Dussin, I., Tassinari, T., Silva, L.C., Gonçalves, L., Alkmim, F.F., Lana, C., Figueiredo, C., Dantas, E., Medeiros, S., De Campos, C., Corrales, F., Heilbron, M., 2016. **The Ediacaran Rio Doce magmatic arc revisited (Araçuaí- Ribeira orogenic system, SE Brazil).** Jounal of South American Earth Sciences, 68, 167–186.

Tedeschi, M., Pedrosa-Soares, A.; Dussin, I., Lanari, P., Novo, T., Pinheiro, M. A. P., Lana, C., Peters, D. 2018. **Protracted zircon geochronological record of UHT garnet-free granulites in the Southern Brasília orogen (SE Brazil): Petrochronological constraints on magmatism and metamorphism**. Precambrian Research, 316, 103 – 126

Tedeschi, M., Rossi Vieira, P. L., Kuchenbecker, M., Ribeiro, B. V., Barrote, V., Reis, H., Stutenbecker, L., Lana, C., Pedrosa-Soares, A., Dussin, I. 2023. **Unravelling and overcoming potential biases in U-Pb detrital zircon records induced by high to ultra-high temperature metamorphism (> 850 ºC)**. Geoscience Frontiers, 14, 101515. https://doi.org/10.1016/j.gsf.2022.101515.

Tindle, A. G. and Webb, P. C. 1990. **Estimation of lithium contents in trioctahedral micas using microprobe data: application to micas from granitic rocks**. European Journal of Mineralogy, 2, 595-610.

Tupinambá, M., Heilbron, M., Valeriano, C.M., Porto Jr., R., Blanco de Dios, F., Machado, N., Silva, L. G. E., Almeida, J.C.H., 2012. **Juvenile contribution of the**

Neoproterozoic Rio Negro magmatic arc (Ribeira Belt, Brazil): implications for western Gondwana amalgamation. Gondwana Research, 21, 422–438;

Van Achterbergh, E., Ryan, C. G., Jackson, S. E., Griffin, W. L. 2001. **Data reduction software for LA-ICP-MS: Supplementary file**. In: Sylvester, P. J. (ed.) 2001. **Laser Ablation – ICP-Mass Spectrometry in the Earth Sciences: Principles and Applications.** Mineralogical Association of Canada Short Course Series, 29, 239-243.

Vervoort, J. D. and Kemp, A. I. S. 2016. **Clarifying the zircon Hf isotope record of crust–mantle evolution**. Geochemical Geology, 425, 65-75.

Vieira, P. L. N. C. R., Vieira, A. C. B., Novo, T. A. 2017. **Condições P-T de formação dos migmatitos da Serra do Caparaó, MG.** Oral presentation/Annals from the 15º Simpósio de Geologia do Sudeste – GEOSUDESTE. Retrieved from: http://geosudeste.com.br/pdf_anais/tema2_OA18.pdf.

Vieira, P. L. N. C. R., Queiroga, G. N., Novo, T. A., Pedrosa-Soares, A. C., Lana, C. 2019. **Ultrahigh temperature (UHT) metamorphic rocks from the Araçuaí Orogen, Southeastern Brazil: tectonic implication from petrography, thermobarometry and phase-equilibria modeling.** Oral presentation/Annals from the XVII Simpósio de Estudos Tectônicos/XI International Symposium on Tectonics and XI Simpósio Sul-Brasileiro de Geologia.p. 133.

Villaseca, C. and Barbero, L. 1994. **Chemical variability of Al-Ti-Fe-Mg minerals in peraluminous granitoid rocks from Central Spain.** European Journal of Mineralogy, 6, 670-691.

Wang, W., Liu, S., Cawood, P. A., Guo, R., Bai, X., and Guo, B. 2017. **Late Neoarchean crust-mantle geodynamics: Evidence from Pingquan Complex of the Northern Hebei Province, North China Craton**. Precambrian Research, 303, 470-493.

Waters, D. J. 1991. **Hercynite quartz granulites phase relations, and implications for crustal processes**. European Journal of Mineralogy, 3, 367-386.

Wheller, C. J. and Powell, R. 2014. **A new thermodynamic model for sapphirine: calculated phase equilibria in K_2O-FeO-MgO-Al_2O_3-SiO_2-H_2O-TiO_2-Fe_2O_3**. Journal of Metamorphic Geology, 32, 287-299.

White, R. W. and Powell, R. 2002. **Melt loss and the preservation of granulite facies mineral assemblages.** Journal of Metamorphic Geology, 20(7), 621-632.

White, R., Powell, R., and Clarke, G. 2002. **The interpretation of reaction textures in Fe-rich metapelitic granulites of the Musgrave Block, central Australia: constraints from mineral equilibria calculations in the system K_2O–FeO–MgO–Al_2O_3–SiO_2–H_2O–TiO_2–Fe_2O_3**. Journal of Metamorphic Geology, 20, 41-55.

White, R. W., Powellm R., and Holland, T. J. B. 2007. **Progress relating to calculation of partial melting equilibria for metapelites**. Journal of Metamorphic Geology, 25, 511-527.

White, R. W., Powell, R., Holland, T. J. B., Johnson, T. E., Green, E. C. R. 2014a. **New mineral activity-composition relations for thermodynamic calculations in metapelitic systems.** Journal of Metamorphic Geology, 32, 261-286.!

White, R. W., Powell, R. and Johnson, T. E. 2014b. **The effect of Mn on mineral stability in metapelites revisited: new a-x relations for manganese-bearing minerals**. Journal of Metamorphic Geology, 32, 809-828.

Whitehouse, M. J. and Kemp, A. I. S. 2010. **On the difficulty of assigning crustal residence, magmatic protolith and metamorphic ages to Lewisian granulites: constraints from combined in situ U–Pb and Lu–Hf isotopes**. Geological Society, London, Special Publication, 335, 81-101.

Whitehouse, M. J., Kumar, G. R. R., and Rimsa, A. 2014. **Behaviour of radiogenic Pb in zircon during ultrahigh-temperature metamorphism: an ion imaging and ion tomography case study from the Kerala Khondalite Belt, southern India.** Contributions to Mineralogy and Petrology, 168:1042.

Whitney, D. L. and Evans. B. W. 2010. **Abbreviations for names of rock-forming minerals.** American Mineralogist, 95, 185-187.

Wisniowski, L., Pedrosa-Soares, A., Medeiros-Junior, E., Belém, J., Dussin, I. Queiroga, G. 2021. **Ultra-high temperature, mid-crustal level, contact metamorphism imprinted on granulite facies paragneisses by a norite intrusion (São Gabriel da Baunilha, Araçuaí orogen, southest Brazil).** Journal of Metamorphic Geology, 00, 1 – 29. DOI: 10.1111/jmg.12594.

Yakymchuk, C., Kirkland, C., and Clark, C. 2018. **Th/U ratios in metamorphic zircon**. Journal of Metamorphic Geology, 36(6), 715-737.

5 DETRITAL ZIRCON U-PB-HF ISOTOPES-BASED RECONSTRUCTION OF THE DEPOSITIONAL HISTORY OF (ULTRA)HIGH-TEMPERATURE METAMORPHIC ROCKS FROM THE SOCORRO-GUAXUPÉ NAPPE (SOUTHERN BRASÍLIA OROGEN, BRAZIL)

Authors: Rossi-Vieira, P. L. N. C[a*]., Tedeschi, M. F.[a,b], Rocha, B. C.[c], Lana, C. C.[d], Barrote, V.[e], Pedrosa-Soares, A. C.[a], Dussin, I. A.[f] and Alkmim, A.[d]

[a] *Programa de Pós-graduação em Geologia da Universidade Federal de Minerais, Centro de Pesquisas Manoel Teixeira da Costa, Institute of Geosciences, Federal University of Minas Gerais, Av. Antônio Carlos, 6627, Belo Horizonte 31270-901, Brazil*

[b] *Institute of Geological Sciences, University of Bern, 3012 Bern, Switzerland*

[c] *Departamento de Mineralogia e Geotectônica, Instituto de Geociências, Universidade de São Paulo, Rua do Lago, 562, CEP 05508-080, São Paulo, SP, Brazil*

[d] *Departamento de Geologia-Escola de Minas, Universidade Federal de Ouro Preto 35400-000, Brazil*

[e] *Freie Universität Berlin, Institut für Geologische Wissenschaften, Geochemie, Malteserstr. 10 74-100, 12249 Berlin, Germany*

[f] *TEKTOS Geotectonic Research Group, Geology Institute, Rio de Janeiro State University, São Francisco Xavier Street, 524/4030-A, Maracanã, Rio de Janeiro 20550-900, Brazil*

Published on Journal of South American Earth Sciences (DOI: https://doi.org/10.1016/j.jsames.2023.104469)

Abstract

Deciphering the provenance of paraderived rocks that underwent high- to ultrahigh (HTUHT) temperature metamorphism is a challenging task. Such metamorphic conditions can generate protracted zircon U-Pb age records of unclear meaning. However, the combination of U-Pb and Lu-Hf in zircon geochronology might be used as a powerful tool in order to retrieve the geological significance of ages and track the signature of possible protosources. Six samples of ortho- and paraderived rocks from the São João da Mata complex in the Socorro-Guaxupé Nappe (SE Brazil), a section mainly containing a continental magmatic arc built at the margins of the Paranapanema paleocontinent affected by HT-UHT metamorphism have been investigated. U-Pb and Lu-Hf isotopic analyses were carried out to evaluate disturbances in the U-Pb system, identify minimum crystallization ages and the Lu-Hf signatures of protosources and protoliths. Five protosources were identified, being four showing crustal Hf signatures ($\varepsilon Hf_{804\text{-}776)}$ = -16 to -2) and minimum U-Pb ages between ca. 804 Ma and ca. 776 Ma, and one with a moderately juvenile Hf signature

(εHf_{816}) = +3 to +9) and a minimum U-Pb age of ca. 816 Ma. The moderately juvenile signature suggests contribution of an island or continental arc-related source. The remaining protosources exhibit similar Lu-Hf signatures to those of orthoderived rocks found within the Socorro-Guaxupé Nappe. We propose that the analyzed paraderived rocks were deposited in a restricted, arc-related setting, that evolved through the following stages: i) an island to early-continental arc stage, with a maximum depositional age of ca. 816 Ma; ii) a continental arc setting, recorded by the protosources with crustal signatures and exhibiting a maximum depositional age of ca. 776 Ma; iii) HT-UHT metamorphism between ca. 690–630 Ma,with high temperature conditions lasting until the end collisional stage of the Orogen (ca. 630–610).

Keywords:

Provenance investigation, Sedimentary basin, Protracted zircon record, Island arc, Continental arc.

1 Introduction

Zircon has been considered one of the best geochronometers for igneous, sedimentary and metamorphic rocks (Mezger and Krogstad, 1997; Rubatto, 2017), mainly due to its high closure temperature for the U-Pb system (>850 °C; e.g. Möller et al., 2002; Cherniak, 2010), resistance to weathering (Hoskin and Schaltegger, 2003) and stability over a wide range of pressure and temperature conditions (Cherniak and Watson, 2001; Finch and Hanchar 2003). It has long played a crucial role in geochronological investigations, from understanding geological processes to the evolution of continents (Hoskin and Schaltegger, 2003; Fedo et al., 2003; Murphy et al., 2004; Cawood et al., 2012; Finch et al., 2021).

Obtaining meaningful ages for high (>850 °C) to ultrahigh (>900 °C) temperature (HTUHT) metamorphic rocks, however, can be a challenging task (e.g., Harley, 1989; Harley, 1998; Kelsey and Hand, 2015). Zircon grains subjected to such high temperatures usually exhibit a protracted (sub)concordant record of (apparent) U-Pb ages spreading over several millions of years (Friend and Kinny, 1995; Whitehouse and Kemp, 2010; Fornelli et al., 2011; Laurent et al., 2018; Kelsey and Hand, 2015; Rocha et al., 2018; Taylor et al., 2020). The smearing of age dates along the Concordia curve may result from i) partial opening of the U-Pb system (Whitehouse and Kemp, 2010; Taylor et al., 2016; Andersen et al., 2019), ii) partial dissolution or crystallization from a melt, particularly during long-lived events (Laurent

et al., 2018), iii) recrystallization, specially from metamictic domains (Laurent et al., 2018), which may involve modification of internal textures without changes to the external shape (Hoskin and Black, 2000; Corfu et al., 2003); as well as other processes described in the literature (e.g. Cherniak and Watson, 2003; Kusiak et al., 2013; Vervoort and Kemp, 2016; Rubatto, 2017).

Cases in which zircon crystals in HT-UHT rocks exhibit preserved internal texture while U-Pb ages show signs of resetting or partial recrystallization, evidencing a decoupling between internal textures and the isotopic system, are commonly described in the literature (Kunz et al., 2018). In these cases, the zircon record often shows scattered Upb dates (Tedeschi et al., 2018) and can exhibit cores younger than the rims (i.e., inverse-age zoning; e.g., Laurent et al., 2018). In heterogeneous rocks such as migmatites, the differential growth of zircon in compositional sub-domains can be particularly important and significantly affect the U-Pb record (Harley, 2016; Tedeschi et al., 2018; Fischer et al., 2021). Within this context, clusters of ages may not necessarily record discrete geological process, but rather variable U-Pb disturbing degrees that record the age interval between the geological processes (Tedeschi et al., 2023) or prolonged thermic events (Rocha et al., 2018; Tedeschi et al., 2018; Motta et al., 2021).

The issues related to these protracted zircon records are enhanced in U-Pb zircon dating-based provenance investigations in which the protosource (i.e. igneous and/or metamorphic rocks in which the zircon grains originally (re)crystallized; Pell et al., 1997) or a metasedimentary rock were somehow affected by HT-UHT metamorphism (c.f., Tedeschi et al., 2023). Ages obtained from the cores of detrital zircon grains are usually expected to reflect the crystallization ages of protosource rocks and are used in maximum depositional age determinations (Andersen et al., 2019) and in the identification of the tectonic settings of sedimentary basins (Cawood, et al., 2012). However, the obtained data can actually represent different scenarios, for instante: i) the genuine ages of paleosources, if sedimentary protosources include (meta)sedimentary rocks (Andersen, et al., 2015; Andersen, et al., 2019); ii) a pseudo-concordant zircon record of ages, owing to post-depositional or metamorphism-related Pb loss (e.g. recrystallization of metamictic domains) that affected source rocks (Mezger and Krogstad, 1997; Andersen, et al., 2019; Tedeschi et al., 2023); iii) ages without a clear geological meaning due to a protracted zircon growth, crystallization and recrystallization record induced by HT-UHT

metamorphism that affected source areas (Tedeschi et al., 2023). HT-UHT metamorphism might even create U-Pb distribution age patterns that could mislead interpreted as specific tectonic settings but with age peaks that are not related to source areas and/or lacking geological meaning (Tedeschi et al., 2023).

The combined use of U-Pb and Lu-Hf analyses in zircon constitute a useful approach to unravel the history behind the U-Pb disturbances (Whitehouse and Kemp, 2010; Taylor et al., 2016; Andersen et al., 2019). Zircon is known to host high concentrations of Hf due to the high partition coefficients with other Hf-hosting phases (i.e., garnet) in a considerable range of melt compositions (Fujimaki, 1986; Luo and Ayers, 2009; Nardi et al., 2013). As a low incorporation of Lu is observed in zircon, $^{176}Lu/^{177}Hf$ ratios tend to be lower than $^{176}Hf/^{177}Hf$ ratios by some orders of magnitude. Thus, variations due to the loss of radiogenic Hf are far lower than those observed on the host rock (Andersen, et al., 2019). The original $^{176}Hf/^{177}Hf$ ratios are likely to be preserved even in zircon grains obtained from rocks that underwent HT-UHT metamorphism (Tedeschi et al., 2018; Andersen et al., 2019; Motta et al., 2021). Consequently, zircon populations can be identified through their $^{176}Hf/^{177}Hf$ ratios and the effects of isotopic disturbance can be assessed (Vervoort and Kemp, 2016). As such, Lu-Hf isotopes are trustworthy markers of petrogenetic processes and crustal evolution through time and are used in a variety of geotectonic and detrital provenance studies (e.g., Gerdes and Zeh, 2009; Kemp et al., 2009; Collins et al., 2011; Westin et al., 2016, 2019; Martin et al., 2020; Ribeiro et al., 2020; Tedeschi et al., 2023).

The Socorro-Guaxupé Nappe (SGN) in the Southern Brasília orogen hosts metaigneous and metasedimentary rocks that record Neoproterozoic high-grade metamorphism (Del Lama et al., 2000; Campos Neto and Caby, 1999, 2000; Reno et al., 2009; Mora et al., 2014; Rocha et al., 2017, 2018; Tedeschi et al., 2018; Motta et al., 2021; Tedeschi et al., 2023). Distinct evolutionary models for this area have been proposed, mainly based on the investigation of the ortho-derived metamorphic rocks (e.g., Campos Neto et al., 2021; Trouw et al., 2013; Rocha et al., 2018; Tedeschi et al., 2018). However, the possible disturbance effects on the U-Pb age record as a result of HT-UHT metamorphism has not been investigated in detail in metasedimentary examples, and little has been discussed regarding their sedimentary provenance (e.g., Rocha et al., 2017). Understanding the deposition and evolution of sedimentary rocks has become crucial, as the time relationship between

magmatism, metamorphism and sedimentation plays an important role in unravelling the tectonic setting in which HT-UHT metamorphism is observed (Kelsey & Hand, 2015; Harley, 2016). In this contribution, U-Pb and Lu-Hf data are combined to unravel the depositional age and signature of protosources of metasedimentary rocks from the SGN. Novel data were integrated to the literature in order to identify possible source areas, depositional settings and further evaluate the effect of the HT-UHT metamorphism in zircon-based investigations. This work discusses the geodynamic context in which the investigated rocks from the SGN were deposited, how the HT-UHT metamorphism affected the U-Pb system conditions and, in a broader sense, the importance of the sedimentary record in identifying the tectonic settings related to extreme crustal conditions.

2 Geological setting

The Brasília Orogen consists of an 1800 km-long orogenic belt, located between the parallels 10 °S and 26 °S in Central Brazil, exhibiting a “boomerang shape” where the inflection (16 °S) corresponds to the boundary between its northern and southern sectors (Campos Neto et al., 2021; Figure 1). The Southern Brasília Orogen results from the convergence and collision between the São Francisco and Paranapanema paleocontinents at ca. 630 Ma (Brito Neves et al., 1999; Campos Neto and Caby, 1999, 2000; Trouw et al., 2000; Campos Neto et al., 2010; Trouw et al., 2013; Cioffi et al., 2016a). During the collision of the Southern Brasília Orogen, a complex nappe system verging eastward towards the São Francisco Craton was developed, where each nappe comprises different tectono-metamorphic domains: i) the Socorro-Guaxupé Nappe, representing the magmatic arc domain (e.g. Campos Neto and Caby, 1999, 2000; Trouw et al., 2000, 2013; Rocha et al., 2017, 2018; Tedeschi et al., 2018; Motta et al., 2021); ii) the Andrelândia Nappe System and Liberdade Nappe, representing the accretionary prism-foreland domain (e.g. Campos Neto et al., 2010, 2011; Coelho et al., 2017; Reno et al., 2009, 2012; Trouw et al., 2000, 2013; Frugis et al., 2018; Kuster et al., 2020); iii) and a passive margin domain associated to the São Francisco paleocontinent, represented by the São Vicente Complex (e.g. Westin et al., 2016), by the Carrancas Nappe System and the Lima Duarte Nappe (e.g. Campos Neto et al., 2004, 2011; Rocha, 2011; Trouw et al., 2013; Westin et al., 2019) and by basement orthogneisses (e.g. Cioffi et al., 2016a,

b, Cioffi et al., 2019; Fetter et al., 2001). An alternative interpretation considers the southern sector of the Socorro-Guaxupé nappe, the eastern sector of the lower nappes (Andrelândia, Carrancas, Lima Duarte) and the São Vicente Complex part of an interference zone between the Brasília and Ribeira orogens (Trouw et al., 2000, 2013; Heilbron et al., 2004, 2008).

2.1 Socorro-Guaxupé Nappe

The Socorro-Guaxupé Nappe (SGN) represents a section of the Neoproterozoic magmatic arc developed at the active margin of the Paranapanema paleocontinent (Campos Neto and Caby, 1999, 2000). The SGN hosts granulite to amphibolite facies metamorphic rocks that are thrusted over the Andrelândia Nappe system (Campos Neto and Figueiredo, 1995; Campos Neto and Caby, 1999, 2000; Campos Neto et al., 2011). It is divided into three main units based on the relative abundance of lithotypes (Figure 1): i) Basal Granulite Unit; ii) Orthogneiss Diatexite Unit; iii) Paragneiss Metatexite Unit (Campos Neto and Caby, 1999, 2000; Campos Neto et al., 2011; Rocha et al., 2017, 2018; Campos Neto et al., 2021).

The Basal Granulite Unit comprises approximately 3 km of enderbitic granulites (Campos Neto and Caby, 2000), and it corresponds to the Elói Mendes unit (Trouw et al., 2014; Tedeschi et al., 2015 (Figures 1 and 2). The Elói Mendes unit occurs at the base of the northern part of the SGN and as tectonic slices enveloped by migmatites of the São João da Mata unit (Tedeschi et al., 2015). It is represented by felsic to mafic granulites and migmatites, presenting clinopyroxene, orthopyroxene, hornblende and (locally) garnet. Charnockitic to enderbitic and granitic leucosomes constitute a common feature and are usually parallel to the regional foliation (Campos Neto and Caby, 2000; Mora et al., 2014; Rocha et al., 2018; Tedeschi et al., 2015, 2018).

The Orthogneiss Diatexite and Paragneiss Metatexite units are roughly composed of the

São João da Mata unit (Figures 1 and 2). It encompasses migmatites and other minor paraderived lithotypes and exhibits an increase in the degree of anatexis from north to south (Campos Neto and Caby, 2000; Janasi, 2002; Tedeschi et al., 2015; Ribeiro et al., 2015a; Rocha et al., 2017; Tedeschi et al., 2017).

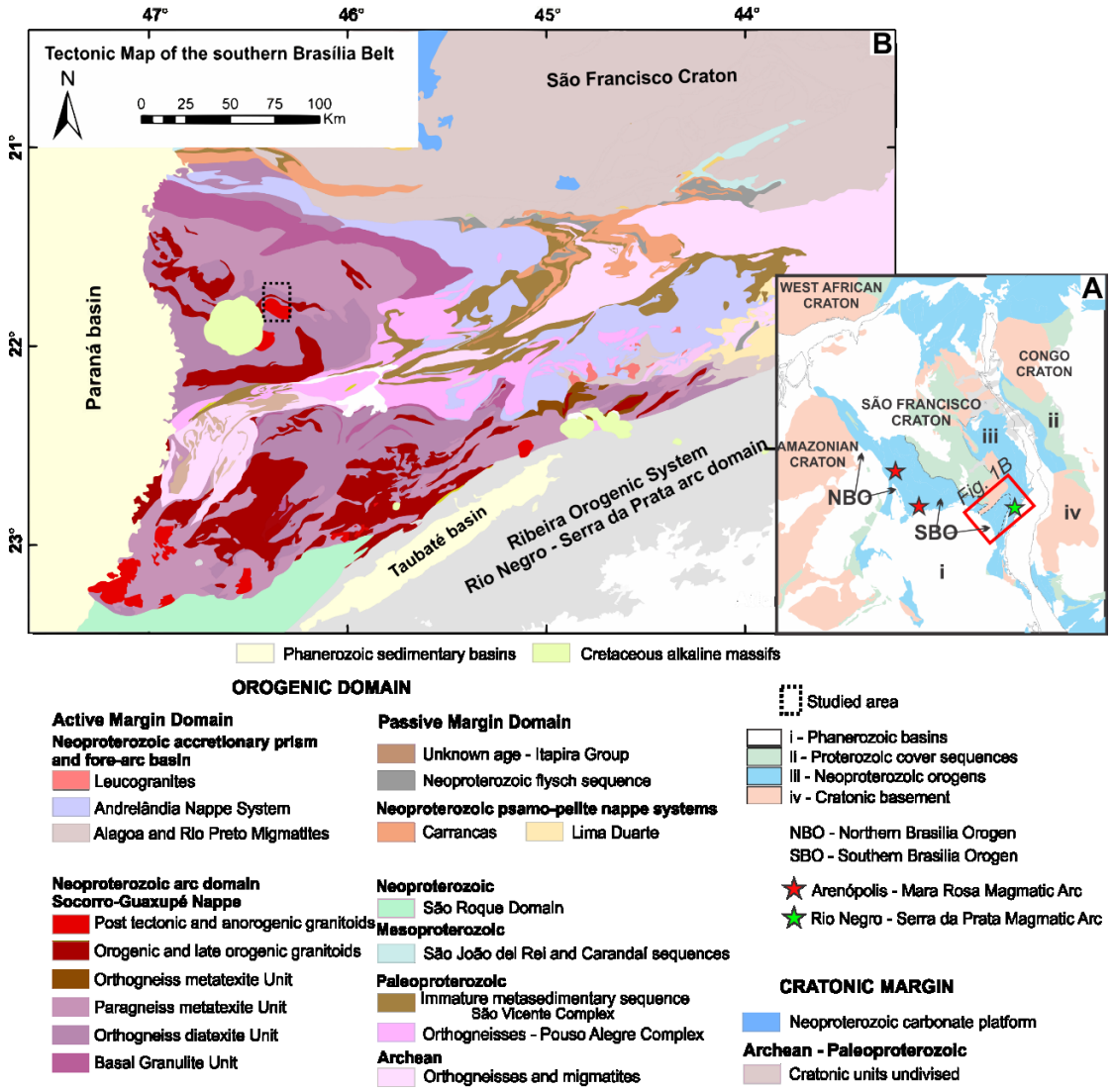

Figure 5-1 - Geological context and map of the Southern Brasília orogen. A) Insert highlighting the location of the Socorro-Guaxupé Nappe in the context of the western Gondwana, with the location of the Northern and Southern Brasília orogens, Arenópolis-Mara Rosa and Rio Negro-Serra da Prata magmatic arcs (modified from Cioffi et al., 2019); B) Sketch map of the Southern Brasília Orogen (modified from Cioffi et al., 2016a), with the studied area indicated in the black dotted rectangle.

The Orthogneiss Diatexite unit consists of (orthopyroxene)-(clinopyroxene)-hornblendebiotite migmatites, exhibiting nebulitic, schollen or schlieren structures, locally with stromatic metatexites (Campos Neto and Caby, 1999, 2000; Tedeschi et al., 2015). Towards the top of the unit, lenses and tectonic slices of calc-silicatic rocks or kinzingites may be observed (Campos Neto and Caby, 2000). Migration and accumulation of melt lead to the formation of leucogranite batholiths as the Serra da Água Limpa Batholith (Vinagre et al., 2014; Tedeschi et al., 2015; Costa et al., 2022). The Paragneiss Metatexite unit comprises (sillimanite)-(garnet)-biotite gneisses and migmatites, with minor occurrences of kinzigites, schists, quartzites, calc-silicatic

rocks, marbles and metamafic intrusives (Campos Neto and Caby, 2000; Ribeiro et al., 2015a; Tedeschi et al., 2015; Rocha et al., 2017; Tedeschi et al, 2017).

The rocks from the SGN are interpreted as remnants of a continental magmatic arc from ca. 790 Ma to ca. 640 Ma (Campos Neto and Figueiredo, 1995; Campos Neto and Caby, 2000; Mora et al., 2014; Rocha et al., 2017, 2018; Tedeschi et al., 2018; Motta et al., 2021), with remnants of island arcs observed locally (e.g., Costa et al., 2022). A high density of U-Pb ages in zircon grains from both arc-related metasedimentary rocks and granulites with arc signature marks a peak for the arc magmatism at ca. 655–650 Ma (Rocha et al., 2018). Peak UHT metamorphic conditions of ca. 900 – 1040 °C at 12 – 14 kbar have been calculated in the previous studies by Del Lama et al. (2000), Rocha et al. (2017, 2018), Tedeschi et al. (2018) and Motta et al. (2021), although different tectonic settings have been associated with this thermal event. Campos Neto and Caby (2000) and Campos Neto et al. (2004) proposed that UHT conditions were reached in the deep roots of the magmatic arc, related to a subduction-collision setting at ca. 630 – 625 Ma. Rocha et al. (2017, 2018) propose a long-lived (~30 Ma), collision-related metamorphic event with a thermal peak at UHT conditions taking place at ca. 630 – 625 Ma due to crustal thickening and radioactive-related heating, followed by extensive melt crystallization during retrograde cooling at ca. 625 – 600 Ma. Tedeschi et al. (2018) advocates for a two-stage, long lived metamorphism: a first stage related to the arc development, between ca. 680 – 640 Ma with the onset of the UHT event at ca. 660 Ma; a second stage, with collision-decompression metamorphism taking place between ca.

640 – 600 Ma.

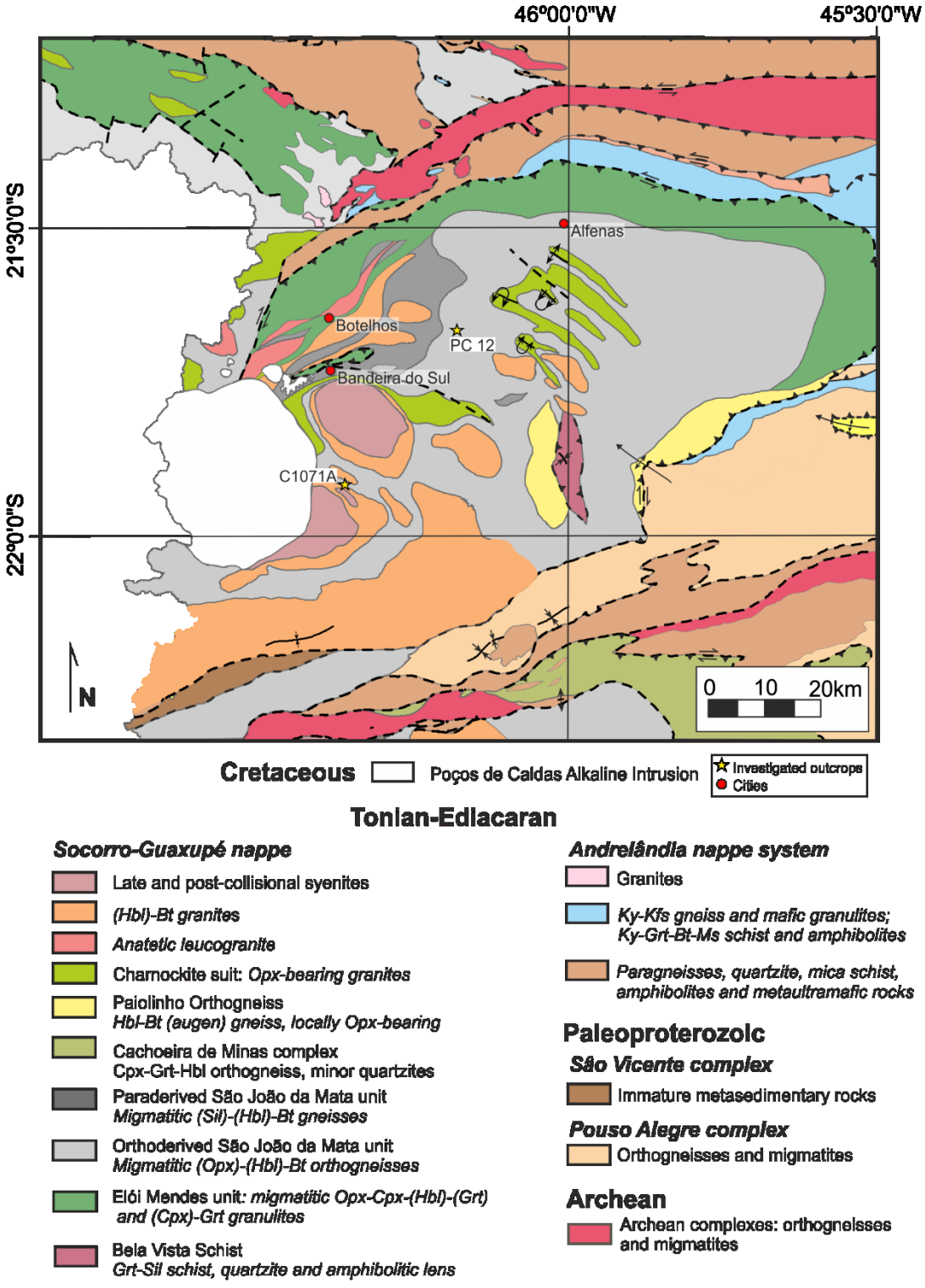

Figure 5-2 - Regional geological map of the Socorro-Guaxupé Nappe showing the location of investigated outcrops (yellow stars) in the Guaxupé domain (modified from Tedeschi et al., 2018; Cioffi et al., 2016a; Westin et al., 2016; Degler et al., 2015; Zogheib et al., 2015; Peixoto et al., 2015; Ribeiro et al., 2015a, b,c; Tedeschi et al., 2015).

3 Materials and Methods

The following procedures were applied for the six analyzed samples in this work. Mineral abbreviations follow Whitney and Evans (2010).

3.1 Field relations

Five samples were collected in an outcrop (PC12) mapped as São João da Mata Complex in Tedeschi et al. (2015), correspondent to the Orthogneiss Diatexite unit from Campos Neto and Caby (1999, 2000), consisting of the following rock types (Figure 3): i) dark gray to black amphibolite enclave (sample PC12.1); ii) a hornblende-biotite stromatic metatexite (sample PC12.2); iii) a biotite-bearing pink leucosome (sample PC12.3); iv) a garnet-biotite stromatic metatexite (sample PC12.4); and v) a garnet-bearing white leucosome (sample PC12.5). One sample was collected in an outcrop 34 km to the southwest of the PC12 outcrop, consisting of a (hornblende)-biotite-bearing stromatic metatexite (sample C1071A). The samples from the hornblende-biotite stromatic metatexite (sample PC12.2) and the pink biotite-bearing pink leucosome (sample PC12.3) have been investigated in Tedeschi et al. (2023) and will be further detailed in this contribution.

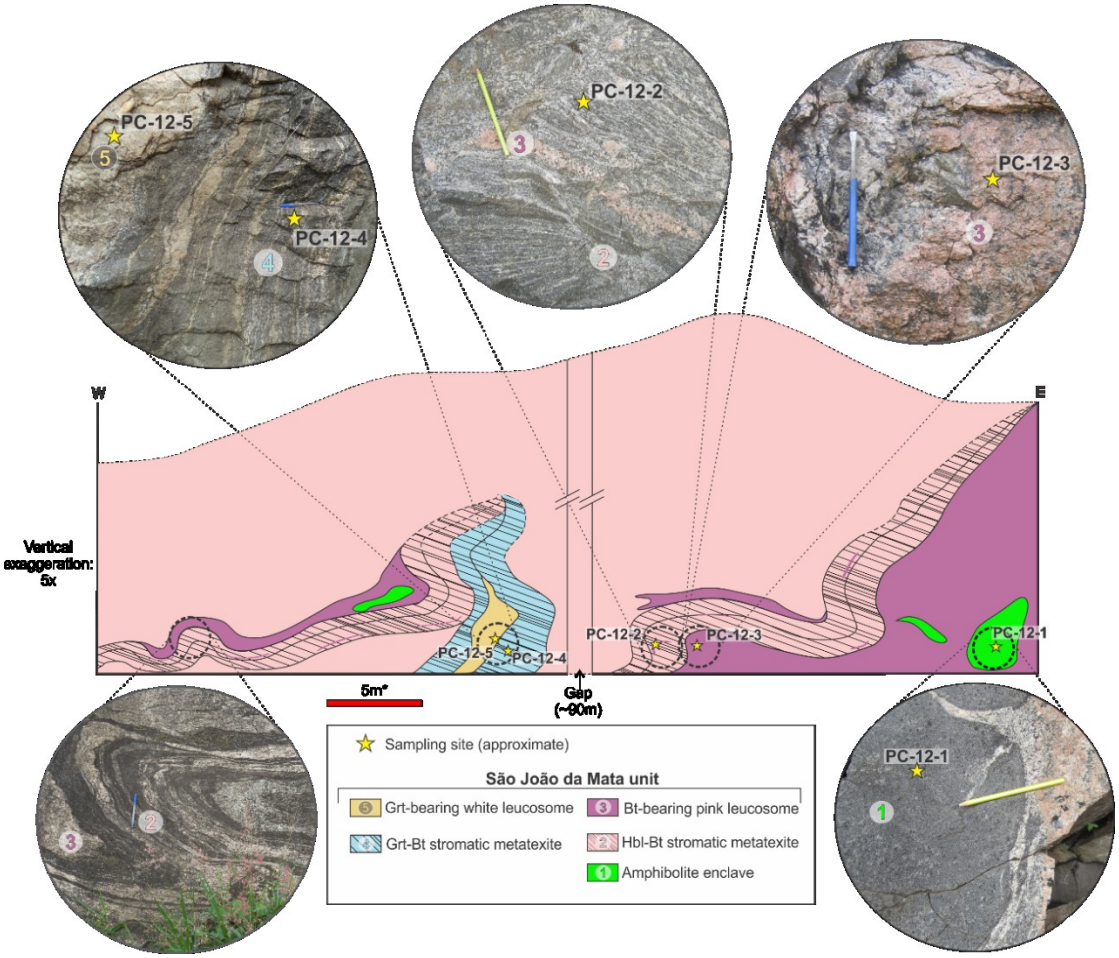

Figure 5-3 - Sketch of the sampled outcrop (PC12), exhibiting the relation between different rock types. PC12.1: Amphibolite enclave; PC12.2: hornblende-biotite stromatic metatexite; PC12.3: Pink biotitebearing pink leucosome; PC12.4: garnet-biotite stromatic gneiss; PC12.5: White garnet-bearing white leucosome. The interrupted bars at the center of the sketch mark a spatial gap (~90m) between the approximate position of the sampling sites along the outcrop. *Scale is approximate.

3.2 LA-ICP-MS isotopic analyses

Zircon was separated using standard rock crushing and heavy mineral separation techniques. Grains were individually selected, picked and mounted in epoxy resin. Grain mounts were polished to expose the grain centers. Zircons were imaged by cathodoluminescence (CL) for domain identification using a Quanta-250-FEI SEM fitted with a CL detector at the Multilab from Universidade do Estado do Rio de Janeiro (UERJ).

3.2.1 U-Pb geochronology

U-Pb isotopic analyses (Supplementary data 1) were performed using two separate LA-ICP-MS systems: i) Samples PC12.1, PC12.3, PC12.4, PC12.5, C1071A and spots PC12_2-001 to PC-12_2-080 from Sample PC12.2 were analyzed with a ArF Excimer Laser 193 nm from the Photon (Machines Inc. Model ATLEX SI) coupled

with a high-resolution Neptune-Plus multicollector (Thermo Fisher Scientific, USA), at the Multilab (UERJ). Instrument set up parameters were 6–7 mJ/cm² laser fluency, a frequency of 10 Hz, 25 µm spot size and laser energy between 60 and 70%. U-Pb data were standardized as following: Sample PC12.1 used the zircon 91500 ($^{206}Pb/^{238}U$ mean age ± 2σ = 1062±6 Ma) (Wiedenbeck et al., 1995) as a primary standard; Samples PC 12.2 used the GJ-1 zircon ($^{206}Pb/^{238}U$ mean age ± 2σ = 608±3 Ma) (Jackson et al., 2004) as primary standard and were tested using the zircon 91500 ($^{206}Pb/^{238}U$ mean age ± 2σ = 1041±3 Ma) (Wiedenbeck et al., 1995) as secondary standard; Samples PC12.3, PC12.4, PC12.5 and C1071A used the GJ-1 zircon ($^{206}Pb/^{238}U$ mean age ± 2σ = 608±4 Ma)

(Jackson et al., 2004) as primary standard and were tested using the Plešovice ($^{206}Pb/^{238}U$ mean age ± 2σ = 337±2 Ma) (Sláma et al. 2008) and/or BB ($^{206}Pb/^{238}U$ mean age ± 2σ = 561±2 Ma) (Santos et al., 2017) zircons as secondary standards. External errors were calculated with the error propagation of individual measurements of GJ-1 and the individual measurements of each spot. Data reduction was done using an Excel program developed by Chemale et al. (2012); ii) Spots PC-12_2-082 to PC-12_2_194 from Sample PC12.2 were analyzed with an Element 2 Thermo Finnigan Neptune multicollector ICP-MS coupled to a Photon-Machines 193 nm at the Universidade Federal de Ouro Preto (UFOP) following the procedure described in Santos et al. (2017).

Instrument set up parameters were a spot size of 30 µm, a frequency of 6 Hz, 1,9 J/cm² fluence, and 10 % energy with an intensity of 0.3 mJ. U-Pb data were standardized using the zircon GJ-1 ($^{206}Pb/^{238}U$ mean age ± 2σ = 601±3 Ma) (Jackson et al., 2004) as primary standard and tested using the Plešovice ($^{206}Pb/^{238}U$ mean age ± 2σ = 338±1 Ma) (Sláma et al. 2008) and BB ($^{206}Pb/^{238}U$ mean age ± 2σ = 561±2 Ma) (Santos et al., 2017) zircons as secondary standards. External errors were propagated considering the internal reproducibility of the individual ratios, external reproducibility of GJ-1, long-term uncertainty of the validation material, ratio uncertainties of the reference material and Pb-common ratio uncertainty (Lana et al., 2017). Data reduction was done using an Excel program developed by Chemale et al. (2012).

Data evaluation for each spot was filtered considering outlier values of common Pb contents (≤ 5% common ^{204}Pb), errors of isotopic ratios (≤ 8%) and

percentage of discordance (≤ 5%). The Concordia diagrams were obtained using the software Isoplot/Ex (Ludwig, 2003) and the histograms and probability density plots with Density Plotter (Vermeesch, 2012). Individual uncertainties are presented at 2σ level. The confidence level for the weighted averages is 95 % (Supplementary data 1).

3.2.2 Lu-Hf isotopes

Data were obtained using a Thermo-Finnigan Neptune multicollector ICP-MS coupled to a Photon-Machines 193 nm laser system (LA-MC-ICP-MS, Photon machines 193/Neptune Thermo Scientific), at Universidade Federal de Ouro Preto, Brazil. Data were collected as described in Santos et al. (2017). Spots were placed in the same Cldomains as U-Pb dating spots. The laser was operated with a spot of 40 μm in diameter, fluence of 4.54 J/cm, and a pulse rate of 8 Hz. Both the acquisition and reduction data were performed in blocks of 80-100 analyses interspersed with the following reference materials: BB (mean $^{176}Hf/^{177}Hf$ ratios = 0.281668 ± 0.000010) (Santos et al., 2017), GJ1 (mean $^{176}Hf/^{177}Hf$ ratios = 0.282000 ± 0.000019) (Morel et al. 2008), Plešovice (mean $^{176}Hf/^{177}Hf$ ratios = 0.282472 ± 0.000019) (Sláma et al., 2008), Mudtank (mean $^{176}Hf/^{177}Hf$ ratios = 0.282495 ± 0.0000018) (Woodhead and Hergt, 2005) and Temora (mean $^{176}Hf/^{177}Hf$ ratios = 0.282696 ± 0.000019) (Woodhead et al., 2004). The results are also within error of recommended values (Supplementary data 1). No interference of Yb on Hf was detected after corrections, and it was assessed through the comparison between $\varepsilon Hf_{(t)}$ and $^{176}Yb/^{177}Hf$ for each sample (Supplementary data 2).

3.3 U-Pb and Lu-Hf data interpreting

A similar approach of Whitehouse and Kemp (2010) was applied: 1) detailed investigation of the internal structure of zircon grains through (CL) imaging, allowing the determination of grains with different growth zones or single-phase grains (without rims); 2) U-Pb zircon core dates from a single source are primary assumed to represent a single magmatic event, therefore the older grains in a single data cluster are considered to represent the crystallization age of that source (Gerdes and Zeh, 2009; Whitehouse and Kemp, 2010); 3) Lu-Hf analyses were carried out on grains from each CL domain and age populations.

$^{176}Hf/^{177}Hf_{(t)}$ ratios (Supplementary data 1) were then compared to the respective U-Pb dates to verify a possible decoupling between the Lu-Hf and U-Pb systems (Gerdes and Zeh, 2009; Whitehouse and Kemp, 2010; Vervoort and Kemp,

2016; Wang et al., 2017) and to identify zircon populations following the approach of Tedeschi et al. (2023): i) check if more than one population of zircon can be identified through U-Pb dates; ii) check if each U-Pb population is related to a specific range of $^{176}Hf/^{177}Hf_{(t)}$ ratios constrained inside the fourth decimal $^{176}Hf/^{177}Hf_{(t)}$ unit (~0.0001); iii) if each U-Pb population cannot be related to a specific range of $^{176}Hf/^{177}Hf_{(t)}$ ratios, then each range of $^{176}Hf/^{177}Hf_{(t)}$ ratios is probably related to a different protosource or different processes; iv) if a single $^{176}Hf/^{177}Hf_{(t)}$ population is identified, then probably the protolith was an igneous rock (or a sedimentary rock derived from a single protosource); v) verify if any of those populations can be related to metamorphism or anatexis; vi) populations that cannot be related to anatexis and/or metamorphism are probably correlated to one or more different protosources, and if two or more protosources can be identified the protolith is probably a multi-sourced sedimentary rock; vii) if all populations present U-Pb dates spreading over the Concordia diagram, then HT-UHT metamorphism was post-depositional; if one or more population does not present U-Pb dates spreading, HT-UHT metamorphism probably affected the source area prior to metamorphism.

Grains from a single population affected by Pb loss define a linear horizontal trend on a $^{176}Hf/^{177}Hf$ ratio versus $^{206}Pb/^{238}U$ age plot (Andersen, et al., 2019), recording a characteristic “signature” for rocks formed from a single source (such as igneous rocks). As discussed by Tedeschi et al. (2023), zircon crystals crystallized from single-source magmas, with little to no influence of magma mixing and without considerable assimilation of host rocks, tend to exhibit well-defined $^{176}Hf/^{177}Hf_{(t)}$ signatures, usually inside a variation of ca. 0.0001 $^{176}Hf/^{177}Hf_{(t)}$ unit, considering the errors of analyses (c.f. Griffin et al., 2002; Andersen et al., 2002; Andersen et al., 2004; Belousova et al., 2006). Different igneous sources belonging to correlated suites might, however, exhibit $^{176}Hf/^{177}Hf_{(t)}$ ratios inside a well-constrained range of values, as observed in the examples from the Sveconorwegian complexes discussed by Andersen et al. (2002, 2004). This is because rocks generated by similar processes in similar tectonic settings might have similar petrogenetic signatures, even though formed at different times. Therefore, detrital zircon obtained from (meta)sedimentary rocks inserted in restricted tectonic settings (as arc-related basins) also tend to have restricted contribution from sources and might exhibit a well constrained $^{176}Hf/^{177}Hf_{(t)}$ signature (c.f. Westin et al., 2016), while multisource basins

exhibit a characteristic broad variation in $^{176}Hf/^{177}Hf_{(t)}$ ratios in zircon (as observed in the detrital zircon from the Heddersvatn Fm. And Vallar Bru Fm. In Griffin et al., 2002).

Based on these works, Tedeschi et al. (2023) explores how zircon populations within the fourth decimal place from a peak $^{176}Hf/^{177}Hf_{(t)}$ value might represent a single protosource and can be used for estimating both crystallization ages for meta igneous rocks and accordingly, minimum crystallization ages in provenance investigations. We proceeded to apply the method proposed by those authors for avoiding biases in provenance studies in the analyzed samples in order to: i) identify zircon populations affected by HT-UHT metamorphism through their Hf signatures; ii) retrieve the minimum crystallization ages of such populations; iii) to determine the nature of the protoliths (magmatic or sedimentary); iv) correlated the identified protosources with other rocks from the orogen; and v) assign the depositional setting of the sedimentary basin of the metasediments.

The term date refers to individual chronological values for $^{206}Pb/^{238}U$ spot data, while the term age refers to groups of $^{206}Pb/^{238}U$ dates with a geological meaning (c.f. Kunz et al., 2018).

4 Results

The results of the investigation are presented by sample. The main aspects of samples are described in this section (Figures 4 and 5), while a detailed petrographic description of samples is presented on Supplementary data 3. U-Pb and Lu-Hf data were analyzed separately for cores and rims of zircon grains from all six samples in this work (Supplementary data 1) (Figure 6). Different zircon textures were identified on most samples (a brief description is provided in sections 4.1 to 4.4), but no correlation between textures, U-Pb dates or Lu-Hf isotopes was observed among the dataset. Zircon populations were identified based on their respective $^{176}Hf/^{177}Hf_{(t)}$ ratios through probability density plots (PDP), and data was compared to their respective U-Pb dates and $\varepsilon H_{(t)}$ values (Table 1, Figures 7, 8, 9 and 10). Zircon analyses did not separate between zircon grains from mafic/mesocratic and leucocratic bands in the stromatic metatexite samples (sections 4.2, 4.3 and 4.4). Only concordant zircon dates were considered for the purpose of this work.

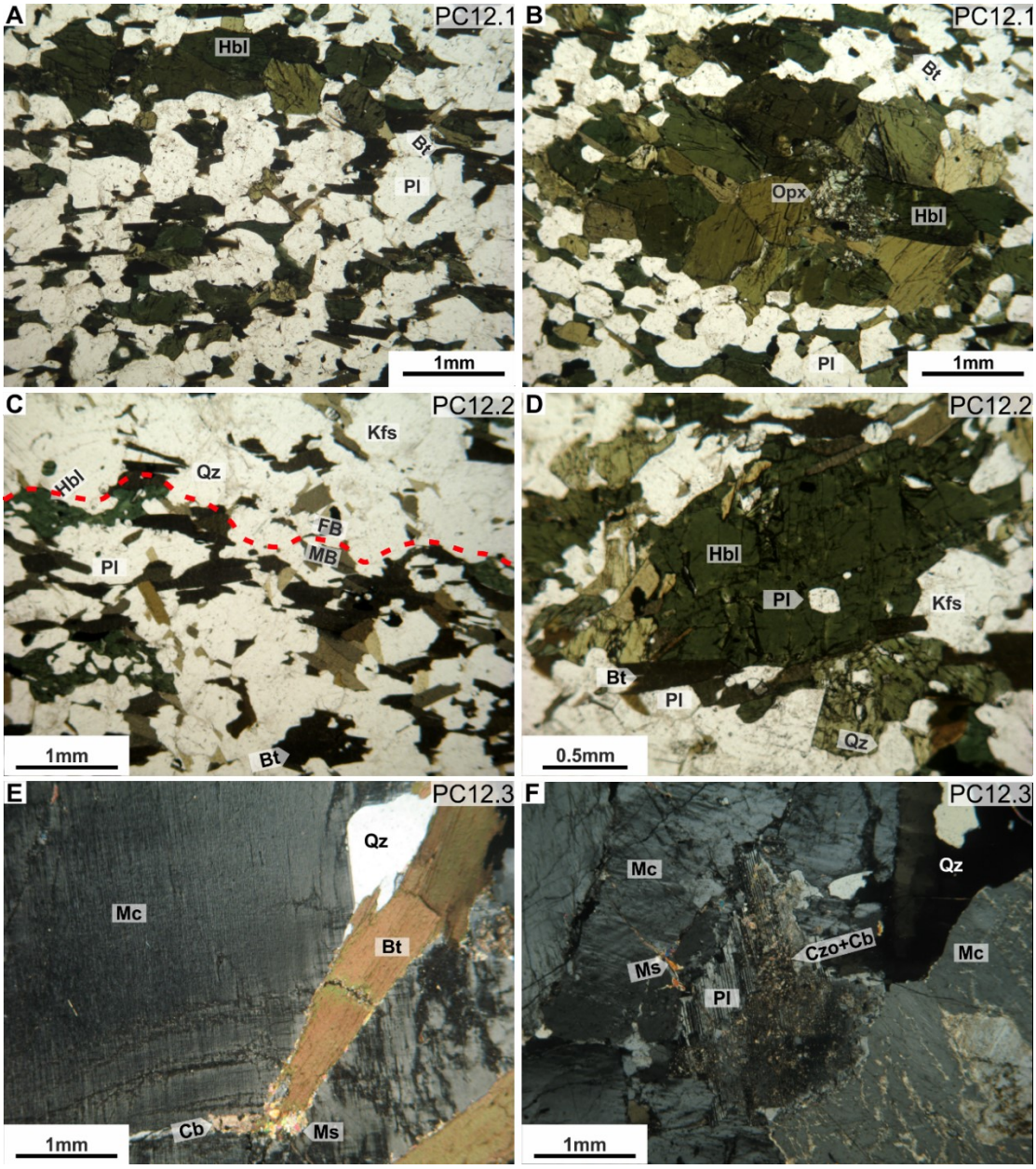

Figure 5-4 - Photomicrographs of the rocks analysed in this work: amphibolite enclave (sample PC12.1) (A-B), hornblende-biotite stromatic metatexite (sample PC12.2) (C-D) and biotite-bearing pink leucosome (sample PC12.3) (E-F). A) Foliation marked by oriented hornblende and biotite crystals. B) Orthopyroxene relict in the middle of the hornblende cluster. C) Contact between mafic band (MB), exhibiting hornblende, plagioclase, quartz and biotite, and felsic band (FB), exhibiting orthoclase, quartz, biotite and minor hornblende. D) Relations between mafic phases. E) Microcline phenocryst, biotite and quartz. F) Late muscovite after microcline and late clinozoisite+carbonate after plagioclase (A-D – plane polarized light; E-F – cross polarized light).

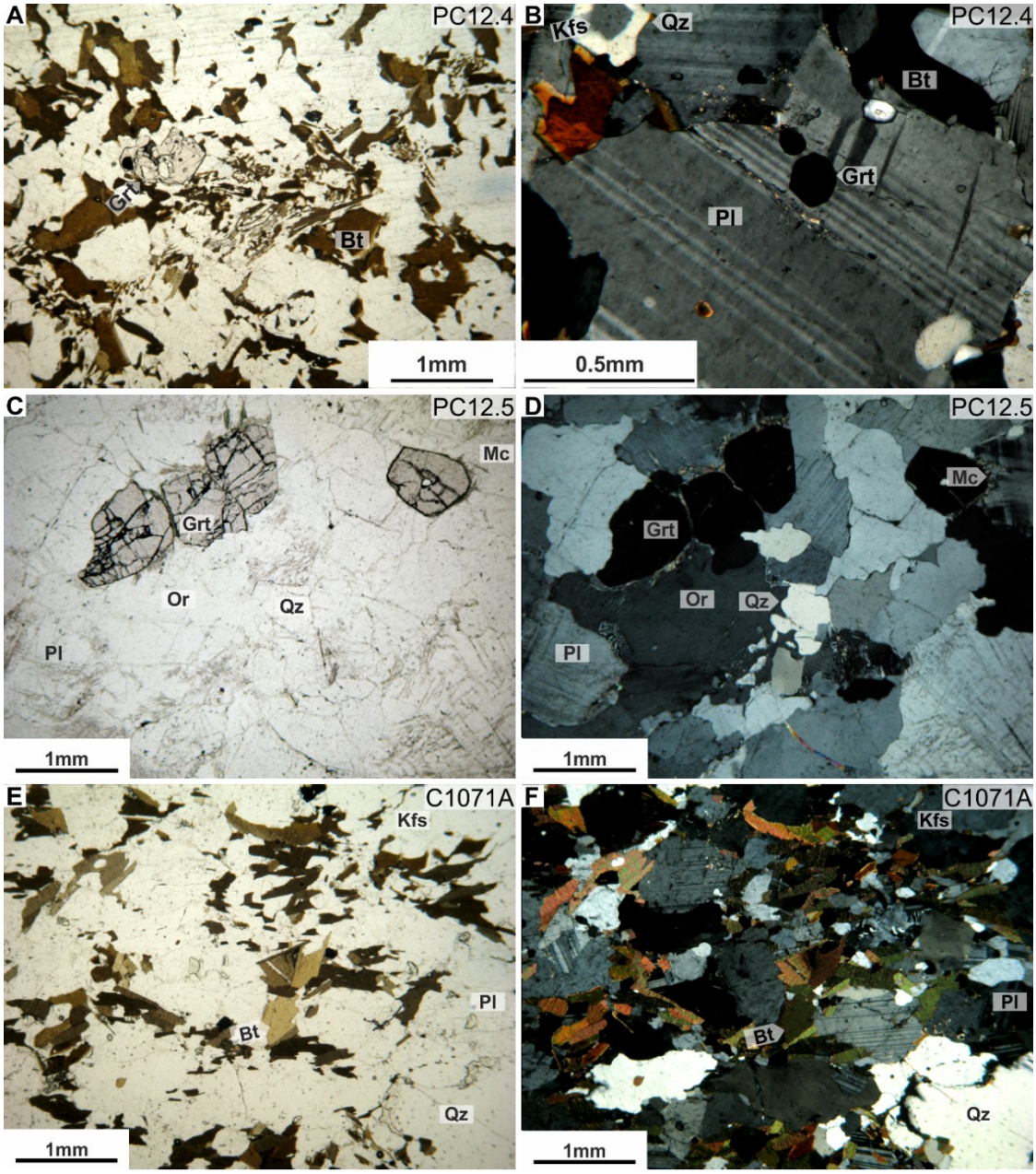

Figure 5-5 - Photomicrographs of the rocks analysed in this work: garnet-biotite stromatic metatexite (sample PC12.4) (A-B), garnet-bearing white leucosome (sample PC12.5) (C-D) and (hornblende)biotite stromatic metatexite (sample C1071A) (E-F). A) Mesocratic band exhibiting euhedral garnet and biotite-plagioclase-quartz skeletal intergrowths. B) Plagioclase crystal exhibiting subhedral garnet inclusions and quartz "pool" surrounding K-feldspar in leucocratic band. C-D) Isotropic texture, exhibiting xenomorphic plagioclase, orthoclase and quartz, and subhedral garnet crystals. E-F) Oriented biotite crystals defining the main foliation in mesocratic band. (A, C, E – plane polarized light; B, D, F – cross-polarized light).

4.1 Amphibolite enclave (PC12.1)

Sample PC12.1 is a fine- to coarse-grained amphibolite enclave in the biotite-bearing pink leucosome (sample PC12.3) (Figure 4A). It is composed of plagioclase (30–50%), hornblende (22 – 40%), biotite (10 – 15%), quartz (5 – 12%) and ilmenite

(3 – 5%), with minor apatite, zircon, titanite, ilmenite and rare pyrite and chalcopyrite. Rare relicts of ortho- and clinopyroxene are also observed (Figure 4B).

Internal textures observed among zircon crystals on CL images include: fir-tree, oscillatory and convolute zoning; high luminescence crystals; and xenocrystic cores. Zoned crystals usually exhibit dark cores and bright rims on CL images, although inverse patterns are also observed. Partial recrystallization or resorption features are seldom observed.

Zircon cores (n=44) (Figures 6; 7A, B) exhibit a protracted record of concordant U-Pb dates from 782±25 Ma to 605±28 Ma, with most data (n = 34) concentrated between 620±9 Ma to 681±14 Ma. Three peaks are identified through a probability density plot (PDP): ca. 675 Ma, ca. 655 Ma and ca. 625 Ma. A single discordant core of Archean age provided an Archean date of 2571±19 Ma (9% discordance).

Zircon rims (n=43) (Figure 6) exhibit concordant U-Pb dates from 780±18 Ma to 599±14 Ma (Figure 7A, B), with most data (n = 33) concentrated between 688±20 Ma and 635±22 Ma. Two older grains were obtained (860±18 Ma and 1304±34 Ma). Three peaks are identified through a PDP: ca. 730 Ma, ca. 665 Ma and ca. 635 Ma.

The $^{176}Hf/^{177}Hf_{(t)}$ for all the zircon population (n=20) provided a homogeneous population (Table 1) with values between 0.28196 and 0.28207, within a range of U-Pb dates between 782±25 Ma and 599±14 Ma (Figure 7C-E). The $^{176}Hf/^{177}Hf_{(t)}$ ratios for cores (n = 11) and rims (n = 9) have a similar range (cores: 0.28196 – 0.28207; rims: 0.28196 –

0.28205). All grains show negative $\varepsilon Hf_{(t)}$ values (cores: -14 to -10; rims: -16 to -9 (Figure 7F). By considering the oldest grain within the core analyses, the minimum age for the amphibolite enclave is interpreted as 782±25 Ma. Recalculated εHf values for the age of the oldest grain of this population $\varepsilon Hf_{(782)}$ lie between -12 and -8 for zircon cores and between -12 and -9 for zircon rims (Figure 7G).

Sample	Domain	Population	Spots (n)	$^{206}Pb/^{238}U$ dates (Ma)	$^{176}Hf/^{177}Hf_{(t)}$	$\varepsilon Hf_{(t)}$	Corrected $\varepsilon Hf_{(t)}$		Avg MORB[a]	T_{DM2} (Ga)[bf]	T_{DM2} (Ga) [c]
PC12.1	Rim	Single	9	780±18 – 599±14	0.28196 – 0.28205	-16 to -9	782	-12 to -9	2.10 – 1.86	2.33 – 2.08	2.07 – 1.82
	Core		11	782±25 – 605±28	0.28196 – 0.28207	-14 to -10	Ma	-12 to -8	2.08 – 1.85	2.30 – 2.08	2.04 – 1.82
PC12.2	Rim	I	3	775±6 – 725±3	0.28190 – 0.28191	-15 to -14	804	-14 to -13	2.17 – 2.14	2.40 – 2.36	2.14 – 2.10
	Core		7	804±5 – 652±4	0.28183 – 0.28192	-18 to -13	Ma	-16 to -13	2.30 – 2.11	2.53 – 2.34	2.27 – 2.07
	Rim	II	7	772±4 – 682±8	0.28198 – 0.28203	-16 to -11	789	-11 to -9	2.08 – 1.93	2.31 – 2.15	2.04 – 1.89
	Core		41	789±10 – 607±17	0.28193 – 0.28203	-16 to -11	Ma	-13 to -9	2.12 – 1.92	2.35 – 2.14	2.09 – 1.88
	Rim	III	5	783±4 – 591±8	028205 – 0.28208	-12 to -8	786	-9 to -8	1.93 – 1.83	2.16 – 2.06	1.90 – 1.80
	Core		21	786±8 – 621±4	0.28204 – 0.28213	-12 to -6	Ma	-9 to -5	1.92 – 1.70	2.14 – 1.92	1.88 – 1.66
	Rim	IV	2	693±4 – 657±2	0.28223	-5 to -4	776	-2	1.55	1.78	1.52 – 1.51
	Core		18	776±14 – 620±3	0.28214 – 0.28224	-8 to -3	Ma	-5 to -2	1.71 – 1.56	1.94 – 1.79	1.68 – 1.52
PC12.3	Rim	Single (Pop. II)	16	691±3 – 597±3	0.28198 – 0.28202	-15 to -11	691	-13 to -12	2.06 – 1.93	2.29 – 2.15	2.03 – 1.89
	Core		18	676±4 – 611±3	0.28198 – 028200	-14 to -13	Ma	-13 to -11	2.06 – 1.96	2.29 – 2.19	2.03 – 1.93
PC12.4	Rim	I	10	829±8 – 632±3	0.28238 – 0.28251	+1 to +7	816	+4 to +8	1.29 – 1.02	1.52 – 1.25	1.25 – 0.98
	Core		47	816±11 – 607±6	0.28239 – 0.28251	+0 to +7	Ma	+4 to +9	1.25 – 0.98	1.48– 1.19	1.22 – 0.93
PC12.5	Rim	Single (Pop. II)	1	592±2	0.28213	-10	661	-10 to -7	1.78	2.01	1.75
	Core		18	661±4 – 572±2	0.28208 – 0.28218	-13 to -7	Ma		1.86 – 1.65	2.08 – 1.88	1.82 – 1.62
C1071A	Rim	Single	6	728±6 – 621±5	0.28212 – 0.28223	-8 to -3	719	-7 to -3	1.75 – 1.53	1.97 – 1.76	1.71 – 1.50
	Core	Single	55	719±15 – 545±5	0.28210 – 0.28223	-11 to -4	Ma	-8 to -4	1.78 – 1.58	2.02 – 1.81	1.75 – 1.54

Table 5-1 - Summary of U-Pb and Lu-Hf data of zircon populations from the analyzed samples. a Chauvel et al. 2008; b Blichert-Toft et al. 2008; c Dhuime et al. (2011).

Figure 5-6 - Representative cathodoluminescence (CL) images, $^{206}Pb/^{238}U$ dates (2σ uncertainties), $^{176}Hf/^{177}Hf$ ratios and εHf values of zircon grains from the analyzed samples in this work (sample PC12.1: amphibolite enclave; sample PC12.2: hornblende-biotite stromatic metatexite; sample PC12.3: biotite-bearing pink leucosome; PC12.4: garnet-biotite stromatic metatexite; PC12.5: garnetbearing white leucosome; sample C1071A: (hornblende)-biotite stromatic metatexite).

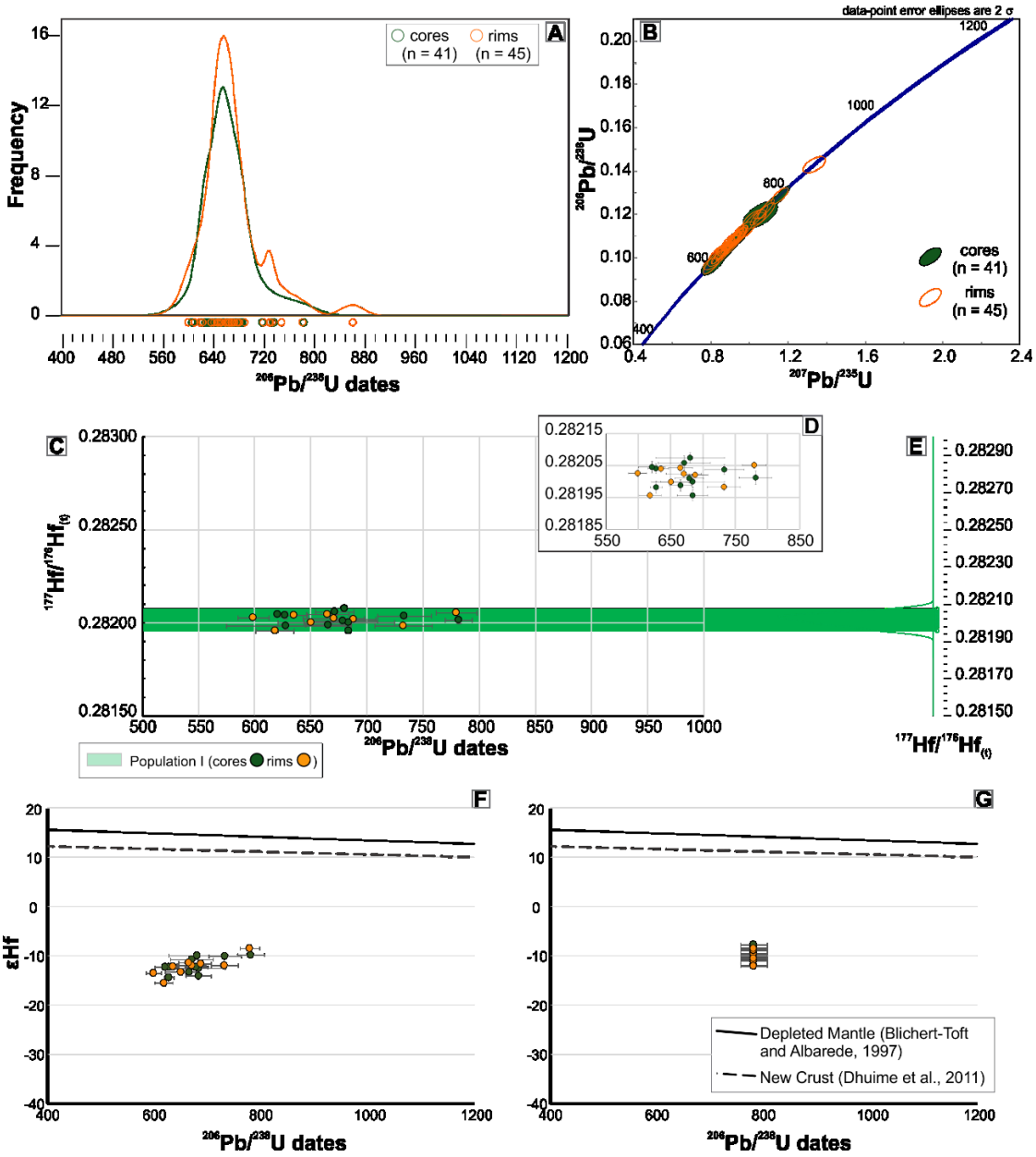

Figure 5-7 - Isotopic data from analyzed zircons in the amphibolite enclave (PC12.1) sample. A) $^{206}Pb/^{238}U$ probability density plot (PDP) for cores (dark green) and rims (orange). B) Concordia diagrams for cores (filled dark green ellipses) and rims (hollow orange ellipses). C) $^{176}Hf/^{177}Hf_{(t)}$ ratios versus $^{206}Pb/^{238}U$ dates. D) Inset on the $^{176}Hf/^{177}Hf_{(t)}$ ratios x $^{206}Pb/^{238}U$ dates chart highlighting the data scatter. E) Probability Density Plot (PDP) for the $^{176}Hf/^{177}Hf_{(t)}$ ratios, compared with I. Green shading indicating a single population of zircon. F-G) εHf ratios versus $^{206}Pb/^{238}U$ dates compared to the depleted mantle (Blichert-Toft and Albarède, 1997) and new crust (Dhuime et al., 2011) evolution trend, with uncorrected ratios considering individual zircon dates and corrected ratios for the oldest zircon grain in the population (outlier excluded), respectively.

4.2 Hornblende-biotite stromatic metatexite (PC12.2) and biotite-bearing pink leucosome (PC12.3

The U-Pb-Hf data from these samples have been published in Tedeschi et al. (2023) but it will be further detailed in this section for sake of comparison with the other samples to explore the full dataset.

The hornblende-biotite stromatic metatexite (PC12.2) exhibits mafic (dark gray to gray) bands interleaved with leucocratic (pink) bands (Figure 4C). Leucocratic bands exhibit variable amounts of plagioclase (23 – 70%), orthoclase (6 – 42%) and quartz (5 – 23%), with biotite (8 – 16%), hornblende (3 – 11%) and opaque minerals (ilmenite and magnetite, 1 – 2%) accounting for 10 – 20 vol% (Figure 4C). Mafic bands (Figure 4C, D) are composed of hornblende (15 – 25%), biotite (25 – 35%), plagioclase (35 – 40%), orthoclase (5 – 15%), quartz (5 – 10%), opaque minerals (ilmenite, magnetite, pyrite and chalcopyrite, 2 – 7%), with minor apatite, monazite, zircon and titanite. Late muscovite is often observed at the contacts between biotite and feldspars.

Zircon grains from the hornblende-biotite stromatic metatexite (PC12.2) exhibit a variety of textures, including: xenocrystic core crystals; fir-tree, oscillatory, sector and convolute zoning; high luminescence crystals; dark, low luminescence crystals; and single-phase crystals. Zoned crystals usually exhibit zones marked by different shades of gray. Partial recrystallization or resorption features are sometimes observed and are usually restricted to well-defined zones in crystals.

U-Pb dates from zircon cores (n=140) (Figure 6) from the hornblende-biotite stromatic metatexite (PC12.2) exhibit a range between 804±5 Ma and 581±14 Ma (Figure 8A, B). A single older (997±7 Ma) and a younger (533±16 Ma) date were obtained and considered outliers. Dates are mainly concentrated between 792±8 and 607±17 Ma, and several peaks were calculated through a PDP: ca. 780 Ma, ca. 770 Ma, ca. 760 Ma, ca. 740 Ma, ca. 730 Ma, ca. 710 Ma, ca. 700 Ma, ca. 680 Ma, ca. 645 Ma and ca. 620 Ma. The U-Pb dates from zircon rims (n=24) (Figure 6) scattered continuously from 787±3 to 591±8 Ma (Figure 8A, B), with an outlier younger date of 565±5 Ma. Several small peaks (frequency < 4) were calculated through a PDP between ca. 785 Ma and ca. 620 Ma.

The biotite-bearing pink leucosome (PC12.3) exhibits perthitic microcline phenocrysts (Figure 4E, F) and a matrix composed of fine- to coarse-grained microcline (35-45%), plagioclase (30 – 35%) and quartz (20 – 30%), with fine- to

coarse-grained biotite (5 – 15%), minor opaque minerals, apatite and zircon (Figure 4F). Late carbonate and clinozoisite are observed after plagioclase, as well as late muscovite after microcline.

Zircon grains from the biotite-bearing pink leucosome (PC12.3) exhibit oscillatory, sector and fir-tree zoning. High luminescence crystals and xenocrystic cores are also observed, as well as crystals with homogeneous CL response (single-phase crystals).

The U-Pb dates from zircon cores (n=44) (Figure 6) from the biotite-bearing pink leucosome (PC12.3) range between 680±6 and 597±3 Ma, except two outliers (573±4

Ma and 710±4 Ma) (Figure 8A, C). Three main peaks were identified through a PDP: ca. 660 Ma, ca. 640 Ma and ca. 620 Ma. The U-Pb dates from zircon rims (n=35) (Figure 6) range between 691±3 and 602±3 Ma, except the 734±5 Ma date (Figure 8A, C) that was considered an outlier. Two main peaks were identified through a PDP: ca. 645 Ma and ca. 625 Ma.

The $^{176}Hf/^{177}Hf_{(t)}$ ratios for the analyzed zircon grains from samples PC12.2 (n=104) and PC12.3 (n=34) provided four populations (Table 1, Figure 8D-G; see section 3.3 for the criteria). No preferable distribution of $^{176}Hf/^{177}Hf_{(t)}$ ratios was observed between analyzed cores and rims, although the lower values for $^{176}Hf/^{177}Hf_{(t)}$ ratios inside each population are usually found on zircon cores. Population I comprises only zircon crystals from the hornblende-biotite stromatic metatexite (sample PC12.2) with cores (n = 7) exhibiting Upb dates between 804±5 Ma – 652±4 Ma and $^{176}Hf/^{177}Hf_{(t)}$ ratios between 0.28183 – 0.28192, while rims (n = 3) present U-Pb dates between 775±6 Ma – 725±3 Ma and $^{176}Hf/^{177}Hf_{(t)}$ ratios between 0.28190 – 0.28191. Population II is represented both by zircon crystals from the hornblende-biotite stromatic metatexite (PC12.2) and from the biotite-bearing pink leucosome (PC12.3). Zircon cores (n = 41) from crystals from sample PC12.2 show U-Pb dates between 789±10 Ma – 607±3 Ma (outlier 997±7 Ma) and $^{176}Hf/^{177}Hf_{(t)}$ ratios between 0.28193 – 0.28203, while rims (n = 7) present U-Pb dates between 772±4 Ma – 682±8 Ma (outlier 556±11 Ma) and $^{176}Hf/^{177}Hf_{(t)}$ ratios between 0.28198 – 0.28203. Zircon cores from sample PC12.3 exhibit U-Pb dates between 676±4 Ma – 611±3 Ma and $^{176}Hf/^{177}Hf_{(t)}$ ratios between 0.28198 – 0.28200, and zircon rims (n = 16) present U-Pb dates between 691±3 Ma – 597±3 Ma (a single outlier at 734±5 Ma) and $^{176}Hf/^{177}Hf_{(t)}$ ratios between 0.28198 – 0.28202. Population

III comprise zircon crystals from sample PC12.2 only, with core (n = 21) U-Pb dates between 786±8 Ma – 621±4 Ma and $^{176}Hf/^{177}Hf_{(t)}$ ratios between 0.28204 – 0.28213, while rims (n = 5) present U-Pb dates between 783±4 Ma – 591±8 Ma and $^{176}Hf/^{177}Hf_{(t)}$ ratios between 0.28205 – 0.28208. Population IV also comprise only zircon crystals from sample PC12.2, with core (n = 18) U-Pb dates between 776±14 Ma – 620±3 Ma and $^{176}Hf/^{177}Hf_{(t)}$ ratios between 0.28214 – 0.28224, while rims (n = 2) exhibit U-Pb dates between 693±4 Ma – 657±2 Ma and $^{176}Hf/^{177}Hf_{(t)}$ = 0.28223.

All four populations exhibit little variation between uncorrected $\varepsilon Hf_{(t)}$ values for their respective zircon cores and rims (Table 1), and partial overlaps are observed between populations I and II and populations III and IV (Figure 8H, Table 1). Corrected $\varepsilon Hf_{(t)}$ values for the oldest dates in each population (excluding outliers; Figure 8I, Table 1) exhibit little to no overlaps and provide slightly less negative values: Population I (804±5 Ma), cores = -16 to -13, rims = -14 to -13; Population II (789±10 Ma), cores =-13 to -9, rims = -11 to -9; Population III (786±8 Ma), cores = -9 to -5, rims = -9 to -8; Population IV (776±14 Ma), cores = -5 to -2, rims = -2. If zircon crystals from the biotite-bearing pink leucosome are considered separately, corrected $\varepsilon Hf_{(t)}$ values for the oldest zircon rim (691±3 Ma) range between $\varepsilon Hf_{(691)}$ = -13 to -11 (Figure 8H).

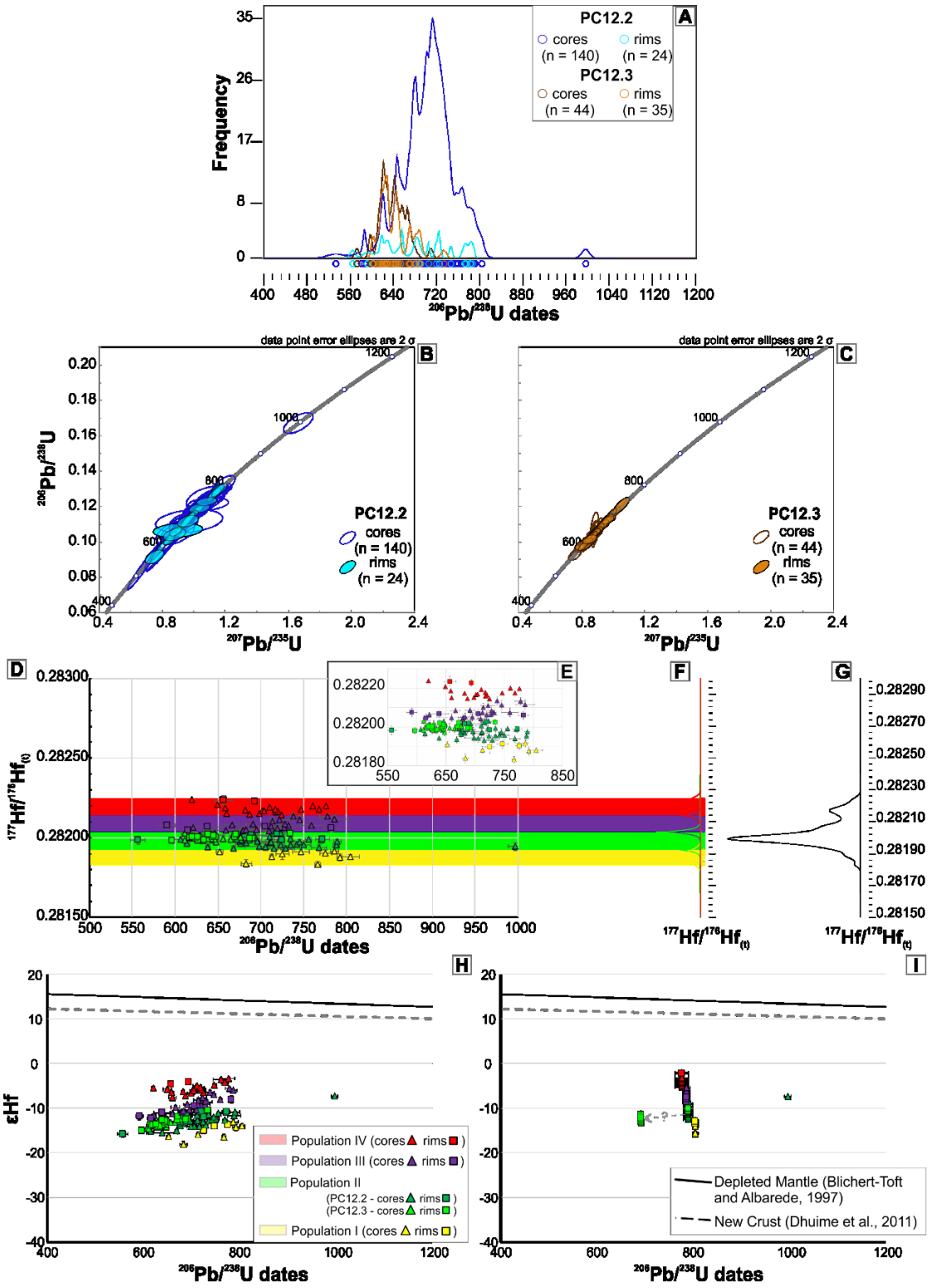

Figure 5-8 - Isotopic data from analyzed zircons in the hornblende-biotite stromatic metatexite (PC12.2) and biotite-bearing pink leucosome (PC12.3) samples. A) $^{206}Pb/^{238}U$ probability density plot (PDP) for cores and rims of both samples (color schemes are the same of the Concordia diagram, BC). B) Concordia diagrams for cores (dark blue ellipses) and rims (light blue ellipses) from sample PC12.2. C) Concordia diagrams for cores (dark brown ellipses) and rims (light brown ellipses) from sample PC12.3. D-G) $^{176}Hf/^{177}Hf_{(t)}$ ratios x $^{206}Pb/^{238}U$ dates (D) and detailed inset I. F-G) Probability density plot (PDP) for $^{176}Hf/^{177}Hf_{(t)}$ ratios from each population (F) and the whole sample (G). Four zircon populations can be identified (Population I, yellow;

Population II, green; Population III, purple; Population IV, red). H-I) εHf ratios x $^{206}Pb/^{238}U$ dates for each population compared to the depleted mantle (Blichert-Toft and Albarède, 1997) and new crust (Dhuime et al., 2011) evolution trend. (H) exhibit the uncorrected ratios considering individual zircon dates, while (I) exhibit ratios corrected for the oldest zircon grain in each population (outliers excluded).

4.3 Garnet-biotite stromatic metatexite (PC12.4) and garnet-bearing white leucosome (PC12.5)

The garnet-biotite stromatic metatexite (PC12.4) exhibits a sharp layering consisting of mesocratic bands interleaved with leucocratic bands. Mesocratic bands (Figure 5A) are composed of garnet (5 – 15%), biotite (15 – 25%), plagioclase (25 – 35%), K-feldspar (predominantly orthoclase, locally microcline; 10 – 20%) and quartz (10 – 20%). Leucocratic bands (Figure 5B) are fine- to coarse- grained, composed of garnet (0 – 5%), biotite (green and brown, 0 – 5%), plagioclase (40 – 45%), K-feldspar (orthoclase and microcline, often perthitic; 30 – 35%) and quartz (25 – 30%). Green biotite is usually found at the borders or along fractures in garnet, and rare late muscovite is associated with partial replacement of feldspars. Minor amounts of apatite and zircon are observed.

Zircon cores (n = 76) (Figure 6) exhibit a range of U-Pb dates between 839±8 Ma to 580±17 Ma (Figure 9A, B), and outliers include younger grains (between 543±13 Ma and 429±15 Ma) as well as an older one (1140±36 Ma). Three main peaks were calculated through a PDP: ca. 745 Ma, ca. 720 Ma and ca. 625 Ma. Zircon rims (n=27) (Figure 6) exhibit a range of U-Pb dates between 829±8 Ma and 582±18 Ma (Figure 9A, B), with three outliers (870±15 Ma, 567±13 Ma and 526±11 Ma). Four main peaks were identified through the probability density plot: ca. 720 Ma, ca. 665 Ma, ca. 625 Ma and ca. 585 Ma.

The garnet-bearing white leucosome (PC12.5) is composed of garnet (5 – 10%), Kfeldspar (microcline>perthitic orthoclase; 35 – 45%), plagioclase (rare antiperthite; 28 – 35%) and quartz (15 – 30%) (Figure 5C, D). Minor biotite, muscovite, zircon, apatite and opaque minerals are observed.

Zircon cores (n=41) (Figure 6) exhibit a main range of U-Pb dates from 661±4 Ma to 572±2 Ma (Figure 9A, C), and four peaks were calculated through a PDP: ca. 650 Ma, ca. 630 Ma, ca. 610 Ma and ca. 585 Ma. Outliers include younger grains (ranging from 547±8 Ma to 483±18 Ma) as well as older ones (738±8 Ma and 721±9 Ma). Zircon rims (n=23) (Figure 6) exhibit a continuous range of U-Pb dates between 663±8 Ma and

579±4 Ma (Figure 9A, C), and three younger outliers (547±8 Ma, 541±6 Ma and 508±8 Ma) were identified. Three peaks were calculated through a PDP: ca. 610 Ma, ca. 590 Ma and ca. 580 Ma.

Zircon grains from samples PC12.4 (n=66) and PC12.5 (n=20) define two distinct populations in terms of $^{176}Hf/^{177}Hf_{(t)}$ ratios (Figures 6 and 9D-G). Population I contains only zircons from sample PC12.4, presenting zircon cores (n = 47) with U-Pb dates between 816±11 Ma – 607±6 Ma and $^{176}Hf/^{177}Hf_{(t)}$ ratios between 0.28239 – 0.28251 (Figures 9D-I). Zircon rims (n = 10) are constrained within similar ranges (U-Pb dates between 829±8 Ma – 632±3 Ma; $^{176}Hf/^{177}Hf_{(t)}$ = 0.28238 – 0.28251). Three outliers exhibit $^{176}Hf/^{177}Hf_{(t)}$ ratios outside those ranges (0.28233, 0.28236 and 0.28256)Population II is constrained mostly by zircons from sample PC12.5, with cores (n = 17) exhibiting U-Pb dates between 661±4 Ma – 572±2 Ma and $^{176}Hf/^{177}Hf_{(t)}$ ratios between 0.28208 – 0.28218, while the single analyzed rim falls into the same ranges . A grain with a higher $^{176}Hf/^{177}Hf_{(t)}$ ratio (0.28228) was considered an outlier. A grain from sample PC12.4 exhibits $^{176}Hf/^{177}Hf_{(t)}$ = 0.28219 (inside the range for Population II) but was considered an outlier in terms of its U-Pb date (774±7 Ma). Eight zircon grains exhibit $^{176}Hf/^{177}Hf_{(t)}$ ratios scattered between 0.28151 and 0.28256 and were also considered outliers.

Uncorrected $\varepsilon Hf_{(t)}$ values also mark a considerable difference between both populations:

Population I exhibit $\varepsilon Hf_{(t)}$ between +0 and +7, while Population II exhibits $\varepsilon Hf_{(t)}$ between -13 and -7 (Table 1; Figure 9H). Recalculated $\varepsilon Hf_{(t)}$ values for the oldest core dates in each population (Figure 9I) provided: Population I (816±11 Ma) with $\varepsilon Hf_{(816)}$ between +4 and +9 for cores and +4 to +8 for rims ; and Population II (661±4 Ma) with $\varepsilon Hf_{(661)}$ between -10 and -7.

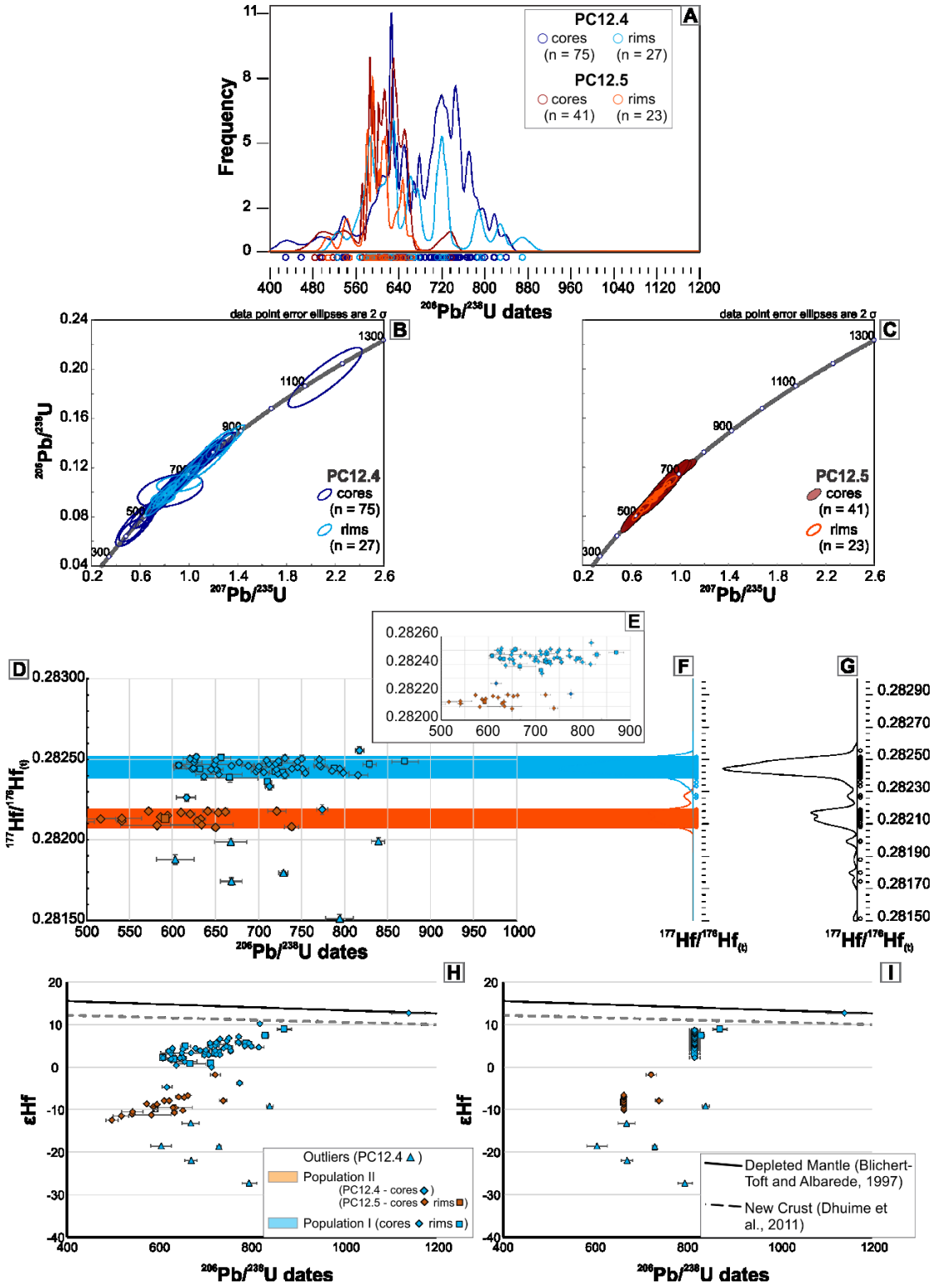

Figure 5-9 - Isotopic data from analyzed zircons in the garnet-biotite stromatic metatexite (PC12.4) and garnet-bearing white leucosome (PC12.5) samples. A) $^{206}Pb/^{238}U$ probability density plot (PDP) for cores and rims of both samples (color schemes are the same of the Concordia diagram, B-C). B) Concordia diagrams for cores and rims (dark blue and light blue ellipses, respectively) from sample PC12.4. C) Concordia diagrams for cores and rims (red and orange ellipses, respectively) from sample PC12.5. D-G) $^{176}Hf/^{177}Hf_{(t)}$ ratios x $^{206}Pb/^{238}U$ dates (D) compared to the PDP for $^{176}Hf/^{177}Hf_{(t)}$ ratios from each population (F) and the whole sample (G). Two zircon populations can be identified (Population I, orange; Population II,

blue). E) Detailed inset on (D). H-I) εHf ratios x $^{206}Pb/^{238}U$ dates for each population compared to the depleted mantle (Blichert-Toft and Albarède, 1997) and new crust (Dhuime et al., 2011) evolution trend. (H) exhibit the uncorrected ratios considering individual zircon dates, while (I) exhibit ratios corrected for the oldest zircon grain in each population (outliers excluded).

4.4 (Hornblende)-biotite stromatic metatexite (C1071A)

The (hornblende)-biotite stromatic metatexite exhibits a layering marked by mesocratic (gray) and leucocratic (pink to gray) bands (Figure 5E, F). It is composed of hornblende (0 – 5%), biotite (5 – 20%), perthitic microcline (20 – 40%), plagioclase (15 – 35%) and quartz (15 – 30%), with minor apatite, opaque minerals and zircon (Figure 5E, F). Hornblende, when observed, is partially replaced by biotite-plagioclase-quartz (±opaque minerals) symplectites.

Zircon cores (n=58) (Figure 6) exhibit a continuous range of U-Pb dates between 719±15 Ma and 564±6 Ma (Figure 10A, B). Older spots (869±7 Ma, 816±7 Ma and 777±6 Ma) as well as younger ones (between 551±8 Ma and 528±5 Ma) constitute outliers. Three main peaks were calculated through a PDP: ca. 678 Ma, ca. 637 Ma and ca. 622 Ma. The U-Pb dates from zircon rims (n=20) (Figure 6) range from 680±8 Ma to 603±6 Ma (Figure 10A, B). Outliers include three younger spots (566±5 Ma, 536±5 Ma and 532±5 Ma) and three older ones (728±6 Ma, 713±4 Ma and 708±4 Ma)

Zircon grains show similar Hf isotopic signature, therefore composing one population

(Figure 10C-E). Cores (n = 55) show $^{176}Hf/^{177}Hf_{(t)}$ ratios between 0.28210 – 0.28223

(Figure 9C, D), U-Pb dates between 719±15 Ma – 564±6 Ma, and εHf values between 11 and -4 (Figure 10F), while rims (n = 6) are constrained within similar ranges (Table 1). Three outliers presented $^{176}Hf/^{177}Hf_{(t)}$ between 0.28205 – 0.28208 and εHf between 10 and -11, and two outliers presented $^{176}Hf/^{177}Hf_{(t)}$ between 0.28225 – 0.28226 and εHf between -5 and -4. Recalculated $\varepsilon Hf_{(t)}$ for the oldest core date (ca. 719 Ma, Figure 10G) provided $\varepsilon Hf_{(719)}$ values between -8 and -4 for cores and between -7 and -3 for rims.

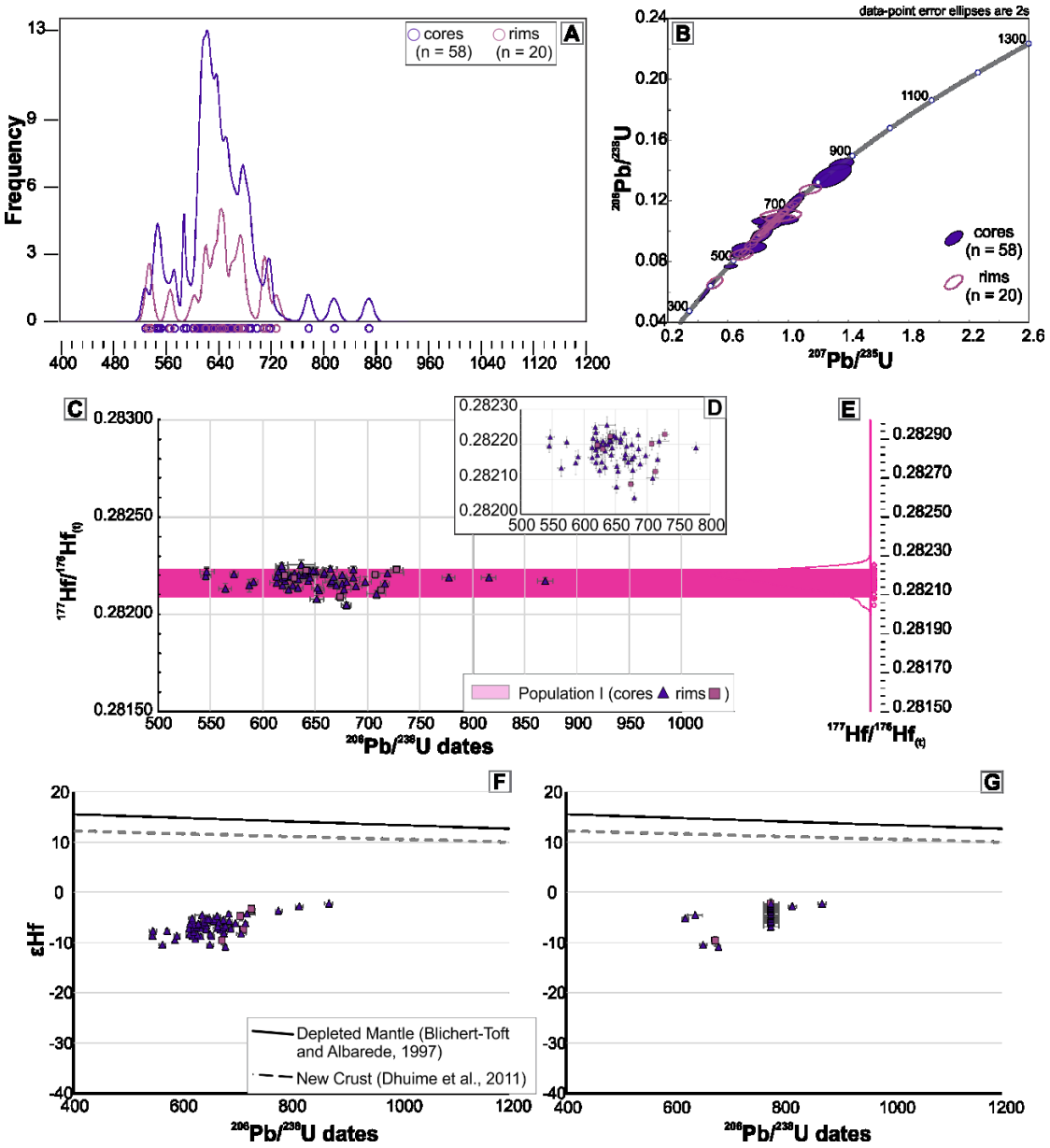

Figure 5-10 - Isotopic data from analyzed zircon in the (hornblende-)biotite-stromatic metatexite (C1071A). A) $^{206}Pb/^{238}U$ probability density plot (PDP) for cores (pink) and rims (brown). B) Concordia diagrams for cores and rims (same color scheme as A). C-E) $^{176}Hf/^{177}Hf_{(t)}$ ratios x $^{206}Pb/^{238}U$ dates I compared to the PDP for $^{176}Hf/^{177}Hf_{(t)}$ ratios (D). A single population of zircons can be identified (highlighted by a pink). E) Detailed inset on I. F-G) εHf ratios x $^{206}Pb/^{238}U$ dates compared to the depleted mantle (Blichert-Toft and Albarède, 1997) and new crust (Dhuime et al., 2011) evolution trend. (F) exhibit the uncorrected ratios considering individual zircon dates, while (G) exhibit ratios corrected for the oldest zircon grain in the population (outliers excluded).

5 Discussion

As a noteworthy feature observed on all analyzed samples, zircon U-Pb spot data smears along the concordia curve. Both date groups and $^{176}Hf/^{177}Hf_{(t)}$ ratios showed no correlation to specific CL domains or zircon textures (Figure 6). Those evidences, associated with the linear horizontal trends defined by zircon populations

in $^{176}Hf/^{177}Hf_{(t)}$ ratios versus $^{206}Pb/^{238}U$ dates plots point to a disturbance in the U-Pb system marked by concealed Pb loss, which is characteristic, but not exclusive, of rocks affected by HTUHT metamorphism (Whitehouse and Kemp, 2010; Taylor et al., 2016; Andersen et al., 2019). Because the SGN records HT-UHT metamorphic conditions, we interpret that the protracted U-Pb record observed is most likely related to a (ultra)high-temperature event.

5.1 Minimum crystallization ages, identification of the protolith and protosources

5.1.1 Amphibolite enclave (sample PC12.1)

The amphibolite enclave (PC12.1) provides a good example to reassure the systematics of the U-Pb and Lu-Hf systems in the context of the studied area. Although it is an orthoderived rock, $^{206}Pb/^{238}U$ dates spread from 782±25 Ma to 605±28 Ma, exhibiting a considerable range of ca. 177 Ma for an igneous rock (cores Figures 7, 11A). All analyzed grains are constrained inside an ~0.0001 range of $^{176}Hf/^{177}Hf_{(t)}$ ratios (0.28196 – 0.28207) as expected for a single sourced igneous protolith, defining a single population. The minimum crystallization age of 782±25 Ma (Figure 11A) can be retrieved for the amphibolite protolith with a crustal Hf signature ($\varepsilon Hf_{(782)}$ between -12 and -8).

5.1.2 Hornblende-biotite stromatic metatexite and biotite-bearing pink leucosome (samples PC12.2 and PC12.3)

The hornblende-biotite stromatic metatexite (PC12.2) and biotite-bearing pink leucosome (PC12.3) exhibit a protracted record of $^{206}Pb/^{238}U$ dates spreading concordantly between ca. 805 Ma and ca. 580 Ma. Though several statistical peaks were identified (Figure 8A), those are not related to specific $^{176}Hf/^{177}Hf_{(t)}$ ranges. Considering the full range of $^{176}Hf/^{177}Hf_{(t)}$ ratios (0.28183 – 0.28225) four zircon populations were identified (Figure 8D-H; Figure 11B; Table 1). The presence of four distinct $^{176}Hf/^{177}Hf_{(t)}$ signatures defines four zircon populations (c.f. Tedeschi et al., 2023) indicating a paraderived origin for the hornblende-biotite stromatic metatexite. Similar mineral assemblages are observed in paraderived rocks with metagraywacke composition (e.g., El-Naby and Frisch, 2006; Santiago et al., 2022). As the main trend of U-Pb dates did not include grains older than ca. 804 Ma, the 997±7 Ma date more likely represents an underrepresented source or an inherited/assimilated grain.

As discussed by Tedeschi et al. (2023) and observed in the orthoderived sample (amphibolite enclave, PC12.1), an igneous protolith without evidence for

magma mixing and/or assimilation of xenoliths would most probably provide a single population of zircon grains well constrained inside a variation in the fourth decimal place (~0.0001) of $^{176}Hf/^{177}Hf_{(t)}$ ratios. Thus, it is less probable that this rock has an igneous protolith.

Four different protosources (and their minimum crystallization ages, Figure 11B) can be identified: Protosource I, with a minimum crystallization age of 804±5 Ma ($^{176}Hf/^{177}Hf_{(804)}$ = 0.28183 – 0.28192, $\varepsilon Hf_{(804)}$ = -16 to -13); Protosource II, with a minimum crystallization age of 789±10 Ma ($^{176}Hf/^{177}Hf_{(789)}$ = 0.28193 – 0.28203, $\varepsilon Hf_{(789)}$ = -13 to -9); Protosource III, with a minimum crystallization age of 786±8 Ma ($^{176}Hf/^{177}Hf_{(786)}$ = 0.28204 – 0.28213, $\varepsilon Hf_{(786)}$ = -9 to -5); and Protosource IV, with a minimum crystallization age of 776±14 Ma ($^{176}Hf/^{177}Hf_{(776)}$ = 0.28214 – 0.28224, $\varepsilon Hf_{(776)}$ = -5 to -2). As such, a metasedimentary protolith is indicated for the hornblende-biotite stromatic metatexite.

The biotite-bearing pink leucosome (PC12.3) exhibits the same isotopic signature than Population II from the hornblende-biotite stromatic metatexite, which is indicative that the leucosome is genetically associated to the metatexite (e.g., instead of being an allochtonous granite). The similarities between the isotopic signature of the leucosome and that of Protosource II might be an effect of the availability of zircons related to that protosource (roughly 46% of the zircon grains from sample PC12.2, see Table 1) on the protolith. However, the oldest zircon grain from Population II less likely provide a minimum crystallization age for the leucosome as it would provide an age older than that of Protosources III and IV. If Population II is considered as representative of the leucosome, two hypotheses can be pointed out: i) the minimum crystallization age for Protosources III and IV is too low and the isotopic composition of older zircon cores were not preserved; ii) older zircon grains in this Population were inherited from the metatexite and thus cannot be used to determine the minimum crystallization age. In a more conservative approach Protosource II and the leucosome are treated separately, thefore the oldest rim from sample PC12.3 is considered as representative of the minimum crystallization age for the leucosome (691±3 Ma; $^{176}Hf/^{177}Hf_{(691)}$ = 0.28197 – 0.28203, $\varepsilon Hf_{(691)}$ = -13 to -11) (Figure 11B).

The four protosources lie in a relatively narrow range of minimum crystallization ages, suggesting that i) the protoliths were crystallized within a narrow

age interval or ii) the zircon populations do not preserve the older dates related to crystallization, reflecting the metamorphism instead.

As the Socorro-Guaxupé Nappe is interpreted to represent the roots of a Neoproterozoic magmatic arc and related metasedimentary rocks, the first hypothesis would agree with the regional geological context (e.g., Campos Neto and Figueiredo 1995; Vinagre et al., 2014; Rocha et al., 2018; Tedeschi et al., 2018). Considering the youngest corrected age between the protosources, a maximum depositional age of ca. 776 Ma can be determined for the protolith of this sample (Figure 11B), based on the minimum crystallization age of Protosource IV.

5.1.3 Garnet-biotite stromatic metatexite and garnet-bearing white leucosome (samples PC12.4 and PC12.5)

The garnet-biotite stromatic metatexite (PC12.4) and the garnet-bearing white leucosome (PC12.5) exhibit a protracted record of concordant zircon $^{206}Pb/^{238}U$ dates from ca. 839 Ma to ca. 580 Ma. Statistical peaks for U-Pb dates do not correspond to specific ranges of $^{176}Hf/^{177}Hf_{(t)}$ ratios. Considering the $^{176}Hf/^{177}Hf_{(t)}$ ratios, two zircon populations were identified: Population I, presenting core U-Pb dates between 816±11 Ma and 607±6 Ma, $^{176}Hf/^{177}Hf_{(t)}$ ratios between 0.28236 – 0.28251 and εHf values between +0 and +7; Population II with core U-Pb dates between 661±4 Ma and 572±2 Ma, $^{176}Hf/^{177}Hf_{(t)}$ ratios between 0.28208 – 0.28219, and εHf between -13 and -7.

Due to the presence of garnet and biotite in its mineral assemblage indicating a more aluminous composition that suggests a sedimentary protolith, it would be expected that the garnet-biotite stromatic metatexite (sample PC12.4) provided several $^{176}Hf/^{177}Hf_{(t)}$ populations. A single population (Population I), however, comprises most of the observed zircon record (57 of 66 grains, ~86%). The difference in $^{176}Hf/^{177}Hf_{(t)}$ ratios observed between this metatexite and the garnet-bearing white leucosome (sample PC12.5) might be a consequence of Hf partitioning between garnet (or other phases) and zircon during partial melting reactions (e.g., Gerdes and Zeh, 2009; Taylor et al., 2016; Finch et al., 2021). It is also possible, however, that the garnet-bearing white leucosome actually corresponds to injection of granitic material derived from a different source. Considering this hypothesis, the garnet-bearing white “leucosome” should be considered a garnet-bearing granite with a minimum crystallization age of 661±4 Ma ($^{176}Hf/^{177}Hf_{(661)}$ = 0.28208 – 0.28218; $\varepsilon Hf_{(661)}$ = -10 – -7) (Figure 11C), though additional data (field relations and geochemistry) would be needed in order to support such interpretation.

The single zircon population identified in the garnet-biotite stromatic metatexite might be indicative of an igneous protolith, with a minimum crystallization age of ca. 816 Ma Ma ($^{176}Hf/^{177}Hf_{(816)}$ = 0.28236 – 0.28251 ; $\varepsilon Hf_{(816)}$ = +3 to +9) (Figure 11C). Alternatively, it could represent a sedimentary protolith derived from a single protosource (Protosource V), thus indicating a deposition in a restricted environment and a maximum depositional age of ca. 816 Ma. The works of Westin et al. (2016) and Santiago et al. (2022) provide examples of metasedimentary rocks from restricted environments with well-defined $^{176}Hf/^{177}Hf_{(t)}$ signatures.

This minimum crystallization age is considerably older than other protolith crystallization ages in the Socorro-Guaxupé Nappe (ca. 790-640 Ma; Campos-Neto and Figueiredo, 1995; Campos Neto and Caby, 2000; Mora et al., 2014; Rocha et al., 2017, 2018; Tedeschi et al., 2018; Motta et al., 2021). Nonetheless, similar ages (ca. 797 Ma) were obtained by Costa et al. (2022) for the protolith of a migmatite from the São João da Mata unit. Similar ages are also observed on the Arenópolis-Mara Rosa magmatic arc (Laux et al., 2004; Matteini et al., 2010) and on the Rio Negro-Serra da Prata magmatic arc (Santiago et al., 2020).

5.1.4 (Hornblende)-biotite stromatic metatexite (sample C1071A)

The (hornblende)-biotite stromatic metatexite (C1071A) exhibits a protracted record of $^{206}Pb/^{238}U$ dates spreading concordantly between ca. 719 Ma and ca. 564 Ma. Statistical peaks calculated for the U-Pb dates cannot be correlated to specific ranges of $^{176}Hf/^{177}Hf_{(t)}$ ratios. Most analyzed grains (56 of 61 grains – excluding outliers –, ~92%) lie in the ~0.0001 range of $^{176}Hf/^{177}Hf_{(t)}$ ratios, defining a single population of zircon grains with $^{176}Hf/^{177}Hf_{(t)}$ = 0.28210 – 0.28223, $\varepsilon Hf_{(t)}$ = -11 to -3.

As a single zircon population was identified, a minimum crystallization age of 719±15 Ma (Figure 11D) ($^{176}Hf/^{177}Hf_{(719)}$ = 0.28210 – 0.28223 and $\varepsilon Hf_{(719)}$ = -8 to -3) is interpreted for this rock. A single population of zircon grains inside a narrow range of $^{176}Hf/^{177}Hf_{(t)}$ ratios is highly suggestive of an orthoderived protolith (Figure 12).

Among the outliers, grains within two $^{176}Hf/^{177}Hf_{(t)}$ ranges were identified (0.28205 – 0.28208, n=3; and 0.28225 – 0.28226, n=2). Those grains might represent inherited zircon cores from the host rocks. The hypothesis that the protolith of this rock consists of a paraderived rock deposited in a restricted basin, thus explaining the presence of a single main population, cannot be completely ruled out.

This minimum crystallization age is younger (~100 Ma – 60 Myr) than those identified among other samples, although it is still constrained within the magmatic arc

ages found on the Socorro-Guaxupé Nappe. This sample has a similar composition to the hornblende-biotite stromatic metatexite (PC12.2) and exhibit Hf signature similar to one of its zircon populations (Population IV: $^{176}Hf/^{177}Hf_{(t)}$ = 0.28214 – 0.28224, and $\varepsilon Hf_{(t)}$ = -8 to -3). Thus, it is either possible this rock served as one of the sources for the protolith of the hornblende-biotite stromatic metatexite or that both share the same protosource, and the difference between minimum crystallization ages (~60 Ma) is an effect of the lack of preservation of the true age of the protolith of the (hornblende)-biotite stromatic metatexite.

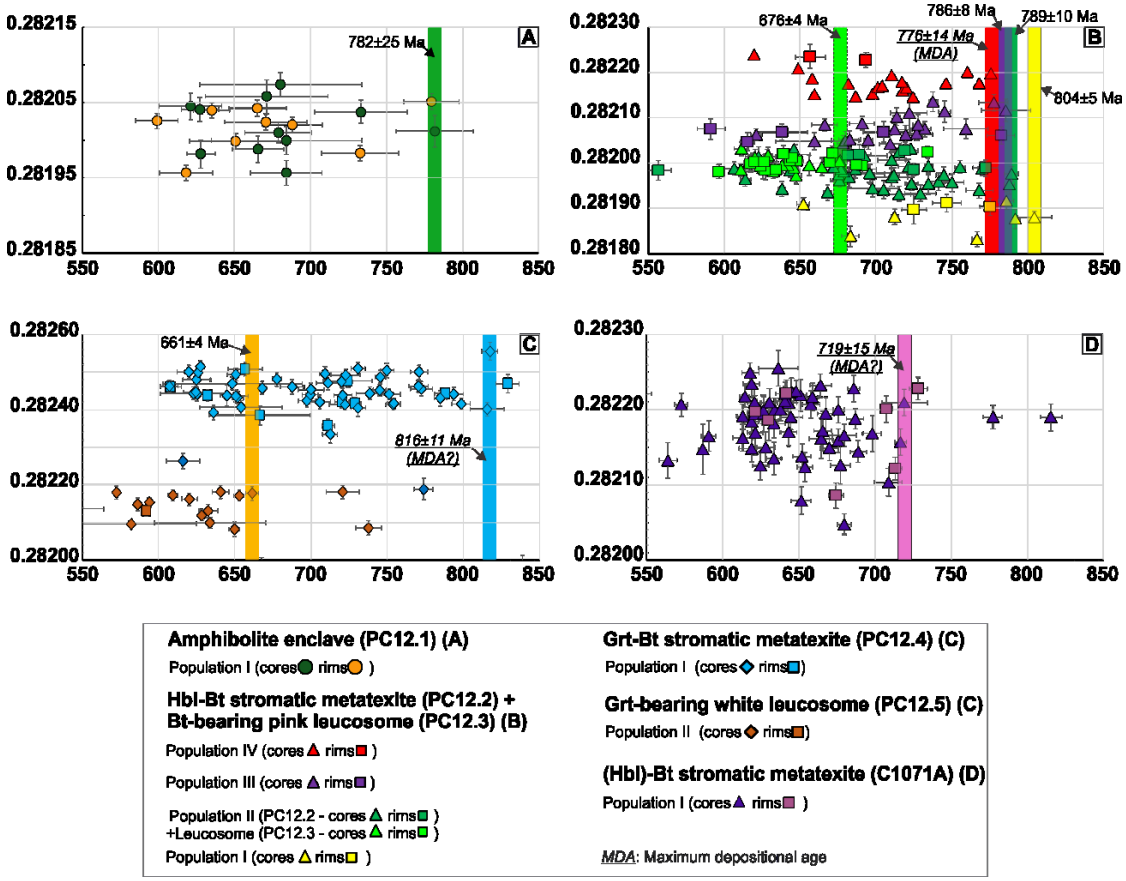

Figure 5-11 - Minimum crystallization ages for the protosources of the rocks analyzed in this work, as well as an estimate of the maximum depositional ages for the paraderived samples. (A) Amphibolite enclave (PC12.1). (B) Hornblende-biotite stromatic metatexite (PC12.2) and biotite-bearing pink leucosome (PC12.3). (C) Garnet-biotite stromatic metatexite (PC12.4) and garnet-bearing white leucosome (PC12.5, see text). (D) (Hornblende-)biotite stromatic metatexite (C1071A).

5.2 Correlations between the amphibolite enclave (Sample PC12.1) and other orthoderived protosources

The Hf isotopic signature from the amphibolite enclave (Sample PC12.1; Figures 12, 13, 14A and 15A) exhibit an almost complete overlap with a banded granulite (C838A) from the Elói Mendes unit (Tedeschi et al., 2018), and partial

overlaps are also observed with an opdalite (C832) from the Elói Mendes unit (Tedeschi et al., 2018) and the charnockites from the Paraguaçu suite (Motta, 2018) (Supplementary data 4). While the minimum crystallization age obtained for the amphibolite enclave (782±25 Ma) differs significantly from those of the banded granulite (691±3 Ma; Tedeschi et al., 2018), it is very similar to the minimum crystallization age of the opdalite (786±10 Ma; Tedeschi et al., 2018). The crustal signature indicated by the Hf isotopes suggests that the amphibolite enclave was formed through the crystallization of a magma derived from the anatexis of the lower crust, similarly to the opdalite and the banded granulite, or that it was derived from a contaminated mafic source.

5.3 Provenance assessment and correlations with sources from the Brasília and Ribeira orogens

A comparison between the $^{176}Hf/^{177}Hf_{(t)}$ ratios versus U-Pb dates (Figures 12 and 14) and $\varepsilon Hf_{(t)}$ ratios versus U-Pb dates (Figures 13 and 15) obtained in this work and the spectra presented in previous works for both ortho and paraderived rocks in the Southern Brasília and Ribeira orogens is presented below (see also Supplementary data 4).

The samples analyzed in this work present horizontal to sub-horizontal trends in $^{176}Hf/^{177}Hf_{(t)}$ ratios versus U-Pb dates diagrams (Figures 7-11, Figure 12), as observed in both individual samples and groups of samples from the São Vicente and Pouso Alegre Complexes (Cioffi et al., 2016a; Westin et al., 2016), Socorro-Guaxupé Nappe (Mora et al., 2014; Tedeschi et al., 2018; Motta, 2018; Motta et al., 2021; Costa et al., 2022), Arenópolis-Mara Rosa magmatic arc (Matteini et al., 2010) and Rio Negro-Serra da Prata magmatic arc (Santiago et al., 2020, 2022) (Figures 12 and 14). In opposition, the spectra observed both for individual samples and groups of samples in the Andrelândia (Frugis et al., 2018; Kuster et al., 2020; Marimon et al., 2021), Carrancas (Westin et al., 2019; Marimon et al., 2020, 2021), Liberdade (Frugis et al., 2018) and Lima Duarte (Kuster et al., 2020) nappes exhibit a prominent slope (Figure 12).

Correlations can be observed both in $^{176}Hf/^{177}Hf_{(t)}$ ratios versus U-Pb dates (Figures 12, 14) and $\varepsilon Hf_{(t)}$ ratios versus U-Pb dates diagrams (Figures 13 and 15) between the analyzed samples and rocks from the Socorro-Guaxupé Nappe (Mora et al., 2014; Tedeschi et al., 2018; Motta, 2018; Motta et al., 2021; Costa et al., 2022), São Roque domain (Balis et al., 2020), Arenópolis-Mara Rosa and Rio Negro-Serra

da Prata magmatic arcs (Matteini et al., 2010; Santiago et al., 2020, 2022). Only partial overlaps are observed between the analyzed samples and the spectra for samples from the Andrelândia, Carrancas, Liberdade and Lima Duarte nappes (Figures 12, 13, 14 and 15). No overlap is observed between analyzed samples and the data from the São Vicente and Pouso Alegre complexes (Cioffi et al., 2016; Westin et al., 2016) (Figures 12 and 13). This suggests that among the samples analyzed in this work a main contribution from sources that belong to the magmatic arc domain (Socorro-Guaxupé Nappe and São Roque domain) can be identified (Figures 12, 13, 14 and 15). Little contribution can be detected from sources observed in the zircon record from the accretionary prism-foreland (Andrelândia and Liberdade nappes) and passive margin (Carrancas and Lima Duarte nappes, São Vicente and Pouso Alegre Complexes) domains, as well as from the Arenópolis-Mara Rosa and Rio Negro-Serra da Prata magmatic arcs (Figures 12, 13, 14 and 15).

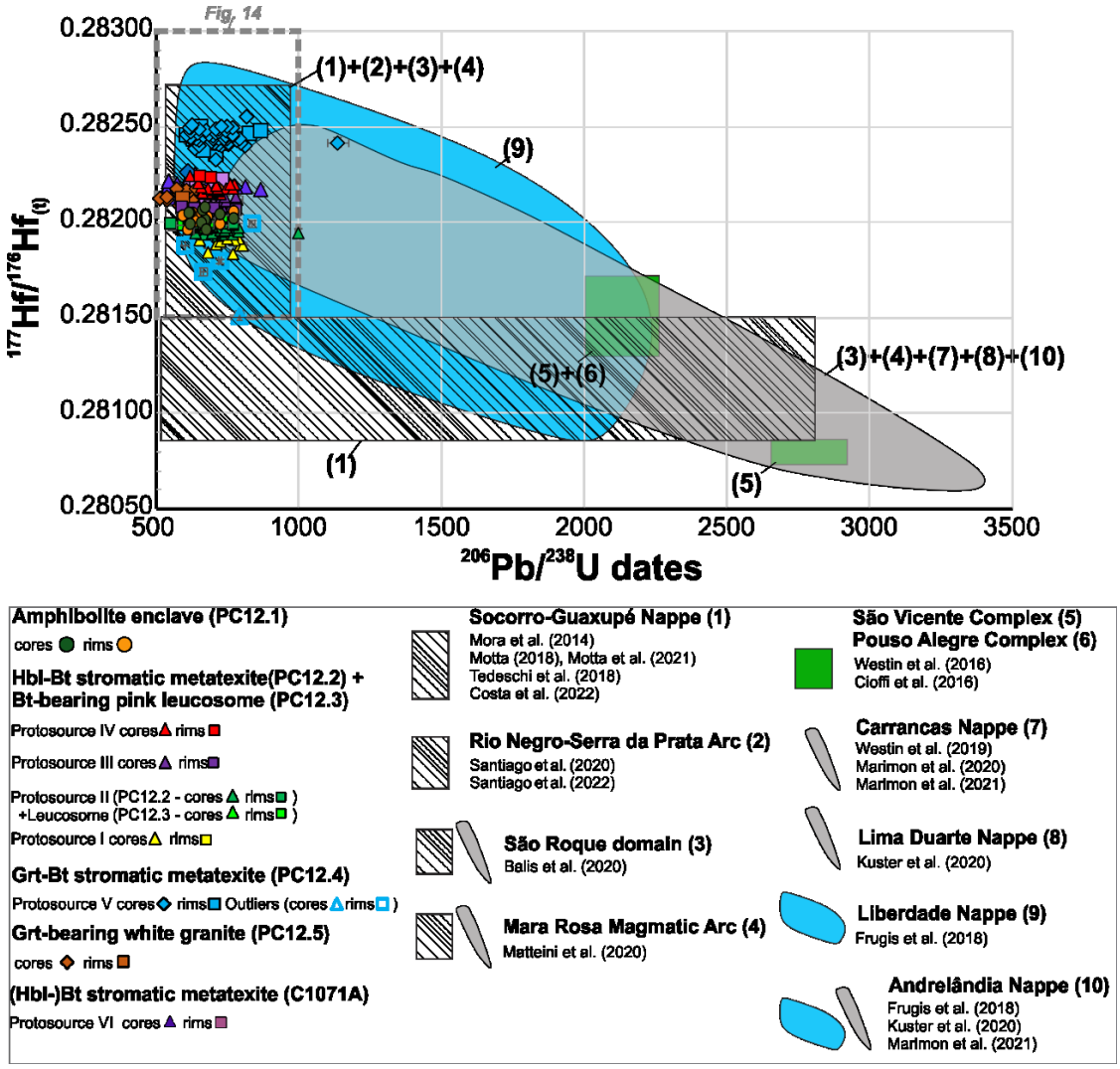

Figure 5-12 - Comparison between $^{176}Hf/^{177}Hf_{(t)}$ ratios x U-Pb dates from the samples analyzed in this work and the spectra obtained in previous works for the: Pouso Alegre (Cioffi et al., 2016) and São Vicente (Westin et al., 2016) complexes; Lima Duarte (Kuster et al., 2020), Liberdade (Frugis et al., 2018), Andrelândia (Frugis et al., 2018; Kuster et al., 2020; Marimon et al., 2021), Carrancas (Westin et al., 2019; Marimon et al., 2020, 2021) and Socorro-Guaxupé (Mora et al., 2014; Tedeschi et al., 2018; Motta, 2018; Motta et al., 2021; Costa et al., 2022) nappes; São Roque domain (Balis et al., 2020); Rio Negro-Serra da Prata (Santiago et al., 2020, 2022) and Mara Rosa (Matteini et al., 2010) magmatic arcs. Shaded and striped areas represent groups of samples from the indicated works.

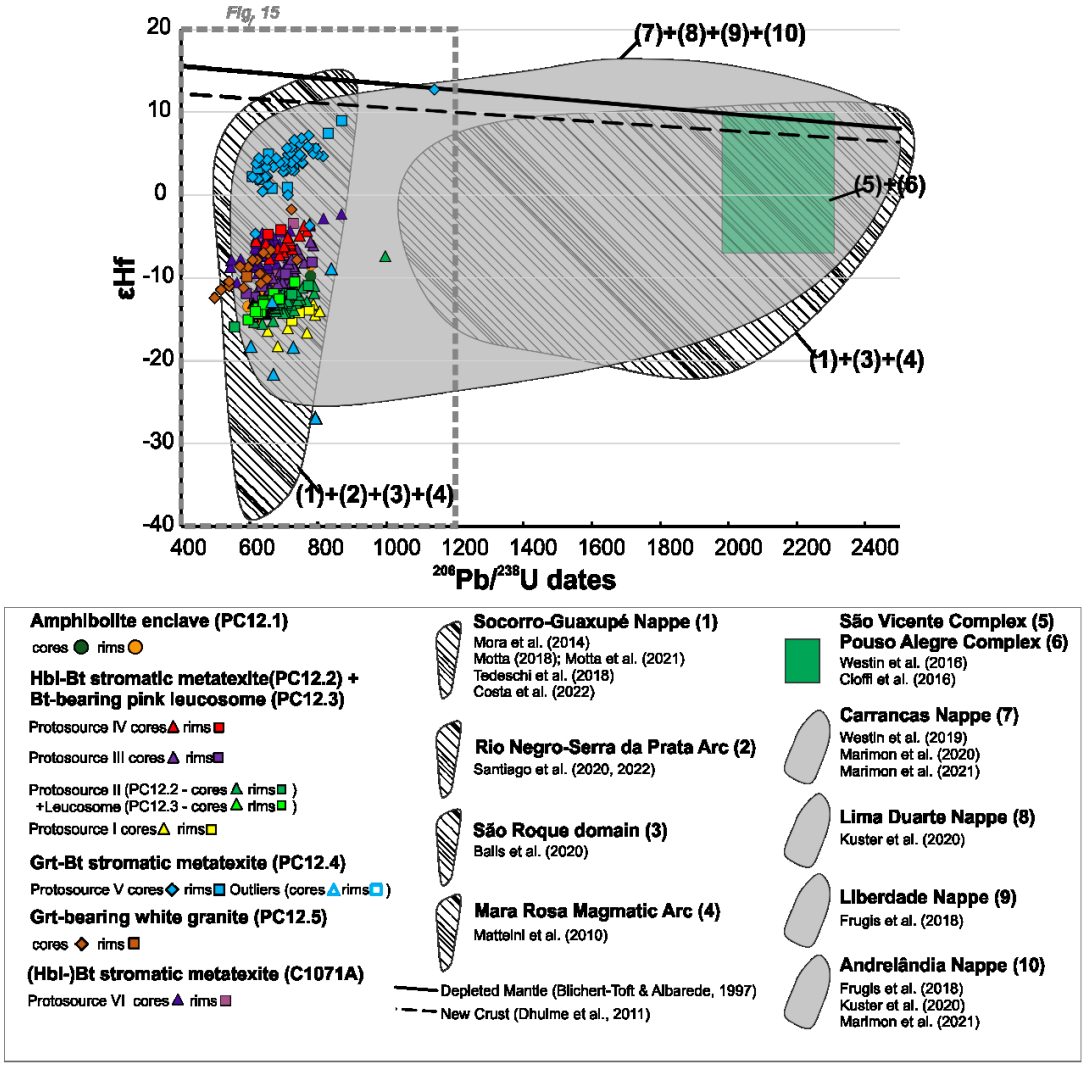

Figure 5-13 - Comparison between $\varepsilon Hf_{(t)}$ ratios x U-Pb dates from the samples analyzed in this work and samples from previous works on the: Pouso Alegre (Cioffi et al., 2016) and São Vicente (Westin et al., 2016) complexes; Lima Duarte (Kuster et al., 2020), Liberdade (Frugis et al., 2018), Andrelândia (Frugis et al., 2018; Kuster et al., 2020; Marimon et al., 2021), Carrancas (Westin et al., 2019; Marimon et al., 2020, 2021) and Socorro-Guaxupé (Mora et al., 2014; Tedeschi et al., 2018; Motta, 2018; Motta et al., 2021; Costa et al., 2022) nappes; São Roque domain (Balis et al., 2020); Rio Negro-Serra da Prata (Santiago et al., 2020, 2022) and Mara Rosa (Matteini et al., 2010) magmatic arcs. Shaded and striped areas represent groups of samples from the indicated works.

5.3.1 Hornblende-biotite stromatic metatexite (Sample PC12.2) and (hornblende)-biotite stromatic metatexite (Sample C1071A)

Among the protosources identified in the hornblende-biotite stromatic metatexite, Protosource I (804±5 Ma) exhibits only partial overlaps with the $^{176}Hf/^{177}Hf_{(t)}$ (Figure 14B) and $\varepsilon Hf_{(t)}$ (Figure 15B) signatures of the opdalite (C832) from Tedeschi et al. (2018). Protosource II (789±10 Ma) exhibits a main correlation (Lu-Hf isotopes and minimum crystallization age) with an opdalite from the Elói Mendes unit (Opdalite C832 786±10 Ma, Tedeschi et al., 2018), while partial overlaps can be traced with a banded

granulite (C838A) from the Elói Mendes suite (Tedeschi et al., 2018) and charnockites of the Paraguaçu suite (Motta, 2018) (Figures 14B, 15B). Protosource III (786±8 Ma) exhibits a similar Lu-Hf signature to that observed in a metapelite from the Serra da Boa Vista unit (Andrelândia Nappe, Frugis et al. 2018), while a partial overlap is also observed with the banded granulite (C838A) from Tedeschi et al. (2018). Protosource IV (776±14 Ma) is analogue to Protosource VI from the (hornblende)-biotite stromatic metatexite (C1071A), and it exhibits similar $^{176}Hf/^{177}Hf_{(t)}$ and $\varepsilon Hf_{(t)}$ signatures than those observed in one underrepresented population (Group 2) from the biotite-bearing granitic leucosome (São João da Mata complex) of Costa et al. (2022) (Figures 14B, 15B). Partial overlaps are also observed between the Lu-Hf signature of this protosource and that of rocks studied in the works of Tedeschi et al. (2018) (mafic granulite enclave, C716B), Motta (2018) and Motta et al. (2021) (felsic granulite, VAB01, VAB19), and Balis et al. (2020) (monzogranitic orthogneiss) (Figures 14B, 15B).

Possible explanations may be pointed out for the lack of a clear correspondence between Protosources I, III and IV and possible sources in the Socorro-Guaxupé Nappe: i) the possibility that the actual sources are not among those studied in previous works; ii) as zircon populations from rocks in the SGN have been affected by U-Pb disturbance due to HT-UHT metamorphism, the U-Pb dates represented in some of the possible sources are not representative of their actual minimum crystallization ages. It is noteworthy that although Protosource III exhibits a partial overlap with a metapelite from the syn-collisional Serra da Boa Vista unit (Frugis et al., 2018) most of the zircon populations from this unit exhibit Paleoproterozoic components (Figures 12, 13; Frugis et al., 2018). It is possible, however, that similar sources contributed to the zircon record of both rocks. The match between Protosource II and the opdalite from Tedeschi et al. (2018) is indicative that both might be derived from the same igneous suite, although a different igneous source with similar Lu-Hf signature cannot be completely disregarded as a possible source. The similarities in the isotopic record also provide an insight on the similarities between the mineral composition of the hornblende-biotite stromatic metatexite and the orthoderived rocks in the surrounding units.

5.3.2 Garnet-biotite stromatic metatexite (Sample PC12.4)

Zircon grains from the garnet-biotite stromatic metatexite are mostly constrained inside the moderately juvenile field (according to the systematics of Reimann et al.,

2010, and Bhalburg et al., 2011) in terms of their $\varepsilon Hf_{(t)}$ signature ($\varepsilon Hf_{(t)}$ = +0 to +7; $\varepsilon Hf_{(816)}$ = +3 to +9; Figure 15C). This juvenile-like signature is observed in rocks related to magmatic arcs in the Northern Brasília Orogen (Mara Rosa-Arenópolis magmatic arc; Laux et al., 2004; Matteini et al. 2010), in the Ribeira Orogen (Rio Negro-Serra da Prata magmatic arc, Santiago et al. 2020, 2022), as well as in a biotite-bearing granitic leucosome from the São João da Mata complex (Socorro-Guaxupé Nappe; Costa et al., 2022). The best correspondence is observed between $^{176}Hf/^{177}Hf_{(t)}$ (Figure 14C) and $\varepsilon Hf_{(t)}$ (Figure 15C) signatures from Protosource V (816±11 Ma) and the main population (Group 1) of the biotite-bearing granitic leucosome (Costa et al., 2022; Figures 14C and 15C), which also exhibits a similar minimum crystallization age (797±9 Ma). A partial overlap is observed with data from the Mara Rosa (Matteini et al., 2010) and Rio Negro-Serra da Prata (Santiago et al., 2022, 2022) magmatic arcs, as well as with a metagraywacke from the Santo Antônio unit (Andrelândia Nappe, Frugis et al., 2018) (Figures 14C, 15C). U-Pb ages between ca. 916 Ma – 815 Ma and a juvenile εNd signature (+1.8 to +5.4) were also obtained by Laux et al. (2004) for the Arenópolis magmatic arc.

Considering that i) the minimum crystallization age of the main protosource of the garnet-biotite stromatic metatexite (Protosource V, 816±11 Ma) is older than most magmatic arc ages found in the Socorro-Guaxupé Nappe (see section 5.1.3), and ii) the isotopic similarities between this sample and the biotite-bearing granitic leucosome discussed in Costa et al. (2022), this signature could represent sources derived from an island arc (e.g. Mara Rosa magmatic arc, Matteini et al., 2010; Rio Negro-Serra da Prata Magmatic arc, Santiago et al., 2020, 2022) or from a transitional setting between an island arc and a continental arc, as originally proposed by Campos Neto et al. (2021) for the Southern (Southernmost) Brasília Orogen (between ca. 930 – 750 Ma).

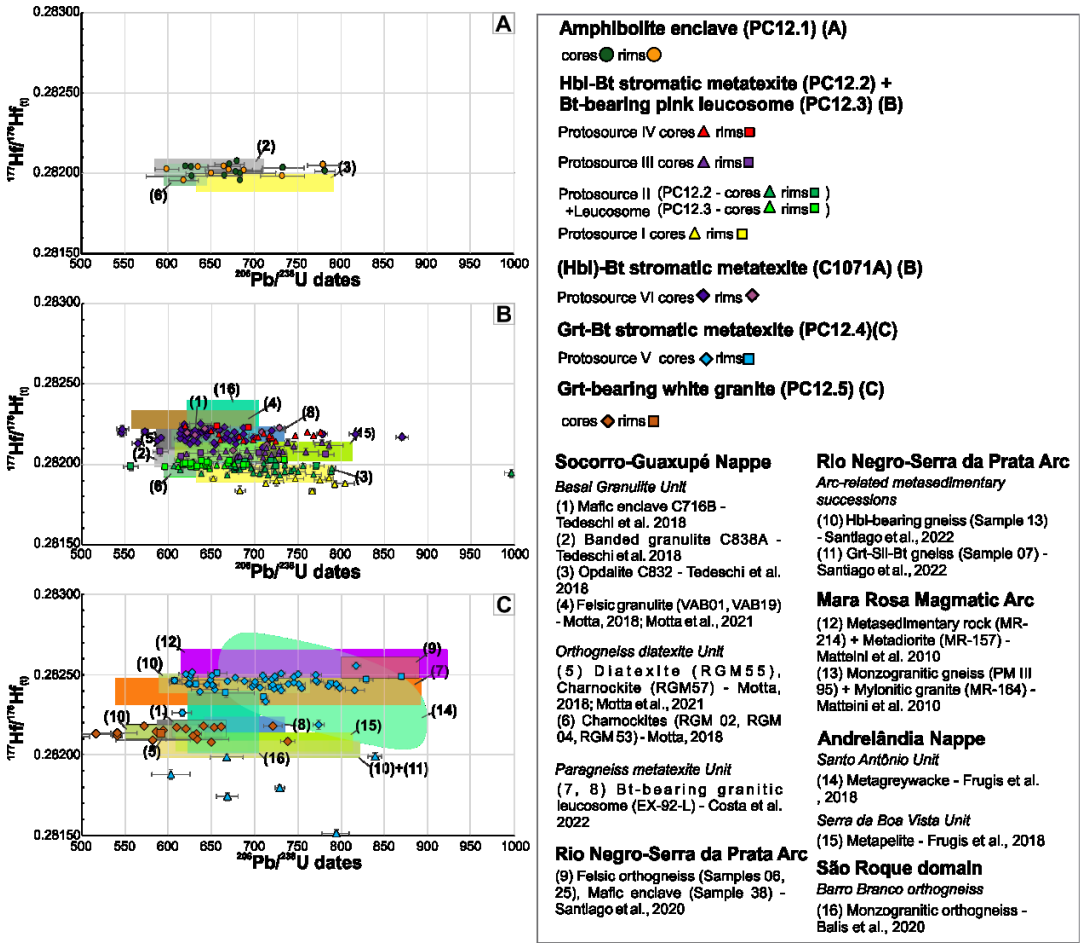

Figure 5-14 - Correlations between $^{176}Hf/^{177}Hf_{(t)}$ ratios x U-Pb dates from the samples analyzed in this work and possible sources in the: Andrelândia Nappe (Frugis et al., 2018; Kuster et al., 2020; Marimon et al., 2021); Socorro-Guaxupé Nappe (Tedeschi et al., 2018; Motta, 2018; Motta et al., 2021; Costa et al., 2022) nappes; São Roque domain (Balis et al., 2020); Rio Negro-Serra da Prata (Santiago et al., 2020, 2022) and Mara Rosa (Matteini et al., 2010) magmatic arcs. Shaded and striped areas represent groups of samples from the indicated works.

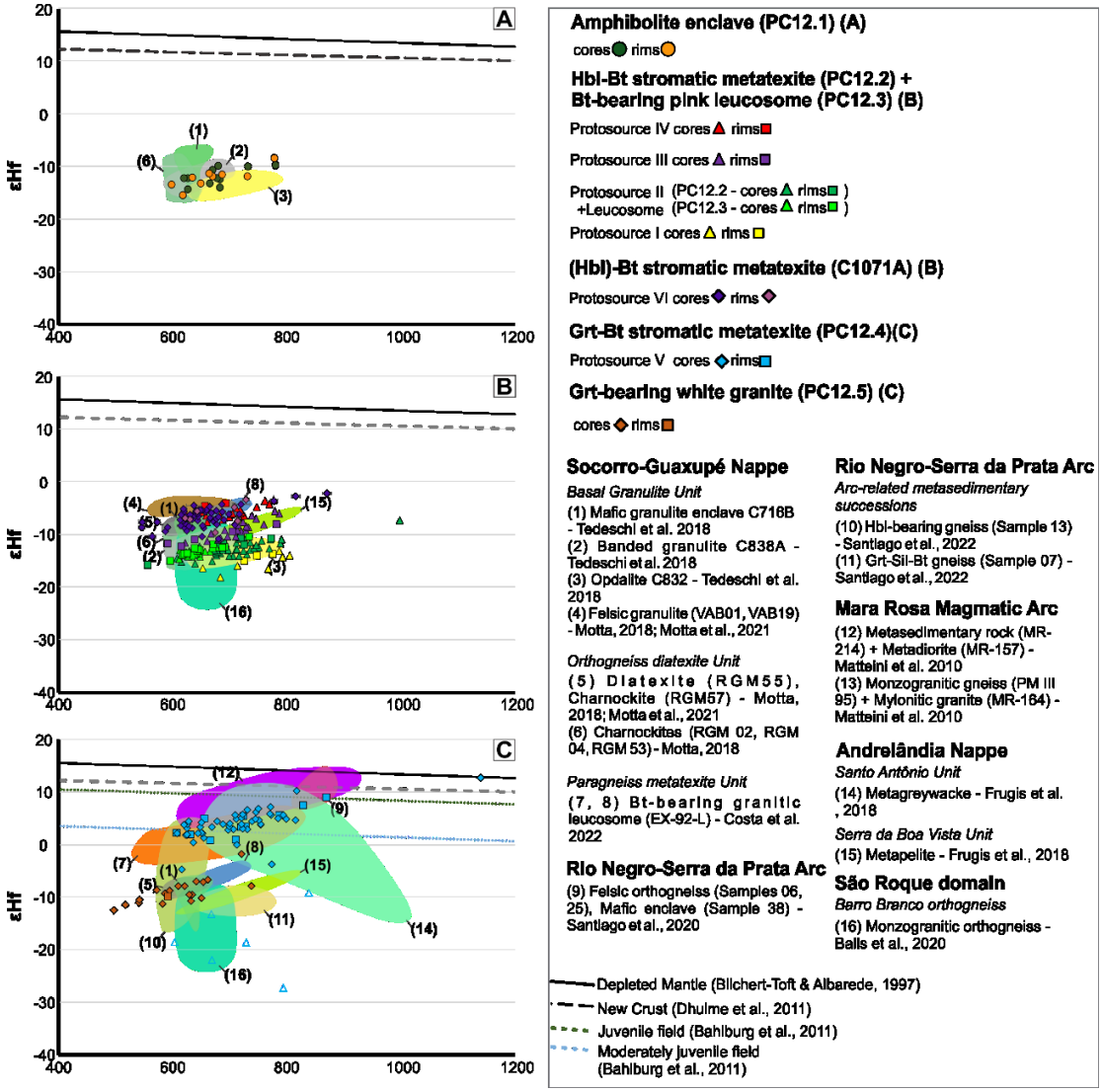

Figure 5-15 - Correlations between $\varepsilon Hf_{(t)}$ ratios x U-Pb dates from the samples analyzed in this work and possible sources in the: Andrelândia Nappe (Frugis et al., 2018; Kuster et al., 2020; Marimon et al., 2021); Socorro-Guaxupé Nappe (Tedeschi et al., 2018; Motta, 2018; Motta et al., 2021; Costa et al., 2022) nappes; São Roque domain (Balis et al., 2020); Rio Negro-Serra da Prata (Santiago et al., 2020, 2022) and Mara Rosa (Matteini et al., 2010) magmatic arcs. Shaded and striped areas represent groups of samples from the indicated works.

5.3.3 Partial melting/granite magmatism of the biotite-bearing pink leucosome (PC12.3) and garnet-bearing white leucosome (PC12.5) and possible insights for the onset of high- to ultrahigh metamorphism

Both the biotite-bearing pink leucosome (Sample PC12.3), related to the hornblende-biotite stromatic metatexite (Sample PC12.2), and the garnet-bearing white leucosome (granite?) (Sample PC12.5) exhibit younger U-Pb minimum crystallization ages (691±3 Ma and 661±4 Ma, respectively) than those observed in the protosources identified in this work. The Lu-Hf signature of the biotite-bearing pink

leucosome ($^{176}Hf/^{177}Hf_{(676)}$ = 0.28197 – 0.28203, $\varepsilon Hf_{(676)}$ = -14 to -12) is constrained inside in the range of the Protosource II of the hornblende-biotite stromatic metatexite. The signature of the garnet-bearing white leucosome (granite?) ($^{176}Hf/^{177}Hf_{(661)}$ = 0.28208 – 0.28218; $\varepsilon Hf_{(661)}$ = -10 to -7), however, is different from that observed in the garnet-biotite stromatic metatexite (sample PC12.4).

While zircon cores tend to reflect the original $^{176}Hf/^{177}Hf_{(t)}$ ratios of the source, metamorphic overgrowths and anatectic zircon might exhibit different signatures, either by additional input from external sources or metamorphic/melting reactions (e.g., Gerdes and Zeh, 2009; Taylor et al., 2016; Finch et al., 2021). It is possible, however, that the garnet-bearing white leucosome corresponds to the intrusion of S-type garnet-bearing white granite.

The minimum crystallization ages ~100-115 Myr younger than those of the youngest protosource identified (776±14 Ma) could be interpreted to record the onset of the HT-UHT thermal event at ca. 690-660 Ma in the Socorro-Guaxupé Nappe (similarly to Tedeschi et al., 2018). A cluster of U-Pb dates at ca. 660-610 Ma (Figures 7-10) can be interpreted to represent the (U)HT event that lasted up to the collisional stage of the Southern Brasília Orogen (ca. 630-610 Ma), in accordance with the observations of Campos Neto and Caby (1999, 2000), Campos Neto et al. (2004), Rocha et al. (2017, 2018) and Motta et al. (2021).

The garnet-bearing white granite (PC12.5) exhibits a better correspondence with a hornblende-bearing gneiss from the Rio Negro-Serra da Prata arc (Santiago et al., 2022) (Figure 15C), while partial overlaps are observed with an underrepresented population (Group 2) from the biotite-bearing granitic leucosome (São João da Mata complex; Costa et al., 2022), a mafic granulite enclave (Tedeschi et al. 2018), a charnockite and a diatexite (Motta, 2018; Motta et al., 2021) from the Basal Granulite unit, and monzonitic orthogneisses from the São Roque domain (Balis et al., 2020).

It is noteworthy that dates younger than the youngest post-collisional intrusions observed in the Socorro-Guaxupé Nappe (ca. 590-580 Ma; Topfner, 1996; Ebert et al., 1996) were obtained in all the analyzed samples with exception of the amphibolite (PC12.2, PC12.3, PC12.4, PC12.5 and C1071A). Those are probably outliers without a clear geological meaning and are suggestive to result from the disturbance of the U-Pb system.

5.4 Tectonic implications: an arc-related, limited basin system?

According to Figures 12 and 14, a remarkable difference can be observed in $^{176}Hf/^{177}Hf_{(t)}$ versus U-Pb dates trends between the Nappe systems belonging to the accretionary prism (Andrelândia and Liberdade nappes) and passive margin (Carrancas and Lima Duarte nappes) and those observed in arc-related rocks (Socorro-Guaxupé Nappe) from the Southern Brasília Orogen. Sub-horizontal, Pb-loss trends have been observed for HT-UHT metamorphic rocks (Whitehouse and Kemp, 2010; Taylor et al., 2016; Andersen et al., 2019) including those from the Socorro-Guaxupé Nappe. Because the Andrelândia nappe system was mostly submitted to lower temperature metamorphic conditions during their tectonic evolution (Campo Neto and Caby, 1999, 2000; Del Lama et al., 2000; Cioffi et al., 2019; Rocha et al., 2017, 2018; Tedeschi et al., 2018; Motta et al., 2021) they exhibit inclined trends related to other crustal evolution processes (i.e. natural decay during the evolution of a crustal source, Spencer et al., 2019; Figure 12). While most of the rocks (and protosources) in an arc-related setting are limited to the timespan of the magmatic arc (Cawood et al., 2012), rocks in the passive margin and accretionary prism receive contributions from several different sources – including rocks from the basement. Although partial overlaps exist between the zircon Lu-Hf record of the studied paraderived rocks and sources in neighbor Nappe systems (Andrelândia Nappe), the best correlations can be traced with other rocks inside the Socorro-Guaxupé Nappe.

As the SGN represents an exposed section of the magmatic arc developed at the margins of the Paranapanema paleocontinent (active margin) during its convergence with the São Francisco paleocontinent, it is suggestive that the deposition of the protoliths of the studied rocks probably took place in an arc-related, limited basin system, and a possible depositional history (Figure 16) can be proposed based on the data presented here:

1) An island arc or a less evolved continental arc system is developed prior to the onset of ocean-continent subduction at the margins of the Paranapanema paleocontinent (Figure 16A), where the protosource of the garnet-biotite stromatic metatexite (816±11 Ma, $\varepsilon Hf_{(816)}$ = +3 to +9) and the protolith of the biotite-bearing leucosome of Costa et al. (2022) (797±9 Ma, $\varepsilon Hf_{(797)}$ = -2 to +7) originally crystallized. A maximum depositional age of 816±11 Ma is assumed as the age of the protosource, being similar to what is observed in other island and continental arc systems in neighbor orogens (Arenópolis-Mara Rosa arc:

ca. 890 – 815 Ma, Laux et al., 2004, and ca. 915 Ma, Matteini et al., 2010; Rio Negro-Serra da Prata arc, ca. 859 – 847 Ma, Santiago et al., 2020);

2) A continental arc setting takes place (Figure 16B), as registered by several protosources with crustal signatures identified in the hornblende-biotite stromatic metatexite (Sample PC12.2) and in the (hornblende-)biotite stromatic gneiss (Sample C1071A) crystallized in a relatively short time span (Protosource I, 804±5 Ma, $\varepsilon Hf_{(804)}$ = -16 to -13; Protosource II, 789±10 Ma, $\varepsilon Hf_{(789)}$ = -13 to -9; Protosource III, 786±8 Ma, $\varepsilon Hf_{(786)}$ = -9 to -5; Protosource IV, 776±14, $\varepsilon Hf_{(776)}$ = -5 to -2), indicative of a contribution of sources derived from the anatexis of the lower crust. A maximum depositional age of 776±14 Ma was obtained for this stage, in accordance with data from previous works (Campos-Neto and Figueiredo, 1995; Campos Neto and Caby, 2000; Mora et al., 2014; Rocha et al., 2017; Rocha et al., 2018; Tedeschi et al., 2018; Motta et al., 2021);
3) Arc-related to collisional high- to ultrahigh temperature metamorphism starts at ca. 690-660 Ma in the magmatic arc (e.g., Tedeschi et al., 2018) (Figure 16C), followed by anatexis (biotite-bearing pink leucosome PC12.3, 691±3 Ma, $\varepsilon Hf_{(691)}$ = -13 to -11) and granite generation (garnet-bearing white granite PC12.5, 661±4 Ma, $\varepsilon Hf_{(661)}$ = -10 to -7). High thermal conditions might have lasted up until the collisional stage (e.g., Campos Neto and Caby, 2000; Campos Neto et al., 2004; Rocha et al., 2017, 2018; Motta et al., 2021) (Figure 16D);

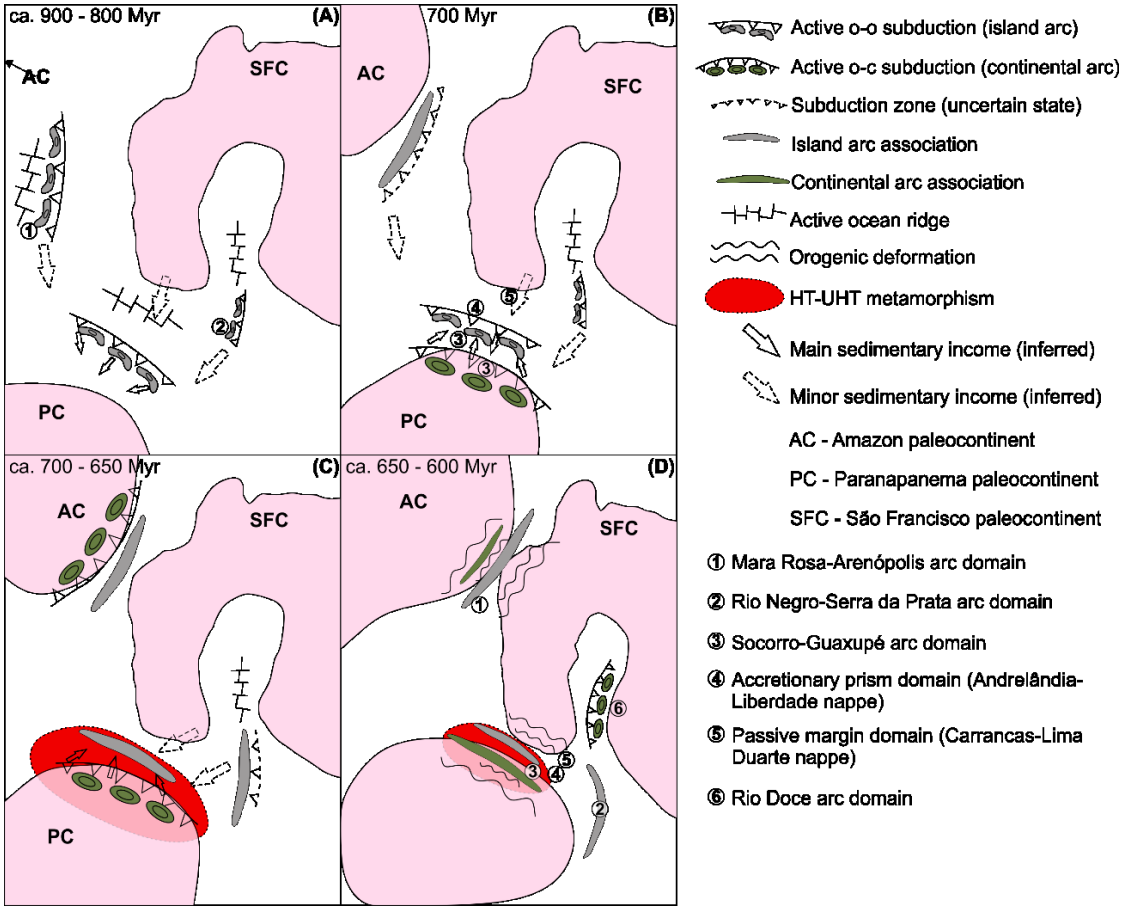

Figure 5-16 - Schematic sketch for the proposed evolution of the arc-related, limited basin system hosted on the Socorro-Guaxupé Nappe in the context of the Southern Brasília orogen (references: Pimentel & Fuck, 1992, 1997; Campos Neto & Caby, 1999, 2000; Pedrosa-Soares et al., 2001, 2008; Campos Neto et al. 2004; Laux et al., 2004, 2005; Matteini et al., 2010; Rocha et al., 2017, 2018; Tedeschi et al., 2018; Frugis et al., 2018; Santiago et al., 2020, 2022; Costa et al., 2022. A) Development of an island arc prior to the onset of subduction at the margins of the Paranapanema paleocontinent, which provided the zircon record of the garnet-biotite stromatic metatexite (ca. 816 Ma, PC12.4); B) Development of the continental arc at the margins of the Paranapanema paleocontinent, which provided most of the zircon record of the hornblende-biotite stromatic metatexite (PC12.2) and (hornblende)-biotite stromatic metatexite (C1071A) maximum depositional age ca. 776 Ma; C) Onset of HT-UHT metamorphism during the development of the continental arc, marked by anatexis (ca. 691 Ma, biotite-bearing pink leucosome, PC12.3; ca. 661 Ma, garnet-bearing white granite, PC12.5); D) HT-UHT metamorphic conditions probably lasted until the end of the collisional stage (ca. 610 Ma).

6 Conclusions

Both ortho- and paraderived samples from the São João da Mata complex exhibit a protracted U-Pb zircon record, a common feature among rocks exposed in the Socorro-Guaxupé Nappe (Rocha et al., 2017, 2018; Tedeschi et al., 2018; Motta et al., 2021; Costa et al., 2022) due to the influence of high- to ultrahigh temperature metamorphism. Through the combination of U-Pb and Lu-Hf in zircon analysis, and following the approach proposed by Tedeschi et al. (2023), five protosources were

identified on the detrital zircon record of the paraderived samples: four with crustal signatures ($\varepsilon Hf_{(804-776)}$ = -16 to -2) and minimum U-Pb ages ranging between ca. 804 Ma and ca. 776 Ma, and one with a moderately juvenile signature ($\varepsilon Hf_{(816)}$ = +3 to +9) and a minimum U-Pb age of ca. 816 Ma.

Those protosources exhibit similar Hf isotopic signatures to rocks observed in the Socorro-Guaxupé Nappe, which represents a section of a Neoproterozoic magmatic arc developed at the margins of the Paranapanema paleocontinent. Only partial correspondences are observed with rocks in neighboring nappe systems (Andrelândia, Carrancas, Lima Duarte and Liberdade Nappes), in the Mara Rosa magmatic arc and in the Serra Negra-Rio da Prata magmatic arc. The moderately juvenile εHf signature observed in one of the protosources (Protosource V, ca. 816 Ma) is similar to rocks previously described by Costa et al. (2022) in the São João da Mata complex, which is suggestive of an island arc-related origin. Therefore, we propose that the paraderived rocks were deposited in a restricted, arc-related setting, starting at an island arc, in which a maximum depositional age of ca. 816 Ma was obtained, and recorded the development of a continental arc between ca. 805 Ma and ca. 776 Ma. Minimum crystallization ages for the leucosome (691±3 Ma) of a paraderived hornblende-biotite stromatic metatexite and a garnet-bearing white granite (661±4 Ma) that outcrops along the studied samples might be indicative of the onset of the high- to ultrahigh temperature thermal event, which might have lasted from ca. 690 Ma to ca. 610.

7 Acknowledgements

The authors are grateful for the financial support from the Universidade Federal de Minas Gerais (UFMG) Edital PRPq 03/2019 and from São Paulo Research Foundation (FAPESP) grant 2021/09437-9. M. Tedeschi was supported by the National Council for Scientific and Technological Development – CNPq through a Research Productivity Grant 308733/2021-5. M. Tedeschi, C. Lana, A.C. Pedrosa-Soares and I.A. Dussin are fellows of the Brazilian Research Council (CNPq). Editorial handling by Andres Folguera and careful reviews by Alice Westin and Rafael Motta helped to improve the manuscript and are greatly acknowledged.

8 References

Andersen, T., Elburg, M., Cawthorn-Blazeby, A. 2015. **U–Pb and Lu–Hf zircon data in young sediments reflect sedimentary recycling in eastern South Africa.** Journal of the Geological Society. Doi:10.1144/jgs2015-006

Andersen, T., Elburg, M., Magwaza, B. 2019. **Sources of bias in detrital zircon geochronology: Discordance, concealed lead loss and common lead correction.** Earth-Science Reviews, 197, 102899. Doi: 10.1016/j.earscirev.2019.102899

Andersen, T., Griffin, W. L., Pearson, N. J. 2002. **Crustal Evolution in the SW Part of the Baltic Shield: the Hf Isotope Evidence.** Journal of Petrology, 43(9), 1725 – 1747

Andersen, T., Griffin, W. L., Jackson, S. E., Knudsen, T. -L, Pearson, N. J. 2004. **Mid-Proterozoic magmatic arc evolution at the southwest margin of the Baltic Shield**. Lithos, 74, 289 – 318

Bahlburg, H., Vervoort, J. D., DuFrane, S. A., Carlotto, V., Reimann, C., Cárdenas, J. 2011. **The U-Pb and Hf isotope evidence of detrital zircons of the Ordovician Ollantaytambo Formation, southern Peru, and the Ordovician provenance and paleogeography of southern Peru and northern Bolivia**. Journal of South American Earth Sciences, 32, 196 – 209

Balis, M., Campos Neto, M. C., Alves, A. 2020. **Serra do Barro Branco orthogneiss: An untimely record of West Gondwana amalgamation in the São Roque Domain.** Precambrian Research, 350, 105913

Belousova, E. A., Griffin, W. L., O'Reilly, S. Y. 2006. **Zircon Crystal Morphology, Trace Element Signatures and Hf Isotope Composition as a Tool for Petrogenetic Modelling: Examples from Eastern Australian Granitoids**. Journal of Petrology, 47(2), 329 – 353

Blichert-Toft, J., Albarède, F. 1997. **The Lu-Hf geochemistry of chondrites and the evolution of the mantle-crust system**. Earth Planet Science Letters, 148, 243 – 258

Blichert-Toft, J., Albarède, F. 2008. **Hafnium isotopes in Jack Hills zircons and the formation of the Hadean crust.** Earth Planet Science Letters, 265(3-4), 686 – 702. https://doi.org/10.1016/j.epsl.2007.10.054

Brito Neves, B. B., Campos Neto, M. C., Fuck, R. A. 1999. **From Rodinia to western Gondwana: an approach to the Brasiliano-Pan African cycle and orogenic collage**. Episodes, 22, 155 – 166

Bouvier, A., Vervoort, J. D., Patchett, P. J. 2008. **The Lu-Hf and Sm-Nd isotopic composition of CHUR: constraints from unequilibrated chondrites and implications for the bulk composition of terrestrial planets**. Earth and Planetary Science Letters, 273, 48 – 57

Campos-Neto, M. C., Basei, M. A. S., Janasi, V. A., Moraes, R. 2011. **Orogen migration and tectonic setting of the Andrelândia Nappe system: An Ediacaran western Gondwana collage, south of São Francisco craton**. Journal of South American Earth Sciences, 32, 393 – 406

Campos Neto, M. C., Basei, M. A., Vlach, S. R. F., Caby, R., Szabó, A. J., Vasconcelos, P. 2004. **Migração de orógenos e superposição de orogêneses:**

um esboço da colagem Brasíliana no sul do Cráton do São Francisco, SE-Brasil. Geologia USP Série Científica, 4 (1), 13 – 40

Campos-Neto, M. C., Caby, R. 1999. **Neoproterozoic high-pressure metamorphism and tectonic constraint from the nappe system south of the Sao Francisco Craton, southeast Brazil**. Precambrian Research, 97 (1 – 2), 3 – 26

Campos-Neto, M. C., Caby, R. 2000. **Terrane accretion and upward extrusion of high-pressure granulites in the Neoproterozoic nappes of southeast Brazil: Petrologic and structural constraints.** Tectonics, 19(4), 669 – 687

Campos Neto, M. C., Cioffi, C. R., Moraes, R., Motta, R. G., Siga Jr., O., Basei, M. A. S. 2010. **Structural and metamorphic control on the exhumation of high-P granulites: the Carvalhos Klippe example, from the oriental Andrelândia nappe system, southern portion of the Brasília Orogen, Brazil**. Precambrian Research, 180, 125 – 142

Campos Neto, M. C., Cioffi, C. R., Westin, A., Rocha, B. C., Frugis, G. L., Tedeschi, M., Pinheiro, M. A. P. 2020. **O orógeno Gondwana meridional.** In: Bartorelli, A., Teixeira, W., Brito Neves, B. B. (Orgs.). **Geocronologia e Evolução Tectônica do Continente Sul-Americano: a contribuição de Umberto Giussepe Cordani**. Solaris Edições Culturais, São Paulo, p. 146 – 180

Campos-Neto, M. C. and Figueiredo, M. C. H. 1995. **The Rio Doce orogeny, southeastem Brazil.** Journal of South American Earth Sciences, 8(2), 143–162

Cawood, P. A., Hawkesworth, C. J., Dhuime, B. 2012. **Detrital zircon record and tectonic setting.** Geology 40, 875–878. Doi:10.1130/G32945.1

Chauvel, C., Lewin, E., Carpentier, M., Arndt, N. T., Marini, J. C. 2008. **Role of recycled oceanic basalt and sediment in generating the Hf–Nd mantle array**. Nature Geoscience, 1(1), 64 – 67

Chemale, F., Kawashita, K., Dussin, I. A., Avila, J. N., Justino, D., Bertotti, A. 2012. **U-Pb zircon in situ dating with LA-MC-ICP-MS using a mixed detector configuration.** Anais da Academia Brasileira de Ciências, 84, 275 – 295

Chen, R. X., Zheng, Y. F 2017. **Metamorphic zirconology of continental subduction zone.** Journal of Asian Earth Sciences, 145, 149 – 176

Cherniak, D. J., Watson, E. B. 2001**. Pb diffusion in zircon**. Chemical Geology,172 (1 – 2), 5 – 24

Cherniak, D. J, Watson, B. E. 2003. **Diffusion in zircon**. Reviews in Mineralogy and Geochemistry, 53, 113 – 143

Cherniak, D. J. 2010. **Diffusion in accessory minerals: zircon, titanite, apatite, monazite and xenotime.** Reviews in Mineralogy and Geochemistry, 72, 827 – 869. https://doi.org/10.2138/rmg.2010.72.18

Cioffi, C. R., Campos Neto, M. C., Möller, A., Rocha, B. C. 2016a. **Paleoproterozoic continental crust generation events at 2.15 and 2.08 Ga in the basement of the southern Brasília Orogen, SE Brazil.** Precambrian Research, 275, 176–196

Cioffi, C. R., Campos Neto, M. C., Möller, A., Rocha, B. C. 2016b. **Tectonic significance of the Meso- to Neoarchean complexes in the basement of the southern Brasília Orogen**. Precambrian Research, 287, 91–107

Cioffi, C. R., Campos Neto, M. C., Moller, A., Rocha, B. C. 2019. **Titanite petrochronology of the southern Brasília Orogen basement: effects of retrograde net-transfer reactions on titanite trace element compositions**. Lithos, 344 – 345, 393 – 408

Coelho, M. B., Trouw, R. A. J., Ganade, C. E., Vinagre, R., Mendes, J. C., Sato, K. 2017. **Constraining timing and P-T conditions of continental collision and late overprinting in the Southern Brasília Orogen (SE-Brazil): U-Pb zircon ages and geothermobarometry of the Andrelândia Nappe System**. Precambrian Research, 292, 194 – 215

Collins, W. J., Belousova, E. A., Kemp, A. I. S., Murphy, J. B. 2011. **Two contrasting Phanerozoic orogenic systems revealed by hafnium isotope data**. Nature Geoscience, 4, 333–337. https://doi.org/10.1038/ngeo1127

Corfu, F., Hanchar, J. M., Hoskin, P. W. O., Kinny, P. 2003. **Atlas of zircon textures.** In: Hanchar, J. M., Hoskin, P. W. O. (Eds.). **Zircon**. Reviews in Mineralogy and Geochemistry, 53, 469 – 500

Costa, F. M., Penna, J. L. A., Martins, L. C. D., Tedeschi, M., Novo, T. A., Araujo, C. S., Vieira Rossi, P. L., Lana, C., Pedrosa-Soares, A. C. 2022. **Zircon petrochronology reveals the moderately juvenile signature of a diatexite from the boundary zone between the Brasília and Ribeira orogens (SE Brazil): Relict of a Tonian arc?** Journal of South American Earth Sciences, 116, 103767. https://doi.org/10.1016/j.jsames.2022.103767

Degler, R., Zogheib, F. F., Martins, L. C. D., Novo, T. 2015. **Geologia das Folha Nova Resende (SF.23-V-D-I) 1:100.000.** Projeto Fronteiras de Minas, CODEMIG-UFMG, Belo Horizonte, Brazil

Del Lama, E. A., Zanardo, A., Oliveira, M. A. F., Moralles, N. 2000. **Exhumation of high-pressure granulites of the Guaxupé Complex, Southeastern Brazil**. Geological Journal, 35, 231 – 249

Dhuime, B., Hawkesworth, C., Cawood, P. 2011. **When continents formed**. Science, 331, 154 – 155

Ebert, H. D.; Chemale Jr., F.; Babinsky, M.; Artur, A. C.; Van Schmus, W. R. 1996. **Tectonic setting and U/Pb zircon dating of the plutonic Socorro Complex in the Transpressive Rio Paraíba do Sul Shear Belt, SE Brazil**. Tectonics, 15 (3), 688 – 699

El-Naby, H. A., Frisch, W. 2006. **Geochemical constraints from the Hafafit Metamorphic Complex (HMC): Evidence of Neoproterozoic back-arc basin**

development in the central Eastern Desert of Egypt. Journal of African Earth Sciences, 45(2), 173 – 186

Fedo, C. M., Sircombe, K. N., Rainbird, R. H. 2003. **Detrital zircon analysis of the sedimentary record.** Reviews in Mineralogy and Geochemistry, 53(1), 278 – 303

Fetter, A. H., Hackspacher, P. C., Ebert, H. D., Dantas, E. L., Costa, A. C. D. 2001. **New Sm-Nd and U-Pb Geochronological Constraints on the Archean to Paleoproterozoic Evolution of the Amparo Basement Complex of the Central Ribeira Belt, South-eastern Brazil**. 3rd South American Symposium on Isotope Geology (Extended Abstracts, CD-ROM)

Finch, M. A., Weinberg, R. F., Barrote, V. R., Cawood, P. A. 2021. **Hf isotopic ratios in zircon reveal processes of anatexis and pluton construction**. Earth and Planetary Science Letters, 576, 117215

Finch, R. J., Hanchar, J. M. 2003. **Structure and chemistry of zircon and zircon-group minerals**. Reviews in Mineralogy and Geochemistry, 53(1), 1 – 25

Fischer, S., Prave, A. R., Johnson, T. E., Cawood, P. A., Hawkesworth, C. J., Horstwood, M. S. A., EIMF. 2021. **Using zircon in mafic migmatites to disentangle complex high-grade gneiss terrains – Terrane spotting in the Lewisian complex, NW Scotland.** Precambrian Research, 355, 106074. https://doi.org/10.1016/j.precamres.2020.106074

Fornelli, A., Langone, A., Micheletti, F., Piccarreta, G. 2011. **Time and duration of Variscan high-temperature metamorphic processes in the south European Variscides: constraints from U–Pb chronology and trace element chemistry of zircon**. Mineralogy and Petrology, 103, 101 – 122. Doi:10.1007/s0071 0-011-0156-8

Friend, C. R. L., Kinny, P. D. 1995. **New evidence for the protolith ages of Lewisian granulites, northwest Scotland**. Geology, 23, 1027 – 1030

Frugis, G. L., Campos Neto, M. C., Lima, R. B. 2018**. Eastern Paranapanema and southern São Francisco orogenic margins: records of enduring Neoproterozoic oceanic convergence and collision in southern Brasília Orogen**. Precambrian Research, 308, 35 – 57

Fujimaki, H. 1986. **Partition coefficients of Hf, Zr, and REE between zircon, apatite, and liquid.** Contributions in Mineralogy and Petrology, 94, 42 – 45. https://doi.org/10.1007/BF00371224

Gerdes, A., Zeh, A. 2009. **Zircon formation versus zircon alteration – New insights from combined U-Pb and Lu-Hf in-situ La-ICP-MS analyses of Archean zircons from the Limpopo Belt.** Chemical Geology, 261(3-4), 230 – 243

Griffin, W. L., Wang, X., Jackson, S. E., Pearson, N. J., O'Reilly, S. Y., Xu, X., Zhou, X. 2002. **Zircon chemistry and magma mixing, SE China: In-situ analysis of Hf isotopes, Tonglu and Pingtan igneous complexes**. Lithos, 61, 237 – 269

Harley, S. L. 2016**. A matter of time: the importance of the duration of UHT metamorphism**. Journal of Mineralogical and Petrological Sciences, 111, 50 – 72. Doi: 10.2465/jmps.160128

Heilbron, M., Pedrosa-Soares, A.C., Campos Neto, M., Silva, L.C., Trouw, R.A.J., Janasi, V.C. 2004. **A Província Mantiqueira**. In: Mantesso-Neto, V., Bartorelli, A.,Carneiro, C.D.R., Brito Neves, B.B. (Eds.). **Geologia do Continente Sul-Americano: Evolução da Obra de Fernando Flávio Marques de Almeida**. Beca, Brazil. P. 203 – 234

Heilbron, M., Valeriano, C. M., Tassinari, C. C. G., Almeida, J. C. H., Tupinambá, M., Siga Jr., O., Trouw, R. A. J., 2008. **Correlation of Neoproterozoic terranes between the Ribeira Belt, SE Brazil and its African counterpart: comparative tectonic evolution and open questions.** In: Pankhurst, R.J., Trouw, R.A.J., Brito-Neves, B.B., de Wit, M. (Eds.). **West Gondwana pre-Cenozoic Correlations across the South Atlantic Region.** Journal Geological Society London, Special Publication, 294, 211 – 232

Hoskin, P. W. O, Black, L. P. 2000. **Metamorphic zircon formation by solid-state recrystallization of protolith igneous zircon.** Journal of Metamorphic Geology, 18, 423 – 439

Hoskin, P. W. O., Schaltegger, U. 2003. **The Composition of Zircon and Igneous and Metamorphic Petrogenesis.** Reviews in Mineralogy and Geochemistry, 53 (1), 27 – 62

Jackson, S. E., Pearson, N. J., Griffin, W. L., and Belousova, E. A. 2004. **The application of laser ablation-inductively coupled plasma-mass spectrometry to in situ U-Pb zircon geochronology**. Chemical Geology, 211, 47 – 69

Janasi, V. A.; Vlach, S. R. F.; Ulbrich, H. G. J. 1993. **Enriched-mantle contributions to the Itu granitoid belt, southeastern Brazil: evidence form K-rich diorites and syenites.** Annals from the Academia Brasileira de Ciências, v. 65, 107 – 118

Janasi, V. A. 2002. **Elemental and Sr-Nd isotope geochemistry of two Neoproterozoic mangerite suites in SE Brazil: implications for the origin of the mangerite-charnockite-granite series**. Precambrian Research, 119, 301 – 327

Kelsey, D. E. 2008. **On ultrahigh-temperature crustal metamorphism.** Gondwana Research, 13, 1 – 29

Kelsey, D. E., Hand, M. 2015. **On ultrahigh temperature crustal metamorphism: Phase equilibria, trace element thermometry, bulk composition, heat sources, timescales and tectonic settings.** Geoscience Frontiers, 6, 311 – 356

Kemp, A. I. S., Hawkesworth, C. J., Collins, W. J., Gray, C. M., Blevin, P. L. 2009. **Isotopic evidence for rapid continental growth in an extensional accretionary orogen: The Tasmanides, eastern Australia.** Earth and Planetary Science Letters, 284, 455 – 466. https://doi.org/10.1016/j.epsl.2009.05.011

Kohn, M. J., Corrie, S. L., Markley, C. 2015. **The fall and rise of metamorphic zircon.** American Mineralogist, 100, 897 – 908. https://doi.org/10.2138/am-2015-5064

Kunz, B. E., Regis, D., Engi, M. 2018. **Zircon ages in granulite facies rocks: decoupling from geochemistry above 850 °C?** Contributions to Mineralogy and Petrology, 173, 26. Doi: 10.1007/s00410-018-1454-5

Kusiak, M. A., Whitehouse M. J., Wilde S. A., Dunkley D. J., Menneken M., Nemchin A. A., Clark, C. 2013a. **Changes in zircon chemistry during archean UHT metamorphism in the Napier Complex, Antarctica.** American Journal of Science, 313, 933 – 967

Kuster, K., Ribeiro, A., Trouw, R. A. J., Dussin, I., Marimon, R. S. 2020. **The Neoproterozoic Andrelândia group: Evolution from an intraplate continental margin to an early collisional basin south of the São Francisco craton, Brazil**. Journal of South American Earth Sciences, 102, 102666

Lana, C., Farina, F., Gerdes, A., Alkmim, A., Gonçalves, G. O., Jardim, A. C. 2017. **Characterization of zircon reference materials via high precision U-Pb LA-MC-ICP-MS.** Journal of Analytical Atomic Spectrometry, 32, 2011 – 2023

Laurent, A., Bingen, B., Duchene, S., Whitehouse, M. J., Seydoux-Guillaume, A. M., Bosse, V. 2018. **Decoding a protracted zircon geochronological record in ultrahigh temperature granulite, and persistence of partial melting in the crust, Rogaland, Norway.** Contributions to Mineralogy and Petrology, 173, 29. https://doi.org/10.1007/s00410-018-1455-4

Laux, J. H., Pimentel, M. M., Dantas, E. L., Armstrong, R., Armele, A., Nilson, A. A. 2004. **Mafic magmatism associated with the Goiás magmatic arc in the Anicuns region, Goiás, central Brazil: Sm–Nd isotopes and new ID-TIMS and SHIMP U–Pb data.** Journal of South American Earth Sciences, 16, 599 – 614

Laux, J. H., Pimentel, M. M., Dantas, E. L., Armstrong, R., Junges, S. L. 2005. **Two neoproterozoic crustal accretion events in the Brasília belt, central Brazil**. Journal of South American Earth Sciences, 18, 183 – 198.

Ludwig, K. R. 2003. **Isoplot Excell version 3.0. A geochronological toolkit for Microsoft Excel.** Berkeley Geochronological Centre Special Publication No. 4, Berkeley, California

Luo, Y. and Ayers, J.C., 2009. **Experimental measurements of zircon/melt trace-element partition coefficients.** Geochimical et Cosmochemical Acta, 73, 3656–3679. https://doi.org/10.1016/j.gca.2009.03.027

Marimon, R. S., Trouw, R. A. J., Dantas, E. L., Ribeiro, A. 2020. U**-Pb and Lu-Hf isotope systematics on detrital zircon from the southern São Francisco Craton's Neoproterozoic passive margin: Tectonic implications**. Journal of South American Earth Sciences, 100, 102539

Marimon, R. S., Trouw, R. A. J., Dantas, E. L., Ribeiro, A., Santos. P., Kuster, K., Vinagre, R. 2021. Pr**ovenance of passive-margin and syn-collisional units:**

Implications for the geodynamic evolution of the Southern Brasília Orogen, West Gondwana. Sedimentary Geology, 413, 105823

Martin, E. L., Collins, W. J., Spencer, C. J. 2020. **Laurentian origin of the Cuyania suspect terrane, western Argentina, confirmed by Hf isotopes in zircon**. Bulletin of the Geological Society of America, 132, 273 – 290. https://doi.org/10.1130/B35150.1

Matteini, M., Junges, S. L., Dantas, E. L., Pimentel, M. M., Bühn, B. 2010. **In situ zircon U-Pb and Lu-Hf isotope systematic on magmatic rocks: insights on the crustal evolution of the Neoproterozoic Goiás Magmatic Arc, Brasília belt, Central Brazil.** Gondwana Research, 17(1), 1 – 12

Möller, A., O'Brien, P. J., Kennedy, A., Kröner, A. 2002. **Polyphase zircon in ultrahigh-temperature granulites (Rogaland, SW Norway): Constraints for Pb diffusion in zircon.** Journal of Metamorphic Geology, 20, 727–740. Doi: 10.1046/j.1525-1314.2002.00400.x

Mora, C. A. S., Campos Neto, M. C., Basei, M. A. S., 2014. **Syn-collisional lower continental crust anataxis in the Neoproterozoic Socorro-Guaxupé Nappe System, southern Brasília Orogen, Brazil: constraints from zircon U-Pb dating, Sr-Nd-Hf signatures and whole-rock geochemistry**. Precambrian Research, 255, 847 – 864

Morel M. L. A., Nebel O., Nebel-Jacobsen Y. J., Miller J. S., Vroon P. Z. 2008. **Hafnium isotope characterization of the GJ-1 zircon reference material by solution and laser-ablation MC-ICP-MS.** Chemical Geology, 255, 231 – 235

Motta, R. G. 2018. **Formação, transformação e evolução da crosta continental inferior: investigando o Orógeno Brasília Meridional.** PhD. Thesis. Instituto de Geociências, Universidade de São Paulo. 210 pp

Motta, R. G., Fitzsimons, I. C. W., Moraes, R., Johnson, T. E., Schuindt, S., Benetti, B. Y. 2021. **Recovering P-T-t paths from ultra-high temperature (UHT) felsic orthogneiss: An example from the Southern Brasília Orogen, Brazil.** Precambrian Research, 359, p. 106222.

Murphy, J. B., Pisarevsky, S. A., Nance, R. D., Keppie, J. D. 2004. **Neoproterozoic–early Paleozoic evolution of peri-Gondwanan terranes implications for Laurentia–Gondwana connections in The Avalonian–Cadomian belt and related peri-Gondwanan terranes**. International Journal of Earth Sciences, 93, 659 – 682. https://doi.org/10.1007/s00531-004-0412-9

Nardi, L. V. S., Formoso, M. L. L., Müller, I. F., Fontana, E., Jarvis, K., Lamarão, C. 2013**. Zircon/rock partition coefficients of REEs, Y, Th, U, Nb, and Ta in granitic rocks: Uses for provenance and mineral exploration purposes.** Chemical Geology, 335, 1 – 7. https://doi.org/10.1016/j.chemgeo.2012.10.043

Pedrosa-Soares, A. C., Noce, C. M., Wiedemann, C. M., Pinto, C. P. 2001. **The Araçuaí-West-Congo Orogen in Brazil: an overview of a confined orogen formed during Gondwanaland assembly.** Precambrian Research, 110, 307 – 323.

Pedrosa-Soares, A. C., Alkmim, F. F., Tack, L., Noce, C. M., Babinski, M. Da Silva, L. C., Martins-Neto, M. A. 2008**. Similarities and differences between the Brazilian and African counterparts of the Neoproterozoic Araçuaí-West-Congo orogen**. Geological Society, London, Special Publications, 294, 153 – 172.

Peixoto, E.I.P., Falci, A., Noronha, R.C., Degler, R., Martins, L.C.D., Nassif, M.T., Freitas, A.R., Novo, T. 2015. **Geologia das Folhas Andradas (SF.23-Y-A-III) e Ouro Fino 1:100.000 (SF.23-Y-B-I).** Projeto Fronteiras de Minas, CODEMIG-UFMG, Belo Horizonte, Brazil

Pell, S. D., Williams, I. S. and Chivas, A. R. 1997. **The use of protolith zircon-age fingerprints in determining the protosource areas for some Australian dune sands.** Sedimentary Geology, 109, 233 – 260

Pimentel, M. M. & Fuck, R. A. 1992. **Neoproterozoic crustal accretion in central Brasil.** Geology, 20, 375 – 379

Pimentel, M. M., Whitehouse, M. J., Viana, M. G., Fuck, R. A., Machado, N. 1997. **The Mara Rosa Arc in the Tocantins Province: further evidence for Neoproterozoic crustal accretion in Central Brazil**. Precambrian Research, 81, 299 – 310.

Reimann, C. R., Bahlburg, H., Koojiman, E., Berndt, J., Gerdes, A., Carlotto, V., López, S. 2010. **Geodynamic evolution of the early Paleozoic Western Gondwana margin 14°–17°S reflected by the detritus of the Devonian and Ordovician basins of southern Peruand northern Bolivia**. Gondwana Research, 18, 370 – 384

Reno, B. L., Brown, M., Kobayashi, K., Nakamura, E., Piccoli, P. M., Trouw, R. A. J. 2009. **Eclogite-high-pressure granulite metamorphism records early collision in west Gondwana: new data from the Southern Brasília belt, Brazil.** Journal of the Geological Society of London, 166, 1013 – 1032

Reno, B. L., Piccoli, P. M., Brown, M., Trouw, R. A. J. 2012. **In situ monazite (U-Th)-Pb ages from the southern Brasília Belt, Brazil: constraints on the high-temperature retro-grade evolution of HP granulites.** Journal of Metamorphic Geology, 30, 81 – 112

Ribeiro, B. V., Cawood, P. A., Faleiros, F. M., Mulder, J. A., Martin, E., Finch, M. A., Raveggi, M., Teixeira, W., Cordani, U. G., Pavan, M. 2020. **A long-lived active margin revealed by zircon U–Pb–Hf data from the Rio Apa Terrane (Brazil): New insights into the Paleoproterozoic evolution of the Amazonian Craton.** Precambrian Research, 350, 105919. https://doi.org/10.1016/j.precamres.2020.105919

Ribeiro, A., Nascimento, D., Bongiolo, E., Trouw, R., Polo, H., Tavares, F., Nepomuceno, F. 2015a. **Geologia da Folha Pouso Alegre (SF.23-Y-B-II) 1:100.000.** Programa Geologia do Brasil, CPRM-UFRJ, Rio de Janeiro, Brazil

Ribeiro, A., Nascimento, D., Campos, M. T., Oliveira, F., Rocha, F. 2015b. **Geologia da Folha Machado (SF.23-V-D-V) 1:100.000.** Programa Geologia do Brasil, CPRM-UFRJ, Rio de Janeiro, Brazil

Ribeiro, A., Campos, M. T., Paciullo, F. V., Carvalho, M. V., Valeriano, C. M., Nascimento, D. 2015c. **Geologia da Folha Alfenas (SF.23-V-D-II) 1:100.000.** Programa Geologia do Brasil, CPRM-UFRJ, Rio de Janeiro, Brazil

Rocha, B. C., Moraes, R., Möller, A., Cioffi, C. R. 2018. **Magmatic inheritance vs. UHT metamorphism: Zircon petrochronology of granulites and petrogenesis of charnockitic leucosomes of the Socorro–Guaxupé nappe, SE Brazil**. Lithos, 314-315, 16 – 39

Rocha, B. C., Moraes, R., Möller, A., Cioffi, C. R., Jercinovic, M. J. 2017. **Timing of anatexis and melt crystallization in the Socorro–Guaxupé Nappe, SE Brazil: Insights from trace element composition of zircon, monazite and garnet coupled to U-Pb geochronology.** Lithos, 277, 337 – 355

Rubatto, D. 2017. **Zircon: the metamorphic mineral.** Reviews in Mineralogy and Geochemistry, 83, 261-295

Santiago, R., Caxito, F. A., Pedrosa-Soares, A., Neves, M. A., Dantas, E. L. 2020. **Tonian island arc remnants in the northern Ribeira orogen of Western Gondwana: The Caxixe batholith (Espírito Santo, SE Brazil).** Precambrian Research, 351, 105944

Santiago, R., Caxito, F. A., Pedrosa-Soares, A., Neves, M. A., Calegari, S. S., Lana, C. 2022**. Detrital zircon U – Pb and Lu – Hf constraints on the age, provenance and tectonic setting of arc-related high-grade units of the transition zone of the Araçuaí and Ribeira orogens (SE Brazil).** Journal of South American Earth Sciences, 116, 103861

Santos, M. M., Lana, C., Scholz, R., Buick, I., Schmitz, M. D., Kamo, S. L., Gerdes, A., Corfu, F., Tapster, S., Lancaster, P., Storey, C.D., Basei, M.A.S., Tohver, E., Alkmim, A., Nalini, H., Krambrock, K., Fantini, C., Wiedenbeck, M. 2017**. A new appraisal of Sri Lankan BB Zircon as a reference material for LA-ICP-MS U-Pb geochronology and Lu-Hf isotope tracing.** Geostandards and Geoanalytical Research, 41(3), 335 – 358

Schaltegger, U., Fanning, C. M., Günther, D., Maurin, J. C., Schulmann, K., and Gebauer, D. 1999. **Growth, annealing and recrystallization of zircon and preservation of monazite in high-grade metamorphism: conventional and in-situ U-Pb isotope, cathodoluminescence and microchemical evidence.** Contributions to Mineralogy and Petrology, 134 (2-3), 186 – 201.

Schulz-Isenbeck, J., Bröcker, M., Berndt, J. 2019. **U–Pb zircon dating of Paleozoic volcanic rocks from the Rheno-Hercynian Zone: new age constraints for the Steinkopf formation, Lahn-Dill area, Germany**. International Journal of Earth Sciences, 108, 1835 – 1855

Sláma, J., Kosler, J., Condon, D. J., Crowley, J. L., Gerdes, A., Gerdes, A., Hanchar, J. M., Horstwood, M. S. A., Morris, G. A., Nasdala, L., Norberg, N., Schaltegger, U., Schoene, B., Tubrett, M. N., Whitehouse, M. J. 2008. **Plesovice zircon—a new natural reference material for U-Pb and Hf isotopic micro-analysis**. Chemical Geology, 249, 1 – 35

Spencer, C. J., Kirkland, C. L., Roberts, N. M. W., Evans, N. J., Liebmann, J. 2019. **Strategies towards robust interpretations of in situ zircon Lu–Hf isotope analyses**. Geoscience Frontiers, 11, 843 – 853. https://doi.org/10.1016/j.gsf.2019.09.004

Taylor, R. J. M., Kirkland, C. L., Clark, C. 2016. **Accessories after the facts: Constraining the timing, duration and conditions of high-temperature metamorphic processes.** Lithos, 264, 239 – 257

Taylor, R. J. M., Johnson, T. E., Clark, C., Harrison, J.R. 2020. **Persistence of melt-bearing Archean lower crust for >200 m.y.—An example from the Lewisian Complex, northwest Scotland.** Geology, 48(3), 221 – 225. Doi: https://doi.org/10.1130/G46834.1

Tedeschi, M., Vieira, P. L. N. C. R., Novo, T. A. 2015. **Geologia e recursos minerais das Folhas Caldas (SF.23-V-D-IV) e Poços de Caldas (SF.23-V-C-VI) 1:100.000.** Projeto Fronteiras de Minas, CODEMIG-UFMG, Belo Horizonte, Brazil

Tedeschi, M., Lanari, P., Rubatto, D., Pedrosa-Soares, A., Hermann, J., Dussin, I., Pinheiro, M. A. P., Bouvier, A.-S., Baumgartner, L. 2017. **Reconstruction of multiple P-T-t stages from retrogressed mafic rocks: Subduction versus collision in the Southern Brasília orogen (SE Brazil).** Lithos, 294–295, 283–303

Tedeschi, M., Pedrosa-Soares, A.; Dussin, I., Lanari, P., Novo, T., Pinheiro, M. A. P., Lana, C., Peters, D. 2018. **Protracted zircon geochronological record of UHT garnet-free granulites in the Southern Brasília orogen (SE Brazil): Petrochronological constraints on magmatism and metamorphism.** Precambrian Research, 316, 103 – 126

Tedeschi, M., Rossi Vieira, P. L., Kuchenbecker, M., Ribeiro, B. V., Barrote, V., Reis, H., Stutenbecker, L., Lana, C., Pedrosa-Soares, A., Dussin, I. 2023. **Unravelling and overcoming potential biases in U-Pb detrital zircon records induced by high to ultra-high temperature metamorphism (> 850 ºC).** Geoscience Frontiers, 14, 101515. https://doi.org/10.1016/j.gsf.2022.101515

Töpfner, C. 1996. **Brasiliano-Granitoide in den Bundes-staaten São Paulo und Minas Gerais- eine vergleichen-de Studie**. Münchner Geologische Hefte, A17, 1 – 258

Trouw, R. A. J., Heilbron, M., Ribeiro, A., Paciullo, F., Valeriano, C. M., Almeida, J. C. H., Tupinambá, M., Andreis, R. R. 2000. **The central segment of Ribeira Belt**. In: Cordani, U.G., Milani, E.J., Thomaz-Filho, A., Campos, D.A. (Eds.). **Tectonic Evolution of South America**. 31th International Geological Congress. Rio de Janeiro, Brasil. P. 287 – 310

Trouw, R. A. J., Peternel, R., Ribeiro, A., Heilbron, M., Vinagre, R., Duffles, P., Trouw, C. C., Fontainha, M., Kussama, H. H. 2013. **A new interpretation for the interference zone between southern Brasília belt and the Central Ribeira belt, SE Brazil.** Journal of South American Earth Sciences, 48, 43 – 57

Trouw, R. A. J., Ribeiro, A., Paciullo, F. V. P., Peternel, R., Vinagre, R., Campos, M. T. R., Duffles, P., Oliveira, A. A., Rocha, F.M. 2014. **Mapeamento das Folhas**

Alfenas, Machado, Pouso Alegre, Campos do Jordão e Pindamonhangaba. In: 47 Congresso Brasileiro de Geologia, Belo Horizonte. Anais. Salvador, SBG-NSA. CD-ROM

Vermeesch, P. 2012. **On the visualization of detrital age distributions**. Chemical Geology, 312 – 313, 190 – 194

Vervoort, J. D., Kemp, A. I. S. 2016. **Clarifying the zircon Hf isotope record of crust–mantle evolution.** Geochemical Geology, 425, 65 – 75

Vinagre, R., Trouw, R. A., Mendes, J. C., Duffles, P., Peternel, R., Matos, G. 2014. **New Evidence of a Magmatic Arc in the Southern Brasília Belt, Brazil: the Serra da Água Limpa Batholith (Socorro-Guaxupé Nappe).** Journal of South American Earth Sciences, 54, 120 – 139

Wang, W., Liu, S., Cawood, P. A., Guo, R., Bai, X., Guo, B. 2017. **Late Neoarchean crust-mantle geodynamics: Evidence from Pingquan Complex of the Northern Hebei Province, North China Craton.** Precambrian Research, 303, 470 – 493

Wasserburg, G. J. 1963. **Diffusion processes in lead-uranium systems**. Journal of Geophysical Research, 68, 4823 – 4846

Westin, A., Campos Neto, M. C., Cawood, P. A., Hawkesworth, C. J., Dhuime, B., Delavault, H. 2019. **The Neoproterozoic southern passive margin of the São Francisco craton: Insights on the pre-amalgamation of West Gondwana from U-Pb and Hf-Nd isotopes**. Precambrian Research, 320, 454 – 471. https://doi.org/10.1016/j.precamres.2018.11.018

Westin, A., Campos Neto, M. C., Hawkesworth, C. J., Cawood, P. A., Dhuime, B., Delavault, H. 2016. **A Paleoproterozoic intra-arc basin associated with a juvenile source in the Southern Brasília Orogen: Application of U-Pb and Hf–Nd isotopic analyses to provenance studies of complex areas**. Precambrian Research, 276, 178 – 193

Whitehouse, M. J., Kemp, A. I. S. 2010. **On the difficulty of assigning crustal residence, magmatic protolith and metamorphic ages to Lewisian granulites: constraints from combined in situ U–Pb and Lu–Hf isotopes**. Geological Society, London, Special Publication, 335, 81 – 101

Whitehouse, M., Ravindra Kumar, G. R., Rimša, A. 2014. **Behaviour of radiogenic Pb in zircon during ultrahigh-temperature metamorphism: An ion imaging and ion tomography case study from the Kerala Khondalite Belt, southern India.** Contributions to Mineralogy and Petrology 168, 1 – 18. Doi:10.1007/s00410-014-1042-2

Whitney, D. L., Evans, B. W., 2010. **Abbreviations for names of rock-forming minerals**. American Mineralogist, 95, 185 – 187

Zogheib, F. F., Degler, R., Martins, L. C. D., Novo, T. 2015. **Geologia das Folha Guaxupé (SF.23-V-C-III) 1:100.000.** Projeto Fronteiras de Minas, CODEMIG-UFMG, Belo Horizonte, Brazil

6 COMPLEMENTARY LU-HF DATA

As explained in Chapter 4, although the distribution of U-Pb dates from the layered orthopyroxene-garnet diatexite (sample P013) exhibit similarities with several units in the Araçuaí orogen and neighbor orogenic belts the isotopic disturbance caused by UHT metamorphism hampers precise correlations.

In order to retrieve information regarding the protosources that contributed to the zircon record obtained for this sample, the approach of Tedeschi et al. (2023) was applied in order to identify zircon populations, minimum crystallization ages and maximum depositional ages based on U-Pb and Lu-Hf isotopes (as with samples PC12.1, PC12.2, PC12.3, PC12.4, PC12.5 and C1071A in Chapter 5). U-Pb and Lu-Hf data is presented in Appendix O.

A detailed description of the layered orthopyroxene-garnet diatexite (sample P013) petrography was provided in Chapter 4 (section 4.2.3).

6.1 Layered orthopyroxene-garnet diatexite (P013) – Caparaó complex, Araçuai orogen

Zircon cores (n = 122) exhibit a range of U-Pb dates between 1179±15 Ma to 589±13 Ma (Figure 3A, B), and outliers include a younger grain (583±5 Ma) and an older one (1704±25 Ma). Most dates (n = 104) are concentrated between 785±8 Ma and 589±13 Ma, and several statistical peaks were calculated through a PDP: ca. 770 Ma, ca. 745, ca. 715 Ma, ca. 665 Ma, ca. 625 Ma, ca. 600 Ma and minor older peaks. Zircon rims (n = 35) exhibit a range of U-Pb dates between 710±11 Ma and 592±5 Ma (Figure 3A, B), with six outliers (1146±19 Ma, 806±13 Ma, 799±12 Ma, 766±7 Ma, 723±11 Ma and 717±12 Ma). Four main peaks were identified through a probability density plot: ca. 705 Ma, ca. 645 Ma, ca. 610 Ma and ca. 595 Ma.

Zircon grains define two distinct populations in terms of $^{176}Hf/^{177}Hf_{(t)}$ ratios and $\varepsilon Hf_{(t)}$ values (Figure 3C – F). Population I exhibit zircon crystals (n = 8) with U-Pb dates between 739±6 Ma – 595±6 Ma, $^{176}Hf/^{177}Hf_{(t)}$ ratios between 0.28186 – 0.28194 and $\varepsilon Hf_{(t)}$ between -19 – -15. Population II exhibit zircon crystals (n = 26) with U-Pb dates between 773±7 Ma – 596±6 Ma, $^{176}Hf/^{177}Hf_{(t)}$ ratios between 0.28195 – 0.28205 and $\varepsilon Hf_{(t)}$ between -16 – -6. Five zircon grains exhibit older U-Pb dates (1179±15 Ma, 1146±16 Ma, 1022±10 Ma, 875±8 Ma and 833±8 Ma) and were considered outliers for this population. Three zircon grains exhibit higher $^{176}Hf/^{177}Hf_{(t)}$ ratios (between 0.28206 and 0.28208) and were also considered outliers.

Recalculated $\varepsilon Hf_{(t)}$ values for the oldest dates in each population provided: Population I (739±6 Ma) with $\varepsilon Hf_{(739)}$ between -16 and -13; and Population II (773±7 Ma) with $\varepsilon Hf_{(773)}$ between -12 and -8. Thus, both populations define different protosources (although Population II is statistically more significand than Population I).

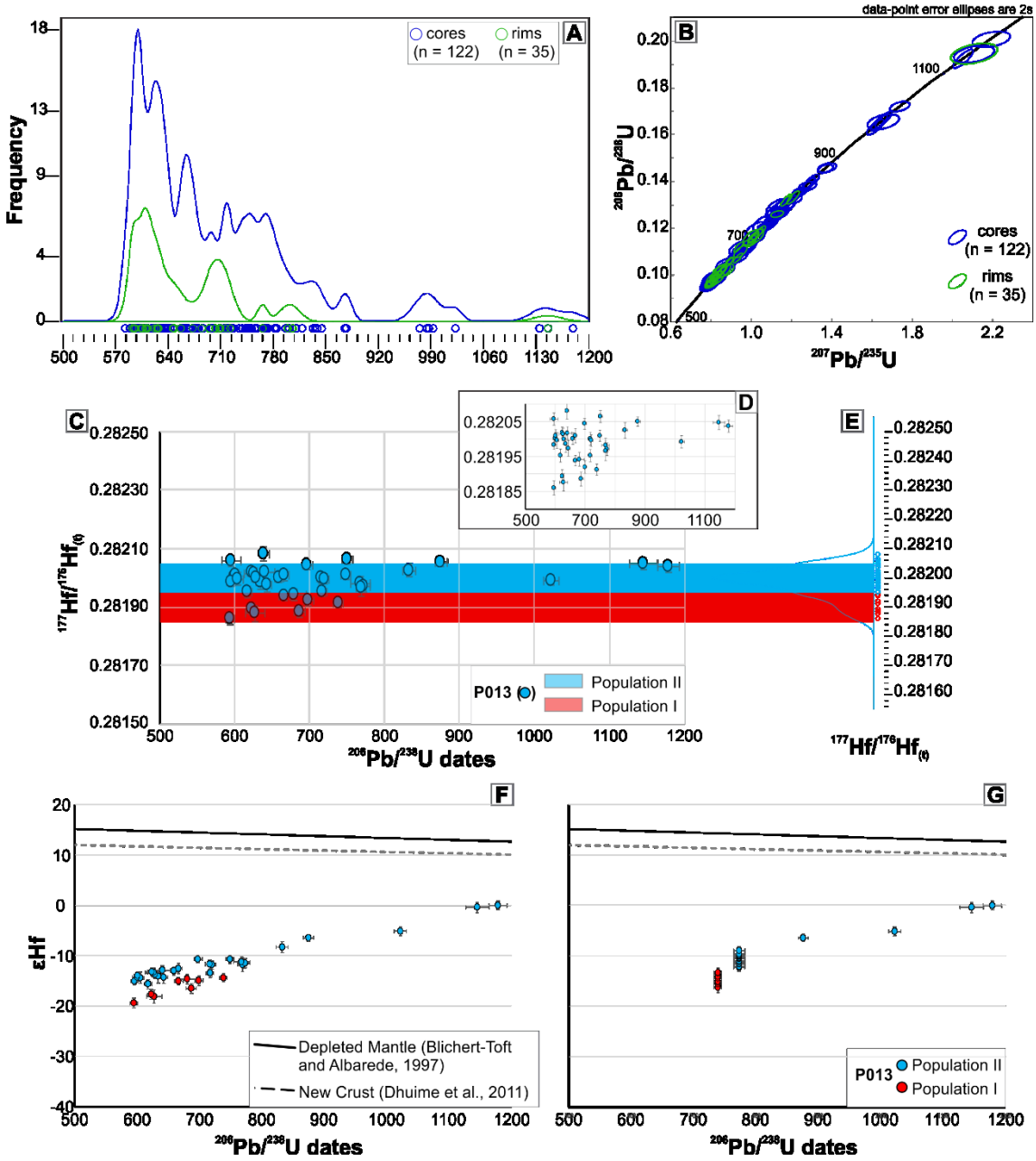

Figure 6-1 – Isotopic data from analyzed zircons in the orthopyroxene-garnet banded diatexite (P013) sample. A) $^{206}Pb/^{238}U$ probability density plot (PDP) for cores and rims (color schemes are the same of the Concordia diagram, B). B) Concordia diagram for cores and rims (dark blue and green ellipses, respectively) from sample P013. C-E) $^{176}Hf/^{177}Hf_{(t)}$ ratios versus $^{206}Pb/^{238}U$ dates (C-D) compared to the PDP for $^{176}Hf/^{177}Hf_{(t)}$ ratios I. Two zircon populations can be identified (Population I, red; Population II, blue). D) Detailed inset on I. F-G) εHf ratios versus $^{206}Pb/^{238}U$ dates for each population compared to the depleted mantle (Blichert-Toft and Albarède, 1997) and new crust (Dhuime et al., 2011) evolution trend. (F) exhibit the uncorrected ratios considering individual zircon dates, while (G) exhibit ratios corrected for the oldest zircon grain in each population (outliers excluded).

6.2 References

Tedeschi, M., Rossi Vieira, P. L., Kuchenbecker, M., Ribeiro, B. V., Barrote, V., Reis, H., Stutenbecker, L., Lana, C., Pedrosa-Soares, A., Dussin, I. 2023. **Unravelling and overcoming potential biases in U-Pb detrital zircon records induced by high to ultra-high temperature metamorphism (> 850 ºC).** Geoscience Frontiers, 14, 101515. https://doi.org/10.1016/j.gsf.2022.101515

7 DISCUSSIONS

Through the development of this thesis, it was observed that the effects of ultrahigh temperature (UHT) metamorphism were imprinted in metasedimentary rocks from the Southern Araçuaí orogen and Southern Brasília orogen (respectively) in different ways (Chapters 4 and 5).

The studied rocks from the Caparaó complex (Southern Araçuaí orogen, Chapter 4) exhibit mineral assemblages typically observed in UHT terrains worldwide (Al-rich orthopyroxene+garnet and hercynite+quartz; Harley, 1998, 2016; Kelsey, 2008; Kelsey and Hand, 2015), although the characteristic sapphirine+quartz assemblage was associated with microdomainial reactions rather than the metamorphic peak. Thermodynamic modelling and thermobarometry confirmed that the region underwent UHT metamorphism, with pressure-temperature conditions between 1020-1035 °C, 7.0-7.1 kbar calculated for hercynite-sillimanite-garnet migmatites and 968-975 °C, 9.5-9.6 kbar calculated for orthopyroxene-garnet migmatites. U-Pb zircon dates between ca. 635 – 610 Ma obtained from both migmatite types are likely associated with the UHT event, although a precise determination of the UHT metamorphism age was not possible through the U-Pb data alone.

The studied rocks from the Socorro-Guaxupé Nappe region (Botelhos-Bandeira do Sul, Southern Brasília orogen; Chapter 5) does not exhibit typical UHT mineral assemblages due to the composition of their protoliths (mostly metapsammites), although UHT occurrences (Al-rich orthopyroxene+garnet assemblages) are reported throughout the nappe (Campos-Neto, 1999, 2000; Del Lama et al., 2000; Campos-Neto et al., 2004; Rocha et al., 2017, 2018; Tedeschi et al., 2018; Motta et al., 2021). Combined U-Pb and Lu-Hf isotopes provided evidence of the contribution of arc-related protosources for the paraderived samples, exhibiting crustal (between ca. 804 – 776 Ma, $\varepsilon Hf_{(t)}$ = -16 to -2) and moderately juvenile (ca. 816 Ma, $\varepsilon Hf_{(t)}$ = +3 to +9) signatures. Crystallization ages for a biotite-bearing pink leucosome (ca. 691 Ma) and a garnet-bearing white granite (ca. 661 Ma) provided an estimate of the onset of UHT metamorphism (between ca. 690 – 660 Ma).

This chapter provides the closing remarks of this thesis by presenting a compilation of UHT metamorphism occurrences in Brazil (Figures 4, 5) and a discussion about the similarities and differences between UHT occurrences in the Southern Araçuaí and Brasília orogens, as well as their possible correlations and implications for the evolution of the West Gondwana.

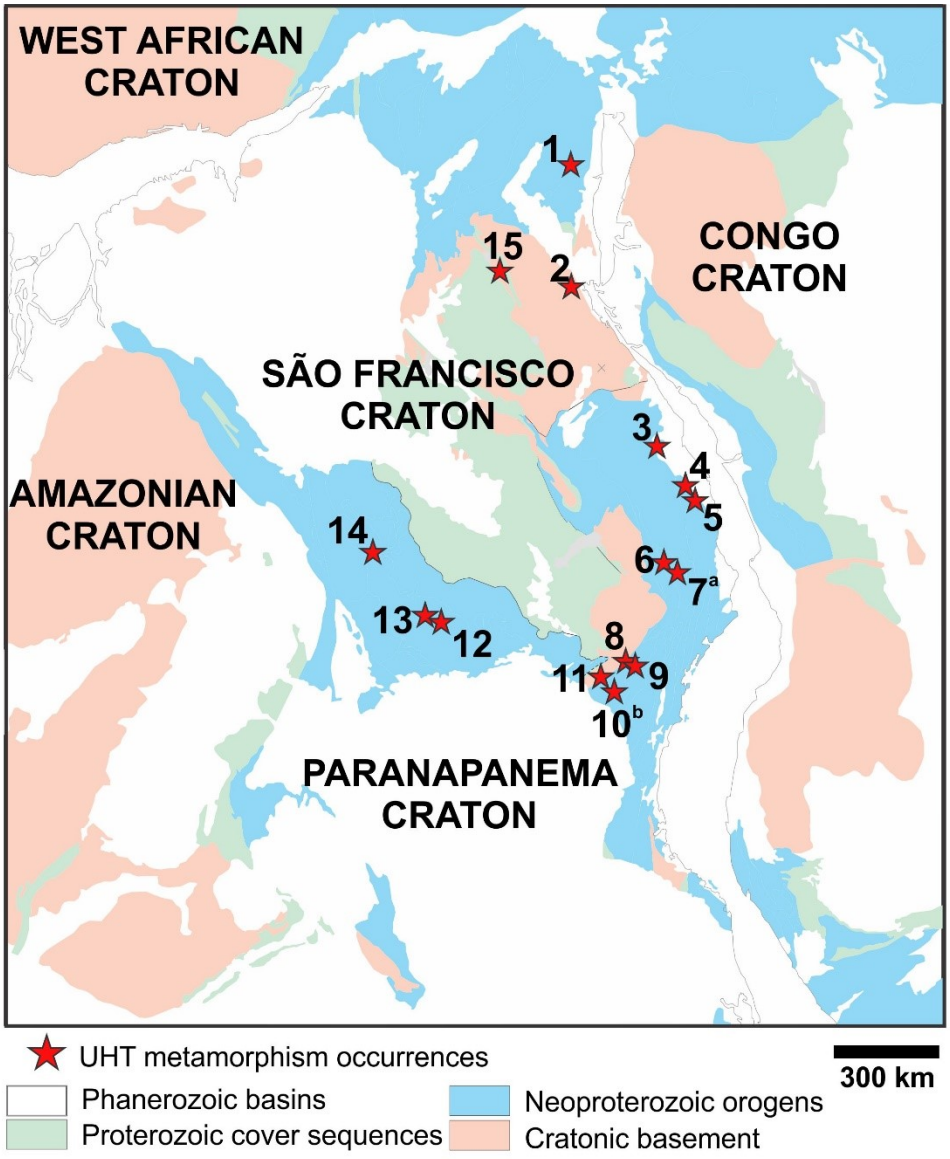

1 – Arapiaca Complex, Borborema Province; 2 – Brejões Dome – Jequié Block, São Francisco Craton; 3 – Jequitinhonha Complex, Araçuaí orogen; 4 – Nova Venécia Complex, Araçuaí orogen; 5 – São Gabriel da Baunilha Norite – Nova Venécia Complex, Araçuaí orogen; 6 – Manhuaçu region, Araçuaí orogen; 7 – Serra do Caparaó region, Caparaó Complex, Araçuaí orogen; 8 – Alfenas region – Socorro-Guaxupé Nappe, Southern Brasilia orogen; 9 – Varginha region – Socorro-Guaxupé Nappe, Southern Brasilia orogen; 10 – Botelhos-Bandeira do Sul region – Socorro-Guaxupé Nappe, Southern Brasilia orogen; 11 – Varginha Shear Zone – Socorro-Guaxupé Nappe, Southern Brasilia orogen; 12 – Goiânia region – Anápolis-Itauçu Complex, Northern Brasilia orogen; 13 – Damolândia region – Anápolis-Itauçu Complex, Northern Brasilia orogen; 14 – Barro Alto Complex, Northern Brasilia orogen; 15 - Itabuna-Salvador-Curaçá Belt.

Figure 7-1 – Occurrences of UHT metamorphic rocks in Brazil (map modified from Cioffi et al., 2019). 1 – Tesser et al. (2021); 2 – Barbosa et al. (2006); 3 – Belém (2006); 4 – Gradim (2013), Gradim et al. (2014); 5 – Wisniowski et al. (2021); 6 – Moreira (1997), Costa (1998); 7ª – Rossi-Vieira et al. (submitted), Chapter 4 from this thesis; 8 – Rocha et al. (2017, 2018); 9 – Reno et al. (2009), Motta et al. (2021); 10 – Tedeschi et al. (2018); 11 – Campos-Neto and Caby (2000), Del Lama et al. (2000); 12 – Moraes et al. (2002), Baldwin et al. (2005, 2007), Baldwin and Brown (2008); 13 – Moraes et al. (2002); 14 – Moraes and Fuck (2000); 15 – Leite et al. (2009).

7.1 Data compilation: known occurrences of ultrahigh temperature metamorphic rocks in Brazil

Considering that the UHT metamorphism occurrences on the South of the Araçuaí and Southern Brasília Orogen exhibit a spatial correlation with arc-related rocks, an initial hypothesis would be that the processes involving subduction probably had a main role in the development of extreme metamorphic temperatures in the context of the West Gondwana amalgamation. In order to test this hypothesis, data from UHT belts along the Brazilian territory were compiled and compared with the data obtained during the development of this thesis. The data compilation discussed in this section is presented in Appendix P.

7.1.1 Paleoproterozoic UHT metamorphism – the São Francisco Craton and Borborema Province

The São Francisco Craton (Jequié Block), the Borborema Province (Arapiaca Complex) and the Itabuna-Salvador-Curaçá belt constrain examples of UHT metamorphism related to the Paleoproterozoic (Rhyacian) orogeny (ca. 2.1 – 2.0 Gyr) in the Gondwana territory (Figure 1, 1-2. It is noteworthy that the Paleoproterozoic Juiz de Fora Complex, in the Araçuaí orogen, also exhibits an occurrence of UHT metamorphism (Figure 1, 6) but it is probably related to the Neoproterozoic orogeny (see section 4.3.1).

Barbosa et al. (2006) reported the occurrence of UHT Al-Mg-rich granulites, exhibiting the mineral assemblage hercynite-sillimanite-garnet-cordierite-plagioclase-quartz, in the Jequié Block, part of the São Francisco Craton. Metamorphic peak conditions between 985 – 1051 °C, 7.5 – 8.2 kbar were calculated using: Al-Opx-Grt barometer (Harley and Green, 1982); Grt-Opx thermometer (Harley, 1984a,c); Grt-Ilm thermometer (Pownceby et al., 1991); Crd-Spl thermometer (Vielzeuf, 1983); and the *average P-T* mode of THERMOCALC (Powell and Holland, 1994; Holland and Powell, 1998) (Figure 2A). Leite et al. (2009) reported metamorphic peak conditions between 900 – 950 °C, 7.0 – 8.0 kbar for sapphirine-bearing granulites and charnockites from the Itabuna-Salvador-Curaçá belt, applying phase-equilibria modeling using the Perple_X'07 software (Conolly and Petrini, 2002). Tesser et al. (2021) reported peak *P-T* conditions of ~970 °C and ~8.5 kbar in sapphirine-bearing diatexites (with several sub-domain assemblages) from the Arapiaca Complex (Borborema Province), based on Al-in-orthopyroxene thermobarometry (Pattison et al., 2003) and ternary feldspar reintegration thermometry (Kroll et al., 1993) (Figure 2A). Those authors proposed that

the UHT metamorphic event was related to continental collision and the accumulation of large volumes of magmas (“magma underplating”) during the ca. 2.1 – 2.0 Gyr orogeny related to the assembly of the Columbia/Nuna supercontinent, possibly associated with a late- to post-collisional orogenic collapse or slab break-off.

7.1.2 UHT metamorphism in the Brasília Orogen

7.1.2.1 Northern Brasília Orogen

UHT metamorphism occurrences in the Northern Brasília Orogen were reported in two different complexes: the Barro Alto Complex (Moraes and Fuck, 2000) (Figure 1, 14) and the Anápolis-Itauçu Complex (Moraes et al., 2002; Baldwin et al., 2005, 2007; Baldwin and Brown, 2008) (Figure 1, 12-13)

Moraes and Fuck (2000) reported *P-T* conditions of ~980 °C, ~8 kbar for orthopyroxene-sillimanite-plagioclase-garnet granulites from the Barro Alto Complex based on the comparison of mineral assemblages with petrogenetic grids (Hensen, 1986; Dasgupta et al., 1995) and in the convergence method of Fitzsimons and Harley (1994). Although no U-Pb data was provided in that work, those authors correlated the UHT metamorphic event to the ca. 820 – 770 Myr ages obtained for the granulite metamorphism by Suita et al. (1994) and Correia et al. (1999). A model involving continental collision, crustal extension and astenospheric heating was suggested to be responsible for the UHT conditions (Figure 2B).

Moraes et al. (2002) did a first detailed characterization of UHT metamorphism in the Anápolis-Itauçu Complex, obtaining *P-T* conditions between 960 – 1012 °C, 8.1 – 9.7 kbar through orthopyroxene-garnet barometers (Harley and Green, 1982; Harley, 1984b) and thermometers (Harley, 1984a) for: a rutile-spinel-orthopyroxene-garnet-sillimanite-cordierite-biotite(±sapphirine) granulite; a sapphirine-spinel-orthopyroxene-garnet-sillimanite-cordierite(±corundum) granulite; a sapphirine-garnet-orthopyroxene-sillimanite(±rutile) quartzite; and an ilmenite-rutile-spinel-orthopyroxene-garnet-sillimanite-cordierite gneiss (Figure 2B). Those authors suggested that UHT metamorphic conditions could have been attained through the ascension of the asthenosphere following the detachment of lithospheric mantle due to the detachment of the orogenic root or to a slab break-off during collision. Those occurrences were further studied in the works of Baldwin et al. (2005, 2007) and Baldwin and Brown (2008), from which *P-T* conditions of 980 – 1025 °C, ~9 kbar were obtained through phase equilibria modeling (THERMOCALC, Powell and Holland, 1988) and Ti-in-zircon thermometry (Watson et al., 2006) (Figure 2B). Baldwin and

Brown (2008) obtained U-Pb zircon ages between ca. 649 – 634 Ma for the UHT metamorphic event, which was associated to thickening of the back arc of the Arenópolis arc driven by terminal collision of the Paraná Block with the arc.

7.1.2.2 Southern Brasília Orogen

UHT metamorphism is reported mainly along the Guaxupé lobe from the Socorro-Guaxupé Nappe (SGN) in the Southern Brasília Orogen (Del Lama et al., 1994, 2000; Campos Neto and Caby, 1999, 2000; Rocha et al., 2017, 2018; Tedeschi et al., 2018; Motta et al., 2021) (Figure 1, 8-11).

Campos Neto and Caby (1999, 2000), Campos-Neto et al. (2004) and Del Lama et al. (1994, 2000) obtained a range of *P-T* values for (orthopyroxene-garnet) felsic and mafic granulites from the northern segment of the SGN (near the Varginha Shear Zone) between 900 – 1040 °C, 12 – 14.4 kbar applying the Grt-Opx thermometers of Ferry and Spear (1978) and Hodges and Spear (1982), the Cpx-Grt and Hbl-Grt thermometers of Powell (1985), the GAPES barometer (Eckert et al., 1991) and the TWEEQU method (Berman, 1988, 1991) (Figure 1, 11; Figure 2C). Rocha et al. (2017, 2018) obtained peak *P-T* values between 900 °C – 1027 °C, 11.7 – 12 kbar through Al-in-orthopyroxene thermobarometry (Pattison et al., 2003) for orthopyroxene-garnet bearing migmatites (Rocha et al., 2017) and granulites (Rocha et al., 2018) near the Alfenas region, close to the northeastern side of the SGN (Figure 1, 8; Figure 2C). Tedeschi et al. (2018) calculated peak *T* conditions of ~998 °C based on the Opx-Cpx calibration of Kretz (1982) for a banded granulite from the Botelhos – Bandeira do Sul region, in the middle of the northern lobe (Guaxupé domain) of the SGN (Figure 1, 10; Figure 2C). Motta et al. (2021) obtained *P-T* values between 1009 – 1020 °C, 11.5 – 14.4 kbar for a garnet-bearing felsic granulite and between 919 – 936 °C, 10.2 – 11 kbar for both a mafic and a felsic garnet-bearing granulite from the eastern side of the SGN (near the Varginha region), applying Al-in-orthopyroxene thermobarometry (Pattison et al., 2003), the *average P-T* mode of THERMOCALC (Powell and Holland, 1994; Holland and Powell, 1998) and phase equilibria modeling (THERMOCALC, Powell and Holland, 1988) (Figure 1, 9; Figure 2C).

Although metamorphic peak conditions are similar throughout different parts of the SGN, different tectonic settings and/or a different timing have been proposed for the UHT metamorphism: i) Reno et al. (2009) proposes that the metamorphic peak was attained during the subduction stage, with near-peak metamorphic ages of ca. 680 Ma obtained from a retroeclogite in the contact zone between the Socorro-Guaxupé

Nappe and the Três Pontas-Vargina Nappe, and that ages between ca. 648 Ma and ca. 622 represent post-peak zircon formation and melt crystallization; ii) Tedeschi et al. (2018) suggests that the Southern Brasília Orogen was affected by a long lived, two-stage metamorphic event, with a first stage encompassing the development of the magmatic arc between ca. 680 – 640 Myr and the onset of UHT conditions at ca. 660 Ma, and a second stage taking place between ca. 640 – 600 Myr, related to the collision-decompression stage; iii) Del Lama et al. (1994, 2000) proposed that the UHT metamorphic peak was achieved between ca. 660 – 630 Myr in a collisional setting; iv) Campos Neto and Caby (1999, 2000) and Campos-Neto et al. (2004) suggested that UHT conditions were achieved in a subduction-collisional setting in the deep roots of the magmatic arc, between ca. 630 – 625 Myr; v) Rocha et al. (2017, 2018) proposes that the UHT metamorphic peak was achieved in a long-lived (~30 Myr) event taking place at ca. 630 – 625 Ma due to crustal thickening and radioactive heat, followed by melt crystallization between ca. 625 – 600 Myr.

Based on crystallization ages of a leucosome and a granite associated to ortho- and paraderived rocks affected by (U)HT metamorphism on the SGN, Rossi-Vieira et al. (2023; Chapter 4) suggested that UHT metamorphism started between ca. 690 – 660 Myr during the development of the magmatic arc (in accordance with Reno et al., 2009, and Tedeschi et al., 2018), and (ultra)high-temperature conditions probably lasted until the collisional stage as suggested by Campos Neto and Caby (1999, 2000), Campos Neto et al. (2004), Rocha et al. (2017, 2018) and Motta et al., (2021).

7.1.3 UHT metamorphism in the Araçuaí Orogen

7.1.3.1 Basement units – the Juiz de Fora Complex

Ultrahigh temperature metamorphism has been firstly reported on the orthoderived orthopyroxene-plagioclase and orthopyroxene-clinopyroxene-plagioclase granulites of the Juiz de Fora Complex by Moreira (1997) and Costa (1998) in the Manhuaçu region. Mean temperature conditions obtained for the metamorphic peak were 990±50 °C, applying conventional Opx-Cpx thermometry (Bertrand and Mercier, 1985) in a range between 4 to 11 kbar (Figure 1, 6; Figure 2D). *P-T* calculations for hornblende-garnet amphibolites in the same region (Tsunogae et al. ,2002) provided peak *P-T* conditions between 830 – 880 °C and 7 – 8 kbar applying conventional Hbl-Pl thermometry (Holland and Blundy, 1994) and GBPQ barometry (Kohn and Spear, 1990). No U-Pb dating was provided in those works, and granulite

metamorphism was correlated to a back arc setting in association with an input of large volumes of magmas (magma underplating) during arc growth (Costa, 1998).

An assessment of U-Pb ages for the Juiz de Fora Complex in the Manhuaçu and Serra do Caparaó region was provided by Da Silva et al. (2002) and Faria et al. (2022). Igneous crystallization ages range between 2290 – 2060 Myr, while metamorphic ages range between ca. 633 – 584 Myr. Those metamorphic ages are older than the regional metamorphic peak for the Araçuaí orogen (ca. 563 Ma; Da Silva et al., 2002, 2011; Pedrosa-Soares et al., 2008, 2020; Gradim, 2013; Peixoto et al., 2015; Gonçalves et al., 2016; Richter et al., 2016; Tedeschi et al., 2016; Degler et al., 2017, 2018; Serrano et al., 2018; Araújo et al., 2020), and are also observed on metasedimentary rocks found along the Caparaó Range (ca. 635 – 581 Ma; Rossi-Vieira et al., submitted). Neoarchean metamorphic ages (ca. 2850 Ma) were obtained for granulitic gneisses from the Juiz de Fora Complex in the Juiz de Fora region (Da Silva et al., 2002), suggesting that at least part of the complex was affected by granulite-facies metamorphism prior to the Brasiliano orogeny.

7.1.3.2 Metasedimentary units – Nova Venécia and Jequitinhonha Complexes; Andrelândia(?) Group

Ultrahigh temperature metamorphic conditions in the Araçuaí orogen are only reported in metasedimentary units: one on the Jequitinhonha Complex (Belém, 2006; Figure 1, 3); two on the Nova Venécia Complex (Gradim, 2013; Gradim et al. 2014; Figure 1, 4; and Wisniowski et al., 2021; Figure 1, 5); and one probably related to the Andrelândia Group (Rossi-Vieira et al., submitted, Chapter 3; Figure 1, 7).

Belém (2006) reported *P-T* conditions of 917±52 °C and 7.4±0.6 kbar in the graphite-sillimanite-garnet-biotite gneisses of the Jequitinhonha Complex, calculated through the *average P-T* mode of THERMOCALC (Powell and Holland, 1994; Holland and Powell, 1998) (Figure 1, 3; Figure 2D). No U-Pb dating was provided in this work and the occurrence was not correlated to a tectonic setting by those authors, although this complex constrains metasedimentary rocks derived from passive margin and arc-related sedimentary sources (Pedrosa-Soares et al., 2001, 2008). Gradim (2013) and Gradim et al. (2014) reported *P-T* conditions of 930±118 °C, 6.1±0.4 kbar in the spinel-cordierite-garnet-sillimanite-biotite gneisses from the Nova Venécia Complex, calculated through the TWEEQU method (Berman, 1988, 1991) (Figure 1, 4; Figure 2D). Although U-Pb zircon dating was not provided for this sample, those authors propose that a thermal anomaly triggered by the subduction of an oceanic ridge (“slab

window") caused an increase in partial melting and granite generation in the back arc during the final pulses of development of the Rio Doce magmatic arc (ca. 590 – 580 Myr).

Rossi-Vieira et al. (submitted) reported two different sets of *P-T* conditions for metasedimentary rocks (probably) correlated to the Andrelândia Group in the Serra do Caparaó region, calculated through phase equilibria modeling (Theriak-Domino software, De Capitani and Petrakakis, 2010) and Al-in-orthopyroxene thermobarometry (Pattison et al., 2003): 1020 – 1035 °C, 7.0 – 7.1 kbar in hercynite-sillimanite-garnet diatexites; and 962 – 978 °C, 9.5 – 9.6 kbar in orthopyroxene-garnet diatexites (Figure 1, 7; Figure 2D; Chapter 3). Those authors associated the pressure difference between both groups to the juxtaposition of rocks from different crustal levels. U-Pb data obtained from both groups point to minimum ages between ca. 635 – 610 Myr for the UHT metamorphic event, within the timespan of the Rio Doce magmatic arc. This occurrence is spatially correlated (~30 km) to high-pressure granulites from the Manhuaçu region (750 °C, 17 kbar; Degler et al., 2019), and the authors interpreted the UHT metamorphism as related to a "slab window" mechanism during the subduction stage of the Araçuaí orogen.

Wisniowski et al. (2021) reported *P-T* conditions of 990 °C, 5.8 kbar in a contact metamorphism aureole in paragneisses from the Nova Venecia complex, employing phase equilibria modeling (Theriak-Domino, op. cit.), *average P-T* (THERMOCALC, op. cit.) and Al-in-orthopyroxene thermobarometry (Pattison et al., 2003) (Figure 1, 5; Figure 2D). This aureole is represented by a plagioclase-garnet-quartz-cordierite-sillimanite-hercynite-K-feldspar hornfels, associated with a norite intrusion. Those authors obtained a ca. 520 Ma age for both the contact metamorphism and the norite, which is associated with the post-collisional stage of the Araçuaí orogen.

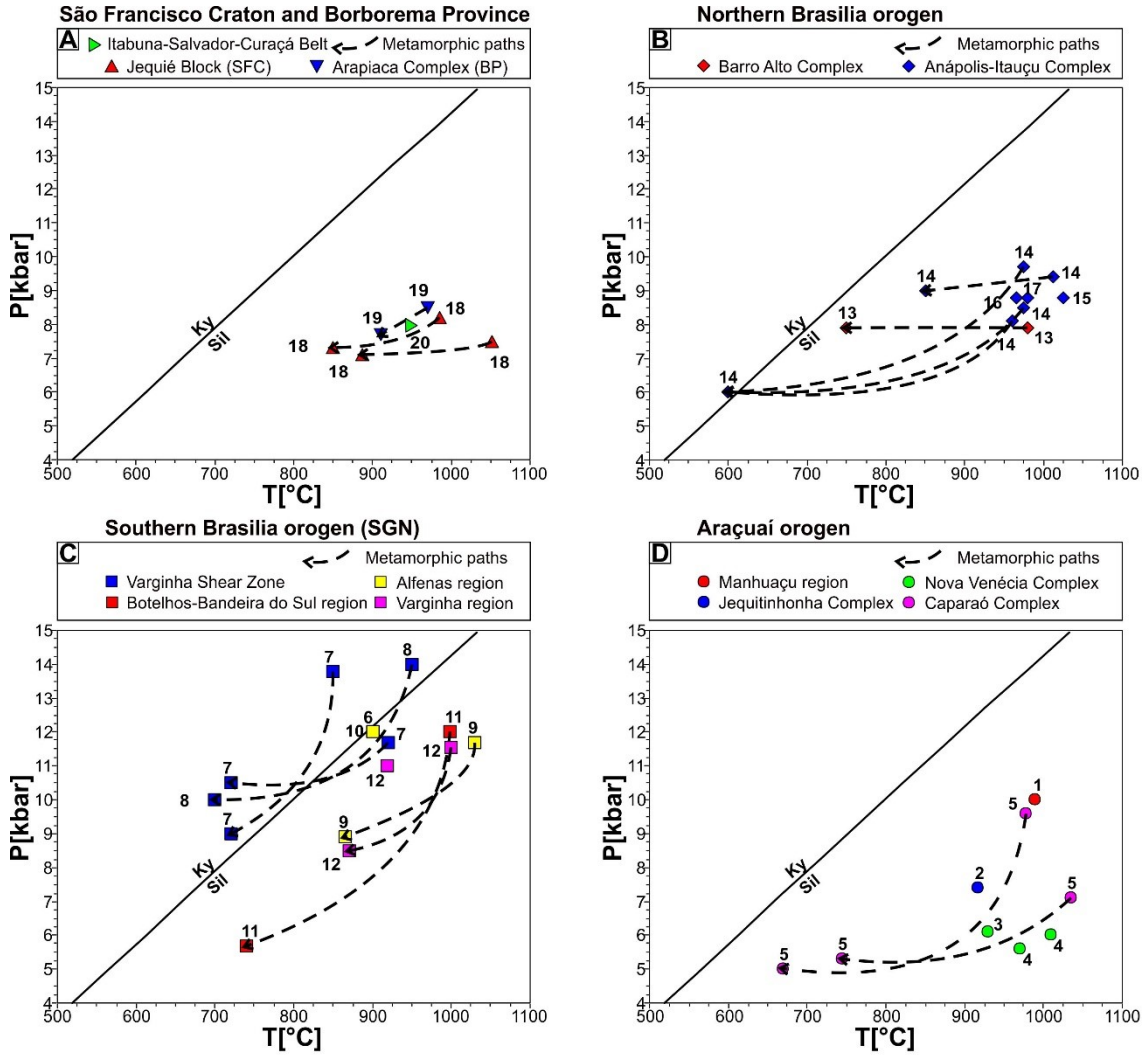

1 – Moreira, 1997; Costa, 1998; 2 – Belém, 2006; 3 – Gradim, 2013; Gradim et al., 2014; 4 – Wisniowski et al., 2021; 5 – Rossi-Vieira et al. (submitted; Chapter 3); 6 – Campos-Neto and Caby, 1999; 7 – Campos-Neto and Caby, 2000; 8 – Del Lama et al., 2000; 9 – Rocha et al., 2017; 10 – Rocha et al., 2018; 11 – Tedeschi et al., 2018; 12 – Motta et al., 2021; 13 – Moraes and Fuck, 2000; 14 – Moraes et al., 2002; 15 – Baldwin et al., 2005; 16 – Baldwin et al., 2007; 17 – Baldwin and Brown, 2008; 18 – Barbosa et al., 2006; 19 – Tesser et al., 2021; 20 - Leite et al., 2009

Figure 7-2 – Temperature-pressure conditions and metamorphic paths from UHT metamorphism occurences in Brazil according to their geological context. A) Araçuaí orogen; B) Southern Brasília orogen (Socorro-Guaxupé Nappe – SGN); C) Northern Brasília orogen; D) Paleoproterozoic occurrences (São Francisco Craton – SFC; Borborema Province – BP).

7.2 UHT metamorphism in the Brasiliano cycle – a link between the Southern Brasília and Araçuaí orogens

Ultrahigh temperature metamorphic rocks are identified on fourteen (14) localities in Brazil and are related to ten (10) different geological units/complexes along the Brasília orogen, Araçuaí orogen, São Francisco Craton and Borborema Province. Despite the differences in terms of metamorphic peak conditions, tectonic setting interpretations and the diachronic evolution of those orogenic systems, occurrences related to the Anápolis-Itauçu Complex (Northern Brasília orogen), Socorro-Guaxupé

Nappe (Southern Brasília orogen) and Caparaó Complex (Southern Araçuaí orogen) were developed in a similar time frame (ca. 690 – 590 Myr or ca. 660 – 590 Myr; Campos Neto and Caby, 2000; Del Lama et al., 2000; Campos-Neto et al., 2004; Baldwin et al., 2007; Baldwin and Brown, 2008; Rocha et al., 2017, 2018; Tedeschi et al., 2018; Motta et al., 2021; Rossi-Vieira et al., 2023; Rossi-Vieira et al., submitted) during the Brasiliano Cycle (Figure 4A-F).

This “time window” encompasses the transition between the pre-collisional, subduction-related stage and the collisional stage for both the Southern Brasília orogen and the Araçuaí orogen. Additional similarities between the UHT occurrences on both orogens include: i) similar clockwise trajectories observed on metamorphic paths; ii) thermal peaks reaching temperatures as high as 1030 °C; iii) protracted zircon U-Pb dates records observed on both paraderived and orthoderived metamorphic rocks, pointing out to a disturbance on the U-Pb system, while Lu-Hf signatures seems to be undisturbed (Figure 4G-K).

On another hand, those occurrences also exhibit remarkable differences: i) the Socorro-Guaxupé Nappe occurrences exhibit higher pressures (11 – 14 kbar) than the Manhuaçu-Caparaó occurrences (7 – 10 kbar), and thus the former were submitted to UHT conditions under higher crustal depths; ii) occurrences on the Southern Brasília orogen are spread throughout the Guaxupé lobe of the SGN, while occurrences on the Southern Araçuaí orogen are spatially limited to the Manhuaçu-Caparaó region; iii) high-pressure (HP) granulites are associated with different nappe systems (Três Pontas-Varginha and Andrelândia Nappe Systems, reaching up to 16-18 kbar; Campos Neto and Caby 1999, 2000; Cioffi et al., 2012) in the Southern Brasília orogen, while a close spatial relation (~35 km apart) is observed between UHT (Serra do Caparaó region) and HP granulites (Mahuaçu region, reaching up to 17 kbar; Degler et al., 2019) in the Araçuaí orogen.

Another distinctive aspect lies in the composition of the protoliths of paraderived rocks and its impact on observed mineral assemblages. In the Araçuaí Orogen there are several examples of hercynite+quartz bearing granulites and migmatites, including those affected by UHT metamorphism (Gradim, 2013; Gradim et al., 2014; Wisniowski et al., 2021) which might also rarely exhibit sapphirine+quartz assemblages (Rossi-Vieira et al., submitted; Chapter 3). Those rocks are typically interpreted as metamorphosed Al- and Mg-rich metapelites and might also exhibit other typical Al-rich phases such as cordierite and sillimanite (Pedrosa-Soares et al., 2001, 2008;

Belém, 2006; Gradim, 2013; Gradim et al., 2014; Richter et al., 2016; Wisniowski et al., 2021; Rossi-VIeira et al., submitted). However, in the Southern Brasília Orogen paraderived granulites and migmatites are typically of metapsammite composition, thus exhibiting high-Al orthopyroxene + garnet assemblages and usually lack Al-rich phases. It is noteworthy, however, that the mineral assemblage observed on the orthopyroxene-garnet migmatites from the Caparaó Complex is similar to those found on UHT paraderived rocks from the Southern Brasília Orogen.

In the Southern Araçuaí orogen, a subduction-related setting was interpreted for the UHT metamorphism in the Manhuaçu-Caparaó region (Costa, 1998; Rossi-Vieira et al., submitted). Rossi-Vieira et al. (submitted) proposes a “slab-window” mechanism as the responsible for the heating, which would explain the restricted occurrences of this type of metamorphism in the Southern Araçuaí orogen. In the Southern Brasília orogen, although different tectonic models have been proposed for the UHT occurrences they can be summarized as: i) subduction-collision models, in which the accumulation of arc-related magmas and crustal thickening is responsible for reaching ultrahigh temperatures (Campos Neto and Caby, 1999, 2000; Reno et al., 2009; Tedeschi et al., 2018; Rossi-Vieira et al., 2023); collisional setting, with the accumulation of radiogenic elements due to crustal thickening during nappe stacking as responsible for attaining ultrahigh temperatures (Del Lama et al., 2000; Rocha et al., 2017, 2018).

In both orogenic systems the UHT occurrences are spatially associated with arc-related rocks (the Elói Mendes and São João da Mata complexes in the SGN and the G1 Supersuite in the Araçuaí orogen). In the SGN, the protoliths of the UHT metamorphic rocks are also related to arc-derived protosources. Those associations and the time intervals (Figure 4A-J) are suggestive that the onset of the UHT metamorphic event in both orogenic systems is related to a subduction setting, although the ocean-continent subduction stage took place diachronically in both orogens (between ca. 635 – 585 Ma in the Araçuaí orogen and between ca. 800 – 630 Ma in the Southern Brasília Orogen; Campos Neto and Figueiredo, 1995; Nalini Jr., 1997; Campos Neto and Caby, 2000; Noce et al., 2000; Hackspacher et al., 2003; Novo et al., 2010; Da Silva et al., 2011; Pedrosa-Soares et al., 2011, 2020; Novo, 2013; Gonçalves et al., 2014, 2016; Mora et al., 2014; Tedeschi et al., 2016; Rocha et al., 2018; Tedeschi et al., 2018; Campos-Neto et al., 2021). Abnormally high heat flux in the lower to middle crust caused by the underplating of arc magmas and/or the

ascension of the asthenosphere is likely to be the trigger for attaining such extreme metamorphic conditions.

It is proposed that the subduction-related, pre-collisional stage of both the Southern Brasília orogen and Araçuaí orogen constrains the UHT metamorphic stage of those orogenic systems, although their onset happened diachronically (ca. 690 – 660 Myr in the Southern Brasília orogen and a minimum estimate between ca. 635 – 610 Myr in the Southern Araçuaí orogen). An overlapping of the proposed ages for the UHT metamorphism can be observed on Figure 4(A-J), which roughly defines a combined interval between ca. 660 – 595 Ma for both orogenic systems. However, although UHT occurrences have been described in detail through several works on the Southern Brasília orogen (Campos Neto and Caby, 1999, 2000; Del Lama et al., 2000; Campos-Neto et al., 2004; Reno et al., 2009; Rocha et al., 2017, 2018; Tedeschi et al., 2018; Motta et al., 2021), only a few detailed reports exist in the Southern Araçuaí orogen up to date (Gradim 2013; Wisniowski et al., 2021; Rossi-Vieira et al., submitted). Additional data is needed in order to better constrain the spatial extent of UHT metamorphism in the Araçuaí orogen as well as better determine their ages.

It is also noteworthy that although spatially unrelated, minimum ages obtained for protosources from the paraderived rocks from the Caparaó complex (layered orthopyroxene-garnet diatexite, sample P013, Figure 4G) and Socorro-Guaxupé Nappe (hornblende-biotite stromatic metatexite, sample PC12.2, Figure 4I; garnet-biotite stromatic metatexite, sample PC12.4, Figure 4J), as well as minimum crystallization ages for orthoderived rocks from the SGN (amphibolite enclave, sample PC12.1, Figure 4H; (hornblende)-biotite stromatic metatexite, sample C1071A, Figure 4K), fall inside a similar range (ca. 816 – 719 Ma). However, in order to suggest the geological context in which the protosources for sample P013 crystallized, a comparison with possible sources in the Araçuaí-West Congo orogen is required.

Although up to date no UHT metamorphism occurrence is known in the Ribeira orogen (considering the SGN as part of the Southern Brasília orogen, as proposed by Campos Neto and Caby, 1999, 2000; Campos-Neto et al., 2004, 2011), it is noteworthy that UHT metamorphism was present in orogenic systems developed on both sides of the São Francisco paleocontinent during the amalgamation of the West Gondwana. The well-marked time frame for those occurrences is in accordance with the observations about the link between the amalgamation of the supercontinents and the occurrence of extreme metamorphism (e.g. Brown, 2007, 2008; Brown and Johnson,

2018). In the systematic reviews presented by Brown (2007, 2008) and Brown and Johnson (2018) it is observed that the time period between ca. 630 – 510 Myr is one of the main “time windows" for the generation of UHT metamorphic rocks, and it is roughly coincident with a major change in the dynamics of plate tectonics. It appears that occurrences of UHT metamorphic rocks roughly define an “UHT metamorphic belt” throughout the Brasiliano orogens (Figure 1). However, further studies are needed in order to identify possible unknown UHT occurrences, provide detailed P-T data, and to better constrain those occurrences in the light of the evolution of the Brasiliano orogens.

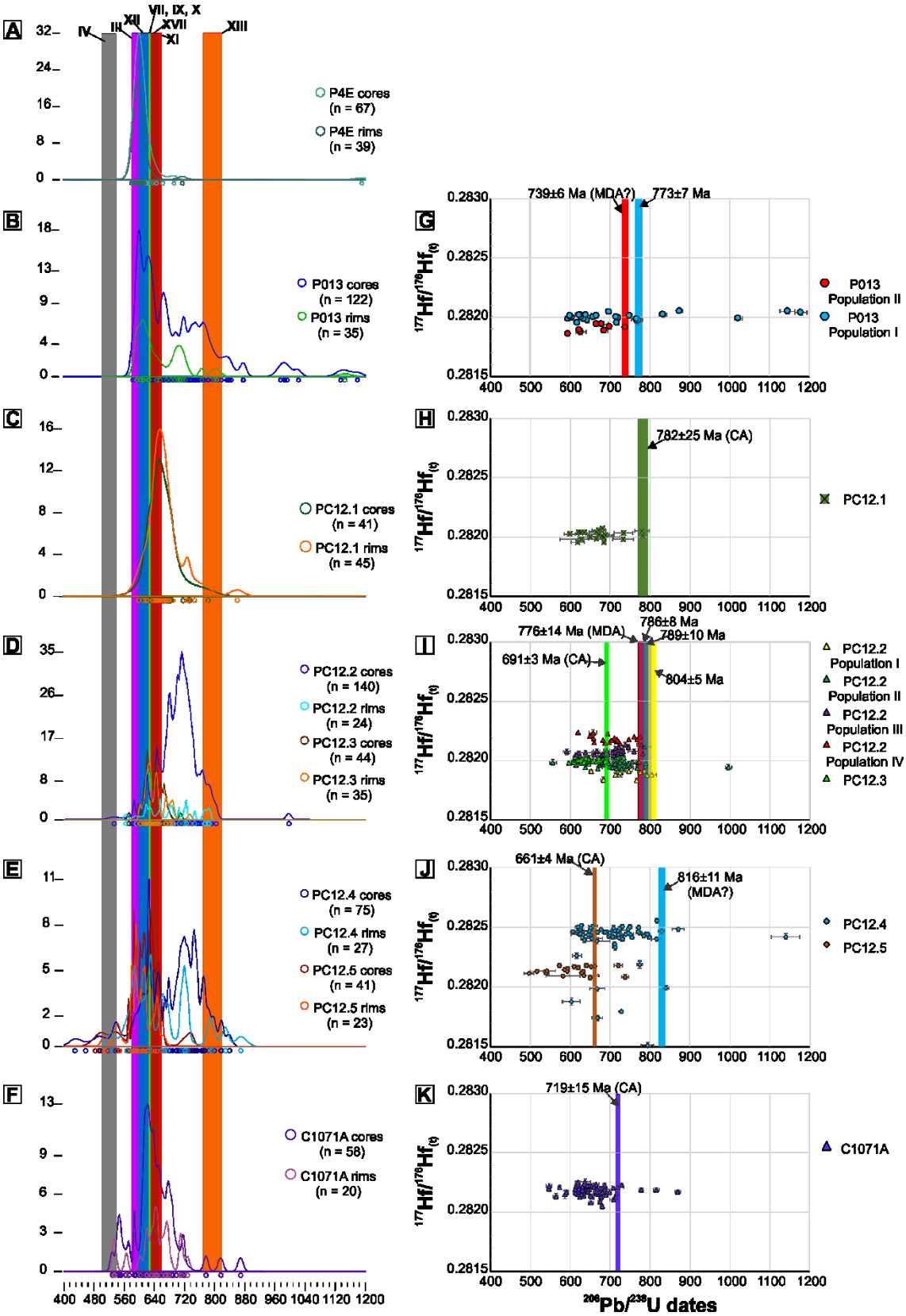

Figure 7-3 – Comparison between U-Pb dates probability density plots (PDP) (A-F), $^{176}Hf/^{177}Hf_{(t)}$ ratios x $^{206}Pb/^{238}U$ dates (G-K), minimum crystallization (CA) and maximum depositional ages (MDA) (G-K) between samples analyzed in this thesis, as well as a comparison with the spectra of UHT metamorphic ages from previous authors. A) schlieren/schollen hercynite-sillimanite-garnet diatexite, P4E; B and G) layered orthopyroxene-garnet diatexite, P013; C and H) amphibolite enclave, PC12.1; D and I) hornblende-biotite

stromatic metatexite, PC12.2, and biotite-bearing pink leucosome, PC12.3; E and J) garnet-biotite stromatic metatexite, PC12.4, and garnet-bearing white granite, PC12.5; F and K) (hornblende)-biotite stromatic metatexite, C1071A. III – Gradim, 2013; Gradim et al., 2014; IV – Wisniowski et al., 2021; VII – Campos Neto and Caby, 2000; IX – Rocha et al., 2017; X – Rocha et al., 2018; XI – Tedeschi et al., 2018; XII – Motta et al., 2021; XIII – Moraes and Fuck, 2000; XVII – Baldwin and Brown, 2008.

7.3 References

Araujo, C., Pedrosa-Soares, A., Lana, C., Dussin, I., Queiroga, G., Serrano, P., Medeiros-Junior, E. 2020. **Zircon in emplacement borders of post-collisional plutons compared to country rocks: A study on morphology, internal texture, U-Th-Pb geochronology and Hf isotopes (Araçuaí orogen, SE Brazil).** Lithos, 352-353, 105252.

Baldwin, J. A. and Brown, M. 2008. **Age and duration of ultrahigh-temperature metamorphism in the Anápolis-Itauçu Complex, Southern Brasília Belt, central Brazil – constraints from U-Pb geochronology, mineral rare earth element chemistry and trace-element thermometry**. Journal of Metamorphic Geology, 26, 213-233. Doi:10.1111/j.1525-1314.2007.00759.x

Baldwin, J. A., Brown, M., Schmitz, M. D. 2007. **First application of titanium-in-zircon thermometry to ultrahigh-temperature metamorphism**. Geology, 35(4), 295-298. Doi: 10.1130/G23285A.1

Baldwin, J. A., Powell, R., Brown, M., Moraes, R. and Fuck, R. A. 2005**. Modelling of mineral equilibria in ultrahigh-temperature metamorphic rocks from the Anápolis-Itauçu Complex, central Brazil.** Journal of Metamorphic Geology, 23, 511 – 531. Doi:10.1111/j.1525-1314.2005.00591.x

Barbosa, J., Nicollet, C., Leite, C., Kienast, J. R., Fuck, R. A., Macedo, E. P. 2006. **Hercynite-quartz-bearing granulites from Brejões Dome area, Jequié Block, Bahia, Brazil: Influence of charnockite intrusion on granulite facies metamorphism**. Lithos, 92(3 – 4), 537 – 556. https://doi.org/10.1016/j.lithos.2006.03.064

Belém, J. 2006. **Caracterização Mineralógica, Física e Termobarométrica de Minérios de Grafita da Província Grafítica Bahia-Minas**. (Unpublished master's thesis). Universidade Federal de Minas Gerais, Belo Horizonte, Brazil.

Berman, R. G. 1988. **Internally-consistent thermodynamic data for minerals in the system Na_2O–K_2O–CaO–MgO–FeO–Fe_2O_3–Al_2O_3–SiO_2–TiO_2–H_2O–CO_2.** Journal of Petrology 29, 445–522.

Berman R. G. 1991. **Thermobarometry using multi-equilibrium calculations: a new technique, with petrological applications.** Canadian Mineralogist, 29, 833-855.

Bertrand, P. and Mercier, J. C. C. 1985. **The mutual solubility of coexisting ortho- and clinopyroxene: toward an absolute geothermometer for the natural system?** Earth Planetary Science Letters, 76(1-2), 109-122.

Blichert-Toft, J. and Albarède, F. 1997. **The Lu-Hf geochemistry of chondrites and the evolution of the mantle-crust system**. Earth Planet Science Letters, 148, 243 – 258

Brown, M. 2007. **Metamorphic conditions in orogenic belts: a record of secular change**. International Geology Reviews, 49(3), 193-234.

Brown, M. 2008. **Characteristic thermal regimes of plate tectonics and their metamorphic imprint throughout Earth history: When did Earth first adopt a plate tectonics mode of behavior?** In K. Condie and V. Pease. (Eds.). **When Did Plate Tectonics Begin?** Geological Society of America Special Paper, 440, 97–128.

Brown, M. and Johnson, T. 2018. **Secular change in metamorphism and the onset of global plate tectonics.** American Mineralogist, 103, 181-196.

Campos-Neto, M. C., Basei, M. A. S., Janasi, V. A., Moraes, R. 2011. **Orogen migration and tectonic setting of the Andrelândia Nappe system: An Ediacaran western Gondwana collage, south of São Francisco craton**. Journal of South American Earth Sciences, 32, 393 – 406

Campos Neto, M. C., Basei, M. A., Vlach, S. R. F., Caby, R., Szabó, A. J., Vasconcelos, P. 2004. **Migração de orógenos e superposição de orogêneses: um esboço da colagem Brasíliana no sul do Cráton do São Francisco, SE-Brasil.** Geologia USP Série Científica, 4 (1), 13 – 40

Campos-Neto, M. C. and Caby, R. 1999. **Neoproterozoic high-pressure metamorphism and tectonic constraint from the nappe system south of the Sao Francisco Craton, southeast Brazil.** Precambrian Research, 97 (1 – 2), 3 – 26

Campos-Neto, M. C. and Caby, R. 2000. **Terrane accretion and upward extrusion of high-pressure granulites in the Neoproterozoic nappes of southeast Brazil: Petrologic and structural constraints**. Tectonics, 19(4), 669 – 687

Campos Neto, M. C., Cioffi, C. R., Westin, A., Rocha, B. C., Frugis, G. L., Tedeschi, M., Pinheiro, M. A. P. 2020. **O orógeno Gondwana meridional.** In: Bartorelli, A., Teixeira, W., Brito Neves, B. B. (Orgs.). **Geocronologia e Evolução Tectônica do Continente Sul-Americano: a contribuição de Umberto Giussepe Cordani**. Solaris Edições Culturais, São Paulo, p. 146 – 180

Campos-Neto, M. C. and Figueiredo, M. C. H. 1995. **The Rio Doce orogeny, southeastem Brazil.** Journal of South American Earth Sciences, 8(2), 143–162

Cioffi, C. R., Campos Neto, M. C., Moller, A., Rocha, B. C. 2019. **Titanite petrochronology of the southern Brasília Orogen basement: effects of retrograde net-transfer reactions on titanite trace element compositions.** Lithos, 344 – 345, 393 – 408

Cioffi, C. R., Campos Neto, M. C., Rocha, B. C., Moraes, R., Henrique-Pinto, R. 2012. **Geochemical signatures of metasedimentary rocks of high-pressure granulite facies and their relation with partial melting: Carvalhos Klippe, southern Brasília Belt, Brazil**. Journal of South American Earth Sciences 40, 63–76.

Conolly, J. A. D. and Petrini, K. 2002. **An automated strategy for calculation of phase diagram sections and retrieval of rock properties as a function of physical conditions**. Journal of Metamorphic Geology, 20, 697–708.

Correia, C. T., Jost, H., Tassinari, C. C. G., Girardi, V. A. V. and Kinni, P. D. 1999. **Ectasian Mesoproterozoic U–Pb ages (SHRIMP II) for the metavolcanosedimentary sequence of Juscelândia and Indaianópolis and for high grade metamorphosed rocks of Barro Alto stratiform igneous Complex, Goiás State, central Brazil.** In: II South American Symposium on Isotope Geology, Cordoba, Actas, pp. 31–33.

Costa, A. G., 1998. **The Granulite-Facies Rocks of the Northern Segment of the Ribeira Belt, Eastern Minas Gerais, SE Brazil.** Gondwana Research, 1(3-4), 367-372.

Costa, F. M., Penna, J. L. A., Martins, L. C. D., Tedeschi, M., Novo, T. A., Araujo, C. S., Vieira Rossi, P. L., Lana, C., Pedrosa-Soares, A. C. 2022. **Zircon petrochronology reveals the moderately juvenile signature of a diatexite from the boundary zone between the Brasília and Ribeira orogens (SE Brazil): Relict of a Tonian arc?** Journal of South American Earth Sciences, 116, 103767. https://doi.org/10.1016/j.jsames.2022.103767.

Da Silva, L. C., Armstrong, R., Noce, C. M., Carneiro, M. A., Pimentel, M., Pedrosa-Soares, A. C., Leite. C. A., Vieira, V. S., Silva, M. A., Paes, V. J. C., Cardoso Filho, J. M. 2002. **Reavaliação da evolução geológica em terrenos Pré-Cambrianos brasileiros com base em novos dados U-Pb SHRIMP, parte II: Orógeno Araçuaí, Cinturão Mineiro e Cráton São Francisco Meridional**. Revista Brasileira de Geociências, 32(4), 513-528.

Da Silva, L. C., Pedrosa-Soares, A. C., Armstrong, R., and Noce, C. M. 2011. **Determinando a duração do período colisional do Orógeno Araçuaí com base em geocronologia U-Pb de alta resolução em zircão: uma contribuição para a história da amalgamação do Gondwana Ocidental**. Geonomos, 19(2), 180-197.

Dasgupta, S., Sengupta, P., Ehl, J., Raith, M., Bardhan, S. 1995. **Reaction textures in a suite of spinel granulites from the isobaric cooling path before the exhumation of the Eastern Ghats Belt, India: evidence for polymetamorphism, a partial petrogenetic grid in the system KFMASH and the roles of ZnO and Fe_2O_3**. Journal of Petrology, 36, 435–461.

De Capitani, C. and Petrakakis, K. 2010. **The computation of equilibrium assemblage diagrams with Theriak/Domino software.** American Mineralogist, 95, 1006-1016. DOI: http://dx.doi.org/10.2138/am.2010.3354

Degler, R., Costa, A. G., Pedrosa-Soares, A. C., Queiroga, G. N. 2019. **High pressure metamorphism related to suture zone in the Araçuaí orogen (SE Brazil): further evidence against ensialic models.** XVII Simpósio Nacional de Estudos Tectônicos (SNET), Annals, p. 124. Sociedade Brasileira de Geologia, SBG.

Degler, R., Pedrosa-Soares, A. C., Dussin, I., Queiroga, G., and Schulz, B. 2017. **Contrasting provenance and timing of metamorphism from paragneisses of the**

Araçuaí-Ribeira orogenic system, Brazil: Hints for Western Gondwana assembly. Gondwana Research, 51, 30-50.

Degler, R., Pedrosa-Soares, A. C., Novo, T. A., Tedeschi, M., Da Silva, L. C., Dussin, I. A., Lana, C. 2018. **Rhyacian-Orosirian isotopic records from the basement of the Araçuaí-Ribeira orogenic system (SE Brazil): Links in the Congo-São Francisco palaeocontinent.** Precambrian Research, 317, 179-195.

Del Lama, E. A., Oliveira, M. A. F. and Zanardo, A. 1994. **Geotermobarometria em rochas do Complexo Campos Gerais ao none da zona de cisalhamento Varginha**. Revista Brasileira de Geociências, 24, 233-239.

Del Lama, E. A., Zanardo, A., Oliveira, M. A. F., Moralles, N. 2000**. Exhumation of high-pressure granulites of the Guaxupé Complex, Southeastern Brazil.** Geological Journal, 35, 231 – 249.

Dhuime, B., Hawkesworth, C., Cawood, P. 2011. **When continents formed**. Science, 331, 154 – 155

Eckert, J. O., Newton, R. C., Kleppa, O. J. 1991. **The ΔH of reaction and recalibration of garnet-pyroxene-plagioclase-quartz geobarometers in the CMAS system by solution calorimetry.** American Mineralogist, 76, 148-160.

Faria, T. G., Alves, M. I., Potratz, G. L., Silva, L. F. R., Rodrigues, S. W. O., Martins, M. V. A., Geraldes, M. C. 2022. **The Serra do Caparaó Complex, Mantiqueira Province, Brazil, revisited: metamorphic age constraints by U-Pb and Lu-Hf method in zircon by LA-ICP-MS.** Journal of the Geological Survey of Brazil, 5(1), 49-80.

Ferry, J. M. and Spear, F. S. 1978. **Experimental calibration of the partitioning of Fe and Mg between biotite and garnet**. Contributions to Mineralogy and Petrology, 66, 113-117.

Fitzimons, I. C. W. and Harley, S. L. 1994. **The influence of retrograde cation exchange on granulite P-T estimates and a convergence technique for the recovery of peak metamorphic conditions.** Journal of Petrology, 35(2), 543-576.

Gonçalves L., Farina F., Lana C., Pedrosa-Soares, A. C., Alkmim, F., Nalini Jr., H. A. 2014. **New U–Pb ages and lithochemical attributes of the Ediacaran Rio Doce magmatic arc, Araçuaí confined orogen, Southeastern Brazil**. Journal of South American Earth Sciences, 52, 129-148.

Gonçalves, L., Alkmim, F. F., Pedrosa-Soares, A. C., Dussin, I. A., Valeriano, C. M., Lana, C., Tedeschi, M. 2016. **Granites of the intracontinental termination of a magmatic arc: an example from the Ediacaran Araçuaí orogen, southeastern Brazil.** Gondwana Research, 36, 439-458.

Gradim, C. 2013. **Complexo Nova Venécia e magmatismo associado, Orógeno Araçuaí, Estado do Espírito Santo** (Unpublished master's thesis). Universidade Federal de Minas Gerais, Belo Horizonte, Brazil.

Gradim, C., Roncato, J., Pedrosa-Soares, A.C., Cordani, U., Dussin, I., Alkmim, F.F., Queiroga, G., Jacobsohn, T., Silva, L. C., Babinski, M. 2014. **The hot back-arc zone of the Araçuaí orogen, Eastern Brazil: from sedimentation to granite generation.** Brazilian Journal of Geology, 44, 155-180. DOI: http://dx.doi.org/10.5327/Z2317-4889201400010012.

Hackspacher, P. C., Fetter, A. H., Ebert, H. D., Janasi, V. A., Dantas, E. L., Oliveira, M. A. F., Braga, I. F., Negri, F. A. 2003. **Magmatismo há ca. 660–640 Ma no Domínio Socorro: registros de convergência pré-colisional na aglutinação do Gondwana Ocidental.** Geologia USP, Série Científica, 3, 85–96.

Harley, S. L. 1984a. **An experimental study of the partitioning of Fe and Mg between garnet and orthopyroxene**. Contributions to Mineralogy and Petrology, 86, 359-373.

Harley, S. L. 1984b. **The solubility of Alumina in orthopyroxene coexisting with garnet in FeO-MgO-Al_2O_3-SiO_2 and CaO-FeO-MgO-Al_2O_3-SiO_2**. Journal of Petrology, 25, 665-696.

Harley, S. L. 1984c. **Comparison of the garnet-orthopyroxene geobarometer with recent experimental studies, and applications to natural assemblages**. Journal of Petrology, 25, 697-712.

Harley, S. L. 1998a. **On the occurrence and characterization of ultrahigh-temperature crustal metamorphism.** In: Treloar, P. J. and O'Brien, P. J. (Eds.). **What drives metamorphism and metamorphic reactions?** Geological Society, London, Special Publications, 138, 81-107.

Harley, S. L. 2016. **A matter of time: the importance of the duration of UHT metamorphism**. Journal of Mineralogical and Petrological Sciences, 111, 50 – 72. Doi: 10.2465/jmps.160128

Harley, S. L. and Green, D. H. 1982. **Garnet-Orthopyroxene barometry for granulites and garnet peridotites.** Nature, 200, 697-700.

Hensen, B. J., 1986. **Theoretical phase relations involving cordierite and garnet revisited: the influence of oxygen fugacity on the stability of sapphirine and spinel in the system Mg–Fe–Al–Si–O.** Contributions to Mineralogy and Petrology, 92, 362–367.

Hodges, K. V. and Spear, F. S. 1982. **Geothermometry, geobarometry and the Al_2SiO_5 triple point at Mt. Moosilauke, New Hampshire**. American Mineralogist, 67, 1118-1134.

Holland T. and Blundy J. 1994. **Non-ideal interactions in calcic amphiboles and their bearing on amphibole-plagioclase thermometry**. Contributions to Mineralogy and Petrology, 116(4), 433-447.

Holland, T. J. B. and Powell, R. 1998. **An internally consistent thermodynamic data set for phases of petrological interest**. Journal of Metamorphic Geology, 16, 309-344.

Kelsey, D. E. 2008. **On ultrahigh-temperature crustal metamorphism**. Gondwana Research, 13, 1 – 29.

Kelsey, D. E., Hand, M. 2015. **On ultrahigh temperature crustal metamorphism: Phase equilibria, trace element thermometry, bulk composition, heat sources, timescales and tectonic settings**. Geoscience Frontiers, 6, 311 – 356.

Kohn M. J., Spear F. S. 1990. **Two new geobarometers for garnet amphibolites, with applications to southeastern Vermont**. American Mineralogist, 75(1-2), 89-96.

Kretz, R. 1982. **Transfer and exchange equilibria in a portion of the pyroxene quadrilateral as deduced from natural and experimental data**. Geochimica et Cosmochimica Acta, 46, 411–421.

Kroll, H., Evangelakakis, C., and Voll, G. 1993. T**wo-feldspar geothermometry: A review and revision for slowly cooled rocks.** Contributions to Mineralogy and Petrology, 114(4), 510 – 518. https://doi.org/10.1007/BF00321755.

Mora, C. A. S., Campos Neto, M. C. and Basei, M. A. S., 2014. **Syn-collisional lower continental crust anataxis in the Neoproterozoic Socorro-Guaxupé Nappe System, southern Brasília Orogen, Brazil: constraints from zircon U-Pb dating, Sr-Nd-Hf signatures and whole-rock geochemistry.** Precambrian Research, 255, 847 – 864.

Moraes, R., Brown, M. Fuck, R. A., Camargo, M. A., Lima, T. M. 2002. **Characterization ant P-T Evolution of Melt-bearing Ultrahigh-temperature Granulites: an Example from the Anápolis-Itauçu Complex of the Brasília Fold Belt, Brazil.** Journal of Petrology, 43(9), 1673 – 1705.

Moraes, R. and Fuck, R. A. 2000. **Ultra-high-temperature metamorphism in Central Brazil: the Barro Alto complex.** Journal of Metamorphic Geology, 18, 345 – 358.

Moreira, L. M. 1997. **Evolução crustal do Leste de Minas Gerais: uma contribuição a partir do estudo geotermobarométrico de metamorfitos da região Simonésia-Manhuaçu (MG).** (Unpublished doctoral thesis). Universidade Federal de Minas Gerais, Belo Horizonte, Brazil.

Motta, R. G., Fitzsimons, I. C. W., Moraes, R., Johnson, T. E., Schuindt, S., Benetti, B. Y. 2021. **Recovering P-T-t paths from ultra-high temperature (UHT) felsic orthogneiss: An example from the Southern Brasília Orogen, Brazil**. Precambrian Research, 359, p. 106222.

Nalini Jr., H.A. 1997. **Caractérisation des suites magmatiques néoprotérozoïques de la région de Conselheiro Pena et Galiléia (Minas Gerais, Brésil): étude géochimique et structurale des 195ondwa Galiléia et Urucum et leur relation avec les pegmatites à éléments rares associées.** Thèse de Doctorat, École des Mines de Saint-Étienne et École des Mines de Paris, Saint-Étienne, 395 p.

Noce, C. M., Macambira, M. B., Pedrosa-Soares, A.C. 2000. **Chronology of Neoproterozoic-Cambrian granitic magmatism in the Araçuaí Belt, Eastern**

Brazil, based on single zircon evaporation dating. Revista Brasileira de Geociências, 30, 25-29.

Novo, T. A. 2013. **Caracterização do Complexo Pocrane, magmatismo básico mesoproterozóico e unidades neoproterozóicas do sistema Araçuaí-Ribeira, com ênfase em geocronologia U-Pb (SHRIMP e LA-ICP-MS).** (Unpublished doctoral thesis). Universidade Federal de Minas Gerais, Belo Horizonte, Brazil.

Novo, T. A., Pedrosa-Soares, A. C., Noce, C. M., Alkmim, F. F., and Dussin, I. A. 2010. **Rochas charnockíticas do sudeste de Minas Gerais: a raiz granulítica do arco magmático do Orógeno Araçuaí.** Revista Brasileira de Geociências, 40(4), 573-592.

Pattison, D. M., Chacko, T., Farquhar, J. and McFarlane, C. R. M. 2003. **Temperatures of granulite-facies metamorphism: constraints from experimental phase equilibria and thermobarometry corrected for retrograde exchange**. Journal of Petrology, 44(5), 867-900. https://rclc.facsci.ualberta.ca/

Pedrosa-Soares, A. C., Noce, C. M., Wiedemann, C. M., Pinto, C. P. 2001. **The Araçuaí-West-Congo Orogen in Brazil: an overview of a confined orogen formed during Gondwanaland assembly.** Precambrian Research, 110, 307-323.

Pedrosa-Soares, A. C., Alkmim, F. F., Tack, L., Noce, C. M., Babinski, M. Da Silva, L. C., Martins-Neto, M. A. 2008. **Similarities and differences between the Brazilian and African counterparts of the Neoproterozoic Araçuaí-West-Congo orogen**. Geological Society, London, Special Publications, 294, 153-172.

Pedrosa-Soares, A. C., Campos, C. P., Noce, C., Da Silva, L. C., Novo, T. A., Roncato, J., Medeiros, S., Castañeda, C., Queiroga, G., Dantas, E., Dussin, I., Alkmim, F. F. 2011. **Late Neoproterozoic–Cambrian granitic magmatism in the Araçuaí orogen (Brazil), the Eastern Brazilian Pegmatite Province and related mineral resources**. Geological Society, London, Special Publications, 350, 25-51.

Pedrosa-Soares, A., Deluca, C., Araujo, C. S., Gradim, C., Lana, C. C., Dussin, I., Da Silva, L. C., Babinski, M. 2020. **O Orógeno Araçuaí à luz da Geocronologia: um tributo a Umberto Cordani.** In: Bartorelli, A., Teixeira, W. and Brito-Neves, B. B. (Eds.). **Geocronologia e evolução tectônica do Continente Sul-Americano: a contribuição de Umberto Cordani.** Sâo Paulo, SP, Brazil: Solaris Edições Culturais. p. 252-271.

Peixoto, E., Pedrosa-Soares, A. C., Alkmim, F. F., Dussin, I. A. 2015. **A suture–related accretionary wedge formed in the Neoproterozoic Araçuaí orogen (SE Brazil) during Western Gondwanaland assembly**. Gondwana Research, 27(2), 878-896.

Powell, R. 1985. **Regression diagnostics and robust regression in geothermometer /geobarometer calibration: The garnet-clinopyroxene geothermometer revisited.** Journal of Metamorphic Geology, 3, 231-243.

Powell, R. and Holland, T. J. B. 1988. **An internally consistent thermodynamic dataset with uncertainties and correlations: 3: application methods, worked examples and a computer program.** Journal of Metamorphic Geology, 6, 173-204.

Powell, R. and Holland, T. J. B. 1994. **Optimal geothermometry and geobarometry.** American Mineralogist, 79, 120-133.

Pownceby, M.I., Wall, V.J., O'Neill, H.St C., 1991. **An experimental study of the effect of Ca upon garnet – ilmenite Fe – Mn exchange equilibria**. American Mineralogist, 76(9 – 10), 1580 – 1588.

Reno, B. L., Brown, M., Kobayashi, K., Nakamura, E., Piccoli, P. M., Trouw, R. A. J. 2009. **Eclogite-high-pressure granulite metamorphism records early collision in west Gondwana: new data from the southern brasília belt, Brazil**. Journal of the Geological Society of London, 166, 1013–1032. https://doi.org/10.1144/0016-76492008-140.

Richter, F., Lana, C., Stevens, G., Buick, I., Pedrosa-Soares, A. C., Alkmim, F. F., Cutts, K. 2016**. Sedimentation, metamorphism and granite generation in a back-arc region: Records from the Ediacaran Nova Venécia Complex (Araçuaí Orogen, Southeastern Brazil)**. Precambrian Research 272, 78-100.

Rocha, B. C., Moraes, R., Möller, A., Cioffi, C. R. 2018. **Magmatic inheritance vs. UHT metamorphism: Zircon petrochronology of granulites and petrogenesis of charnockitic leucosomes of the Socorro–Guaxupé nappe, SE Brazil**. Lithos, 314-315, 16 – 39

Rocha, B. C., Moraes, R., Möller, A., Cioffi, C. R., Jercinovic, M. J. 2017. **Timing of anatexis and melt crystallization in the Socorro–Guaxupé Nappe, SE Brazil: Insights from trace element composition of zircon, monazite and garnet coupled to U-Pb geochronology**. Lithos, 277, 337 – 355

Rossi-Vieira, P. L. N. C., Tedeschi, M., Queiroga, G. N., Novo, T. A., Pedrosa-Soares, A., Lana, C. *submitted*. **Unveilling the P-T Evolution of ultrahigh temperature metamorphism from sapphirine-bearing and orthopyroxene-garnet migmatites – Tectonic implications for the Ediacaran evolution of the Araçuaí orogen (SE Brazil).** Gondwana Research.

Rossi-Vieira, P. L. N. C., Tedeschi, M., Rocha, B. C., Lana, C. C., Barrote, V., Pedrosa-Soares, A. C., Dussin, I. A., Alkmim, A. 2023**. Detrital zircon U-Pb-Hf isotopes-based reconstruction of the depositional history of (ultra)high-temperature metamorphic rocks from the Socorro-Guaxupé Nappe (southern Brasília orogen, Brazil).** Journal of South American Earth Sciences, 128, 104469. https://doi.org/10.1016/j.jsames.2023.104469.

Serrano, P., Pedrosa-Soares, A., Medeiros-Junior, E., Fonte-Boa, T., Araujo, C., Dussin, I., Queiroga, G., Lana, C., 2018. A**-type Medina batholith and post-collisional anatexis in the Araçuaí orogen (SE Brazil).** Lithos, 320-321, 515-536.

Suita, M. T. F., Kamo, S. L., Krogh, T. E., Fyfe, W. S. and Hartmann, L. A., 1994. **U–Pb ages from high-grade Barro Alto mafic–ultramafic complex (Goiás, central Brazil): middle Proterozoic continental magmatism and Upper Proterozoic continental collision.** ICOG 8 by Golden Gate Berkeley, California, USA. US Geological Survey Circular, 1107, 309.

Tedeschi, M., Novo, T., Pedrosa-Soares, A.C., Dussin, I., Tassinari, T., Silva, L.C., Gonçalves, L., Alkmim, F.F., Lana, C., Figueiredo, C., Dantas, E., Medeiros, S., De Campos, C., Corrales, F., Heilbron, M., 2016. **The Ediacaran Rio Doce magmatic arc revisited (Araçuaí- Ribeira orogenic system, SE Brazil).** Jounal of South American Earth Sciences, 68, 167–186.

Tedeschi, M., Pedrosa-Soares, A.; Dussin, I., Lanari, P., Novo, T., Pinheiro, M. A. P., Lana, C., Peters, D. 2018. **Protracted zircon geochronological record of UHT garnet-free granulites in the Southern Brasília orogen (SE Brazil): Petrochronological constraints on magmatism and metamorphism.** Precambrian Research, 316, 103 – 126

Tedeschi, M., Rossi Vieira, P. L., Kuchenbecker, M., Ribeiro, B. V., Barrote, V., Reis, H., Stutenbecker, L., Lana, C., Pedrosa-Soares, A., Dussin, I. 2023. **Unravelling and overcoming potential biases in U-Pb detrital zircon records induced by high to ultra-high temperature metamorphism (> 850 ºC).** Geoscience Frontiers, 14, 101515. https://doi.org/10.1016/j.gsf.2022.101515

Tesser, L. R., Ganade, C. E., Weinberg, R. F., Basei, M. A. S., Moraes, R., Batista, L. 2021. **Ultrahigh-temperature Paleoproterozoic rocks in the Neoproterozoic Borborema Province, implications for São Francisco Craton dispersion in NE Brazil**. Journal or Metamorphic Geology, 40, 359 – 387. DOI: 10.1111/jmg.12632.

Tsunogae, T., Costa, A. G., Rosière, C. A., Dayan, H., Miyano, T., Van Reenen, D. D. 2002. **Metamorphic P-T conditions of the Juiz de Fora Complex in Manhuaçu Area, northern Ribeira Belt, Brazil.** Annual Report of the Institute of Geosciences of the University of Tsukuba 28: 23-28.

Vielzeuf, D. 1983. **The spinel and quartz associations in high-grade xenoliths from Tallante (SE Spain) and their potential use in geothermometry and barometry.** Contributions to Mineralalogy and Petrology, 82(4), 301 – 311.

Watson, E.B., Wark, D.A., and Thomas, J.B., 2006, **Crystallization thermometers for zircon and rutile.** Contributions to Mineralogy and Petrology, 151, 413–433. Doi: 10.1007/s00410–006–0068–5.

Wisniowski, L., Pedrosa-Soares, A., Medeiros-Junior, E., Belém, J., Dussin, I. Queiroga, G. 2021. **Ultra-high temperature, mid-crustal level, contact metamorphism imprinted on granulite facies paragneisses by a norite intrusion (São Gabriel da Baunilha, Araçuaí orogen, southest Brazil).** Journal of Metamorphic Geology, 00, 1 – 29. DOI: 10.1111/jmg.12594.

8 CONCLUSION

Ultrahigh temperature metamorphic rocks from the Southern Brasília and Araçuaí orogens provide important insights on the evolution of the Brasiliano orogenic systems.

Paraderived migmatites from the Caparaó complex, located in the Rio Doce Arc domain in the Araçuaí Orogen, exhibit the highest temperature-pressure conditions ever disclosed for this orogen. They are divided in two types: hercynite-sillimanite-garnet migmatites exhibiting hercynite+quartz assemblages typical of metapelitic UHT rocks, which provided P-T conditions of 1020-1035 °C, 7.0-7.1 kbar; orthopyroxene-garnet migmatites exhibiting Al-rich orthopyroxene, which provided P-T conditions of 962-978 °C, 9.5-9.6 kbar. Both rock types exhibit a protracted zircon U-Pb record owing to UHT isotopic disturbance. Protosource ages for a layered orthopyroxene-garnet diatexite are ca. 773 Ma and ca. 739 Ma, and both migmatite types provided minimum metamorphic ages between ca. 635-610 Myr. This age interval fits inside the timespan of the Rio Doce Magmatic arc, pointing to a pre-collisional, subduction-related UHT metamorphic peak for the Araçuaí Orogen. A “slab window” mechanism associated with accumulation of large volumes of arc magmas and crustal thickening is interpreted as responsible for attaining UHT metamorphic conditions.

Para- and orthoderived migmatites from the Socorro-Guaxupé Nappe, in the Southern Brasília Orogen, also exhibit a protracted zircon U-Pb dates record owing to the influence of high- to ultrahigh temperature metamorphism. Zircon Lu-Hf and U-Pb isotopes obtained from the paraderived rocks revealed five protosources, among which four exhibit crustal signatures ($\varepsilon Hf(804\text{-}776)$ = -16 to -2) and minimum U-Pb ages ranging between ca. 804 Ma and ca. 776 Ma, and one exhibit a moderately juvenile signature ($\varepsilon Hf(816)$ = +3 to +9) and a minimum U-Pb age of ca. 816 Ma. Protosources with crustal signatures exhibit similarities with rocks found along the Socorro-Guaxupé Nappe, and the moderately juvenile protosource points to contributions from an island arc older than the continental arc built at the margins of the Paranapanema paleocontinent. Minimum crystallization ages for a biotite-bearing granitic leucosome (ca. 691 Ma) and a garnet-bearing granite (ca. 661 Ma) suggest that the onset of UHT metamorphism might be related to this ca. 690-660 Myr time window, and the thermal event might have lasted until the collisional stage (until ca. 610 Ma).

Metamorphic ages for most UHT occurrences in the Southern Brasília and Araçuaí orogens are related to this ca. 690-590 Myr interval. Although those orogenic

systems evolved diachronically and lie in opposing sides of the São Francisco paleocontinent, this is suggestive that UHT metamorphism occurrences from both orogens are strongly related to the subduction-collision transition setting. Those observations corroborate the idea that UHT metamorphism occurrences are part of the evolution of the supercontinent cycle rather than exotic events. Further studies are needed in order to map, determine the P-T conditions and better establish links between UHT occurrences along the Brasiliano orogenic systems.

9 APPENDICES

The appendices of this work are divided as it follows:

- Appendix A to J: Supplementary files 1 to 6 and Supplementary images 1 to 4 from Chapter 4, “Unveiling the P-T evolution of ultrahigh temperature metamorphism from sapphirine-bearing and orthopyroxene-garnet migmatites - Tectonic implications for the Ediacaran evolution of the Araçuaí orogen (SE Brazil)”;
- Appendix K to N: Supplementary data 1 to 4 from Chapter 5, “Detrital zircon U-Pb-Hf isotopes-based reconstruction of the depositional history of (ultra)high-temperature metamorphic rocks from the Socorro-Guaxupé Nappe (Southern Brasília orogen, Brazil)”;
- Appendix O: Lu-Hf and U-Pb data presented in Chapter 6, “Complementary Lu-Hf data;
- Appendix P: Compilation of UHT occurrences in Brazil, presented in Chapter 7 “Discussions”.

9.1 APPENDIX A – Supplementary file 1 (Chapter 4): Standards for EMPA and WRG preparation

9.1.1 Analytical standards for electron microprobe analysis (EMPA)

Element	Count. Time (Peak) [s]	Count. Time (Background) [s]	X-ray	Spectometer	Channel	Standard
Na	10	5	Kα	TAPH	1	Anorthoclase
F	10	5	Kα	TAPH	1	CaF_2
Si	10	5	Kα	TAP	2	Quartz
Al	10	5	Kα	TAP	2	Corundum
Mg	10	5	Kα	TAP	2	Olivine
Zn	10	5	Kα	LIFH	3	Gahnite
Fe	10	5	Kα	LIFH	3	Fe
Cl	30	15	Kα	PETH	3	Scapolite (Meionite)
Cr	30	15	Kα	LIFH	3	Chromite
Ca	10	5	Kα	PETJ	4	Fluor-Apatite
Ti	10	5	Kα	PETL	5	Rutile
K	10	5	Kα	PETL	5	Microcline
Mn	10	5	Kα	LIFL	5	MnO_2

9.1.2 Analytical procedures for whole-rock geochemical analysis

Preparation of samples P1, P1D (schlieren orthopyroxene-garnet diatexite), P008 (sapphirine-bearing hercynite-sillimanite-garnet diatexite) and P013 (layered orthopyroxene-garnet diatexite) for whole-rock geochemical analysis at the SGS GEOSOL Laboratories (Brazil) were performed under the following protocol. Samples were dried at 105 °C, crushed to 3mm, homogenized, submitted to quartering and then 250-300g of the sample was pulverized to 150 mesh at a steel (95%) mill. Loss on Ignition (LOI) was determinated by calcination under 1000 °C. 10g of each sample was then submitted to fusion with lithium metaborate (LiBO2), underwent dissolution with an acid solution of C4H6O6+HNO3 for complete opening and then analysed under ICP/OES (Inductively Coupled Plasma Optical Emission Spectrometry) for determining major element compositions.

Preparation of sample P4E (schlieren/schöllen hercynite-sillimanite-garnet diatexite) for whole-rock geochemical analysis at the GeoX Laboratory (Federal University of Ouro Preto – UFOP, Brazil) were performed under the following protocol. Samples were dried at 105 °C, crushed to 3mm, homogenized, submitted to quartering and then 250-300g of the sample was pulverized to 150 mesh at a steel (95%) mill. Loss on Ignition (LOI) was determinated by calcination under 1000 °C. 1g of each

sample was used for preparing glass disks with 6g of Li2B4O7 and LiBO2 (1:1 proportion) for X-Ray Fluorescence analysis. Analysis were conducted using a Phillips PANanalyical MagiX X-Ray Fluorescence Spectometer.

9.2 APPENDIX B – Supplementary file 2 (Chapter 4): Representative mineral compositions

Representative major element compositions of biotite (Bt) crystals

Structura formulas calculated after Tindle & Webb (199)

spot/analysis	type	SiO2	TiO2	Al2O3	FeO	MnO	MgO	CaO	Na2O	K2O	ZnO	F	Cl	Cr2O3	O=F,CL	Total	Si	Al iv	Al vi	Ti	Cr	Fe	Mn	Mg	Zn	Ca	Na	K	Total cations	XMg
Sample P008																														
Bt1																														
P008F02Mbt59	Inclusion	40.08	1.56	15.45	5.93	0.04	22.52	0.01	0.02	10.31	0.00	2.75	0.03	0.01	1.17	97.55	5.69	2.31	0.27	0.17	0.00	0.70	0.00	4.76	0.00	0.00	0.01	1.87	15.79	**0.8712**
P008F02Mbt60	Inclusion	39.34	1.42	15.16	6.16	0.02	22.13	0.03	0.05	10.21	0.02	2.45	0.02	0.00	1.04	95.97	5.68	2.32	0.26	0.15	0.00	0.74	0.00	4.76	0.00	0.01	0.01	1.88	15.82	**0.8649**
Bt2																														
P008F03Mbt88	Inclusion	38.39	6.26	15.11	7.33	0.02	18.40	0.03	0.28	9.65	0.00	1.87	0.01	0.02	0.79	96.57	5.52	2.48	0.08	0.68	0.00	0.88	0.00	3.95	0.00	0.00	0.08	1.77	15.44	**0.8173**
P008F03Mbt89	Inclusion	37.60	6.07	14.96	7.84	0.02	17.49	0.03	0.28	9.42	0.03	1.89	0.02	0.03	0.80	94.86	5.52	2.48	0.11	0.67	0.00	0.96	0.00	3.83	0.00	0.00	0.08	1.76	15.43	**0.7991**
Sample P4E(L)																														
Bt1																														
P4EF01Cbt30	Inclusion	38.48	3.71	15.26	7.11	0.01	20.13	0.06	0.40	9.82	0.00	2.64	0.00	0.00	1.11	96.50	5.56	2.44	0.16	0.40	0.00	0.86	0.00	4.34	0.00	0.01	0.11	1.81	15.70	0.8346
P4EF01Cbt33	Inclusion	38.19	3.68	16.17	7.20	0.02	19.61	0.02	0.33	9.85	0.00	2.68	0.00	0.00	1.13	96.62	5.51	2.49	0.26	0.40	0.00	0.87	0.00	4.22	0.00	0.00	0.09	1.81	15.66	0.8292
P4EF02Cbt63	Inclusion	38.27	5.04	14.71	7.51	0.03	18.84	0.02	0.36	9.56	0.00	1.99	0.00	0.00	0.84	95.49	5.58	2.42	0.10	0.55	0.00	0.92	0.00	4.09	0.00	0.00	0.10	1.78	15.55	0.8171
P4EF02Cbt65	Inclusion	38.54	3.23	15.81	6.70	0.02	20.05	0.08	0.46	9.11	0.00	1.61	0.00	0.00	0.68	94.94	5.59	2.41	0.29	0.35	0.00	0.81	0.00	4.33	0.00	0.01	0.13	1.69	15.62	0.8420
P4EF02Cbt66	Inclusion	38.30	3.33	15.93	6.78	0.00	19.80	0.61	0.48	9.16	0.00	1.49	0.00	0.00	0.63	95.24	5.55	2.45	0.27	0.36	0.00	0.82	0.00	4.27	0.00	0.09	0.13	1.69	15.64	0.8388
P4EF02Cbt67	Inclusion	38.19	3.34	15.95	7.00	0.00	20.03	0.08	0.48	9.06	0.00	1.59	0.00	0.00	0.67	95.06	5.54	2.46	0.27	0.36	0.00	0.85	0.00	4.33	0.00	0.01	0.13	1.68	15.64	0.8361
P4EF02Cbt88	Inclusion	38.03	3.78	15.49	8.08	0.01	19.39	0.08	0.25	9.32	0.00	1.36	0.00	0.00	0.57	95.21	5.54	2.46	0.20	0.41	0.00	0.98	0.00	4.21	0.00	0.01	0.07	1.73	15.62	0.8105
Bt2																														
P4EF02Mbt90	Matrix	37.10	5.65	14.49	12.75	0.02	15.11	0.05	0.12	9.53	0.00	1.18	0.00	0.00	0.50	98.97	5.52	2.48	0.07	0.63	0.00	1.59	0.00	3.35	0.00	0.01	0.04	1.81	15.50	0.6787
P4EF02Mbt89	Matrix	37.38	5.17	15.21	12.46	0.04	14.79	0.06	0.09	9.18	0.00	1.29	0.00	0.00	0.54	95.12	5.56	2.44	0.23	0.58	0.00	1.55	0.00	3.28	0.00	0.01	0.03	1.74	15.41	0.6790
P4EF02Mbt19	Matrix	37.64	4.36	14.98	12.83	0.02	15.47	0.03	0.16	9.62	0.09	1.46	0.55	0.05	0.74	96.50	5.57	2.43	0.19	0.49	0.01	1.59	0.00	3.41	0.01	0.00	0.04	1.82	15.56	0.6824
P4EF02Mbt23	Matrix	37.61	4.61	15.10	12.75	0.06	15.25	0.00	0.11	9.49	0.00	1.40	0.55	0.03	0.72	96.23	5.57	2.43	0.21	0.51	0.00	1.58	0.01	3.37	0.00	0.00	0.03	1.79	15.51	0.6807
P4EF03Mbt39	Matrix	36.97	5.51	14.63	13.91	0.04	14.01	0.02	0.11	9.50	0.05	1.21	0.53	0.03	0.63	95.89	5.54	2.46	0.12	0.62	0.00	1.74	0.01	3.13	0.01	0.00	0.03	1.81	15.47	0.6423
P4EF03Mbt40	Matrix	36.89	5.41	14.77	13.87	0.04	13.70	0.02	0.12	9.28	0.00	1.25	0.53	0.00	0.65	95.24	5.55	2.45	0.17	0.61	0.00	1.75	0.01	3.08	0.00	0.00	0.04	1.78	15.43	0.6378

P4EF03Mbt41	Matrix	36.88	5.44	14.66	14.07	0.04	13.75	0.03	0.13	9.31	0.03	1.05	0.53	0.01	0.56	98.72	5.55	2.45	0.14	0.62	0.00	1.77	0.01	3.08	0.00	0.00	0.04	1.79	15.45	0.6354
Bt3																														
P4EF01Mbt48	Matrix	37.65	2.02	15.59	10.75	0.04	18.29	0.09	0.10	9.64	0.00	1.71	0.00	0.00	0.72	98.39	5.58	2.42	0.30	0.22	0.00	1.33	0.01	4.04	0.00	0.01	0.03	1.82	15.76	0.7520
P4EF01Mbt49	Matrix	37.65	2.02	15.59	10.75	0.04	18.29	0.09	0.10	9.64	0.00	1.71	0.00	0.00	0.72	95.16	5.58	2.42	0.30	0.22	0.00	1.33	0.01	4.04	0.00	0.01	0.03	1.82	15.76	0.7520
P4EF01Mbt50	Matrix	37.38	2.05	15.70	10.83	0.01	18.32	0.08	0.09	9.46	0.00	1.59	0.00	0.00	0.67	94.83	5.55	2.45	0.30	0.23	0.00	1.34	0.00	4.06	0.00	0.01	0.03	1.79	15.76	0.7510
P4EF01Mbt51	Matrix	37.14	2.83	15.68	10.66	0.02	17.93	0.06	0.07	9.56	0.00	1.59	0.00	0.00	0.67	94.86	5.52	2.48	0.26	0.32	0.00	1.32	0.00	3.97	0.00	0.01	0.02	1.81	15.71	0.7499
P4EF01Mbt52	Matrix	36.80	2.92	15.80	11.98	0.06	17.38	0.06	0.10	9.52	0.00	1.54	0.00	0.00	0.65	95.51	5.47	2.53	0.23	0.33	0.00	1.49	0.01	3.85	0.00	0.01	0.03	1.80	15.74	0.7212
P4EF01Cbt36	Inclusion	37.47	1.23	18.76	9.14	0.04	18.66	0.03	0.21	9.72	0.00	0.61	0.00	0.00	0.26	95.61	5.43	2.57	0.63	0.13	0.00	1.11	0.01	4.03	0.00	0.00	0.06	1.80	15.77	0.7845
Sample P4E(R)																														
Bt1																														
P4E'F01Cbt13	Inclusion	37.05	4.47	15.65	9.37	0.00	17.51	0.02	0.16	10.11	0.00	1.27	0.00	0.00	0.54	95.07	5.47	2.53	0.19	0.50	0.00	1.16	0.00	3.85	0.00	0.00	0.04	1.90	15.65	0.7691
P4E'F03Cbt101	Inclusion	37.51	4.55	15.87	9.41	0.02	17.78	0.08	0.15	9.60	0.00	1.58	0.00	0.00	0.66	95.88	5.48	2.52	0.21	0.50	0.00	1.15	0.00	3.87	0.00	0.01	0.04	1.79	15.57	0.7710
P4E'F03Cbt102	Inclusion	38.16	4.31	15.63	9.35	0.04	18.38	0.07	0.14	9.77	0.00	1.61	0.00	0.00	0.68	96.78	5.52	2.48	0.18	0.47	0.00	1.13	0.00	3.96	0.00	0.01	0.04	1.80	15.60	0.7781
P4E'F03Mbt117	Matrix	38.41	4.18	15.06	9.48	0.04	18.10	0.04	0.08	9.98	0.00	1.58	0.00	0.00	0.66	96.28	5.59	2.41	0.17	0.46	0.00	1.15	0.00	3.93	0.00	0.01	0.02	1.85	15.60	0.7729
P4E'F03Mbt118	Matrix	38.18	4.01	14.82	9.39	0.02	18.10	0.03	0.10	9.86	0.00	1.75	0.00	0.00	0.74	95.53	5.60	2.40	0.17	0.44	0.00	1.15	0.00	3.96	0.00	0.00	0.03	1.85	15.61	0.7745
Bt2																														
P4E'F01Mbt12	Matrix	37.25	5.08	15.40	10.87	0.01	16.35	0.00	0.13	10.07	0.00	1.12	0.00	0.00	0.47	95.81	5.49	2.51	0.16	0.56	0.00	1.34	0.00	3.59	0.00	0.00	0.04	1.89	15.58	0.7283
P4E'F01Mbt09	Matrix	36.83	5.72	14.76	11.41	0.00	15.29	0.03	0.15	9.93	0.00	1.00	0.00	0.00	0.42	94.69	5.50	2.50	0.10	0.64	0.00	1.43	0.00	3.41	0.00	0.01	0.04	1.89	15.52	0.7049
P4E'F01Mbt10	Matrix	37.25	5.33	14.83	11.41	0.02	15.59	0.04	0.12	9.82	0.00	1.18	0.00	0.00	0.50	95.08	5.54	2.46	0.14	0.60	0.00	1.42	0.00	3.46	0.00	0.01	0.03	1.86	15.51	0.7091
P4E'F01Mbt29	Matrix	37.21	4.82	15.09	11.69	0.00	15.66	0.03	0.13	9.93	0.00	1.27	0.00	0.00	0.54	95.31	5.53	2.47	0.18	0.54	0.00	1.45	0.00	3.47	0.00	0.01	0.04	1.88	15.57	0.7048
P4E'F01Mbt30	Matrix	36.84	4.70	15.01	11.61	0.03	15.62	0.03	0.07	9.87	0.00	1.29	0.00	0.00	0.54	94.52	5.52	2.48	0.18	0.53	0.00	1.46	0.00	3.49	0.00	0.00	0.02	1.89	15.57	0.7058
P4E'F02Mbt65	Matrix	37.67	5.01	14.75	11.22	0.00	16.29	0.08	0.14	9.72	0.00	1.37	0.00	0.00	0.58	99.08	5.56	2.44	0.13	0.56	0.00	1.39	0.00	3.58	0.00	0.01	0.04	1.83	15.53	0.7212
Sample P013(Rr)																														
Bt1																														
P013F01Cbt145	Inclusion	36.84	1.99	17.26	9.86	0.01	17.83	0.06	0.10	9.27	0.05	1.10	0.29	0.02	0.53	94.15	5.47	2.53	0.49	0.22	0.00	1.22	0.00	3.95	0.01	0.01	0.03	1.76	15.69	0.7632
P013F01Cbt146	Inclusion	37.40	1.89	17.12	9.64	0.03	18.10	0.00	0.11	9.78	0.00	1.07	0.29	0.00	0.52	94.91	5.51	2.49	0.48	0.21	0.00	1.19	0.00	3.98	0.00	0.00	0.03	1.84	15.73	0.7700
Bt2																														
P013F02Mbt107	Matrix	37.32	5.34	13.87	13.14	0.03	14.58	0.06	0.10	9.44	0.05	1.27	0.21	0.10	0.58	94.94	5.61	2.39	0.07	0.60	0.01	1.65	0.00	3.27	0.01	0.01	0.03	1.81	15.47	0.6641
P013F02Mbt108	Matrix	37.93	5.28	14.04	13.23	0.02	14.89	0.01	0.02	9.55	0.03	1.43	0.20	0.08	0.65	96.07	5.63	2.37	0.09	0.59	0.01	1.64	0.00	3.30	0.00	0.00	0.01	1.81	15.45	0.6673

P013F02Mbt109	Matrix	38.17	5.17	14.08	13.01	0.02	14.83	0.03	0.10	9.58	0.02	1.35	0.21	0.06	0.61	96.00	5.66	2.34	0.12	0.58	0.01	1.61	0.00	3.28	0.00	0.00	0.03	1.81	15.45	0.6701
P013F01Mbt139	Matrix	37.77	5.32	14.13	13.49	0.00	14.72	0.00	0.03	9.50	0.00	1.27	0.23	0.06	0.59	95.94	5.62	2.38	0.10	0.60	0.01	1.68	0.00	3.26	0.00	0.00	0.01	1.80	15.45	0.6605
P013F01Mbt140	Matrix	37.27	5.17	13.86	13.59	0.02	14.41	0.05	0.07	9.17	0.01	1.44	0.24	0.10	0.66	94.73	5.62	2.38	0.09	0.59	0.01	1.72	0.00	3.24	0.00	0.01	0.02	1.77	15.44	0.6540
P013F02Mbt103	Matrix	38.11	4.93	14.28	11.49	0.03	16.41	0.02	0.06	9.64	0.11	1.64	0.21	0.07	0.74	96.26	5.61	2.39	0.09	0.55	0.01	1.42	0.00	3.60	0.01	0.00	0.02	1.81	15.51	0.7179
P013F02Mbt104	Matrix	37.96	5.08	14.29	11.79	0.00	15.90	0.04	0.07	9.62	0.03	1.55	0.21	0.07	0.70	95.92	5.61	2.39	0.11	0.56	0.01	1.46	0.00	3.51	0.00	0.01	0.02	1.82	15.49	0.7063
P013F02Mbt105	Matrix	38.14	4.99	14.36	11.75	0.01	16.12	0.02	0.04	9.60	0.00	1.38	0.21	0.08	0.63	96.06	5.62	2.38	0.11	0.55	0.01	1.45	0.00	3.54	0.00	0.00	0.01	1.80	15.48	0.7098
P013F02Mbt106	Matrix	37.82	4.92	14.35	11.57	0.03	16.23	0.04	0.06	9.67	0.00	1.59	0.21	0.08	0.71	95.86	5.60	2.40	0.10	0.55	0.01	1.43	0.00	3.58	0.00	0.01	0.02	1.83	15.52	0.7143
Sample P013(Lr)																														
Bt1																														
P013F04Cbt41	Inclusion	39.88	2.34	14.66	7.72	0.04	20.52	0.02	0.05	9.61	0.01	2.52	0.03	0.02	1.07	96.34	5.75	2.25	0.25	0.25	0.00	0.93	0.00	4.41	0.00	0.00	0.01	1.77	15.64	0.8257
P013F04Cbt42	Inclusion	40.11	2.24	15.64	9.02	0.02	17.84	0.09	0.08	8.45	0.00	1.71	0.03	0.00	0.73	94.50	5.85	2.15	0.53	0.25	0.00	1.10	0.00	3.87	0.00	0.01	0.02	1.57	15.36	0.7789
P013F04Cbt43	Inclusion	39.90	1.95	14.87	7.37	0.02	20.75	0.03	0.05	9.68	0.02	2.26	0.02	0.03	0.95	95.98	5.76	2.24	0.29	0.21	0.00	0.89	0.00	4.47	0.00	0.00	0.01	1.78	15.66	0.8339
Bt2																														
P013F05Mbt20	Matrix	37.05	4.89	13.78	13.36	0.05	14.63	0.05	0.04	9.13	0.08	1.40	0.12	0.09	0.62	94.04	5.62	2.38	0.09	0.56	0.01	1.70	0.01	3.31	0.01	0.01	0.01	1.77	15.47	0.6612
P013F05Mbt22	Matrix	37.56	4.78	14.36	13.49	0.01	14.79	0.06	0.05	9.00	0.03	1.52	0.13	0.09	0.67	95.19	5.62	2.38	0.15	0.54	0.01	1.69	0.00	3.30	0.00	0.01	0.02	1.72	15.44	0.6614
P013F04Mbt44	Matrix	37.37	5.19	14.39	13.17	0.05	14.89	0.02	0.06	9.31	0.11	1.40	0.18	0.08	0.63	95.60	5.58	2.42	0.11	0.58	0.01	1.64	0.01	3.31	0.01	0.00	0.02	1.77	15.47	0.6682
P013F04Mbt45	Matrix	37.46	4.91	14.13	12.85	0.03	15.08	0.02	0.06	9.46	0.04	1.33	0.17	0.06	0.60	94.99	5.62	2.38	0.11	0.55	0.01	1.61	0.00	3.37	0.00	0.00	0.02	1.81	15.49	0.6766
P013F03Mbt72	Matrix	37.62	4.72	14.15	13.84	0.01	14.96	0.05	0.03	9.53	0.04	1.28	0.15	0.08	0.57	99.26	5.61	2.39	0.10	0.53	0.01	1.73	0.00	3.33	0.00	0.01	0.01	1.81	15.52	0.6584
P013F03Mbt74	Matrix	37.74	4.69	13.88	13.76	0.01	14.62	0.07	0.04	9.37	0.02	1.19	0.13	0.09	0.53	95.08	5.66	2.34	0.12	0.53	0.01	1.73	0.00	3.27	0.00	0.01	0.01	1.79	15.48	0.6543
P013F03Mbt75	Matrix	36.88	4.98	13.71	14.24	0.02	13.97	0.13	0.04	9.48	0.02	1.47	0.15	0.08	0.65	94.50	5.61	2.39	0.07	0.57	0.01	1.81	0.00	3.17	0.00	0.02	0.01	1.84	15.51	0.6360
Bt3																														
P013F02Cbt110	Inclusion	37.40	6.35	14.24	10.57	0.02	16.05	0.09	0.09	9.57	0.11	1.30	0.20	0.09	0.59	95.49	5.53	2.47	0.01	0.71	0.01	1.31	0.00	3.54	0.01	0.01	0.03	1.80	15.43	0.7303
P013F02Cbt111	Inclusion	37.15	6.23	14.24	11.28	0.06	15.57	0.18	0.11	9.07	0.07	1.27	0.18	0.10	0.57	94.92	5.53	2.47	0.03	0.70	0.01	1.40	0.01	3.46	0.01	0.03	0.03	1.72	15.39	0.7110
Sample P1(R)																														
Bt1																														
P1mF05Cbt137	Inclusion	37.23	6.25	14.11	11.88	0.00	14.84	0.00	0.13	9.68	0.00	1.46	0.00	0.00	0.61	94.96	5.57	2.43	0.05	0.70	0.00	1.48	0.00	3.31	0.00	0.00	0.04	1.84	15.43	0.6902
P1mF05Cbt139	Inclusion	37.55	6.34	14.22	11.80	0.03	15.23	0.04	0.15	9.62	0.00	1.51	0.00	0.00	0.63	95.86	5.56	2.44	0.04	0.71	0.00	1.46	0.00	3.36	0.00	0.01	0.04	1.82	15.43	0.6970
P1mF05Cbt140	Inclusion	37.47	6.21	14.17	11.98	0.02	15.38	0.01	0.19	9.62	0.00	1.52	0.00	0.00	0.64	95.92	5.55	2.45	0.02	0.69	0.00	1.48	0.00	3.39	0.00	0.00	0.05	1.82	15.46	0.6959
Bt2																														

P1mFDMbt52	Matrix	37.99	4.69	13.91	12.95	0.02	14.65	0.50	0.32	9.68	0.01	1.41	0.28	0.08	0.66	95.83	5.67	2.33	0.11	0.53	0.01	1.62	0.00	3.26	0.00	0.08	0.09	1.84	15.54	0.6685
P1mFDMbt56	Matrix	37.49	5.26	13.72	13.84	0.00	14.46	0.04	0.11	10.05	0.00	1.65	0.28	0.08	0.76	96.21	5.61	2.39	0.03	0.59	0.01	1.73	0.00	3.23	0.00	0.01	0.03	1.92	15.55	0.6505
P1mF05Mbt152	Matrix	37.30	4.84	13.98	13.47	0.02	14.82	0.05	0.10	9.65	0.00	1.48	0.00	0.00	0.62	98.37	5.61	2.39	0.09	0.55	0.00	1.69	0.00	3.32	0.00	0.01	0.03	1.85	15.54	0.6622
P1mF05Mbt153	Matrix	37.46	5.27	13.72	13.86	0.00	14.44	0.03	0.07	9.78	0.00	1.45	0.00	0.00	0.61	98.78	5.62	2.38	0.05	0.60	0.00	1.74	0.00	3.23	0.00	0.01	0.02	1.87	15.51	0.6499
P1mF05Mbt154	Matrix	37.49	5.54	13.90	14.14	0.00	14.38	0.00	0.08	9.75	0.00	1.44	0.00	0.00	0.61	96.11	5.59	2.41	0.04	0.62	0.00	1.76	0.00	3.20	0.00	0.00	0.02	1.86	15.50	0.6445
P1mF07Mbt81	Matrix	38.39	3.71	13.80	10.86	0.00	17.81	0.03	0.06	9.95	0.00	2.05	0.00	0.00	0.86	95.78	5.68	2.32	0.08	0.41	0.00	1.34	0.00	3.92	0.00	0.00	0.02	1.88	15.66	0.7452
P1mF07Mbt82	Matrix	37.97	4.04	13.78	11.34	0.00	17.40	0.03	0.03	9.98	0.00	1.94	0.00	0.00	0.82	95.69	5.64	2.36	0.05	0.45	0.00	1.41	0.00	3.85	0.00	0.00	0.01	1.89	15.66	0.7322
P1mF07Mbt83	Matrix	38.00	3.64	13.80	10.95	0.01	17.56	0.05	0.06	9.83	0.00	1.98	0.00	0.00	0.83	95.04	5.66	2.34	0.09	0.41	0.00	1.37	0.00	3.90	0.00	0.01	0.02	1.87	15.66	0.7408
P1mFBMbt85	Matrix	37.07	5.01	13.41	13.57	0.04	14.39	0.03	0.16	10.17	0.03	1.52	0.30	0.09	0.71	98.24	5.62	2.38	0.02	0.57	0.01	1.72	0.01	3.25	0.00	0.01	0.05	1.97	15.61	0.6540
P1mF07Mbt87	Matrix	37.41	4.88	13.66	12.64	0.00	15.51	0.03	0.03	9.80	0.00	1.60	0.00	0.00	0.67	94.88	5.63	2.37	0.05	0.55	0.00	1.59	0.00	3.48	0.00	0.00	0.01	1.88	15.56	0.6863
P1mF07Mbt88	Matrix	37.78	4.74	13.51	12.35	0.00	15.48	0.02	0.05	9.67	0.00	1.69	0.00	0.00	0.71	94.57	5.68	2.32	0.08	0.54	0.00	1.55	0.00	3.47	0.00	0.00	0.01	1.86	15.52	0.6909
P1mF06Mbt115	Inclusion	38.65	4.58	13.61	11.54	0.00	17.05	0.02	0.09	9.93	0.00	1.87	0.00	0.00	0.79	96.54	5.68	2.32	0.03	0.51	0.00	1.42	0.00	3.73	0.00	0.00	0.03	1.86	15.58	0.7247
P1mF06Mbt117	Matrix	37.22	5.10	13.82	12.32	0.04	15.80	0.02	0.08	9.72	0.00	1.62	0.00	0.00	0.68	95.05	5.58	2.42	0.02	0.58	0.00	1.54	0.01	3.53	0.00	0.00	0.02	1.86	15.56	0.6957
Sample P1(L)																														
Bt1																														
P1lF01Cbt20	Inclusion	37.76	6.03	14.01	11.59	0.03	15.80	0.03	0.12	9.87	0.00	1.63	0.00	0.00	0.69	96.18	5.57	2.43	0.01	0.67	0.00	1.43	0.00	3.48	0.00	0.01	0.03	1.86	15.48	0.7084
P1lF01Cbt21	Inclusion	38.07	6.00	14.02	11.42	0.01	15.95	0.00	0.11	9.82	0.00	1.57	0.00	0.00	0.66	96.30	5.60	2.40	0.03	0.66	0.00	1.40	0.00	3.49	0.00	0.00	0.03	1.84	15.46	0.7135
Bt2																														
P1lFGMbt5	Matrix	38.01	4.27	13.86	12.32	0.08	16.13	0.04	0.12	9.81	0.00	1.70	0.28	0.12	0.78	95.97	5.65	2.35	0.08	0.48	0.01	1.53	0.01	3.58	0.00	0.01	0.04	1.86	15.60	0.7000
P1lFGMbt6	Matrix	38.46	4.15	13.65	13.90	0.01	16.16	0.08	0.11	8.92	0.02	1.74	0.26	0.06	0.79	96.74	5.68	2.32	0.06	0.46	0.01	1.72	0.00	3.56	0.00	0.01	0.03	1.68	15.52	0.6745
P1lF01Mbt24	Matrix	37.77	5.03	14.04	12.75	0.05	15.42	0.05	0.05	9.86	0.00	1.68	0.00	0.00	0.71	95.99	5.61	2.39	0.07	0.56	0.00	1.59	0.01	3.42	0.00	0.01	0.01	1.87	15.54	0.6831
P1lF01Mbt26	Matrix	37.54	4.91	14.25	12.32	0.04	15.60	0.06	0.12	9.75	0.00	1.65	0.00	0.00	0.69	95.53	5.59	2.41	0.10	0.55	0.00	1.53	0.00	3.47	0.00	0.01	0.03	1.85	15.55	0.6930
P1lF02Mbt59	Matrix	37.32	5.47	13.84	12.95	0.02	14.99	0.00	0.10	9.68	0.00	1.51	0.00	0.00	0.64	95.24	5.59	2.41	0.04	0.62	0.00	1.62	0.00	3.35	0.00	0.00	0.03	1.85	15.51	0.6735
P1lF02Mbt60	Matrix	37.32	5.49	13.99	12.67	0.03	15.07	0.01	0.08	9.58	0.00	1.46	0.00	0.00	0.61	95.08	5.59	2.41	0.06	0.62	0.00	1.59	0.00	3.36	0.00	0.00	0.02	1.83	15.49	0.6794
P1lF02Mbt61	Matrix	37.69	5.49	14.15	12.53	0.00	15.46	0.01	0.05	9.69	0.00	1.64	0.00	0.00	0.69	96.00	5.59	2.41	0.06	0.61	0.00	1.55	0.00	3.42	0.00	0.00	0.01	1.83	15.49	0.6875
P1lFFMbt24	Matrix	37.56	3.60	13.72	13.13	0.03	16.23	0.04	0.08	9.16	0.00	1.76	0.26	0.07	0.80	94.83	5.66	2.34	0.10	0.41	0.01	1.65	0.00	3.65	0.00	0.01	0.02	1.76	15.60	0.6879
P1lFFMbt25	Matrix	38.30	3.99	13.99	11.76	0.04	16.81	0.06	0.10	9.97	0.00	2.02	0.30	0.07	0.92	96.49	5.66	2.34	0.10	0.44	0.01	1.45	0.00	3.70	0.00	0.01	0.03	1.88	15.63	0.7181
P1lF02Mbt51	Inclusion	39.21	2.27	15.64	9.91	0.00	19.40	0.06	0.10	9.84	0.00	2.29	0.00	0.00	0.97	97.76	5.63	2.37	0.28	0.25	0.00	1.19	0.00	4.15	0.00	0.01	0.03	1.80	15.71	0.7772
P1lF02Mbt52	Inclusion	38.90	2.49	14.85	9.73	0.01	19.27	0.07	0.07	9.94	0.00	2.16	0.00	0.00	0.91	96.57	5.66	2.34	0.21	0.27	0.00	1.18	0.00	4.18	0.00	0.01	0.02	1.85	15.72	0.7792
P1lF02Mbt55	Matrix	38.94	3.65	13.60	11.43	0.00	17.41	0.02	0.09	9.67	0.00	2.33	0.00	0.00	0.98	96.16	5.74	2.26	0.11	0.40	0.00	1.41	0.00	3.83	0.00	0.00	0.03	1.82	15.59	0.7308
P1lF02Mbt56	Matrix	38.24	3.48	13.76	12.61	0.00	16.76	0.00	0.09	9.60	0.00	2.08	0.00	0.00	0.88	95.74	5.69	2.31	0.11	0.39	0.00	1.57	0.00	3.72	0.00	0.00	0.03	1.82	15.63	0.7031

Sample P1D Bt1																												
P1DF02Cbt59	Inclusion	37.25	4.91	16.06	12.36	0.00	15.09	0.00	0.06	10.00	0.00	1.04	0.00	0.00	0.44	96.33	5.48	2.52	0.27	0.54	0.00	1.52	0.00	3.31	0.00	0.00	0.02	1.88	15.53	0.6852
P1DF02Cbt60	Inclusion	37.05	4.68	16.01	12.50	0.02	14.78	0.02	0.06	9.97	0.00	1.13	0.00	0.00	0.48	95.72	5.49	2.51	0.29	0.52	0.00	1.55	0.00	3.27	0.00	0.00	0.02	1.88	15.54	0.6782
P1DF04Cbt99	Inclusion	38.14	4.43	15.21	10.60	0.00	16.71	0.05	0.14	9.73	0.00	0.96	0.00	0.00	0.40	95.55	5.59	2.41	0.22	0.49	0.00	1.30	0.00	3.65	0.00	0.01	0.04	1.82	15.53	0.7375
P1DF01Mbt10	Matrix	37.69	4.07	15.50	11.43	0.02	15.97	0.05	0.08	9.98	0.00	1.30	0.00	0.00	0.55	95.52	5.57	2.43	0.27	0.45	0.00	1.41	0.00	3.52	0.00	0.01	0.02	1.88	15.58	0.7135
P1DF01Mbt12	Matrix	37.90	4.13	15.60	11.33	0.00	15.99	0.00	0.03	10.04	0.00	1.38	0.00	0.00	0.58	95.81	5.58	2.42	0.29	0.46	0.00	1.40	0.00	3.51	0.00	0.00	0.01	1.89	15.55	0.7154
P1DF01Mbt14	Matrix	37.76	4.73	15.33	11.68	0.06	15.55	0.03	0.07	9.93	0.00	1.00	0.00	0.00	0.42	95.71	5.57	2.43	0.23	0.52	0.00	1.44	0.01	3.42	0.00	0.00	0.02	1.87	15.52	0.7035
P1DF01Mbt15	Matrix	37.66	4.21	15.55	12.07	0.01	15.78	0.02	0.05	9.93	0.00	1.60	0.00	0.00	0.67	96.20	5.55	2.45	0.26	0.47	0.00	1.49	0.00	3.47	0.00	0.00	0.01	1.87	15.57	0.6996
P1DF04Mbt104	Matrix	36.46	5.19	15.28	13.43	0.00	14.35	0.05	0.07	9.23	0.00	0.95	0.00	0.00	0.40	94.60	5.48	2.52	0.19	0.59	0.00	1.69	0.00	3.22	0.00	0.01	0.02	1.77	15.47	0.6557
P1DF04Mbt105	Matrix	36.72	4.98	15.42	13.77	0.01	13.93	0.08	0.11	8.74	0.00	0.90	0.00	0.00	0.38	94.28	5.52	2.48	0.26	0.56	0.00	1.73	0.00	3.12	0.00	0.01	0.03	1.68	15.40	0.6433
P1DF03Mbt76	Matrix	37.34	3.98	15.23	10.35	0.00	16.90	0.09	0.07	9.54	0.00	1.16	0.00	0.00	0.49	94.16	5.56	2.44	0.24	0.45	0.00	1.29	0.00	3.75	0.00	0.01	0.02	1.81	15.57	0.7443
P1DF03Mbt77	Matrix	37.56	4.59	15.26	10.96	0.00	16.17	0.01	0.06	9.84	0.00	1.04	0.00	0.00	0.44	95.04	5.56	2.44	0.22	0.51	0.00	1.36	0.00	3.57	0.00	0.00	0.02	1.86	15.53	0.7245
P1DF03Mbt78	Matrix	37.49	4.81	15.11	10.95	0.00	15.89	0.01	0.02	9.92	0.00	1.04	0.00	0.00	0.44	94.78	5.57	2.43	0.21	0.54	0.00	1.36	0.00	3.52	0.00	0.00	0.01	1.88	15.51	0.7212
P1DF03Mbt79	Matrix	37.40	4.56	15.26	11.17	0.00	16.11	0.00	0.06	9.61	0.00	1.07	0.00	0.00	0.45	94.78	5.55	2.45	0.22	0.51	0.00	1.39	0.00	3.57	0.00	0.00	0.02	1.82	15.52	0.7200

(L) = leucosome; (R) = residue; (Rr) = residue-rich band; (Lr) = leucosome-rich band

Representative major element compositions of cordierite (Crd) crystals

Structural formulas calculated after Deer et al. (1992)

spot/analysis	type	SiO2	TiO2	Al2O3	FeO	MnO	MgO	CaO	Na2O	K2O	TOTAL	Si	Ti	Al	Fe	Mn	Mg	Ca	Na	K	Total cations	XMg
Sample P4E																						
Crd1																						
P4EF03Mcrd47	Core	51.26	0.04	33.89	3.69	0.03	11.59	0.01	0.00	0.02	100.52	5.09	0.00	3.97	0.31	0.00	1.72	0.00	0.00	0.00	11.10	0.8483
P4EF03Mcrd48	Core	50.74	0.01	33.68	3.80	0.07	11.59	0.01	0.05	0.00	99.95	5.04	0.00	3.95	0.32	0.01	1.72	0.00	0.01	0.00	11.04	0.8447
P4EF03Mcrd49	Rim	50.36	0.01	33.68	3.83	0.07	11.43	0.01	0.00	0.00	99.39	5.00	0.00	3.94	0.32	0.01	1.69	0.00	0.00	0.00	10.97	0.8418
P4EF02Mcrd04	Core	50.07	0.00	33.31	3.58	0.00	11.59	0.12	0.08	0.01	98.75	4.98	0.00	3.90	0.30	0.00	1.72	0.01	0.02	0.00	10.92	0.8522
P4EF02Mcrd09	Rim	50.41	0.03	33.68	3.72	0.06	11.66	0.00	0.04	0.01	99.59	5.01	0.00	3.95	0.31	0.01	1.73	0.00	0.01	0.00	11.01	0.8482
P4EF02Mcrd12	Core	50.30	0.01	33.84	3.70	0.06	11.74	0.02	0.05	0.01	99.73	5.00	0.00	3.96	0.31	0.01	1.74	0.00	0.01	0.00	11.03	0.8499
P4EF02Mcrd13	Rim	50.04	0.01	33.75	3.74	0.08	11.45	0.03	0.05	0.01	99.15	4.97	0.00	3.95	0.31	0.01	1.70	0.00	0.01	0.00	10.95	0.8452
Crd2																						
P4E'F01Mcrd43	Moat	50.84	0.00	34.06	3.37	0.01	12.13	0.05	0.03	0.02	100.51	5.00	0.00	3.95	0.28	0.00	1.78	0.01	0.01	0.00	11.02	0.8647
P4E'F01Mcrd44	Moat	50.86	0.00	34.44	3.34	0.05	11.94	0.03	0.06	0.02	100.73	5.00	0.00	3.99	0.27	0.00	1.75	0.00	0.01	0.00	11.05	0.8627
P4E'F01Mcrd45	Moat	51.16	0.00	34.53	3.29	0.04	12.03	0.02	0.03	0.01	101.11	5.04	0.00	4.00	0.27	0.00	1.77	0.00	0.01	0.00	11.09	0.8657
P4E'F01Mcrd46	Moat	51.05	0.00	34.51	3.30	0.05	12.15	0.02	0.03	0.01	101.12	5.02	0.00	4.00	0.27	0.00	1.78	0.00	0.01	0.00	11.09	0.8660
P4EF01Mcrd53	Moat	50.30	0.03	34.02	3.41	0.06	11.67	0.00	0.03	0.01	99.53	5.00	0.00	3.98	0.28	0.01	1.73	0.00	0.01	0.00	11.01	0.8590
P4EF01Mcrd54	Moat	50.29	0.02	34.02	3.53	0.04	11.90	0.00	0.03	0.01	99.84	5.00	0.00	3.99	0.29	0.00	1.76	0.00	0.01	0.00	11.05	0.8571
Crd3																						
P4EF03Mcrd24	Pinitized	50.27	0.01	33.60	4.05	0.07	11.34	0.04	0.01	0.01	99.39	5.00	0.00	3.94	0.34	0.01	1.68	0.00	0.00	0.00	10.96	0.8330
P4EF03Mcrd25	Pinitized	50.63	0.00	33.66	3.96	0.03	11.42	0.02	0.02	0.02	99.75	5.03	0.00	3.94	0.33	0.00	1.69	0.00	0.00	0.00	11.00	0.8369
P4EF03Mcrd26	Pinitized	50.39	0.01	33.56	3.91	0.04	11.30	0.02	0.03	0.01	99.25	5.01	0.00	3.93	0.33	0.00	1.67	0.00	0.01	0.00	10.95	0.8373
P4EF03Mcrd53	Pinitized	50.00	0.06	33.41	4.02	0.09	11.15	0.04	0.05	0.02	98.84	4.97	0.00	3.91	0.33	0.01	1.65	0.00	0.01	0.00	10.90	0.8318
P4EF03Mcrd54	Pinitized	50.65	0.19	33.69	4.06	0.03	11.52	0.03	0.06	0.00	100.23	5.03	0.01	3.95	0.34	0.00	1.71	0.00	0.01	0.00	11.06	0.8351

Representative major element compositions of orthoclase (Or) and plagioclase (Pl) crystals

Structural formulas calculated after Perkins (2007)

spot/analysis	Mineral	type	SiO2	Al2O3	FeO	CaO	Na2O	K2O	Total	Si	Al	Fe3+	Ca	Na	K	Total cations	An%	Ab%	Or%
Sample P008																			
P008F02Mpl41	Pl	Matrix	58.55	25.89	0.05	7.75	7.16	0.13	99.53	2.63	1.37	0.00	0.37	0.62	0.01	5.00	37.13	62.12	0.75
P008F02Mpl42	Pl	Matrix	58.28	24.79	1.85	6.97	6.97	0.17	99.03	2.65	1.33	0.07	0.34	0.61	0.01	5.00	35.22	63.76	1.02
P008F02Mpl43	Pl	Matrix	59.21	26.17	0.02	7.74	7.21	0.15	100.50	2.63	1.37	0.00	0.37	0.62	0.01	5.00	36.91	62.22	0.87
P008F03Cpl83	Pl	Inclusion	58.13	26.14	0.15	8.21	6.38	0.58	99.59	2.61	1.39	0.01	0.40	0.56	0.03	4.99	40.16	56.47	3.37
P008F03Cpl87	Pl	Inclusion	59.20	25.88	0.08	7.41	6.97	0.29	99.83	2.64	1.36	0.00	0.35	0.60	0.02	4.98	36.38	61.93	1.69
P008F01Mor15	Or	Matrix	64.50	19.02	0.02	0.40	1.23	14.65	99.82	2.97	1.03	0.00	0.02	0.11	0.86	5.00	2.01	11.08	86.91
P008F01Mor16	Or	Matrix	64.37	18.94	0.04	0.41	1.20	14.52	99.48	2.97	1.03	0.00	0.02	0.11	0.86	4.99	2.07	10.95	86.98
P008F01Mor46	Or	Matrix	64.54	18.64	0.00	0.14	1.45	14.36	99.14	2.99	1.02	0.00	0.01	0.13	0.85	4.99	0.70	13.23	86.06
Sample P4E Pl																			
P4EF01Cpl26	Pl	Inclusion	59.05	26.57	0.23	8.04	6.86	0.18	100.92	2.62	1.39	0.01	0.38	0.59	0.01	5.00	38.90	60.10	1.00
P4EF01Cpl27	Pl	Inclusion	58.58	26.59	0.09	8.27	6.66	0.20	100.37	2.61	1.40	0.00	0.39	0.57	0.01	4.98	40.20	58.60	1.10
P4EF01Mpl55	Pl	Matrix	59.82	25.79	0.12	7.32	7.26	0.09	100.40	2.65	1.35	0.00	0.35	0.62	0.00	4.97	35.60	63.90	0.50
P4EF01Mpl56	Pl	Matrix	58.29	26.56	0.07	7.97	7.05	0.10	100.03	2.60	1.40	0.00	0.38	0.61	0.01	5.00	38.30	61.20	0.50
P4EF02Cpl68	Pl	Inclusion	58.09	26.75	0.13	8.45	6.76	0.09	100.26	2.59	1.41	0.00	0.40	0.58	0.01	4.99	40.70	58.80	0.50
P4EF02Cpl69	Pl	Inclusion	58.15	26.93	0.27	8.35	6.78	0.10	100.58	2.59	1.41	0.01	0.40	0.59	0.01	5.01	40.30	59.20	0.60
P4EF04Mpl74	Pl	Matrix	65.63	21.87	0.05	5.74	6.67	0.13	100.10	2.87	1.13	0.00	0.27	0.57	0.01	4.85	31.95	67.19	0.85
P4EF02Mpl99	Pl	Matrix	59.92	25.49	0.01	6.98	7.52	0.10	100.02	2.67	1.34	0.00	0.33	0.65	0.01	5.00	33.70	65.70	0.60
P4EF02Mpl100	Pl	Matrix	59.80	25.95	0.05	7.15	7.47	0.12	100.53	2.65	1.36	0.00	0.34	0.64	0.01	5.00	34.37	64.95	0.68
P4E'F04Mpl137	Pl	Matrix	58.12	26.76	0.06	8.28	6.74	0.16	100.11	2.60	1.41	0.00	0.40	0.58	0.01	5.00	40.08	59.01	0.91
P4E'F01Mpl35	Pl	Matrix	59.42	25.95	0.02	7.50	7.12	0.14	100.15	2.64	1.36	0.00	0.36	0.61	0.01	4.98	36.50	62.70	0.80
P4E'F01Mpl37	Pl	Matrix	59.36	26.57	0.05	7.88	6.90	0.13	100.87	2.62	1.38	0.00	0.37	0.59	0.01	4.97	38.40	60.90	0.70
P4E'F01Mpl38	Pl	Matrix	59.21	26.26	0.05	7.87	7.00	0.10	100.49	2.63	1.37	0.00	0.37	0.60	0.01	4.98	38.10	61.30	0.60

Or																			
P4EF01Mor43	Or	Matrix	65.04	19.20	0.00	0.29	2.00	13.52	100.04	2.98	1.04	0.00	0.01	0.18	0.79	5.00	1.50	18.10	80.50
P4EF02Cor84	Or	Inclusion	64.70	18.85	0.21	0.22	1.68	13.85	99.50	2.98	1.02	0.01	0.01	0.15	0.81	4.98	1.10	15.40	83.50
P4EF02Cor85	Or	Inclusion	64.70	18.95	0.12	0.28	1.95	13.53	99.52	2.98	1.03	0.00	0.01	0.17	0.79	4.98	1.40	17.70	80.90
P4EF02Mor94	Or	Matrix	65.22	18.83	0.00	0.15	2.11	13.50	99.80	2.99	1.02	0.00	0.01	0.19	0.79	5.00	0.70	19.00	80.20
P4EF02Mor97	Or	Matrix	65.22	18.83	0.00	0.15	2.11	13.50	99.80	2.99	1.02	0.00	0.01	0.19	0.79	4.99	0.74	19.04	80.22
P4E'F01Cor14	Or	Inclusion	64.41	18.98	0.22	0.12	1.84	13.85	99.42	2.97	1.03	0.01	0.01	0.16	0.82	5.00	0.60	16.70	82.70
P4E'F01Mor31	Or	Matrix	64.82	18.92	0.00	0.15	1.90	14.00	99.79	2.98	1.03	0.00	0.01	0.17	0.82	5.01	0.80	17.00	82.30
P4EF02Mor35	Or	Matrix	65.69	18.76	0.02	0.13	1.43	14.16	100.18	3.00	1.01	0.00	0.01	0.13	0.83	4.97	0.65	13.24	86.11
P4E'F02Mor71	Or	Matrix	65.04	18.86	0.01	0.20	1.94	13.67	99.72	2.99	1.02	0.00	0.01	0.17	0.80	4.99	1.01	17.59	81.40
P4E'F03Mor113	Or	Matrix	65.38	18.98	0.05	0.12	1.65	14.14	100.31	2.99	1.02	0.00	0.01	0.15	0.82	4.99	0.58	15.00	84.42
P4EF02Mor81	Or	Matrix	64.31	19.47	0.05	0.48	2.80	12.15	99.26	2.96	1.05	0.00	0.02	0.25	0.71	4.99	2.40	25.30	72.30
P4EF02Mor82	Or	Matrix	63.83	19.18	0.02	0.47	2.40	12.84	98.75	2.96	1.05	0.00	0.02	0.22	0.76	5.01	2.30	21.60	76.00
P4E'F02Mor69	Or	Matrix	64.20	19.29	0.45	0.19	2.31	12.56	99.00	2.96	1.05	0.02	0.01	0.21	0.74	4.99	1.00	21.70	77.40
P4E'F02Mor70	Or	Matrix	63.88	19.93	0.25	0.23	3.11	11.27	98.66	2.94	1.08	0.01	0.01	0.28	0.66	4.98	1.20	29.20	69.60
Sample P013(Rr)																			
Pl (inclusions)																			
P013F01Cpl127	Pl	Inclusion	54.08	29.60	0.16	11.95	4.41	0.27	100.46	2.43	1.57	0.01	0.58	0.38	0.02	4.99	59.00	39.40	1.60
P013F01Cpl128	Pl	Inclusion	51.08	31.36	0.30	13.89	3.22	0.15	100.00	2.32	1.68	0.01	0.68	0.28	0.01	4.98	69.80	29.30	0.90
P013F01Cpl129	Pl	Inclusion	50.61	31.56	0.19	13.71	3.26	0.17	99.50	2.31	1.70	0.01	0.67	0.29	0.01	4.99	69.20	29.80	1.00
P013F01Cpl131	Pl	Inclusion	49.50	32.44	0.17	15.46	2.61	0.07	100.26	2.25	1.74	0.01	0.75	0.23	0.00	4.98	76.30	23.30	0.40
Pl (matrix)																			
P013F02Mpl114	Pl	Matrix	56.75	27.33	0.09	9.46	5.99	0.12	99.74	2.55	1.45	0.00	0.46	0.52	0.01	4.99	46.30	53.00	0.70
P013F02Mpl115	Pl	Matrix	56.90	27.25	0.06	9.56	6.08	0.17	100.02	2.55	1.44	0.00	0.46	0.53	0.01	4.99	46.10	53.00	1.00
P013F02Mpl117	Pl	Matrix	58.17	26.76	0.05	8.60	6.41	0.21	100.19	2.60	1.41	0.00	0.41	0.55	0.01	4.98	42.10	56.70	1.20
P013F01Cpl132	Pl	Matrix	56.97	27.02	0.03	8.98	6.26	0.23	99.50	2.57	1.44	0.00	0.43	0.55	0.01	5.00	43.60	55.10	1.30
P013F01Cpl134	Pl	Matrix	57.52	27.00	0.09	9.33	6.07	0.15	100.15	2.57	1.42	0.00	0.45	0.53	0.01	4.98	45.50	53.60	0.90
Or																			
P013F02Mpl118	Or	Matrix	64.71	18.71	0.07	0.09	0.94	14.50	99.02	3.00	1.02	0.00	0.00	0.08	0.86	4.96	0.50	9.00	90.60
P013F02Mpl121	Or	Matrix	64.77	18.70	0.11	0.10	1.12	14.34	99.15	2.99	1.02	0.00	0.01	0.10	0.85	4.97	0.50	10.60	88.90
P013F01Mpl136	Or	Matrix	64.47	18.88	0.00	0.11	0.97	14.46	98.89	2.99	1.03	0.00	0.01	0.09	0.85	4.97	0.60	9.20	90.20

P013F01Mpl137	Or	Matrix	65.29	18.44	0.04	0.07	0.91	14.60	99.36	3.01	1.00	0.00	0.00	0.08	0.86	4.95	0.40	8.60	91.00
Sample P013(Lr)																			
Pl																			
P013F05Mpl27	Pl	Core	57.98	26.83	0.08	9.10	6.13	0.24	100.35	2.59	1.41	0.00	0.43	0.53	0.01	4.98	44.44	54.17	1.40
P013F05Mpl28	Pl	Core	57.72	26.86	0.05	8.60	6.08	0.26	99.57	2.59	1.42	0.00	0.41	0.53	0.01	4.96	43.20	55.30	1.50
P013F05Mpl29	Pl	Rim	58.05	26.85	0.10	8.90	6.24	0.26	100.39	2.59	1.41	0.00	0.43	0.54	0.01	4.98	43.44	55.08	1.48
P013F04Cpl51	Pl	Inclusion	58.30	27.02	0.07	8.90	6.40	0.19	100.89	2.59	1.41	0.00	0.42	0.55	0.01	4.98	43.00	55.90	1.10
P013F04Cpl58	Pl	Core	57.38	27.08	0.06	9.27	6.16	0.18	100.13	2.57	1.43	0.00	0.44	0.54	0.01	4.99	44.90	54.00	1.10
P013F04Cpl60	Pl	Rim	56.77	26.89	0.39	8.95	6.01	0.36	99.37	2.57	1.43	0.01	0.43	0.53	0.02	4.99	44.20	53.70	2.10
P013F03Cpl78	Pl	Core	57.60	26.78	0.02	8.81	6.28	0.24	99.73	2.59	1.42	0.00	0.42	0.55	0.01	4.99	43.10	55.60	1.40
Or																			
P013F05Mor30	Or	Core	64.65	18.44	0.56	0.13	0.90	14.08	98.76	3.00	1.01	0.02	0.01	0.08	0.83	4.95	0.70	8.80	90.50
P013F05Mor31	Or	Rim	64.63	18.61	0.16	0.08	0.85	14.22	98.54	3.00	1.02	0.01	0.00	0.08	0.84	4.95	0.40	8.30	91.30
P013F04Mor53	Or	Inclusion	64.32	18.56	0.14	0.17	1.05	14.08	98.32	3.00	1.02	0.01	0.01	0.10	0.84	4.98	0.90	10.10	89.00
P013F04Mor54	Or	Inclusion	64.49	18.85	0.09	0.18	1.25	13.92	98.78	2.99	1.03	0.00	0.01	0.11	0.82	4.96	0.90	11.90	87.20
P013F04Mor55	Or	Rim	65.35	18.62	0.05	0.04	0.97	14.51	99.54	3.01	1.01	0.00	0.00	0.09	0.85	4.96	0.20	9.20	90.60
Sample P1(R)																			
Pl																			
P1mFAMpl90	Pl	Matrix	56.66	26.98	0.07	9.32	5.95	0.19	99.17	2.56	1.44	0.00	0.45	0.52	0.01	4.99	45.88	52.98	1.14
P1mFAMpl91	Pl	Matrix	56.18	28.16	0.07	9.84	5.44	0.22	99.90	2.52	1.49	0.00	0.47	0.47	0.01	4.96	49.30	49.30	1.30
P1mFAMpl92	Pl	Matrix	55.71	28.59	0.04	10.40	5.32	0.17	100.23	2.50	1.51	0.00	0.50	0.46	0.01	4.98	51.40	47.60	1.00
P1mF07Mpl93	Pl	Matrix	56.24	27.77	0.18	9.99	5.70	0.22	100.10	2.53	1.47	0.01	0.48	0.50	0.01	4.99	48.57	50.15	1.29
P1mF07Mpl95	Pl	Matrix	56.44	27.95	0.06	9.86	5.86	0.30	100.47	2.53	1.47	0.00	0.47	0.51	0.02	5.00	47.36	50.94	1.70
P1mF05Mpl141	Pl	Inclusion	56.46	27.78	0.12	10.01	5.75	0.29	100.40	2.53	1.47	0.00	0.48	0.50	0.02	5.00	48.20	50.10	1.70
P1mF05Mpl142	Pl	Inclusion	56.48	27.93	0.15	10.14	5.69	0.29	100.68	2.52	1.47	0.01	0.49	0.49	0.02	5.00	48.80	49.60	1.60
P1mF05Mpl143	Pl	Inclusion	56.21	27.84	0.05	10.02	5.68	0.33	100.14	2.52	1.47	0.00	0.48	0.49	0.02	4.98	48.40	49.60	1.90
P1mF05Mpl148	Pl	Matrix	56.55	27.85	0.04	10.02	5.58	0.31	100.34	2.53	1.47	0.00	0.48	0.48	0.02	4.98	48.90	49.30	1.80
P1mF05Mpl149	Pl	Matrix	56.42	28.00	0.08	10.18	5.66	0.33	100.68	2.52	1.48	0.00	0.49	0.49	0.02	5.00	48.90	49.19	1.91
P1mF05Mpl150	Pl	Matrix	55.97	27.99	0.02	10.23	5.54	0.27	100.03	2.52	1.48	0.00	0.49	0.48	0.02	4.99	49.72	48.72	1.56
P1mF05Mpl151	Pl	Matrix	55.65	28.27	0.06	10.50	5.49	0.28	100.25	2.50	1.50	0.00	0.51	0.48	0.02	5.00	50.58	47.81	1.61

Or																			
P1mFAMor93	Or	Matrix	63.94	18.11	0.03	0.03	0.62	15.91	98.62	3.00	1.00	0.00	0.00	0.06	0.95	5.01	0.10	5.60	94.30
P1mFAMor94	Or	Matrix	63.66	18.23	0.00	0.01	0.65	15.82	98.36	2.99	1.01	0.00	0.00	0.06	0.95	5.01	0.00	5.90	94.10
P1mFAMor95	Or	Matrix	64.35	18.55	0.03	0.03	0.68	15.85	99.48	2.99	1.02	0.00	0.00	0.06	0.94	5.01	0.20	6.10	93.80
P1mFAMor97	Or	Matrix	64.13	18.42	0.05	0.05	0.65	15.94	99.23	2.99	1.01	0.00	0.00	0.06	0.95	5.01	0.22	5.85	93.93
Sample P1(L)																			
Pl																			
P1lFEMpl39	Pl	Matrix	56.72	27.41	0.06	9.40	5.92	0.31	99.81	2.55	1.45	0.00	0.45	0.52	0.02	4.99	45.90	52.30	1.80
P1lFEMpl40	Pl	Matrix	56.97	27.20	0.03	8.79	6.00	0.25	99.24	2.57	1.45	0.00	0.42	0.52	0.01	4.97	44.10	54.40	1.50
P1lF01Mpl32	Pl	Matrix	56.77	27.82	0.05	9.72	6.06	0.18	100.60	2.53	1.46	0.00	0.47	0.52	0.01	4.99	46.50	52.40	1.00
P1lF01Mpl34	Pl	Matrix	56.33	28.29	0.10	10.15	5.77	0.20	100.84	2.51	1.49	0.00	0.49	0.50	0.01	5.00	48.70	50.10	1.20
P1lF02Mpl64	Pl	Matrix	55.82	28.11	0.08	10.29	5.74	0.12	100.15	2.51	1.49	0.00	0.50	0.50	0.01	5.01	49.40	49.90	0.70
P1lF02Mpl65	Pl	Matrix	56.83	27.82	0.02	9.87	5.96	0.20	100.70	2.53	1.46	0.00	0.47	0.52	0.01	4.99	47.20	51.60	1.20
Or																			
P1lF01Mor13	Or	Inclusion	64.51	18.80	0.06	0.19	1.29	14.60	99.44	2.98	1.02	0.00	0.01	0.12	0.86	4.99	0.90	11.70	87.40
P1lF01Mor14	Or	Inclusion	64.99	18.97	0.10	0.18	1.38	14.19	99.81	2.98	1.03	0.00	0.01	0.12	0.83	4.97	0.90	12.80	86.30
P1lF01Mor18	Or	Inclusion	64.54	18.77	0.12	0.11	1.04	14.77	99.33	2.99	1.02	0.00	0.01	0.09	0.87	4.98	0.50	9.60	89.90
P1lF01Mor19	Or	Inclusion	64.61	18.83	0.13	0.10	1.18	14.79	99.64	2.98	1.02	0.00	0.00	0.11	0.87	4.98	0.50	10.70	88.80
P1lF02Mor49	Or	Inclusion	64.68	18.43	0.07	0.06	1.19	14.99	99.43	2.99	1.01	0.00	0.00	0.11	0.89	5.00	0.30	10.70	89.00
P1lF02Mor50	Or	Inclusion	65.35	18.66	0.17	0.04	1.08	15.03	100.33	3.00	1.01	0.01	0.00	0.10	0.88	5.00	0.20	9.80	90.00
Sample P1D																			
P1DF01Mpl26	Pl	Matrix	58.93	26.35	0.04	7.91	6.89	0.19	100.31	2.62	1.38	0.00	0.38	0.59	0.01	4.98	38.40	60.50	1.10
P1DF01Mpl27	Pl	Matrix	58.93	26.40	0.05	8.25	6.75	0.20	100.56	2.62	1.38	0.00	0.39	0.58	0.01	4.98	39.90	59.00	1.10
P1DF01Mpl28	Pl	Matrix	58.87	25.83	0.03	7.57	6.92	0.18	99.41	2.64	1.37	0.00	0.36	0.60	0.01	4.98	37.20	61.70	1.10
P1DF03Mpl80	Pl	Matrix	59.59	25.79	0.07	7.42	6.81	0.37	100.06	2.65	1.35	0.00	0.35	0.59	0.02	4.96	36.70	61.10	2.20
P1DF04Mpl111	Pl	Matrix	59.27	25.81	0.09	7.68	6.90	0.14	99.88	2.65	1.36	0.00	0.37	0.60	0.01	4.99	37.80	61.40	0.80
P1DF04Mpl112	Pl	Matrix	59.84	25.31	0.23	5.88	6.98	0.15	98.38	2.69	1.34	0.01	0.28	0.61	0.01	4.94	31.50	67.60	0.90
P1DF01Mor18	Or	Matrix	64.69	18.91	0.03	0.02	0.80	15.37	99.82	2.98	1.03	0.00	0.00	0.07	0.90	4.98	0.10	7.30	92.60
P1DF01Mor24	Or	Matrix	65.15	18.76	0.01	0.03	0.97	15.39	100.31	2.99	1.02	0.00	0.00	0.09	0.90	5.00	0.10	8.80	91.10
P1DF01Mor29	Or	Matrix	64.61	18.84	0.00	0.13	1.15	14.92	99.64	2.98	1.03	0.00	0.01	0.10	0.88	5.00	0.60	10.40	89.00
P1DF02Mor62	Or	Inclusion	64.93	18.62	0.29	0.27	1.15	14.84	100.10	2.99	1.01	0.01	0.01	0.10	0.87	4.99	1.40	10.40	88.20

P1DF03Mor86	Or	Matrix	65.33	18.79	0.16	0.06	0.94	15.11	100.39	2.99	1.01	0.01	0.00	0.08	0.88	4.97	0.30	8.60	91.00
P1DF04Mor107	Or	Matrix	64.61	18.87	0.00	0.05	1.23	14.58	99.34	2.99	1.03	0.00	0.00	0.11	0.86	4.99	0.20	11.30	88.40
P1DF04Mor109	Or	Matrix	64.61	18.68	0.01	0.11	1.11	14.84	99.35	2.99	1.02	0.00	0.01	0.10	0.88	5.00	0.50	10.20	89.30

(L) = leucosome; (R) = residue; (Rr) = residue-rich band; (Lr) = leucosome-rich band

Representative major element compositions of garnet (Grt) crystals

*Structural formulas and Fe3+ contents calculated after Perkins (2007)

spot/analysis	type	SiO2	TiO2	Al2O3	Cr2O3	FeO	Fe2O3	MnO	MgO	CaO	Total	Si	Ti	Al	Cr	Fe3+*	Fe2+	Mn	Mg	Ca	Total cations	Alm%	Sps%	Prp%	Grs%
Sample P008																									
P008F03Cg74	Rim	39.65	0.07	22.36	0.02	23.53	0.00	1.23	12.42	1.05	100.32	2.98	0.00	1.98	0.00	0.05	1.43	0.08	1.39	0.08	8.00	47.91	2.62	46.64	2.75
P008F03Cg76	Core	39.76	0.05	22.04	0.03	23.21	0.00	1.19	12.47	1.00	99.75	3.03	0.00	1.95	0.00	0.00	1.62	0.22	1.00	0.17	8.00	53.75	7.26	33.24	5.75
P008F03Cg79	Core	40.02	0.03	22.14	0.03	23.17	0.00	1.10	12.49	1.18	100.16	3.01	0.00	1.96	0.00	0.01	1.45	0.07	1.40	0.10	8.00	48.01	2.32	46.51	3.14
P008F03Cg80	Core	39.66	0.04	22.08	0.03	23.15	0.00	1.16	12.21	1.19	99.51	3.01	0.00	1.97	0.00	0.01	1.46	0.07	1.38	0.10	8.00	48.46	2.48	45.86	3.18
P008F03Mg81	Rim	40.25	0.05	22.53	0.02	23.17	0.00	1.17	12.67	1.12	100.97	3.00	0.00	1.98	0.00	0.01	1.43	0.07	1.41	0.09	8.00	47.71	2.46	46.86	2.94
P008F03Mg82	Rim	39.95	0.05	22.25	0.02	23.29	0.00	1.17	12.49	0.99	100.20	3.00	0.00	1.97	0.00	0.01	1.45	0.07	1.40	0.08	8.00	48.32	2.47	46.56	2.63
P008F02Cg34	Rim	40.06	0.05	22.21	0.03	23.20	0.00	1.10	12.54	1.01	100.20	3.01	0.00	1.97	0.00	0.00	1.46	0.07	1.41	0.08	8.00	48.35	2.33	46.63	2.69
P008F02Cg35	Rim	40.12	0.05	22.54	0.00	23.07	0.00	1.18	12.67	1.10	100.72	3.00	0.00	1.98	0.00	0.01	1.43	0.07	1.41	0.09	8.00	47.55	2.49	47.04	2.90
P008F02Cg54	Core	40.41	0.07	22.26	0.02	22.81	0.00	1.28	12.60	1.19	100.63	3.02	0.00	1.96	0.00	0.00	1.43	0.08	1.41	0.10	8.00	47.42	2.70	46.70	3.17
P008F02Cg55	Core	40.27	0.04	22.25	0.02	23.05	0.00	1.14	12.32	1.27	100.36	3.02	0.00	1.97	0.00	0.00	1.45	0.07	1.38	0.10	8.00	48.23	2.41	45.95	3.40
P008F02Mg57	Rim	39.88	0.08	22.09	0.02	23.45	0.00	1.15	12.25	1.37	100.28	3.00	0.00	1.96	0.00	0.03	1.45	0.07	1.37	0.11	8.00	48.18	2.43	45.71	3.62
P008F02Mg58	Rim	39.73	0.06	22.13	0.04	23.78	0.00	1.15	12.02	1.20	100.10	3.00	0.00	1.97	0.00	0.02	1.48	0.07	1.35	0.10	8.00	49.26	2.45	45.06	3.18
Sample P4E																									
Grt (very coarse to coarse)																									
P4EF02Mg01	Rim	40.12	0.06	22.15	0.00	24.26	0.00	1.31	11.27	1.31	100.47	3.03	0.00	1.97	0.00	0.00	1.53	0.08	1.27	0.11	8.00	51.23	2.80	42.41	3.55
P4EF02Mg02	Rim	39.85	0.05	22.17	0.00	24.41	0.00	1.30	11.44	1.32	100.54	3.01	0.00	1.97	0.00	0.01	1.53	0.08	1.29	0.11	8.00	50.96	2.76	42.73	3.53
P4EF02Mg20	Rim	39.75	0.03	22.12	0.00	0.00	24.51	1.42	11.42	1.26	100.51	3.00	0.00	1.97	0.00	0.02	1.52	0.09	1.29	0.10	8.00	50.77	3.02	42.82	3.35
P4EF02Cg10	Core	40.18	0.03	22.42	0.00	23.46	0.00	1.21	12.12	1.61	101.02	3.00	0.00	1.97	0.00	0.02	1.45	0.08	1.35	0.13	8.00	48.22	2.55	44.95	4.24
P4EF02Cg11	Core	40.16	0.00	22.43	0.00	23.03	0.00	1.29	12.29	1.46	100.66	3.01	0.00	1.98	0.00	0.01	1.44	0.08	1.37	0.12	8.00	47.76	2.72	45.62	3.89
P4EF02Cg12	Core	40.29	0.03	22.23	0.00	23.22	0.00	1.21	12.24	1.16	100.37	3.03	0.00	1.97	0.00	0.00	1.46	0.08	1.37	0.09	8.00	48.65	2.56	45.69	3.10
P4EF02Cg14	Core	40.10	0.05	22.36	0.00	0.00	23.03	1.21	12.42	1.43	100.58	3.00	0.00	1.97	0.00	0.01	1.43	0.08	1.39	0.11	8.00	47.53	2.55	46.12	3.78
P4EF02Cg36	Core	39.71	0.02	21.86	0.00	23.59	0.00	1.15	12.08	1.35	99.75	3.01	0.00	1.95	0.00	0.03	1.46	0.07	1.36	0.11	8.00	48.60	2.45	45.32	3.58
P4EF02Cg37	Core	39.94	0.03	22.36	0.00	23.36	0.00	1.20	12.08	1.57	100.54	3.00	0.00	1.98	0.00	0.02	1.45	0.08	1.35	0.13	8.00	48.19	2.54	45.06	4.16
P4EF02Mg61	Rim	39.84	0.01	22.00	0.00	24.59	0.00	1.34	11.23	1.39	100.40	3.01	0.00	1.96	0.00	0.01	1.55	0.09	1.27	0.11	8.00	51.40	2.85	42.01	3.73

P4EF02Mg62	Rim	39.53	0.06	21.89	0.00	24.89	0.00	1.37	10.97	1.41	100.12	3.01	0.00	1.96	0.00	0.02	1.56	0.09	1.24	0.11	8.00	51.95	2.94	41.31	3.76
Grt (coarse to medium)																									
P4EF01Mg05	Rim	39.26	0.04	22.16	0.00	27.35	0.00	1.23	10.00	1.20	101.24	2.98	0.00	1.98	0.00	0.06	1.67	0.08	1.13	0.10	8.00	56.12	2.65	37.95	3.18
P4EF01Mg06	Rim	39.33	0.07	21.98	0.00	26.08	0.00	1.32	10.40	1.53	100.71	2.99	0.00	1.97	0.00	0.05	1.60	0.08	1.18	0.12	8.00	53.63	2.84	39.38	4.03
P4EF01Cg10	Core	39.46	0.03	22.22	0.00	25.56	0.00	1.45	10.89	1.58	101.19	2.97	0.00	1.97	0.00	0.08	1.53	0.09	1.22	0.13	8.00	51.48	3.11	41.12	4.12
P4EF01Cg11	Core	39.88	0.08	22.37	0.00	25.56	0.00	1.47	10.90	1.50	101.76	2.99	0.00	1.98	0.00	0.04	1.56	0.09	1.22	0.12	8.00	52.18	3.12	40.67	3.94
P4EF01Cg17	Core	39.62	0.04	22.33	0.00	25.42	0.00	1.50	11.05	1.70	101.66	2.97	0.00	1.97	0.00	0.09	1.50	0.10	1.23	0.14	8.00	50.64	3.21	41.55	4.39
P4EF01Cg18	Core	39.42	0.05	22.26	0.00	25.15	0.00	1.43	11.18	1.46	100.94	2.97	0.00	1.98	0.00	0.08	1.51	0.09	1.26	0.12	8.00	50.75	3.06	42.23	3.80
P4EF01Mg23	Rim	39.69	0.04	22.23	0.00	25.95	0.00	1.46	10.67	1.40	101.44	2.99	0.00	1.97	0.00	0.05	1.59	0.09	1.20	0.11	8.00	53.08	3.12	40.02	3.68
P4EF01Mg24	Rim	38.98	0.05	21.88	0.00	25.75	0.00	1.42	10.61	1.34	100.02	2.98	0.00	1.97	0.00	0.07	1.57	0.09	1.21	0.11	8.00	52.72	3.08	40.52	3.53
P4E'F02grt48	Rim	39.59	0.04	22.08	0.00	0.00	25.53	1.16	10.37	1.63	100.40	3.01	0.00	1.98	0.00	0.00	1.62	0.07	1.18	0.13	8.00	54.00	2.48	39.10	4.41
P4E'F02grt49	Core	39.47	0.02	22.22	0.00	0.00	24.78	1.16	10.87	1.74	100.26	2.99	0.00	1.99	0.00	0.02	1.55	0.07	1.23	0.14	8.00	51.75	2.49	41.03	4.67
P4E'F02grt52	Core	39.66	0.03	22.11	0.00	0.00	24.52	1.21	11.26	1.57	100.35	3.00	0.00	1.97	0.00	0.02	1.53	0.08	1.27	0.13	8.00	50.89	2.57	42.29	4.19
P4E'F02grt53	Core	39.68	0.03	22.20	0.00	0.00	24.69	1.25	10.98	1.74	100.57	3.00	0.00	1.98	0.00	0.02	1.54	0.08	1.24	0.14	8.00	51.39	2.67	41.24	4.66
P4E'F02grt54	Core	39.90	0.03	22.24	0.00	0.00	24.07	1.33	11.33	1.86	100.75	3.00	0.00	1.97	0.00	0.02	1.50	0.08	1.27	0.15	8.00	49.89	2.81	42.31	4.95
P4E'F02grt59	Core	39.78	0.01	22.21	0.00	0.00	24.48	1.13	11.19	1.39	100.19	3.01	0.00	1.98	0.00	0.00	1.55	0.07	1.26	0.11	8.00	51.70	2.42	42.12	3.76
P4E'F02grt60	Rim	39.79	0.02	22.18	0.00	0.00	24.52	1.16	11.16	1.27	100.08	3.02	0.00	1.98	0.00	0.00	1.56	0.07	1.26	0.10	8.00	51.95	2.48	42.14	3.43
P4E'F01Mg01	Rim	39.49	0.03	22.42	0.00	25.99	0.00	1.15	10.15	1.09	100.31	3.01	0.00	2.01	0.00	0.00	1.66	0.07	1.15	0.09	8.00	55.72	2.50	38.80	2.98
P4E'F01Cg03	Core	39.42	0.07	22.25	0.00	25.52	0.00	1.17	10.72	1.25	100.40	2.99	0.00	1.99	0.00	0.01	1.61	0.08	1.21	0.10	8.00	53.60	2.51	40.49	3.37
P4E'F01Cg04	Core	39.22	0.04	22.02	0.00	25.78	0.00	1.17	10.30	1.15	99.67	3.01	0.00	1.99	0.00	0.00	1.65	0.08	1.18	0.09	8.00	55.09	2.53	39.22	3.16
P4E'F01Mg06	Rim	39.37	0.06	22.15	0.00	26.07	0.00	1.18	10.47	1.12	100.42	3.00	0.00	1.99	0.00	0.01	1.65	0.08	1.19	0.09	8.00	54.84	2.54	39.59	3.01
P4E'F01Mg07	Rim	39.30	0.01	21.81	0.00	27.21	0.00	1.20	9.32	1.03	99.89	3.03	0.00	1.98	0.00	0.00	1.75	0.08	1.07	0.08	8.00	58.70	2.62	35.85	2.84
P4E'F03Mg82	Rim	39.39	0.04	22.26	0.00	26.68	0.00	1.12	9.82	1.04	100.35	3.01	0.00	2.01	0.00	0.00	1.71	0.07	1.12	0.09	8.00	57.19	2.42	37.52	2.86
P4E'F03Cg87	Core	39.31	0.02	22.15	0.00	26.47	0.00	1.09	10.32	1.04	100.40	3.00	0.00	1.99	0.00	0.02	1.67	0.07	1.17	0.08	8.00	55.72	2.35	39.10	2.80
P4E'F03Cg88	Core	39.33	0.00	21.83	0.00	26.60	0.00	1.26	9.80	1.13	99.95	3.02	0.00	1.98	0.00	0.00	1.71	0.08	1.12	0.09	8.00	56.86	2.72	37.33	3.09
P4E'F03Mg91	Rim	39.81	0.03	22.29	0.00	25.58	0.00	1.16	10.62	1.00	100.50	3.02	0.00	1.99	0.00	0.00	1.62	0.07	1.20	0.08	8.00	54.45	2.50	40.31	2.74
Grt (overgrowths)																									
P4E'F02Mg77	Rim (bt)	39.29	0.01	22.04	0.00	27.44	0.00	1.07	9.46	1.05	100.37	3.01	0.00	1.99	0.00	0.00	1.76	0.07	1.08	0.09	8.00	58.71	2.33	36.08	2.88
P4E'F02Mg78	Rim (bt)	39.10	0.07	21.96	0.00	27.19	0.00	1.12	9.68	1.09	100.21	3.00	0.00	1.98	0.00	0.01	1.73	0.07	1.11	0.09	8.00	57.72	2.43	36.86	2.97
P4E'F02Mg79	Rim (bt)	39.38	0.08	22.02	0.00	28.15	0.00	1.12	8.99	1.05	100.78	3.02	0.00	1.99	0.00	0.00	1.80	0.07	1.03	0.09	8.00	60.33	2.44	34.35	2.87

P4E'F04Mg149	Rim (ilm)	39.36	0.06	22.04	0.00	0.00	27.91	1.21	9.15	1.00	100.73	3.01	0.00	1.99	0.00	0.00	1.79	0.08	1.04	0.08	8.00	59.73	2.63	34.89	2.74
P4E'F04Mg151	Rim (ilm)	39.42	0.14	21.84	0.00	26.86	0.00	1.19	9.67	1.08	100.19	3.02	0.01	1.97	0.00	0.00	1.72	0.08	1.11	0.09	8.00	57.54	2.57	36.92	2.96
P4E'F04Mg152	Rim (ilm)	39.70	0.09	22.16	0.00	27.07	0.00	1.24	9.78	1.14	101.18	3.01	0.01	1.98	0.00	0.00	1.72	0.08	1.11	0.09	8.00	57.34	2.66	36.93	3.07
P4E'F04Mg153	Rim (ilm)	38.15	0.10	21.83	0.00	27.08	0.00	1.07	9.44	1.06	98.74	2.97	0.01	2.00	0.00	0.04	1.72	0.07	1.10	0.09	8.00	57.84	2.38	36.81	2.91
Sample P013(Rr)																									
P013F01Mgrt122	Rim	39.00	0.04	21.32	0.01	28.30	0.00	0.98	8.22	2.33	100.19	3.02	0.00	1.94	0.00	0.02	1.81	0.06	0.95	0.19	8.00	60.08	2.12	31.40	6.34
P013F01Mgrt125	Core	39.06	0.06	21.29	0.01	26.79	0.00	0.91	8.48	3.21	99.81	3.02	0.00	1.94	0.00	0.01	1.72	0.06	0.98	0.27	8.00	56.93	1.97	32.32	8.71
P013F01Mgrt141	Core	39.11	0.05	21.40	0.00	26.57	0.00	0.92	8.42	3.29	99.76	3.02	0.00	1.95	0.00	0.00	1.72	0.06	0.97	0.27	8.00	56.86	1.99	32.12	9.01
P013F01Mgrt143	Rim	38.77	0.07	21.54	0.01	27.56	0.00	0.87	8.63	2.08	99.52	3.01	0.00	1.97	0.00	0.00	1.78	0.06	1.00	0.17	8.00	59.23	1.89	33.15	5.71
P013F02Mgrt93	Rim	38.74	0.04	21.43	0.03	28.98	0.00	0.84	7.75	2.01	99.82	3.02	0.00	1.97	0.00	0.00	1.89	0.06	0.90	0.17	8.00	62.71	1.84	29.89	5.55
P013F02Mgrt95	Core	38.91	0.08	21.64	0.02	26.90	0.00	0.85	8.25	3.07	99.72	3.01	0.00	1.98	0.00	0.00	1.74	0.06	0.95	0.26	8.00	57.98	1.85	31.68	8.46
P013F02Mgrt96	Core	39.22	0.06	21.46	0.03	26.95	0.00	0.91	8.26	2.78	99.68	3.04	0.00	1.96	0.00	0.00	1.75	0.06	0.95	0.23	8.00	58.38	2.00	31.90	7.70
P013F02Mgrt98	Rim	38.85	0.06	21.11	0.05	28.53	0.00	0.91	8.20	1.99	99.69	3.02	0.00	1.94	0.00	0.01	1.85	0.06	0.95	0.17	8.00	61.10	1.98	31.44	5.45
Sample P013(Lr)																									
Grt																									
P013F03Mgrt84	Rim	39.08	0.04	21.17	0.04	28.79	0.00	0.96	7.78	2.00	99.84	3.04	0.00	1.94	0.00	0.00	1.88	0.06	0.90	0.17	8.00	62.32	2.10	30.03	5.54
P013F03Mgrt85	Core	39.45	0.06	21.28	0.02	28.26	0.00	0.88	8.60	2.12	100.66	3.03	0.00	1.93	0.00	0.00	1.82	0.06	0.99	0.17	8.00	59.89	1.89	32.48	5.73
P013F03Mgrt86	Core	38.94	0.07	21.46	0.02	27.89	0.00	0.97	8.55	2.36	100.25	3.00	0.00	1.95	0.00	0.03	1.77	0.06	0.98	0.19	8.00	58.75	2.10	32.67	6.36
P013F03Mgrt87	Core	39.02	0.05	21.33	0.03	27.19	0.00	0.87	8.33	2.62	99.43	3.03	0.00	1.95	0.00	0.00	1.77	0.06	0.96	0.22	8.00	58.76	1.91	32.07	7.24
P013F03Mgrt89	Rim	38.77	0.06	21.18	0.05	29.53	0.00	0.90	7.36	2.04	99.88	3.03	0.00	1.95	0.00	0.00	1.93	0.06	0.86	0.17	8.00	63.95	1.98	28.42	5.63
P013F04Mgrt35	Rim	38.88	0.06	21.59	0.05	0.00	28.83	1.07	8.07	1.75	100.29	3.01	0.00	1.97	0.00	0.00	1.87	0.07	0.93	0.14	8.00	61.95	2.32	30.92	4.79
P013F04Mgrt37	Core	38.98	0.06	21.48	0.02	0.00	27.14	0.96	8.88	1.91	99.42	3.02	0.00	1.96	0.00	0.00	1.76	0.06	1.03	0.16	8.00	58.52	2.09	34.12	5.26
P013F04Mgrt38	Core	39.16	0.09	21.63	0.01	0.00	27.34	0.95	9.08	1.93	100.17	3.01	0.00	1.96	0.00	0.00	1.75	0.06	1.04	0.16	8.00	58.16	2.04	34.52	5.25
P013F04Mgrt39	Core	38.99	0.05	21.63	0.02	0.00	27.38	0.93	8.81	1.89	99.69	3.02	0.00	1.97	0.00	0.00	1.77	0.06	1.02	0.16	8.00	58.96	2.02	33.82	5.19
P013F04Mgrt65	Core	39.65	0.06	21.30	0.01	0.00	27.38	0.84	8.76	2.07	100.06	3.06	0.00	1.94	0.00	0.00	1.77	0.05	1.01	0.17	8.00	58.90	1.82	33.58	5.68
P013F04Mgrt67	Rim	38.84	0.03	21.40	0.04	0.00	28.33	0.94	8.33	1.86	99.77	3.02	0.00	1.96	0.00	0.00	1.84	0.06	0.96	0.16	8.00	60.85	2.06	31.95	5.12
P013F05Mgrt01	Rim	39.25	0.04	21.40	0.05	27.86	0.00	0.91	8.63	2.02	100.16	3.03	0.00	1.95	0.00	0.00	1.80	0.06	0.99	0.17	8.00	59.60	1.96	32.89	5.53
P013F05Mgrt02	Core	39.28	0.05	21.36	0.03	28.23	0.00	0.79	8.72	1.92	100.38	3.03	0.00	1.94	0.00	0.00	1.82	0.05	1.00	0.16	8.00	60.01	1.70	33.05	5.23

P013F05Mgrt03	Core	38.88	0.05	21.38	0.02	28.00	0.00	0.82	8.56	1.93	99.65	3.02	0.00	1.96	0.00	0.00	1.81	0.05	0.99	0.16	8.00	60.08	1.79	32.80	5.31
P013F05Mgrt05	Core	38.94	0.05	21.55	0.05	28.24	0.00	0.76	8.38	1.83	99.79	3.02	0.00	1.97	0.00	0.00	1.83	0.05	0.97	0.15	8.00	61.01	1.67	32.25	5.06
P013F05Mgrt06	Rim	38.62	0.01	21.44	0.04	29.41	0.00	0.80	7.46	2.13	99.91	3.01	0.00	1.97	0.00	0.00	1.91	0.05	0.87	0.18	8.00	63.57	1.74	28.78	5.88
Grt (xenomorphic)																									
P013F05Mgrt07	Xenomorphic	38.64	0.00	21.35	0.01	28.65	0.00	0.74	6.68	3.26	99.32	3.03	0.00	1.98	0.00	0.00	1.88	0.05	0.78	0.27	8.00	62.98	1.66	26.17	9.19
P013F05Mgrt08	Xenomorphic	38.60	0.00	21.43	0.06	28.96	0.00	0.77	7.22	2.54	99.58	3.02	0.00	1.98	0.00	0.00	1.89	0.05	0.84	0.21	8.00	63.14	1.70	28.06	7.09
P013F05Mgrt09	Xenomorphic	39.10	0.04	21.63	0.05	28.79	0.00	0.80	7.40	2.59	100.39	3.03	0.00	1.98	0.00	0.00	1.87	0.05	0.86	0.21	8.00	62.44	1.76	28.62	7.17
P013F05Mgrt10	Xenomorphic	38.69	0.01	21.46	0.07	29.70	0.00	0.71	6.85	2.77	100.26	3.01	0.00	1.97	0.00	0.00	1.94	0.05	0.80	0.23	8.00	64.31	1.56	26.45	7.66
Sample P1(R)																									
P1mF05Mgrt131	Rim	38.92	0.03	21.60	0.00	28.73	0.00	1.02	7.61	2.46	100.36	3.01	0.00	1.97	0.00	0.00	1.86	0.07	0.88	0.20	8.00	61.81	2.22	29.20	6.77
P1mF05Cgrt132	Core	38.90	0.04	21.66	0.00	28.34	0.00	0.97	8.00	2.58	100.49	3.00	0.00	1.97	0.00	0.02	1.81	0.06	0.92	0.21	8.00	60.16	2.10	30.64	7.01
P1mF05Cgrt133	Core	38.73	0.09	21.37	0.00	27.60	0.00	1.06	7.78	2.76	99.38	3.02	0.00	1.97	0.00	0.00	1.80	0.07	0.90	0.23	8.00	59.91	2.32	30.09	7.66
P1mF05Cgrt134	Core	38.86	0.08	21.67	0.00	27.85	0.00	1.05	7.84	2.79	100.14	3.01	0.00	1.98	0.00	0.00	1.80	0.07	0.91	0.23	8.00	59.94	2.28	30.08	7.68
P1mF05Cgrt135	Core	39.07	0.09	21.44	0.00	28.03	0.00	1.03	7.79	2.69	100.15	3.03	0.01	1.96	0.00	0.00	1.82	0.07	0.90	0.22	8.00	60.40	2.25	29.92	7.42
P1mF05Mgrt136	Rim	38.48	0.02	21.61	0.00	28.73	0.00	1.07	7.67	2.53	100.11	2.99	0.00	1.98	0.00	0.05	1.82	0.07	0.89	0.21	8.00	60.90	2.35	29.71	6.88
P1mF06Mgrt106	Rim	38.76	0.00	21.39	0.00	28.08	0.00	0.94	7.57	3.14	99.87	3.01	0.00	1.96	0.00	0.01	1.81	0.06	0.88	0.26	8.00	60.16	2.06	29.11	8.61
P1mF06Cgrt107	Core	38.74	0.04	21.28	0.00	28.97	0.00	1.07	7.22	2.45	99.77	3.03	0.00	1.96	0.00	0.00	1.89	0.07	0.84	0.21	8.00	62.89	2.35	27.94	6.81
P1mF06Cgrt108	Core	38.49	0.06	21.56	0.00	29.28	0.00	1.02	7.60	2.27	100.27	2.99	0.00	1.97	0.00	0.05	1.86	0.07	0.88	0.19	8.00	62.03	2.23	29.42	6.16
P1mF06Cgrt109	Core	38.79	0.03	21.39	0.00	28.85	0.00	0.94	7.26	2.54	99.79	3.03	0.00	1.97	0.00	0.00	1.88	0.06	0.85	0.21	8.00	62.73	2.06	28.14	7.06
P1mF06Cgrt110	Core	38.63	0.02	21.39	0.00	29.04	0.00	1.04	7.63	2.31	100.06	3.00	0.00	1.96	0.00	0.03	1.86	0.07	0.88	0.19	8.00	61.86	2.28	29.45	6.31
P1mF06Cgrt111	Core	38.79	0.02	21.28	0.00	29.06	0.00	1.05	7.44	2.34	99.98	3.02	0.00	1.95	0.00	0.00	1.89	0.07	0.86	0.20	8.00	62.65	2.28	28.60	6.46
P1mF06Mgrt112	Rim	38.63	0.02	21.26	0.00	29.08	0.00	1.02	7.33	2.42	99.75	3.02	0.00	1.96	0.00	0.00	1.90	0.07	0.85	0.20	8.00	62.78	2.24	28.26	6.70
P1mF07Mgrt73	Rim	38.96	0.08	21.44	0.00	0.00	29.25	1.01	7.06	2.69	100.48	3.03	0.00	1.96	0.00	0.00	1.90	0.07	0.82	0.22	8.00	63.19	2.21	27.17	7.42
P1mF07Mgrt74	Rim	38.84	0.04	21.24	0.00	0.00	29.40	1.04	6.74	3.02	100.31	3.03	0.00	1.95	0.00	0.00	1.92	0.07	0.78	0.25	8.00	63.45	2.28	25.93	8.34
P1mF07Mgrt75	Core	38.87	0.03	21.32	0.00	0.00	29.20	1.01	7.28	2.68	100.38	3.02	0.00	1.95	0.00	0.01	1.89	0.07	0.84	0.22	8.00	62.55	2.19	27.88	7.34
P1mF07Mgrt76	Core	38.81	0.04	21.28	0.00	0.00	29.10	1.12	7.17	2.68	100.20	3.02	0.00	1.95	0.00	0.00	1.89	0.07	0.83	0.22	8.00	62.64	2.45	27.50	7.40
P1mF07Mgrt77	Core	38.75	0.05	21.34	0.00	0.00	28.79	1.02	7.41	2.45	99.80	3.02	0.00	1.96	0.00	0.00	1.88	0.07	0.86	0.21	8.00	62.36	2.23	28.60	6.80
P1mF07Mgrt78	Core	38.83	0.21	21.26	0.00	0.00	29.13	1.14	7.30	2.46	100.33	3.02	0.01	1.95	0.00	0.00	1.89	0.08	0.85	0.20	8.00	62.72	2.48	28.01	6.74
P1mF07Mgrt79	Core	38.75	0.08	21.15	0.00	0.00	29.16	1.03	7.24	2.33	99.74	3.03	0.00	1.95	0.00	0.00	1.91	0.07	0.84	0.19	8.00	63.27	2.26	28.01	6.45
P1mF07Mgrt80	Rim	38.61	0.07	21.04	0.00	0.00	29.33	0.96	7.18	2.49	99.68	3.02	0.00	1.94	0.00	0.00	1.92	0.06	0.84	0.21	8.00	63.33	2.10	27.67	6.88

Sample P1(L)																								
P1lF02Mgrt37	Rim	39.22	0.05	21.82	0.00	29.04	0.00	0.94	7.64	3.01	101.72	3.00	0.00	1.97	0.00	0.03	1.82	0.06	0.87	0.25	8.00	60.74	2.03	29.01	8.06
P1lF02Cgrt38	Core	38.94	0.03	21.65	0.00	28.88	0.00	1.02	7.85	2.28	100.65	3.01	0.00	1.97	0.00	0.02	1.85	0.07	0.90	0.19	8.00	61.48	2.21	30.03	6.23
P1lF02Cgrt39	Core	38.74	0.21	21.61	0.00	28.58	0.00	0.97	8.01	2.34	100.47	2.99	0.01	1.97	0.00	0.02	1.83	0.06	0.92	0.19	8.00	60.75	2.11	30.70	6.35
P1lF02Cgrt40	Core	38.72	0.04	21.50	0.00	28.13	0.00	0.99	7.98	2.38	99.72	3.01	0.00	1.97	0.00	0.00	1.83	0.06	0.92	0.20	8.00	60.58	2.15	30.70	6.55
P1lF02Cgrt41	Core	38.73	0.01	21.37	0.00	28.18	0.00	0.91	7.88	2.52	99.60	3.02	0.00	1.96	0.00	0.00	1.83	0.06	0.91	0.21	8.00	60.73	1.99	30.31	6.96
P1lF02Cgrt42	Core	38.98	0.07	21.48	0.00	28.24	0.00	0.90	8.05	2.32	100.03	3.02	0.00	1.96	0.00	0.00	1.83	0.06	0.93	0.19	8.00	60.77	1.97	30.87	6.38
P1lF02Cgrt43	Core	38.98	0.02	21.58	0.00	28.32	0.00	1.03	7.90	2.34	100.16	3.02	0.00	1.97	0.00	0.00	1.83	0.07	0.91	0.19	8.00	60.98	2.25	30.33	6.44
P1lF02Mgrt44	Rim	38.49	0.00	21.56	0.00	28.68	0.00	1.00	7.39	2.57	99.68	3.00	0.00	1.98	0.00	0.01	1.86	0.07	0.86	0.22	8.00	62.02	2.21	28.61	7.13
Sample P1D																								
P1DF02Mgrt33	Rim	38.96	0.06	21.83	0.00	28.81	0.00	0.79	8.21	1.79	100.45	3.01	0.00	1.99	0.00	0.00	1.86	0.05	0.94	0.15	8.00	61.91	1.71	31.46	4.91
P1DF02Cgrt34	Core	39.18	0.09	21.85	0.00	28.46	0.00	0.81	8.35	1.74	100.48	3.02	0.01	1.99	0.00	0.00	1.83	0.05	0.96	0.14	8.00	61.35	1.77	32.08	4.78
P1DF02Cgrt35	Core	38.66	0.06	21.67	0.00	29.39	0.00	0.80	7.74	1.71	100.03	3.01	0.00	1.99	0.00	0.00	1.91	0.05	0.90	0.14	8.00	63.63	1.75	29.87	4.74
P1DF02Cgrt36	Core	39.07	0.05	21.84	0.00	28.77	0.00	0.77	7.99	1.76	100.25	3.02	0.00	1.99	0.00	0.00	1.86	0.05	0.92	0.15	8.00	62.48	1.70	30.92	4.90
P1DF02Cgrt37	Core	39.22	0.07	22.00	0.00	28.32	0.00	0.75	8.62	1.71	100.69	3.01	0.00	1.99	0.00	0.00	1.82	0.05	0.99	0.14	8.00	60.73	1.64	32.94	4.68
P1DF02Cgrt38	Core	39.13	0.05	21.70	0.00	28.13	0.00	0.79	8.53	1.81	100.15	3.02	0.00	1.97	0.00	0.00	1.82	0.05	0.98	0.15	8.00	60.54	1.73	32.73	4.99
P1DF02Cgrt39	Core	39.09	0.07	22.02	0.00	28.55	0.00	0.83	8.51	1.76	100.83	3.00	0.00	1.99	0.00	0.00	1.83	0.05	0.97	0.14	8.00	60.97	1.80	32.43	4.79
P1DF02Cgrt40	Core	39.14	0.06	21.93	0.00	28.42	0.00	0.76	8.34	1.79	100.44	3.02	0.00	1.99	0.00	0.00	1.83	0.05	0.96	0.15	8.00	61.31	1.67	32.07	4.94
P1DF02Cgrt41	Core	38.95	0.02	21.78	0.00	28.96	0.00	0.76	7.96	1.80	100.22	3.02	0.00	1.99	0.00	0.00	1.88	0.05	0.92	0.15	8.00	62.64	1.66	30.71	4.99
P1DF02Cgrt42	Core	39.08	0.04	21.74	0.00	29.17	0.00	0.78	8.03	1.73	100.55	3.02	0.00	1.98	0.00	0.00	1.88	0.05	0.92	0.14	8.00	62.74	1.70	30.79	4.76
P1DF02Mgrt43	Rim	38.74	0.04	21.69	0.00	29.46	0.00	0.83	7.78	1.70	100.24	3.01	0.00	1.98	0.00	0.00	1.91	0.05	0.90	0.14	8.00	63.56	1.82	29.93	4.68

(L) = leucosome; (R) = residue; (Rr) = residue-rich band; (Lr) = leucosome-rich band

Representative major element compositions of ilmenite (Ilm) and hematite (Hem) crystals

*Structural formulas and Fe3+ contents calculated after Droop (1987)

spot/analysis	Mineral	type	SiO2	TiO2	Al2O3	Cr2O3	Fe2O3	FeO	MnO	MgO	CaO	ZnO	Total	Si	Ti	Al	Cr	Fe3+*	Fe2+	Mn	Mg	Ca	Zn	Total cations	Hem	Ilm	Pph	Gk
Sample P008																												
P008F01Milm29	Ilm-lamellae	Rim	0.09	46.18	0.10	0.07	0.00	48.46	0.13	1.88	0.00	0.00	96.91	0.00	1.77	0.01	0.00	0.44	1.63	0.01	0.14	0.00	0.00	4.00	11.03	81.52	0.28	7.17
P008F01Milm32	Hem-lamellae	Core	0.04	16.09	0.20	0.29	0.00	73.46	0.08	0.47	0.00	0.03	90.66	0.00	0.65	0.01	0.01	2.68	0.61	0.00	0.04	0.00	0.00	4.00	67.40	30.54	0.18	1.88
P008F02Milm47	Ilm-lamellae	Core	0.02	46.37	0.03	0.08	0.00	49.21	0.18	1.39	0.01	0.02	97.31	0.00	1.78	0.00	0.00	0.44	1.66	0.01	0.11	0.00	0.00	4.00	10.90	83.39	0.40	5.31
P008F02Milm50	Hem-lamellae	Core	0.04	17.91	0.27	0.22	0.00	71.94	0.05	0.38	0.00	0.03	90.85	0.00	0.72	0.02	0.01	2.53	0.69	0.00	0.03	0.00	0.00	4.00	63.68	34.67	0.11	1.54
Sample P4E																												
P4EF02Cilm05	Ilm-lamellae	Inclusion	0.02	47.55	0.02	0.03	0.00	47.49	0.17	1.39	0.04	0.00	96.73	0.00	1.84	0.00	0.00	0.32	1.72	0.01	0.11	0.00	0.00	4.00	7.98	86.30	0.38	5.34
P4EF04Milm68	Ilm-lamellae	Core	0.05	47.19	0.00	0.04	0.00	49.28	0.31	1.02	0.00	0.04	97.92	0.00	1.81	0.00	0.00	0.38	1.72	0.01	0.08	0.00	0.00	4.00	9.53	85.93	0.66	3.88
P4EF04Milm69	Hem-lamellae	Core	0.01	18.29	0.14	0.11	0.00	72.12	0.07	0.31	0.00	0.00	91.06	0.00	0.74	0.01	0.00	2.51	0.71	0.00	0.02	0.00	0.00	4.00	63.10	35.50	0.15	1.25
P4E'F01Cilm24	Ilm-lamellae	Inclusion	0.03	44.70	0.03	0.00	0.00	51.54	0.15	1.09	0.02	0.00	97.57	0.00	1.71	0.00	0.00	0.57	1.62	0.01	0.08	0.00	0.00	4.00	14.31	81.21	0.33	4.15
P4E'F01Cilm25	Hem-lamellae	Inclusion	0.00	20.30	0.12	0.00	0.00	70.25	0.04	0.42	0.02	0.00	91.15	0.00	0.82	0.01	0.00	2.36	0.78	0.00	0.03	0.00	0.00	4.00	59.15	39.07	0.10	1.69
P4E'F03Cilm95	Hem-lamellae	Inclusion	0.00	13.49	0.08	0.00	0.00	76.29	0.01	0.24	0.02	0.00	90.13	0.00	0.55	0.01	0.00	2.90	0.52	0.00	0.02	0.00	0.00	4.00	72.72	26.30	0.02	0.97
P4E'F03Cilm96	Ilm-lamellae	Inclusion	0.05	48.93	0.00	0.00	0.00	48.26	0.14	1.23	0.00	0.00	98.60	0.00	1.86	0.00	0.00	0.28	1.76	0.01	0.09	0.00	0.00	4.00	6.91	88.17	0.29	4.63
P4E'F04Cilm146	Ilm-lamellae	Core	0.00	46.29	0.00	0.00	0.00	50.46	0.09	1.00	0.00	0.00	97.84	0.00	1.77	0.00	0.00	0.46	1.69	0.00	0.08	0.00	0.00	4.00	11.40	84.61	0.20	3.79
Sample P013																												
P013F05Milm33	Ilmenite	Core	0.00	45.35	0.03	0.11	0.00	51.43	0.19	0.53	0.02	0.00	97.65	0.00	1.74	0.00	0.00	0.50	1.70	0.01	0.04	0.00	0.00	4.00	12.63	84.95	0.40	2.01
P013F05Milm34	Ilmenite	Rim	0.26	45.85	0.07	0.08	0.00	50.51	0.13	0.52	0.02	0.02	97.45	0.01	1.77	0.00	0.00	0.43	1.73	0.01	0.04	0.00	0.00	4.00	10.86	86.87	0.27	2.00
Sample P1)																												
P1MFDMilm48	Ilmenite	Rim	0.13	45.05	0.03	0.08	0.00	48.73	0.21	0.42	0.02	0.00	94.66	0.01	1.79	0.00	0.00	0.40	1.75	0.01	0.03	0.00	0.00	4.00	10.02	87.87	0.46	1.65
P1MFDMilm49	Ilmenite	Rim	0.07	47.06	0.00	0.08	0.00	49.55	0.14	0.35	0.01	0.00	97.26	0.00	1.82	0.00	0.00	0.34	1.79	0.01	0.03	0.00	0.00	4.00	8.54	89.81	0.31	1.34
P1MFDMilm50	Ilmenite	Rim	0.08	46.45	0.00	0.08	0.00	49.63	0.14	0.34	0.03	0.00	96.75	0.00	1.81	0.00	0.00	0.37	1.78	0.01	0.03	0.00	0.00	4.00	9.28	89.09	0.30	1.33
P1MFBMilm87	Ilmenite	Core	0.10	45.20	0.40	0.08	0.00	48.74	0.29	0.43	0.04	0.11	95.39	0.01	1.78	0.02	0.00	0.40	1.73	0.01	0.03	0.00	0.00	4.00	10.16	87.49	0.65	1.70

Representative major element compositions of orthopyroxene (Opx) crystals

Structural formulas calculated after Perkins (2007)

spot/analysis	type	SiO2	TiO2	Al2O3	Cr2O3	FeO	MnO	MgO	CaO	Na2O	K2O	ZnO	Total	Si	Ti	Al	Cr	Fe	Mg	Mn	Zn	Ca	Na	K	Total cations	En	Fs	Wo	XAl	XMg
Sample P013(Rr)																														
P013F05Mopx11	Skeletal	50.26	0.08	4.58	0.06	24.81	0.19	19.33	0.22	0.00	0.00	0.19	99.72	1.90	0.00	0.20	0.00	0.78	1.09	0.01	0.01	0.01	0.00	0.00	4.00	0.58	0.42	0.00	0.10	0.5814
P013F05Copx12	Skeletal	49.46	0.11	5.02	0.07	25.09	0.25	18.86	0.20	0.05	0.01	0.17	99.28	1.88	0.00	0.23	0.00	0.80	1.07	0.01	0.00	0.01	0.00	0.00	4.00	0.57	0.43	0.00	0.11	0.5726
P013F05Copx14	Skeletal	50.26	0.10	4.23	0.09	24.98	0.21	19.33	0.19	0.02	0.01	0.09	99.51	1.90	0.00	0.19	0.00	0.79	1.09	0.01	0.00	0.01	0.00	0.00	4.00	0.58	0.42	0.00	0.09	0.5797
P013F05Mopx15	Skeletal	49.90	0.09	4.91	0.07	25.43	0.18	18.84	0.16	0.02	0.00	0.11	99.71	1.89	0.00	0.22	0.00	0.81	1.06	0.01	0.00	0.01	0.00	0.00	4.00	0.57	0.43	0.00	0.11	0.5690
P013F05Mopx19	Rim	49.81	0.09	4.69	0.09	24.69	0.24	19.18	0.18	0.00	0.02	0.17	99.13	1.89	0.00	0.21	0.00	0.78	1.09	0.01	0.00	0.01	0.00	0.00	4.00	0.58	0.42	0.00	0.10	0.5807
P013F04Mopx61	Rim	49.74	0.11	5.03	0.06	25.61	0.25	18.82	0.20	0.03	0.01	0.12	99.98	1.88	0.00	0.22	0.00	0.81	1.06	0.01	0.00	0.01	0.00	0.00	4.00	0.56	0.43	0.00	0.11	0.5670
P013F04Copx62	Core	49.12	0.10	5.15	0.05	25.37	0.22	18.63	0.17	0.04	0.00	0.02	98.86	1.88	0.00	0.23	0.00	0.81	1.06	0.01	0.00	0.01	0.00	0.00	4.00	0.56	0.43	0.00	0.12	0.5668
P013F03Mopx68	Core	50.18	0.15	4.42	0.07	24.94	0.26	19.26	0.19	0.03	0.00	0.13	99.60	1.90	0.00	0.20	0.00	0.79	1.09	0.01	0.00	0.01	0.00	0.00	4.00	0.58	0.42	0.00	0.10	0.5792
P013F03Mopx69	Rim	48.90	0.06	5.03	0.09	25.24	0.22	18.65	0.14	0.02	0.01	0.05	98.41	1.88	0.00	0.23	0.00	0.81	1.07	0.01	0.00	0.01	0.00	0.00	4.01	0.57	0.43	0.00	0.11	0.5684
P013F03Copx70	Core	49.50	0.08	4.92	0.09	25.08	0.25	19.03	0.19	0.00	0.01	0.05	99.19	1.88	0.00	0.22	0.00	0.80	1.08	0.01	0.00	0.01	0.00	0.00	4.00	0.57	0.42	0.00	0.11	0.5749
P013F03Copx71	Core	48.86	0.30	4.44	0.04	25.19	0.29	18.66	0.14	0.01	0.00	0.15	98.07	1.89	0.01	0.20	0.00	0.81	1.07	0.01	0.00	0.01	0.00	0.00	4.00	0.57	0.43	0.00	0.10	0.5690
Sample P1(R)																														
Opx1																														
P1mFBMopx72	Rim	50.10	0.11	3.86	0.06	25.08	0.34	19.22	0.27	0.03	0.01	0.17	99.23	1.91	0.00	0.17	0.00	0.80	1.09	0.01	0.00	0.01	0.00	0.00	4.00	0.57	0.42	0.01	0.09	0.5773
P1mFBCopx74	Core	50.09	0.35	3.86	0.06	25.25	0.31	19.04	0.28	0.04	0.02	0.01	99.29	1.91	0.01	0.17	0.00	0.80	1.08	0.01	0.00	0.01	0.00	0.00	4.00	0.57	0.42	0.01	0.09	0.5735
P1mFBCopx75	Core	49.57	0.10	4.41	0.07	24.95	0.31	18.83	0.24	0.04	0.00	0.12	98.63	1.90	0.00	0.20	0.00	0.80	1.07	0.01	0.00	0.01	0.00	0.00	4.00	0.57	0.42	0.01	0.10	0.5737
P1mFBCopx76	Core	50.02	0.09	4.28	0.05	25.32	0.36	19.11	0.23	0.03	0.02	0.09	99.58	1.90	0.00	0.19	0.00	0.80	1.08	0.01	0.00	0.01	0.00	0.00	4.00	0.57	0.42	0.00	0.10	0.5736
P1mFBMopx77	Rim	50.29	0.07	3.86	0.04	25.15	0.35	19.06	0.26	0.03	0.01	0.03	99.15	1.91	0.00	0.17	0.00	0.80	1.08	0.01	0.00	0.01	0.00	0.00	4.00	0.57	0.42	0.01	0.09	0.5746
P1mFBMopx78	Rim	50.64	0.07	3.44	0.07	25.08	0.27	19.53	0.27	0.01	0.01	0.07	99.45	1.92	0.00	0.15	0.00	0.80	1.10	0.01	0.00	0.01	0.00	0.00	4.00	0.58	0.42	0.01	0.08	0.5812
Opx2																														
P1mF07Copx100	Core	51.57	0.11	3.11	0.00	24.21	0.26	20.52	0.27	0.03	0.02	0.00	100.11	1.93	0.00	0.14	0.00	0.76	1.15	0.01	0.00	0.01	0.00	0.00	4.00	0.60	0.40	0.01	0.07	0.6017
P1mF07Copx105	Rim	50.99	0.09	2.69	0.00	24.58	0.24	19.76	0.34	0.02	0.01	0.00	98.72	1.94	0.00	0.12	0.00	0.78	1.12	0.01	0.00	0.01	0.00	0.00	4.00	0.58	0.41	0.01	0.06	0.5889
P1mF05Copx144	Core	51.42	0.10	2.25	0.00	25.43	0.30	19.92	0.33	0.00	0.02	0.00	99.77	1.95	0.00	0.10	0.00	0.80	1.12	0.01	0.00	0.01	0.00	0.00	4.00	0.58	0.41	0.01	0.05	0.5827
P1mF05Copx145	Core	51.42	0.08	2.28	0.00	25.14	0.32	19.75	0.29	0.04	0.01	0.00	99.33	1.95	0.00	0.10	0.00	0.80	1.12	0.01	0.00	0.01	0.00	0.00	4.00	0.58	0.41	0.01	0.05	0.5834

P1mF05Mopx146	Rim	51.27	0.08	3.18	0.00	25.09	0.22	20.00	0.28	0.00	0.01	0.00	100.13	1.93	0.00	0.14	0.00	0.79	1.12	0.01	0.00	0.01	0.00	0.00	4.00	0.58	0.41	0.01	0.07	0.5869
P1mF05Mopx147	Rim	51.08	0.06	2.09	0.00	26.69	0.29	18.71	0.31	0.03	0.00	0.00	99.25	1.96	0.00	0.09	0.00	0.85	1.07	0.01	0.00	0.01	0.00	0.00	4.00	0.55	0.44	0.01	0.05	0.5554

(R) = residue; (Rr) = residue-rich band

Representative major element compositions of sapphirine (Spr) crystals

*Structural formulas and Fe3+ contents calculated after Higgins (1979), Grew et al. (2008) and Taylor-Jones & Powell (2010)

spot/analysis	type	SiO2	TiO2	Al2O3	Cr2O3	FeO	Fe2O3	MnO	MgO	CaO	Na2O	K2O	ZnO	Total	Si	Ti	Al (IV)	Al (VI)	Cr	Fe3+*	Fe 2+	Mg	Mn	Zn	Ca	Na	K	Total cations	Al (t)	Fe (t)	XMg
Sample P008																														
P008F01Mspr1	Core	12.59	0.03	59.71	0.03	10.11	0.00	0.08	15.35	0.03	0.04	0.03	0.02	98.02	1.55	0.00	4.45	4.22	0.00	0.22	0.82	2.82	0.01	0.00	0.00	0.01	0.00	14.12	8.67	1.04	0.7751
P008F01Mspr2	Core	12.64	0.01	60.36	0.03	9.33	0.00	0.10	15.52	0.05	0.02	0.01	0.00	98.06	1.55	0.00	4.45	4.27	0.00	0.18	0.78	2.84	0.01	0.00	0.01	0.00	0.00	14.09	8.72	0.96	0.7843
P008F01Mspr3	Core	12.69	0.01	60.28	0.04	9.28	0.00	0.08	15.43	0.01	0.00	0.01	0.00	97.84	1.56	0.00	4.44	4.28	0.00	0.15	0.80	2.82	0.01	0.00	0.00	0.00	0.00	14.08	8.73	0.95	0.7796
P008F01Mspr5	Core	13.24	0.01	61.44	0.02	8.27	0.00	0.10	16.14	0.04	0.01	0.00	0.00	99.26	1.59	0.00	4.41	4.30	0.00	0.10	0.73	2.89	0.01	0.00	0.00	0.00	0.00	14.05	8.71	0.83	0.7984
P008F01Mspr6	Core	12.63	0.03	60.31	0.04	9.06	0.00	0.13	15.24	0.01	0.02	0.00	0.00	97.48	1.56	0.00	4.44	4.31	0.00	0.13	0.80	2.80	0.01	0.00	0.00	0.00	0.00	14.07	8.75	0.93	0.7771

Representative major element compositions of sillimanite (Sil) crystals

Structural formulas calculated after Deer et al. (1992)

spot/analysis	type	SiO2	TiO2	Al2O3	FeOT	MnO	MgO	CaO	Na2O	K2O	Total	Si	Ti	Al	Fe3+	Mn	Mg	Ca	Na	K	Total cations
Sample P008																					
P008F01Msil19	Core	37.27	0.06	61.60	1.15	0.00	0.00	0.02	0.01	0.00	100.10	1.01	0.00	1.97	0.03	0.00	0.00	0.00	0.00	0.00	3.01
P008F01Msil20	Rim	36.51	0.03	60.90	1.20	0.01	0.00	0.02	0.02	0.01	98.70	1.00	0.00	1.97	0.03	0.00	0.00	0.00	0.00	0.00	3.01
P008F01Msil38	Core	36.71	0.01	61.27	1.12	0.00	0.03	0.00	0.00	0.00	99.14	1.00	0.00	1.98	0.03	0.00	0.00	0.00	0.00	0.00	3.01
P008F01Msil39	Rim	36.83	0.01	61.60	1.13	0.02	0.02	0.00	0.06	0.02	99.69	1.00	0.00	1.98	0.03	0.00	0.00	0.00	0.00	0.00	3.01
P008F01Msil40	Core	37.29	0.00	61.40	1.10	0.04	0.00	0.00	0.01	0.01	99.85	1.01	0.00	1.97	0.02	0.00	0.00	0.00	0.00	0.00	3.00
Sample P4E																					
P4EF02Msil14	Rim	37.15	0.01	61.16	0.98	0.00	0.00	0.00	0.01	0.01	99.31	1.01	0.00	1.97	0.02	0.00	0.00	0.00	0.00	0.00	3.00
P4EF02Msil15	Core	36.92	0.02	60.88	1.22	0.01	0.03	0.02	0.02	0.00	99.11	1.01	0.00	1.96	0.03	0.00	0.00	0.00	0.00	0.00	3.01
P4EF02Msil16	Rim	37.07	0.00	61.11	1.00	0.00	0.00	0.02	0.01	0.01	99.22	1.01	0.00	1.97	0.02	0.00	0.00	0.00	0.00	0.00	3.00
P4EF02Msil17	Core	37.24	0.02	61.26	1.20	0.00	0.01	0.03	0.03	0.01	99.79	1.01	0.00	1.96	0.03	0.00	0.00	0.00	0.00	0.00	3.01
P4EF02Msil18	Core	36.82	0.01	61.12	1.05	0.04	0.03	0.00	0.02	0.02	99.11	1.01	0.00	1.97	0.02	0.00	0.00	0.00	0.00	0.00	3.01

Representative major element compositions of hercynite (Hc) and magnetite (Mag) crystals

*Structural formulas and Fe3+ contents calculated using the Spinel End-Member generator software (Ferracutti et al., 2015)

spot/analysis	Mineral	type	SiO2	TiO2	Al2O3	Cr2O3	Fe2O3	FeO	MnO	MgO	CaO	ZnO	Total	Si	Ti	Al	Cr	Fe3+*	Fe2+	Mn	Mg	Ca	Zn	Sum	Sp	Hc	Ghn	Mfr	Mag	XMg
Sample P008																														
P008F01Mhc22	Hercynite	Core	0.76	0.01	60.63	0.09	0.00	24.28	0.17	11.00	0.00	0.32	97.27	0.02	0.00	1.96	0.00	0.00	0.56	0.00	0.45	0.00	0.01	3	44.4	55.0	0.6	0.0	0.0	0.447
P008F02Mhc61	Hercynite	Core	0.00	0.01	59.49	0.15	0.00	26.09	0.10	11.66	0.00	0.58	98.10	0.00	0.00	1.91	0.00	0.08	0.51	0.00	0.47	0.00	0.01	3	45.6	49.2	1.1	2.0	2.2	0.481
P008F02Mhc62	Hercynite	Rim	0.00	0.01	59.23	0.14	0.00	26.61	0.08	11.49	0.00	0.41	98.00	0.00	0.00	1.91	0.00	0.09	0.52	0.00	0.47	0.00	0.01	3	44.9	50.0	0.8	2.0	2.3	0.473
P008F02Mhc64	Hercynite	Core	0.00	0.02	59.47	0.12	0.00	27.01	0.09	11.06	0.00	0.44	98.28	0.00	0.00	1.92	0.00	0.08	0.54	0.00	0.45	0.00	0.01	3	43.4	51.8	0.9	1.8	2.2	0.456
Sample P4E(L)																														
Hc1																														
P4EF02Chc74	Hercynite	Inclusion	0.00	0.00	58.95	0.00	0.00	27.84	0.13	11.28	0.00	0.00	98.20	0.00	0.00	1.90	0.00	0.10	0.54	0.00	0.46	0.00	0.00	3	43.8	51.2	0.0	2.3	2.7	0.461
P4EF02Chc75	Hercynite	Inclusion	0.06	0.07	58.10	0.00	0.00	28.11	0.16	11.19	0.01	0.00	97.69	0.00	0.00	1.89	0.00	0.11	0.54	0.00	0.46	0.00	0.00	3	43.5	51.1	0.0	2.5	2.9	0.460
P4EF02Chc86	Spinel	Inclusion	0.00	0.00	59.02	0.00	0.00	25.24	0.07	12.80	0.02	0.00	97.15	0.00	0.00	1.90	0.00	0.10	0.48	0.00	0.52	0.00	0.00	3	49.6	45.4	0.0	2.6	2.4	0.522
P4EF02Chc87	Spinel	Inclusion	0.00	0.03	59.01	0.00	0.00	25.40	0.07	12.71	0.01	0.00	97.25	0.00	0.00	1.90	0.00	0.10	0.48	0.00	0.52	0.00	0.00	3	49.3	45.8	0.0	2.6	2.4	0.518
Hc2																														
P4EF01Mhc01	Hercynite	Core	0.01	0.05	59.10	0.00	0.00	29.26	0.02	9.75	0.00	0.00	98.19	0.00	0.00	1.92	0.00	0.08	0.60	0.00	0.40	0.00	0.00	3	38.6	57.7	0.0	1.5	2.3	0.401
P4EF01Mhc02	Hercynite	Rim	0.05	0.01	57.26	0.00	0.00	30.56	0.11	9.84	0.01	0.00	97.83	0.00	0.00	1.88	0.00	0.12	0.59	0.00	0.41	0.00	0.00	3	38.4	55.6	0.0	2.5	3.6	0.409
P4EF01Mhc03	Hercynite	Core	0.02	0.02	59.24	0.00	0.00	28.40	0.05	10.26	0.03	0.00	98.02	0.00	0.00	1.92	0.00	0.08	0.58	0.00	0.42	0.00	0.00	3	40.5	55.7	0.0	1.6	2.2	0.421
P4EF03Mhc32	Hercynite	Rim	0.00	0.01	57.38	0.22	0.00	30.30	0.23	8.66	0.02	0.30	97.12	0.00	0.00	1.91	0.00	0.09	0.62	0.01	0.36	0.00	0.01	3	35.0	60.0	0.6	1.6	2.8	0.368
P4EF03Mhc34	Hercynite	Core	0.00	0.02	58.37	0.26	0.00	29.36	0.18	8.81	0.01	0.24	97.24	0.00	0.00	1.93	0.01	0.07	0.62	0.00	0.37	0.00	0.00	3	35.8	60.5	0.5	1.2	2.0	0.371
Sample P4E(R)																														
Hc2																														
P4E'F01Mhc39	Hercynite	Rim	0.00	0.00	59.73	0.00	0.00	28.58	0.11	9.84	0.00	0.00	98.26	0.00	0.00	1.94	0.00	0.06	0.59	0.00	0.40	0.00	0.00	3	39.2	57.7	0.0	1.3	1.9	0.404
P4E'F01Mhc40	Hercynite	Core	0.04	0.03	59.65	0.00	0.00	27.99	0.08	9.91	0.00	0.00	97.69	0.00	0.00	1.94	0.00	0.05	0.59	0.00	0.41	0.00	0.00	3	39.7	57.6	0.0	1.1	1.6	0.408
P4E'F02Mhc66	Hercynite	Rim	0.00	0.00	59.10	0.00	0.00	28.29	0.05	10.14	0.00	0.00	97.60	0.00	0.00	1.93	0.00	0.07	0.58	0.00	0.42	0.00	0.00	3	40.3	56.0	0.0	1.5	2.1	0.418
P4E'F03Chc107	Hercynite	Inclusion	0.03	0.08	59.42	0.00	0.00	27.87	0.08	10.43	0.02	0.00	97.94	0.00	0.00	1.93	0.00	0.07	0.57	0.00	0.43	0.00	0.00	3	41.3	55.3	0.0	1.5	2.0	0.427
P4E'F03Chc108	Hercynite	Inclusion	0.02	0.00	59.76	0.00	0.00	27.58	0.06	10.56	0.00	0.00	97.97	0.00	0.00	1.93	0.00	0.07	0.57	0.00	0.43	0.00	0.00	3	41.8	54.9	0.0	1.4	1.9	0.432
P4E'F03Chc110	Hercynite	Rim	0.03	0.01	60.54	0.00	0.00	26.32	0.01	11.37	0.01	0.00	98.28	0.00	0.00	1.94	0.00	0.06	0.54	0.00	0.46	0.00	0.00	3	44.7	52.4	0.0	1.4	1.6	0.460

Mag																													
P4E'F03Cmt109	Magnetite	Mt-lamellae	0.08	0.05	26.98	0.00	0.00	64.16	0.02	5.48	0.07	0.00	96.84	0.00	0.00	1.02	0.00	0.98	0.74	0.00	0.26	0.00	0.00	3	13.3	37.7	0.0	12.8	36.2	0.261
P4E'F03Cmt112	Magnetite	Mt-lamellae	0.06	0.00	27.91	0.00	0.00	61.69	0.06	5.81	0.00	0.00	95.52	0.00	0.00	1.06	0.00	0.94	0.72	0.00	0.28	0.00	0.00	3	14.8	38.3	0.0	13.1	33.9	0.278

(L) = leucosome; (R) = residue

9.3 APPENDIX C – Supplementary file 3 (Chapter 4): Al-in-orthopyroxene thermobarometry for analyzed samples

Layered orthopyroxene-garnet diatexite (P013)

Assemblage	X_{Ca} Grt	M/FM Grt	M/FM Opx	X_{Al} Opx	T (°C)	P (kbar)
Grt cores/high-Al Opx cores (mean compositions)						
P013_Grt96_Opx63_Pl49	0.077	0.366	0.542	0.053	990	10
P013_Grt87_Opx63_Pl49	0.073	0.366	0.543	0.053	977	9.7
P013_Grt86_Opx70_Pl49	0.065	0.37	0.545	0.055	969	9.2
P013_Grt95_Opx63_Pl49	0.085	0.369	0.54	0.055	1021	10.8
P013_Grt86_Opx63_Pl49	0.065	0.368	0.547	0.053	956	9.1
P013_Grt97_Opx63_Pl49	0.062	0.364	0.544	0.053	948	8.8
P013_Grt87_Opx17_Pl49	0.073	0.363	0.539	0.054	984	9.8
Average					***977.9***	***9.6***
standard deviation					***24.1***	***0.7***
Grt cores/high-Al Opx cores (higher XGrs and XAl compositions)						
P013_Grt141_Opx62_Pl117	0.09	0.392	0.558	0.058	1054	11.9
P013_Grt125_Opx62_Pl117	0.088	0.391	0.558	0.058	1048	11.7
P013_Grt125_Opx62_Pl28	0.088	0.391	0.559	0.058	1044	11.5
P013_Grt141_Opx69_Pl117	0.09	0.392	0.56	0.057	1046	11.7
P013_Grt125_Opx69_Pl117	0.088	0.391	0.56	0.057	1040	11.6
Average					***1043.0***	***11.7***
standard deviation					***4.2***	***0.1***
Xenomorphic Grt and Opx (higher XGrs and XAl)						
P013_Grt11_Opx12_Pl28	0.077	0.326	0.492	0.056	1028	10.1
P013_Grt11_Opx15_Pl28	0.077	0.325	0.493	0.055	1018	10
P013_Grt07_Opx12_Pl28	0.092	0.33	0.493	0.056	1066	11.3
P013_Grt07_Opx15_Pl28	0.092	0.327	0.493	0.055	1055	11.2
Average					***1041.8***	***10.7***
standard deviation					***22.5***	***0.7***
Xenomorphic Grt and Opx (lower XGrs and XAl)						
P013_Grt08_Opx11_Pl28	0.071	0.337	0.515	0.051	969	9.3
P013_Grt08_Opx14_Pl28	0.071	0.334	0.52	0.047	940	9
P013_Grt09_Opx14_Pl28	0.072	0.338	0.525	0.047	940	9.1
P013_Grt09_Opx11_Pl28	0.072	0.341	0.52	0.051	970	9.4
Average					***954.8***	***9.2***
standard deviation					***17.0***	***0.2***

Grt rims/low-Al Opx cores and Opx rims (retrograde stage)						
P013_Grt84_Opx68_Pl78	0.056	0.346	0.531	0.049	912	7.9
P013_Grt89_Opx69_Pl80	0.056	0.336	0.505	0.057	975	8.4
P013_Grt101_Opx19_Pl29	0.055	0.368	0.551	0.052	923	8.2
P013_Grt35_Opx61_Pl58	0.048	0.352	0.526	0.056	934	7.5
Average					***936.0***	***8.0***
standard deviation					***27.5***	***0.4***

Schlieren orthopyroxene-garnet diatexite (P1)

Assemblage	X_{Ca} Grt	M/FM Grt	M/FM Opx	X_{Al} Opx	T (°C)	P (kbar)
Grt cores/high-Al Opx cores (peak stage)						
P1-F05-Grt134-Pl142_FB-Opx75	0.077	0.361	0.545	0.05	953	9.2
P1-FA-Pl92_F5-Grt132_FB-Opx75	0.071	0.361	0.548	0.05	932	8.6
P1-F6-Grt106_FB-Opx75_FA-Pl92	0.087	0.357	0.54	0.05	971	9.68
P1-F6-Grt106_FB-Opx75_FA-Pl90	0.087	0.358	0.539	0.05	983	10.2
P1-F5-Grt134_FB-Opx75_FA-Pl90	0.077	0.362	0.544	0.05	959	9.51
P1-F6-Grt106-Pl122_FB-Opx75	0.087	0.358	0.54	0.05	977	9.97
Average					***962.5***	***9.5***
standard deviation					***18.6***	***0.6***
Grt rims/low-Al Opx cores and Opx rims (retrograde stage)						
P1MF05-Grt131-Opx146-Pl151	0.068	0.342	0.564	0.035	807	7.17
P1MF05-Grt136-Opx146-Pl151	0.07	0.346	0.568	0.035	810	7.36
P1MF05-Grt136-Opx146-Pl149	0.07	0.346	0.568	0.035	812	7.45
P1MF05-Grt131-Opx146-Pl149	0.068	0.342	0.565	0.035	808	7.28
P1MF07-Grt73-Opx100-Pl93	0.074	0.338	0.562	0.034	816	7.66
P1MF07-Grt73-Opx100-Pl95	0.074	0.339	0.562	0.034	818	7.73
P1MF07-Grt73-Opx105-Pl95	0.074	0.326	0.562	0.03	782	7.33
P1MF07-Grt74-Opx100-Pl95	0.083	0.335	0.555	0.034	839	8.23
P1MF07-Grt74-Opx105-Pl95	0.083	0.322	0.555	0.03	802	7.8
P1MF05-Grt131-Opx146-Pl150	0.068	0.342	0.565	0.035	808	7.22
P1MF05-Grt131-Opx146-Pl150-Bt153	0.068	0.361	0.588	0.035	795	7.38
P1MF05-Grt131-Opx146-Pl149_FB-Bt85	0.07	0.365	0.59	0.035	801	7.61
Average					***808.2***	***7.5***
standard deviation					***13.7***	***0.3***

M/FM = Mg/(Fe+Mg); XAl Opx = Al cations (for a 6-oxygen formula)/4; T rclc and P rclc: temperature and pressure estimates using RCLC of Pattison et al. (2003)

9.4 APPENDIX D – Supplementary file 4 (Chapter 4): Bulk-rock compositions of analyzed samples

														Theriak-Domino input										
Sample	**SiO_2**	**TiO_2**	**Al_2O_3**	**Cr_2O_3**	**Fe_2O_3T[a]**	**MnO**	**MgO**	**CaO**	**Na_2O**	**K_2O**	**P_2O_5**	**LOI[b]**	**Total**	**Si**	**Ti**	**Al**	**Fe^{2+}**	**Mg**	**Mn**	**Ca**	**Na**	**K**	**O**	**H[d]**	**O[c]**
P1(L)	64.51	0.79	16.50	0.02	8.59	0.19	2.06	2.20	1.52	6.28	0.06	0.50	100.22	-	-	-	-	-	-	-	-	-	-	-	-
P1(R)	58.54	1.36	17.92	0.03	11.24	0.21	4.17	4.92	2.25	2.14	0.16	0.27	100.21	-	-	-	-	-	-	-	-	-	-	-	-
P1D	68.00	0.81	14.54	0.02	7.15	0.14	2.15	2.46	2.21	3.18	0.05	0.17	100.88	-	-	-	-	-	-	-	-	-	-	-	-
P013	**62.82**	**1.15**	**16.81**	**0.02**	**10.67**	**0.22**	**3.39**	**4.06**	**2.27**	**1.69**	**0.19**	**-0.52**	**100.83**	**1.026**	**0.014**	**0.324**	**0.131**	**0.083**	**0.003**	**0.071**	**0.072**	**0.035**	**2.980**	**0.006**	**0.002**
P10A	57.06	1.38	17.80	0.02	9.25	0.17	3.84	4.47	2.72	3.71	0.19	0.04	100.63	-	-	-	-	-	-	-	-	-	-	-	-
P4E	**66.53**	**1.18**	**16.11**	**0.00**	**8.93**	**0.17**	**2.95**	**0.53**	**0.72**	**2.86**	**0.06**	**0.25**	**100.28**	**1.107**	**0.015**	**0.316**	**0.112**	**0.073**	**0.002**	**0.009**	**0.023**	**0.061**	**2.962**	**0.017**	**0.010**
P008B	**69.00**	**1.43**	**13.54**	**0.03**	**9.79**	**0.18**	**2.38**	**0.63**	**0.64**	**1.43**	**0.04**	**-0.15**	**98.94**	**1.148**	**0.018**	**0.266**	**0.123**	**0.059**	**0.003**	**0.011**	**0.021**	**0.030**	**2.951**	**0.003**	**0.017**
P008B replicate	69.54	1.46	13.78	0.03	10.00	0.19	2.43	0.65	0.67	1.46	0.04	-	100.25	-	-	-	-	-	-	-	-	-	-	-	-
BRANCO_PREP standard	>90	<0,01	0.05	<0,01	1.72	0.02	<0,01	0.02	<0,01	<0,01	<0,01	-0.45	-	-	-	-	-	-	-	-	-	-	-	-	-
TILL-3 standard	69.86	0.53	12.70	0.02	4.26	0.07	1.74	2.71	2.93	2.58	0.11	-	97.51	-	-	-	-	-	-	-	-	-	-	-	-

[a] Fe_2O_3T - total iron analysed as Fe_2O_3 by XRF and ICP/OES

[b] LOI - loss on ignition

[c] Fe^{3+} contents calculated as additional "O" entry with T-X phase-equilibria diagrams at Theriak-Domino

[d] H contents calculated with T-X phase-equilibria diagrams at Theriak-Domino

(L) - leucosome
(R) - residue

9.5 APPENDIX E – Supplementary file 5 (Chapter 4): U-Pb LA-ICP-MS analyses

U-Pb LA-ICP-MS analysis and ages of sample P4E

grain/spot position	spot site	U	Th	Th/U	Isotopic ratios							Ages (in Ma)[a]						Discordance[b]
		ppm	ppm		$^{206}Pb/^{238}U$	2σ	$^{207}Pb/^{235}U$	2σ	$^{207}Pb/^{206}Pb$	2σ	Rho	$^{206}Pb/^{238}U$	2σ	$^{207}Pb/^{206}Pb$	2σ	$^{207}Pb/^{235}U$	2σ	(%)
Schlieren/schollen hercynite-sillimanite-garnet diatexite (P4E)																		
P4E007	Core	74.83071	27.22741	0.363853	0.099946	2.621673	0.83491	4.46957	0.06058601	3.61993	0.58656	614.09	15.33	624.57	78.05	616.33	20.83	0.36
P4E008	Rim	41.09479	56.71553	1.380115	0.09815	3.645373	0.801028	6.765651	0.05919076	5.699587	0.538806	603.56	20.98	574.12	123.94	597.41	30.97	-1.03
P4E009	Core	112.1822	65.91346	0.587557	0.096014	1.65082	0.792449	2.278409	0.05986	1.570331	0.72455	591.01	9.30	598.52	34.01	592.56	10.26	0.26
P4E010	Core	47.35781	88.89352	1.877061	0.097839	1.738146	0.807924	2.528619	0.0598901	1.836508	0.68739	601.74	9.96	599.61	39.76	601.29	11.52	-0.07
P4E011	Rim	44.44688	24.49544	0.551117	0.096937	1.717893	0.802472	2.499408	0.06004	1.815456	0.68732	596.43	9.77	605.02	39.27	598.22	11.34	0.30
P4E013	Core	194.5798	16.51447	0.084872	0.099756	1.641859	0.828268	2.030321	0.06021883	1.194363	0.80867	612.98	9.58	611.45	25.81	612.65	9.37	-0.05
P4E014	Rim	55.68656	37.44545	0.672432	0.098291	1.653399	0.81165	2.268273	0.05989	1.552847	0.728924	604.39	9.52	599.60	33.62	603.38	10.35	-0.17
P4E015	Core	342.349	69.09344	0.201822	0.108232	2.457097	0.923127	4.194611	0.06185905	3.399622	0.585775	662.47	15.44	669.24	72.76	664.01	20.62	0.23
P4E016	Core	99.74015	20.90217	0.209566	0.09796	1.658986	0.809862	2.171371	0.05996	1.400934	0.764027	602.44	9.52	602.13	30.32	602.38	9.90	-0.01
P4E017	Core	83.22209	52.56051	0.631569	0.097579	1.644906	0.810074	2.14616	0.06021	1.378509	0.766442	600.20	9.41	611.13	29.79	602.50	9.78	0.38
P4E018	Rim	44.14352	37.30141	0.845003	0.097177	1.672344	0.801785	2.364189	0.05984	1.671123	0.707365	597.85	9.53	597.79	36.19	597.84	10.72	0.00
P4E019	Core	24.46266	50.15761	2.050375	0.097067	1.839603	0.800607	3.042962	0.05982	2.423938	0.604544	597.20	10.47	597.07	52.51	597.17	13.81	0.00
P4E020	Rim	70.45223	42.73692	0.606609	0.095131	1.645049	0.784376	2.196081	0.0598	1.454849	0.749084	585.81	9.19	596.35	31.52	587.98	9.83	0.37
P4E027	Rim	74.83744	32.77077	0.437893	0.097127	1.652551	0.806193	2.152172	0.0602	1.378738	0.767853	597.55	9.41	610.77	29.80	600.32	9.78	0.46
P4E028	Core	46.64283	41.65846	0.893138	0.096224	1.709758	0.794586	2.484992	0.05989	1.803306	0.688034	592.24	9.65	599.60	39.05	593.77	11.21	0.26
P4E029	Core	61.34494	35.70699	0.582069	0.096355	1.728267	0.794068	2.440609	0.05977	1.723273	0.708129	593.01	9.77	595.26	37.34	593.48	11.01	0.08
P4E030	Rim	64.22211	38.21995	0.595121	0.097007	1.675284	0.802652	2.293514	0.06001	1.566406	0.730445	596.84	9.53	603.94	33.89	598.32	10.40	0.25
P4E031	Rim	81.11415	12.10534	0.149238	0.096826	1.636966	0.803027	2.130289	0.06015	1.363259	0.768424	595.78	9.30	608.97	29.47	598.53	9.66	0.46
P4E032	Rim	95.28109	29.88552	0.313656	0.096656	1.639855	0.798148	2.11505	0.05989	1.335782	0.775327	594.78	9.30	599.60	28.92	595.78	9.56	0.17
P4E033	Core	201.2425	7.811446	0.038816	0.097769	1.695836	0.809613	2.173154	0.06005838	1.358948	0.780357	601.32	9.72	605.68	29.39	602.24	9.90	0.15
P4E034	Core	80.69495	37.14629	0.46033	0.096335	1.666146	0.797224	2.219396	0.06002	1.466178	0.75072	592.89	9.42	604.30	31.72	595.26	10.03	0.40
P4E035	Rim	57.75181	36.0272	0.623828	0.095863	1.674341	0.793454	2.269841	0.06003	1.532567	0.737647	590.12	9.42	604.66	33.16	593.13	10.23	0.51
P4E036	Core	67.06058	37.69401	0.562089	0.098321	1.673299	0.814746	2.201713	0.0601	1.430948	0.759998	604.56	9.64	607.18	30.94	605.11	10.07	0.09
P4E037	Core	53.71473	36.67539	0.682781	0.095322	1.831193	0.787393	2.738639	0.05991	2.036388	0.668651	586.93	10.25	600.33	44.09	589.69	12.30	0.47
P4E038	Core	49.79931	27.48447	0.551905	0.096766	1.948994	0.794923	3.065814	0.05958	2.366566	0.635718	595.43	11.06	588.36	51.34	593.96	13.86	-0.25
P4E039	Core	46.80831	36.15388	0.772382	0.096826	2.111522	0.797806	3.552718	0.05975888	2.857146	0.59434	595.78	11.99	594.86	61.91	595.59	16.11	-0.03
P4E047	Rim	37.0696	38.90248	1.049444	0.095933	1.714943	0.793109	2.427325	0.05996	1.717812	0.706516	590.53	9.66	602.13	37.18	592.93	10.94	0.40

P4E048	Core	42.36208	38.05079	0.898228	0.099144	1.720125	0.824843	2.518506	0.06034	1.839576	0.682994	609.39	9.98	615.79	39.72	610.75	11.60	0.22
P4E049	Core	540.7286	42.35133	0.078323	0.099806	1.588099	0.801453	1.94105	0.05824	1.116071	0.818165	613.27	9.27	538.80	24.41	597.65	8.79	-2.61
P4E051	Rim	75.8089	18.94322	0.249881	0.096907	1.697723	0.802624	2.286459	0.06007	1.531547	0.742512	596.25	9.65	606.10	33.13	598.31	10.37	0.34
P4E052	Core	124.7441	18.11849	0.145245	0.097679	1.643217	0.776968	2.084593	0.05769	1.282718	0.788268	600.79	9.41	518.01	28.16	583.75	9.28	-2.92
P4E053	Rim	50.67532	34.57091	0.682204	0.097298	1.732137	0.805998	2.437089	0.06008	1.714381	0.71074	598.55	9.88	606.46	37.08	600.21	11.08	0.28
P4E054	Core	54.47555	34.75484	0.63799	0.099264	1.697827	0.826803	2.269753	0.06041	1.506373	0.748023	610.09	9.86	618.29	32.51	611.84	10.47	0.28
P4E055	Core	91.77927	39.35418	0.428792	0.098983	1.702645	0.826101	2.238885	0.06053	1.453825	0.760488	608.45	9.86	622.57	31.36	611.45	10.32	0.49
P4E056	Core	38.69962	26.80231	0.692573	0.096325	1.749635	0.793555	2.503632	0.05975	1.790795	0.698839	592.83	9.89	594.53	38.81	593.19	11.29	0.06
P4E057	Core	58.08815	22.19559	0.382102	0.099124	1.720474	0.823446	2.402119	0.06025	1.676349	0.716232	609.27	9.98	612.56	36.22	609.97	11.06	0.11
P4E058	Core	195.1371	39.06092	0.200172	0.096626	1.66113	0.797899	2.060357	0.05989	1.218901	0.806234	594.60	9.41	599.60	26.39	595.64	9.31	0.17
P4E059	Core	50.46395	19.78161	0.391995	0.096174	1.773235	0.791254	2.55788	0.05967	1.843472	0.693244	591.95	10.01	591.63	39.97	591.88	11.52	-0.01
P4E060	Rim	63.83727	32.94768	0.51612	0.096415	1.852375	0.79322	2.662384	0.05966891	1.912328	0.695758	593.37	10.48	591.59	41.46	593.00	12.01	-0.06
P4E067	Core	89.91374	45.14757	0.502121	0.098833	1.664637	0.824027	2.147061	0.06047	1.356044	0.775309	607.56	9.63	620.43	29.26	610.29	9.88	0.45
P4E068	Core	44.86277	23.86203	0.531889	0.100408	1.738435	0.836051	2.482235	0.06039	1.771817	0.700351	616.80	10.20	617.58	38.25	616.96	11.52	0.03
P4E069	Rim	45.0885	41.23336	0.914498	0.099144	1.740362	0.824296	2.415439	0.0603	1.674959	0.720516	609.39	10.10	614.36	36.18	610.44	11.12	0.17
P4E070	Core	32.71003	27.46268	0.83958	0.09794	1.787522	0.809693	2.667997	0.05995978	1.980649	0.669987	602.32	10.26	602.12	42.87	602.28	12.17	-0.01
P4E071	Core	23.4345	17.97667	0.767103	0.09811	1.860941	0.81043	3.053021	0.05991	2.420297	0.609541	603.33	10.70	600.33	52.40	602.70	13.95	-0.10
P4E072	Rim	27.27936	17.19885	0.630471	0.099856	1.788226	0.831044	2.723613	0.06036	2.054341	0.656564	613.56	10.44	616.50	44.36	614.19	12.61	0.10
P4E073	Rim	48.52022	24.64502	0.507933	0.097609	1.747174	0.808978	2.412517	0.06011	1.663617	0.724212	600.38	9.99	607.54	35.97	601.88	10.99	0.25
P4E074	Core	59.31075	26.70924	0.450327	0.09812	2.670455	0.81344	4.548869	0.06012636	3.68251	0.587059	603.38	15.36	608.12	79.62	604.38	20.90	0.17
P4E075	Core	158.468	16.65999	0.105132	0.102133	1.669777	0.853376	2.078429	0.0606	1.237624	0.803384	626.90	9.95	625.07	26.68	626.50	9.75	-0.06
P4E076	Core	375.418	73.75741	0.196467	0.103467	1.774272	0.827952	2.393541	0.05803647	1.606549	0.741275	634.70	10.70	531.14	35.19	612.48	11.05	-3.63
P4E077	Core	34.12288	16.78261	0.491829	0.101712	1.854226	0.853081	2.854291	0.06083	2.169982	0.649628	624.43	11.01	633.23	46.72	626.34	13.41	0.30
P4E078	Rim	34.79728	25.02691	0.71922	0.098742	7.169419	0.795012	13.89304	0.05839412	11.90025	0.516044	607.03	41.55	544.58	260.07	594.01	64.37	-2.19
P4E079	Core	72.88431	19.15596	0.262827	0.095532	1.903202	0.7854	2.731554	0.05962656	1.95939	0.696747	588.17	10.68	590.05	42.49	588.56	12.25	0.07
P4E080	Rim	29.576	30.93998	1.046118	0.100077	1.864475	0.833571	2.948678	0.06041	2.28439	0.632309	614.86	10.91	618.29	49.31	615.59	13.68	0.12
P4E087	Core	43.32101	37.35329	0.862244	0.094382	1.740977	0.77729	2.510051	0.05973	1.808137	0.693602	581.40	9.67	593.81	39.19	583.94	11.20	0.43
P4E088	Rim	46.06895	40.26346	0.873982	0.095905	1.692436	0.791419	2.390015	0.05985	1.687552	0.708128	590.37	9.54	598.16	36.55	591.98	10.77	0.27
P4E089	Core	88.91444	23.5595	0.264968	0.100865	1.648952	0.841525	2.134354	0.06051	1.355148	0.772576	619.47	9.73	621.86	29.23	619.99	9.94	0.08
P4E090	Rim	40.97037	31.4401	0.767386	0.099241	1.918223	0.830035	3.142629	0.06066	2.489285	0.610388	609.96	11.15	627.20	53.65	613.63	14.56	0.60
P4E091	Core	48.16417	30.72685	0.637961	0.097228	1.772465	0.803137	2.712336	0.05991	2.05308	0.653483	598.14	10.11	600.33	44.45	598.60	12.33	0.08
P4E092	Core	178.0524	60.92819	0.342193	0.103109	2.538113	0.86293	4.307423	0.06069858	3.480212	0.589242	632.60	15.28	628.57	74.99	631.72	20.44	-0.14
P4E093	Rim	44.24122	36.56584	0.826511	0.098891	2.65376	0.812178	4.608925	0.05956544	3.768255	0.575787	607.90	15.39	587.83	81.75	603.68	21.17	-0.70
P4E094	Core	331.0626	571.4992	1.726258	0.202731	1.685062	2.225896	2.059682	0.07963124	1.184421	0.818118	1189.97	18.31	1187.87	23.39	1189.23	14.53	-0.06
P4E095	Core	125.8606	21.41043	0.170112	0.09827	1.651713	0.815403	2.184108	0.06018	1.429046	0.756241	604.26	9.52	610.05	30.89	605.48	10.00	0.20

P4E096	Rim	32.00498	35.95437	1.123399	0.0983	1.977372	0.818363	3.632691	0.06038	3.047367	0.544327	604.44	11.40	617.22	65.79	607.13	16.72	0.44
P4E097	Rim	166.676	174.7361	1.048358	0.117226	1.6987	1.020177	2.193811	0.06311753	1.388246	0.774315	714.58	11.48	712.19	29.50	714.00	11.30	-0.08
P4E098	Core	182.2479	87.57546	0.480529	0.096165	1.646176	0.791712	2.020955	0.05971	1.172333	0.814553	591.90	9.30	593.08	25.41	592.14	9.10	0.04
P4E099	Core	244.7552	53.30994	0.217809	0.101035	1.626339	0.842806	1.967587	0.0605	1.107438	0.826565	620.47	9.61	621.50	23.89	620.69	9.17	0.04
P4E100	Rim	173.4849	20.63149	0.118924	0.09869	1.725888	0.821072	2.546719	0.06034	1.872721	0.677691	606.73	9.98	615.79	40.44	608.65	11.71	0.31
P4E107	Core	48.28552	19.2646	0.398973	0.099201	1.696798	0.829153	2.309773	0.06062	1.56714	0.734617	609.73	9.86	625.78	33.78	613.14	10.68	0.56
P4E108	Core	75.04844	24.29991	0.32379	0.097207	1.710987	0.803374	2.378115	0.05994	1.651652	0.719472	598.02	9.76	601.41	35.75	598.73	10.80	0.12
P4E109	Rim	27.2644	48.58117	1.781854	0.095574	1.928923	0.790799	3.468658	0.06001	2.882853	0.556101	588.42	10.84	603.94	62.38	591.63	15.66	0.54
P4E110	Core	28.71383	29.98035	1.044108	0.096727	2.00953	0.796865	3.663157	0.05975	3.062762	0.548579	595.20	11.42	594.53	66.37	595.06	16.61	-0.02
P4E112	Core	67.4749	34.04048	0.504491	0.099362	1.714228	0.825013	2.296202	0.06022	1.527732	0.746549	610.67	9.98	611.49	33.01	610.84	10.58	0.03
P4E113	Core	54.49204	31.82288	0.583991	0.098049	1.675863	0.815331	2.168527	0.06031	1.376223	0.772812	602.97	9.64	614.71	29.72	605.44	9.93	0.41
P4E115	Core	127.0653	39.55588	0.311304	0.096216	1.666146	0.799023	2.205111	0.06023	1.444463	0.755584	592.19	9.42	611.85	31.21	596.28	9.98	0.69
P4E116	Core	324.22	70.27544	0.216752	0.105483	1.690729	0.890823	2.059221	0.06125	1.17551	0.821053	646.46	10.39	648.02	25.25	646.81	9.89	0.05
P4E117	Rim	41.35604	27.67963	0.669301	0.096466	1.724138	0.799241	2.575901	0.06009	1.913796	0.669334	593.67	9.77	606.82	41.39	596.40	11.67	0.46
P4E118	Rim	33.54641	25.45392	0.758767	0.095534	1.950708	0.794814	3.413168	0.06034	2.800795	0.571524	588.18	10.96	615.79	60.48	593.90	15.45	0.96
P4E119	Rim	42.35357	24.40655	0.576257	0.095604	1.802557	0.798298	2.740363	0.06056	2.064069	0.65778	588.60	10.13	623.64	44.51	595.87	12.41	1.22
P4E120	Core	35.62911	19.90445	0.558657	0.094993	1.856344	0.780752	3.006828	0.05961	2.365375	0.617376	585.00	10.37	589.45	51.30	585.91	13.46	0.16
P4E127	Core	37.70477	31.5512	0.836796	0.099722	2.66348	0.83769	4.603275	0.06092421	3.754466	0.578606	612.78	15.56	636.56	80.79	617.87	21.51	0.82
P4E128	Core	106.5761	37.54995	0.35233	0.099712	5.346539	0.811259	10.19852	0.05900778	8.684714	0.524247	612.72	31.27	567.38	189.07	603.16	47.42	-1.59
P4E129	Rim	29.1995	43.90958	1.503778	0.096707	1.761293	0.7979	2.656469	0.05984	1.988636	0.66302	595.08	10.00	597.79	43.07	595.64	12.03	0.09
P4E130	Rim	46.91041	41.85417	0.892215	0.097799	1.782604	0.811361	2.529703	0.06017	1.794914	0.704669	601.50	10.23	609.69	38.80	603.22	11.56	0.29
P4E132	Core	52.03378	27.65125	0.53141	0.09844	1.709924	0.813152	2.366355	0.05991	1.635787	0.722598	605.26	9.87	600.33	35.41	604.22	10.82	-0.17
P4E133	Rim	53.90939	32.32933	0.599698	0.099402	1.713537	0.824934	2.36372	0.06019	1.628177	0.724932	610.90	9.98	610.41	35.19	610.80	10.90	-0.02
P4E134	Core	129.1083	89.3677	0.692192	0.096005	1.69067	0.798203	2.368242	0.0603	1.658375	0.713892	590.95	9.54	614.36	35.82	595.81	10.72	0.82
P4E135	Rim	138.8622	70.7604	0.509573	0.097288	1.647786	0.809402	2.146463	0.06034	1.375539	0.767675	598.49	9.41	615.79	29.70	602.12	9.79	0.60
P4E137	Rim	56.40118	28.75336	0.509801	0.099101	1.698514	0.823396	2.340097	0.06026	1.609691	0.72583	609.14	9.86	612.92	34.78	609.94	10.78	0.13
P4E138	Core	62.53974	20.26209	0.323987	0.10349	1.684577	0.867849	2.331122	0.06082	1.611312	0.722647	634.83	10.17	632.87	34.70	634.40	11.05	-0.07
P4E139	Core	43.64735	24.66566	0.565112	0.09864	3.055505	0.810663	5.422865	0.05960531	4.480106	0.563449	606.44	17.68	589.28	97.17	602.83	24.93	-0.60
P4E140	Core	30.03981	25.55246	0.85062	0.099372	2.818039	0.82559	5.111811	0.06025604	4.264888	0.55128	610.73	16.41	612.78	92.14	611.16	23.72	0.07
P4E147	Rim	27.28738	22.89045	0.838866	0.09828	2.018554	0.836761	3.233703	0.06175	2.526316	0.624224	604.32	11.63	665.46	54.10	617.36	15.05	2.11
P4E148	Core	337.1727	201.2058	0.596744	0.098209	1.639023	0.81323	2.054827	0.06005638	1.239321	0.797645	603.91	9.44	605.61	26.81	604.26	9.39	0.06
P4E149	Core	183.3886	147.9757	0.806897	0.113419	1.64311	0.977699	1.997368	0.06252	1.135637	0.822637	692.57	10.78	691.94	24.22	692.42	10.07	-0.02
P4E150	Core	50.2777	26.72552	0.531558	0.096366	2.368334	0.789332	3.884393	0.0594067	3.07888	0.609705	593.08	13.41	582.03	66.86	590.79	17.53	-0.39
P4E151	Rim	68.06387	24.93085	0.366286	0.097388	2.660932	0.810676	4.497559	0.06037285	3.625945	0.591639	599.08	15.21	616.96	78.28	602.83	20.63	0.62
P4E152	Core	101.261	19.35948	0.191184	0.096186	1.666667	0.796121	2.154922	0.06003	1.365984	0.773423	592.02	9.42	604.66	29.55	594.64	9.73	0.44

P4E153	Core	34.53609	36.80142	1.065593	0.094913	5.579241	0.763918	10.7562	0.058374	9.196079	0.5187	584.53	31.20	543.83	201.00	576.27	48.38	-1.43
P4E154	Core	36.08411	28.11391	0.779121	0.098039	1.819111	0.810517	2.704534	0.05996	2.001334	0.672615	602.91	10.46	602.13	43.32	602.74	12.36	-0.03
P4E155	Core	37.7825	23.39446	0.619188	0.09844	1.852417	0.814645	2.837405	0.06002	2.149284	0.652856	605.26	10.69	604.30	46.50	605.06	13.00	-0.03
P4E156	Core	40.09581	23.85509	0.594952	0.095654	1.780664	0.790935	2.678576	0.05997	2.001001	0.66478	588.89	10.01	602.49	43.31	591.70	12.07	0.47
P4E157	Rim	45.00641	18.82667	0.418311	0.103159	1.756515	0.864261	2.497171	0.06076267	1.774969	0.703402	632.89	10.58	630.84	38.23	632.45	11.81	-0.07
P4E158	Core	266.2933	22.33371	0.083869	0.099542	1.630599	0.828432	2.020328	0.06036	1.192843	0.807096	611.72	9.51	616.50	25.75	612.74	9.33	0.17
P4E159	Rim	31.14721	34.0721	1.093906	0.094322	1.912046	0.776665	3.038145	0.05972	2.361018	0.629346	581.05	10.61	593.44	51.17	583.58	13.56	0.43
P4E160	Core	120.4884	57.29829	0.47555	0.095073	1.749394	0.791897	2.374581	0.06041	1.605694	0.736717	585.47	9.78	618.29	34.66	592.25	10.70	1.14

U-Pb LA-ICP-MS analysis and ages of reference materials

spot/grain position		U	Th	Th/U	Isotopic ratios								Ages (in Ma)[a]						Discordance[b]
		ppm	ppm		$^{206}Pb/^{238}U$	2σ	$^{207}Pb/^{235}U$	2σ	$^{207}Pb/^{206}Pb$	2σ	Rho		$^{206}Pb/^{238}U$	2σ	$^{207}Pb/^{206}Pb$	2σ	$^{207}Pb/^{235}U$	2σ	(%)
PRIMARY REFERENCE MATERIAL (BB, Santos et al. 2017)																			
1.sSMPABC002		571.1753	262.3859	0.459379	0.09183	1.589894	0.745637	1.906875	0.05889	1.05281	0.833769		566.3509	8.625943	563.03185	22.93652	565.689694	8.30425	-0.12
1.sSMPABC021		498.7065	225.1019	0.451371	0.09154	1.845324	0.745278	2.571731	0.05904809	1.791251	0.717542		564.6385	9.983855	568.86966	38.98571	565.480643	11.21256	0.15
1.sSMPABC022		486.6629	217.1866	0.446277	0.09226	1.604174	0.741857	1.924503	0.05831835	1.063174	0.833552		568.8892	8.740805	541.74247	23.24602	563.488412	8.35684	-0.96
1.sSMPABC042		463.9878	209.6917	0.451934	0.09264	1.619171	0.745061	1.936881	0.05833	1.062918	0.835968		571.1316	8.855858	542.1791	23.23869	565.354601	8.431718	-1.02
1.sSMPABC061		405.4203	180.7321	0.44579	0.09119	1.644917	0.727238	1.972849	0.05784	1.089212	0.833777		562.5711	8.867634	523.70648	23.88854	554.93101	8.469511	-1.38
1.sSMPABC062		398.3368	169.9475	0.426643	0.09155	1.638449	0.738314	1.979774	0.05849	1.111301	0.827594		564.6975	8.864707	548.16493	24.27182	561.421349	8.574145	-0.58
1.sSMPABC081		424.2188	198.6504	0.468273	0.09067	2.73101	0.732112	4.511548	0.05856152	3.591051	0.605338		559.4984	14.65228	550.8334	78.39633	557.791742	19.54929	-0.31
1.sSMPABC102		428.3097	196.1871	0.45805	0.09103	1.603867	0.736129	1.979051	0.05865	1.15942	0.810422		561.6258	8.632272	554.12836	25.29721	560.144013	8.556328	-0.26
1.sSMPABC121		397.1808	185.7892	0.46777	0.09151	1.661021	0.748716	2.027578	0.05934	1.162791	0.819214		564.4613	8.983315	579.59287	25.26186	567.479371	8.85314	0.53
1.sSMPABC122		406.8547	182.6451	0.44892	0.0922	1.626898	0.758303	1.958117	0.05965	1.08969	0.830848		568.5351	8.859428	590.90209	23.62874	573.030421	8.611082	0.78
1.sSMPABC141		422.6812	196.713	0.465393	0.09168	1.657941	0.749728	2.025393	0.05931	1.163379	0.818577		565.4652	8.981915	578.49415	25.27932	568.066628	8.850419	0.46
1.sSMPABC161		409.2244	187.8641	0.459074	0.08973	1.710348	0.726986	2.216378	0.05876071	1.409624	0.771686		553.9401	9.085052	558.2418	30.73495	554.782609	9.517979	0.15
1.sSMPABC162		380.0672	170.0978	0.447546	0.0897	1.627653	0.732038	1.982588	0.05918885	1.131989	0.820974		553.7626	8.642846	574.04938	24.61567	557.74863	8.544064	0.71
Weighted average 206Pb/238U Age = 563.7±3.2 Ma (2σ, MSWD 1.4)																			

SECONDARY REFERENCE MATERIAL (GJ1, Jackson et al. 2004; Morel et al. 2008)																			
1.sSMPABC003		651.4834	21.06468	0.032333	0.09815	1.625754	0.811393	1.98663	0.05995672	1.141764	0.818347		603.5609	9.346849	602.01285	24.7118	603.235449	9.060282	-0.05
1.sSMPABC004		616.7649	20.33783	0.032975	0.09803	1.596398	0.811659	1.90118	0.06005	1.032473	0.839688		602.8542	9.167692	605.37672	22.33377	603.384379	8.670483	0.09
1.sSMPABC023		505.6737	16.7213	0.033067	0.09791	1.659836	0.811337	1.999463	0.0601	1.114809	0.830141		602.1474	9.521597	607.17681	24.10753	603.204044	9.118723	0.18
1.sSMPABC024		541.0933	17.53383	0.032404	0.097288	1.670448	0.804708	2.037636	0.05999	1.166861	0.819797		598.4944	9.526983	603.21392	25.24991	599.480904	9.25128	0.16
1.sSMPABC043		486.9422	15.88106	0.032614	0.097478	1.646599	0.804806	2.00975	0.05988	1.152305	0.819305		599.6141	9.407649	599.24111	24.95153	599.536109	9.12472	-0.01
1.sSMPABC044		502.5627	15.88771	0.031613	0.098552	1.628664	0.814891	1.975029	0.05997	1.117225	0.824628		605.916	9.398477	602.49233	24.17875	605.19423	9.028658	-0.12
1.sSMPABC063		453.5403	14.59614	0.032183	0.09806	1.639523	0.81113	1.989656	0.05999244	1.127251	0.824023		603.0308	9.418164	603.30186	24.39242	603.087797	9.072506	0.01
1.sSMPABC064		456.726	14.46983	0.031682	0.098532	1.649359	0.813503	1.993071	0.05988	1.118904	0.827546		605.7982	9.516218	599.24111	24.22829	604.417049	9.102892	-0.23
1.sSMPABC083		463.8877	15.243	0.032859	0.09855	1.613514	0.812911	1.94288	0.05982526	1.082292	0.830475		605.9061	9.321348	597.26046	23.44329	604.085509	8.875163	-0.30
1.sSMPABC084		486.8646	15.89704	0.032652	0.097398	1.584199	0.803738	1.959292	0.05985	1.152882	0.808557		599.1412	9.054284	598.15589	24.96858	598.935302	8.89418	-0.03
1.sSMPABC103		473.5527	15.45344	0.032633	0.097278	1.630161	0.803848	1.954933	0.05993218	1.079044	0.833871		598.4349	9.306673	601.12674	23.35778	598.997235	8.874981	0.09
1.sSMPABC123		453.8325	14.6295	0.032235	0.09872	1.623871	0.817511	1.942283	0.06006	1.065601	0.836063		606.9055	9.395994	605.7369	23.04898	606.658714	8.900191	-0.04
1.sSMPABC124		410.7098	13.29302	0.032366	0.098169	2.601351	0.814413	4.415499	0.06016829	3.567857	0.589141		603.6715	14.98182	609.63221	77.12256	604.926725	20.30444	0.21
1.sSMPABC143		460.4352	14.66315	0.031846	0.0985	1.647849	0.806993	2.006252	0.05942	1.144396	0.821357		605.6121	9.515438	582.51909	24.84998	600.765976	9.128837	-0.81
1.sSMPABC144		435.8551	14.06912	0.032279	0.09833	1.74272	0.808435	2.283853	0.05962929	1.476114	0.763061		604.6125	10.04784	590.14915	32.01197	601.575966	10.4088	-0.50
1.sSMPABC163		414.1282	13.68918	0.033055	0.097989	1.697342	0.812265	2.126345	0.06012	1.280772	0.798244		602.6128	9.755098	607.89628	27.69312	603.723586	9.712976	0.18
1.sSMPABC164		431.9506	13.65998	0.031624	0.096907	1.770663	0.80173	2.339313	0.06000289	1.528769	0.756916		596.2566	10.07428	603.67867	33.07872	597.803988	10.61351	0.26
Weighted average 206Pb/238U Age = 602.6±2.3 Ma (2σ, MSWD 0.44)																			
TERTIARY REFERENCE MATERIAL (Plešovice, Sláma et al. 2008)																			
1.sSMPABC005		851.7699	138.5089	0.162613	0.05377	1.641791	0.394267	2.058088	0.05318	1.241068	0.797726		337.6264	5.386499	336.48434	28.12075	337.481634	5.913097	-0.04
1.sSMPABC006		883.3655	138.4672	0.15675	0.053961	1.561629	0.396557	1.914159	0.0533	1.106942	0.81583		338.7923	5.140633	341.58913	25.05894	339.148262	5.521406	0.10

1.sSMPABC025		817.2914	141.1434	0.172697	0.05383	1.602684	0.394857	1.959738	0.0532	1.12782	0.817805		337.9946	5.263728	337.33626	25.55084	337.911058	5.6358	-0.02
1.sSMPABC045		707.0355	110.7682	0.156666	0.054081	1.63235	0.396696	2.084888	0.0532	1.296992	0.782944		339.5285	5.384913	337.33626	29.38347	339.249326	6.016852	-0.08
1.sSMPABC046		701.7492	108.2434	0.154248	0.053921	1.674419	0.395668	2.094891	0.05322	1.258925	0.799287		338.5469	5.508187	338.18773	28.51674	338.50122	6.034532	-0.01
1.sSMPABC065		658.4468	103.2256	0.156771	0.054262	1.700869	0.398395	2.115671	0.05325	1.258216	0.803938		340.6328	5.628827	339.4641	28.49422	340.483445	6.124727	-0.04
1.sSMPABC066		673.3858	100.6029	0.149399	0.054232	1.627821	0.392342	1.967663	0.05247	1.105394	0.827287		340.4487	5.384147	305.94664	25.18322	336.078516	5.632672	-1.30
1.sSMPABC085		711.2146	113.0561	0.158962	0.053674	4.063958	0.393949	5.633661	0.05323272	3.901587	0.721371		337.0356	13.33444	338.7291	88.36891	337.250043	16.27375	0.06
1.sSMPABC086		754.5107	119.479	0.158353	0.053834	1.637819	0.394734	1.999542	0.05318	1.147048	0.819097		338.0163	5.385834	336.48434	25.99039	337.821907	5.754434	-0.06
1.sSMPABC105		693.7407	106.0368	0.152848	0.053754	2.660844	0.392005	3.577586	0.05289106	2.39145	0.743754		337.5259	8.739877	324.12629	54.30589	335.833052	10.26744	-0.50
1.sSMPABC106		768.5103	116.684	0.151831	0.054215	1.645945	0.398299	2.087221	0.05328344	1.283494	0.788582		340.3448	5.448897	340.88566	29.05935	340.413919	6.046448	0.02
1.sSMPABC125		732.6087	116.1828	0.158588	0.054305	1.697417	0.399235	2.145866	0.05332	1.312828	0.791017		340.8962	5.62824	342.43836	29.71531	341.093535	6.22734	0.06
1.sSMPABC126		732.2238	112.7415	0.153971	0.053914	1.797712	0.396012	2.24208	0.05327279	1.339834	0.801805		338.5066	5.920226	340.43287	30.33737	338.751495	6.46967	0.07
1.sSMPABC146		606.2542	91.32539	0.150639	0.05408	1.627219	0.398031	2.13767	0.05338	1.386287	0.761211		339.522	5.384045	344.98338	31.36386	340.218891	6.198625	0.20
Weighted average 206Pb/238U Age = 339.1±1.5 (2σ, MSWD 0.17)																			

[a]Ages and errors calculated with ISOPLOT (Ludwig, 2003)

[b]Discordance in % = 100*(1-^{206}Pb/^{238}U age/^{207}Pb/^{235}U age))

U-Pb LA-ICP-MS analysis and ages of sample P013

grain/spot position	spot site	U	Th	Th/U	Isotopic ratios							Ages (in Ma)[a]						Discordance[b]
		ppm	ppm		$^{206}Pb/^{238}U$	2σ	$^{207}Pb/^{235}U$	2σ	$^{207}Pb/^{206}Pb$	2σ	Rho	$^{206}Pb/^{238}U$	2σ	$^{207}Pb/^{235}U$	2σ	$^{207}Pb/^{206}Pb$	2σ	(%)
Layered orthopyroxene-garnet diatexite (P013)																		
P013-009	Core	436.2544	185.2948	0.42474	0.119264	1.612091	1.045188	1.900718	0.06356	1.006923	0.848148	726.33	11.07	726.50	9.90	727.02	21.35	0.06
P013-010	Rim	191.5878	48.97645	0.255634	0.115158	1.652182	1.008224	2.068252	0.0634981	1.244169	0.798831	702.64	10.99	707.98	10.59	724.95	26.39	0.79
P013-011	Rim	292.4087	93.9557	0.321316	0.105665	1.592115	0.888134	2.042553	0.06096	1.279528	0.779473	647.52	9.80	645.37	9.80	637.82	27.53	-0.31
P013-012	Core	71.48141	262.8372	3.677001	0.099437	1.711984	0.831258	2.388706	0.06063	1.665842	0.716699	611.11	9.98	614.31	11.06	626.13	35.91	0.55
P013-014	Core	205.4034	112.1583	0.546039	0.098235	1.610601	0.814575	1.948951	0.06014	1.097439	0.826394	604.06	9.28	605.02	8.92	608.62	23.73	0.19
P013-015	Core	132.848	79.64688	0.599534	0.13846	1.605554	1.281191	2.044999	0.06711	1.266577	0.785112	835.95	12.58	837.38	11.72	841.19	26.36	0.21
P013-016	Rim	74.3973	19.71567	0.265005	0.099587	1.66918	0.828806	2.162641	0.06036	1.375083	0.771825	611.99	9.74	612.95	9.99	616.50	29.69	0.18
P013-032	Rim	510.0263	418.5529	0.82065	0.098235	1.590214	0.812679	1.905592	0.06	1.05	0.834499	604.06	9.16	603.96	8.71	603.57	22.72	0.01
P013-033	Core	580.6048	765.3571	1.318207	0.099637	1.592528	0.817329	1.913888	0.0594942	1.06152	0.83209	612.28	9.30	606.56	8.77	585.23	23.04	-0.92
P013-035	Core	412.9344	213.6793	0.517466	0.10169	1.647385	0.852468	2.02903	0.0607994	1.184519	0.811908	624.30	9.80	626.00	9.52	632.15	25.51	0.30
P013-036	Rim	127.6756	232.9587	1.824614	0.099787	1.647884	0.832052	2.128029	0.0604748	1.346472	0.774371	613.16	9.63	614.75	9.85	620.61	29.05	0.29
P013-047	Core	15.84704	10.88628	0.68696	0.122158	2.500159	1.070871	4.747026	0.0635791	4.035277	0.526679	742.97	17.55	739.17	25.22	727.66	85.54	-0.48
P013-048	Core	82.32488	309.6203	3.760956	0.096393	1.703719	0.803018	2.209479	0.06042	1.406819	0.771095	593.23	9.65	598.53	10.03	618.65	30.36	0.91
P013-050	Core	386.9247	322.0541	0.832343	0.163224	1.620743	1.615785	2.091301	0.0717955	1.32164	0.774993	974.67	14.66	976.36	13.20	980.15	26.92	0.21
P013-051	Core	694.9006	356.9748	0.513706	0.110612	1.611443	0.949692	1.894227	0.06227	0.995664	0.850713	676.30	10.34	677.94	9.41	683.39	21.26	0.27
P013-052	Rim	661.0009	178.4044	0.2699	0.105435	1.614588	0.889687	1.906098	0.0612	1.013072	0.847065	646.18	9.92	646.20	9.15	646.27	21.77	0.03
P013-053	Core	806.2868	232.565	0.28844	0.127165	1.574927	1.100402	1.90265	0.06276	1.067559	0.827754	771.67	11.45	753.54	10.17	700.11	22.73	-2.37
P013-054	Rim	158.0822	103.1992	0.65282	0.118713	1.61957	1.042653	2.059111	0.0637	1.271586	0.786539	723.15	11.07	725.24	10.72	731.68	26.94	0.32
P013-056	Core	439.341	45.23052	0.102951	0.102871	1.596418	0.842383	1.91672	0.05939	1.060785	0.832891	631.21	9.59	620.46	8.93	581.42	23.04	-1.70
P013-057	Core	670.3886	274.3843	0.409291	0.122729	1.599217	1.088582	1.883417	0.06433	0.99487	0.849104	746.25	11.27	747.81	10.01	752.50	21.01	0.24
P013-059	Core	426.2571	90.65698	0.212681	0.107237	1.58745	0.909924	1.943485	0.06154	1.121222	0.816806	656.68	9.91	657.02	9.44	658.16	24.04	0.08
P013-060	Core	209.0603	95.77265	0.45811	0.129097	1.644431	1.160736	2.127267	0.06521	1.349486	0.773025	782.71	12.12	782.30	11.66	781.12	28.36	-0.02
P013-067	Rim	626.7193	69.18876	0.110398	0.11617	2.366077	1.009359	4.082985	0.0630161	3.327528	0.579497	708.48	15.87	708.55	21.03	708.77	70.76	0.04
P013-068	Core	50.82333	68.36601	1.34517	0.139942	1.745975	1.298378	2.302461	0.06729	1.500966	0.758308	844.34	13.82	845.01	13.29	846.76	31.22	0.11
P013-069	Core	510.9109	29.13015	0.057016	0.122498	1.618573	1.086877	1.916173	0.06435	1.025641	0.84469	744.93	11.38	746.99	10.18	753.16	21.65	0.31
P013-072	Core	50.49398	71.07103	1.407515	0.097033	1.857585	0.80247	2.779313	0.05998	2.067356	0.668361	597.00	10.59	598.22	12.63	602.85	44.74	0.23
P013-073	Core	1117.463	1315.231	1.176979	0.119394	1.660758	1.043909	1.968667	0.063413	1.057133	0.843595	727.08	11.41	725.86	10.25	722.11	22.43	-0.14
P013-074	Core	222.6946	186.8895	0.839219	0.102841	1.635833	0.862555	1.981308	0.06083	1.117869	0.825633	631.04	9.83	631.52	9.35	633.23	24.07	0.10
P013-075	Core	87.22694	758.7419	8.698481	0.103452	1.664892	0.852274	2.200804	0.05975	1.439331	0.756493	634.61	10.06	625.90	10.33	594.53	31.19	-1.36

P013-077	Core	377.2688	133.7503	0.354523	0.105405	1.615048	0.886236	1.93509	0.06098	1.065923	0.834611	646.01	9.92	644.35	9.27	638.53	22.93	-0.23
P013-078	Core	363.2938	314.8371	0.866618	0.122839	1.63039	1.086341	1.944777	0.06414	1.060181	0.838343	746.88	11.49	746.72	10.33	746.25	22.41	0.01
P013-079	Rim	35.58575	139.6956	3.925604	0.109971	1.857585	0.945402	2.840687	0.06235	2.149158	0.653921	672.58	11.86	675.71	14.10	686.14	45.87	0.49
P013-088	Core	161.8465	400.5108	2.474633	0.10175	1.633697	0.855786	2.054565	0.061	1.245902	0.795155	624.66	9.72	627.82	9.66	639.23	26.80	0.53
P013-089	Rim	245.2569	213.1505	0.869091	0.10199	1.728816	0.852741	2.228368	0.0606397	1.405995	0.775821	626.06	10.31	626.15	10.46	626.48	30.31	0.04
P013-090	Core	163.4785	206.4347	1.262764	0.097053	1.733388	0.801432	2.219298	0.05989	1.385874	0.781053	597.12	9.88	597.64	10.07	599.60	30.01	0.11
P013-091	Core	843.6694	321.1937	0.38071	0.131421	1.645843	1.188483	2.004102	0.0655885	1.143514	0.821237	795.97	12.32	795.26	11.10	793.27	23.99	-0.06
P013-092	Rim	564.171	174.3301	0.309002	0.11607	1.604428	1.00767	2.025365	0.0629649	1.236089	0.792167	707.90	10.75	707.70	10.37	707.05	26.29	0.00
P013-093	Core	126.1581	215.8677	1.711089	0.101009	1.66551	0.853035	2.136877	0.06125	1.338776	0.779413	620.32	9.85	626.31	10.03	648.02	28.75	0.99
P013-094	Core	214.3699	327.177	1.526227	0.097614	1.685532	0.800217	2.182378	0.0594557	1.386274	0.772337	600.41	9.66	596.95	9.89	583.82	30.10	-0.55
P013-095	Core	378.2384	77.60315	0.20517	0.111363	1.672511	0.955219	2.015792	0.06221	1.125221	0.829704	680.66	10.80	680.82	10.04	681.34	24.04	0.05
P013-096	Core	199.5615	399.0644	1.999706	0.10162	1.665567	0.847456	2.077216	0.0604836	1.241255	0.801826	623.89	9.90	623.25	9.71	620.92	26.78	-0.07
P013-097	Core	422.585	243.3279	0.575808	0.126794	1.626915	1.137055	1.925625	0.06504	1.030135	0.844876	769.55	11.80	771.11	10.45	775.63	21.67	0.24
P013-098	Rim	37.54881	44.70258	1.190519	0.096643	1.947985	0.802172	3.22862	0.0602	2.574751	0.603349	594.70	11.06	598.05	14.69	610.77	55.65	0.59
P013-099	Core	409.1361	204.6055	0.500091	0.192455	1.65839	2.052765	2.01396	0.0773588	1.142706	0.823448	1134.66	17.26	1133.22	13.84	1130.45	22.76	-0.08
P013-100	Rim	71.18085	92.52881	1.299912	0.098405	1.767085	0.814584	2.529918	0.0600366	1.810496	0.698475	605.06	10.20	605.02	11.59	604.89	39.17	0.02
P013-107	Core	1056.087	188.8707	0.17884	0.107988	1.654742	0.920033	1.962833	0.061791	1.055718	0.843038	661.06	10.39	662.38	9.59	666.88	22.60	0.23
P013-108	Rim	176.6738	165.5039	0.936777	0.099407	1.677294	0.826526	2.252738	0.0603031	1.503832	0.744558	610.93	9.77	611.68	10.40	614.47	32.48	0.15
P013-109	Core	879.2837	64.82328	0.073723	0.107608	1.619595	0.917196	1.940811	0.0618182	1.069421	0.834494	658.84	10.14	660.88	9.46	667.83	22.89	0.34
P013-110	Core	357.8309	202.4806	0.565855	0.114147	1.631723	0.989002	1.931964	0.0628393	1.03439	0.844593	696.79	10.77	698.21	9.79	702.80	22.02	0.23
P013-111	Rim	136.2724	168.711	1.238042	0.096563	1.765086	0.792202	2.364732	0.0595011	1.573667	0.746421	594.23	10.02	592.42	10.66	585.48	34.15	-0.28
P013-113	Core	774.2077	561.8025	0.725648	0.119104	2.366168	1.020292	4.129865	0.0621295	3.384824	0.572941	725.40	16.23	714.06	21.39	678.57	72.33	-1.56
P013-114	Rim	430.4312	502.1049	1.166516	0.117562	1.720844	1.028393	2.161601	0.0634442	1.308135	0.796097	716.51	11.67	718.12	11.18	723.16	27.75	0.26
P013-118	Rim	152.4135	235.6397	1.546055	0.11644	1.633987	1.012092	2.059212	0.06304	1.253173	0.793501	710.04	10.98	709.93	10.56	709.58	26.64	0.02
P013-120	Core	736.9377	268.1647	0.363891	0.138941	1.672072	1.285639	1.962892	0.06711	1.028163	0.851841	838.67	13.15	839.36	11.27	841.19	21.40	0.12
P013-127	Core	180.366	559.1583	3.100131	0.097624	2.469327	0.799028	4.118445	0.0593613	3.29606	0.599578	600.47	14.16	596.28	18.73	580.37	71.60	-0.68
P013-128	Rim	59.71592	139.1586	2.330343	0.10217	1.685779	0.856787	2.275962	0.06082	1.529102	0.740688	627.12	10.07	628.37	10.71	632.87	32.93	0.23
P013-130	Rim	189.2015	92.92885	0.491163	0.10169	2.572105	0.850571	4.365135	0.0606641	3.526851	0.589238	624.30	15.30	624.96	20.56	627.35	76.01	0.13
P013-135	Core	435.1641	110.3187	0.253511	0.127425	1.661991	1.143659	2.103946	0.0650938	1.290107	0.78994	773.16	12.11	774.24	11.45	777.37	27.13	0.17
P013-136	Core	243.9279	152.2677	0.624233	0.128917	2.241378	1.157312	3.968811	0.0651086	3.275315	0.564748	781.69	16.50	780.69	21.84	777.85	68.87	-0.09
P013-137	Core	116.7859	464.5005	3.977366	0.100468	1.694408	0.836001	2.121065	0.06035	1.275891	0.798848	617.15	9.97	616.94	9.85	616.15	27.55	-0.01
P013-138	Core	63.58631	221.8629	3.489161	0.097374	1.912793	0.815087	2.945689	0.06071	2.240158	0.649353	599.00	10.94	605.30	13.51	628.98	48.27	1.07
P013-140	Core	446.36	337.402	0.755897	0.128887	2.253127	1.130133	4.009633	0.0635944	3.316712	0.561929	781.51	16.58	767.82	21.82	728.17	70.31	-1.75
P013-147	Rim	329.3785	121.4308	0.368667	0.112064	1.644178	0.934809	1.955089	0.0605	1.057851	0.840974	684.72	10.68	670.16	9.63	621.50	22.82	-2.14
P013-148	Core	279.9695	198.1123	0.707621	0.118823	1.618068	1.040671	1.975594	0.06352	1.133501	0.819029	723.79	11.07	724.25	10.27	725.69	24.04	0.10

P013-149	Rim	155.3913	134.6298	0.866392	0.11613	1.655601	1.009234	2.076524	0.06303	1.253371	0.797294	708.25	11.10	708.49	10.64	709.24	26.65	0.06
P013-150	Core	96.81998	277.5792	2.866961	0.096723	1.801429	0.803371	2.44966	0.06024	1.660027	0.735379	595.18	10.24	598.73	11.13	612.21	35.87	0.62
P013-151	Core	800.2961	411.9427	0.514738	0.117231	1.674212	1.022363	1.989679	0.06325	1.075099	0.841448	714.61	11.32	715.10	10.26	716.65	22.83	0.10
P013-152	Core	134.2729	193.921	1.44423	0.097865	1.657628	0.812987	2.063067	0.06025	1.228216	0.803478	601.88	9.52	604.13	9.43	612.56	26.54	0.40
P013-153	Core	245.8295	176.787	0.719145	0.134014	1.643877	1.22416	2.022005	0.06625	1.177358	0.812993	810.73	12.52	811.68	11.36	814.28	24.61	0.15
P013-154	Core	1039.374	322.8913	0.310659	0.108459	1.624965	0.922982	1.963254	0.06172	1.10175	0.82769	663.79	10.25	663.94	9.61	664.42	23.60	0.05
P013-155	Rim	537.1374	233.1796	0.434115	0.107237	1.643477	0.931955	1.940233	0.06303	1.031255	0.847051	656.68	10.26	668.66	9.54	709.24	21.93	1.82
P013-157	Rim	168.635	397.7432	2.358604	0.098535	2.628482	0.818142	4.419511	0.0602192	3.552909	0.594745	605.82	15.20	607.01	20.38	611.46	76.78	0.22
P013-158	Core	420.1827	168.7486	0.401608	0.164947	1.689291	1.633774	2.000247	0.0718368	1.071115	0.844541	984.21	15.42	983.32	12.67	981.32	21.81	-0.05
P013-159	Core	165.3181	192.9989	1.16744	0.302646	1.687457	4.362333	1.983597	0.10454	1.042663	0.850705	1704.42	25.30	1705.23	16.51	1706.24	19.19	0.10
P013-160	Core	1801.309	163.652	0.090852	0.129278	2.246321	1.16263	3.933446	0.0652254	3.228938	0.571082	783.74	16.58	783.19	21.69	781.61	67.86	-0.04
P013-167	Rim	892.2131	193.8004	0.217213	0.131991	1.640419	1.175258	1.938729	0.0645782	1.033294	0.846131	799.22	12.33	789.10	10.69	760.63	21.79	-1.25
P013-168	Core	306.1804	246.9378	0.806511	0.103693	1.647959	0.869906	1.996944	0.0608448	1.127836	0.825241	636.01	9.98	635.52	9.47	633.75	24.28	-0.05
P013-171	Core	109.5719	303.1625	2.766792	0.097594	1.701665	0.804097	2.16416	0.0597562	1.337133	0.786294	600.29	9.75	599.14	9.83	594.76	28.98	-0.17
P013-172	Rim	355.0667	115.7065	0.325873	0.133103	1.715317	1.205926	2.060354	0.06571	1.141379	0.832535	805.54	12.99	803.32	11.49	797.15	23.93	-0.24
P013-173	Core	976.8949	733.101	0.75044	0.110923	2.478005	0.952655	4.204391	0.0622895	3.396526	0.589385	678.10	15.95	679.48	21.03	684.06	72.52	0.23
P013-174	Rim	126.9435	319.5033	2.516893	0.096963	1.755654	0.800554	2.236875	0.05988	1.386106	0.784869	596.59	10.00	597.14	10.14	599.24	30.01	0.12
P013-175	Core	188.3777	131.7279	0.699276	0.124251	1.660643	1.104909	2.102167	0.064495	1.288942	0.789967	754.98	11.83	755.72	11.26	757.90	27.19	0.13
P013-177	Core	239.7776	64.78427	0.270185	0.166499	1.659951	1.656797	1.973263	0.07217	1.066925	0.841221	992.79	15.27	992.15	12.57	990.74	21.70	-0.02
P013-178	Rim	442.4204	144.6407	0.32693	0.102	1.649337	0.853221	1.966814	0.0606679	1.071469	0.838583	626.12	9.84	626.42	9.23	627.48	23.09	0.08
P013-180	Rim	174.6828	82.38591	0.471632	0.101259	1.700949	0.85138	2.070584	0.06098	1.180715	0.821483	621.78	10.08	625.41	9.71	638.53	25.40	0.61

U-Pb LA-ICP-MS analysis and ages of reference materials

spot/grain position		U	Th	Th/U	Isotopic ratios								Ages (in Ma)[a]						Discordance[b]
		ppm	ppm		$^{206}Pb/^{238}U$	2σ	$^{207}Pb/^{235}U$	2σ	$^{207}Pb/^{206}Pb$	2σ	Rho		$^{206}Pb/^{238}U$	2σ	$^{207}Pb/^{206}Pb$	2σ	$^{207}Pb/^{235}U$	2σ	(%)
PRIMARY REFERENCE MATERIAL (BB, Santos et al. 2017)																			
1.sSMPABC002		407.9418	182.9876	0.448563	0.09047	1.613795	0.737713	1.933683	0.05914	1.065269	0.83457		558.3162	8.636708	572.2537	23.17183	561.06984	8.369764	0.49
1.sSMPABC021		408.2526	189.4644	0.464086	0.0912	2.715139	0.735908	4.487473	0.0585231	3.572874	0.605049		562.6302	14.64516	549.4003	78.01847	560.01473	19.5026	-0.47
1.sSMPABC022		421.6326	190.0377	0.450719	0.09072	1.609347	0.738375	1.949999	0.05903	1.101135	0.825307		559.7939	8.634727	568.2027	23.96837	561.45695	8.44506	0.30
1.sSMPABC042		442.8278	198.6085	0.448501	0.09278	2.694546	0.739302	4.511221	0.0577918	3.618085	0.597299		571.9575	14.76464	521.8782	79.37641	561.99822	19.65932	-1.77

1.sSMPABC081		402.5749	183.0035	0.454582	0.0922	1.64859	0.748514	2.003168	0.05888	1.137908	0.822991		568.5351	8.977636	562.6619	24.792	567.36189	8.744741	-0.21
1.sSMPABC101		421.7416	197.7078	0.468789	0.09283	1.637402	0.759516	2.018079	0.05934	1.179643	0.811367		572.2525	8.972457	579.5929	25.62797	573.73103	8.884037	0.26
1.sSMPABC121		404.7006	175.1469	0.432782	0.09131	2.737926	0.735191	4.519669	0.0583957	3.595994	0.60578		563.28	14.78455	544.6388	78.58677	559.59549	19.63276	-0.66
1.sSMPABC141		420.702	193.5024	0.459951	0.08987	1.624569	0.72774	1.975379	0.05873	1.123787	0.822409		554.7682	8.641466	557.1017	24.50738	555.22564	8.483812	0.08
1.sSMPABC142		415.6109	190.9158	0.459362	0.09178	1.818835	0.746362	2.406616	0.0589794	1.575957	0.755764		566.0557	9.864082	566.3357	34.31463	566.11151	10.49773	0.01
1.sSMPABC161		390.5938	163.7912	0.419339	0.09185	1.654872	0.740734	1.983906	0.05849	1.094204	0.834148		566.469	8.980516	548.1649	23.89841	562.83357	8.608361	-0.65
Weighted average 206Pb/238U Age = 563.8±4.3 Ma (2σ, MSWD 1.5)																			
SECONDARY REFERENCE MATERIAL (GJ1, Jackson et al. 2004; Morel et al. 2008)																			
1.sSMPABC003		471.1294	14.9311	0.031692	0.097174	1.586974	0.804032	1.912037	0.06001	1.066489	0.829991		597.8238	9.055688	603.9352	23.07515	599.10039	8.683196	0.21
1.sSMPABC004		445.8647	14.02035	0.031445	0.097224	1.586157	0.804982	1.901725	0.06005	1.049126	0.834062		598.118	9.055275	605.3767	22.69399	599.63522	8.641851	0.25
1.sSMPABC023		459.637	14.75466	0.032101	0.098265	1.599981	0.810853	1.938045	0.0598469	1.093653	0.825565		604.2337	9.223415	598.0419	23.68628	602.93217	8.843257	-0.22
1.sSMPABC024		476.6338	15.23135	0.031956	0.098596	1.645338	0.811719	1.98215	0.05971	1.105342	0.830077		606.1731	9.514137	593.0817	23.95938	603.41787	9.050771	-0.46
1.sSMPABC043		480.7329	15.29077	0.031807	0.098165	1.611752	0.813047	1.922934	0.06007	1.048776	0.838173		603.6459	9.282688	606.097	22.6837	604.16166	8.787168	0.09
1.sSMPABC044		480.1148	15.09574	0.031442	0.097865	1.598017	0.810664	1.933727	0.0600778	1.088871	0.826392		601.8822	9.177853	606.3792	23.54978	602.82655	8.82233	0.16
1.sSMPABC064		458.1022	14.81862	0.032348	0.098145	1.652893	0.81261	1.975781	0.06005	1.082431	0.836577		603.5283	9.518039	605.3767	23.41443	603.91716	9.027051	0.06
1.sSMPABC083		470.4403	15.15198	0.032208	0.098045	2.641636	0.815317	4.391322	0.0603116	3.507915	0.601558		602.9405	15.2042	614.7722	75.76173	605.43258	20.21088	0.41
1.sSMPABC084		476.6858	15.05628	0.031585	0.098786	1.601622	0.807156	1.931726	0.05926	1.079987	0.829115		607.2894	9.277445	576.6613	23.47451	600.85737	8.791952	-1.07
1.sSMPABC103		465.8535	14.67983	0.031512	0.097744	1.618687	0.802286	1.93394	0.05953	1.05829	0.836989		601.1766	9.286242	586.5339	22.96472	598.11709	8.772459	-0.51
1.sSMPABC104		464.954	14.84447	0.031927	0.098806	1.662106	0.816856	2.002799	0.05996	1.117412	0.829891		607.4069	9.629841	602.1314	24.18425	606.2929	9.177504	-0.18
1.sSMPABC123		472.1268	14.48162	0.030673	0.097794	1.617968	0.796286	2.016002	0.0590546	1.202683	0.802562		601.4706	9.286451	569.108	26.17476	594.73123	9.108107	-1.13
1.sSMPABC124		447.9185	14.0326	0.031328	0.097804	1.617692	0.808712	1.947232	0.05997	1.083875	0.830765		601.5294	9.285734	602.4923	23.457	601.73136	8.872332	0.03
1.sSMPABC143		431.5215	14.06163	0.032586	0.097744	1.641615	0.805034	1.965757	0.0597339	1.081342	0.835106		601.1766	9.417876	593.9495	23.43573	599.66416	8.934426	-0.25
1.sSMPABC144		452.593	14.35281	0.031712	0.097634	1.641026	0.809324	1.974371	0.06012	1.097804	0.831164		600.5297	9.404819	607.8963	23.73696	602.07468	9.000314	0.26
1.sSMPABC163		456.926	14.86488	0.032532	0.098886	1.660759	0.814519	2.003982	0.05974	1.121527	0.82873		607.8769	9.62914	594.1704	24.30574	604.98584	9.168393	-0.48
1.sSMPABC164		415.1443	13.39762	0.032272	0.097714	2.612014	0.781741	4.485285	0.0580234	3.646253	0.582352		601.0002	14.98729	530.6449	79.87496	586.47582	20.16546	-2.48

1.sSMPABC183		425.6794	13.90379	0.032663	0.098125	1.667136	0.813076	2.026873	0.0600967	1.152766	0.822516		603.4108	9.598335	607.0567	24.92886	604.1779	9.264489	0.13
1.sSMPABC184		421.9926	13.60807	0.032247	0.097484	1.736864	0.789919	2.259537	0.0587689	1.445272	0.768681		599.6475	9.940531	558.5456	31.51058	591.12567	10.16804	-1.44
Weighted average 206Pb/238U Age = 602.7±2.2 Ma (2σ, MSWD 0.39)																			
TERTIARY REFERENCE MATERIAL (Plešovice, Sláma et al. 2008)																			
1.sSMPABC005		782.5095	175.3796	0.224125	0.053694	1.857976	0.395078	2.359606	0.0533651	1.454534	0.787409		337.1598	6.098267	344.3516	32.91159	338.07215	6.801099	0.27
1.sSMPABC006		770.1912	183.2488	0.237926	0.053474	1.610487	0.393493	1.922148	0.05337	1.049279	0.837858		335.8119	5.265028	344.5595	23.74105	336.918	5.52078	0.33
1.sSMPABC025		849.7217	196.4233	0.231162	0.053834	1.5625	0.396443	1.902806	0.05341	1.085939	0.821156		338.0174	5.140779	346.2544	24.56314	339.06504	5.494502	0.31
1.sSMPABC045		845.7192	196.4646	0.232305	0.053614	1.865988	0.392563	2.355978	0.0531047	1.438305	0.792023		336.6697	6.1159	333.271	32.60845	336.24022	6.759452	-0.13
1.sSMPABC065		945.881	216.5445	0.228934	0.053674	1.604478	0.394671	1.938338	0.05333	1.087568	0.82776		337.0373	5.264028	342.8628	24.61479	337.77581	5.579392	0.22
1.sSMPABC066		885.7244	203.2131	0.229431	0.053864	1.59881	0.388792	2.047975	0.05235	1.279847	0.780678		338.2012	5.263079	300.7279	29.18487	333.48643	5.832449	-1.41
1.sSMPABC086		890.6097	208.0589	0.233614	0.054515	4.043817	0.403884	5.631638	0.0537328	3.919552	0.718053		342.1815	13.47286	359.8688	88.44405	344.46125	16.56926	0.66
1.sSMPABC105		906.0689	206.0587	0.227421	0.054475	1.884949	0.399657	2.374716	0.0532096	1.444384	0.793758		341.9366	6.272238	337.7446	32.72025	341.39952	6.901693	-0.16
1.sSMPABC106		898.8227	203.4884	0.226394	0.054074	1.759313	0.396756	2.255213	0.0532146	1.410959	0.780109		339.4874	5.813132	337.957	31.96188	339.29247	6.519073	-0.06
1.sSMPABC125		849.8712	193.9999	0.22827	0.054505	4.029343	0.402691	5.620804	0.0535839	3.918907	0.716862		342.1202	13.42224	353.604	88.52751	343.59793	16.50199	0.43
1.sSMPABC126		878.4644	201.2469	0.229089	0.053914	4.058395	0.396105	5.630522	0.0532852	3.902845	0.720785		338.5075	13.37992	340.961	88.36241	338.81948	16.33547	0.09
1.sSMPABC145		457.3991	62.50016	0.136642	0.05362	1.862282	0.393714	2.359124	0.053254	1.448231	0.789396		336.7082	6.112408	339.636	32.79639	337.07875	6.789518	0.11
1.sSMPABC146		796.5942	112.7325	0.141518	0.05449	2.545129	0.399796	3.461449	0.0532133	2.34605	0.735278		342.0289	8.483754	337.9013	53.14462	341.49997	10.08828	-0.15
1.sSMPABC166		765.0012	110.3527	0.144252	0.05388	1.633259	0.39485	1.974786	0.05315	1.110066	0.827056		338.2987	5.385067	335.2056	25.15815	337.90615	5.692085	-0.12
1.sSMPABC185		835.8824	194.0961	0.232205	0.05408	1.675335	0.398717	2.090035	0.0534721	1.2496	0.801582		339.522	5.543316	348.8824	28.25187	340.71758	6.067582	0.35
1.sSMPABC186		904.5308	204.4821	0.226064	0.05343	1.707054	0.39307	2.103098	0.053356	1.228409	0.811685		335.5456	5.58384	343.9641	27.797	336.60923	6.043351	0.32
Weighted average 206Pb/238U Age = 338.1±1.5 (2σ, MSWD 0.39)																			

[a]Ages and errors calculated with ISOPLOT (Ludwig, 2003)

[b]Discordance in % = 100*(1-$^{206}Pb/^{238}U$ age/$^{207}Pb/^{235}U$ age))

9.6 APPENDIX F – Supplementary file 6 (Chapter 4): Compilation of ages from the Araçuaí orogen

Author[1]	Unit	Method	Type	Age
Sollner et al. 1991	Caparao Suite/Juiz de Fora Complex granulite	U-Pb	Magmatic crystallization	ca. 2176 Ma
Sollner et al. 1991	Caparao Suite/Juiz de Fora Complex granulite	U-Pb	Metamorphism	ca. 586 Ma
Pedrosa-Soares et al. 1998 Tassinari et al. 2001 Queiroga et al. 2007 Schmitt et al 2008 Queiroga et al. 2010 Amaral et al., 2020	Araçuai orogen ophiolite assemblages	U-Pb	Magmatic crystallization	ca. 660 - 600 Myr
Da Silva et al. 2002	Galileia Suite (G1) Grt-charnockite	U-Pb	Magmatic crystallization	584±5 Ma
Da Silva et al. 2002	Caparao Suite/Juiz de Fora Complex granulite	U-Pb	Magmatic crystallization	2195±15 Ma
Da Silva et al. 2002	Caparao Suite/Juiz de Fora Complex granulite	U-Pb	Metamorphism	587±9 Ma
Da Silva et al. 2002	Juiz de Fora Complex (alloctonous) granulite	U-Pb	Magmatic crystallization	2985±17 Ma
Da Silva et al. 2002	Juiz de Fora Complex (alloctonous) granulite	U-Pb	Metamorphism	808±360 Ma
Da Silva et al. 2002	Juiz de Fora Complex (alloctonous) enderbite	U-Pb	Metamorphism	2856±44 Ma
De Campos et al. 2004 Bento dos Santos et al. 2011 Gradim et al. 2014 Bento dos Santos et al. 2015 Dias et al. 2016 Richter et al. 2016	G2 Supersuite and regional metamorphic peak ages	U-Pb	Magmatic crystallization and metamorphism	ca. 575 - 560 Myr
Noce et al. 2007	Juiz de Fora Complex mafic granulite	U-Pb	Magmatic crystallization	2119 Ma
Noce et al. 2007	Juiz de Fora Complex granitic vein	U-Pb	Metamorphism	ca. 584 - 574 Myr
Noce et al. 2007	Juiz de Fora Complex enderbitic migmatite	U-Pb	Magmatic crystallization	2084 Ma
Noce et al. 2007	Juiz de Fora Complex enderbitic migmatite	U-Pb	Metamorphism	594 Ma
Rosa et al. 2007	Southern Bahia alkaline province	U-Pb	Magmatic crystallization	ca. 732 - 696 Myr
Pedrosa-Soares et al. 2008	G1 Supersuite ages	U-Pb	Magmatic crystallization	ca. 630 - 585 Myr
Novo et al. 2010	Divino Suite (G1) charnockite	U-Pb	Magmatic crystallization	ca. 603 - 592 Myr
Heilbron et al. 2010	Juiz de Fora Complex mafic granulite	U-Pb	Magmatic crystallization	2427±9 Ma
Heilbron et al. 2010	Juiz de Fora Complex mafic granulite	U-Pb	Metamorphism	654±12 Ma

Heilbron et al. 2010	Juz de Fora Complex enderbitic granulite	U-Pb	Magmatic crystallization	1966±38 Ma
Heilbron et al. 2010	Juz de Fora Complex enderbitic granulite	U-Pb	Metamorphism	587±15 Ma
Heilbron et al. 2010	Juiz de Fora Complex Charnockite	U-Pb	Magmatic crystallization	2199±17 Ma
Heilbron et al. 2010	Juiz de Fora Complex Charnockite	U-Pb	Metamorphism	633±140 Ma
Heilbron et al. 2010	Juiz de Fora Complex Charnockite	U-Pb	Magmatic crystallization	2154±11 Ma
Heilbron et al. 2010	Juiz de Fora Complex alkaline mafic granulite	U-Pb	Magmatic crystallization	1765±34 Ma
Heilbron et al. 2010	Juiz de Fora Complex alkaline mafic granulite	U-Pb	Metamorphism	586±14 Ma
Heilbron et al. 2010	Juiz de Fora Complex alkaline mafic granulite	U-Pb	Magmatic crystallization	1687±48 Ma
Heilbron et al. 2010	Juiz de Fora Complex alkaline mafic granulite	U-Pb	Metamorphism	619±21 Ma
Heilbron et al. 2010	Juiz de Fora Complex alkaline mafic granulite	U-Pb	Metamorphism	584±2 Ma
Heilbron et al. 2010	Juiz de Fora Complex calc-alkaline enderbite	U-Pb	Magmatic crystallization	1656±69 Ma
Heilbron et al. 2010	Juiz de Fora Complex calc-alkaline enderbite	U-Pb	Metamorphism	591±5 Ma
Da Silva et al. 2011	Caparao Suite/Juiz de Fora Complex charnockitic granulite	U-Pb	Metamorphism	2095±9 Ma
Da Silva et al. 2011	Caparao Suite/Juiz de Fora Complex charnockitic granulite	U-Pb	Metamorphism	587±9 Ma
Da Silva et al. 2011	Caparao Suite/Juiz de Fora Complex charnockitic granulite	U-Pb	Magmatic crystallization	2195±15 Ma
Tupinambá et al. 2012	Rio Negro-Serra da Prata magmatic arc	U-Pb	Magmatic crystallization	ca. 860 - 600 Myr
Gradim et al. 2014	Ataléia Suite S-type granites	U-Pb	Magmatic crystallization	ca. 590 - 580 Myr
Gradim et al. 2014	Carlos Chagas S-type granites (G2 Supersuite)	U-Pb	Magmatic crystallization	ca. 576 - 565 Myr
Gradim et al. 2014	Ataléia and Carlos Chagas S-type granites	U-Pb	Metamorphism	ca. 571 - 563 Myr
Alves et al. 2015	Andrelândia Group quartzite	U-Pb	Metamorphism	ca. 598 - 583 Myr
Alves et al. 2015	Andrelândia Group quartzite	U-Pb	Sedimentary provenance	ca. 2670 - 675 Myr
Richter et al. 2016	Nova Venecia Complex peraluminous granodiorite	U-Pb	Magmatic crystallization	593±8 Ma
Richter et al. 2016	Nova Venecia Complex peraluminous granodiorite	U-Pb	Metamorphism	ca. 571 - 501 Myr
Richter et al. 2016	Nova Venecia Complex granite	U-Pb	Magmatic crystallization	519.3±2 Ma
Richter et al. 2016	Nova Venecia Complex granite	U-Pb	Metamorphism	ca. 507 - 498 Myr

Richter et al. 2016	Nova Venecia Complex metatexite (Bt-Grt-Opx-metagreywacke)	U-Pb	Sedimentary provenance	ca. 877 - 606 Myr
Richter et al. 2016	Nova Venecia Complex metatexite (Bt-Grt-Opx-metagreywacke)	U-Pb	Metamorphism	ca. 590 - 495 Myr
Richter et al. 2016	Nova Venecia Complex metatexite (Bt-Grt-Crd-metagreywacke)	U-Pb	Sedimentary provenance	ca. 903 - 607 Myr
Richter et al. 2016	Nova Venecia Complex metatexite (Bt-Grt-Crd-metagreywacke)	U-Pb	Metamorphism	ca. 561 - 499 Myr
Richter et al. 2016	Nova Venecia Complex diatexite (Crd-Grt-granulite)	U-Pb	Sedimentary provenance	ca. 790 - 607 Myr
Richter et al. 2016	Nova Venecia Complex diatexite (Crd-Grt-granulite)	U-Pb	Metamorphism	565±5 Ma
Richter et al. 2016	Nova Venecia Complex metatexite (Bt-Grt-metagreywacke)	U-Pb	Metamorphism	502±6 Ma
Tedeschi et al., 2016	Gabbronorite (Chaves pluton - central Rio Doce Arc)	U-Pb	Magmatic crystallization	599±15 Ma
Tedeschi et al., 2016	Tonalite (Brasilândia pluton - central Rio Doce Arc)	U-Pb	Magmatic crystallization	581±11 Ma
Tedeschi et al., 2016	Granodiorite (Guarataia pluton - central Rio Doce Arc)	U-Pb	Magmatic crystallization	576±9 Ma
Tedeschi et al., 2016	Tonalitic orthogneiss (Baixo Guandu batholith - central Rio Doce Arc)	U-Pb	Magmatic crystallization	621±5 Ma
Tedeschi et al., 2016	Gabbronorite (Serra do Valentim pluton - southern Rio Doce Arc)	U-Pb	Magmatic crystallization	605±8 Ma
Tedeschi et al., 2016	Gabbronorite (Serra do Valentim pluton - southern Rio Doce Arc)	U-Pb	Metamorphism	590±7 Ma
Tedeschi et al., 2016	Granodioritic paleosome (Muriaé batolith - southern Rio Doce Arc)	U-Pb	Magmatic crystallization	620±3 Ma
Tedeschi et al., 2016	Granodioritic paleosome (Muriaé batolith - southern Rio Doce Arc)	U-Pb	Migmatization	592±4 Ma
Tedeschi et al., 2016	Biotite granite (Muriaé batolith - Southern Rio Doce Arc)	U-Pb	Magmatic crystallization	593±4 Ma
Tedeschi et al., 2016	Tonalitic orthogneiss (southern Rio Doce arc)	U-Pb	Magmatic crystallization	586±7 Ma
Degler et al. 2017	Metassedimentary Sequence paragneiss	U-Pb	Sedimentary provenance	ca. 2803 - 614 Myr
Degler et al. 2017	Metassedimentary Sequence paragneiss	U-Pb	Metamorphism	ca. 613 - 482 Myr
Degler et al. 2017	Metassedimentary Sequence paragneiss	U-Pb	Sedimentary provenance	ca. 1988 - 579 Myr
Degler et al. 2017	Metassedimentary Sequence paragneiss	U-Pb	Metamorphism	ca. 618 - 573 Myr
Novo et al. 2018	Rio Doce Group quartzite	U-Pb	Sedimentary provenance	ca. 2976 - 619 Myr

Novo et al. 2018	Rio Doce Group Grt-schist	U-Pb	Sedimentary provenance	ca. 3252 - 766 Myr
Novo et al. 2018	Rio Doce Group metapyroclastic rhyolite tuff	U-Pb	Magmatic crystallization	595±13 Ma
Novo et al. 2018	Rio Doce Group metapyroclastic dacite tuff	U-Pb	Magmatic crystallization	584±5 Ma
Novo et al. 2018	Rio Doce Group dacitic metavolcaniclastic	U-Pb	Magmatic crystallization	585±4 Ma
Faria et al. 2022	Caparao Suite/Juiz de Fora Complex orthogneiss+migmatite	U-Pb	Magmatic crystallization	ca. 2209 - 2121 Myr
Faria et al. 2022	Caparao Suite/Juiz de Fora Complex orthogneiss+migmatites	U-Pb	Metamorphism	ca. 633-584 Myr

[1]References are listed in the main file of this paper

9.7 APPENDIX G – Supplementary figure 1 (Chapter 4)

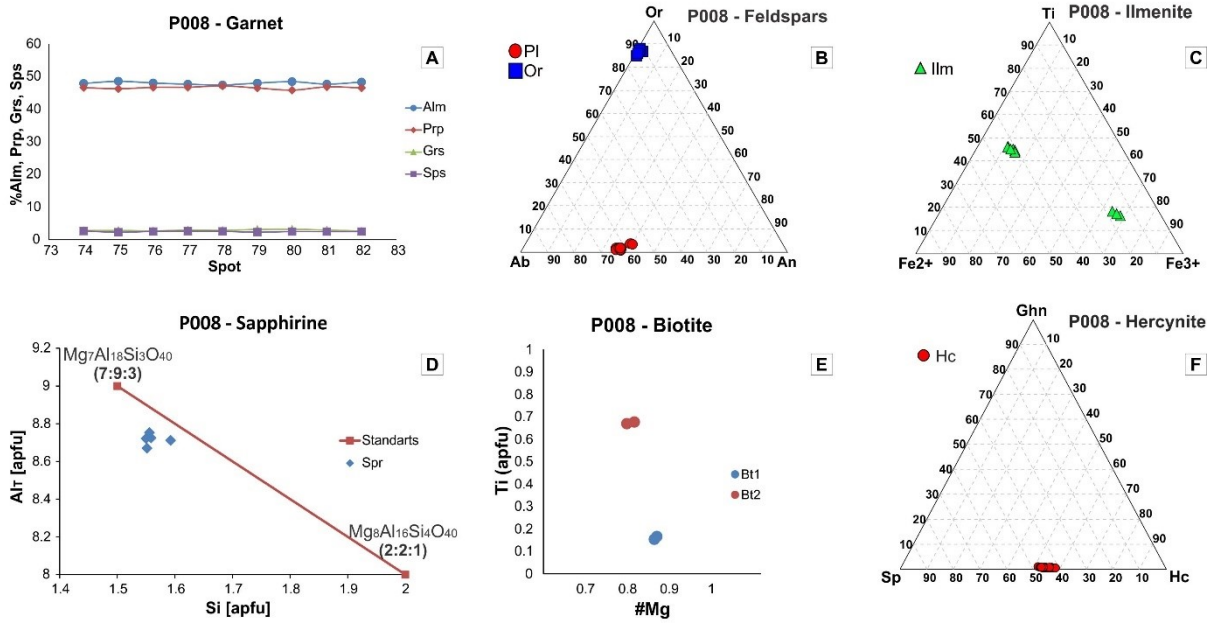

Supplementary figure 1 - Compositional plots for the main phases of sample P008. A) Garnet; B) Feldspars; C) Ilmenite; D) Classification plot of sapphirine adapted after Barbosa et al. (2017) with end-member compositions of Higgins et al. (1979) and Grew et al. (2008); E) Biotite; F) Hercynite. AlT – total aluminium. #Mg = XMg = $Mg/(Fe^{2+}+Mg)$.

9.8 APPENDIX H – Supplementary figure 2 (Chapter 4)

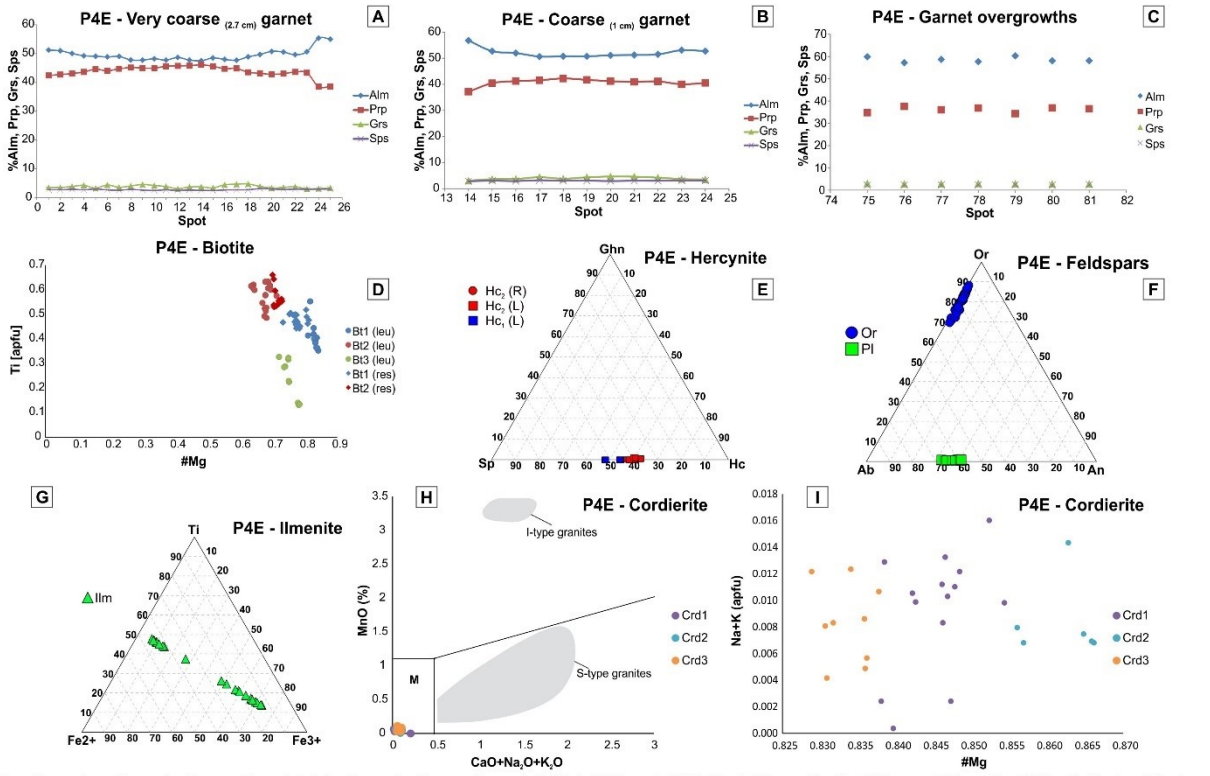

Supplementary figure 2 - Compositional plots for the main phases of sample P4E. A-C) Garnet; D) Biotite; E) Hercynite; F) Feldspars; G) Ilmenite; H) Cordierite classification diagram by Barbero & Villaseca (1992) and Villaseca & Barbero (1994); I) Cordierite Na+K x #Mg plot. #Mg = X_{Mg} = $Mg/(Fe^{2+}+Mg)$. M - metamorphic. R - residuum. L - leucosome.

9.9 APPENDIX I – Supplementary figure 3 (Chapter 4)

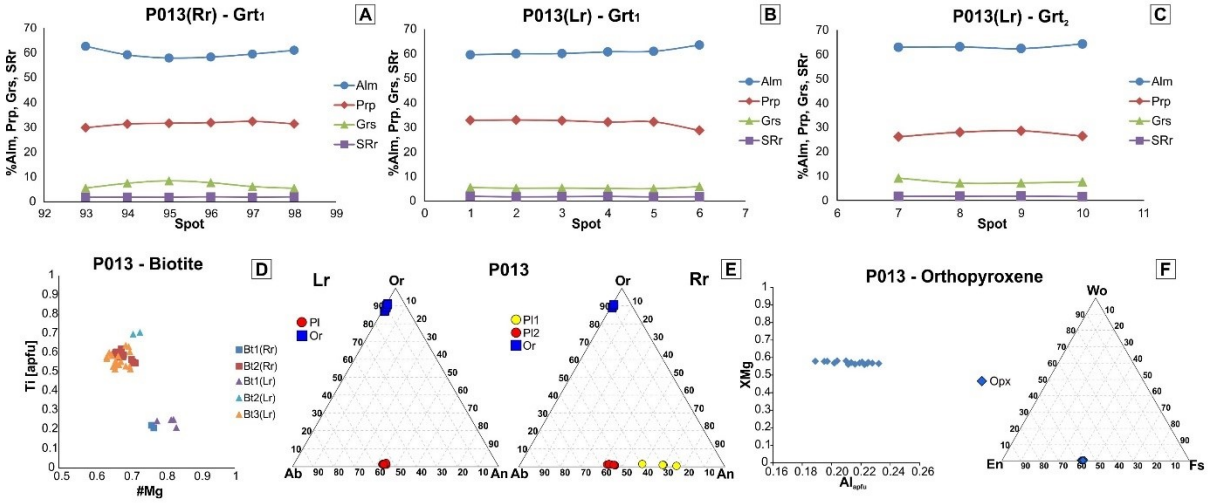

Supplementary figure 3 - Compositional plots for the main phases of sample P013. A-C) Garnet; D) Biotite; E) Feldspars; F) Orthopyroxene. Lr – leucosome-rich bands; Rr - residue-rich bands. #Mg = XMg = Mg/(Fe^{2+}+Mg).

9.10 APPENDIX J – Supplementary figure 4 (Chapter 4)

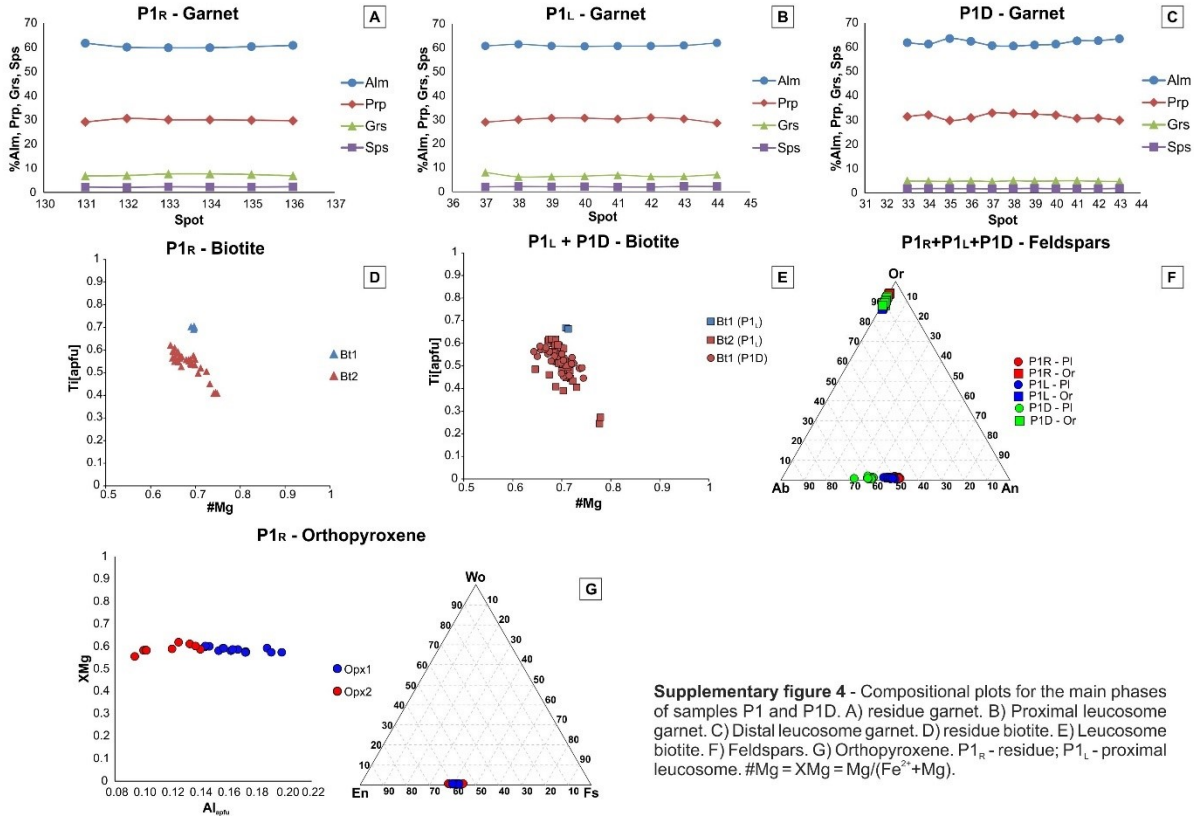

Supplementary figure 4 - Compositional plots for the main phases of samples P1 and P1D. A) residue garnet. B) Proximal leucosome garnet. C) Distal leucosome garnet. D) residue biotite. E) Leucosome biotite. F) Feldspars. G) Orthopyroxene. $P1_R$ - residue; $P1_L$ - proximal leucosome. #Mg = XMg = Mg/(Fe^{2+}+Mg).

9.11 APPENDIX K – Supplementary data 1 (Chapter 5): Zircon LA-MC-ICP-MS results

Zircon LA-MC-ICP-MS U-Pb results - Amphibolite enclave (PC12.1)

							Isotope ratios[c]							Ages (Ma)						
Spot number	CL-domain	f_{206}[a]	Pb ppm	Th ppm	U ppm	Th/U[b]	207Pb/ 206Pb[e]	2 s [%]	207Pb/ 235U	2 s [%]	206Pb/ 238U	2 s [%]	Rho[d]	^{206}Pb/ ^{238}U	2 s abs	^{207}Pb/ ^{235}U	2 s abs	^{207}Pb/ ^{206}Pb	2 s abs	% Disc.[e]
PC-12-1_01	**c**	0.0209	4	33	22	1.50	0.19840	5.00	13.40514	5.05	0.49003	0.74	0.15	2571	19	2709	137	2813	141	9
PC-12-1_02	**r**	0.0050	3	26	26	0.98	0.06132	3.21	0.90833	4.43	0.10744	3.05	0.69	658	20	656	29	650	21	-1
PC-12-1_03	**r**	0.0021	13	136	92	1.47	0.06131	2.66	0.88767	2.96	0.10500	1.29	0.44	644	8	645	19	650	17	1
PC-12-1_04	**r**	0.0050	35	599	199	3.02	0.06209	3.03	0.93852	4.23	0.10963	2.95	0.70	671	20	672	28	677	21	1
PC-12-1_05	**c**	0.0010	38	554	223	2.48	0.06199	1.78	0.94208	3.27	0.11023	2.75	0.84	674	19	674	22	674	12	0
PC-12-1_06	**c**	0.0048	23	360	132	2.73	0.06232	2.15	0.96208	7.53	0.11196	7.21	0.96	684	49	684	52	685	15	0
PC-12-1_08	**r**	0.0033	19	269	107	2.51	0.06264	3.30	0.97297	4.37	0.11265	2.87	0.66	688	20	690	30	696	23	1
PC-12-1_09	**r**	0.0055	8	73	64	1.15	0.08605	3.35	2.65909	4.22	0.22411	2.58	0.61	1304	34	1317	56	1339	45	3
PC-12-1_10	**r**	0.0018	10	58	72	0.81	0.06209	1.99	0.94669	3.75	0.11058	3.18	0.85	676	21	676	25	677	13	0
PC-12-1_11	**c**	0.0022	29	361	135	2.67	0.06378	1.80	1.06024	5.81	0.12056	5.52	0.95	734	41	734	43	734	13	0
PC-12-1_12	**r**	0.0049	24	317	122	2.58	0.06484	2.27	1.07590	4.12	0.12035	3.44	0.84	733	25	742	31	769	17	5
PC-12-1_14	**r**	0.0015	36	557	200	2.79	0.06357	1.61	1.04894	3.52	0.11967	3.13	0.89	729	23	728	26	727	12	0
PC-12-1_15	**r**	0.0035	43	754	219	3.45	0.06388	2.16	1.05315	2.36	0.11957	0.96	0.41	728	7	730	17	738	16	1
PC-12-1_16	**r**	0.0036	42	696	221	3.15	0.06205	2.25	0.94884	3.79	0.11090	3.06	0.81	678	21	677	26	676	15	0
PC-12-1_17	**r**	0.0037	32	441	199	2.22	0.06195	2.05	0.93635	4.54	0.10962	4.05	0.89	671	27	671	30	672	14	0
PC-12-1_18	**r**	0.0047	29	492	172	2.86	0.06188	2.83	0.93009	4.64	0.10901	3.68	0.79	667	25	668	31	670	19	0
PC-12-1_19	**r**	0.0024	15	177	96	1.84	0.06035	1.96	0.83758	3.41	0.10066	2.79	0.82	618	17	618	21	616	12	0
PC-12-1_20	**c**	0.0038	21	285	109	2.60	0.06526	1.60	1.15991	3.61	0.12891	3.24	0.90	782	25	782	28	783	13	0
PC-12-1_21	**c**	0.0029	22	157	150	1.05	0.06072	2.59	0.86051	6.51	0.10279	5.97	0.92	631	38	630	41	629	16	0
PC-12-1_22	**r**	0.0026	10	99	73	1.35	0.06121	1.91	0.88936	5.63	0.10538	5.29	0.94	646	34	646	36	647	12	0
PC-12-1_23	**r**	0.0007	58	901	306	2.94	0.06157	1.55	0.91188	3.96	0.10742	3.64	0.92	658	24	658	26	659	10	0
PC-12-1_24	**r**	0.0015	45	696	223	3.12	0.06175	1.48	0.92982	3.54	0.10920	3.21	0.91	668	21	668	24	666	10	0
PC-12-1_25	**c**	0.0023	58	980	285	3.44	0.06167	1.76	0.90752	2.19	0.10674	1.31	0.60	654	9	656	14	663	12	1
PC-12-1_26	**r**	0.0036	10	117	67	1.74	0.05988	3.30	0.80388	4.04	0.09737	2.33	0.58	599	14	599	24	599	20	0
PC-12-1_27	**c**	0.0129	32	528	174	3.04	0.06228	2.16	0.94903	3.50	0.11052	2.76	0.79	676	19	678	24	684	15	1

PC-12-1_28	**r**	0.0064	6	42	45	0.92	0.06043	3.79	0.84393	5.69	0.10128	4.24	0.75	622	26	621	35	619	23	0
PC-12-1_29	**c**	0.0039	33	495	187	2.65	0.06212	1.97	0.95116	3.78	0.11104	3.22	0.85	679	22	679	26	678	13	0
PC-12-1_30	**r**	0.0016	16	184	90	2.04	0.06087	2.66	0.86879	3.25	0.10352	1.86	0.57	635	12	635	21	635	17	0
PC-12-1_31	**r**	0.0003	27	410	156	2.63	0.06146	1.64	0.91613	2.23	0.10812	1.51	0.68	662	10	660	15	655	11	-1
PC-12-1_32	**c**	0.0016	8	65	52	1.27	0.06184	2.29	0.93576	6.43	0.10975	6.01	0.93	671	40	671	43	669	15	0
PC-12-1_33	**c**	0.0029	33	525	175	3.00	0.06104	1.74	0.88334	5.28	0.10497	4.98	0.94	643	32	643	34	640	11	0
PC-12-1_34	**c**	0.0012	10	125	67	1.87	0.06115	3.10	0.88296	5.13	0.10473	4.08	0.80	642	26	643	33	644	20	0
PC-12-1_35	**r**	0.0021	31	463	161	2.88	0.06125	3.20	0.89609	3.64	0.10610	1.73	0.48	650	11	650	24	648	21	0
PC-12-1_36	**c**	0.0093	7	76	44	1.71	0.06114	3.01	0.89895	3.44	0.10664	1.68	0.49	653	11	651	22	644	19	-1
PC-12-1_37	**c**	0.0085	8	87	50	1.73	0.06007	4.37	0.81474	6.39	0.09837	4.67	0.73	605	28	605	39	606	26	0
PC-12-1_38	**r**	0.0040	24	370	130	2.85	0.06416	1.58	1.08615	3.25	0.12278	2.84	0.87	747	21	747	24	747	12	0
PC-12-1_39	**c**	0.0021	18	249	96	2.60	0.06084	2.31	0.86764	3.08	0.10343	2.04	0.66	634	13	634	20	634	15	0
PC-12-1_40	**r**	0.0011	19	245	125	1.95	0.06145	1.69	0.91667	2.53	0.10818	1.87	0.74	662	12	661	17	655	11	-1
PC-12-1_41	**c**	0.0023	41	608	233	2.62	0.06147	2.07	0.90684	2.87	0.10699	1.99	0.69	655	13	655	19	656	14	0
PC-12-1_42	**r**	0.0053	18	183	130	1.41	0.06182	2.28	0.93149	3.93	0.10928	3.20	0.81	669	21	668	26	668	15	0
PC-12-1_43	**c**	0.0028	37	337	271	1.24	0.06076	1.55	0.85605	2.49	0.10219	1.95	0.78	627	12	628	16	631	10	1
PC-12-1_44	**r**	0.0044	20	288	114	2.52	0.06030	3.01	0.82321	5.99	0.09901	5.17	0.86	609	31	610	37	614	19	1
PC-12-1_45	**r**	0.0040	33	523	175	2.99	0.06120	1.69	0.89289	2.82	0.10582	2.25	0.80	648	15	648	18	646	11	0
PC-12-1_46	**r**	0.0018	10	55	81	0.68	0.06192	2.69	0.92784	3.37	0.10869	2.02	0.60	665	13	666	22	671	18	1
PC-12-1_47	**r**	0.0031	26	375	137	2.74	0.06209	2.40	0.95108	3.27	0.11109	2.23	0.68	679	15	679	22	677	16	0
PC-12-1_48	**r**	0.0047	39	173	274	0.63	0.06794	2.91	1.33764	3.61	0.14279	2.14	0.59	860	18	862	31	867	25	1
PC-12-1_49	**r**	0.0042	13	137	83	1.65	0.06140	2.10	0.90016	3.87	0.10632	3.25	0.84	651	21	652	25	653	14	0
PC-12-1_50	**r**	0.0008	12	114	80	1.41	0.06191	2.65	0.93928	3.27	0.11003	1.91	0.58	673	13	673	22	671	18	0
PC-12-1_51	**r**	0.0023	32	495	172	2.87	0.06127	1.54	0.89726	4.90	0.10620	4.66	0.95	651	30	650	32	649	10	0
PC-12-1_52	**r**	0.0015	33	472	179	2.64	0.06096	1.54	0.87728	4.27	0.10438	3.99	0.93	640	26	640	27	638	10	0
PC-12-1_53	**c**	0.0035	5	28	41	0.68	0.06365	5.70	1.05711	7.04	0.12046	4.13	0.59	733	30	732	52	730	42	0
PC-12-1_54	**r**	0.0020	7	47	54	0.88	0.06177	1.60	0.92594	3.27	0.10871	2.85	0.87	665	19	665	22	666	11	0
PC-12-1_55	**c**	0.0042	7	69	44	1.57	0.06189	3.37	0.93685	4.37	0.10979	2.78	0.64	672	19	671	29	670	23	0
PC-12-1_56	**c**	0.0042	28	485	141	3.45	0.06159	1.82	0.91771	2.57	0.10806	1.81	0.70	661	12	661	17	660	12	0
PC-12-1_57	**c**	0.0048	11	111	84	1.32	0.06193	2.55	0.92528	8.19	0.10837	7.78	0.95	663	52	665	54	672	17	1
PC-12-1_58	**c**	0.0024	27	447	159	2.81	0.06136	2.13	0.90230	3.05	0.10666	2.17	0.71	653	14	653	20	652	14	0
PC-12-1_59	**c**	0.0014	35	614	195	3.16	0.06171	2.03	0.92545	3.25	0.10876	2.54	0.78	666	17	665	22	664	13	0
PC-12-1_60	**c**	0.0014	17	238	100	2.38	0.06213	2.11	0.95232	2.57	0.11117	1.47	0.57	680	10	679	17	679	14	0

PC-12-1_61	**c**	0.0015	22	303	121	2.50	0.06110	1.68	0.88245	2.86	0.10476	2.31	0.81	642	15	642	18	643	11	0
PC-12-1_62	**c**	0.0031	37	576	198	2.90	0.06114	1.83	0.88662	5.57	0.10517	5.26	0.94	645	34	645	36	644	12	0
PC-12-1_63	**c**	0.0009	15	205	92	2.23	0.06078	1.87	0.84664	2.34	0.10102	1.41	0.60	620	9	623	15	632	12	2
PC-12-1_64	**c**	0.0026	49	297	389	0.76	0.06072	1.76	0.85653	2.31	0.10231	1.49	0.65	628	9	628	15	629	11	0
PC-12-1_65	**r**	0.0014	33	547	180	3.03	0.06187	1.59	0.92673	2.93	0.10864	2.47	0.84	665	16	666	20	669	11	1
PC-12-1_66	**c**	0.0023	35	519	174	2.98	0.06117	2.09	0.89242	5.07	0.10581	4.62	0.91	648	30	648	33	645	13	0
PC-12-1_67	**r**	0.0020	34	527	191	2.76	0.06163	1.79	0.91557	2.56	0.10775	1.83	0.72	660	12	660	17	661	12	0
PC-12-1_68	**r**	0.0028	24	400	141	2.85	0.06125	2.54	0.88955	2.88	0.10534	1.37	0.47	646	9	646	19	648	16	0
PC-12-1_69	**c**	0.0033	9	75	64	1.18	0.06086	2.31	0.86985	4.78	0.10367	4.19	0.88	636	27	635	30	634	15	0
PC-12-1_70	**r**	0.0047	18	218	133	1.63	0.06523	2.01	1.15621	3.08	0.12856	2.33	0.76	780	18	780	24	782	16	0
PC-12-1_71	**c**	0.0014	21	339	124	2.74	0.06111	1.94	0.88388	2.55	0.10489	1.66	0.65	643	11	643	16	643	12	0
PC-12-1_72	**c**	0.0029	24	136	181	0.75	0.06076	1.96	0.85420	3.32	0.10196	2.68	0.81	626	17	627	21	631	12	1
PC-12-1_73	**r**	0.0022	44	523	264	1.98	0.06147	1.54	0.91053	4.96	0.10742	4.72	0.95	658	31	657	33	656	10	0
PC-12-1_74	**c**	0.0043	11	117	73	1.60	0.06226	2.28	0.95621	3.06	0.11139	2.03	0.66	681	14	681	21	683	16	0
PC-12-1_75	**c**	0.0016	25	337	160	2.10	0.06219	2.49	0.95183	3.21	0.11100	2.03	0.63	679	14	679	22	681	17	0
PC-12-1_76	**r**	0.0024	10	98	62	1.58	0.06080	2.63	0.86745	4.33	0.10347	3.44	0.79	635	22	634	27	632	17	0
PC-12-1_77	**c**	0.0042	15	82	106	0.77	0.06114	1.94	0.89330	2.59	0.10597	1.71	0.66	649	11	648	17	644	13	-1
PC-12-1_78	**r**	0.0018	47	654	239	2.73	0.06162	1.53	0.92080	3.80	0.10837	3.48	0.92	663	23	663	25	661	10	0
PC-12-1_79	**r**	0.0049	15	185	98	1.90	0.06095	2.75	0.87109	4.17	0.10365	3.13	0.75	636	20	636	27	638	18	0
PC-12-1_80	**c**	0.0045	10	106	64	1.65	0.06195	2.77	0.93587	5.11	0.10956	4.30	0.84	670	29	671	34	672	19	0
PC-12-1_81	**c**	0.0024	37	548	213	2.57	0.06180	1.96	0.92001	4.17	0.10797	3.68	0.88	661	24	662	28	667	13	1
PC-12-1_82	**r**	0.0021	27	358	159	2.25	0.06322	3.80	1.02734	4.82	0.11786	2.97	0.62	718	21	718	35	716	27	0
PC-12-1_83	**r**	0.0008	17	248	106	2.34	0.06143	1.62	0.90171	2.36	0.10646	1.72	0.73	652	11	653	15	654	11	0
PC-12-1_84	**c**	0.0033	53	855	242	3.53	0.06238	1.59	0.96268	3.82	0.11193	3.47	0.91	684	24	685	26	687	11	0
PC-12-1_85	**c**	0.0035	24	303	135	2.25	0.06327	1.75	1.02452	5.07	0.11744	4.76	0.94	716	34	716	36	717	13	0
PC-12-1_86	**r**	0.0027	34	105	297	0.35	0.06045	1.37	0.84293	3.57	0.10114	3.29	0.92	621	20	621	22	620	8	0
PC-12-1_87	**r**	0.0031	14	191	77	2.49	0.06252	2.03	0.95952	8.09	0.11132	7.82	0.97	680	53	683	55	692	14	2
PC-12-1_88	**c**	0.0045	25	360	132	2.72	0.06154	2.35	0.91398	3.47	0.10771	2.55	0.74	659	17	659	23	658	15	0
PC-12-1_89	**c**	0.0016	25	137	195	0.70	0.06160	2.15	0.91829	3.90	0.10812	3.25	0.83	662	22	661	26	660	14	0
PC-12-1_90	**c**	0.0014	24	338	152	2.22	0.06184	1.75	0.93626	4.77	0.10981	4.44	0.93	672	30	671	32	668	12	0

aFraction of the non-radiogenic ^{206}Pb in the analyzed zircon spot, where f_{206}=[$^{206}Pb/^{204}Pb$]c/[$^{206}Pb/^{204}Pb$]s (c=common; s=sample)

bTh/U ratios and amount of Pb, Th and U (in pmm) are calculated relative to 91500 reference zircon

cCorrected for background and within-run Pb/U fractionation and normalised to reference zircon GJ-1 (ID-TIMS values/measured value); $^{207}Pb/^{235}U$ calculated using ($^{207}Pb/^{206}Pb$)/($^{238}U/^{206}Pb$ * 1/137.88)

dRho is the error correlation defined as the quotient of the propagated errors of the $^{206}Pb/^{238}U$ and the $^{207}/^{235}U$ ratio

eDegree of discordance = 100 - ($^{206}Pb/^{238}U$ age * 100/$^{207}Pb/^{206}U$ age)

c-core

r-rim

s-single phase

Hf isotopes results determined by LA-ICP-MS - Amphibolite enclave (PC12.1)

Grain#	CL-Domain	$^{176}Yb/^{177}Hf$ [a]	±2s	$^{176}Lu/^{177}Hf$ [a]	±2s	$^{178}Hf/^{177}Hf$	$^{180}Hf/^{177}Hf$	Sig_{Hf} [b] (V)	$^{176}Hf/^{177}Hf$	±2s [c]	age [f] (Ma)	±2s	$^{176}Hf/^{177}Hf_{(t)}$ [d]	eHf(t) [d]	±2s [c]	age [f] (Ma)	±2s	eHf(t) [d]	±2s [c]
											(measured)					(pref./min.)			
PC-12-1_06	**c**	0.056963	46	0.001707	10	1.467246	1.886757	13.709733	0.282021	18	684	49	0.281999	-12.5	0.79	782	25	-10.4	0.79
PC-12-1_08	**r**	0.043920	36	0.001320	8	1.467175	1.886671	14.800869	0.282037	17	688	20	0.282020	-11.7	0.73	782	25	-9.7	0.73
PC-12-1_12	**r**	0.051239	41	0.001608	10	1.467191	1.886950	13.697324	0.282005	19	733	25	0.281983	-12.0	0.76	782	25	-11.0	0.76
PC-12-1_17	**r**	0.043395	36	0.001417	9	1.467197	1.886751	9.636598	0.282042	16	671	27	0.282024	-12.0	0.74	782	25	-9.6	0.74
PC-12-1_19	**r**	0.083093	67	0.002600	16	1.467225	1.886708	12.207516	0.281986	17	618	17	0.281956	-15.5	0.92	782	25	-12.2	0.92
PC-12-1_20	**c**	0.051271	47	0.001545	11	1.467198	1.886683	13.804868	0.282034	21	782	25	0.282011	-9.9	0.79	782	25	-9.9	0.79
PC-12-1_26	**r**	0.039991	41	0.001221	10	1.467230	1.886789	15.502279	0.282039	25	599	14	0.282025	-13.5	0.76	782	25	-9.6	0.76
PC-12-1_29	**c**	0.050214	42	0.001565	10	1.467212	1.886889	14.094015	0.282029	14	679	22	0.282009	-12.3	0.76	782	25	-10.1	0.76
PC-12-1_30	**r**	0.030818	25	0.001071	7	1.467264	1.886687	11.755867	0.282052	16	635	12	0.282039	-12.2	0.69	782	25	-9.0	0.69
PC-12-1_32	**c**	0.019385	17	0.000583	4	1.467195	1.886803	18.222236	0.282065	22	671	40	0.282058	-10.8	0.66	782	25	-8.3	0.66
PC-12-1_44	**c**	0.031642	26	0.000994	6	1.467236	1.886830	15.335769	0.282052	16	627	12	0.282040	-12.4	0.69	782	25	-9.0	0.69
PC-12-1_50	**r**	0.084615	75	0.002448	17	1.467272	1.887004	12.485566	0.282028	17	651	30	0.281998	-13.3	0.99	782	25	-10.6	0.99
PC-12-1_53	**c**	0.042198	35	0.001394	9	1.467332	1.886685	7.073004	0.282056	15	733	30	0.282037	-10.1	0.73	782	25	-9.0	0.73
PC-12-1_54	**r**	0.021353	17	0.000749	5	1.467302	1.886914	10.043916	0.282051	19	665	19	0.282042	-11.4	0.66	782	25	-8.9	0.66
PC-12-1_59	**c**	0.070378	58	0.002040	13	1.467243	1.886781	15.298003	0.282013	18	666	17	0.281988	-13.4	0.86	782	25	-10.9	0.86

PC-12-1_64	**c**	0.047275	38	0.001534	9	1.467234	1.886698	10.612906	0.282000	19	628	9	0.281981	-14.4	0.74	782	25	-11.1	0.74
PC-12-1_70	**r**	0.025304	21	0.000757	5	1.467236	1.886802	16.325610	0.282062	18	780	18	0.282051	-8.5	0.67	782	25	-8.5	0.67
PC-12-1_84	**c**	0.076146	63	0.002315	15	1.467189	1.886939	13.789396	0.281986	16	684	24	0.281956	-14.1	0.90	782	25	-12.0	0.90
PC-12-1_86	**c**	0.016493	13	0.000569	4	1.467247	1.886800	12.677075	0.282051	18	621	20	0.282044	-12.3	0.65	782	25	-8.8	0.65
PC-12-1_87	**c**	0.019159	15	0.000667	4	1.467296	1.886739	9.878690	0.282082	16	680	53	0.282074	-10.0	0.66	782	25	-7.7	0.66

(a) $^{176}Yb/^{177}Hf = (^{176}Yb/^{173}Yb)_{true} \times (^{173}Yb/^{177}Hf)_{meassured} \times (M_{173(Yb)}/M_{177(Hf)})^{b(Hf)}$, $b(Hf) = \ln(^{179}Hf/^{177}Hf_{\ true} / {}^{179}Hf/^{177}Hf_{measured}) / \ln (M_{179(Hf)}/M_{177(Hf)})$

M=mass of respective isotope. The $^{176}Lu/^{177}Hf$ were calculated in a similar way by using the $^{175}Lu/^{177}Hf$ and b(Yb)

(b) Mean Hf signal in volt

(c) Uncertainties are quadratic additions of the within-run precision and the daily reproducibility of the zircon standards. Uncertainties for the standard quoted at 2SD (2 standard deviation)

(d) Initial $^{176}Hf/^{177}Hf$ and ƐHf calculated using the apparent Pb-Pb ages of respective zircon domains, and the CHUR parameters: $^{176}Lu/^{177}Hf = 0.0336$, and $^{176}Hf/^{177}Hf = 0.282785$ (Bouvier et al., 2008)

(e) Two stage model age in billion years using the measured $^{176}Lu/^{177}Lu$ of each spot (first stage = age of zircon), a value of 0.0113 for the average continental crust (second stage), and a average MORB (DM) $^{176}Lu/^{177}Hf$ and $^{176}Hf/^{177}Hf$ of 0.0384 and 0.283164

Bouvier, A., Vervoort, J.D., Patchett, P.J., 2008. The Lu-Hf and Sm-Nd isotopic composition of CHUR: constraints from unequilibrated chondrites and implications for the bulk composition of terrestrial planets. Earth and Planetary Science Letters 273, 48-57.

(f) $^{206}Pb/^{238}U$ age

c-core

r-rim

s-single phase

Zircon LA-MC-ICP-MS U-Pb results - Hornblende-biotite stromatic metatexite (PC12.2)

							Isotope ratios[c]							Ages (Ma)						
Spot number	CL-domain	f_{206}[a]	Pb ppm	Th ppm	U ppm	Th/U[b]	207Pb/ 206Pb[e]	2 s [%]	207Pb/ 235U	2 s [%]	206Pb/ 238U	2 s [%]	Rho[d]	^{206}Pb/ ^{238}U	2 s abs	^{207}Pb/ ^{235}U	2 s abs	^{207}Pb/ ^{206}Pb	2 s abs	% Disc.[e]
PC-12_2-002	r	0.2360	35	74	316	0.24	0.06049	2.33	0.84923	3.80	0.10182	3.00	0.79	625	4	624	4	621	13	-1
PC-12_2-004	r	0.0000	66	212	598	0.36	0.05940	1.80	0.78697	5.86	0.09608	5.58	0.95	591	8	589	7	582	10	-2
PC-12_2-005	r	0.0000	68	186	521	0.36	0.06189	1.87	0.95189	5.25	0.11156	4.91	0.93	682	8	679	7	670	10	-2
PC-12_2-006	c	0.0000	11	43	68	0.63	0.06355	3.32	1.07585	4.12	0.12278	2.43	0.59	747	4	742	5	727	18	-3
PC-12_2-007	c	0.0000	87	102	919	0.11	0.05932	1.80	0.77962	2.63	0.09531	1.92	0.73	587	3	585	3	579	10	-1
PC-12_2-008	c	0.0000	97	251	774	0.32	0.06181	1.82	0.94356	2.51	0.11072	1.73	0.69	677	3	675	3	667	10	-1
PC-12_2-009	c	0.0000	85	220	668	0.33	0.06192	2.04	0.94817	3.04	0.11106	2.26	0.74	679	4	677	4	671	11	-1
PC-12_2-010	r	2.5843	31	105	245	0.43	0.06117	13.62	0.89966	13.95	0.10668	3.04	0.22	653	5	652	17	645	73	-1
PC-12_2-012	c	0.6016	100	69	977	0.07	0.06097	3.56	0.88241	17.05	0.10497	16.67	0.98	643	26	642	20	638	19	-1
PC-12_2-013	r	0.0000	72	102	696	0.15	0.06055	1.91	0.85816	3.12	0.10279	2.47	0.79	631	4	629	4	623	10	-1
PC-12_2-014	c	0.0637	67	191	479	0.40	0.06335	1.90	1.05147	3.46	0.12038	2.89	0.84	733	5	730	5	720	10	-2
PC-12_2-015	r	0.0000	46	44	412	0.11	0.06216	1.98	0.96430	3.66	0.11251	3.08	0.84	687	5	686	5	680	11	-1
PC-12_2-016	r	0.0000	68	159	533	0.30	0.06263	2.06	0.99844	2.48	0.11563	1.38	0.56	705	2	703	3	696	11	-1
PC-12_2-017	c	0.0000	108	215	858	0.25	0.06279	1.75	1.01198	2.56	0.11689	1.87	0.73	713	3	710	3	701	9	-2
PC-12_2-018	c	0.0000	54	146	478	0.30	0.06021	1.93	0.83964	3.59	0.10115	3.03	0.84	621	4	619	4	611	10	-2
PC-12_2-019	c	0.0000	79	147	626	0.23	0.06309	1.75	1.03350	2.50	0.11881	1.80	0.72	724	3	721	3	711	9	-2
PC-12_2-021	c	0.6023	20	19	113	0.17	0.07209	3.55	1.66215	4.58	0.16722	2.91	0.63	997	7	994	7	989	18	-1
PC-12_2-022	c	0.0000	66	139	552	0.25	0.06116	1.83	0.89772	3.09	0.10646	2.50	0.81	652	4	651	4	645	10	-1
PC-12_2-023	c	0.0000	76	164	616	0.27	0.06170	1.87	0.93483	3.08	0.10989	2.45	0.79	672	4	670	4	664	10	-1
PC-12_2-024	c	0.7272	14	33	106	0.31	0.06296	17.13	0.97047	17.81	0.11179	4.86	0.27	683	8	689	23	707	91	3
PC-12_2-025	c	0.0000	77	143	629	0.23	0.06239	1.85	0.98124	3.86	0.11406	3.38	0.88	696	6	694	5	688	10	-1
PC-12_2-026	c	0.0000	123	120	1126	0.11	0.06163	1.77	0.93943	3.64	0.11056	3.18	0.87	676	5	673	4	661	9	-2
PC-12_2-027	r	0.0000	54	54	538	0.10	0.06017	1.89	0.83493	2.48	0.10064	1.60	0.65	618	2	616	3	610	10	-1
PC-12_2-028	c	8.2731	104	102	1112	0.09	0.05922	43.71	0.77001	44.80	0.09431	9.86	0.22	581	14	580	51	575	238	-1
PC-12_2-029	r	1.1026	63	163	601	0.27	0.05958	5.31	0.75223	6.32	0.09157	3.42	0.54	565	5	570	7	588	29	4
PC-12_2-030	c	0.0000	54	68	504	0.13	0.06102	4.13	0.88825	4.36	0.10557	1.37	0.32	647	2	645	5	640	22	-1
PC-12_2-032	c	0.0000	103	341	765	0.45	0.06109	2.26	0.88823	3.32	0.10545	2.43	0.73	646	4	645	4	642	12	-1

PC-12_2-033	**r**	0.0000	49	43	415	0.10	0.06295	1.89	1.02459	2.37	0.11804	1.44	0.60	719	2	716	3	707	10	-2
PC-12_2-034	**c**	0.0000	17	17	201	0.08	0.05767	2.72	0.68596	12.80	0.08627	12.51	0.98	533	16	530	13	517	15	-3
PC-12_2-035	**r**	0.0000	81	152	638	0.24	0.06312	1.90	1.03628	2.26	0.11907	1.23	0.54	725	2	722	3	712	10	-2
PC-12_2-036	**r**	0.0000	103	107	917	0.12	0.06203	1.76	0.96468	6.48	0.11280	6.24	0.96	689	10	686	8	675	9	-2
PC-12_2-037	**c**	0.0000	56	144	404	0.36	0.06320	1.83	1.04159	2.66	0.11953	1.93	0.72	728	3	725	3	715	10	-2
PC-12_2-038	**r**	0.0000	51	59	437	0.14	0.06248	5.09	0.96259	5.63	0.11174	2.40	0.43	683	4	685	7	691	27	1
PC-12_2-039	**c**	0.2752	12	46	83	0.56	0.06183	3.02	0.95129	3.41	0.11159	1.59	0.47	682	3	679	4	668	16	-2
PC-12_2-040	**s**	0.0000	22	114	146	0.78	0.06119	2.34	0.90507	2.62	0.10728	1.18	0.45	657	2	654	3	646	13	-2
PC-12_2-041	**c**	0.0000	61	91	482	0.19	0.06363	1.76	1.05934	2.44	0.12074	1.68	0.69	735	3	733	3	729	9	-1
PC-12_2-042	**c**	2.1324	43	46	333	0.14	0.06504	9.28	1.09163	9.59	0.12173	2.40	0.25	741	4	749	13	776	49	5
PC-12_2-043	**c**	0.0000	102	202	756	0.27	0.06408	2.00	1.09861	2.85	0.12434	2.03	0.71	755	4	753	4	744	11	-1
PC-12_2-044	**c**	0.0000	57	64	467	0.14	0.06359	1.96	1.06905	2.75	0.12193	1.93	0.70	742	3	738	4	728	10	-2
PC-12_2-045	**c**	0.0000	127	280	947	0.30	0.06342	1.77	1.05568	2.75	0.12072	2.10	0.77	735	4	732	4	722	9	-2
PC-12_2-046	**c**	0.5921	93	44	997	0.04	0.05990	3.72	0.81512	12.55	0.09869	11.99	0.96	607	17	605	14	600	20	-1
PC-12_2-047	**c**	0.0000	47	106	346	0.31	0.06368	2.01	1.07623	2.98	0.12257	2.20	0.74	745	4	742	4	731	11	-2
PC-12_2-048	**r**	0.0000	67	122	483	0.25	0.06448	1.99	1.13165	2.95	0.12728	2.17	0.74	772	4	769	4	758	10	-2
PC-12_2-049	**r**	0.0000	97	200	686	0.29	0.06489	1.83	1.15472	2.94	0.12907	2.30	0.78	783	4	779	4	771	10	-2
PC-12_2-050	**c**	0.0000	141	106	1220	0.09	0.06298	1.68	1.03097	9.54	0.11873	9.39	0.98	723	16	719	12	708	9	-2
PC-12_2-051	**c**	0.0000	82	157	595	0.26	0.06459	1.87	1.12718	3.14	0.12656	2.53	0.80	768	5	766	4	761	10	-1
PC-12_2-052	**c**	0.2677	60	220	429	0.51	0.06195	2.30	0.96008	2.98	0.11241	1.89	0.64	687	3	683	4	672	12	-2
PC-12_2-053	**c**	0.0000	60	98	494	0.20	0.06250	1.83	0.99068	2.35	0.11496	1.48	0.63	701	2	699	3	691	10	-1
PC-12_2-054	**c**	0.0536	60	106	499	0.21	0.06206	1.99	0.95558	2.51	0.11168	1.53	0.61	682	2	681	3	676	11	-1
PC-12_2-055	**c**	0.1837	72	172	625	0.27	0.06077	4.67	0.84991	5.24	0.10144	2.37	0.45	623	4	625	6	631	25	1
PC-12_2-056	**c**	0.0000	112	383	811	0.47	0.06162	1.87	0.92836	2.63	0.10927	1.85	0.70	669	3	667	3	661	10	-1
PC-12_2-058	**r**	0.8801	124	304	917	0.33	0.06316	4.90	1.03693	5.24	0.11907	1.85	0.35	725	3	722	7	714	26	-2
PC-12_2-059	**r**	0.0000	43	57	318	0.18	0.06456	2.02	1.13775	3.74	0.12782	3.14	0.84	775	6	771	5	760	11	-2
PC-12_2-060	**c**	0.2563	11	36	79	0.45	0.06190	2.99	0.94728	3.44	0.11099	1.71	0.50	679	3	677	4	671	16	-1
PC-12_2-061	**c**	0.0000	47	46	470	0.10	0.06029	2.03	0.83897	3.06	0.10093	2.29	0.75	620	3	619	4	614	11	-1
PC-12_2-062	**c**	0.5368	80	84	801	0.11	0.06033	3.58	0.83138	5.87	0.09995	4.65	0.79	614	7	614	7	615	19	0
PC-12_2-064	**c**	0.0000	88	202	615	0.33	0.06461	1.98	1.13041	4.53	0.12689	4.08	0.90	770	7	768	6	762	10	-1
PC-12_2-065	**r**	0.0000	129	240	967	0.25	0.06388	4.64	1.08205	4.90	0.12285	1.57	0.32	747	3	745	6	738	25	-1
PC-12_2-066	**c**	0.0000	62	200	410	0.49	0.06416	1.94	1.10593	2.78	0.12501	1.99	0.72	759	4	756	4	747	10	-2
PC-12_2-067	**c**	0.0000	51	77	402	0.19	0.06346	2.60	1.04818	3.22	0.11980	1.89	0.59	729	3	728	4	724	14	-1

PC-12_2-070	**r**	0.0000	50	89	354	0.25	0.06483	2.91	1.16100	3.46	0.12989	1.87	0.54	787	3	782	5	769	15	-2
PC-12_2-071	**c**	0.0000	55	100	404	0.25	0.06429	2.84	1.11943	3.62	0.12629	2.25	0.62	767	4	763	5	751	15	-2
PC-12_2-072	**c**	0.0000	27	68	223	0.31	0.06119	3.77	0.90702	4.76	0.10751	2.92	0.61	658	5	655	6	646	20	-2
PC-12_2-073	**c**	0.0000	58	108	425	0.25	0.06426	5.72	1.09338	7.04	0.12340	4.10	0.58	750	7	750	9	750	30	0
PC-12_2-074	**c**	0.0000	30	41	256	0.16	0.06220	3.33	0.97758	5.37	0.11400	4.21	0.78	696	7	692	7	681	18	-2
PC-12_2-075	**r**	0.0000	26	24	276	0.09	0.05923	7.77	0.79927	20.50	0.09787	18.97	0.93	602	27	596	23	575	42	-5
PC-12_2-076	**c**	0.1171	44	67	346	0.19	0.06325	4.92	1.02348	5.87	0.11736	3.19	0.54	715	5	716	8	717	26	0
PC-12_2-077	**c**	1.0827	38	166	256	0.65	0.06158	7.15	0.93488	8.08	0.11010	3.77	0.47	673	6	670	10	660	38	-2
PC-12_2-078	**c**	0.4947	90	193	736	0.26	0.06133	23.75	0.88020	31.71	0.10408	21.02	0.66	638	32	641	38	651	127	2
PC-12_2-079	**c**	1.0824	6	25	38	0.65	0.06085	9.90	0.88390	11.24	0.10535	5.31	0.47	646	8	643	13	634	53	-2
PC-12_2-080	**c**	0.0000	35	38	255	0.15	0.06524	3.53	1.19561	4.56	0.13291	2.89	0.63	804	5	799	6	782	19	-3
PC-12_2-082	**c**	0.1772		153	319	0.48	0.06538	2.45	1.17864	2.67	0.13074	1.07	0.40	792	8	791	15	787	51	0
PC-12_2-083	**c**	0.0692		314	826	0.38	0.06500	2.78	1.14940	3.02	0.12824	1.19	0.39	778	9	777	17	774	58	0
PC-12_2-084	**c**	0.0000		853	946	0.90	0.06551	3.54	1.17107	3.83	0.12965	1.47	0.38	786	11	787	21	791	74	0
PC-12_2-085	**c**	1.0000		374	635	0.59	0.06560	3.79	1.15697	4.23	0.12791	1.88	0.44	776	14	781	23	794	80	-1
PC-12_2-086	**c**	0.1389		155	910	0.17	0.06278	2.34	0.98987	2.57	0.11435	1.06	0.41	698	7	699	13	701	50	0
PC-12_2-087	**c**	1.0000		569	315	1.81	0.06353	3.94	1.04173	4.41	0.11893	2.00	0.45	724	14	725	23	726	83	0
PC-12_2-088	**c**	1.0000		145	340	0.43	0.06583	3.80	1.18035	4.23	0.13004	1.86	0.44	788	14	791	24	801	80	0
PC-12_2-089	**c**	0.2452		240	332	0.72	0.06521	3.04	1.17127	3.32	0.13027	1.33	0.40	789	10	787	18	781	64	0
PC-12_2-090	**c**	0.0185		159	1499	0.11	0.06181	2.88	0.91843	3.14	0.10777	1.26	0.40	660	8	662	15	667	62	0
PC-12_2-092	**c**	0.0000		170	298	0.57	0.06455	3.10	1.07923	3.34	0.12126	1.24	0.37	738	9	743	18	760	65	-1
PC-12_2-093	**c**	1.0000		372	717	0.52	0.06461	4.98	1.11566	5.48	0.12523	2.29	0.42	761	16	761	30	762	105	0
PC-12_2-094	**c**	0.0000		281	380	0.74	0.06486	2.28	1.13199	2.53	0.12658	1.09	0.43	768	8	769	14	770	48	0
PC-12_2-096	**c**	0.0060		673	835	0.81	0.06528	2.24	1.16679	2.46	0.12964	1.03	0.42	786	8	785	14	783	47	0
PC-12_2-097	**c**	0.1408		769	766	1.00	0.06553	2.30	1.17120	2.54	0.12963	1.09	0.43	786	8	787	14	791	48	0
PC-12_2-099	**c**	0.0808		314	347	0.90	0.06343	2.28	1.02297	2.55	0.11697	1.14	0.45	713	8	715	13	723	48	0
PC-12_2-100	**c**	1.0000		108	260	0.42	0.06331	3.95	1.01016	4.47	0.11572	2.10	0.47	706	14	709	23	719	84	0
PC-12_2-102	**c**	1.0000		165	222	0.75	0.06394	3.93	1.06006	4.41	0.12024	2.01	0.46	732	14	734	23	740	83	0
PC-12_2-104	**c**	0.1452		222	404	0.55	0.06414	2.41	1.07515	2.70	0.12158	1.21	0.45	740	8	741	14	746	51	0
PC-12_2-105	**c**	0.0266		191	1531	0.12	0.06103	2.52	0.88942	2.77	0.10569	1.14	0.41	648	7	646	13	640	54	0
PC-12_2-107	**c**	0.1044		146	230	0.64	0.06355	2.48	1.03935	2.75	0.11861	1.19	0.43	723	8	724	14	727	53	0
PC-12_2-108	**c**	0.0803		307	427	0.72	0.06367	2.28	1.03632	2.55	0.11805	1.16	0.45	719	8	722	13	731	48	0
PC-12_2-109	**c**	0.0905		218	421	0.52	0.06350	2.63	1.03466	2.90	0.11817	1.23	0.42	720	8	721	15	725	56	0

PC-12_2-110	**c**	1.3343	68	178	0.38	0.06233	5.72	1.01156	6.45	0.11771	2.99	0.46	717	20	710	33	685	122	1
PC-12_2-111	**c**	0.0000	226	388	0.58	0.06297	2.57	0.99890	2.84	0.11505	1.20	0.42	702	8	703	15	707	55	0
PC-12_2-112	**c**	0.0339	799	1283	0.62	0.06354	2.17	1.02518	2.45	0.11702	1.13	0.46	713	8	717	13	726	46	0
PC-12_2-114	**c**	0.1080	489	595	0.82	0.06233	2.56	0.95089	2.89	0.11064	1.33	0.46	676	9	679	14	686	55	0
PC-12_2-116	**c**	0.0000	224	391	0.57	0.06298	2.73	1.01217	3.04	0.11656	1.34	0.44	711	9	710	16	708	58	0
PC-12_2-117	**c**	0.0000	68	332	0.21	0.06330	2.84	1.02176	3.15	0.11707	1.37	0.43	714	9	715	16	718	60	0
PC-12_2-118	**c**	0.0917	308	632	0.49	0.06355	2.35	1.03117	2.67	0.11768	1.27	0.48	717	9	720	14	727	50	0
PC-12_2-119	**c**	0.0000	58	59	0.98	0.06086	3.52	0.85735	3.88	0.10217	1.64	0.42	627	10	629	18	634	76	0
PC-12_2-121	**c**	0.0000	247	452	0.55	0.06331	2.46	1.02987	2.76	0.11798	1.24	0.45	719	8	719	14	719	52	0
PC-12_2-122	**c**	0.3217	429	783	0.55	0.06333	2.58	1.02506	2.94	0.11740	1.41	0.48	716	10	716	15	719	55	0
PC-12_2-123	**c**	0.0000	170	154	1.10	0.06362	2.58	1.03281	2.88	0.11774	1.29	0.45	718	9	720	15	729	55	0
PC-12_2-125	**c**	0.1167	226	466	0.48	0.06288	2.48	0.99889	2.76	0.11522	1.21	0.44	703	8	703	14	704	53	0
PC-12_2-126	**c**	0.0000	167	753	0.22	0.06061	3.43	0.88291	3.75	0.10565	1.51	0.40	647	9	643	18	625	74	1
PC-12_2-127	**c**	0.0556	128	287	0.45	0.06412	2.97	1.07291	3.27	0.12135	1.37	0.42	738	10	740	17	746	63	0
PC-12_2-128	**c**	0.0000	209	381	0.55	0.06353	3.37	1.04589	3.71	0.11940	1.56	0.42	727	11	727	19	726	71	0
PC-12_2-130	**c**	0.0000	20	38	0.52	0.06347	3.25	1.03107	3.59	0.11782	1.53	0.43	718	10	719	19	724	69	0
PC-12_2-131	**c**	0.0244	634	825	0.77	0.06396	2.82	1.05454	3.11	0.11957	1.32	0.43	728	9	731	16	740	60	0
PC-12_2-132	**c**	0.2010	288	473	0.61	0.06397	2.07	1.03657	2.43	0.11752	1.27	0.52	716	9	722	13	741	44	-1
PC-12_2-133	**c**	2.4858	125	331	0.38	0.06256	8.36	1.07573	9.43	0.12472	4.36	0.46	758	31	742	51	693	178	2
PC-12_2-134	**c**	0.0000	182	331	0.55	0.06348	2.33	1.03727	2.64	0.11851	1.25	0.47	722	9	723	14	724	49	0
PC-12_2-135	**c**	0.1375	168	377	0.45	0.06275	2.40	0.98508	2.71	0.11385	1.27	0.47	695	8	696	14	700	51	0
PC-12_2-136	**c**	0.1998	62	429	0.14	0.06181	2.61	0.92684	2.94	0.10876	1.36	0.46	666	9	666	14	667	56	0
PC-12_2-138	**c**	0.0000	349	382	0.91	0.06277	2.93	0.97374	3.27	0.11251	1.44	0.44	687	9	690	16	700	62	0
PC-12_2-140	**c**	0.0351	79	697	0.11	0.06144	2.18	0.90836	2.51	0.10723	1.23	0.49	657	8	656	12	655	47	0
PC-12_2-141	**c**	0.0000	129	214	0.60	0.06433	2.27	1.06979	2.60	0.12061	1.28	0.49	734	9	739	14	752	48	-1
PC-12_2-143	**c**	0.0077	143	486	0.29	0.06350	2.14	1.01021	2.47	0.11539	1.23	0.50	704	8	709	13	725	45	-1
PC-12_2-144	**c**	0.0272	48	271	0.18	0.06277	2.01	0.98167	2.38	0.11342	1.27	0.53	693	8	694	12	701	43	0
PC-12_2-145	**c**	0.0000	109	344	0.32	0.06217	2.03	0.95329	2.43	0.11121	1.35	0.55	680	9	680	12	680	43	0
PC-12_2-148	**c**	0.2779	435	493	0.88	0.06331	2.12	1.01683	2.52	0.11648	1.36	0.54	710	9	712	13	719	45	0
PC-12_2-149	**c**	0.1202	228	419	0.54	0.06376	2.69	1.02731	3.04	0.11685	1.40	0.46	712	9	718	16	734	57	-1
PC-12_2-150	**c**	0.1095	289	399	0.72	0.06389	1.97	1.02900	2.34	0.11681	1.26	0.54	712	9	718	12	738	42	-1
PC-12_2-151	**c**	0.3592	1208	2249	0.54	0.06155	2.11	0.89912	2.56	0.10595	1.45	0.57	649	9	651	12	658	45	0
PC-12_2-152	**c**	1.0739	131	898	0.15	0.06113	4.16	0.96224	4.83	0.11417	2.47	0.51	697	16	684	24	644	89	2

PC-12_2-153	**c**	0.0000	52	1058	0.05	0.06212	2.00	0.94045	2.36	0.10980	1.26	0.53	672	8	673	12	678	43	0
PC-12_2-154	**c**	1.0000	75	247	0.31	0.06388	3.86	1.03388	4.41	0.11738	2.14	0.49	715	15	721	23	738	82	-1
PC-12_2-155	**c**	0.0332	82	245	0.33	0.06272	2.08	0.99950	2.44	0.11558	1.28	0.53	705	9	704	12	699	44	0
PC-12_2-156	**c**	0.0000	186	418	0.44	0.06264	2.30	0.98598	2.63	0.11416	1.28	0.49	697	8	697	13	696	49	0
PC-12_2-157	**c**	0.2225	91	396	0.23	0.06470	2.07	1.12645	2.49	0.12628	1.39	0.56	767	10	766	13	764	44	0
PC-12_2-158	**c**	0.1078	322	561	0.57	0.06313	2.15	1.01426	2.50	0.11652	1.27	0.51	711	9	711	13	713	46	0
PC-12_2-159	**c**	0.0000	120	801	0.15	0.06201	2.68	0.93100	3.04	0.10889	1.43	0.47	666	9	668	15	674	57	0
PC-12_2-160	**c**	0.0000	31	159	0.20	0.06125	2.22	0.87340	2.61	0.10342	1.37	0.53	634	8	637	12	648	48	0
PC-12_2-161	**c**	0.0000	98	216	0.46	0.06314	2.41	1.00212	2.76	0.11511	1.36	0.49	702	9	705	14	713	51	0
PC-12_2-162	**c**	0.0000	98	214	0.46	0.06376	2.10	1.05785	2.48	0.12033	1.31	0.53	732	9	733	13	734	45	0
PC-12_2-163	**c**	1.2194	56	178	0.31	0.06347	4.54	1.08833	5.20	0.12437	2.53	0.49	756	18	748	28	724	96	1
PC-12_2-164	**c**	0.4897	302	401	0.75	0.06384	2.57	1.07847	3.05	0.12253	1.63	0.53	745	11	743	16	736	55	0
PC-12_2-166	**c**	0.0236	360	398	0.91	0.06295	2.10	0.98210	2.47	0.11316	1.31	0.53	691	9	695	13	706	45	-1
PC-12_2-167	**c**	0.0000	587	738	0.80	0.06425	3.08	1.07643	3.46	0.12151	1.56	0.45	739	11	742	18	750	65	0
PC-12_2-168	**c**	0.7544	609	1042	0.58	0.06181	3.14	1.01365	3.72	0.11894	1.99	0.53	724	14	711	19	668	67	2
PC-12_2-169	**c**	1.0000	136	414	0.33	0.06300	3.91	1.00391	4.48	0.11557	2.18	0.49	705	15	706	23	708	83	0
PC-12_2-171	**c**	0.0000	267	477	0.56	0.06323	2.21	1.02953	2.69	0.11809	1.52	0.57	720	10	719	14	716	47	0
PC-12_2-172	**c**	0.1454	111	591	0.19	0.06276	2.25	0.97036	2.62	0.11214	1.35	0.51	685	9	689	13	700	48	-1
PC-12_2-173	**c**	0.0000	109	326	0.33	0.06279	2.17	0.97665	2.55	0.11281	1.35	0.53	689	9	692	13	701	46	0
PC-12_2-174	**c**	0.0220	619	2850	0.22	0.06238	2.28	0.96067	2.63	0.11170	1.31	0.50	683	8	684	13	687	49	0
PC-12_2-175	**c**	1.4944	71	603	0.12	0.05945	5.60	0.86442	6.52	0.10546	3.35	0.51	646	21	633	31	584	121	2
PC-12_2-176	**r**	0.0652	46	209	0.22	0.06070	3.04	0.88590	3.63	0.10585	1.99	0.55	649	12	644	17	629	65	1
PC-12_2-177	**c**	1.0000	184	620	0.30	0.06163	3.96	0.91542	4.58	0.10773	2.30	0.50	660	14	660	22	661	85	0
PC-12_2-178	**r**	0.1899	56	347	0.16	0.06074	2.80	0.83888	3.19	0.10016	1.53	0.48	615	9	619	15	630	60	-1
PC-12_2-179	**c**	1.0000	359	690	0.52	0.06338	3.85	1.01843	4.42	0.11654	2.18	0.49	711	15	713	23	721	82	0
PC-12_2-181	**r**	0.0000	54	161	0.33	0.06114	6.08	0.87756	6.68	0.10410	2.75	0.41	638	17	640	32	644	131	0
PC-12_2-182	**c**	0.1449	48	220	0.22	0.06277	2.43	1.00038	2.82	0.11559	1.42	0.50	705	10	704	14	700	52	0
PC-12_2-183	**c**	0.2786	235	509	0.46	0.06344	2.17	1.03002	2.60	0.11775	1.42	0.55	718	10	719	13	723	46	0
PC-12_2-184	**c**	0.0116	211	419	0.50	0.06360	2.48	1.02060	2.86	0.11638	1.41	0.49	710	9	714	15	728	53	-1
PC-12_2-185	**c**	0.9050	33	171	0.19	0.06176	4.07	0.98049	4.73	0.11515	2.42	0.51	703	16	694	24	666	87	1
PC-12_2-187	**c**	0.0000	90	206	0.44	0.06297	2.16	0.97580	2.57	0.11239	1.39	0.54	687	9	691	13	707	46	-1
PC-12_2-188	**c**	1.0000	84	279	0.30	0.06245	4.02	0.95117	4.64	0.11047	2.31	0.50	675	15	679	23	689	86	0
PC-12_2-189	**c**	0.3479	294	418	0.70	0.06320	2.31	1.02188	2.69	0.11727	1.39	0.52	715	9	715	14	715	49	0

PC-12_2-190	**c**	0.0000	148	342	0.43	0.06271	2.39	0.98189	2.72	0.11356	1.30	0.48	693	9	695	14	698	51	0
PC-12_2-191	**c**	1.6674	588	871	0.68	0.05989	6.04	0.92046	6.96	0.11146	3.47	0.50	681	22	663	34	600	131	3
PC-12_2-192	**c**	0.0000	90	221	0.41	0.06297	2.51	0.99282	2.82	0.11435	1.29	0.46	698	9	700	14	707	53	0
PC-12_2-193	**c**	0.5599	202	280	0.72	0.06303	3.12	1.02002	3.58	0.11738	1.75	0.49	715	12	714	19	709	66	0
PC-12_2-194	**c**	0.1597	313	433	0.72	0.06356	3.40	1.03829	3.77	0.11848	1.61	0.43	722	11	723	20	727	72	0

aFraction of the non-radiogenic ^{206}Pb in the analyzed zircon spot, where f_{206}=[$^{206}Pb/^{204}Pb$]c/[$^{206}Pb/^{204}Pb$]s (c=common; s=sample)

bTh/U ratios and amount of Pb, Th and U (in pmm) are calculated relative to 91500 reference zircon

cCorrected for background and within-run Pb/U fractionation and normalised to reference zircon GJ-1 (ID-TIMS values/measured value); $^{207}Pb/^{235}U$ calculated using ($^{207}Pb/^{206}Pb$)/($^{238}U/^{206}Pb$ * 1/137.88)

dRho is the error correlation defined as the quotient of the propagated errors of the $^{206}Pb/^{238}U$ and the $^{207}/^{235}U$ ratio

eDegree of discordance = 100 - ($^{206}Pb/^{238}U$ age * 100/$^{207}Pb/^{206}U$ age)

c-core

r-rim

s-single phase

Hf isotopes results determined by LA-ICP-MS - Hornblende-biotite stromatic metatexite (PC12.2)

Grain#	CL-Domain	$^{176}Yb/^{177}Hf$ [a]	±2s	$^{176}Lu/^{177}Hf$ [a]	±2s	$^{178}Hf/^{177}Hf$	$^{180}Hf/^{177}Hf$	Sig_{Hf} [b] (V)	$^{176}Hf/^{177}Hf$	±2s [c]	age [f] (Ma)	±2s	$^{176}Hf/^{177}Hf_{(t)}$ [d]	eHf(t) [d]	±2s [c]	age [f] (Ma)	±2s	eHf(t) [d]	±2s [c]
											(measured)					(pref./min.)			
PC-12-2_01	**r**	0.024751	20	0.000997	7	1.467180	1.886818	20.478544	0.281994	13	557	11	0.281984	-15.9	0.97	789	10	-10.9	0.97
PC-12-2_03	**c**	0.020221	16	0.000809	5	1.467167	1.886855	21.033306	0.282003	13	755	4	0.281991	-11.2	0.95	789	10	-10.5	0.95
PC-12-2_04	**r**	0.018701	15	0.000715	4	1.467191	1.886789	14.120506	0.282083	24	591	8	0.282075	-11.9	0.96	786	8	-7.6	0.96
PC-12-2_05	**r**	0.022200	18	0.000889	5	1.467164	1.886899	20.561613	0.282029	17	682	8	0.282018	-11.9	0.97	789	10	-9.6	0.97
PC-12-2_06	**c**	0.027061	22	0.001096	7	1.467153	1.886814	13.135065	0.282191	13	747	4	0.282176	-4.9	0.95	776	14	-4.2	0.95
PC-12-2_08	**c**	0.021735	19	0.000856	6	1.467215	1.886138	14.166473	0.282000	19	770	7	0.281987	-11.0	0.95	789	10	-10.6	0.95
PC-12-2_09	**c**	0.024687	21	0.000941	6	1.467258	1.886090	13.713349	0.281993	17	679	4	0.281981	-13.3	0.95	789	10	-10.9	0.95

PC-12-2_12	**c**	0.015813	16	0.000551	4	1.467217	1.886007	13.177385	0.281991	19	643	26	0.281984	-14.0	0.95	789	10	-10.7	0.95
PC-12-2_15	**r**	0.010947	10	0.000441	3	1.467260	1.884553	12.294717	0.282010	20	687	5	0.282004	-12.3	0.96	789	10	-10.0	0.96
PC-12-2_16	**r**	0.020352	17	0.000794	5	1.467253	1.885830	13.430758	0.282079	16	705	2	0.282069	-9.6	0.97	786	8	-7.8	0.97
PC-12-2_17	**c**	0.040384	32	0.001552	9	1.467178	1.886857	16.097653	0.281902	17	713	3	0.281882	-16.1	0.95	804	5	-14.1	0.95
PC-12-2_18	**c**	0.030736	25	0.001147	7	1.467213	1.886816	18.523887	0.282076	21	621	4	0.282063	-11.7	0.95	786	8	-8.1	0.95
PC-12-2_19	**c**	0.016354	20	0.000645	6	1.467270	1.885733	13.854870	0.281963	15	724	3	0.281954	-13.2	0.95	789	10	-11.8	0.95
PC-12-2_21	**c**	0.010551	8	0.000425	3	1.467190	1.886924	19.460954	0.281953	15	997	7	0.281945	-7.4	0.95	997	7	-7.4	0.95
PC-12-2_22	**c**	0.017536	21	0.000672	7	1.467229	1.885377	12.281226	0.281918	23	652	4	0.281910	-16.4	0.95	804	5	-13.1	0.95
PC-12-2_23	**c**	0.020221	16	0.000809	5	1.467167	1.886855	21.033306	0.282003	13	722	11	0.281992	-12.0	0.95	789	10	-10.5	0.95
PC-12-2_24	**c**	0.034095	34	0.001286	10	1.467225	1.886260	12.175223	0.281856	20	683	8	0.281839	-18.2	0.96	804	5	-15.6	0.96
PC-12-2_25	**c**	0.022504	34	0.000862	11	1.467279	1.886247	12.408044	0.281988	17	696	6	0.281976	-13.1	0.96	789	10	-11.0	0.96
PC-12-2_26	**c**	0.016482	28	0.000643	9	1.467356	1.884252	8.761386	0.281970	32	676	5	0.281962	-14.0	0.96	789	10	-11.5	0.96
PC-12-2_30	**c**	0.010376	9	0.000397	2	1.467372	1.882370	8.020597	0.282030	45	715	12	0.282024	-10.9	0.95	789	10	-9.3	0.95
PC-12-2_32	**c**	0.038313	46	0.001523	16	1.467314	1.885470	9.158260	0.282052	25	723	16	0.282031	-10.5	0.96	786	8	-9.2	0.96
PC-12-2_33	**r**	0.008017	16	0.000329	6	1.467168	1.886442	15.289718	0.282031	17	719	2	0.282027	-10.8	0.96	789	10	-9.2	0.96
PC-12-2_35	**r**	0.014150	15	0.000558	5	1.467244	1.886301	13.413611	0.281993	17	725	2	0.281986	-12.1	0.96	789	10	-10.7	0.96
PC-12-2_36	**r**	0.022453	19	0.000814	6	1.467257	1.885345	12.384610	0.282029	18	689	10	0.282018	-11.7	0.97	789	10	-9.5	0.97
PC-12-2_37	**c**	0.035085	45	0.001314	14	1.467177	1.886324	11.992440	0.282102	18	728	3	0.282084	-8.5	0.96	786	8	-7.3	0.96
PC-12-2_39	**c**	0.024701	20	0.000981	6	1.467156	1.886879	10.345184	0.282187	18	682	3	0.282175	-6.4	0.95	776	14	-4.3	0.95
PC-12-2_40	**s**	0.031206	28	0.001185	8	1.467215	1.886564	8.798158	0.282249	23	657	2	0.282235	-4.8	0.99	776	14	-2.2	0.99
PC-12-2_41	**c**	0.013796	11	0.000533	3	1.467192	1.886914	16.648682	0.281961	22	735	3	0.281954	-13.0	0.95	789	10	-11.8	0.95
PC-12-2_43	**c**	0.030942	25	0.001224	7	1.467190	1.886796	15.904277	0.282002	21	687	9	0.281986	-12.9	0.95	789	10	-10.7	0.95
PC-12-2_44	**c**	0.019391	16	0.000761	5	1.467225	1.885881	14.581167	0.281970	14	742	3	0.281959	-12.7	0.95	789	10	-11.6	0.95
PC-12-2_45	**c**	0.034683	33	0.001330	10	1.467203	1.886839	15.163588	0.282025	14	676	9	0.282008	-12.4	0.96	789	10	-10.0	0.96
PC-12-2_46	**c**	0.009359	8	0.000374	2	1.467239	1.886185	15.144921	0.281992	19	677	3	0.281987	-13.1	0.95	789	10	-10.6	0.95
PC-12-2_47	**c**	0.019285	31	0.000742	8	1.467230	1.886570	14.032636	0.282124	17	745	4	0.282113	-7.1	0.95	786	8	-6.2	0.95
PC-12-2_48	**r**	0.034166	27	0.001318	8	1.467164	1.886788	15.389011	0.282008	14	772	4	0.281989	-10.9	0.99	789	10	-10.5	0.99
PC-12-2_49	**r**	0.028092	22	0.001094	7	1.467202	1.886860	15.018975	0.282077	20	783	4	0.282061	-8.1	0.98	786	8	-8.0	0.98
PC-12-2_50	**c**	0.017845	16	0.000651	5	1.467218	1.886431	13.878670	0.282050	18	710	9	0.282042	-10.4	0.95	786	8	-8.8	0.95
PC-12-2_51	**c**	0.018905	15	0.000746	5	1.467208	1.886900	13.000834	0.281950	16	768	5	0.281939	-12.8	0.95	789	10	-12.3	0.95
PC-12-2_52	**c**	0.040044	32	0.001553	9	1.467145	1.886978	9.715014	0.282167	15	687	3	0.282147	-7.2	0.96	776	14	-5.3	0.96
PC-12-2_53	**c**	0.052714	42	0.001983	12	1.467203	1.886878	17.850888	0.282194	14	701	2	0.282168	-6.2	0.96	776	14	-4.6	0.96
PC-12-2_54	**c**	0.010061	8	0.000410	2	1.467185	1.886841	15.352513	0.281975	20	682	2	0.281969	-13.6	0.95	789	10	-11.3	0.95

PC-12-2_55	**c**	0.014620	12	0.000480	3	1.467212	1.886903	13.400897	0.282021	15	693	8	0.282015	-11.8	0.95	789	10	-9.6	0.95
PC-12-2_56	**c**	0.021219	17	0.000843	5	1.467182	1.886862	13.182021	0.281946	20	669	3	0.281935	-15.2	0.95	789	10	-12.5	0.95
PC-12-2_58	**r**	0.026652	21	0.001039	6	1.467225	1.886737	12.834379	0.281912	16	725	3	0.281898	-15.2	0.97	804	5	-13.5	0.97
PC-12-2_59	**r**	0.015765	16	0.000610	6	1.467201	1.886084	12.152797	0.281913	23	775	6	0.281904	-13.9	0.96	804	5	-13.2	0.96
PC-12-2_60	**c**	0.008400	7	0.000351	2	1.467201	1.886418	13.159228	0.282052	18	660	14	0.282047	-11.4	0.95	786	8	-8.6	0.95
PC-12-2_61	**c**	0.017150	18	0.000671	6	1.467229	1.886183	9.751029	0.282246	17	620	3	0.282238	-5.5	0.95	776	14	-2.1	0.95
PC-12-2_62	**c**	0.016853	15	0.000638	4	1.467264	1.886063	15.700657	0.281973	17	614	7	0.281965	-15.3	0.95	789	10	-11.4	0.95
PC-12-2_63	**r**	0.023500	25	0.001011	9	1.467225	1.886524	9.615375	0.282241	22	693	4	0.282228	-4.2	0.98	776	14	-2.4	0.98
PC-12-2_64	**c**	0.023450	19	0.000956	6	1.467241	1.886847	15.614073	0.282003	15	672	4	0.281991	-13.1	0.95	789	10	-10.5	0.95
PC-12-2_65	**r**	0.021514	17	0.000839	5	1.467240	1.886938	15.552792	0.281924	21	747	3	0.281912	-14.2	0.97	804	5	-13.0	0.97
PC-12-2_66	**c**	0.023555	19	0.000937	6	1.467211	1.886754	14.504053	0.282089	21	759	4	0.282076	-8.1	0.95	786	8	-7.6	0.95
PC-12-2_67	**c**	0.017190	21	0.000653	6	1.467236	1.886461	13.638782	0.281942	17	729	3	0.281933	-13.9	0.95	789	10	-12.5	0.95
PC-12-2_71	**c**	0.017637	14	0.000690	4	1.467132	1.886752	13.305423	0.281842	15	767	4	0.281832	-16.6	0.95	804	5	-15.8	0.95
PC-12-2_72	**c**	0.019638	16	0.000809	5	1.467177	1.886786	11.609493	0.282196	20	658	5	0.282186	-6.5	0.95	776	14	-3.9	0.95
PC-12-2_73	**c**	0.017875	14	0.000727	4	1.467164	1.886860	15.632574	0.281967	14	750	7	0.281957	-12.5	0.95	789	10	-11.7	0.95
PC-12-2_74	**c**	0.014712	18	0.000558	6	1.467212	1.886163	14.122489	0.281986	19	696	7	0.281978	-13.0	0.95	789	10	-10.9	0.95
PC-12-2_76	**c**	0.018984	15	0.000708	4	1.467214	1.886893	16.353892	0.281941	18	715	5	0.281932	-14.2	0.95	789	10	-12.6	0.95
PC-12-2_78	**c**	0.021571	21	0.000801	6	1.467267	1.885335	11.327349	0.281952	20	638	32	0.281943	-15.6	0.95	789	10	-12.2	0.95
PC-12-2_80	**c**	0.024774	20	0.000938	6	1.467191	1.886850	18.090945	0.281895	15	804	5	0.281880	-14.0	0.95	804	5	-14.0	0.95
PC-12_2-082	**c**	0.026491	21	0.001031	6	1.467209	1.886890	9.615332	0.281892	19	792	8	0.281877	-14.4	0.95	804	5	-14.2	0.95
PC-12_2-083	**c**	0.029163	23	0.001143	7	1.467223	1.886891	9.685784	0.282150	22	778	9	0.282133	-5.7	0.95	786	8	-5.5	0.95
PC-12_2-084	**c**	0.033757	27	0.001354	8	1.467298	1.886892	8.286156	0.281937	20	786	11	0.281917	-13.1	0.95	804	5	-12.7	0.95
PC-12_2-085	**c**	0.031082	25	0.001188	7	1.467177	1.886933	9.882498	0.282215	23	776	14	0.282198	-3.4	0.95	776	14	-3.4	0.95
PC-12_2-086	**c**	0.013877	11	0.000568	3	1.467278	1.886799	10.715469	0.282160	19	698	7	0.282153	-6.8	0.95	776	14	-5.1	0.95
PC-12_2-087	**c**	0.047854	38	0.001790	11	1.467174	1.886781	8.708572	0.282169	17	724	14	0.282145	-6.5	0.96	776	14	-5.4	0.96
PC-12_2-088	**c**	0.016095	16	0.000682	6	1.467243	1.886835	9.592867	0.281964	18	788	14	0.281953	-11.8	0.95	789	10	-11.8	0.95
PC-12_2-089	**c**	0.027379	22	0.001048	6	1.467254	1.886923	9.403405	0.281991	23	789	10	0.281976	-11.0	0.95	789	10	-11.0	0.95
PC-12_2-090	**c**	0.036994	30	0.001328	8	1.467152	1.886967	6.730797	0.282167	33	660	8	0.282151	-7.7	0.95	776	14	-5.2	0.95
PC-12_2-092	**c**	0.022720	18	0.000903	5	1.467224	1.886777	9.917840	0.282148	19	738	9	0.282135	-6.5	0.95	786	8	-5.5	0.95
PC-12_2-093	**c**	0.029917	47	0.001160	20	1.467219	1.886760	11.545634	0.282218	18	761	16	0.282201	-3.7	0.97	776	14	-3.3	0.97
PC-12_2-094	**c**	0.024604	33	0.000983	11	1.467260	1.886861	10.940013	0.282191	22	768	8	0.282177	-4.4	0.96	776	14	-4.2	0.96
PC-12_2-096	**c**	0.037812	43	0.001451	15	1.467211	1.886823	10.390806	0.282138	18	786	8	0.282117	-6.1	0.96	786	8	-6.1	0.96
PC-12_2-109	**c**	0.024130	47	0.000986	19	1.467207	1.886835	10.083896	0.282179	22	720	8	0.282166	-5.8	0.97	776	14	-4.6	0.97

PC-12_2-114	**c**	0.014806	12	0.000588	4	1.467151	1.886730	9.735314	0.282014	22	711	15	0.282006	-11.7	0.95	789	10	-9.9	0.95
PC-12_2-116	**c**	0.031293	68	0.001259	27	1.467272	1.886905	10.208367	0.282210	19	711	9	0.282193	-5.1	0.99	776	14	-3.7	0.99
PC-12_2-117	**c**	0.026364	21	0.001054	6	1.467195	1.886956	10.687688	0.282116	21	714	9	0.282102	-8.2	0.95	786	8	-6.7	0.95
PC-12_2-118	**c**	0.025696	35	0.000962	10	1.467267	1.886784	10.752268	0.282191	20	717	9	0.282178	-5.4	0.96	776	14	-4.2	0.96
PC-12_2-128	**c**	0.034134	36	0.001297	14	1.467234	1.886773	8.594260	0.282084	24	727	11	0.282066	-9.2	0.96	786	8	-7.9	0.96
PC-12_2-134	**c**	0.033054	29	0.001301	9	1.467263	1.886799	9.539262	0.282129	23	722	9	0.282111	-7.7	0.96	786	8	-6.3	0.96
PC-12_2-135	**c**	0.037015	34	0.001381	10	1.467259	1.886857	9.250504	0.282071	19	683	4	0.282053	-10.7	0.96	786	8	-8.4	0.96
PC-12_2-143	**c**	0.026822	22	0.001119	7	1.467230	1.886837	10.348074	0.282185	18	704	8	0.282170	-6.0	0.95	776	14	-4.5	0.95
PC-12_2-144	**c**	0.011023	21	0.000459	9	1.467248	1.886792	9.677833	0.282024	20	647	2	0.282018	-12.7	0.95	789	10	-9.5	0.95
PC-12_2-145	**c**	0.015679	17	0.000623	6	1.467261	1.886802	10.775488	0.282058	19	695	8	0.282050	-10.5	0.95	786	8	-8.5	0.95
PC-12_2-148	**c**	0.031657	26	0.001214	8	1.467275	1.886818	8.726263	0.281985	19	710	9	0.281969	-13.0	0.95	789	10	-11.3	0.95
PC-12_2-149	**c**	0.029213	46	0.001083	17	1.467243	1.886789	8.744760	0.281988	22	745	11	0.281973	-12.1	0.97	789	10	-11.1	0.97
PC-12_2-150	**c**	0.026818	22	0.001063	7	1.467214	1.886888	10.493198	0.282089	16	712	9	0.282075	-9.2	0.95	786	8	-7.6	0.95
PC-12_2-151	**c**	0.056917	47	0.002385	15	1.467196	1.886840	10.704210	0.282237	23	649	9	0.282208	-5.9	0.96	776	14	-3.3	0.96
PC-12_2-159	**c**	0.015855	13	0.000633	4	1.467231	1.886767	10.605760	0.282092	19	666	9	0.282084	-9.9	0.95	786	8	-7.3	0.95
PC-12_2-162	**c**	0.033431	28	0.001299	8	1.467209	1.886778	8.605542	0.282093	28	732	9	0.282075	-8.7	0.95	786	8	-7.6	0.95
PC-12_2-164	**c**	0.027694	23	0.001044	7	1.467186	1.886798	7.986067	0.281987	22	712	9	0.281974	-12.8	0.95	789	10	-11.1	0.95
PC-12_2-166	**c**	0.016771	14	0.000652	4	1.467196	1.886859	10.333002	0.282096	25	691	9	0.282087	-9.3	0.95	786	8	-7.2	0.95
PC-12_2-171	**c**	0.027148	25	0.001070	8	1.467250	1.886806	8.769363	0.282076	22	720	10	0.282062	-9.5	0.95	786	8	-8.1	0.95
PC-12_2-177	**c**	0.031325	25	0.001201	7	1.467202	1.886676	9.529891	0.282064	21	680	9	0.282049	-10.9	0.95	786	8	-8.6	0.95
PC-12_2-178	**r**	0.010237	8	0.000389	2	1.467244	1.886902	8.709657	0.282051	17	615	9	0.282047	-12.4	0.95	786	8	-8.6	0.95
PC-12_2-179	**c**	0.048948	39	0.001820	11	1.467263	1.886751	7.669010	0.282035	24	623	4	0.282014	-13.4	0.96	789	10	-9.9	0.96
PC-12_2-181	**r**	0.009559	8	0.000381	2	1.467273	1.886762	10.226001	0.282073	18	638	17	0.282069	-11.1	0.95	786	8	-7.8	0.95
PC-12_2-182	**c**	0.010979	9	0.000462	3	1.467256	1.886802	9.776711	0.281947	22	705	10	0.281941	-14.1	0.95	789	10	-12.3	0.95
PC-12_2-183	**c**	0.031398	41	0.001242	15	1.467231	1.886858	8.780612	0.282176	20	718	10	0.282159	-6.1	0.96	776	14	-4.8	0.96
PC-12_2-184	**c**	0.024067	19	0.000956	6	1.467266	1.886845	9.698061	0.282056	21	679	3	0.282044	-11.1	0.95	786	8	-8.7	0.95
PC-12_2-187	**c**	0.038740	47	0.001460	16	1.467265	1.886861	8.672869	0.282005	21	607	17	0.281989	-14.6	0.96	789	10	-10.7	0.96
PC-12_2-188	**c**	0.014427	19	0.000595	7	1.467215	1.886905	11.111954	0.281983	20	675	15	0.281975	-13.6	0.95	789	10	-11.1	0.95
PC-12_2-192	**c**	0.018179	19	0.000734	7	1.467247	1.886773	10.196338	0.281954	21	698	9	0.281944	-14.2	0.95	789	10	-12.2	0.95
PC-12_2-193	**c**	0.034977	42	0.001344	14	1.467275	1.886626	9.086398	0.282047	24	646	4	0.282031	-12.3	0.96	786	8	-9.3	0.96
PC-12_2-194	**c**	0.025538	31	0.000994	11	1.467239	1.886962	8.877102	0.282008	17	735	4	0.281994	-11.6	0.96	789	10	-10.4	0.96

(a) $^{176}Yb/^{177}Hf = (^{176}Yb/^{173}Yb)_{true} \times (^{173}Yb/^{177}Hf)_{meassured} \times (M_{173(Yb)}/M_{177(Hf)})^{b(Hf)}$, $b(Hf) = \ln(^{179}Hf/^{177}Hf_{true} / {}^{179}Hf/^{177}Hf_{measured}) / \ln (M_{179(Hf)}/M_{177(Hf)})$

M=mass of respective isotope. The $^{176}Lu/^{177}Hf$ were calculated in a similar way by using the $^{175}Lu/^{177}Hf$ and b(Yb)

(b) Mean Hf signal in volt

(c) Uncertainties are quadratic additions of the within-run precision and the daily reproducibility of the zircon standards. Uncertainties for the standard quoted at 2SD (2 standard deviation)

(d) Initial $^{176}Hf/^{177}Hf$ and ƐHf calculated using the apparent Pb-Pb ages of respective zircon domains, and the CHUR parameters: $^{176}Lu/^{177}Hf = 0.0336$, and $^{176}Hf/^{177}Hf = 0.282785$ (Bouvier et al., 2008)

(e) Two stage model age in billion years using the measured $^{176}Lu/^{177}Lu$ of each spot (first stage = age of zircon), a value of 0.0113 for the average continental crust (second stage), and a average MORB (DM) $^{176}Lu/^{177}Hf$ and $^{176}Hf/^{177}Hf$ of 0.0384 and 0.283164

Bouvier, A., Vervoort, J.D., Patchett, P.J., 2008. The Lu-Hf and Sm-Nd isotopic composition of CHUR: constraints from unequilibrated chondrites and implications for the bulk composition of terrestrial planets. Earth and Planetary Science Letters 273, 48-57.

(f) $^{206}Pb/^{238}U$ age

c-core

r-rim

s-single phase

Zircon LA-MC-ICP-MS U-Pb results - Biotite-bearing pink leucosome (PC12.3)

							Isotope ratios[c]							Ages (Ma)						
Spot number	CL-domain	f_{206}[a]	Pb ppm	Th ppm	U ppm	Th/U[b]	207Pb/ 206Pb[e]	2 s [%]	207Pb/ 235U	2 s [%]	206Pb/ 238U	2 s [%]	Rho[d]	^{206}Pb/ ^{238}U	2 s abs	^{207}Pb/ ^{235}U	2 s abs	^{207}Pb/ ^{206}Pb	2 s abs	% Disc.[e]
PC-12-3_01	**c**	0.0000	15	56	112	0.50	0.06082	2.16	0.88425	3.59	0.10544	2.87	0.80	646	4	643	4	633	12	-2
PC-12-3_02	**r**	0.0000	15	48	114	0.42	0.06144	1.96	0.92695	3.26	0.10943	2.61	0.80	669	4	666	4	655	10	-2
PC-12-3_03	**c**	0.0000	19	83	130	0.64	0.06163	2.36	0.93952	3.47	0.11056	2.55	0.73	676	4	673	4	661	13	-2
PC-12-3_04	**c**	0.0000	20	80	133	0.60	0.06253	2.14	1.00328	3.24	0.11636	2.44	0.75	710	4	705	4	692	11	-2
PC-12-3_05	**r**	0.0000	13	40	101	0.40	0.06204	1.90	0.96815	4.48	0.11319	4.05	0.91	691	7	688	6	675	10	-2
PC-12-3_06	**c**	0.0000	8	24	71	0.33	0.06060	2.78	0.86976	3.84	0.10410	2.64	0.69	638	4	635	5	625	15	-2
PC-12-3_07	**c**	0.0000	19	86	135	0.64	0.06130	2.07	0.91737	3.12	0.10855	2.34	0.75	664	4	661	4	650	11	-2
PC-12-3_08	**r**	0.0000	19	66	137	0.49	0.06172	2.15	0.94575	4.44	0.11113	3.89	0.87	679	6	676	5	664	12	-2
PC-12-3_09	**r**	0.0000	11	31	82	0.38	0.06321	2.39	1.05173	3.95	0.12067	3.13	0.79	734	5	730	5	715	13	-3
PC-12-3_10	**c**	0.0000	13	46	99	0.47	0.06108	1.97	0.90121	3.96	0.10702	3.44	0.87	655	5	652	5	642	11	-2
PC-12-3_11	**c**	1.1382	23	95	157	0.61	1.62523	1.41	0.88318	2.46	0.10764	6.95	0.35	656	4	656	8	654	35	0
PC-12-3_12	**c**	0.0000	22	91	159	0.58	0.49427	2.88	0.87991	2.06	0.10819	2.85	0.72	637	3	637	3	637	11	0
PC-12-3_13	**c**	0.0293	21	91	156	0.58	0.50598	2.91	0.87796	2.15	0.10460	2.95	0.73	626	3	626	3	627	11	0
PC-12-3_14	**c**	0.1555	18	59	153	0.38	0.57429	2.40	0.87635	1.72	0.10552	2.87	0.60	616	3	617	3	617	12	0
PC-12-3_15	**r**	0.0000	20	68	155	0.44	0.50008	2.91	0.87825	2.12	0.10478	2.91	0.73	628	3	627	3	626	11	0
PC-12-3_16	**c**	0.0047	15	52	115	0.45	0.55379	2.70	0.87852	2.03	0.10326	3.00	0.68	629	3	629	4	629	12	0
PC-12-3_17	**c**	0.0799	12	39	91	0.43	0.62677	3.37	0.88730	3.93	0.10739	4.66	0.84	680	6	679	6	676	13	-1
PC-12-3_18	**r**	0.0000	16	60	125	0.48	0.52358	2.81	0.87550	2.07	0.10255	2.94	0.70	611	3	612	3	612	11	0
PC-12-3_19	**c**	0.3123	15	45	126	0.36	0.65739	1.98	0.87704	1.50	0.10350	3.03	0.50	621	2	621	4	621	14	0
PC-12-3_20	**c**	0.0000	23	87	171	0.51	0.54148	3.20	0.88136	2.88	0.10499	3.60	0.80	646	4	645	4	644	12	0
PC-12-3_21	**c**	0.5452	17	55	140	0.39	0.92185	1.39	0.87709	1.37	0.10191	3.93	0.35	621	2	621	5	621	20	0
PC-12-3_22	**r**	0.2618	22	96	167	0.57	0.06104	2.76	0.88400	3.70	0.10503	2.46	0.67	644	4	643	4	641	15	0
PC-12-3_23	**c**	0.0802	19	71	153	0.47	0.06037	2.75	0.83177	3.52	0.09993	2.20	0.62	614	3	615	4	617	15	0
PC-12-3_24	**c**	0.0000	28	104	233	0.45	0.06042	2.16	0.83915	2.98	0.10073	2.06	0.69	619	3	619	3	619	12	0
PC-12-3_25	**c**	0.3867	22	91	184	0.50	0.05918	3.48	0.75902	4.48	0.09302	2.82	0.63	573	4	573	5	574	19	0
PC-12-3_26	**c**	0.0000	21	78	170	0.46	0.06046	2.67	0.84391	3.27	0.10123	1.87	0.57	622	3	621	4	620	14	0
PC-12-3_27	**c**	0.0105	20	70	160	0.44	0.06066	2.58	0.85468	3.30	0.10218	2.05	0.62	627	3	627	4	627	14	0

PC-12-3_28	**r**	0.2633	26	110	203	0.54	0.06062	2.55	0.85329	3.69	0.10208	2.66	0.72	627	4	626	4	626	14	0
PC-12-3_29	**r**	0.0627	36	157	278	0.57	0.06068	2.30	0.85487	3.38	0.10217	2.48	0.73	627	4	627	4	628	12	0
PC-12-3_30	**c**	0.0000	14	40	118	0.34	0.06069	2.63	0.85680	3.30	0.10240	1.99	0.60	628	3	628	4	628	14	0
PC-12-3_31	**c**	0.1562	26	110	203	0.54	0.06072	2.39	0.85917	2.89	0.10262	1.62	0.56	630	2	630	3	629	13	0
PC-12-3_32	**r**	0.0000	24	77	194	0.40	0.06136	2.44	0.90378	3.54	0.10682	2.57	0.73	654	4	654	4	652	13	0
PC-12-3_33	**c**	0.4775	39	31	395	0.08	0.06054	3.49	0.83691	4.30	0.10026	2.51	0.58	616	4	617	5	623	19	1
PC-12-3_34	**r**	0.0923	22	69	185	0.37	0.06116	2.35	0.88914	2.90	0.10543	1.70	0.59	646	3	646	3	645	13	0
PC-12-3_35	**c**	0.1238	41	185	316	0.58	0.06057	2.22	0.84843	2.98	0.10159	1.98	0.67	624	3	624	3	624	12	0
PC-12-3_36	**r**	0.0000	21	79	172	0.46	0.06072	2.39	0.85986	2.86	0.10271	1.57	0.55	630	2	630	3	629	13	0
PC-12-3_37	**c**	0.0455	25	84	211	0.40	0.06040	2.40	0.83634	3.52	0.10043	2.57	0.73	617	4	617	4	618	13	0
PC-12-3_38	**r**	0.0000	21	73	176	0.42	0.06097	2.43	0.87607	3.05	0.10421	1.84	0.60	639	3	639	4	638	13	0
PC-12-3_39	**r**	0.0544	26	85	216	0.39	0.06089	2.37	0.86805	3.03	0.10340	1.89	0.62	634	3	635	4	635	13	0
PC-12-3_40	**c**	0.0000	33	142	246	0.58	0.06109	2.29	0.88556	2.79	0.10513	1.59	0.57	644	2	644	3	642	12	0
PC-12-3_41	**r**	0.0000	21	67	174	0.38	0.06117	2.20	0.88789	2.83	0.10528	1.78	0.63	645	3	645	3	645	12	0
PC-12-3_42	**r**	0.0000	24	96	172	0.56	0.06180	2.33	0.93324	3.37	0.10953	2.43	0.72	670	4	669	4	667	12	0
PC-12-3_43	**r**	0.0574	20	87	160	0.54	0.06003	4.63	0.81266	5.28	0.09819	2.55	0.48	604	4	604	6	605	25	0
PC-12-3_44	**r**	0.0501	21	76	172	0.44	0.06046	2.54	0.84118	3.11	0.10090	1.79	0.58	620	3	620	4	620	14	0
PC-12-3_45	**r**	0.0000	26	72	206	0.35	0.06184	2.79	0.93639	3.33	0.10982	1.81	0.54	672	3	671	4	669	15	0
PC-12-3_46	**c**	0.2110	34	157	256	0.62	0.05994	2.38	0.80523	3.33	0.09743	2.33	0.70	599	3	600	4	602	13	0
PC-12-3_47	**c**	0.0000	29	110	209	0.52	0.06169	2.43	0.92646	3.28	0.10892	2.21	0.67	666	3	666	4	663	13	0
PC-12-3_48	**c**	0.6063	34	148	269	0.55	0.05983	4.02	0.79997	4.60	0.09697	2.22	0.48	597	3	597	5	598	22	0
PC-12-3_49	**r**	0.2265	20	66	169	0.39	0.06031	2.58	0.83207	3.23	0.10006	1.94	0.60	615	3	615	4	615	14	0
PC-12-3_50	**r**	0.0547	27	126	215	0.58	0.06000	1.94	0.81031	2.91	0.09795	2.17	0.75	602	3	603	3	604	10	0
PC-12-3_51	**r**	0.0000	22	67	194	0.35	0.06044	2.29	0.84029	3.20	0.10083	2.23	0.70	619	3	619	4	619	12	0
PC-12-3_52	**c**	0.3448	47	74	366	0.20	0.06101	2.78	0.88089	3.18	0.10472	1.54	0.48	642	2	641	4	640	15	0
PC-12-3_53	**c**	0.0000	18	28	144	0.19	0.06150	2.20	0.91169	3.06	0.10752	2.13	0.70	658	3	658	4	657	12	0
PC-12-3_54	**c**	0.0000	18	27	133	0.21	0.06195	2.27	0.93792	2.74	0.10980	1.54	0.56	672	2	672	3	672	12	0
PC-12-3_55	**c**	0.0000	20	30	157	0.19	0.06168	2.26	0.92363	3.29	0.10861	2.39	0.73	665	4	664	4	663	12	0
PC-12-3_56	**c**	0.0000	24	36	180	0.20	0.06175	2.48	0.92772	2.88	0.10897	1.46	0.51	667	2	666	4	665	13	0
PC-12-3_57	**c**	0.0000	19	29	144	0.20	0.06142	2.68	0.90384	3.15	0.10673	1.66	0.53	654	3	654	4	654	14	0
PC-12-3_58	**c**	0.0000	25	39	190	0.21	0.06145	2.31	0.91045	3.07	0.10745	2.03	0.66	658	3	657	4	655	12	0
PC-12-3_59	**r**	0.0571	16	23	122	0.19	0.06231	2.68	0.96670	3.16	0.11251	1.67	0.53	687	3	687	4	685	14	0
PC-12-3_60	**r**	0.0000	17	25	126	0.20	0.06210	2.56	0.95365	3.19	0.11137	1.91	0.60	681	3	680	4	678	14	0

PC-12-3_61	**r**	0.0000	15	22	117	0.19	0.06239	2.91	0.97369	3.32	0.11319	1.59	0.48	691	3	690	4	687	16	-1
PC-12-3_62	**r**	0.2449	15	23	117	0.20	0.06057	2.74	0.84899	4.48	0.10166	3.54	0.79	624	5	624	5	624	15	0
PC-12-3_63	**c**	0.0000	16	24	117	0.21	0.06092	2.28	0.87237	3.01	0.10386	1.97	0.65	637	3	637	4	636	12	0
PC-12-3_64	**c**	0.1000	14	21	108	0.19	0.06078	2.58	0.86416	3.94	0.10312	2.97	0.76	633	4	632	5	631	14	0
PC-12-3_65	**r**	0.0000	9	13	73	0.19	0.06121	3.08	0.89261	3.76	0.10576	2.16	0.58	648	3	648	5	647	17	0
PC-12-3_66	**c**	0.0457	22	35	164	0.21	0.06022	2.70	0.82565	3.34	0.09943	1.97	0.59	611	3	611	4	612	15	0
PC-12-3_67	**r**	0.0343	14	23	118	0.20	0.06042	3.11	0.83765	3.46	0.10055	1.53	0.44	618	2	618	4	619	17	0
PC-12-3_68	**r**	0.0000	18	28	139	0.20	0.06124	2.55	0.89550	3.29	0.10605	2.08	0.63	650	3	649	4	648	14	0
PC-12-3_69	**c**	0.0000	16	25	130	0.19	0.06098	4.04	0.87930	4.52	0.10458	2.03	0.45	641	3	641	5	639	22	0
PC-12-3_71	**r**	0.0000	13	21	110	0.19	0.06068	2.28	0.85561	3.09	0.10227	2.09	0.68	628	3	628	4	628	12	0
PC-12-3_72	**c**	0.0000	17	26	133	0.19	0.06120	2.52	0.89179	3.15	0.10568	1.89	0.60	648	3	647	4	646	14	0
PC-12-3_73	**r**	0.5122	15	24	122	0.20	0.06091	3.99	0.85246	4.42	0.10151	1.90	0.43	623	3	626	5	636	21	2
PC-12-3_74	**r**	0.0000	16	24	126	0.19	0.06112	2.50	0.88510	3.17	0.10503	1.96	0.62	644	3	644	4	644	13	0
PC-12-3_75	**r**	0.0000	14	23	117	0.19	0.06051	2.99	0.84646	3.61	0.10146	2.03	0.56	623	3	623	4	622	16	0
PC-12-3_76	**c**	0.0000	27	44	216	0.20	0.06055	2.09	0.84813	2.61	0.10159	1.57	0.60	624	2	624	3	623	11	0
PC-12-3_77	**r**	0.0000	19	30	164	0.18	0.06107	2.19	0.88152	3.11	0.10470	2.21	0.71	642	3	642	4	642	12	0
PC-12-3_78	**c**	0.0000	14	22	121	0.18	0.06121	2.57	0.89332	3.28	0.10584	2.04	0.62	649	3	648	4	647	14	0
PC-12-3_79	**c**	0.0000	28	45	214	0.21	0.06106	2.74	0.88226	3.80	0.10480	2.63	0.69	642	4	642	5	641	15	0
PC-12-3_81	**r**	0.0127	18	28	144	0.20	0.06067	2.48	0.85421	3.19	0.10212	2.01	0.63	627	3	627	4	628	13	0

aFraction of the non-radiogenic ^{206}Pb in the analyzed zircon spot, where f_{206}=[$^{206}Pb/^{204}Pb$]c/[$^{206}Pb/^{204}Pb$]s (c=common; s=sample)

bTh/U ratios and amount of Pb, Th and U (in pmm) are calculated relative to 91500 reference zircon

cCorrected for background and within-run Pb/U fractionation and normalised to reference zircon GJ-1 (ID-TIMS values/measured value); $^{207}Pb/^{235}U$ calculated using ($^{207}Pb/^{206}Pb$)/($^{238}U/^{206}Pb$ * 1/137.88)

dRho is the error correlation defined as the quotient of the propagated errors of the $^{206}Pb/^{238}U$ and the $^{207}/^{235}U$ ratio

eDegree of discordance = 100 - ($^{206}Pb/^{238}U$ age * 100/$^{207}Pb/^{206}U$ age)

c-core

r-rim

s-single phase

Hf isotopes results determined by LA-ICP-MS - Biotite-bearing pink leucosome (PC12.3)

Grain#	CL-Domain	$^{176}Yb/^{177}Hf$ [a]	±2s	$^{176}Lu/^{177}Hf$ [a]	±2s	$^{178}Hf/^{177}Hf$	$^{180}Hf/^{177}Hf$	Sig_{Hf} [b] (V)	$^{176}Hf/^{177}Hf$	±2s [c]	age [f] (Ma)	±2s	$^{176}Hf/^{177}Hf_{(t)}$ [d]	eHf(t) [d]	±2s [c]	age [f] (Ma)	±2s	eHf(t) [d]	±2s [c]
											(measured)					(pref./min.)			
PC-12-3_01	**c**	0.022007	18	0.000825	5	1.467191	1.886894	17.549665	0.282000	17	646	4	0.281990	-13.7	0.8	691	3	-12.7	0.8
PC-12-3_03	**c**	0.018108	19	0.000690	6	1.467180	1.886969	15.037799	0.282013	14	676	4	0.282004	-12.5	0.8	691	3	-12.2	0.8
PC-12-3_06	**c**	0.020458	28	0.000778	10	1.467163	1.886840	15.965671	0.282005	18	638	4	0.281995	-13.7	0.8	691	3	-12.5	0.8
PC-12-3_09	**r**	0.014083	13	0.000553	4	1.467165	1.886821	18.233849	0.282032	15	734	5	0.282024	-10.5	0.8	789	10	-9.3	0.8
PC-12-3_11	**c**	0.021435	19	0.000807	6	1.467214	1.886828	15.130588	0.282005	19	656	4	0.281995	-13.3	0.8	691	3	-12.5	0.8
PC-12-3_13	**c**	0.024649	21	0.000935	6	1.467197	1.886895	15.926958	0.282000	20	626	3	0.281989	-14.2	0.8	691	3	-12.8	0.8
PC-12-3_16	**c**	0.011779	9	0.000456	3	1.467170	1.886871	18.706585	0.282022	15	629	3	0.282017	-13.1	0.8	691	3	-11.8	0.8
PC-12-3_19	**c**	0.020423	23	0.000786	7	1.467186	1.886713	13.890774	0.282022	19	621	2	0.282013	-13.5	0.8	691	3	-11.9	0.8
PC-12-3_21	**c**	0.021736	22	0.000838	7	1.467224	1.886855	13.123614	0.282024	19	628	3	0.282014	-13.2	0.8	691	3	-11.9	0.8
PC-12-3_23	**c**	0.022165	18	0.000836	5	1.467192	1.886802	14.350815	0.282011	16	616	3	0.282001	-14.0	0.8	691	3	-12.4	0.8
PC-12-3_27	**c**	0.013103	11	0.000514	3	1.467219	1.886944	13.770145	0.282037	13	611	3	0.282031	-13.0	0.8	691	3	-11.3	0.8
PC-12-3_28	**r**	0.020405	23	0.000780	8	1.467177	1.886880	14.625266	0.282011	22	621	2	0.282002	-13.9	0.8	691	3	-12.3	0.8
PC-12-3_28	**r**	0.018208	15	0.000699	4	1.467205	1.886966	14.821775	0.282011	18	627	4	0.282002	-13.7	0.8	691	3	-12.3	0.8
PC-12-3_29	**r**	0.020731	30	0.000800	10	1.467212	1.886878	15.148107	0.281993	17	627	4	0.281983	-14.4	0.8	691	3	-13.0	0.8
PC-12-3_31	**c**	0.020063	21	0.000762	7	1.467198	1.886884	14.183791	0.282000	16	630	2	0.281991	-14.1	0.8	691	3	-12.7	0.8
PC-12-3_38	**r**	0.016099	13	0.000629	4	1.467239	1.886820	14.527505	0.282028	16	639	3	0.282020	-12.8	0.8	691	3	-11.6	0.8
PC-12-3_39	**r**	0.016052	23	0.000621	8	1.467137	1.886832	13.427387	0.281993	14	634	3	0.281986	-14.1	0.8	691	3	-12.9	0.8
PC-12-3_40	**c**	0.021042	17	0.000794	5	1.467221	1.886893	13.974287	0.282018	15	644	2	0.282009	-13.1	0.8	691	3	-12.1	0.8
PC-12-3_41	**r**	0.011991	12	0.000466	4	1.467151	1.886854	14.057561	0.282018	18	645	3	0.282012	-13.0	0.8	691	3	-11.9	0.8
PC-12-3_42	**r**	0.021340	27	0.000813	9	1.467203	1.886892	14.075180	0.282011	14	670	4	0.282001	-12.8	0.8	691	3	-12.3	0.8
PC-12-3_45	**r**	0.012935	13	0.000504	4	1.467173	1.886830	13.748955	0.282029	17	672	3	0.282022	-12.0	0.8	691	3	-11.6	0.8
PC-12-3_48	**r**	0.021184	20	0.000817	6	1.467159	1.886893	15.234668	0.281990	18	597	3	0.281981	-15.1	0.8	691	3	-13.1	0.8
PC-12-3_52	**c**	0.026230	22	0.001016	7	1.467202	1.886953	13.957462	0.282007	18	642	2	0.281995	-13.6	0.8	691	3	-12.6	0.8
PC-12-3_55	**c**	0.017358	14	0.000674	4	1.467116	1.886752	18.122154	0.282000	17	665	4	0.281992	-13.2	0.8	691	3	-12.7	0.8
PC-12-3_59	**r**	0.014802	14	0.000588	4	1.467172	1.886878	16.909312	0.282002	20	687	3	0.281995	-12.6	0.8	691	3	-12.5	0.8
PC-12-3_61	**r**	0.013770	11	0.000538	3	1.467058	1.886853	16.362372	0.282001	16	691	3	0.281994	-12.6	0.8	691	3	-12.6	0.8
PC-12-3_62	**r**	0.014245	13	0.000553	4	1.467222	1.886884	17.110251	0.281999	24	624	5	0.281992	-14.1	0.8	691	3	-12.6	0.8

PC-12-3_64	**c**	0.022495	18	0.000875	5	1.467101	1.886841	15.390488	0.281993	16	633	4	0.281983	-14.3	0.8	691	3	-13.0	0.8
PC-12-3_65	**r**	0.012418	18	0.000497	6	1.467135	1.886779	13.587183	0.282010	18	648	3	0.282003	-13.2	0.8	691	3	-12.2	0.8
PC-12-3_66	**c**	0.020099	18	0.000784	5	1.467178	1.886860	15.286841	0.281994	16	611	3	0.281985	-14.7	0.8	691	3	-12.9	0.8
PC-12-3_67	**r**	0.017438	14	0.000667	4	1.467199	1.886930	16.893604	0.282006	20	618	2	0.281998	-14.1	0.8	691	3	-12.5	0.8
PC-12-3_72	**c**	0.019182	24	0.000747	8	1.467122	1.886812	15.038717	0.281982	18	648	3	0.281973	-14.3	0.8	691	3	-13.3	0.8
PC-12-3_74	**r**	0.023558	41	0.000894	13	1.467093	1.886828	15.679412	0.282015	20	644	3	0.282004	-13.3	0.9	691	3	-12.2	0.9
PC-12-3_80	**c**	0.019604	16	0.000742	5	1.467202	1.886883	13.613629	0.282010	16	619	8	0.282002	-13.9	0.8	691	3	-12.3	0.8

(a) $^{176}Yb/^{177}Hf = (^{176}Yb/^{173}Yb)_{true} \times (^{173}Yb/^{177}Hf)_{meassured} \times (M_{173(Yb)}/M_{177(Hf)})^{b(Hf)}$, $b(Hf) = \ln(^{179}Hf/^{177}Hf_{\ true} / {}^{179}Hf/^{177}Hf_{measured}) / \ln (M_{179(Hf)}/M_{177(Hf)})$

M=mass of respective isotope. The $^{176}Lu/^{177}Hf$ were calculated in a similar way by using the $^{175}Lu/^{177}Hf$ and b(Yb)

(b) Mean Hf signal in volt

(c) Uncertainties are quadratic additions of the within-run precision and the daily reproducibility of the zircon standards. Uncertainties for the standard quoted at 2SD (2 standard deviation)

(d) Initial $^{176}Hf/^{177}Hf$ and ƐHf calculated using the apparent Pb-Pb ages of respective zircon domains, and the CHUR parameters: $^{176}Lu/^{177}Hf = 0.0336$, and $^{176}Hf/^{177}Hf = 0.282785$ (Bouvier et al., 2008)

(e) Two stage model age in billion years using the measured $^{176}Lu/^{177}Lu$ of each spot (first stage = age of zircon), a value of 0.0113 for the average continental crust (second stage), and a average MORB (DM) $^{176}Lu/^{177}Hf$ and $^{176}Hf/^{177}Hf$ of 0.0384 and 0.283164

Bouvier, A., Vervoort, J.D., Patchett, P.J., 2008. The Lu-Hf and Sm-Nd isotopic composition of CHUR: constraints from unequilibrated chondrites and implications for the bulk composition of terrestrial planets. Earth and Planetary Science Letters 273, 48-57.

(f) $^{206}Pb/^{238}U$ age

c-core

r-rim

s-single phase

Zircon LA-MC-ICP-MS U-Pb results - Garnet-biotite stromatic metatexite (PC12.4)

							Isotope ratios[c]							Ages (Ma)						
Spot number	CL-domain	f_{206}[a]	Pb ppm	Th ppm	U ppm	Th/U[b]	$^{207}Pb/^{206}Pb$[e]	2 s [%]	$^{207}Pb/^{235}U$	2 s [%]	$^{206}Pb/^{238}U$	2 s [%]	Rho[d]	$^{206}Pb/^{238}U$	2 s abs	$^{207}Pb/^{235}U$	2 s abs	$^{207}Pb/^{206}Pb$	2 s abs	% Disc.[e]
PC-12-4_01	**c**	0.5842	37	57	409	0.14	0.06007	2.64	0.81864	5.69	0.09884	5.04	0.89	608	10	607	9	606	19	0
PC-12-4_02	**c**	1.1788	116	520	949	0.55	0.06048	4.88	0.79868	6.00	0.09578	3.48	0.58	590	7	596	9	621	35	5
PC-12-4_03	**r**	0.0000	203	928	1376	0.67	0.06350	2.29	1.04119	14.72	0.11892	13.99	0.95	724	16	725	13	725	16	0
PC-12-4_04	**c**	0.9366	23	50	270	0.18	0.05881	3.73	0.70617	5.71	0.08709	4.32	0.76	538	7	542	8	560	27	4
PC-12-4_05	**r**	2.7471	175	1135	1095	1.04	0.06194	15.52	0.91597	16.43	0.10726	5.38	0.33	657	11	660	27	672	111	2
PC-12-4_06	**c**	0.0000	151	850	1023	0.83	0.06128	1.33	0.90238	13.08	0.10679	13.01	0.99	654	27	653	21	649	10	-1
PC-12-4_08	**r**	0.1405	112	187	1085	0.17	0.06162	1.39	0.92694	8.88	0.10911	8.77	0.99	668	19	666	15	661	10	-1
PC-12-4_09	**c**	1.6060	48	157	540	0.29	0.05828	6.40	0.69633	28.36	0.08665	27.62	0.97	536	48	537	40	540	47	1
PC-12-4_10	**c**	0.1925	43	65	473	0.14	0.06000	1.65	0.81722	3.39	0.09878	2.96	0.87	607	6	606	5	604	12	-1
PC-12-4_11	**r**	0.0000	15	31	189	0.16	0.05734	1.30	0.67201	4.44	0.08500	4.25	0.86	526	11	522	9	504	14	-4
PC-12-4_12	**r**	0.0000	14	33	115	0.29	0.06280	1.95	1.01024	5.34	0.11667	3.64	0.68	711	4	709	5	702	14	-1
PC-12-4_13	**c**	0.4763	37	55	396	0.14	0.06035	2.34	0.84003	4.58	0.10095	3.94	0.86	620	8	619	7	616	17	-1
PC-12-4_14	**c**	0.0000	26	87	181	0.48	0.06427	1.56	1.10011	4.80	0.12415	3.65	0.76	754	4	753	4	750	11	-1
PC-12-4_15	**c**	0.0000	86	132	916	0.14	0.06049	1.34	0.84850	6.49	0.10174	6.17	0.85	625	8	624	7	621	10	-1
PC-12-4_16	**c**	0.0000	70	136	709	0.19	0.06060	1.35	0.85480	3.73	0.10231	3.13	0.84	628	4	627	4	625	10	0
PC-12-4_17	**c**	0.0000	125	382	1086	0.35	0.06167	1.28	0.92890	9.24	0.10924	9.04	0.88	668	13	667	10	663	9	-1
PC-12-4_18	**c**	0.0028	45	127	364	0.35	0.06294	1.47	1.00445	6.61	0.11574	5.92	0.90	706	7	706	6	706	10	0
PC-12-4_19	**r**	1.2760	115	538	958	0.56	0.06041	6.95	0.79450	7.37	0.09539	2.45	0.33	587	5	594	11	618	50	5
PC-12-4_20	**r**	0.0000	28	86	319	0.27	0.05833	4.75	0.73881	6.74	0.09186	4.79	0.71	567	13	562	15	542	52	-4
PC-12-4_21	**r**	0.0000	18	34	208	0.16	0.05900	5.58	0.77208	13.15	0.09492	11.91	0.91	585	22	581	20	567	41	-3
PC-12-4_22	**r**	0.4800	41	62	445	0.14	0.06001	2.31	0.81818	4.33	0.09889	3.66	0.85	608	7	607	7	604	17	-1
PC-12-4_23	**r**	0.0000	44	65	462	0.14	0.06044	1.39	0.84848	7.10	0.10182	6.79	0.86	625	9	624	7	619	10	-1
PC-12-4_24	**c**	0.0000	72	110	765	0.14	0.06051	1.31	0.84978	2.56	0.10185	1.63	0.64	625	2	625	3	622	9	-1
PC-12-4_25	**c**	0.0000	110	192	1193	0.16	0.05997	1.34	0.81064	12.90	0.09803	12.83	0.99	603	25	603	20	603	10	0

PC-12-4_26	**c**	0.2367	58	117	607	0.19	0.06024	1.63	0.83309	5.87	0.10030	5.65	0.96	616	11	615	9	612	12	-1
PC-12-4_27	**c**	0.0000	57	85	598	0.14	0.06079	1.36	0.86944	1.69	0.10373	1.00	0.59	636	2	635	3	632	10	-1
PC-12-4_28	**r**	0.4967	44	76	462	0.17	0.06037	2.38	0.84302	4.53	0.10128	3.86	0.85	622	8	621	7	617	17	-1
PC-12-4_29	**c**	0.9031	99	695	615	1.13	0.06129	3.60	0.88892	4.11	0.10519	1.98	0.48	645	4	646	7	649	26	1
PC-12-4_30	**c**	0.0000	42	62	449	0.14	0.06051	1.38	0.85074	2.67	0.10197	1.68	0.63	626	2	625	3	622	10	-1
PC-12-4_31	**c**	0.0000	42	60	442	0.14	0.06057	1.39	0.85400	2.61	0.10226	1.58	0.61	628	2	627	3	624	10	-1
PC-12-4_32	**c**	0.0000	50	69	512	0.13	0.06115	1.33	0.89550	8.23	0.10620	7.79	0.95	651	8	649	7	645	10	-1
PC-12-4_34	**c**	0.0000	37	50	373	0.14	0.06132	2.05	0.89816	6.59	0.10622	5.15	0.78	651	5	651	5	651	15	0
PC-12-4_35	**r**	2.4352	28	61	304	0.20	0.05976	9.03	0.78752	9.91	0.09557	4.08	0.41	588	8	590	15	595	65	1
PC-12-4_36	**r**	0.0000	127	651	721	0.90	0.06562	3.24	1.18631	14.31	0.13111	12.76	0.89	794	16	794	13	794	23	0
PC-12-4_38	**c**	0.0000	81	134	587	0.23	0.06653	1.46	1.27501	6.65	0.13900	5.98	0.90	839	8	835	6	823	10	-2
PC-12-4_39	**r**	0.0000	57	85	594	0.14	0.06080	1.33	0.86394	2.83	0.10305	2.02	0.71	632	3	632	3	632	10	0
PC-12-4_40	**c**	1.5160	15	36	134	0.27	0.06207	5.93	0.95260	6.33	0.11131	2.21	0.35	680	5	679	11	676	42	-1
PC-12-4_41	**c**	0.0000	24	95	168	0.57	0.06318	2.23	1.02974	7.89	0.11820	6.50	0.82	720	7	719	7	714	16	-1
PC-12-4_42	**c**	0.0000	10	25	125	0.20	0.05760	2.96	0.69755	5.94	0.08783	5.15	0.87	543	13	537	12	515	32	-5
PC-12-4_43	**c**	0.0000	61	86	607	0.14	0.06158	1.30	0.92741	3.61	0.10923	2.50	0.69	668	3	666	3	660	9	-1
PC-12-4_44	**c**	0.0000	57	70	512	0.14	0.06333	1.39	1.04457	11.16	0.11963	10.80	0.97	728	12	726	10	719	10	-1
PC-12-4_45	**c**	0.0000	50	101	388	0.26	0.06467	1.96	1.13292	6.26	0.12706	4.89	0.78	771	6	769	6	764	14	-1
PC-12-4_46	**r**	0.3787	55	75	534	0.14	0.06181	1.95	0.94244	2.97	0.11058	2.24	0.75	676	5	674	5	668	14	-1
PC-12-4_47	**c**	0.4679	50	82	445	0.19	0.06281	2.35	1.01058	4.19	0.11668	3.47	0.83	711	8	709	7	702	17	-1
PC-12-4_48	**c**	0.0000	75	101	708	0.14	0.06235	1.25	0.98230	5.80	0.11426	5.23	0.90	697	6	695	5	686	9	-2
PC-12-4_49	**c**	0.0000	16	44	120	0.36	0.06348	2.01	1.05092	5.68	0.12007	4.03	0.71	731	5	729	5	724	14	-1
PC-12-4_50	**r**	0.0277	50	67	503	0.13	0.06149	1.34	0.91719	5.79	0.10819	5.14	0.89	662	5	661	5	656	10	-1
PC-12-4_51	**c**	0.0000	21	64	158	0.41	0.06384	1.83	1.07949	4.84	0.12263	3.18	0.66	746	4	743	4	736	13	-1
PC-12-4_52	**c**	0.0000	73	95	662	0.14	0.06305	1.33	1.03095	9.41	0.11858	9.02	0.96	722	10	719	8	710	9	-2
PC-12-4_53	**c**	0.0000	32	42	294	0.14	0.06276	1.40	1.01172	5.08	0.11691	4.24	0.84	713	5	710	4	700	10	-2
PC-12-4_54	**r**	0.0000	54	77	478	0.16	0.06322	1.37	1.04376	2.09	0.11974	1.57	0.75	729	4	726	4	716	10	-2
PC-12-4_55	**c**	0.0000	85	186	708	0.26	0.06332	1.29	1.04471	2.59	0.11967	2.25	0.87	729	5	726	4	719	9	-1
PC-12-4_56	**c**	0.0000	45	61	409	0.15	0.06303	1.39	1.02741	2.37	0.11823	1.93	0.81	720	4	718	4	709	10	-2

PC-12-4_58	**r**	0.0000	45	61	409	0.15	0.06303	1.39	1.02741	2.37	0.11823	1.93	0.81	720	4	718	4	709	10	-2
PC-12-4_59	**c**	0.0000	106	132	920	0.14	0.06384	1.35	1.08804	3.39	0.12361	3.11	0.92	751	7	748	6	736	10	-2
PC-12-4_60	**c**	0.0000	49	62	454	0.14	0.06267	1.53	1.00541	4.59	0.11635	3.41	0.74	709	4	707	4	697	11	-2
PC-12-4_61	**c**	0.0000	13	58	139	0.42	0.05912	1.57	0.76811	6.39	0.09423	9.30	0.97	580	17	579	14	572	17	-2
PC-12-4_62	**c**	0.0000	59	71	515	0.14	0.06390	1.32	1.09349	4.70	0.12411	3.89	0.83	754	5	750	4	738	9	-2
PC-12-4_63	**r**	0.0000	75	133	656	0.20	0.06300	1.30	1.02672	4.76	0.11820	3.99	0.84	720	5	717	4	708	9	-2
PC-12-4_64	**c**	6.2899	63	316	475	0.67	0.06056	23.37	0.84696	25.76	0.10144	10.85	0.42	623	22	623	41	624	168	0
PC-12-4_65	**c**	0.0000	31	73	222	0.33	0.06590	1.64	1.22861	5.30	0.13522	4.17	0.79	818	5	814	5	803	11	-2
PC-12-4_66	**c**	1.8024	68	102	316	0.32	0.07937	5.59	2.11640	11.69	0.19339	10.27	0.88	1140	36	1154	27	1181	37	4
PC-12-4_67	**r**	0.0000	12	20	138	0.14	0.05937	1.76	0.78393	5.83	0.09577	5.56	0.95	590	16	588	13	581	19	-2
PC-12-4_68	**c**	0.1158	93	126	877	0.14	0.06239	1.37	0.98698	4.10	0.11473	3.87	0.94	700	9	697	7	688	10	-2
PC-12-4_69	**c**	0.0000	89	341	620	0.55	0.06384	1.31	1.08606	4.67	0.12339	3.87	0.83	750	5	747	4	736	9	-2
PC-12-4_70	**c**	0.0000	32	59	254	0.23	0.06452	2.15	1.13262	7.44	0.12732	6.08	0.82	773	7	769	7	759	15	-2
PC-12-4_71	**c**	0.0000	29	46	225	0.21	0.06525	2.05	1.18672	6.29	0.13191	4.78	0.76	799	6	794	6	782	14	-2
PC-12-4_72	**r**	0.0000	67	78	552	0.14	0.06491	1.52	1.16416	6.38	0.13009	5.61	0.88	788	7	784	6	771	11	-2
PC-12-4_73	**c**	0.0000	12	22	118	0.18	0.06137	2.35	0.94263	13.36	0.11140	12.51	0.94	681	13	674	11	652	17	-4
PC-12-4_75	**c**	0.0000	80	112	694	0.16	0.06379	1.36	1.06805	8.14	0.12144	7.67	0.94	739	9	738	7	735	10	-1
PC-12-4_76	**r**	0.0000	10	38	102	0.37	0.05917	2.91	0.77046	6.93	0.09444	6.29	0.91	582	18	580	15	573	32	-1
PC-12-4_77	**c**	0.0000	34	53	276	0.19	0.06460	1.86	1.13140	6.39	0.12701	5.20	0.81	771	6	768	6	761	13	-1
PC-12-4_78	**c**	0.0000	74	196	582	0.34	0.06332	1.58	1.05249	15.11	0.12055	14.78	0.98	734	17	730	13	719	11	-2
PC-12-4_79	**c**	0.0000	56	68	498	0.14	0.06361	1.41	1.06980	5.38	0.12198	4.58	0.85	742	5	739	5	729	10	-2
PC-12-4_80	**c**	0.0000	63	73	515	0.14	0.06511	1.59	1.17664	5.87	0.13107	4.93	0.84	794	6	790	5	778	11	-2
PC-12-4_81	**c**	0.0000	46	84	406	0.21	0.06281	1.43	1.01556	6.86	0.11727	6.23	0.91	715	7	712	6	702	10	-2
PC-12-4_82	**c**	0.0000	88	142	719	0.20	0.06426	1.61	1.11805	12.15	0.12618	12.04	0.99	766	29	762	22	750	11	-2
PC-12-4_83	**c**	0.0000	11	27	109	0.24	0.06026	2.53	0.86938	11.04	0.10463	10.37	0.84	642	14	635	12	613	18	-5
PC-12-4_84	**r**	0.0000	46	108	317	0.34	0.06618	2.29	1.25254	7.40	0.13727	5.82	0.79	829	8	825	7	812	16	-2
PC-12-4_85	**c**	0.0000	16	71	150	0.47	0.05975	3.09	0.80673	15.51	0.09792	15.20	0.98	602	29	601	24	595	22	-1
PC-12-4_86	**c**	0.0370	25	56	261	0.21	0.05998	2.37	0.81121	11.90	0.09808	11.66	0.88	603	22	603	18	603	17	0
PC-12-4_87	**c**	0.0000	94	190	729	0.26	0.06462	1.30	1.13663	5.94	0.12757	5.34	0.90	774	6	771	5	762	9	-2

PC-12-4_88	**r**	0.1026	127	576	683	0.84	0.06751	3.21	1.34586	6.54	0.14458	5.70	0.87	870	15	866	13	854	22	-2
PC-12-4_89	**c**	0.0000	33	55	334	0.16	0.06104	2.36	0.89071	22.29	0.10584	22.17	0.99	649	46	647	36	641	17	-1
PC-12-4_90	**r**	1.0288	62	103	604	0.17	0.06158	4.85	0.92505	16.46	0.10894	15.73	0.96	667	33	665	27	660	35	-1
PC-12-4_91	**c**	0.0000	8	20	114	0.18	0.05570	13.77	0.56570	24.07	0.07366	19.74	0.82	458	29	455	30	440	102	-4
PC-12-4_92	**c**	0.0000	9	26	122	0.21	0.05648	10.14	0.61911	13.57	0.07950	9.01	0.66	493	14	489	18	471	75	-5
PC-12-4_93	**r**	0.0000	11	17	127	0.13	0.05909	3.23	0.78628	7.73	0.09651	7.02	0.91	594	20	589	17	570	35	-4
PC-12-4_94	**c**	0.0000	64	203	447	0.46	0.06491	1.98	1.15897	2.56	0.12950	1.63	0.64	785	4	781	5	771	14	-2
PC-12-4_95	**c**	0.0000	30	72	370	0.20	0.05779	5.07	0.67568	14.11	0.08480	13.17	0.93	525	22	524	19	522	37	-1
PC-12-4_96	**c**	0.0000	75	88	638	0.14	0.06430	1.79	1.11954	5.30	0.12627	3.90	0.74	767	5	763	5	752	13	-2
PC-12-4_97	**c**	0.0000	76	94	671	0.14	0.06369	1.76	1.07628	5.06	0.12256	3.63	0.72	745	4	742	4	731	12	-2
PC-12-4_98	**c**	0.0000	39	70	336	0.21	0.06312	2.16	1.03005	6.75	0.11836	5.17	0.77	721	6	719	6	712	15	-1
PC-12-4_99	**c**	0.0000	39	49	348	0.14	0.06357	2.11	1.06858	6.17	0.12191	4.51	0.73	742	5	738	5	727	15	-2
PC-12-4_100	**c**	0.0000	40	51	363	0.14	0.06332	2.07	1.04826	5.85	0.12007	4.14	0.71	731	5	728	5	719	15	-2
PC-12-4_102	**c**	0.0000	58	76	545	0.14	0.06256	1.88	0.98876	6.11	0.11463	4.80	0.79	700	5	698	5	693	13	-1
PC-12-4_103	**c**	0.4542	17	60	125	0.48	0.06315	3.30	1.03317	5.41	0.11867	4.29	0.79	723	10	721	9	713	23	-1
PC-12-4_104	**c**	0.0000	51	69	496	0.14	0.06181	1.87	0.94487	4.58	0.11088	2.64	0.58	678	3	675	4	667	13	-2
PC-12-4_105	**c**	0.0000	60	83	574	0.15	0.06223	1.81	0.96602	8.05	0.11259	7.19	0.89	688	8	686	7	682	13	-1
PC-12-4_107	**c**	0.0000	8	24	130	0.18	0.05536	11.85	0.52548	15.98	0.06884	10.72	0.67	429	15	429	19	427	88	-1
PC-12-4_108	**c**	0.0000	75	108	759	0.14	0.06110	1.73	0.89665	3.68	0.10643	2.61	0.71	652	4	650	4	643	12	-1
PC-12-4_109	**r**	0.0000	51	80	536	0.15	0.06035	1.87	0.84832	4.51	0.10194	3.54	0.78	626	5	624	5	616	13	-2
PC-12-4_110	**c**	0.0000	122	140	974	0.14	0.06570	1.64	1.22201	9.28	0.13490	8.68	0.94	816	11	811	9	797	11	-2

aFraction of the non-radiogenic ^{206}Pb in the analyzed zircon spot, where $f_{206}=[^{206}Pb/^{204}Pb]c/[^{206}Pb/^{204}Pb]s$ (c=common; s=sample)

bTh/U ratios and amount of Pb, Th and U (in pmm) are calculated relative to 91500 reference zircon

cCorrected for background and within-run Pb/U fractionation and normalised to reference zircon GJ-1 (ID-TIMS values/measured value); $^{207}Pb/^{235}U$ calculated using $(^{207}Pb/^{206}Pb)/(^{238}U/^{206}Pb * 1/137.88)$

dRho is the error correlation defined as the quotient of the propagated errors of the $^{206}Pb/^{238}U$ and the $^{207}/^{235}U$ ratio

eDegree of discordance = 100 - ($^{206}Pb/^{238}U$ age * 100/$^{207}Pb/^{206}U$ age)

c-core

r-rim

s-single phase

Hf isotopes results determined by LA-ICP-MS - Garnet-biotite stromatic metatexite (PC12.4)

Grain#	CL-Domain	$^{176}Yb/^{177}Hf$ [a]	±2s	$^{176}Lu/^{177}Hf$ [a]	±2s	$^{178}Hf/^{177}Hf$	$^{180}Hf/^{177}Hf$	Sig_{Hf} [b] (V)	$^{176}Hf/^{177}Hf$	±2s [c]	age [f] (Ma)	±2s	$^{176}Hf/^{177}Hf_{(t)}$ [d]	eHf(t) [d]	±2s [c]	age [f] (Ma)	±2s	eHf(t) [d]	±2s [c]
											(measured)					(pref./min.)			
PC-12-4_03	**r**	0.021113	17	0.000874	5	1.467235	1.885881	14.293068	0.282488	17	724	16	0.282477	5.3	1.0	816	11	7.3	1.0
PC-12-4_05	**r**	0.037605	40	0.001621	15	1.467263	1.885940	10.601403	0.282527	17	657	11	0.282507	4.8	1.0	816	11	8.3	1.0
PC-12-4_06	**c**	0.123863	111	0.005047	35	1.467198	1.886777	14.565509	0.282468	18	654	27	0.282406	1.2	1.5	816	11	4.3	1.5
PC-12-4_08	**r**	0.013275	11	0.000534	3	1.467222	1.886010	14.162298	0.281997	18	668	19	0.281990	-13.2	1.0	668	19	-13.2	1.0
PC-12-4_10	**c**	0.006094	5	0.000206	1	1.467238	1.886129	14.907099	0.282464	16	607	6	0.282462	2.1	1.0	816	11	6.8	1.0
PC-12-4_12	**r**	0.004879	4	0.000205	1	1.467228	1.886561	12.871746	0.282361	17	711	4	0.282358	0.8	1.0	816	11	3.1	1.0
PC-12-4_13	**c**	0.010816	9	0.000426	3	1.467276	1.886622	15.457098	0.282506	18	620	8	0.282501	3.8	1.0	816	11	8.1	1.0
PC-12-4_14	**c**	0.011149	9	0.000489	3	1.467230	1.886525	14.341963	0.282423	15	754	4	0.282416	3.8	1.0	816	11	5.2	1.0
PC-12-4_15	**c**	0.018831	15	0.000689	4	1.467236	1.886347	14.791085	0.282454	16	625	8	0.282446	1.9	1.0	816	11	6.2	1.0
PC-12-4_17	**c**	0.027038	22	0.001245	7	1.467269	1.885868	6.749036	0.281759	23	668	13	0.281743	-22.0	1.0	668	13	-22.0	1.0
PC-12-4_18	**c**	0.017872	14	0.000759	5	1.467195	1.885755	12.224215	0.282430	18	706	7	0.282420	2.9	1.0	816	11	5.3	1.0
PC-12-4_22	**r**	0.007326	6	0.000255	2	1.467221	1.886184	14.970047	0.282463	16	608	7	0.282460	2.1	1.0	816	11	6.7	1.0
PC-12-4_23	**c**	0.078707	64	0.003256	20	1.467251	1.885807	11.985274	0.282518	19	625	9	0.282480	3.2	1.1	816	11	7.0	1.1
PC-12-4_24	**c**	0.019874	16	0.000722	4	1.467223	1.886103	15.123118	0.282449	18	625	2	0.282440	1.8	1.0	816	11	6.0	1.0
PC-12-4_26	**c**	0.011075	11	0.000436	3	1.467277	1.886325	14.022963	0.282269	20	616	11	0.282264	-4.7	1.0	616	11	-4.7	1.0
PC-12-4_27	**c**	0.018870	15	0.000732	4	1.467207	1.886379	16.039977	0.282402	19	636	2	0.282393	0.3	1.0	816	11	4.3	1.0
PC-12-4_29	**c**	0.067928	55	0.002841	17	1.467173	1.885500	9.551818	0.282472	27	645	4	0.282438	2.1	1.1	816	11	5.6	1.1
PC-12-4_30	**c**	0.003237	3	0.000102	1	1.467215	1.886563	16.319323	0.282500	15	626	2	0.282499	3.8	1.0	816	11	8.1	1.0
PC-12-4_31	**c**	0.011291	9	0.000429	3	1.467244	1.886218	14.741073	0.282519	15	628	2	0.282514	4.4	1.0	816	11	8.6	1.0
PC-12-4_32	**c**	0.006075	5	0.000206	1	1.467233	1.886137	15.291483	0.282439	16	651	8	0.282436	2.2	1.0	816	11	5.9	1.0
PC-12-4_34	**c**	0.021947	18	0.000814	5	1.467226	1.886040	14.909527	0.282504	17	651	5	0.282494	4.2	1.0	816	11	7.9	1.0
PC-12-4_36	**r**	0.056256	46	0.002020	12	1.467291	1.885496	11.130005	0.281544	27	794	16	0.281514	-27.3	1.1	794	16	-27.3	1.1
PC-12-4_38	**c**	0.017569	14	0.000687	4	1.467273	1.886205	11.995671	0.282005	18	839	8	0.281995	-9.2	1.0	839	8	-9.2	1.0

PC-12-4_39	**r**	0.021220	17	0.000747	4	1.467252	1.886227	15.302876	0.282446	16	632	3	0.282437	1.8	1.0	816	11	5.9	1.0
PC-12-4_41	**c**	0.026480	21	0.001040	6	1.467235	1.886357	12.957066	0.282488	14	720	7	0.282474	5.1	1.0	816	11	7.2	1.0
PC-12-4_43	**c**	0.014012	11	0.000491	3	1.467231	1.886131	14.462834	0.282464	17	668	3	0.282458	3.3	1.0	816	11	6.6	1.0
PC-12-4_45	**c**	0.046078	37	0.001858	11	1.467200	1.886182	9.794323	0.282527	18	771	6	0.282500	7.2	1.0	816	11	8.1	1.0
PC-12-4_47	**c**	0.027880	22	0.001087	7	1.467253	1.886421	15.523455	0.282486	19	711	8	0.282471	4.8	1.0	816	11	7.1	1.0
PC-12-4_48	**c**	0.015868	13	0.000555	3	1.467176	1.886295	15.059705	0.282432	18	697	6	0.282424	2.8	1.0	816	11	5.4	1.0
PC-12-4_49	**c**	0.027852	22	0.001101	7	1.467202	1.886485	12.705513	0.282524	17	731	5	0.282509	6.6	1.0	816	11	8.4	1.0
PC-12-4_51	**c**	0.029941	24	0.001211	7	1.467263	1.886274	11.368618	0.282504	17	746	4	0.282487	6.1	1.0	816	11	7.7	1.0
PC-12-4_52	**c**	0.005961	5	0.000210	1	1.467220	1.885973	16.263382	0.282416	14	722	10	0.282413	3.0	1.0	816	11	5.1	1.0
PC-12-4_53	**c**	0.020362	16	0.000762	5	1.467221	1.886414	14.769732	0.282344	23	713	5	0.282334	0.0	1.0	816	11	2.2	1.0
PC-12-4_54	**r**	0.020121	16	0.000784	5	1.467213	1.885997	14.420291	0.282428	15	729	4	0.282417	3.3	1.0	816	11	5.2	1.0
PC-12-4_55	**c**	0.007796	6	0.000330	2	1.467258	1.885780	16.475646	0.281802	13	729	5	0.281798	-18.7	1.0	729	5	-18.7	1.0
PC-12-4_58	**r**	0.011782	10	0.000438	3	1.467219	1.886508	15.818241	0.282427	16	720	4	0.282421	3.2	1.0	816	11	5.3	1.0
PC-12-4_59	**c**	0.016984	14	0.000593	4	1.467280	1.886324	14.868610	0.282450	14	751	7	0.282442	4.6	1.0	816	11	6.1	1.0
PC-12-4_60	**c**	0.012072	10	0.000463	3	1.467259	1.886295	13.100033	0.282501	20	709	4	0.282495	5.6	1.0	816	11	7.9	1.0
PC-12-4_62	**c**	0.006097	5	0.000244	1	1.467289	1.886404	14.902368	0.282418	15	754	5	0.282414	3.7	1.0	816	11	5.1	1.0
PC-12-4_64	**c**	0.107362	87	0.004618	28	1.467227	1.885958	10.654169	0.282498	17	623	22	0.282444	1.8	1.3	816	11	5.6	1.3
PC-12-4_65	**c**	0.049512	40	0.001884	11	1.467203	1.886415	10.906892	0.282584	23	818	5	0.282555	10.2	1.0	818	5	-7.1	1.0
PC-12-4_66	**c**	0.005743	5	0.000206	1	1.467318	1.884461	9.723036	0.282425	24	1140	36	0.282420	12.7	1.0	1140	36	12.7	1.0
PC-12-4_68	**c**	0.010141	8	0.000362	2	1.467238	1.886143	15.265935	0.282459	17	700	9	0.282454	3.9	1.0	816	11	6.5	1.0
PC-12-4_69	**c**	0.028977	23	0.001233	7	1.467303	1.886243	13.123053	0.282521	20	750	5	0.282504	6.8	1.0	816	11	8.3	1.0
PC-12-4_70	**c**	0.044361	35	0.001778	11	1.467237	1.886474	13.758891	0.282481	20	773	7	0.282455	5.6	1.0	816	11	6.5	1.0
PC-12-4_71	**c**	0.042518	34	0.001671	10	1.467218	1.886443	13.575067	0.282441	15	799	6	0.282416	4.8	1.0	816	11	5.2	1.0
PC-12-4_72	**r**	0.014171	11	0.000519	3	1.467237	1.886134	16.976606	0.282450	14	788	7	0.282442	5.5	1.0	816	11	6.1	1.0
PC-12-4_75	**c**	0.020973	17	0.000831	5	1.467257	1.886153	16.541913	0.282455	17	739	9	0.282444	4.4	1.0	816	11	6.1	1.0
PC-12-4_77	**c**	0.054921	44	0.002254	14	1.467239	1.885991	12.111166	0.282495	16	771	6	0.282462	5.8	1.0	816	11	6.8	1.0
PC-12-4_80	**c**	0.013590	11	0.000473	3	1.467256	1.886217	15.242770	0.282448	17	794	6	0.282441	5.6	1.0	816	11	6.1	1.0
PC-12-4_84	**r**	0.068321	55	0.002956	18	1.467300	1.886022	8.948756	0.282515	24	829	8	0.282469	7.4	1.1	829	8	7.4	1.1
PC-12-4_86	**c**	0.010104	8	0.000403	2	1.467258	1.885374	13.412917	0.281884	31	603	22	0.281879	-18.6	1.0	603	22	-18.6	1.0
PC-12-4_87	**c**	0.035539	33	0.001435	11	1.467225	1.886247	12.452334	0.282210	29	774	6	0.282189	-3.8	1.0	774	6	-3.8	1.0
PC-12-4_88	**c**	0.035386	28	0.001498	9	1.467212	1.886620	15.263600	0.282509	14	870	15	0.282484	8.8	1.0	870	15	8.8	1.0
PC-12-4_89	**c**	0.021594	17	0.000901	5	1.467227	1.886396	14.853068	0.282481	16	649	46	0.282470	3.3	1.0	816	11	7.0	1.0
PC-12-4_90	**r**	0.016637	13	0.000681	4	1.467279	1.885024	12.705940	0.282393	26	667	33	0.282385	0.7	1.0	816	11	4.0	1.0

PC-12-4_94	**c**	0.064543	52	0.002436	15	1.467193	1.886545	9.072057	0.282466	20	785	4	0.282430	5.0	1.1	816	11	5.6	1.1
PC-12-4_97	**c**	0.006321	5	0.000207	1	1.467229	1.886149	14.740387	0.282455	15	745	4	0.282452	4.9	1.0	816	11	6.5	1.0
PC-12-4_98	**c**	0.040455	32	0.001700	10	1.467252	1.886037	11.438445	0.282461	19	721	6	0.282438	3.8	1.0	816	11	5.9	1.0
PC-12-4_100	**c**	0.017788	14	0.000653	4	1.467228	1.885616	13.077292	0.282413	22	731	5	0.282404	2.9	1.0	816	11	4.7	1.0
PC-12-4_102	**c**	0.016823	14	0.000594	4	1.467249	1.886454	15.095723	0.282447	16	700	5	0.282439	3.4	1.0	816	11	6.0	1.0
PC-12-4_103	**c**	0.038907	36	0.001438	11	1.467282	1.886332	11.786394	0.282511	16	723	10	0.282491	5.8	1.0	816	11	7.8	1.0
PC-12-4_104	**c**	0.005892	5	0.000212	1	1.467222	1.885999	14.087332	0.282483	18	678	3	0.282481	4.4	1.0	816	11	7.5	1.0
PC-12-4_105	**c**	0.020696	17	0.000775	5	1.467318	1.885738	14.044972	0.282470	19	688	8	0.282460	3.9	1.0	816	11	6.7	1.0
PC-12-4_108	**c**	0.017782	14	0.000626	4	1.467223	1.886499	13.950726	0.282440	16	652	4	0.282432	2.1	1.0	816	11	5.7	1.0
PC-12-4_110	**c**	0.029068	29	0.001069	9	1.467213	1.886317	13.784608	0.282417	18	816	11	0.282401	4.6	1.0	816	11	4.6	1.0

(a) $^{176}Yb/^{177}Hf = (^{176}Yb/^{173}Yb)_{true} \times (^{173}Yb/^{177}Hf)_{meassured} \times (M_{173(Yb)}/M_{177(Hf)})^{b(Hf)}$, $b(Hf) = \ln(^{179}Hf/^{177}Hf_{true} / {}^{179}Hf/^{177}Hf_{measured}) / \ln(M_{179(Hf)}/M_{177(Hf)})$
M=mass of respective isotope. The $^{176}Lu/^{177}Hf$ were calculated in a similar way by using the $^{175}Lu/^{177}Hf$ and b(Yb)

(b) Mean Hf signal in volt

(c) Uncertainties are quadratic additions of the within-run precision and the daily reproducibility of the zircon standards. Uncertainties for the standard quoted at 2SD (2 standard deviation)

(d) Initial $^{176}Hf/^{177}Hf$ and ƐHf calculated using the apparent Pb-Pb ages of respective zircon domains, and the CHUR parameters: $^{176}Lu/^{177}Hf = 0.0336$, and $^{176}Hf/^{177}Hf = 0.282785$ (Bouvier et al., 2008)

(e) Two stage model age in billion years using the measured $^{176}Lu/^{177}Lu$ of each spot (first stage = age of zircon), a value of 0.0113 for the average continental crust (second stage), and a average MORB (DM) $^{176}Lu/^{177}Hf$ and $^{176}Hf/^{177}Hf$ of 0.0384 and 0.283164

Bouvier, A., Vervoort, J.D., Patchett, P.J., 2008. The Lu-Hf and Sm-Nd isotopic composition of CHUR: constraints from unequilibrated chondrites and implications for the bulk composition of terrestrial planets. Earth and Planetary Science Letters 273, 48-57.

(f) $^{206}Pb/^{238}U$ age

c-core

r-rim

s-single phase

Zircon LA-MC-ICP-MS U-Pb results - Garnet-bearing white leucosome (PC12.5)

							Isotope ratios[c]							Ages (Ma)						
Spot number	CL-domain	f_{206}[a]	Pb ppm	Th ppm	U ppm	Th/U[b]	$^{207}Pb/^{206}Pb$[e]	2 s [%]	$^{207}Pb/^{235}U$	2 s [%]	$^{206}Pb/^{238}U$	2 s [%]	Rho[d]	$^{206}Pb/^{238}U$	2 s abs	$^{207}Pb/^{235}U$	2 s abs	$^{207}Pb/^{206}Pb$	2 s abs	% Disc.[e]
PC-12-5_01	**c**	0.2787	10	1	135	0.01	0.05737	3.69	0.66007	10.81	0.08344	10.17	0.94	517	17	515	15	506	27	-2
PC-12-5_02	**c**	0.5589	13	1	157	0.01	0.05808	4.31	0.70108	14.11	0.08754	13.43	0.95	541	23	539	20	533	31	-2
PC-12-5_04	**c**	0.0000	32	162	271	0.60	0.06114	1.63	0.88771	2.88	0.10530	2.37	0.82	645	5	645	5	644	12	0
PC-12-5_05	**c**	5.4833	67	13	765	0.02	0.05953	22.95	0.77557	32.48	0.09449	22.98	0.71	582	43	583	49	586	166	1
PC-12-5_06	**c**	1.5593	99	8	1042	0.01	0.06090	6.61	0.86744	19.28	0.10331	18.11	0.94	634	37	634	31	636	47	0
PC-12-5_07	**c**	1.4224	17	61	154	0.40	0.06040	6.25	0.83786	6.58	0.10061	2.06	0.31	618	4	618	10	618	45	0
PC-12-5_08	**c**	0.7839	57	33	494	0.07	0.06384	3.58	1.06767	5.09	0.12129	3.63	0.71	738	8	738	9	736	25	0
PC-12-5_09	**c**	0.0000	31	139	273	0.51	0.06067	1.45	0.85612	2.38	0.10234	1.88	0.79	628	4	628	4	628	10	0
PC-12-5_11	**c**	0.0494	22	104	211	0.49	0.05965	1.95	0.78369	2.23	0.09528	1.08	0.48	587	2	588	3	591	14	1
PC-12-5_12	**c**	0.2160	22	92	218	0.43	0.05960	1.88	0.78233	2.19	0.09521	1.11	0.51	586	2	587	3	589	14	0
PC-12-5_13	**r**	6.5819	44	11	496	0.02	0.05959	27.00	0.78226	29.52	0.09520	11.93	0.40	586	22	587	45	589	195	0
PC-12-5_14	**r**	0.0223	23	105	218	0.48	0.05974	1.44	0.79277	1.90	0.09625	1.24	0.65	592	2	593	3	594	10	0
PC-12-5_15	**r**	0.5804	36	33	454	0.07	0.05777	3.02	0.65343	5.83	0.08203	4.98	0.86	508	8	511	8	521	22	2
PC-12-5_16	**c**	0.3498	15	42	154	0.27	0.05976	2.22	0.79562	2.45	0.09656	1.04	0.42	594	2	594	4	595	16	0
PC-12-5_17	**c**	0.0000	13	3	179	0.02	0.05665	6.16	0.60755	12.86	0.07778	11.29	0.88	483	18	482	17	478	45	-1
PC-12-5_18	**r**	0.7798	27	32	318	0.10	0.05859	3.61	0.71563	5.89	0.08859	4.65	0.79	547	8	548	8	552	26	1
PC-12-5_19	**c**	0.0982	11	8	139	0.06	0.05788	3.21	0.69824	7.54	0.08749	6.82	0.90	541	12	538	11	525	23	-3
PC-12-5_20	**c**	0.0042	35	55	372	0.15	0.05974	1.36	0.79237	1.82	0.09619	1.21	0.66	592	2	593	3	594	10	0
PC-12-5_21	**c**	0.0000	36	255	228	1.12	0.06337	1.56	1.03379	4.97	0.11832	4.72	0.85	721	11	721	9	721	11	0
PC-12-5_22	**c**	0.0000	11	1	146	0.01	0.05697	6.64	0.62907	10.40	0.08009	8.00	0.77	497	13	496	14	490	49	-1
PC-12-5_23	**r**	0.0957	21	86	204	0.42	0.05973	1.64	0.79196	2.33	0.09616	1.65	0.71	592	3	592	3	594	12	0
PC-12-5_24	**c**	0.0000	24	84	208	0.40	0.06132	1.56	0.90129	2.21	0.10660	1.57	0.71	653	3	652	4	651	11	0
PC-12-5_26	**r**	0.0000	22	80	200	0.40	0.06115	1.41	0.88902	3.04	0.10544	2.70	0.89	646	6	646	5	644	10	0
PC-12-5_27	**c**	0.0000	21	86	189	0.46	0.06101	1.81	0.87924	3.41	0.10452	2.89	0.85	641	6	641	5	640	13	0
PC-12-5_29	**r**	0.1085	23	103	207	0.50	0.06046	1.62	0.84217	3.09	0.10103	2.64	0.85	620	5	620	5	620	12	0
PC-12-5_30	**c**	0.0000	31	152	281	0.54	0.06029	1.39	0.82746	2.42	0.09954	1.98	0.82	612	4	612	4	614	10	0
PC-12-5_31	**c**	0.0000	21	87	180	0.48	0.06116	1.61	0.88925	2.77	0.10545	2.26	0.81	646	5	646	4	645	12	0

PC-12-5_32	**c**	0.0316	41	24	417	0.06	0.06084	1.46	0.86490	3.35	0.10310	3.01	0.90	633	6	633	5	634	10	0
PC-12-5_33	**r**	0.1127	35	30	357	0.08	0.06083	1.46	0.86595	3.05	0.10325	2.68	0.88	633	5	633	5	633	10	0
PC-12-5_34	**c**	0.0000	31	143	257	0.56	0.06159	1.86	0.91099	2.43	0.10728	1.56	0.64	657	3	658	4	660	13	0
PC-12-5_35	**c**	0.0000	19	69	184	0.37	0.06025	1.64	0.82885	2.20	0.09978	1.46	0.66	613	3	613	3	613	12	0
PC-12-5_37	**c**	0.2330	22	91	207	0.44	0.06009	1.78	0.81622	2.15	0.09851	1.20	0.56	606	2	606	3	607	13	0
PC-12-5_38	**r**	0.6431	17	61	171	0.35	0.05947	3.32	0.77393	3.49	0.09438	1.07	0.31	581	2	582	5	584	24	1
PC-12-5_39	**c**	0.1339	22	95	207	0.46	0.05985	1.65	0.79847	2.13	0.09676	1.35	0.63	595	3	596	3	598	12	0
PC-12-5_40	**c**	0.4716	20	77	200	0.38	0.05948	2.62	0.77438	2.85	0.09442	1.11	0.39	582	2	582	4	585	19	1
PC-12-5_41	**c**	0.0000	20	67	206	0.33	0.05921	1.69	0.75805	2.09	0.09285	1.23	0.59	572	2	573	3	575	12	0
PC-12-5_42	**r**	0.1923	26	128	232	0.55	0.06040	1.97	0.83300	2.55	0.10002	1.61	0.63	615	3	615	4	618	14	1
PC-12-5_43	**c**	0.5038	23	104	213	0.49	0.06031	2.72	0.83185	3.47	0.10004	2.15	0.62	615	4	615	5	615	20	0
PC-12-5_44	**c**	0.0000	30	131	270	0.48	0.06086	1.55	0.86848	3.08	0.10350	2.66	0.86	635	5	635	5	634	11	0
PC-12-5_45	**c**	0.0000	26	114	228	0.50	0.06079	1.74	0.86378	2.95	0.10306	2.38	0.81	632	5	632	5	632	12	0
PC-12-5_46	**r**	0.0000	33	34	365	0.09	0.05953	1.76	0.77559	2.92	0.09448	2.33	0.80	582	4	583	4	587	13	1
PC-12-5_47	**c**	0.8963	29	129	272	0.48	0.06019	4.14	0.82292	4.46	0.09916	1.65	0.37	609	3	610	7	610	30	0
PC-12-5_48	**r**	0.0000	20	63	187	0.34	0.06103	1.54	0.87960	3.23	0.10453	2.84	0.88	641	6	641	5	640	11	0
PC-12-5_49	**r**	0.0000	27	40	265	0.15	0.06125	2.00	0.89341	2.59	0.10578	1.64	0.63	648	3	648	4	648	14	0
PC-12-5_50	**r**	0.9405	13	48	132	0.36	0.05938	4.52	0.76939	5.05	0.09397	2.27	0.45	579	4	579	7	581	33	0
PC-12-5_51	**c**	0.0381	25	100	238	0.42	0.05960	2.67	0.78384	2.83	0.09539	0.94	0.33	587	2	588	4	589	19	0
PC-12-5_53	**c**	0.0000	23	85	193	0.44	0.06158	2.67	0.91751	3.37	0.10806	2.06	0.61	661	4	661	5	660	19	0
PC-12-5_54	**c**	0.0000	29	135	249	0.54	0.06095	2.46	0.86832	2.90	0.10333	1.53	0.53	634	3	635	5	637	18	1
PC-12-5_55	**r**	0.0000	18	79	162	0.48	0.06026	3.39	0.83009	3.66	0.09991	1.37	0.38	614	3	614	6	613	24	0
PC-12-5_56	**r**	0.4779	84	24	1021	0.02	0.05852	4.33	0.70597	5.38	0.08749	3.18	0.59	541	6	542	8	549	32	2
PC-12-5_57	**r**	0.0765	17	69	161	0.43	0.06002	3.06	0.81099	3.24	0.09799	1.09	0.34	603	2	603	5	604	22	0
PC-12-5_58	**r**	0.0742	28	31	308	0.10	0.05977	2.56	0.79533	5.37	0.09651	4.72	0.88	594	9	594	8	595	18	0
PC-12-5_59	**r**	0.4124	23	67	228	0.29	0.06016	3.13	0.82182	3.28	0.09908	0.97	0.29	609	2	609	5	609	23	0
PC-12-5_60	**c**	0.3591	15	49	143	0.34	0.06071	3.53	0.85732	3.74	0.10241	1.24	0.33	629	2	629	6	629	25	0
PC-12-5_61	**c**	1.3751	24	119	200	0.60	0.06158	5.97	0.90080	6.18	0.10609	1.61	0.26	650	3	652	10	660	43	1
PC-12-5_62	**r**	0.2249	19	76	184	0.41	0.05967	3.10	0.78955	3.28	0.09596	1.05	0.32	591	2	591	5	592	22	0
PC-12-5_63	**c**	0.0588	29	152	265	0.57	0.05997	2.48	0.80880	2.76	0.09781	1.19	0.43	602	2	602	4	603	18	0
PC-12-5_64	**c**	0.1973	25	106	233	0.45	0.06007	2.75	0.81034	2.97	0.09783	1.14	0.38	602	2	603	5	606	20	1
PC-12-5_65	**r**	0.1870	30	161	267	0.60	0.05985	2.60	0.80045	2.99	0.09700	1.47	0.49	597	3	597	5	598	19	0
PC-12-5_66	**r**	0.0834	19	79	176	0.45	0.06023	2.81	0.82535	3.96	0.09939	2.79	0.70	611	5	611	6	612	20	0

PC-12-5_67	**c**	0.2389	30	134	263	0.51	0.06074	5.34	0.83995	5.65	0.10030	1.84	0.33	616	4	619	9	630	38	2
PC-12-5_68	**c**	0.1058	19	75	170	0.44	0.06097	2.90	0.87730	4.18	0.10436	3.01	0.72	640	6	640	7	638	21	0
PC-12-5_69	**r**	0.2479	20	80	172	0.47	0.06167	3.23	0.92149	4.91	0.10837	3.70	0.75	663	8	663	8	663	23	0
PC-12-5_70	**c**	0.0411	25	106	224	0.47	0.06067	2.69	0.85481	3.77	0.10218	2.65	0.70	627	5	627	6	628	19	0

aFraction of the non-radiogenic ^{206}Pb in the analyzed zircon spot, where f_{206}=[$^{206}Pb/^{204}Pb$]c/[$^{206}Pb/^{204}Pb$]s (c=common; s=sample)

bTh/U ratios and amount of Pb, Th and U (in pmm) are calculated relative to 91500 reference zircon

cCorrected for background and within-run Pb/U fractionation and normalised to reference zircon GJ-1 (ID-TIMS values/measured value); $^{207}Pb/^{235}U$ calculated using ($^{207}Pb/^{206}Pb$)/($^{238}U/^{206}Pb$ * 1/137.88)

dRho is the error correlation defined as the quotient of the propagated errors of the $^{206}Pb/^{238}U$ and the $^{207}/^{235}U$ ratio

eDegree of discordance = 100 - ($^{206}Pb/^{238}U$ age * 100/$^{207}Pb/^{206}U$ age)

c-core

r-rim

s-single phase

Hf isotopes results determined by LA-ICP-MS - Garnet-bearing white leucosome (PC12.5)

Grain#	CL-Domain	$^{176}Yb/^{177}Hf$ [a]	±2s	$^{176}Lu/^{177}Hf$ [a]	±2s	$^{178}Hf/^{177}Hf$	$^{180}Hf/^{177}Hf$	Sig_{Hf} [b] (V)	$^{176}Hf/^{177}Hf$	±2s [c]	age [f] (Ma)	±2s	$^{176}Hf/^{177}Hf_{(t)}$ [d]	eHf(t) [d]	±2s [c]	age [f] (Ma)	±2s	eHf(t) [d]	±2s [c]
											(measured)					(pref./min.)			
PC-12-5_01	**c**	0.028403	23	0.000950	6	1.467202	1.886206	18.614964	0.282145	14	517	17	0.282136	-11.4	1.0	661	4	-8.3	1.0
PC-12-5_02	**c**	0.016879	14	0.000560	3	1.467201	1.886197	19.094962	0.282153	13	541	23	0.282148	-10.5	1.0	661	4	-7.8	1.0
PC-12-5_05	**c**	0.004584	4	0.000135	1	1.467240	1.885781	27.513407	0.282101	11	582	43	0.282100	-11.3	1.0	661	4	-9.5	1.0
PC-12-5_06	**c**	0.010941	9	0.000351	2	1.467222	1.886063	23.240739	0.282120	14	634	37	0.282116	-9.5	1.0	661	4	-8.9	1.0
PC-12-5_08	**c**	0.012742	10	0.000445	3	1.467246	1.886114	16.359842	0.282101	19	738	8	0.282095	-7.9	1.0	738	8	-7.9	1.0
PC-12-5_12	**c**	0.014602	12	0.000462	3	1.467220	1.886470	17.755257	0.282158	17	586	2	0.282153	-9.3	1.0	661	4	-7.6	1.0
PC-12-5_16	**c**	0.004112	4	0.000120	1	1.467215	1.886501	18.271478	0.282163	14	594	2	0.282162	-8.8	1.0	661	4	-7.3	1.0
PC-12-5_20	**r**	0.002168	2	0.000059	1	1.467214	1.885928	19.326330	0.282132	14	592	2	0.282131	-9.9	1.0	661	4	-8.4	1.0
PC-12-5_21	**c**	0.017023	14	0.000655	4	1.467237	1.886139	12.665210	0.282287	18	721	11	0.282278	-1.8	1.0	721	11	-1.8	1.0
PC-12-5_22	**c**	0.014650	12	0.000480	3	1.467212	1.886173	21.065699	0.282124	14	497	13	0.282119	-12.5	1.0	661	4	-8.8	1.0

PC-12-5_24	**c**	0.014970	12	0.000464	3	1.467255	1.886305	16.023979	0.282178	13	653	3	0.282172	-7.1	1.0	661	4	-6.9	1.0
PC-12-5_29	**c**	0.014065	11	0.000452	3	1.467205	1.886547	15.412026	0.282176	17	620	5	0.282171	-7.9	1.0	661	4	-7.0	1.0
PC-12-5_32	**c**	0.013543	11	0.000479	3	1.467202	1.887062	26.323417	0.282088	18	633	6	0.282082	-10.8	1.0	661	4	-10.1	1.0
PC-12-5_41	**c**	0.007647	6	0.000229	1	1.467203	1.886225	16.323322	0.282183	17	572	2	0.282181	-8.6	1.0	661	4	-6.6	1.0
PC-12-5_47	**c**	0.010304	8	0.000327	2	1.467228	1.886206	16.932562	0.282182	15	609	3	0.282178	-7.9	1.0	661	4	-6.7	1.0
PC-12-5_48	**c**	0.010055	8	0.000321	2	1.467200	1.886199	16.616608	0.282185	18	641	6	0.282181	-7.1	1.0	661	4	-6.6	1.0
PC-12-5_53	**c**	0.017024	14	0.000529	3	1.467288	1.886524	16.165189	0.282186	18	661	4	0.282180	-6.7	1.0	661	4	-6.7	1.0
PC-12-5_56	**c**	0.014813	12	0.000513	3	1.467214	1.886291	20.394809	0.282136	14	541	6	0.282131	-11.1	1.0	661	4	-8.4	1.0
PC-12-5_60	**c**	0.033828	27	0.001025	6	1.467245	1.886101	17.087722	0.282131	15	629	2	0.282119	-9.5	1.0	661	4	-8.8	1.0
PC-12-5_61	**c**	0.010559	8	0.000364	2	1.467276	1.886073	11.948734	0.282090	19	650	3	0.282086	-10.2	1.0	661	4	-10.0	1.0

(a) $^{176}Yb/^{177}Hf = (^{176}Yb/^{173}Yb)_{true} \times (^{173}Yb/^{177}Hf)_{meassured} \times (M_{173(Yb)}/M_{177(Hf)})^{b(Hf)}$, $b(Hf) = \ln(^{179}Hf/^{177}Hf_{true} / {}^{179}Hf/^{177}Hf_{measured}) / \ln (M_{179(Hf)}/M_{177(Hf)})$

M=mass of respective isotope. The $^{176}Lu/^{177}Hf$ were calculated in a similar way by using the $^{175}Lu/^{177}Hf$ and b(Yb)

(b) Mean Hf signal in volt

(c) Uncertainties are quadratic additions of the within-run precision and the daily reproducibility of the zircon standards. Uncertainties for the standard quoted at 2SD (2 standard deviation)

(d) Initial $^{176}Hf/^{177}Hf$ and ℇHf calculated using the apparent Pb-Pb ages of respective zircon domains, and the CHUR parameters: $^{176}Lu/^{177}Hf = 0.0336$, and $^{176}Hf/^{177}Hf = 0.282785$ (Bouvier et al., 2008)

(e) Two stage model age in billion years using the measured $^{176}Lu/^{177}Lu$ of each spot (first stage = age of zircon), a value of 0.0113 for the average continental crust (second stage), and a average MORB (DM) $^{176}Lu/^{177}Hf$ and $^{176}Hf/^{177}Hf$ of 0.0384 and 0.283164

Bouvier, A., Vervoort, J.D., Patchett, P.J., 2008. The Lu-Hf and Sm-Nd isotopic composition of CHUR: constraints from unequilibrated chondrites and implications for the bulk composition of terrestrial planets. Earth and Planetary Science Letters 273, 48-57.

(f) $^{206}Pb/^{238}U$ age

c-core

r-rim

s-single phase

Zircon LA-MC-ICP-MS U-Pb results - (Hornblende)-biotite stromatic metatexite (C1071A)

							Isotope ratios[c]							Ages (Ma)						
Spot number	CL-domain	f_{206}[a]	Pb ppm	Th ppm	U ppm	Th/U[b]	$^{207}Pb/^{206}Pb$[e]	2 s [%]	$^{207}Pb/^{235}U$	2 s [%]	$^{206}Pb/^{238}U$	2 s [%]	Rho[d]	$^{206}Pb/^{238}U$	2 s abs	$^{207}Pb/^{235}U$	2 s abs	$^{207}Pb/^{206}Pb$	2 s abs	% Disc.[e]
C-1071A_01	c	1.4539	2562	1375	2632	0.52	0.06020	5.42	0.81922	6.10	0.09870	2.80	0.46	607	6	608	11	611	47	1
C-1071A_02	r	0.0000	1467	1942	3961	0.49	0.06293	1.91	1.00663	2.37	0.11601	1.41	0.59	708	4	707	5	706	16	0
C-1071A_03	c	0.0000	2495	1327	3320	0.40	0.06052	1.88	0.83993	3.03	0.10066	2.37	0.78	618	6	619	6	622	16	1
C-1071A_04	c	0.6643	2914	290	1034	0.28	0.06081	2.81	0.86143	3.62	0.10275	2.28	0.63	630	5	631	7	632	24	0
C-1071A_05	c	0.4137	2078	878	2573	0.34	0.06211	2.43	0.95220	2.96	0.11119	1.70	0.57	680	4	679	6	678	21	0
C-1071A_06	c	0.1551	2802	2079	3131	0.66	0.06138	4.16	0.89996	4.91	0.10635	2.60	0.53	652	6	652	9	652	36	0
C-1071A_08	c	2.0898	2907	2269	2785	0.81	0.06188	8.03	0.92647	8.37	0.10859	2.34	0.28	665	6	666	16	670	69	1
C-1071A_09	r	0.0000	19815	2659	4513	0.59	0.06084	1.36	0.87863	1.88	0.10474	1.29	0.69	642	3	640	4	634	12	-1
C-1071A_11	c	0.0000	5801	1539	2267	0.68	0.06617	1.83	1.23044	2.92	0.13486	2.28	0.78	816	7	815	7	812	15	0
C-1071A_12	c	0.4066	4747	2172	5439	0.40	0.06321	3.34	1.02876	6.41	0.11804	5.47	0.85	719	15	718	13	715	28	-1
C-1071A_13	c	1.0521	3731	522	1252	0.42	0.06181	4.35	0.92729	4.94	0.10880	2.34	0.47	666	6	666	10	668	37	0
C-1071A_14	c	0.0000	4607	2543	4603	0.55	0.06250	2.78	0.96772	3.11	0.11230	1.40	0.45	686	4	687	6	691	24	1
C-1071A_15	c	0.2585	4846	1345	4185	0.32	0.06237	2.19	0.96692	3.12	0.11243	2.22	0.71	687	6	687	6	687	19	0
C-1071A_17	r	0.0412	3380	3190	5672	0.56	0.06123	1.37	0.89272	1.81	0.10574	1.17	0.65	648	3	648	3	647	12	0
C-1071A_18	c	1.2650	8121	2806	3429	0.82	0.06792	4.39	1.35214	4.91	0.14438	2.21	0.45	869	7	868	12	866	36	0
C-1071A_19	c	0.5833	4942	2363	7311	0.32	0.06177	3.22	0.92491	4.37	0.10860	2.95	0.67	665	7	665	9	666	28	0
C-1071A_21	r	0.0000	5498	7523	4117	1.83	0.06199	2.12	0.94513	2.53	0.11058	1.38	0.55	676	4	676	5	674	18	0
C-1071A_22	c	0.0000	5436	1614	3716	0.43	0.06312	2.32	1.02355	2.76	0.11761	1.49	0.54	717	4	716	6	712	20	-1
C-1071A_25	r	0.7524	3690	1669	3433	0.49	0.06308	3.16	1.01783	3.55	0.11702	1.62	0.46	713	4	713	7	711	27	0
C-1071A_26	r	0.2701	4852	1060	4525	0.23	0.06215	1.85	0.95321	3.53	0.11123	3.00	0.85	680	8	680	7	679	16	0
C-1071A_27	c	1.9153	4189	6925	4172	1.66	0.06094	6.82	0.87150	7.02	0.10372	1.67	0.24	636	4	636	13	637	59	0
C-1071A_28	c	0.0000	4068	1818	3893	0.47	0.06198	1.52	0.94478	2.09	0.11056	1.44	0.69	676	4	675	4	673	13	0
C-1071A_29	r	0.0000	3390	8051	4627	1.74	0.06356	2.37	1.04794	3.18	0.11959	2.12	0.67	728	6	728	7	727	20	0
C-1071A_30	c	1.2390	3384	8894	5630	1.58	0.06270	4.50	0.98868	5.01	0.11436	2.21	0.44	698	6	698	10	698	38	0
C-1071A_31	c	0.0000	2997	5184	4985	1.04	0.06080	2.72	0.85833	3.64	0.10240	2.43	0.67	628	6	629	7	632	23	1
C-1071A_32	c	0.3058	3476	535	4710	0.11	0.05880	1.71	0.71895	3.43	0.08867	2.97	0.87	548	6	550	6	560	15	2
C-1071A_33	c	0.8246	3821	2386	4669	0.51	0.06005	3.55	0.80917	6.53	0.09772	5.48	0.84	601	13	602	12	606	31	1

C-1071A_34	**c**	0.3800	2681	216	4977	0.04	0.05979	2.11	0.78571	2.34	0.09531	1.01	0.43	587	2	589	4	596	18	2
C-1071A_35	**c**	0.0344	2572	3474	4242	0.82	0.06133	4.65	0.90012	5.20	0.10644	2.33	0.45	652	6	652	10	651	40	0
C-1071A_36	**c**	0.0000	4270	2935	4625	0.63	0.06137	1.71	0.89903	2.42	0.10625	1.71	0.71	651	4	651	5	652	15	0
C-1071A_37	**r**	0.0000	2534	2440	3719	0.66	0.06189	2.75	0.93481	3.54	0.10955	2.23	0.63	670	6	670	7	670	24	0
C-1071A_41	**c**	0.0000	1005	100	553	0.18	0.05952	3.23	0.76253	3.74	0.09291	1.89	0.51	573	4	575	7	586	28	2
C-1071A_42	**r**	0.0000	2013	137	597	0.23	0.06110	2.64	0.87105	3.10	0.10340	1.62	0.52	634	4	636	6	643	23	1
C-1071A_43	**r**	0.0000	3045	449	903	0.50	0.06178	1.37	0.91635	2.13	0.10758	1.63	0.77	659	4	660	4	666	12	1
C-1071A_44	**r**	0.9064	2519	409	651	0.63	0.06135	4.24	0.88994	5.22	0.10521	3.06	0.59	645	8	646	10	651	36	1
C-1071A_45	**r**	0.3001	1110	225	592	0.38	0.06072	2.44	0.84716	3.09	0.10119	1.90	0.62	621	5	623	6	629	21	1
C-1071A_46	**c**	0.2767	3551	614	979	0.63	0.06044	1.60	0.83138	2.19	0.09977	1.50	0.68	613	4	614	4	619	14	1
C-1071A_47	**c**	0.9291	2327	209	716	0.29	0.06221	3.48	0.94623	3.94	0.11031	1.85	0.47	675	5	676	8	681	30	1
C-1071A_48	**r**	0.0234	1211	155	599	0.26	0.06135	2.30	0.89038	3.21	0.10526	2.24	0.70	645	6	647	6	652	20	1
C-1071A_49	**c**	0.0000	25418	394	670	0.59	0.06074	2.11	0.83771	2.51	0.10003	1.36	0.54	615	3	618	5	630	18	2
C-1071A_50	**c**	0.2651	2274	581	734	0.79	0.06123	2.05	0.87840	2.69	0.10405	1.74	0.65	638	4	640	5	647	18	1
C-1071A_53	**c**	1.3190	1005	406	533	0.76	0.06143	6.11	0.88509	6.62	0.10450	2.56	0.39	641	6	644	13	654	52	2
C-1071A_54	**r**	1.9038	1109	143	577	0.25	0.06203	7.16	0.93319	7.47	0.10911	2.14	0.29	668	5	669	15	675	61	1
C-1071A_56	**c**	0.1821	8013	183	593	0.31	0.06098	2.71	0.86823	4.13	0.10326	3.12	0.76	633	8	635	8	639	23	1
C-1071A_57	**c**	3.9243	350	1325	2412	0.55	0.06145	13.51	0.91055	13.71	0.10747	2.30	0.17	658	6	657	27	655	116	0
C-1071A_58	**c**	0.0814	1186	508	4896	0.10	0.05901	1.42	0.74395	3.05	0.09144	2.70	0.89	564	6	565	5	567	12	1
C-1071A_59	**c**	0.0000	2444	1061	3149	0.34	0.06058	1.81	0.85266	2.86	0.10209	2.21	0.77	627	5	626	5	624	16	0
C-1071A_60	**c**	3.5928	4140	3946	3665	1.08	0.06228	11.50	0.95153	11.76	0.11081	2.45	0.21	677	6	679	24	684	98	1
C-1071A_61	**c**	0.0623	4675	1758	4135	0.43	0.06052	1.80	0.84377	2.62	0.10112	1.90	0.73	621	5	621	5	622	16	0
C-1071A_62	**r**	1.5861	2414	2455	3955	0.62	0.05836	5.61	0.69168	6.11	0.08595	2.42	0.40	532	5	534	10	543	49	2
C-1071A_63	**c**	0.3157	3636	4299	4157	1.03	0.06115	2.48	0.87509	5.95	0.10379	5.41	0.91	637	13	638	11	645	21	1
C-1071A_65	**r**	0.6418	4444	149	4836	0.03	0.05933	3.97	0.75039	4.54	0.09174	2.21	0.49	566	5	568	8	579	34	2
C-1071A_66	**r**	0.0000	4419	5444	3942	1.38	0.06065	1.52	0.85891	2.96	0.10271	2.54	0.86	630	6	630	6	627	13	-1
C-1071A_67	**c**	0.1123	3623	697	3436	0.20	0.06064	1.39	0.85390	2.44	0.10213	2.01	0.82	627	5	627	5	626	12	0
C-1071A_68	**r**	0.0000	2458	1740	3941	0.44	0.06042	1.24	0.83990	2.25	0.10082	1.87	0.83	619	4	619	4	619	11	0
C-1071A_69	**c**	0.0000	4776	13483	4263	3.16	0.06074	1.34	0.86507	2.38	0.10329	1.97	0.83	634	5	633	4	630	12	-1
C-1071A_70	**c**	0.2758	4219	262	3169	0.08	0.05985	2.57	0.79219	3.35	0.09599	2.15	0.64	591	5	592	6	598	22	1
C-1071A_71	**c**	1.2656	3936	1253	4017	0.31	0.06482	4.75	1.14510	5.19	0.12813	2.09	0.40	777	6	775	11	768	40	-1
C-1071A_73	**r**	0.9432	4360	2994	4442	0.67	0.06033	4.42	0.81579	5.05	0.09808	2.44	0.48	603	6	606	9	615	38	2
C-1071A_74	**c**	0.0000	4393	2442	4167	0.59	0.06013	1.51	0.82197	2.45	0.09915	1.93	0.79	609	4	609	5	608	13	0

C-1071A_75	**c**	0.0000	3962	979	4068	0.24	0.06094	1.34	0.87844	2.71	0.10455	2.35	0.87	641	6	640	5	637	12	-1
C-1071A_78	**c**	0.2662	4902	668	3589	0.19	0.05858	2.29	0.71315	3.25	0.08830	2.30	0.71	545	5	547	6	551	20	1
C-1071A_79	**c**	0.0000	3730	450	2257	0.20	0.06035	1.46	0.83882	3.87	0.10082	3.59	0.93	619	8	618	7	616	13	-1
C-1071A_80	**c**	0.2805	4803	2447	5031	0.49	0.06103	1.61	0.88507	2.70	0.10495	2.17	0.80	643	5	643	5	640	14	0
C-1071A_81	**c**	0.2805	2803	2447	5031	0.49	0.06103	1.61	0.88307	2.70	0.10495	2.17	0.80	643	5	643	5	640	14	0
C-1071A_82	**c**	0.8069	4555	4279	4458	0.96	0.06281	3.18	1.00648	4.61	0.11621	3.34	0.72	709	9	707	9	702	27	-1
C-1071A_83	**c**	0.1160	3595	2329	3392	0.69	0.06054	2.69	0.84149	3.50	0.10080	2.24	0.64	619	5	620	7	623	23	1
C-1071A_84	**c**	0.0000	3125	125941	47871	2.63	0.06057	2.33	0.84985	3.24	0.10176	2.25	0.70	625	5	625	6	624	20	0
C-1071A_85	**c**	0.7973	3750	347	4573	0.08	0.05852	3.14	0.71431	4.55	0.08852	3.28	0.72	547	7	547	8	549	27	0
C-1071A_86	**c**	0.0177	4978	2164	4856	0.45	0.06029	1.89	0.82959	3.24	0.09980	2.64	0.81	613	6	613	6	614	16	0
C-1071A_87	**c**	0.0000	3368	941	4335	0.22	0.06156	4.20	0.92160	5.02	0.10857	2.75	0.55	664	7	663	10	659	36	-1
C-1071A_89	**c**	0.0000	4251	4338	4320	1.00	0.06220	1.73	0.96765	2.66	0.11283	2.02	0.76	689	5	687	5	681	15	-1
C-1071A_90	**c**	0.3083	4016	1846	3319	0.56	0.06038	2.13	0.84214	2.88	0.10115	1.94	0.67	621	5	620	5	617	18	-1
C-1071A_91	**c**	1.4818	2977	4787	4925	0.97	0.05861	5.50	0.72139	6.78	0.08927	3.96	0.58	551	8	551	12	553	48	0
C-1071A_92	**c**	0.0000	2581	3160	3055	1.03	0.06033	3.46	0.84177	4.04	0.10120	2.08	0.51	621	5	620	8	615	30	-1
C-1071A_93	**c**	1.8003	4789	2455	4663	0.53	0.05801	6.43	0.68334	6.89	0.08544	2.46	0.36	528	5	529	11	530	56	0
C-1071A_95	**c**	0.2403	4170	1448	4110	0.35	0.06129	1.65	0.90249	2.61	0.10679	2.02	0.77	654	5	653	5	650	14	-1
C-1071A_96	**r**	0.5392	5610	2678	4493	0.60	0.05846	2.29	0.69911	3.20	0.08673	2.23	0.70	536	5	538	5	547	20	2

aFraction of the non-radiogenic ^{206}Pb in the analyzed zircon spot, where f_{206}=[$^{206}Pb/^{204}Pb$]c/[$^{206}Pb/^{204}Pb$]s (c=common; s=sample)

bTh/U ratios and amount of Pb, Th and U (in pmm) are calculated relative to 91500 reference zircon

cCorrected for background and within-run Pb/U fractionation and normalised to reference zircon GJ-1 (ID-TIMS values/measured value); $^{207}Pb/^{235}U$ calculated using ($^{207}Pb/^{206}Pb$)/($^{238}U/^{206}Pb$ * 1/137.88)

dRho is the error correlation defined as the quotient of the propagated errors of the $^{206}Pb/^{238}U$ and the $^{207}/^{235}U$ ratio

eDegree of discordance = 100 - ($^{206}Pb/^{238}U$ age * 100/$^{207}Pb/^{206}U$ age)

c-core

r-rim

s-single phase

Hf isotopes results determined by LA-ICP-MS - (Hornblende)-biotite stromatic metatexite (C1071A)

Grain#	CL-Domain	$^{176}Yb/^{177}Hf$ [a]	±2s	$^{176}Lu/^{177}Hf$ [a]	±2s	$^{178}Hf/^{177}Hf$	$^{180}Hf/^{177}Hf$	Sig_{Hf} [b] (V)	$^{176}Hf/^{177}Hf$	±2s [c]	age [f] (Ma)	±2s	$^{176}Hf/^{177}Hf_{(t)}$ [d]	eHf(t) [d]	±2s [c]	age [f] (Ma)	±2s	eHf(t) [d]	±2s [c]
											(measured)					(pref./min.)			
C1071A_02	**r**	0.018785	15	0.000835	5	1.467212	1.886250	13.672144	0.282212	18	708	4	0.282201	-4.9	0.96	719	15	-4.6	0.96
C1071A_03	**c**	0.021674	17	0.000849	5	1.467247	1.886317	12.432277	0.282259	13	618	6	0.282249	-5.2	0.97	618	6	-5.2	0.97
C1071A_04	**c**	0.020214	16	0.000888	5	1.467184	1.886679	13.968932	0.282220	19	630	5	0.282210	-6.3	0.97	719	15	-4.3	0.97
C1071A_05	**c**	0.002188	2	0.000070	0	1.467240	1.886634	13.369546	0.282049	14	680	4	0.282048	-10.9	0.95	680	4	-10.9	0.95
C1071A_06	**c**	0.027887	27	0.001043	8	1.467217	1.886736	14.421892	0.282091	19	652	6	0.282079	-10.5	0.80	652	6	-10.5	0.80
C1071A_09	**r**	0.016484	20	0.000688	8	1.467209	1.886807	15.404871	0.282230	18	642	3	0.282222	-5.6	0.78	719	15	-3.9	0.78
C1071A_11	**c**	0.045027	36	0.001577	9	1.467207	1.886448	10.655532	0.282214	18	816	7	0.282190	-2.8	1.02	816	7	-2.8	1.02
C1071A_12	**c**	0.013724	11	0.000621	4	1.467232	1.886234	13.534640	0.282218	17	719	15	0.282209	-4.3	0.96	719	15	-4.3	0.96
C1071A_13	**c**	0.030929	25	0.001153	7	1.467282	1.885070	10.002359	0.282186	26	666	6	0.282172	-6.8	0.98	719	15	-5.7	0.98
C1071A_14	**c**	0.025993	21	0.001052	6	1.467254	1.886384	12.993641	0.282241	18	686	4	0.282228	-4.4	0.97	719	15	-3.7	0.97
C1071A_15	**c**	0.010820	9	0.000439	3	1.467225	1.885969	15.280063	0.282194	13	687	6	0.282188	-5.8	0.96	719	15	-5.1	0.96
C1071A_17	**c**	0.020799	18	0.000863	6	1.467256	1.886076	14.181350	0.282235	15	648	3	0.282224	-5.4	0.97	719	15	-3.8	0.97
C1071A_18	**c**	0.040280	37	0.001570	12	1.467237	1.886333	11.416941	0.282197	18	869	7	0.282172	-2.3	1.02	869	7	-2.3	1.02
C1071A_19	**c**	0.029767	25	0.001121	7	1.467284	1.884479	10.673516	0.282176	27	665	7	0.282162	-7.2	0.98	719	15	-6.0	0.98
C1071A_21	**c**	0.019529	16	0.000842	5	1.467211	1.886099	11.569378	0.282211	17	676	4	0.282200	-5.6	0.96	719	15	-4.6	0.96
C1071A_22	**c**	0.015856	18	0.000622	6	1.467141	1.886797	15.715617	0.282165	18	717	4	0.282157	-6.2	0.77	719	15	-6.2	0.77
C1071A_25	**r**	0.028381	40	0.001089	13	1.467190	1.886884	15.232707	0.282137	15	713	4	0.282122	-7.5	0.85	719	15	-7.4	0.85
C1071A_26	**c**	0.024762	20	0.000924	6	1.467224	1.886527	13.823442	0.282177	15	680	8	0.282166	-6.7	0.97	719	15	-5.9	0.97
C1071A_28	**c**	0.024489	20	0.000951	6	1.467225	1.886872	15.999518	0.282171	16	676	4	0.282159	-7.1	0.78	719	15	-6.1	0.78
C1071A_29	**r**	0.019975	16	0.000862	5	1.467189	1.886894	15.132984	0.282240	15	728	6	0.282228	-3.4	0.77	728	6	-3.4	0.77
C1071A_30	**c**	0.049966	40	0.001794	11	1.467234	1.886076	8.610303	0.282192	24	698	6	0.282168	-6.2	1.03	719	15	-5.8	1.03
C1071A_31	**c**	0.037137	30	0.001400	8	1.467233	1.886273	10.453387	0.282167	21	628	6	0.282150	-8.4	1.00	719	15	-6.5	1.00
C1071A_34	**c**	0.044238	38	0.001613	10	1.467401	1.884767	10.020950	0.282165	33	587	2	0.282147	-9.5	1.02	719	15	-6.6	1.02
C1071A_35	**c**	0.028530	23	0.001112	7	1.467135	1.886819	16.056716	0.282152	17	652	6	0.282138	-8.3	0.78	719	15	-6.9	0.78
C1071A_36	**c**	0.019546	17	0.000774	5	1.467254	1.886548	12.961096	0.282229	21	651	4	0.282219	-5.5	0.97	719	15	-4.0	0.97
C1071A_37	**c**	0.027402	42	0.001064	12	1.467155	1.886763	13.622852	0.282163	17	670	6	0.282149	-7.5	0.86	719	15	-6.5	0.86
C1071A_41	**c**	0.018233	20	0.000704	6	1.467245	1.886506	10.871051	0.282214	15	573	4	0.282207	-7.7	0.97	719	15	-4.5	0.97

C1071A_42	**c**	0.025642	21	0.000960	6	1.467205	1.886288	14.454440	0.282211	16	634	4	0.282200	-6.6	0.97	719	15	-4.7	0.97
C1071A_43	**c**	0.015634	13	0.000731	4	1.467219	1.886033	15.201118	0.282226	18	659	4	0.282217	-5.4	0.96	719	15	-4.1	0.96
C1071A_44	**c**	0.019551	16	0.000896	5	1.467251	1.885682	13.637244	0.282201	16	645	8	0.282191	-6.6	0.96	719	15	-5.0	0.96
C1071A_45	**r**	0.014639	17	0.000584	6	1.467208	1.886858	12.390872	0.282204	16	621	5	0.282197	-6.9	0.77	719	15	-4.8	0.77
C1071A_46	**c**	0.023964	19	0.000864	5	1.467219	1.885954	18.315851	0.282201	17	613	4	0.282191	-7.3	0.97	719	15	-5.0	0.97
C1071A_47	**r**	0.033484	28	0.001225	8	1.467173	1.886926	11.959166	0.282101	17	675	5	0.282086	-9.7	0.80	675	5	-9.7	0.80
C1071A_48	**c**	0.013433	11	0.000619	4	1.467222	1.886199	14.823571	0.282231	18	645	6	0.282224	-5.5	0.96	719	15	-3.8	0.96
C1071A_49	**c**	0.010390	8	0.000460	3	1.467226	1.886325	15.033642	0.282223	15	615	3	0.282218	-6.3	0.95	719	15	-4.0	0.95
C1071A_50	**c**	0.016811	13	0.000684	4	1.467276	1.886666	14.951459	0.282208	15	638	4	0.282200	-6.5	0.96	719	15	-4.7	0.96
C1071A_53	**c**	0.014025	11	0.000557	3	1.467215	1.886606	10.303227	0.282228	16	641	6	0.282221	-5.7	0.96	719	15	-3.9	0.96
C1071A_54	**c**	0.016810	13	0.000651	4	1.467183	1.886171	11.581540	0.282203	22	668	5	0.282195	-6.0	0.96	719	15	-4.8	0.96
C1071A_56	**c**	0.022421	18	0.000859	5	1.467205	1.886461	10.373962	0.282192	19	633	8	0.282181	-7.2	0.97	719	15	-5.3	0.97
C1071A_57	**c**	0.022724	18	0.000877	5	1.467266	1.886218	11.226713	0.282218	19	658	6	0.282207	-5.8	0.97	719	15	-4.4	0.97
C1071A_58	**c**	0.029747	24	0.001098	7	1.467190	1.886788	15.200199	0.282144	24	564	6	0.282133	-10.5	0.98	719	15	-7.1	0.98
C1071A_59	**c**	0.031195	25	0.001008	6	1.467156	1.885897	14.343509	0.282206	24	627	5	0.282194	-6.9	0.98	719	15	-4.9	0.98
C1071A_60	**c**	0.048176	39	0.001442	9	1.467347	1.886609	9.674863	0.282145	26	677	6	0.282127	-8.2	1.03	719	15	-7.3	1.03
C1071A_61	**c**	0.015438	14	0.000652	5	1.467272	1.886223	10.183149	0.282217	18	621	5	0.282209	-6.5	0.96	719	15	-4.3	0.96
C1071A_63	**c**	0.029989	26	0.001210	8	1.467285	1.886199	9.809220	0.282270	23	637	13	0.282255	-4.5	0.99	637	13	-4.5	0.99
C1071A_66	**r**	0.023087	20	0.000841	6	1.467328	1.885918	10.959123	0.282196	27	630	6	0.282186	-7.1	0.97	719	15	-5.2	0.97
C1071A_67	**c**	0.012759	12	0.000502	4	1.467250	1.886036	11.051615	0.282205	18	627	5	0.282199	-6.7	0.96	719	15	-4.7	0.96
C1071A_68	**c**	0.029805	24	0.000997	6	1.467256	1.886064	17.325770	0.282196	14	619	4	0.282184	-7.4	0.98	719	15	-5.3	0.98
C1071A_69	**c**	0.055391	45	0.002090	13	1.467240	1.886850	11.416383	0.282160	22	634	5	0.282135	-8.9	1.05	719	15	-7.1	1.05
C1071A_70	**c**	0.026489	21	0.001001	6	1.467217	1.886134	11.625711	0.282176	20	591	5	0.282165	-8.8	0.97	719	15	-6.0	0.97
C1071A_71	**c**	0.023229	19	0.000867	5	1.467197	1.886016	15.075906	0.282203	16	777	6	0.282190	-3.7	0.97	816	7	-2.8	0.97
C1071A_75	**c**	0.025991	21	0.000996	6	1.467253	1.886155	12.639580	0.282224	19	641	6	0.282212	-6.0	0.97	719	15	-4.3	0.97
C1071A_78	**c**	0.037600	30	0.001493	9	1.467258	1.885591	9.488796	0.282211	19	545	5	0.282195	-8.7	1.00	719	15	-5.0	1.00
C1071A_79	**c**	0.022386	18	0.000833	5	1.467200	1.886415	13.465132	0.282158	18	619	8	0.282149	-8.7	0.97	719	15	-6.5	0.97
C1071A_80	**c**	0.025583	23	0.000937	7	1.467203	1.886266	13.558753	0.282181	19	643	5	0.282170	-7.4	0.98	719	15	-5.7	0.98
C1071A_81	**c**	0.024771	22	0.001005	7	1.467194	1.886233	13.666897	0.282221	20	643	5	0.282208	-6.0	0.98	719	15	-4.4	0.98
C1071A_82	**c**	0.072401	61	0.002066	13	1.467307	1.886084	13.134776	0.282131	18	709	9	0.282103	-8.3	1.13	719	15	-8.1	1.13
C1071A_83	**c**	0.033010	36	0.001419	13	1.467191	1.887158	11.559634	0.282250	17	619	5	0.282234	-5.7	1.02	719	15	-3.5	1.02
C1071A_84	**c**	0.032065	27	0.001124	7	1.467283	1.885350	10.551753	0.282139	18	625	5	0.282126	-9.4	0.99	719	15	-7.3	0.99
C1071A_85	**c**	0.016140	13	0.000673	5	1.467271	1.886328	14.551021	0.282228	21	547	7	0.282221	-7.8	0.96	719	15	-4.0	0.96

C1071A_86	**c**	0.021892	18	0.000811	5	1.467170	1.886100	13.315560	0.282172	18	613	6	0.282163	-8.3	0.97	719	15	-6.0	0.97
C1071A_87	**c**	0.016746	15	0.000765	6	1.467245	1.885985	10.628018	0.282242	15	664	7	0.282232	-4.7	0.96	719	15	-3.5	0.96
C1071A_89	**c**	0.023744	21	0.000892	6	1.467218	1.886024	12.501820	0.282156	14	689	5	0.282144	-7.3	0.97	719	15	-6.6	0.97
C1071A_90	**c**	0.030680	34	0.001169	11	1.467202	1.886105	10.090135	0.282208	24	621	5	0.282194	-7.0	1.01	719	15	-4.9	1.01
C1071A_92	**c**	0.030337	25	0.001074	7	1.467303	1.885058	8.768531	0.282182	29	621	5	0.282169	-7.9	0.98	719	15	-5.8	0.98
C1071A_95	**c**	0.047401	40	0.001688	11	1.467324	1.884878	8.965763	0.282145	19	654	5	0.282124	-8.8	1.03	719	15	-7.4	1.03

(a) $^{176}Yb/^{177}Hf = (^{176}Yb/^{173}Yb)_{true} \times (^{173}Yb/^{177}Hf)_{meassured} \times (M_{173(Yb)}/M_{177(Hf)})^{b(Hf)}$, $b(Hf) = \ln(^{179}Hf/^{177}Hf_{true} / {}^{179}Hf/^{177}Hf_{measured}) / \ln (M_{179(Hf)}/M_{177(Hf)})$

M=mass of respective isotope. The $^{176}Lu/^{177}Hf$ were calculated in a similar way by using the $^{175}Lu/^{177}Hf$ and b(Yb)

(b) Mean Hf signal in volt

(c) Uncertainties are quadratic additions of the within-run precision and the daily reproducibility of the zircon standards. Uncertainties for the standard quoted at 2SD (2 standard deviation)

(d) Initial $^{176}Hf/^{177}Hf$ and ƐHf calculated using the apparent Pb-Pb ages of respective zircon domains, and the CHUR parameters: $^{176}Lu/^{177}Hf = 0.0336$, and $^{176}Hf/^{177}Hf = 0.282785$ (Bouvier et al., 2008)

(e) Two stage model age in billion years using the measured $^{176}Lu/^{177}Lu$ of each spot (first stage = age of zircon), a value of 0.0113 for the average continental crust (second stage), and a average MORB (DM) $^{176}Lu/^{177}Hf$ and $^{176}Hf/^{177}Hf$ of 0.0384 and 0.283164

Bouvier, A., Vervoort, J.D., Patchett, P.J., 2008. The Lu-Hf and Sm-Nd isotopic composition of CHUR: constraints from unequilibrated chondrites and implications for the bulk composition of terrestrial planets. Earth and Planetary Science Letters 273, 48-57.

(f) $^{206}Pb/^{238}U$ age

c-core

r-rim

s-single phase

Zircon LA-MC-ICP-MS U-Pb results - Standards - 91500, GJ-1, Plesovice, BB

						Isotope ratios[c]							Ages (Ma)						
Spot number	f_{206}[a]	Pb ppm	Th ppm	U ppm	Th/U[b]	207Pb/ 206Pb[e]	2 s [%]	207Pb/ 235U	2 s [%]	206Pb/ 238U	2 s [%]	Rho[d]	^{206}Pb/ ^{238}U	2 s abs	^{207}Pb/ ^{235}U	2 s abs	^{207}Pb/ ^{206}Pb	2 s abs	% Disc.[e]
Amphibolite enclave (PC12.1)																			
91500 Ref. Mat.																			
91500_001	0.0054	11	22	52	0.41	0.07426	1.95	1.79326	4.06	0.18	3.57	0.88	1040	37	1043	42	1049	20	1
91500_002	0.0039	13	24	64	0.38	0.07583	1.99	1.87654	2.59	0.18	1.66	0.64	1064	18	1073	28	1091	22	2
91500_003	0.0036	11	18	51	0.36	0.07412	1.69	1.79003	3.29	0.18	2.82	0.86	1040	29	1042	34	1045	18	0
91500_004	0.0052	10	18	51	0.35	0.07440	1.84	1.83290	3.37	0.18	2.83	0.84	1060	30	1057	36	1052	19	-1
91500_005	0.0024	9	17	50	0.33	0.07436	1.73	1.85590	2.52	0.18	1.84	0.73	1072	20	1066	27	1051	18	-2
91500_006	0.0032	10	19	53	0.36	0.07422	1.94	1.83411	2.57	0.18	1.69	0.65	1063	18	1058	27	1048	20	-1
91500_007	0.0034	12	21	57	0.37	0.07485	2.34	1.85266	3.84	0.18	3.05	0.79	1064	32	1064	41	1064	25	0
91500_008	0.0031	11	20	56	0.35	0.07489	1.82	1.85526	3.45	0.18	2.93	0.85	1065	31	1065	37	1066	19	0
91500_009	0.0039	11	19	56	0.34	0.07504	2.51	1.86708	3.52	0.18	2.47	0.70	1069	26	1069	38	1070	27	0
91500_010	0.0033	11	19	55	0.35	0.07487	2.18	1.85709	3.32	0.18	2.50	0.75	1066	27	1066	35	1065	23	0
Hornblende-biotite stromatic metatexite (PC12.2) - PC-12_2-001 - PC-12_2-080																			
GJ-1 Ref. Mat.																			
GJ-1_1	0.0000	33	5	360	0.01	0.05982	2.08	0.81460	2.91	0.10	2.04	0.70	607	3	605	3	597	11	-2
GJ-1_2	0.0000	31	5	340	0.02	0.05985	2.07	0.81615	3.16	0.10	2.38	0.75	608	3	606	4	598	11	-2
GJ-1_3	2.6857	31	5	337	0.01	0.05992	14.64	0.81648	14.84	0.10	2.47	0.17	608	4	606	17	601	79	-1
GJ-1_5	0.0000	34	5	371	0.01	0.05991	2.44	0.81945	2.81	0.10	1.40	0.50	610	2	608	3	600	13	-2
GJ-1_21	1.2832	32	5	345	0.01	0.05984	7.15	0.81446	7.30	0.10	1.46	0.20	607	2	605	8	598	39	-2
GJ-1_22	0.0000	31	5	338	0.01	0.05991	1.86	0.81960	2.86	0.10	2.17	0.76	610	3	608	3	600	10	-2
GJ-1_23	0.7707	30	5	324	0.02	0.05989	4.66	0.81833	5.28	0.10	2.48	0.47	609	4	607	6	600	25	-2
GJ-1_24	0.0689	31	5	332	0.02	0.05988	2.06	0.81836	3.19	0.10	2.43	0.76	609	4	607	4	599	11	-2

GJ-1_25	0.0000	31	5	332	0.02	0.05986	2.20	0.81712	2.79	0.10	1.72	0.61	609	2	606	3	599	12	-2
GJ-1_41	1.0169	31	5	340	0.02	0.05988	5.97	0.81868	6.46	0.10	2.45	0.38	609	4	607	7	599	32	-2
GJ-1_42	0.1443	30	5	331	0.02	0.05991	2.38	0.81744	3.18	0.10	2.10	0.66	608	3	607	4	600	13	-1
GJ-1_43	0.1745	30	5	329	0.01	0.05990	2.32	0.81857	5.76	0.10	5.28	0.92	609	8	607	7	600	13	-2
GJ-1_44	1.4314	31	5	340	0.02	0.06001	8.02	0.82088	8.27	0.10	2.00	0.24	610	3	609	10	604	43	-1
GJ-1_45	0.6995	32	5	347	0.01	0.05992	4.32	0.82058	4.64	0.10	1.69	0.36	610	2	608	5	601	23	-2
GJ-1_1	0.0000	33	5	359	0.01	0.05987	2.09	0.81901	4.01	0.10	3.43	0.85	610	5	607	5	599	11	-2
GJ-1_2	0.0000	32	5	352	0.01	0.05986	1.91	0.81844	3.55	0.10	2.99	0.84	609	4	607	4	599	10	-2
GJ-1_5	0.0000	32	5	345	0.01	0.05984	1.85	0.81747	2.97	0.10	2.33	0.78	609	3	607	3	598	10	-2
GJ-1_22	0.0000	33	5	358	0.01	0.05992	1.92	0.82093	4.69	0.10	4.28	0.91	611	6	609	5	601	10	-2
GJ-1_23	0.0000	32	5	349	0.01	0.05997	2.00	0.82444	3.22	0.10	2.52	0.78	613	4	611	4	603	11	-2
GJ-1_24	1.0007	36	6	385	0.01	0.06000	5.80	0.82191	6.47	0.10	2.86	0.44	611	4	609	7	604	31	-1
GJ-1_25	1.2373	32	5	346	0.01	0.05995	7.01	0.81938	8.09	0.10	4.04	0.50	609	6	608	9	602	38	-1
GJ-1_26	0.0000	32	5	346	0.01	0.05990	1.92	0.82051	3.25	0.10	2.62	0.81	611	4	608	4	600	10	-2
GJ-1_42	0.2527	33	5	358	0.01	0.05995	2.66	0.81797	3.72	0.10	2.61	0.70	608	4	607	4	602	14	-1
GJ-1_43	0.0000	33	5	353	0.01	0.05990	1.80	0.82111	3.56	0.10	3.07	0.86	611	4	609	4	600	10	-2
GJ-1_44	0.0000	32	5	350	0.01	0.05992	1.85	0.82112	4.83	0.10	4.47	0.92	611	7	609	6	601	10	-2
GJ-1_45	1.3677	31	5	335	0.01	0.05994	7.67	0.82076	8.04	0.10	2.40	0.30	610	3	608	9	602	41	-1
GJ-1_46	1.5652	31	5	338	0.01	0.05991	8.65	0.81684	9.15	0.10	2.99	0.33	608	4	606	10	600	47	-1
GJ-1_62	0.0000	30	5	321	0.01	0.05991	1.95	0.82012	4.39	0.10	3.93	0.90	610	6	608	5	600	11	-2
GJ-1_63	0.0000	31	5	332	0.01	0.05993	2.51	0.82104	3.98	0.10	3.09	0.78	611	4	609	5	601	14	-2
GJ-1_64	0.0000	30	5	330	0.01	0.05991	2.18	0.82065	3.63	0.10	2.90	0.80	611	4	608	4	600	12	-2
GJ-1_65	0.0000	31	5	341	0.01	0.05993	2.02	0.82010	3.08	0.10	2.32	0.75	610	3	608	4	601	11	-1
GJ-1_66	0.0000	27	4	293	0.01	0.05991	2.22	0.81937	3.75	0.10	3.02	0.81	610	4	608	4	600	12	-2
GJ-1_82	0.0000	27	4	293	0.01	0.05984	1.91	0.82115	3.55	0.10	3.00	0.84	612	4	609	4	598	10	-2
GJ-1_83	0.0000	27	4	293	0.01	0.06000	2.16	0.82094	3.52	0.10	2.78	0.79	610	4	609	4	603	12	-1
GJ-1_84	0.1071	29	4	315	0.01	0.05989	2.05	0.81948	4.27	0.10	3.74	0.88	610	5	608	5	600	11	-2
GJ-1_85	0.0000	28	4	303	0.01	0.05993	1.91	0.82111	3.85	0.10	3.34	0.87	611	5	609	4	601	10	-2

GJ-1_86	0.0000	29	4	314	0.01	0.05995	2.11	0.82166	4.54	0.10	4.01	0.89	611	6	609	5	602	11	-2
GJ-1_102	0.0000	29	5	317	0.01	0.05990	3.30	0.81996	4.70	0.10	3.34	0.71	610	5	608	5	600	18	-2
GJ-1_103	0.0000	29	4	319	0.01	0.05991	3.17	0.82074	4.35	0.10	2.98	0.68	611	4	608	5	600	17	-2
GJ-1_104	0.0000	28	4	304	0.01	0.05989	3.26	0.82227	4.87	0.10	3.62	0.74	612	5	609	6	600	18	-2
GJ-1_105	0.7823	30	5	322	0.01	0.05990	5.21	0.81873	5.87	0.10	2.71	0.46	609	4	607	7	600	28	-2
GJ-1_106	0.0000	30	5	330	0.01	0.05989	3.13	0.82026	5.18	0.10	4.13	0.80	610	6	608	6	600	17	-2
GJ-1_122	1.2114	27	4	294	0.01	0.06008	7.34	0.82394	9.02	0.10	5.24	0.58	611	8	610	10	606	40	-1
GJ-1_123	0.0000	28	4	303	0.01	0.05994	3.40	0.82362	5.36	0.10	4.14	0.77	612	6	610	6	602	18	-2
GJ-1_124	0.0000	31	5	324	0.01	0.06051	3.23	0.86299	5.88	0.10	4.91	0.84	635	7	632	7	622	17	-2
GJ-1_125	0.0000	29	4	311	0.01	0.05997	3.37	0.81856	5.77	0.10	4.68	0.81	609	7	607	7	602	18	-1
GJ-1_126	0.0000	27	4	296	0.01	0.06002	3.22	0.82791	7.43	0.10	6.70	0.90	615	10	612	9	604	17	-2
91500 Ref. Mat.																			
91500_6	0.0000	31	30	171	0.18	0.07350	2.28	1.77291	3.12	0.17	2.13	0.68	1039	5	1036	5	1028	12	-1
91500_7	0.0000	29	28	160	0.18	0.07348	2.63	1.77022	3.65	0.17	2.53	0.69	1038	6	1035	6	1027	13	-1
91500_8	0.0000	28	27	157	0.17	0.07349	2.11	1.76904	3.66	0.17	2.99	0.82	1037	7	1034	6	1028	11	-1
91500_9	0.0000	29	28	162	0.17	0.07353	2.17	1.77174	4.02	0.17	3.39	0.84	1038	8	1035	7	1029	11	-1
91500_27	0.0000	26	24	140	0.17	0.07353	2.65	1.77613	3.50	0.18	2.29	0.65	1041	5	1037	6	1029	13	-1
91500_28	0.0000	26	25	145	0.17	0.07360	2.06	1.77926	3.12	0.18	2.34	0.75	1041	6	1038	5	1031	10	-1
91500_29	0.0000	25	24	136	0.17	0.07365	2.19	1.78459	3.23	0.18	2.36	0.73	1044	6	1040	5	1032	11	-1
91500_46	0.0000	27	25	147	0.17	0.07344	2.22	1.76829	4.09	0.17	3.44	0.84	1038	8	1034	7	1026	11	-1
91500_47	0.0000	31	30	169	0.18	0.07349	2.39	1.77025	4.20	0.17	3.46	0.82	1038	8	1035	7	1027	12	-1
91500_48	0.0000	26	25	143	0.17	0.07340	2.22	1.76432	3.93	0.17	3.24	0.82	1036	8	1032	6	1025	11	-1
91500_49	0.0000	26	24	142	0.17	0.07349	2.25	1.77018	3.70	0.17	2.94	0.79	1038	7	1035	6	1028	11	-1
91500_6	0.0000	23	21	126	0.17	0.07358	2.06	1.77843	3.74	0.18	3.12	0.83	1041	7	1038	6	1030	10	-1
91500_7	0.0000	22	20	119	0.17	0.07372	2.38	1.79032	3.63	0.18	2.75	0.76	1046	7	1042	6	1034	12	-1
91500_8	1.0167	21	19	113	0.17	0.07364	5.00	1.78343	6.23	0.18	3.72	0.60	1043	9	1039	10	1032	25	-1
91500_9	0.0000	20	18	108	0.16	0.07376	2.01	1.79354	3.36	0.18	2.70	0.80	1047	7	1043	5	1035	10	-1

91500_10	0.0000	20	17	107	0.16	0.07368	2.23	1.78470	3.53	0.18	2.74	0.78	1043	7	1040	6	1033	11	-1
91500_27	0.0000	28	27	155	0.17	0.07351	2.16	1.77466	2.89	0.18	1.91	0.66	1040	5	1036	5	1028	11	-1
91500_28	0.0000	29	27	160	0.17	0.07370	2.07	1.78777	2.55	0.18	1.49	0.59	1045	4	1041	4	1033	10	-1
91500_29	0.0000	25	22	134	0.16	0.07363	2.83	1.78354	3.47	0.18	2.01	0.58	1043	5	1039	6	1031	14	-1
91500_30	0.0000	22	19	118	0.16	0.07359	2.20	1.77892	2.79	0.18	1.72	0.62	1041	4	1038	5	1030	11	-1
91500_31	0.0000	24	21	130	0.16	0.07377	2.44	1.78358	2.90	0.18	1.58	0.54	1042	4	1039	5	1035	12	-1
91500_47	0.0000	23	21	128	0.16	0.07364	2.10	1.78148	2.65	0.18	1.62	0.61	1042	4	1039	4	1032	11	-1
91500_48	0.0000	24	21	130	0.16	0.07357	1.93	1.77722	2.55	0.18	1.68	0.66	1041	4	1037	4	1030	10	-1
91500_49	0.0000	24	22	133	0.16	0.07361	1.88	1.78027	2.34	0.18	1.39	0.60	1042	3	1038	4	1031	10	-1
91500_50	0.0000	24	22	133	0.16	0.07363	2.22	1.78041	2.75	0.18	1.64	0.59	1042	4	1038	4	1031	11	-1
91500_51	0.0000	26	23	140	0.16	0.07388	2.28	1.78372	3.06	0.18	2.04	0.67	1040	5	1040	5	1038	12	0
91500_67	0.0000	23	20	123	0.17	0.07353	2.33	1.77662	2.88	0.18	1.69	0.59	1041	4	1037	5	1029	12	-1
91500_68	0.0000	25	23	136	0.17	0.07355	1.99	1.77598	2.67	0.18	1.78	0.67	1040	4	1037	4	1029	10	-1
91500_69	0.0000	27	24	145	0.16	0.07369	1.92	1.78784	2.43	0.18	1.49	0.61	1045	4	1041	4	1033	10	-1
91500_70	0.0000	25	22	134	0.16	0.07366	2.12	1.78404	2.62	0.18	1.54	0.59	1043	4	1040	4	1032	11	-1
91500_71	0.0000	25	23	139	0.16	0.07361	2.21	1.78007	2.61	0.18	1.40	0.53	1042	3	1038	4	1031	11	-1
91500_87	0.0000	31	28	168	0.17	0.07370	2.15	1.77647	2.54	0.17	1.35	0.53	1039	3	1037	4	1033	11	-1
91500_88	0.0000	28	25	154	0.16	0.07370	1.96	1.78206	2.61	0.18	1.72	0.66	1042	4	1039	4	1033	10	-1
91500_89	0.2579	29	28	154	0.18	0.07401	4.90	1.81040	5.97	0.18	3.41	0.57	1053	8	1049	10	1042	25	-1
91500_90	0.0000	33	30	179	0.17	0.07392	4.26	1.78681	4.54	0.18	1.57	0.35	1041	4	1041	7	1039	22	0
91500_91	0.0000	34	31	181	0.17	0.07414	7.56	1.81002	7.72	0.18	1.56	0.20	1051	4	1049	13	1045	38	-1
91500_107	0.0000	34	32	188	0.17	0.07348	2.90	1.77590	3.26	0.18	1.49	0.46	1041	4	1037	5	1027	15	-1
91500_108	0.0000	31	28	170	0.17	0.07391	3.23	1.78651	3.87	0.18	2.13	0.55	1041	5	1041	6	1039	16	0
91500_109	0.0000	29	26	157	0.17	0.07358	3.07	1.78017	3.38	0.18	1.41	0.42	1042	3	1038	6	1030	16	-1
91500_110	0.0000	29	27	161	0.17	0.07355	3.24	1.78090	3.69	0.18	1.76	0.48	1043	4	1039	6	1029	16	-1
91500_111	0.0000	34	32	186	0.17	0.07383	3.17	1.78874	3.54	0.18	1.58	0.45	1044	4	1041	6	1037	16	-1
91500_127	0.0000	21	19	113	0.17	0.07360	3.52	1.78500	4.15	0.18	2.19	0.53	1044	5	1040	7	1031	18	-1
91500_128	0.0000	21	19	117	0.16	0.07359	3.52	1.77877	4.04	0.18	1.98	0.49	1041	5	1038	7	1030	18	-1
91500_129	0.0836	23	20	123	0.16	0.07388	4.04	1.77746	4.43	0.17	1.80	0.41	1037	4	1037	7	1038	20	0

91500_130	0.0000	22	19	119	0.16	0.07356	3.49	1.77826	3.90	0.18	1.73	0.44	1041	4	1038	6	1029	18	-1
91500_131	0.0000	24	21	130	0.16	0.07406	3.87	1.79034	4.74	0.18	2.74	0.58	1041	7	1042	8	1043	20	0

Hornblende-biotite stromatic metatexite (PC12.2) - PC-12_2-082 - PC-12_2-194

GJ-1 Ref. Mat.

GJ-1_021	1.0000	31	7	441	0.02	0.05955	4.30	0.80617	4.90	0.10	2.34	0.48	604	14	600	22	587	93	-1
GJ-1_041	0.0000	31	6	324	0.02	0.05936	2.39	0.79955	2.65	0.10	1.15	0.43	601	7	597	12	580	52	-1
GJ-1_042	0.0000	34	6	318	0.02	0.06078	2.40	0.81985	2.66	0.10	1.14	0.43	602	7	608	12	631	52	1
GJ-1_061	0.0130	32	5	287	0.02	0.06003	2.50	0.80662	2.78	0.10	1.21	0.44	599	7	601	13	605	54	0
GJ-1_062	0.0000	31	5	271	0.02	0.06076	2.73	0.81564	3.02	0.10	1.29	0.43	599	7	606	14	631	59	1
GJ-1_081	0.2707	30	5	253	0.02	0.05994	2.76	0.80807	3.10	0.10	1.42	0.46	601	8	601	14	601	60	0
GJ-1_082	0.0020	31	5	251	0.02	0.06095	2.59	0.81633	2.91	0.10	1.32	0.45	598	8	606	13	637	56	1
GJ-1_101	0.1667	31	5	235	0.02	0.05988	2.79	0.80787	3.16	0.10	1.47	0.47	602	8	601	14	599	61	0
GJ-1_102	0.0000	28	5	226	0.02	0.05974	2.75	0.80524	3.10	0.10	1.43	0.46	601	8	600	14	594	59	0

GJ-1_101	0.1666	31	5	325	0.01	0.05968	2.31	0.80107	2.64	0.10	1.28	0.48	599	7	597	12	592	50	0
GJ-1_102	0.0000	30	5	313	0.02	0.05948	2.22	0.79690	2.54	0.10	1.23	0.49	598	7	595	12	585	48	0
GJ-1_121	0.0000	31	5	312	0.02	0.06002	2.23	0.80720	2.56	0.10	1.25	0.49	600	7	601	12	604	48	0
GJ-1_161	1.0000	27	5	286	0.02	0.05944	4.09	0.81428	4.75	0.10	2.42	0.51	611	14	605	22	583	89	-1
GJ-1_162	0.0000	27	5	279	0.02	0.06068	2.31	0.81373	2.68	0.10	1.36	0.51	598	8	605	12	628	50	1
GJ-1_182	0.0222	28	5	275	0.02	0.06062	2.34	0.80895	2.73	0.10	1.41	0.51	596	8	602	12	626	51	1
GJ-1_142	0.1428	27	5	287	0.02	0.05883	2.33	0.79114	2.69	0.10	1.34	0.50	600	8	592	12	561	51	-1

GJ-1_181	0.1530	29	4	263	0.02	0.05814	2.43	0.78072	2.82	0.10	1.43	0.51	599	8	586	13	535	53	-2
Plesovice Ref. Mat.																			
PLES_023	0.0000	31	43	638	0.07	0.05301	4.00	0.39593	4.30	0.05	1.59	0.37	340	5	339	12	329	91	0
PLES_043	0.0000	30	70	885	0.08	0.05306	2.53	0.39557	2.79	0.05	1.18	0.42	339	4	338	8	331	57	0
PLES_044	0.0000	28	76	779	0.10	0.05292	2.42	0.39278	2.68	0.05	1.15	0.43	338	4	336	8	325	55	0
PLES_063	0.3530	44	69	681	0.10	0.05341	2.80	0.39392	3.33	0.05	1.81	0.54	336	6	337	10	346	63	0
PLES_064	0.0000	41	69	753	0.09	0.05293	2.46	0.39241	2.75	0.05	1.23	0.45	338	4	336	8	326	56	0
PLES_083	0.0000	14	62	690	0.09	0.05281	2.92	0.39269	3.26	0.05	1.45	0.44	339	5	336	9	321	66	-1
PLES_084	0.0000	11	59	662	0.09	0.05353	2.58	0.39435	2.89	0.05	1.31	0.45	336	4	338	8	351	58	1
PLES_103	0.0000	12	54	594	0.09	0.05273	2.73	0.39282	3.07	0.05	1.41	0.46	339	5	336	9	317	62	-1
PLES_104	0.0000	30	47	536	0.09	0.05311	2.79	0.39536	3.14	0.05	1.44	0.46	339	5	338	9	333	63	0
PLES_103	0.0000	22	56	817	0.07	0.05311	2.18	0.39631	2.50	0.05	1.22	0.49	340	4	339	7	333	50	0
PLES_104	0.0000	21	50	749	0.07	0.05338	2.21	0.39685	2.53	0.05	1.22	0.48	339	4	339	7	345	50	0
PLES_123	0.0000	22	56	803	0.07	0.05267	2.24	0.39324	2.57	0.05	1.26	0.49	340	4	337	7	315	51	-1
PLES_124	0.0000	24	49	714	0.07	0.05343	2.10	0.39303	2.43	0.05	1.24	0.51	335	4	337	7	347	47	0
PLES_143	0.0000	23	53	743	0.07	0.05252	2.21	0.39097	2.56	0.05	1.30	0.51	339	4	335	7	308	50	-1
PLES_144	0.0000	30	24	390	0.06	0.05327	2.37	0.39486	2.70	0.05	1.30	0.48	338	4	338	8	340	54	0
PLES_163	0.0000	15	23	373	0.06	0.05344	2.43	0.39428	2.80	0.05	1.38	0.49	336	5	337	8	348	55	0
PLES_164	0.0000	15	24	369	0.06	0.05383	2.42	0.39753	2.78	0.05	1.38	0.50	336	5	340	8	364	54	1
PLES_183	0.0000	18	21	303	0.07	0.05344	2.54	0.39524	2.91	0.05	1.42	0.49	337	5	338	8	348	58	0
PLES_184	0.0000	25	24	359	0.07	0.05301	2.45	0.39352	2.83	0.05	1.41	0.50	338	5	337	8	329	56	0
BB Ref. Mat.																			
BB_025	0.0000	36	121	527	0.23	0.05937	2.63	0.74467	2.87	0.09	1.14	0.40	561	6	565	12	581	57	1
BB_026	0.1140	39	124	542	0.23	0.05951	2.58	0.74301	2.84	0.09	1.18	0.41	559	6	564	12	586	56	1
BB_045	0.1759	36	114	441	0.26	0.05826	2.48	0.73048	2.77	0.09	1.23	0.44	561	7	557	12	539	54	-1
BB_046	0.0000	38	115	440	0.26	0.05823	2.40	0.73198	2.67	0.09	1.16	0.44	562	6	558	12	538	53	-1

BB_085	0.0000	34	103	354	0.29	0.05841	2.74	0.73771	3.07	0.09	1.38	0.45	565	7	561	13	545	60	-1
BB_086	0.0000	31	98	346	0.28	0.05901	2.68	0.73617	3.01	0.09	1.37	0.46	558	7	560	13	567	58	0
BB_105	0.0000	33	102	336	0.30	0.05949	2.79	0.74175	3.16	0.09	1.48	0.47	558	8	563	14	585	61	1
BB_106	0.0000	32	92	314	0.29	0.05926	2.73	0.74428	3.09	0.09	1.45	0.47	562	8	565	13	577	59	1
BB_105	0.0000	35	106	458	0.23	0.05937	2.26	0.74034	2.59	0.09	1.26	0.49	558	7	563	11	581	49	1
BB_106	0.0000	32	96	429	0.22	0.05846	2.26	0.73858	2.59	0.09	1.27	0.49	565	7	562	11	547	49	-1
BB_125	0.1132	32	91	404	0.23	0.05830	2.33	0.73154	2.68	0.09	1.32	0.49	561	7	557	12	541	51	-1
BB_126	0.0000	31	94	416	0.23	0.05855	2.22	0.73205	2.55	0.09	1.26	0.49	560	7	558	11	550	48	0
BB_145	0.2075	32	91	397	0.23	0.05920	2.73	0.73818	3.09	0.09	1.45	0.47	558	8	561	13	574	59	1
BB_146	0.0000	46	94	395	0.24	0.05865	2.39	0.73136	2.74	0.09	1.35	0.49	558	7	557	12	554	52	0
BB_165	0.0000	41	78	344	0.23	0.05852	2.46	0.73377	2.82	0.09	1.39	0.49	561	7	559	12	549	54	0
BB_166	0.0928	42	86	363	0.24	0.05786	2.48	0.72960	2.85	0.09	1.41	0.50	564	8	556	12	524	54	-1
BB_185	0.0626	42	87	358	0.24	0.05794	2.70	0.73222	3.08	0.09	1.49	0.48	565	8	558	13	528	59	-1
BB_186	0.0000	42	86	358	0.24	0.05770	2.77	0.72890	3.17	0.09	1.53	0.48	565	8	556	14	518	61	-2

Biotite-bearing pink leucosome (PC12.3)

GJ-1 Ref. Mat.

GJ-1_22	0.0000	31	5	340	0.02	0.06019	2.13	0.82073	3.12	0.10	2.29	0.73	608	3	608	4	610	12	0
GJ-1_23	0.0000	30	5	332	0.02	0.06013	1.98	0.82066	2.83	0.10	2.03	0.72	608	3	608	3	608	11	0
GJ-1_24	0.0537	31	5	337	0.02	0.06002	2.10	0.81154	4.70	0.10	4.21	0.90	603	6	603	5	604	11	0
GJ-1_25	0.4070	31	5	342	0.02	0.06008	2.99	0.81669	3.63	0.10	2.06	0.57	606	3	606	4	606	16	0
GJ-1_41	0.0990	32	6	346	0.02	0.06010	2.17	0.81706	3.72	0.10	3.03	0.81	606	4	606	4	607	12	0
GJ-1_42	0.3371	32	6	351	0.02	0.06019	2.75	0.82312	3.37	0.10	1.95	0.58	610	3	610	4	611	15	0
GJ-1_43	0.0000	30	5	326	0.02	0.06018	1.97	0.82246	2.72	0.10	1.87	0.69	609	3	609	3	610	11	0
GJ-1_44	0.0000	29	5	317	0.02	0.06011	2.07	0.81711	2.79	0.10	1.87	0.67	606	3	606	3	607	11	0
GJ-1_45	0.0919	28	5	309	0.02	0.06012	2.66	0.81675	3.51	0.10	2.29	0.65	606	3	606	4	608	14	0

GJ-1_61	0.1358	33	5	356	0.02	0.06009	2.34	0.81793	3.44	0.10	2.53	0.73	607	4	607	4	607	13	0
GJ-1_62	0.1744	32	5	349	0.02	0.06013	2.24	0.82055	2.85	0.10	1.75	0.62	608	3	608	3	608	12	0
GJ-1_63	0.0236	29	5	315	0.02	0.06011	2.05	0.81900	2.67	0.10	1.71	0.64	607	2	607	3	607	11	0
GJ-1_64	0.0040	30	5	326	0.01	0.06014	1.95	0.82091	3.24	0.10	2.58	0.80	609	4	609	4	609	11	0
GJ-1_65	0.5143	31	5	333	0.02	0.06011	3.63	0.81866	4.39	0.10	2.46	0.56	607	4	607	5	608	20	0
GJ-1_82	0.0000	34	5	337	0.01	0.06011	2.03	0.82201	3.15	0.10	2.41	0.77	610	4	609	4	608	11	0
GJ-1_83	0.0000	32	5	311	0.02	0.06014	3.14	0.82351	3.98	0.10	2.45	0.62	610	4	610	5	609	17	0
GJ-1_84	0.0000	31	5	308	0.01	0.06008	2.16	0.82013	2.74	0.10	1.69	0.62	609	2	608	3	607	12	0
GJ-1_85	0.0000	33	5	326	0.02	0.06015	2.32	0.82289	3.03	0.10	1.95	0.64	610	3	610	3	609	13	0
GJ-1_121	0.0649	20	5	217	0.02	0.06014	2.38	0.81949	2.68	0.10	1.23	0.46	608	2	608	3	609	13	0
GJ-1_122	0.0321	21	5	233	0.02	0.06008	2.47	0.81754	2.98	0.10	1.67	0.56	607	2	607	3	607	13	0
GJ-1_123	0.0482	21	5	230	0.02	0.06011	2.10	0.81838	2.51	0.10	1.38	0.55	607	2	607	3	608	11	0
GJ-1_124	0.1378	20	5	217	0.02	0.06012	3.50	0.81890	4.11	0.10	2.14	0.52	607	3	607	5	608	19	0
GJ-1_125	0.3425	21	5	225	0.02	0.06010	3.52	0.81805	3.81	0.10	1.46	0.38	607	2	607	4	607	19	0
GJ-1_141	0.0375	22	5	236	0.02	0.06008	2.66	0.81541	3.24	0.10	1.84	0.57	605	3	605	4	606	14	0
GJ-1_142	0.0292	22	5	234	0.02	0.06015	2.51	0.82073	3.00	0.10	1.65	0.55	608	2	608	3	609	14	0
GJ-1_143	0.0000	21	5	228	0.02	0.06013	2.61	0.82083	3.01	0.10	1.50	0.50	609	2	609	3	608	14	0
GJ-1_144	0.0592	21	5	232	0.02	0.06011	2.50	0.81792	3.14	0.10	1.90	0.61	607	3	607	4	608	14	0
GJ-1_145	0.8036	24	6	261	0.02	0.06014	5.12	0.81875	5.68	0.10	2.44	0.43	607	4	607	7	609	28	0
BB Ref. Mat.																			
BB-9_26	0.0316	41	67	442	0.15	0.05886	2.45	0.73910	3.76	0.09	2.85	0.76	562	4	562	4	562	13	0
BB-9_27	0.0000	42	67	443	0.15	0.05889	2.37	0.73960	3.50	0.09	2.58	0.74	562	3	562	4	563	13	0
BB-9_28	0.0386	44	71	472	0.15	0.05888	2.02	0.73899	2.77	0.09	1.89	0.68	562	3	562	3	563	11	0
BB-9_29	0.4535	44	74	473	0.16	0.05887	3.31	0.73859	3.87	0.09	1.99	0.51	561	3	562	4	562	18	0
BB-9_30	0.0415	41	65	444	0.15	0.05886	2.07	0.73878	3.47	0.09	2.78	0.80	562	4	562	4	562	11	0
BB-9_46	0.0145	45	74	479	0.15	0.05886	2.07	0.73880	2.97	0.09	2.14	0.72	562	3	562	3	562	11	0
BB-9_47	0.0000	47	78	504	0.16	0.05884	2.12	0.73624	2.94	0.09	2.03	0.69	560	3	560	3	561	12	0
BB-9_48	0.0000	42	65	447	0.15	0.05882	2.01	0.73626	2.86	0.09	2.03	0.71	560	3	560	3	560	11	0

BB-9_49	0.0000	47	77	499	0.15	0.05890	2.08	0.74043	3.20	0.09	2.44	0.76	562	3	563	3	563	11	0
BB-9_50	0.0000	46	76	494	0.15	0.05889	2.09	0.73922	3.27	0.09	2.51	0.77	562	3	562	4	563	11	0
BB-9_66	0.0243	41	67	441	0.15	0.05886	2.40	0.73862	3.15	0.09	2.04	0.65	562	3	562	3	562	13	0
BB-9_67	0.2988	42	67	453	0.15	0.05886	2.62	0.73886	3.18	0.09	1.79	0.56	562	2	562	3	562	14	0
BB-9_68	0.0000	42	66	452	0.15	0.05888	2.21	0.73899	2.79	0.09	1.71	0.61	562	2	562	3	563	12	0
BB-9_69	0.0000	42	68	452	0.15	0.05884	1.84	0.73665	2.55	0.09	1.76	0.69	560	2	560	3	561	10	0
BB-9_70	0.0534	43	70	455	0.15	0.05887	2.05	0.73777	2.99	0.09	2.18	0.73	561	3	561	3	562	11	0
BB-9_86	0.2611	32	50	343	0.14	0.05890	2.51	0.73979	3.34	0.09	2.20	0.66	562	3	562	4	563	14	0
BB-9_87	0.5498	33	52	358	0.15	0.05879	3.84	0.73302	4.27	0.09	1.86	0.44	558	2	558	5	559	21	0
BB-9_88	0.3101	31	48	329	0.15	0.05885	3.05	0.73850	3.76	0.09	2.20	0.58	562	3	562	4	562	17	0
BB-9_89	0.0000	32	50	343	0.14	0.05882	1.92	0.73540	2.73	0.09	1.94	0.71	560	3	560	3	560	10	0
BB-9_90	0.0221	33	51	350	0.15	0.05892	1.94	0.74156	2.80	0.09	2.02	0.72	563	3	563	3	564	11	0
BB-9_101	0.7365	36	56	389	0.14	0.05881	4.66	0.73536	5.00	0.09	1.82	0.36	560	2	560	5	560	25	0
BB-9_102	0.0000	39	62	426	0.15	0.05885	2.08	0.73753	2.73	0.09	1.77	0.65	561	2	561	3	561	11	0
BB-9_103	0.0198	36	57	391	0.15	0.05882	1.94	0.73599	2.61	0.09	1.74	0.67	560	2	560	3	560	11	0
BB-9_104	0.0000	38	59	409	0.15	0.05889	1.84	0.74036	2.49	0.09	1.69	0.68	562	2	563	3	563	10	0
BB-9_105	0.0522	37	59	407	0.15	0.05883	1.91	0.73570	2.53	0.09	1.66	0.66	560	2	560	3	561	10	0
BB-9_106	0.1478	32	50	343	0.15	0.05888	2.25	0.73915	2.94	0.09	1.89	0.64	562	3	562	3	563	12	0
BB-9_107	0.0348	34	53	362	0.15	0.05891	2.17	0.74039	2.75	0.09	1.68	0.61	562	2	563	3	564	12	0
BB-9_108	0.1951	31	49	333	0.15	0.05884	2.24	0.73620	2.94	0.09	1.91	0.65	560	3	560	3	561	12	0
BB-9_109	0.0000	33	51	350	0.15	0.05882	2.07	0.73674	3.01	0.09	2.19	0.73	561	3	561	3	560	11	0
BB-9_110	0.2372	32	50	342	0.15	0.05883	2.44	0.73647	3.01	0.09	1.77	0.59	560	2	560	3	561	13	0
BB-9_126	0.1666	32	50	341	0.15	0.05887	2.21	0.73861	2.93	0.09	1.93	0.66	561	3	562	3	562	12	0
BB-9_127	0.0473	35	54	373	0.15	0.05885	2.08	0.73768	2.91	0.09	2.04	0.70	561	3	561	3	561	11	0
BB-9_128	0.0553	32	49	337	0.15	0.05885	2.37	0.73856	2.91	0.09	1.69	0.58	562	2	562	3	561	13	0
BB-9_129	0.0553	32	49	337	0.15	0.05885	2.37	0.73856	2.91	0.09	1.69	0.58	562	2	562	3	561	13	0
BB-9_130	0.0073	31	48	332	0.15	0.05883	2.45	0.73757	2.86	0.09	1.49	0.52	561	2	561	3	561	13	0
BB-9_146	0.3310	31	48	330	0.15	0.05886	2.75	0.73921	3.44	0.09	2.07	0.60	562	3	562	4	562	15	0

BB-9_147	0.0466	29	45	312	0.15	0.05883	2.48	0.73603	3.18	0.09	1.98	0.62	560	3	560	3	561	14	0
BB-9_148	0.0467	31	49	334	0.15	0.05885	2.12	0.73749	2.56	0.09	1.44	0.56	561	2	561	3	561	12	0
BB-9_149	0.0000	31	48	330	0.15	0.05892	2.00	0.74113	2.54	0.09	1.57	0.62	563	2	563	3	564	11	0
BB-9_150	0.0000	30	47	321	0.15	0.05886	2.11	0.73828	2.72	0.09	1.71	0.63	561	2	561	3	562	12	0
Garnet-biotite stromatic metatexite (PC12.4)																			
GJ-1 Ref. Mat.																			
GJ-1_1	0.0000	31	5	340	0.02	0.05984	1.33	0.81602	1.99	0.10	1.47	0.74	608	3	606	3	598	10	-2
GJ-1_2	0.0000	31	5	342	0.02	0.05990	1.46	0.81815	2.23	0.10	1.68	0.76	609	3	607	3	600	11	-1
GJ-1_3	0.0000	29	5	313	0.02	0.05997	1.73	0.82220	2.16	0.10	1.30	0.60	611	3	609	3	602	12	-1
GJ-1_17	0.3996	24	4	265	0.01	0.05986	2.42	0.81447	7.30	0.10	6.89	0.94	607	13	605	11	599	17	-1
GJ-1_18	0.0000	24	4	260	0.01	0.05993	1.63	0.82068	4.00	0.10	3.65	0.91	610	7	608	6	601	12	-2
GJ-1_19	0.0000	25	4	272	0.01	0.05983	1.69	0.81413	3.74	0.10	3.33	0.89	607	6	605	6	598	12	-2
GJ-1_33	0.0000	26	4	285	0.01	0.05991	1.68	0.81818	5.39	0.10	5.12	0.95	609	10	607	8	600	12	-1
GJ-1_34	0.0000	26	4	282	0.01	0.05986	1.76	0.81480	5.67	0.10	5.39	0.95	607	10	605	9	599	13	-1
GJ-1_35	0.0000	28	4	304	0.01	0.05989	1.50	0.81812	2.82	0.10	2.39	0.85	609	5	607	4	600	11	-2
GJ-1_49	0.0000	31	5	334	0.01	0.05986	1.56	0.81609	4.45	0.10	4.17	0.94	608	8	606	7	599	11	-2
GJ-1_50	0.0000	30	5	330	0.01	0.05985	1.59	0.81648	5.20	0.10	4.96	0.95	608	10	606	8	598	11	-2
GJ-1_51	0.0000	31	5	340	0.02	0.05989	1.86	0.82040	4.44	0.10	4.04	0.91	611	8	608	7	600	13	-2
GJ-1_65	0.0000	32	5	345	0.01	0.05979	1.69	0.81608	3.22	0.10	2.74	0.85	608	5	606	5	596	12	-2
GJ-1_66	0.0000	30	5	329	0.01	0.05999	12.11	0.82480	12.35	0.10	2.45	0.20	613	5	611	19	603	87	-2
GJ-1_67	0.0000	31	5	337	0.01	0.05995	1.80	0.82196	3.71	0.10	3.25	0.88	611	6	609	6	602	13	-2
GJ-1_11	0.0000	33	5	359	0.01	0.05990	1.55	0.81871	1.80	0.10	0.91	0.50	609	2	607	3	600	11	-2
GJ-1_12	0.0000	32	5	345	0.01	0.05985	1.41	0.81555	1.70	0.10	0.94	0.56	608	2	606	3	598	10	-2
GJ-1_14	0.5548	31	5	337	0.01	0.05987	2.77	0.81540	3.04	0.10	1.25	0.41	607	2	605	5	599	20	-1
GJ-1_29	0.0000	24	1	237	0.00	0.06146	1.48	0.91859	2.63	0.11	2.17	0.83	663	5	662	4	656	11	-1
GJ-1_30	0.0000	31	5	339	0.01	0.06004	1.65	0.82236	2.04	0.10	1.19	0.59	611	2	609	3	605	12	-1
GJ-1_31	0.0000	31	5	332	0.02	0.05992	1.52	0.81989	1.89	0.10	1.13	0.60	610	2	608	3	601	11	-2
GJ-1_32	0.0000	30	5	333	0.02	0.05982	1.48	0.81409	3.00	0.10	2.62	0.87	607	5	605	5	597	11	-2
GJ-1_33	0.6016	31	5	334	0.01	0.05984	2.91	0.81440	3.08	0.10	1.02	0.33	607	2	605	5	598	21	-1

GJ-1_48	0.0000	31	5	338	0.01	0.05997	1.60	0.82295	1.94	0.10	1.10	0.57	612	2	610	3	602	12	-2
GJ-1_49	0.0000	32	5	343	0.01	0.05990	1.53	0.81931	1.96	0.10	1.22	0.62	610	2	608	3	600	11	-2
GJ-1_50	0.3196	33	5	354	0.01	0.05991	1.96	0.81996	2.29	0.10	1.17	0.51	610	2	608	3	600	14	-2
GJ-1_51	0.0000	32	5	351	0.01	0.05989	1.74	0.82020	2.14	0.10	1.25	0.58	610	2	608	3	600	13	-2
GJ-1_66	0.0000	32	5	346	0.01	0.05990	1.51	0.81910	1.79	0.10	0.96	0.54	610	2	608	3	600	11	-2
GJ-1_67	0.0000	33	5	355	0.01	0.05988	1.42	0.81782	1.65	0.10	0.85	0.52	609	2	607	3	599	10	-2
GJ-1_68	0.0000	31	5	334	0.01	0.05985	1.57	0.81594	1.92	0.10	1.10	0.57	608	2	606	3	598	11	-2
GJ-1_69	0.0000	30	5	322	0.02	0.05988	1.50	0.81773	2.72	0.10	2.27	0.83	609	4	607	4	599	11	-2
GJ-1_84	0.0000	25	4	268	0.02	0.05994	1.53	0.81649	3.14	0.10	2.74	0.87	607	5	606	5	601	11	-1
GJ-1_85	0.0000	24	4	265	0.02	0.05986	1.61	0.81628	5.85	0.10	5.63	0.96	608	11	606	9	599	12	-2
GJ-1_86	1.1174	26	4	288	0.02	0.05985	4.87	0.81733	6.71	0.10	4.63	0.69	609	9	607	10	598	35	-2
GJ-1_87	0.0000	25	4	267	0.01	0.05993	1.87	0.82005	2.63	0.10	1.85	0.70	610	4	608	4	601	13	-2
GJ-1_102	0.5929	28	5	301	0.02	0.05983	2.82	0.81460	4.41	0.10	3.39	0.77	607	7	605	7	598	20	-2
GJ-1_103	0.0000	25	4	276	0.02	0.05985	1.54	0.81745	2.71	0.10	2.23	0.82	609	4	607	4	598	11	-2
GJ-1_104	1.8770	26	4	284	0.02	0.05986	8.16	0.81723	8.68	0.10	2.94	0.34	609	6	607	13	599	59	-2
GJ-1_105	0.2234	25	4	268	0.02	0.05985	1.87	0.81599	5.09	0.10	4.73	0.93	608	9	606	8	598	13	-2
GJ-1_120	0.1506	28	5	302	0.02	0.05987	2.43	0.81790	3.57	0.10	2.61	0.73	609	5	607	5	599	18	-2
GJ-1_121	1.4966	29	5	314	0.02	0.05983	6.44	0.81474	6.57	0.10	1.28	0.20	607	2	605	10	598	46	-2
GJ-1_122	0.0000	28	5	308	0.01	0.05984	2.73	0.81580	2.99	0.10	1.20	0.40	608	2	606	5	598	20	-2
GJ-1_123	2.2495	29	5	311	0.02	0.05985	9.39	0.81790	9.48	0.10	1.29	0.14	609	2	607	15	598	68	-2
GJ-1_138	1.9771	28	5	301	0.02	0.05986	8.31	0.81614	8.46	0.10	1.57	0.19	608	3	606	13	599	60	-2
GJ-1_139	0.0000	27	5	298	0.02	0.05982	2.39	0.81527	2.96	0.10	1.75	0.59	608	3	605	5	597	17	-2
GJ-1_140	1.2517	28	5	305	0.02	0.05991	5.53	0.81919	5.83	0.10	1.82	0.31	610	4	608	9	600	40	-2
GJ-1_141	0.6168	28	5	309	0.02	0.05987	3.44	0.81907	3.71	0.10	1.38	0.37	610	3	608	6	599	25	-2
Plesovice Ref. Mat.																			
Ples_4	0.0000	28	24	560	0.04	0.05304	1.61	0.39505	6.36	0.05	6.16	0.97	339	7	338	6	331	12	-3
Ples_5	0.0000	44	36	864	0.04	0.05307	1.56	0.39532	2.88	0.05	2.42	0.84	339	3	338	3	332	12	-2
Ples_6	0.0000	41	33	839	0.04	0.05274	1.46	0.37548	4.35	0.05	4.10	0.94	325	4	324	4	318	11	-2
Ples_20	0.0000	14	11	267	0.04	0.05308	2.05	0.39506	2.96	0.05	2.15	0.72	339	2	338	3	332	15	-2
Ples_21	0.0886	11	8	225	0.04	0.05304	2.63	0.39404	7.40	0.05	6.92	0.93	338	8	337	7	330	20	-2
Ples_22	0.0000	12	9	245	0.04	0.05303	1.97	0.39388	3.50	0.05	2.90	0.83	338	3	337	3	330	15	-3

Ples_36	0.0000	24	19	479	0.04	0.05301	2.45	0.39230	3.26	0.05	2.15	0.66	337	2	336	3	329	19	-2
Ples_37	0.9822	26	22	525	0.04	0.05300	4.78	0.39125	5.77	0.05	3.24	0.56	336	4	335	6	329	36	-2
Ples_38	0.0000	27	22	531	0.04	0.05303	1.88	0.39468	2.62	0.05	1.83	0.70	339	2	338	3	330	14	-3
Ples_52	0.0000	34	34	665	0.05	0.05302	1.97	0.39237	2.49	0.05	1.52	0.61	337	2	336	2	330	15	-2
Ples_53	0.0000	34	34	666	0.05	0.05300	1.77	0.39356	2.41	0.05	1.63	0.68	338	2	337	2	329	13	-3
Ples_54	0.0000	33	33	645	0.05	0.05300	1.45	0.39230	2.27	0.05	1.75	0.77	337	2	336	2	329	11	-2
Ples_68	0.0000	33	28	660	0.04	0.05306	1.60	0.39489	6.51	0.05	6.31	0.97	339	7	338	6	331	12	-2
Ples_69	0.0000	31	26	609	0.04	0.05308	13.73	0.39551	14.19	0.05	3.58	0.25	339	4	338	14	332	104	-2
Ples_70	0.0000	32	26	623	0.04	0.05306	2.54	0.39570	4.98	0.05	4.28	0.86	340	5	339	5	331	19	-2
91500 Ref. Mat.																			
91500_15	0.0000	18	17	97	0.18	0.07380	1.64	1.79590	2.82	0.18	2.29	0.81	1048	7	1044	6	1036	11	-1
91500_16	0.0000	18	17	97	0.18	0.07370	1.48	1.78665	3.06	0.18	2.69	0.88	1044	9	1041	7	1033	10	-1
91500_17	0.0000	17	17	95	0.17	0.07365	1.63	1.78216	2.61	0.18	2.04	0.78	1042	7	1039	6	1032	11	-1
91500_18	0.0000	18	17	99	0.18	0.07361	1.62	1.77886	2.62	0.18	2.06	0.79	1041	7	1038	6	1031	11	-1
91500_34	0.0000	17	16	91	0.17	0.07364	1.54	1.78139	2.82	0.18	2.36	0.84	1042	8	1039	6	1032	10	-1
91500_35	0.0000	18	17	98	0.18	0.07380	1.50	1.79153	2.73	0.18	2.28	0.83	1045	7	1042	6	1036	10	-1
91500_36	0.0000	21	20	112	0.18	0.07352	1.56	1.77294	3.38	0.17	2.99	0.89	1039	10	1036	7	1028	11	-1
91500_37	0.0000	19	18	101	0.17	0.07364	1.58	1.78117	4.41	0.18	4.12	0.93	1042	13	1039	10	1032	11	-1
91500_52	0.0000	17	17	93	0.18	0.07374	1.47	1.79099	2.80	0.18	2.38	0.85	1046	8	1042	6	1034	10	-1
91500_53	0.0000	16	16	88	0.18	0.07369	1.50	1.78784	2.62	0.18	2.15	0.82	1045	7	1041	6	1033	10	-1
91500_54	0.0000	17	17	92	0.18	0.07383	1.44	1.79787	5.28	0.18	5.08	0.96	1048	16	1045	12	1037	10	-1
91500_55	0.0000	18	17	99	0.17	0.07375	1.43	1.79221	2.93	0.18	2.56	0.87	1046	8	1043	6	1035	10	-1
91500_70	0.0000	23	22	123	0.18	0.07361	1.48	1.78031	2.96	0.18	2.56	0.87	1042	8	1038	6	1031	10	-1
91500_71	0.0000	23	23	126	0.18	0.07352	2.23	1.77255	2.88	0.17	1.82	0.63	1039	6	1035	6	1028	15	-1
91500_72	0.0000	24	24	129	0.18	0.07362	1.50	1.78249	2.78	0.18	2.34	0.84	1043	8	1039	6	1031	10	-1
91500_73	0.0873	24	25	132	0.19	0.07329	2.39	1.75635	4.10	0.17	3.34	0.81	1033	11	1030	9	1022	16	-1
91500_88	0.0000	23	23	125	0.18	0.07357	1.42	1.77865	2.35	0.18	1.87	0.80	1041	6	1038	5	1030	10	-1
91500_89	0.0000	22	22	120	0.18	0.07360	1.61	1.77984	2.64	0.18	2.09	0.79	1042	7	1038	6	1030	11	-1
91500_90	0.0000	20	19	106	0.18	0.07371	1.53	1.78742	2.17	0.18	1.54	0.71	1044	5	1041	5	1033	10	-1
91500_91	0.0000	19	18	102	0.17	0.07377	1.74	1.78109	2.89	0.18	2.31	0.80	1040	7	1039	6	1035	12	0
91500_106	0.0000	22	22	122	0.18	0.07346	1.67	1.77022	2.90	0.17	2.36	0.82	1038	8	1035	6	1027	11	-1

91500_107	0.0000	18	17	95	0.18	0.07353	1.85	1.77548	2.83	0.18	2.15	0.76	1040	7	1037	6	1029	12	-1
91500_124	0.0000	23	23	128	0.18	0.07363	2.37	1.78199	2.69	0.18	1.27	0.47	1042	4	1039	6	1031	16	-1
91500_125	0.0000	22	21	119	0.17	0.07358	2.50	1.77919	2.99	0.18	1.64	0.55	1042	5	1038	7	1030	17	-1
91500_126	0.0000	22	21	120	0.17	0.07353	2.42	1.77354	2.92	0.17	1.64	0.56	1039	5	1036	6	1029	16	-1
91500_127	0.0000	22	21	120	0.18	0.07362	2.36	1.77766	2.99	0.18	1.83	0.61	1040	6	1037	6	1031	16	-1
91500_142	0.0000	17	16	94	0.18	0.07338	2.70	1.76444	3.17	0.17	1.67	0.53	1036	5	1032	7	1025	18	-1
91500_143	0.0000	19	18	104	0.17	0.07349	2.70	1.77138	3.30	0.17	1.90	0.58	1039	6	1035	7	1027	18	-1
91500_145	0.0000	17	16	93	0.17	0.07338	3.10	1.76445	3.72	0.17	2.06	0.55	1036	7	1032	8	1025	21	-1
Garnet-bearing white leucosome (PC12.5)																			
GJ-1 Ref. Mat.																			
GJ-1_1	0.0136	31	5	340	0.01	0.06014	1.40	0.81980	2.67	0.10	2.28	0.85	608	4	608	4	608	10	0
GJ-1_2	0.7281	31	5	340	0.02	0.06017	3.37	0.82119	4.33	0.10	2.71	0.63	608	5	609	7	610	24	0
GJ-1_3	0.0170	30	5	330	0.02	0.06013	1.45	0.81972	3.42	0.10	3.09	0.90	608	6	608	5	608	10	0
GJ-1_20	0.0965	31	5	343	0.01	0.06013	1.53	0.81743	2.46	0.10	1.93	0.78	606	4	607	4	608	11	0
GJ-1_21	0.0331	30	5	330	0.01	0.06012	1.44	0.81886	2.76	0.10	2.35	0.85	607	5	607	4	608	10	0
GJ-1_22	0.1998	29	5	321	0.02	0.06017	1.72	0.82135	2.29	0.10	1.51	0.66	609	3	609	4	610	12	0
GJ-1_40	0.0376	26	4	284	0.01	0.06018	1.64	0.82271	2.93	0.10	2.44	0.83	609	5	610	4	610	12	0
GJ-1_41	0.0000	28	5	307	0.01	0.06013	1.43	0.82057	3.40	0.10	3.08	0.91	608	6	608	5	608	10	0
GJ-1_58	0.0451	26	4	280	0.02	0.06018	1.48	0.82197	3.17	0.10	2.81	0.88	609	5	609	5	610	11	0
GJ-1_59	0.0490	26	4	279	0.01	0.06020	1.69	0.82280	2.34	0.10	1.63	0.69	609	3	610	4	611	12	0
GJ-1_60	0.0000	25	4	275	0.01	0.06020	1.48	0.82358	2.26	0.10	1.71	0.76	610	3	610	3	611	11	0
GJ-1_77	0.5193	25	4	272	0.01	0.06011	2.65	0.81855	3.37	0.10	2.08	0.62	607	4	607	5	608	19	0
GJ-1_78	0.0379	22	3	242	0.01	0.06010	1.69	0.81811	2.47	0.10	1.81	0.73	607	3	607	4	607	12	0
GJ-1_79	0.0000	28	4	306	0.01	0.06017	1.54	0.82232	2.31	0.10	1.72	0.75	609	3	609	4	610	11	0
GJ-1_96	0.0000	26	4	283	0.01	0.06014	1.56	0.82038	2.64	0.10	2.14	0.81	608	4	608	4	608	11	0
GJ-1_115	0.0363	25	4	275	0.01	0.06018	2.40	0.82244	3.02	0.10	1.82	0.60	609	4	609	5	610	17	0
GJ-1_116	0.0292	24	4	263	0.01	0.06015	2.54	0.82094	3.08	0.10	1.73	0.56	608	3	609	5	609	18	0
GJ-1_117	0.0000	25	4	277	0.01	0.06014	2.52	0.82145	2.98	0.10	1.60	0.54	609	3	609	5	609	18	0
GJ-1_134	0.0248	26	4	289	0.01	0.06017	2.46	0.82181	3.50	0.10	2.49	0.71	609	5	609	5	610	18	0

Plesovice Ref. Mat.																			
PLES_4	0.0179	25	42	501	0.08	0.05322	1.52	0.39391	2.69	0.05	2.22	0.83	337	2	337	3	338	11	0
PLES_5	0.0469	24	37	470	0.08	0.05328	1.65	0.39755	2.73	0.05	2.17	0.80	340	2	340	3	341	12	0
PLES_6	0.6167	27	45	542	0.08	0.05323	3.40	0.39361	3.96	0.05	2.03	0.51	337	2	337	4	338	26	0
PLES_23	0.0000	16	23	320	0.07	0.05319	1.71	0.39525	2.80	0.05	2.22	0.79	338	2	338	3	337	13	0
PLES_24	0.1211	22	39	429	0.09	0.05328	1.91	0.39753	2.74	0.05	1.96	0.71	340	2	340	3	341	14	0
PLES_25	0.0431	25	47	496	0.10	0.05322	1.61	0.39469	3.94	0.05	3.60	0.91	338	4	338	4	338	12	0
PLES_42	0.1019	25	39	491	0.08	0.05326	1.58	0.39539	2.36	0.05	1.75	0.74	338	2	338	2	340	12	1
PLES_43	0.0000	24	38	476	0.08	0.05324	2.12	0.39470	3.36	0.05	2.61	0.78	338	3	338	3	339	16	0
PLES_44	0.0726	32	47	636	0.07	0.05323	1.78	0.39397	2.71	0.05	2.05	0.76	337	2	337	3	339	13	0
PLES_61	0.0877	22	35	435	0.08	0.05331	1.92	0.39785	4.28	0.05	3.83	0.89	340	4	340	4	342	14	1
PLES_62	0.1659	21	29	421	0.07	0.05325	1.65	0.39658	2.55	0.05	1.94	0.76	339	2	339	2	340	12	0
PLES_63	0.2271	22	33	442	0.07	0.05325	1.98	0.39752	2.77	0.05	1.93	0.70	340	2	340	3	340	15	0
PLES_80	0.8881	24	34	466	0.07	0.05326	4.51	0.39730	5.11	0.05	2.40	0.47	340	3	340	5	340	34	0
PLES_81	0.0508	23	34	464	0.07	0.05324	1.62	0.39542	2.89	0.05	2.39	0.83	338	3	338	3	339	12	0
PLES_82	0.0000	30	41	582	0.07	0.05329	1.58	0.39774	3.56	0.05	3.19	0.90	340	4	340	3	341	12	0
PLES_99	0.0093	15	21	305	0.07	0.05322	3.06	0.39503	4.39	0.05	3.15	0.72	338	3	338	4	338	23	0
PLES_100	0.0000	15	21	292	0.07	0.05324	3.49	0.39617	4.25	0.05	2.42	0.57	339	3	339	4	339	26	0
PLES_101	0.1105	18	25	350	0.07	0.05326	3.06	0.39584	4.86	0.05	3.78	0.78	338	4	339	5	340	23	0
PLES_118	0.0441	25	36	498	0.07	0.05325	2.52	0.39557	3.42	0.05	2.31	0.67	338	3	338	3	339	19	0
PLES_119	0.6402	20	33	380	0.09	0.05334	4.43	0.39814	6.67	0.05	4.98	0.75	340	5	340	6	343	33	1
PLES_120	0.0877	18	34	351	0.10	0.05326	2.79	0.39545	3.60	0.05	2.28	0.63	338	3	338	3	340	21	1
BB Ref. Mat.																			
BB-9_7	0.0365	43	56	489	0.11	0.05888	1.45	0.73980	2.95	0.09	2.57	0.87	562	5	562	4	563	11	0
BB-9_8	0.0128	44	58	498	0.12	0.05888	1.46	0.74010	2.61	0.09	2.16	0.83	562	4	562	4	563	11	0
BB-9_9	1.0376	46	63	523	0.12	0.05890	4.74	0.74073	5.37	0.09	2.52	0.47	563	5	563	8	564	34	0
BB-9_26	0.0000	43	57	495	0.12	0.05887	1.33	0.73875	2.75	0.09	2.40	0.87	562	4	562	4	562	10	0
BB-9_27	0.1370	42	56	484	0.12	0.05886	1.53	0.73864	2.18	0.09	1.55	0.71	562	3	562	3	562	11	0
BB-9_28	0.0316	44	59	501	0.12	0.05891	1.40	0.74154	3.62	0.09	3.34	0.92	563	6	563	5	564	10	0
BB-9_45	0.0000	45	60	508	0.12	0.05891	1.35	0.74154	2.95	0.09	2.62	0.89	563	5	563	4	564	10	0

BB-9_46	0.2136	42	57	483	0.12	0.05887	1.65	0.73900	2.42	0.09	1.77	0.73	562	3	562	3	562	12	0
BB-9_47	0.1696	44	59	501	0.12	0.05885	1.73	0.73699	2.52	0.09	1.84	0.73	560	3	561	4	562	13	0
BB-9_64	0.3617	42	56	480	0.12	0.05901	2.26	0.73890	2.70	0.09	1.47	0.54	560	3	562	4	567	16	1
BB-9_65	0.0902	35	45	394	0.12	0.05888	1.54	0.73806	2.05	0.09	1.35	0.66	561	2	561	3	563	11	0
BB-9_66	0.0000	40	54	461	0.12	0.05878	1.71	0.73729	2.55	0.09	1.90	0.74	561	3	561	4	559	12	0
BB-9_83	0.0000	33	42	377	0.11	0.05889	2.70	0.73949	4.34	0.09	3.39	0.78	562	6	562	6	563	20	0
BB-9_84	0.1540	40	55	460	0.12	0.05884	1.76	0.73666	3.06	0.09	2.50	0.82	560	4	560	4	561	13	0
BB-9_85	0.0000	42	55	473	0.12	0.05893	1.33	0.74279	2.59	0.09	2.22	0.86	564	4	564	4	565	10	0
BB-9_102	0.0000	43	57	486	0.12	0.05887	2.14	0.74011	3.50	0.09	2.77	0.79	563	5	562	5	562	16	0
BB-9_103	0.0088	40	52	450	0.12	0.05893	2.24	0.74258	3.02	0.09	2.03	0.67	564	4	564	4	564	16	0
BB-9_104	0.4435	38	52	437	0.12	0.05891	2.87	0.74158	3.45	0.09	1.91	0.55	563	3	563	5	564	21	0
BB-9_121	0.2686	40	53	457	0.12	0.05889	2.44	0.74092	3.04	0.09	1.83	0.60	563	3	563	4	563	18	0
BB-9_122	0.0181	40	54	461	0.12	0.05884	2.14	0.73766	2.71	0.09	1.65	0.61	561	3	561	4	561	16	0
BB-9_123	0.0000	39	52	447	0.12	0.05885	3.09	0.73957	4.08	0.09	2.66	0.65	562	5	562	6	562	22	0
BB-9_135	0.0353	23	4	270	0.01	0.06018	2.18	0.78035	2.71	0.09	1.60	0.59	579	3	586	4	610	16	5
BB-9_136	0.0325	23	4	266	0.01	0.06018	2.16	0.78140	2.75	0.09	1.70	0.62	580	3	586	4	610	16	5
(Hornblende)-biotite stromatic metatexite (C1071A)																			
GJ-1 Ref. Mat.																			
GJ1-1	0.3198	15005	11	737	0.01	0.06003	2.22	0.81315	3.01	0.10	2.04	0.68	604	5	604	5	605	19	0
GJ1-2	0.0000	15069	20	1413	0.01	0.06002	1.69	0.81357	2.43	0.10	1.74	0.72	605	4	604	4	604	15	0
GJ1-3	0.0000	14742	11	725	0.01	0.05995	1.42	0.80840	2.49	0.10	2.05	0.82	602	5	602	5	602	12	0
GJ1-20	0.0099	13251	10	698	0.01	0.05999	1.62	0.81188	2.88	0.10	2.38	0.83	604	5	604	5	603	14	0
GJ1-21	0.4812	15225	23	1676	0.01	0.06009	2.33	0.80894	3.30	0.10	2.34	0.71	601	5	602	6	607	20	1
GJ1-22	0.0000	14355	21	1601	0.01	0.05996	1.42	0.81051	2.54	0.10	2.11	0.83	603	5	603	5	602	12	0
GJ1-39	0.0000	15277	23	1718	0.01	0.06014	1.60	0.81272	2.17	0.10	1.47	0.68	603	3	604	4	608	14	1
GJ1-40	0.0000	14458	6	410	0.01	0.05996	1.35	0.80919	2.25	0.10	1.80	0.80	602	4	602	4	602	12	0
GJ1-41	0.5682	14609	10	730	0.01	0.06010	2.37	0.81768	2.93	0.10	1.72	0.59	607	4	607	5	607	21	0
GJ1-58	0.0000	13555	12	851	0.01	0.06001	1.60	0.81320	2.12	0.10	1.39	0.66	604	3	604	4	604	14	0
GJ1-59	0.0288	13458	15	992	0.01	0.06013	1.66	0.81885	3.11	0.10	2.63	0.85	607	6	607	6	608	14	0
GJ1-60	0.3391	14273	17	1071	0.02	0.06003	1.82	0.81430	2.34	0.10	1.46	0.62	605	3	605	4	605	16	0

GJ1_77	0.0000	11795	8	627	0.01	0.06019	1.40	0.81720	3.59	0.10	3.30	0.92	605	8	606	7	610	12	1
GJ1_78	0.0000	11839	5	414	0.01	0.06008	1.46	0.81378	2.67	0.10	2.23	0.84	604	5	605	5	606	13	0
GJ1_79	0.0201	11925	6	433	0.01	0.06007	1.67	0.81683	3.41	0.10	2.98	0.87	606	7	606	6	606	14	0
GJ-1_96	0.0582	1926	187	292	0.64	0.06014	1.52	0.81215	2.07	0.10	1.40	0.68	602	3	604	4	609	13	1
GJ-1_97	0.4474	1929	201	324	0.62	0.06015	2.09	0.81410	2.98	0.10	2.13	0.71	604	5	605	5	609	18	1
GJ-1_98	0.1745	1927	184	294	0.62	0.06024	1.59	0.81880	2.81	0.10	2.32	0.83	606	5	607	5	612	14	1
Plesovice Ref. Mat.																			
Ples_4	0.1110	12194	137	1083	0.13	0.05327	1.92	0.39537	2.17	0.05	1.00	0.46	338	1	338	2	340	17	1
Ples_5	0.0197	10250	87	721	0.12	0.05321	1.69	0.39526	2.02	0.05	1.10	0.55	338	1	338	2	338	15	0
Ples_6	0.0000	10332	79	650	0.12	0.05321	1.75	0.39267	2.03	0.05	1.04	0.51	336	1	336	2	338	16	0
Ples_23	0.5036	16866	137	1186	0.12	0.05332	2.55	0.39251	2.83	0.05	1.23	0.44	335	2	336	3	342	23	2
Ples_24	0.0077	16812	128	1095	0.12	0.05322	1.54	0.39507	2.16	0.05	1.51	0.70	338	2	338	2	338	14	0
Ples_25	0.0000	16642	94	821	0.11	0.05319	1.35	0.39329	2.02	0.05	1.50	0.74	337	2	337	2	337	12	0
Ples_42	0.3906	17360	174	1496	0.12	0.05320	2.36	0.39498	2.67	0.05	1.26	0.47	338	2	338	3	337	21	0
Ples_43	0.2049	17052	151	1306	0.12	0.05326	1.68	0.39525	2.03	0.05	1.14	0.56	338	1	338	2	340	15	1
Ples_44	0.0413	16759	107	937	0.11	0.05324	1.50	0.39462	3.53	0.05	3.19	0.91	338	4	338	4	339	14	0
Ples_61	0.1830	16868	127	1126	0.11	0.05321	1.73	0.39371	2.54	0.05	1.87	0.73	337	2	337	3	338	16	0
Ples_62	0.1612	16363	112	977	0.11	0.05321	1.83	0.39402	2.48	0.05	1.68	0.68	337	2	337	3	338	17	0
Ples_63	0.0770	15950	100	879	0.11	0.05320	2.51	0.39678	2.98	0.05	1.62	0.54	340	2	339	3	337	23	-1
Ples_80	0.0507	5848	68	606	0.11	0.05328	1.74	0.39736	3.21	0.05	2.70	0.84	340	4	340	4	341	16	0
Ples_82	0.0055	6333	76	663	0.11	0.05326	2.28	0.39745	2.85	0.05	1.71	0.60	340	2	340	3	340	21	0
PLES_99	0.2114	1834	3237	654	4.95	0.05334	1.96	0.39606	2.39	0.05	1.37	0.57	338	2	339	3	343	18	1
PLES_100	0.0000	1833	3223	635	5.08	0.05332	1.75	0.39542	2.27	0.05	1.45	0.64	338	2	338	3	342	16	1
PLES_101	0.5112	1833	3275	645	5.08	0.05329	2.58	0.39310	4.27	0.05	3.41	0.80	336	4	337	5	341	23	1
BB Ref. Mat.																			
BB9_7	0.0000	1913	79	386	0.20	0.05887	1.61	0.73923	3.14	0.09	2.69	0.86	562	6	562	5	562	14	0
BB9_8	0.0000	1854	46	224	0.21	0.05882	1.27	0.73813	1.83	0.09	1.32	0.72	562	3	561	3	560	11	0
BB9_9	0.0000	1934	122	592	0.21	0.05897	1.57	0.74255	2.12	0.09	1.42	0.67	563	3	564	4	566	14	0
BB9_26	0.0000	20193	88	431	0.21	0.05887	1.44	0.74056	1.78	0.09	1.05	0.59	563	2	563	3	562	13	0

BB9_27	0.1783	21336	129	628	0.21	0.05893	1.72	0.74354	2.29	0.09	1.52	0.66	564	3	564	4	564	15	0
BB9_45	0.0000	20327	77	382	0.20	0.05896	2.45	0.74517	2.84	0.09	1.43	0.51	565	3	565	5	566	21	0
BB9_46	0.0000	20458	94	459	0.20	0.05892	1.41	0.74327	2.25	0.09	1.75	0.78	564	4	564	4	564	12	0
BB9_47	0.0000	20242	50	244	0.20	0.05892	2.02	0.74196	2.31	0.09	1.11	0.48	563	2	564	4	564	18	0
BB-9_102	0.2439	888	2039	439	4.64	0.05872	1.60	0.72251	2.49	0.09	1.90	0.76	551	4	552	4	557	14	1
BB-9_103	0.0000	887	2033	435	4.67	0.05881	1.47	0.72836	2.02	0.09	1.39	0.69	554	3	556	3	560	13	1
BB-9_104	0.1444	887	2028	432	4.69	0.05872	1.50	0.72103	3.06	0.09	2.66	0.87	550	6	551	5	557	13	1
BB_64	0.0960	11256	70	338	0.21	0.05888	1.85	0.73731	2.32	0.09	1.41	0.61	560	3	561	4	563	16	0
BB_65	0.0000	12149	60	296	0.20	0.05898	1.47	0.74535	3.73	0.09	3.42	0.92	565	7	566	6	566	13	0
BB_66	0.1892	12667	79	381	0.21	0.05890	1.66	0.73941	2.53	0.09	1.91	0.75	562	4	562	4	563	14	0
BB_83	0.0373	15010	87	421	0.21	0.05904	1.70	0.74812	2.68	0.09	2.08	0.78	567	5	567	5	568	15	0
BB_84	0.0282	14934	89	433	0.21	0.05895	1.45	0.74280	2.82	0.09	2.41	0.86	564	5	564	5	565	13	0
BB_85	0.0442	15127	85	414	0.21	0.05902	1.46	0.74854	2.83	0.09	2.42	0.86	567	5	567	5	568	13	0

aFraction of the non-radiogenic ^{206}Pb in the analyzed zircon spot, where f_{206}=[$^{206}Pb/^{204}Pb$]c/[$^{206}Pb/^{204}Pb$]s (c=common; s=sample)

bTh/U ratios and amount of Pb, Th and U (in pmm) are calculated relative to 91500 reference zircon

cCorrected for background and within-run Pb/U fractionation and normalised to reference zircon GJ-1 (ID-TIMS values/measured value); $^{207}Pb/^{235}U$ calculated using ($^{207}Pb/^{206}Pb$)/($^{238}U/^{206}Pb$ * 1/137.88)

dRho is the error correlation defined as the quotient of the propagated errors of the $^{206}Pb/^{238}U$ and the $^{207}/^{235}U$ ratio

eDegree of discordance = 100 - ($^{206}Pb/^{238}U$ age * 100/$^{207}Pb/^{206}U$ age)

c-core
r-rim
s-single phase

Hf isotopes results determined by LA-ICP-MS - Standards - BB, GJ-1, PLESOVICE, MUDTANK, TEMORA

Grain#	$^{176}Yb/^{177}Hf$ [a]	±2s	$^{176}Lu/^{177}Hf$ [a]	±2s	$^{178}Hf/^{177}Hf$	$^{180}Hf/^{177}Hf$	Sig_{Hf} [b] (V)	$^{176}Hf/^{177}Hf$	±2s [c]	age [f] (Ma)	±2s	$^{176}Hf/^{177}Hf_{(t)}$ [d]	eHf(t) [d]	±2s [c]
										(measured)				
Amphibolite enclave (PC12.1)														
BB-0003.dat	0.010523	8	0.000293	2	1.467194	1.886821	12.074716	0.281678	17	560	1	0.281675	-26.8	0.64
BB-0033.dat	0.012614	10	0.000351	2	1.467269	1.886962	12.746038	0.281662	19	560	1	0.281659	-27.4	0.65
BB-0034.dat	0.012659	10	0.000351	2	1.467195	1.886867	13.048240	0.281673	24	560	1	0.281669	-27.0	0.65
BB-0035.dat	0.012274	10	0.000343	2	1.467213	1.886787	12.666458	0.281680	21	560	1	0.281677	-26.7	0.65
BB-0065.dat	0.011365	11	0.000320	2	1.467194	1.886754	13.101085	0.281655	17	560	1	0.281652	-27.6	0.65
BB-0066.dat	0.011536	9	0.000326	2	1.467196	1.886785	13.073753	0.281669	17	560	1	0.281666	-27.1	0.65
BB-0067.dat	0.012415	11	0.000344	2	1.467241	1.886822	13.536218	0.281681	14	560	1	0.281678	-26.7	0.65
BB-0107.dat	0.009266	7	0.000260	2	1.467245	1.886750	12.643688	0.281684	26	560	1	0.281681	-26.6	0.64
BB-0108.dat	0.009710	10	0.000272	2	1.467249	1.886957	12.690430	0.281673	17	560	1	0.281671	-27.0	0.65
BB-0109.dat	0.012601	10	0.000347	2	1.467203	1.886902	13.353967	0.281662	15	560	1	0.281659	-27.4	0.65
BB-0143.dat	0.009112	8	0.000252	2	1.467198	1.886928	12.629340	0.281662	30	560	1	0.281659	-27.4	0.64
BB-0144.dat	0.006399	5	0.000181	1	1.467180	1.886832	12.283331	0.281669	15	560	1	0.281668	-27.1	0.64
BB-0145.dat	0.008988	8	0.000252	2	1.467228	1.886872	12.386913	0.281662	16	560	1	0.281659	-27.4	0.64
BB (560Ma): $^{176}Hf/^{177}Hf$=0.2816713±0.0000028							**Average:**	**0.281670**						
GJ-1-0008.dat	0.007742	6	0.000246	1	1.467213	1.886794	10.179596	0.282016	20	608	1	0.282013	-13.7	0.64
GJ-1-0009.dat	0.007734	6	0.000246	1	1.467254	1.886885	10.152856	0.282000	22	608	1	0.281997	-14.3	0.64
GJ-1-0039.dat	0.007622	6	0.000245	1	1.467159	1.886985	10.550631	0.281965	19	608	1	0.281963	-15.5	0.64
GJ-1-0040.dat	0.007611	6	0.000245	2	1.467194	1.886952	10.529247	0.281990	15	608	1	0.281987	-14.7	0.64
GJ-1-0041.dat	0.007592	6	0.000245	2	1.467207	1.886759	10.636046	0.282012	19	608	1	0.282009	-13.9	0.64
GJ-1-0071.dat	0.007643	6	0.000245	1	1.467190	1.886785	10.571257	0.282012	23	608	1	0.282009	-13.9	0.64
GJ-1-0072.dat	0.007660	6	0.000246	1	1.467160	1.886910	10.576879	0.281975	21	608	1	0.281973	-15.2	0.64
GJ-1-0073.dat	0.007669	6	0.000246	1	1.467217	1.886863	10.823880	0.282020	20	608	1	0.282017	-13.6	0.64
GJ-1-0113.dat	0.007663	6	0.000246	2	1.467267	1.886945	10.808528	0.282009	21	608	1	0.282006	-14.0	0.64
GJ-1-0149.dat	0.007704	6	0.000246	2	1.467181	1.886800	10.784029	0.282015	33	608	1	0.282013	-13.8	0.64

GJ-1-0150.dat	0.007550	6	0.000243	2	1.467244	1.886758	10.660509	0.282010	15	608	1	0.282007	-14.0	0.64
GJ-1-0151.dat	0.007625	6	0.000242	2	1.467182	1.886751	10.499054	0.282029	18	608	1	0.282026	-13.3	0.64
GJ-1 (608Ma): $^{176}Hf/^{177}Hf$=0.282000±0.000005							**Average:**	**0.282004**						
PLES-0010.dat	0.006274	5	0.000129	1	1.467204	1.886838	20.151537	0.282462	21	337	1	0.282462	-3.9	0.64
PLES-0011.dat	0.006562	5	0.000140	1	1.467250	1.886875	20.062893	0.282475	23	337	1	0.282474	-3.5	0.64
PLES-0012.dat	0.004242	3	0.000092	1	1.467236	1.886882	20.629369	0.282476	26	337	1	0.282475	-3.5	0.64
PLES-0042.dat	0.004883	4	0.000104	1	1.467222	1.886813	21.219281	0.282464	16	337	1	0.282463	-3.9	0.64
PLES-0043.dat	0.007465	6	0.000157	1	1.467196	1.886837	20.280690	0.282452	20	337	1	0.282451	-4.3	0.64
PLES-0074.dat	0.005031	4	0.000108	1	1.467189	1.886783	21.016911	0.282470	20	337	1	0.282470	-3.7	0.64
PLES-0075.dat	0.006389	5	0.000137	1	1.467188	1.886862	20.855517	0.282475	18	337	1	0.282474	-3.5	0.64
PLES-0076.dat	0.004697	4	0.000102	1	1.467210	1.886803	21.649136	0.282468	22	337	1	0.282467	-3.7	0.64
PLES-0117.dat	0.005537	4	0.000120	1	1.467247	1.886758	21.251749	0.282479	16	337	1	0.282478	-3.4	0.64
PLES-0118.dat	0.008414	8	0.000183	1	1.467178	1.886790	20.282363	0.282469	15	337	1	0.282468	-3.7	0.65
PLES-0152.dat	0.008109	7	0.000180	1	1.467230	1.886865	16.303282	0.282469	18	337	1	0.282468	-3.7	0.64
PLES-0153.dat	0.009653	8	0.000216	1	1.467204	1.886784	16.271684	0.282464	17	337	1	0.282462	-3.9	0.65
PLESOVICE (337Ma): $^{176}Hf/^{177}Hf$=0.282482±0.000013							**Average:**	**0.282469**						
Hornblende-biotite stromatic metatexite (PC12.2), Biotite-bearing pink leucosome (PC12.3), (Hornblende)-biotite stromatic metatexite (C1071A)														
BB-0001.dat	0.004359	3	0.000158	1	1.467177	1.886864	10.746166	0.281679	35	560	1	0.281677	-26.7	0.75
BB-0003.dat	0.004327	4	0.000157	1	1.467183	1.886833	10.991572	0.281682	17	560	1	0.281681	-26.6	0.75
BB-0004.dat	0.004339	4	0.000157	1	1.467155	1.886947	10.852379	0.281659	30	560	1	0.281657	-27.4	0.75
BB-0041.dat	0.004338	3	0.000156	1	1.467231	1.886903	10.771158	0.281663	16	560	1	0.281662	-27.3	0.75
BB-0042.dat	0.004323	5	0.000157	1	1.467215	1.886895	11.015562	0.281670	18	560	1	0.281668	-27.0	0.75
BB-0043.dat	0.004441	5	0.000161	1	1.467188	1.886888	11.033714	0.281656	16	560	1	0.281654	-27.5	0.75
BB-0044.dat	0.004331	5	0.000156	1	1.467224	1.886965	10.918817	0.281680	16	560	1	0.281679	-26.7	0.75
BB-0090.dat	0.007106	6	0.000254	2	1.467237	1.886887	11.108867	0.281660	18	560	1	0.281657	-27.4	0.75
BB-0093.dat	0.008702	7	0.000312	2	1.467224	1.886931	11.633616	0.281681	18	560	1	0.281678	-26.7	0.75
BB-0140.dat	0.003946	3	0.000143	1	1.467138	1.886726	11.092954	0.281667	16	560	1	0.281666	-27.1	0.75

BB-0142.dat	0.004345	4	0.000157	1	1.467207	1.886829	11.033291	0.281659	16	560	1	0.281657	-27.4	0.75
BB-0181.dat	0.003864	3	0.000139	1	1.467188	1.886939	11.029465	0.281663	14	560	1	0.281661	-27.3	0.75
BB-0183.dat	0.003930	3	0.000142	1	1.467215	1.886753	10.951878	0.281685	13	560	1	0.281683	-26.5	0.75
BB (560Ma): $^{176}Hf/^{177}Hf$=0.2816713±0.0000028							**Average:**	**0.281669**						
PLES-0011.dat	0.005916	5	0.000158	1	1.467209	1.886855	16.233226	0.282471	17	337	1	0.282470	-3.7	0.75
PLES-0012.dat	0.007384	6	0.000192	1	1.467208	1.886816	15.608156	0.282466	17	337	1	0.282465	-3.8	0.75
PLES-0051.dat	0.005432	4	0.000144	1	1.467162	1.886812	15.592879	0.282465	21	337	1	0.282465	-3.8	0.75
PLES-0101.dat	0.005520	4	0.000151	1	1.467186	1.886909	15.780586	0.282473	19	337	1	0.282472	-3.6	0.75
PLES-0149.dat	0.005857	5	0.000156	1	1.467210	1.886840	15.123549	0.282467	17	337	1	0.282466	-3.8	0.75
PLES-0150.dat	0.005920	5	0.000157	1	1.467183	1.886715	15.548247	0.282458	16	337	1	0.282457	-4.1	0.75
PLES-0151.dat	0.005534	4	0.000151	1	1.467214	1.886789	16.514334	0.282469	16	337	1	0.282468	-3.7	0.75
PLES-0191.dat	0.005293	4	0.000145	1	1.467214	1.886798	15.298513	0.282477	17	337	1	0.282476	-3.4	0.75
PLESOVICE (337Ma): $^{176}Hf/^{177}Hf$=0.282482±0.000013							**Average:**	**0.282468**						
GJ-1-0013.dat	0.006224	7	0.000245	2	1.467188	1.886857	9.216948	0.281999	14	608	1	0.281997	-14.3	0.75
GJ-1-0014.dat	0.006191	6	0.000247	2	1.467180	1.886863	9.136292	0.282004	16	608	1	0.282001	-14.2	0.75
GJ-1-0015.dat	0.006099	6	0.000246	2	1.467235	1.886996	9.318175	0.281989	16	608	1	0.281986	-14.7	0.75
GJ-1-0016.dat	0.006172	5	0.000247	2	1.467199	1.886986	9.306733	0.281981	15	608	1	0.281978	-15.0	0.75
GJ-1-0053.dat	0.006247	6	0.000249	2	1.467264	1.886860	8.998201	0.281988	16	608	1	0.281985	-14.8	0.75
GJ-1-0054.dat	0.006150	5	0.000248	2	1.467217	1.886794	8.594940	0.282028	18	608	1	0.282025	-13.3	0.75
GJ-1-0055.dat	0.006087	5	0.000249	2	1.467194	1.886950	8.683998	0.281995	15	608	1	0.281992	-14.5	0.75
GJ-1-0056.dat	0.006093	5	0.000248	2	1.467183	1.886822	8.772768	0.282030	14	608	1	0.282027	-13.2	0.75
GJ-1-0102.dat	0.006186	5	0.000249	1	1.467118	1.887008	9.032882	0.281976	17	608	1	0.281973	-15.2	0.75
GJ-1-0103.dat	0.006157	5	0.000249	1	1.467159	1.886823	8.738024	0.281996	20	608	1	0.281993	-14.5	0.75
GJ-1-0104.dat	0.006137	5	0.000248	1	1.467129	1.886814	8.746046	0.281982	20	608	1	0.281979	-14.9	0.75
GJ-1-0105.dat	0.006199	5	0.000249	1	1.467188	1.886800	8.756440	0.281985	21	608	1	0.281982	-14.9	0.75
GJ-1-0152.dat	0.006155	5	0.000248	2	1.467222	1.886814	9.031531	0.282005	15	608	1	0.282002	-14.1	0.75
GJ-1-0153.dat	0.006158	5	0.000247	1	1.467118	1.886855	9.145246	0.281994	16	608	1	0.281991	-14.5	0.75
GJ-1-0154.dat	0.006239	5	0.000248	2	1.467097	1.886773	9.135639	0.281983	16	608	1	0.281980	-14.9	0.75

GJ-1-0155.dat	0.006155	6	0.000248	2	1.467013	1.886802	9.631711	0.281960	14	608	1	0.281958	-15.7	0.75
GJ-1-0192.dat	0.006227	5	0.000247	1	1.467151	1.886749	8.920486	0.282019	13	608	1	0.282016	-13.6	0.75
GJ-1-0193.dat	0.006141	5	0.000246	2	1.467184	1.886837	8.889837	0.282000	19	608	1	0.281997	-14.3	0.75
GJ-1-0194.dat	0.006167	5	0.000248	2	1.467187	1.886716	8.820663	0.281989	14	608	1	0.281986	-14.7	0.75
GJ-1-0195.dat	0.006117	6	0.000247	2	1.467233	1.886872	8.739111	0.281995	16	608	1	0.281992	-14.5	0.75

GJ-1 (608Ma): $^{176}Hf/^{177}Hf$=0.282000±0.000005 **Average: 0.281995**

Hornblende-biotite stromatic metatexite (PC12.2), Garnet-biotite stromatic metatexite (PC12.4), Garnet-bearing white leucosome (PC12.5), (Hornblende)-biotite stromatic metatexite (C1071A)

BB-004.dat	0.004596	4	0.000161	1	1.467271	1.886155	12.231647	0.281659	18	560	1	0.281658	-27.4	0.95
BB-005.dat	0.004460	4	0.000157	1	1.467284	1.886004	12.286617	0.281670	19	560	1	0.281668	-27.1	0.95
BB-006.dat	0.004473	4	0.000157	1	1.467289	1.886096	12.249973	0.281667	19	560	1	0.281665	-27.2	0.95
BB-051.dat	0.004593	5	0.000160	1	1.467240	1.886145	12.346711	0.281662	23	560	1	0.281661	-27.3	0.95
BB-052.dat	0.004493	6	0.000157	2	1.467179	1.886154	12.290405	0.281659	19	560	1	0.281657	-27.4	0.95
BB-151.dat	0.004670	4	0.000163	1	1.467272	1.886260	12.722228	0.281675	17	560	1	0.281674	-26.9	0.95
BB-153.dat	0.004636	6	0.000161	2	1.467233	1.886328	12.791378	0.281669	18	560	1	0.281667	-27.1	0.95
BB-154.dat	0.004442	4	0.000156	1	1.467229	1.886096	14.510019	0.281657	25	560	1	0.281655	-27.5	0.95
BB-222.dat	0.004356	4	0.000153	1	1.467261	1.886068	13.141757	0.281661	17	560	1	0.281660	-27.3	0.95
BB-223.dat	0.004457	4	0.000155	1	1.467243	1.886024	13.110520	0.281672	21	560	1	0.281671	-27.0	0.95
BB-224.dat	0.004432	4	0.000155	1	1.467263	1.886360	13.330114	0.281667	20	560	1	0.281666	-27.1	0.95
BB-225.dat	0.004442	4	0.000156	1	1.467227	1.885976	13.274272	0.281657	18	560	1	0.281656	-27.5	0.95

BB (560Ma): $^{176}Hf/^{177}Hf$=0.2816713±0.0000028 **Average: 0.281665**

MUD-013.dat	0.000924	1	0.000030	0	1.467220	1.886049	12.300595	0.282504	17	732	1	0.282504	6.4	0.95
MUD-014.dat	0.000872	1	0.000028	0	1.467292	1.886165	12.509102	0.282491	18	732	1	0.282491	6.0	0.95
MUD-015.dat	0.000879	1	0.000028	0	1.467253	1.885955	12.849601	0.282481	19	732	1	0.282481	5.6	0.95
MUD-016.dat	0.000909	1	0.000029	0	1.467254	1.886110	12.735564	0.282490	19	732	1	0.282490	5.9	0.95
MUD-057.dat	0.000954	1	0.000031	0	1.467270	1.886027	12.485574	0.282497	16	732	1	0.282497	6.2	0.95
MUD-058.dat	0.000934	1	0.000030	0	1.467233	1.885908	12.574764	0.282485	19	732	1	0.282484	5.7	0.95
MUD-059.dat	0.000929	1	0.000030	0	1.467245	1.885954	12.657573	0.282482	20	732	1	0.282482	5.6	0.95

MUD-060.dat	0.000916	1	0.000029	0	1.467218	1.886205	12.961075	0.282496	17	732	1	0.282496	6.1	0.95
MUD-158.dat	0.000979	1	0.000031	0	1.467233	1.886100	13.086126	0.282491	18	732	1	0.282491	6.0	0.95
MUD-159.dat	0.001011	1	0.000033	0	1.467287	1.886231	13.309559	0.282514	14	732	1	0.282514	6.8	0.95
MUD-160.dat	0.000948	1	0.000030	0	1.467250	1.886311	13.273056	0.282508	18	732	1	0.282508	6.6	0.95
MUD-229.dat	0.000892	1	0.000029	0	1.467262	1.886251	13.482478	0.282508	18	732	1	0.282508	6.6	0.95
MUD-230.dat	0.000953	1	0.000031	0	1.467204	1.886324	13.051854	0.282485	17	732	1	0.282484	5.7	0.95
MUD-231.dat	0.001067	1	0.000034	0	1.467195	1.885941	12.973979	0.282491	20	732	1	0.282491	6.0	0.95
Mudtank(732Ma): $^{176}Hf/^{177}Hf$=0.282504±0.0000044							**Average:**	**0.282495**						
GJ-1-009.dat	0.006292	5	0.000253	2	1.467177	1.886053	8.867688	0.281977	19	602	1	0.281974	-15.3	0.95
GJ-1-010.dat	0.006272	8	0.000253	3	1.467237	1.885904	8.982469	0.282006	21	602	1	0.282003	-14.3	0.95
GJ-1-011.dat	0.006261	6	0.000253	2	1.467207	1.886208	8.794998	0.282015	23	602	1	0.282012	-13.9	0.95
GJ-1-012.dat	0.006284	6	0.000253	2	1.467258	1.886352	8.740408	0.282008	20	602	1	0.282005	-14.2	0.95
GJ-1-053.dat	0.006278	6	0.000253	2	1.467235	1.886095	8.822742	0.281991	21	602	1	0.281988	-14.8	0.95
GJ-1-054.dat	0.006281	5	0.000253	2	1.467269	1.886173	8.918123	0.281988	20	602	1	0.281985	-14.9	0.95
GJ-1-056.dat	0.006328	6	0.000253	2	1.467248	1.885915	10.538158	0.282000	30	602	1	0.281998	-14.4	0.95
GJ-1-155.dat	0.006276	6	0.000252	2	1.467225	1.885980	9.122700	0.282022	20	602	1	0.282019	-13.7	0.95
GJ-1-156.dat	0.006287	6	0.000252	2	1.467217	1.886027	9.113542	0.282022	21	602	1	0.282019	-13.7	0.95
GJ-1-157.dat	0.006287	5	0.000252	2	1.467267	1.886205	9.043459	0.282005	25	602	1	0.282002	-14.3	0.95
GJ-1-226.dat	0.006328	5	0.000251	2	1.467255	1.885794	9.703028	0.281996	19	602	1	0.281993	-14.6	0.95
GJ-1-227.dat	0.006344	5	0.000253	2	1.467299	1.885806	9.279988	0.282014	19	602	1	0.282012	-13.9	0.95
GJ-1-228.dat	0.006353	5	0.000253	2	1.467226	1.885980	9.251908	0.282009	20	602	1	0.282006	-14.1	0.95
Gj-1(602Ma): $^{176}Hf/^{177}Hf$=0.2820000±0.0000005							**Average:**	**0.282004**						
PLES-017.dat	0.002672	2	0.000069	0	1.467235	1.886126	14.231143	0.282492	17	337	1	0.282492	-2.9	0.95
PLES-018.dat	0.002892	3	0.000075	1	1.467220	1.886134	14.276097	0.282465	17	337	1	0.282465	-3.8	0.95
PLES-019.dat	0.002870	2	0.000074	0	1.467218	1.886388	14.453668	0.282497	15	337	1	0.282497	-2.7	0.95
PLES-020.dat	0.002851	3	0.000074	1	1.467271	1.886352	14.537214	0.282473	16	337	1	0.282473	-3.5	0.95
PLES-061.dat	0.002037	2	0.000053	0	1.467235	1.886175	14.969446	0.282482	16	337	1	0.282482	-3.2	0.95
PLES-062.dat	0.002128	2	0.000056	0	1.467181	1.885927	14.802227	0.282490	19	337	1	0.282489	-3.0	0.95

PLES-063.dat	0.002090	2	0.000054	0	1.467185	1.886103	14.939023	0.282460	18	337	1	0.282460	-4.0	0.95
PLES-064.dat	0.002404	3	0.000062	1	1.467193	1.886198	14.658916	0.282458	16	337	1	0.282458	-4.1	0.95
PLES-161.dat	0.001897	2	0.000049	0	1.467219	1.886104	15.225472	0.282493	18	337	1	0.282493	-2.8	0.95
PLES-162.dat	0.001701	2	0.000044	0	1.467229	1.886073	15.414409	0.282485	15	337	1	0.282484	-3.1	0.95
PLES-163.dat	0.002640	2	0.000068	0	1.467191	1.886012	14.941312	0.282477	16	337	1	0.282476	-3.4	0.95
PLES-232.dat	0.003478	3	0.000090	1	1.467267	1.886393	15.006851	0.282468	18	337	1	0.282467	-3.7	0.95
PLES-233.dat	0.004618	4	0.000124	1	1.467213	1.886229	14.665592	0.282473	16	337	1	0.282472	-3.6	0.95
PLES-234.dat	0.003772	3	0.000099	1	1.467224	1.886407	15.115748	0.282478	18	337	1	0.282478	-3.4	0.95

Plesovice(337Ma): $^{176}Hf/^{177}Hf$=0.2820000±0.0000005 **Average: 0.282478**

Hornblende-biotite stromatic metatexite (PC12.2)

TEM-004.dat	0.022231	19	0.000970	6	1.467242	1.886930	8.935610	0.282692	15	417	1	0.282684	5.7	0.77
TEM-005.dat	0.028229	23	0.001173	7	1.467196	1.886941	9.248201	0.282706	21	417	1	0.282697	6.2	1.05
TEM-006.dat	0.021518	20	0.000872	7	1.467234	1.886791	10.886013	0.282686	19	417	1	0.282679	5.5	0.94
TEM-007.dat	0.011699	10	0.000487	3	1.467295	1.886966	10.592472	0.282675	20	417	1	0.282671	5.3	0.99
TEM-008.dat	0.034633	28	0.001471	9	1.467246	1.886949	9.276234	0.282703	20	417	1	0.282692	6.0	0.98
TEM-009.dat	0.031934	26	0.001294	9	1.467169	1.886883	9.656625	0.282708	20	417	1	0.282698	6.2	0.99
TEM-010.dat	0.018161	15	0.000727	5	1.467184	1.886755	8.804496	0.282699	20	417	1	0.282694	6.1	0.99

Temora (417Ma): $^{176}Hf/^{177}Hf$=0.282686±0.000007 **Average: 0.282696**

[a] $^{176}Yb/^{177}Hf = (^{176}Yb/^{173}Yb)_{true} \times (^{173}Yb/^{177}Hf)_{meassured} \times (M_{173(Yb)}/M_{177(Hf)})^{b(Hf)}$, $b(Hf) = \ln(^{179}Hf/^{177}Hf_{true} / {}^{179}Hf/^{177}Hf_{measured}) / \ln (M_{179(Hf)}/M_{177(Hf)})$

M=mass of respective isotope. The $^{176}Lu/^{177}Hf$ were calculated in a similar way by using the $^{175}Lu/^{177}Hf$ and b(Yb)

[b] Mean Hf signal in volt

[c] Uncertainties are quadratic additions of the within-run precision and the daily reproducibility of the zircon standards. Uncertainties for the standard quoted at 2SD (2 standard deviation)

(d) Initial $^{176}Hf/^{177}Hf$ and ƐHf calculated using the apparent Pb-Pb ages of respective zircon domains, and the CHUR parameters: $^{176}Lu/^{177}Hf = 0.0336$, and $^{176}Hf/^{177}Hf = 0.282785$ (Bouvier et al., 2008)
(e) Two stage model age in billion years using the measured $^{176}Lu/^{177}Lu$ of each spot (first stage = age of zircon), a value of 0.0113 for the average continental crust (second stage), and a average MORB (DM) $^{176}Lu/^{177}Hf$ and $^{176}Hf/^{177}Hf$ of 0.0384 and 0.283164

Bouvier, A., Vervoort, J.D., Patchett, P.J., 2008. The Lu-Hf and Sm-Nd isotopic composition of CHUR: constraints from unequilibrated chondrites and implications for the bulk composition of terrestrial planets. Earth and Planetary Science Letters 273, 48-57.
(f) $^{206}Pb/^{238}U$ age

9.12 APPENDIX L – Supplementary data 2 (Chapter 5): Interference of Yb on Hf

Interference of Yb on Hf

Data quality and interference of elements with similar masses were assessed through the comparison between $\varepsilon Hf_{(t)}$ and $^{176}Yb/^{177}Hf$. No apparent correlation was detected between $\varepsilon Hf_{(t)}$ and $^{176}Yb/^{177}Hf$ for any of the analyzed samples, which suggests isobaric corrections for the interference of Yb on Hf were effective.

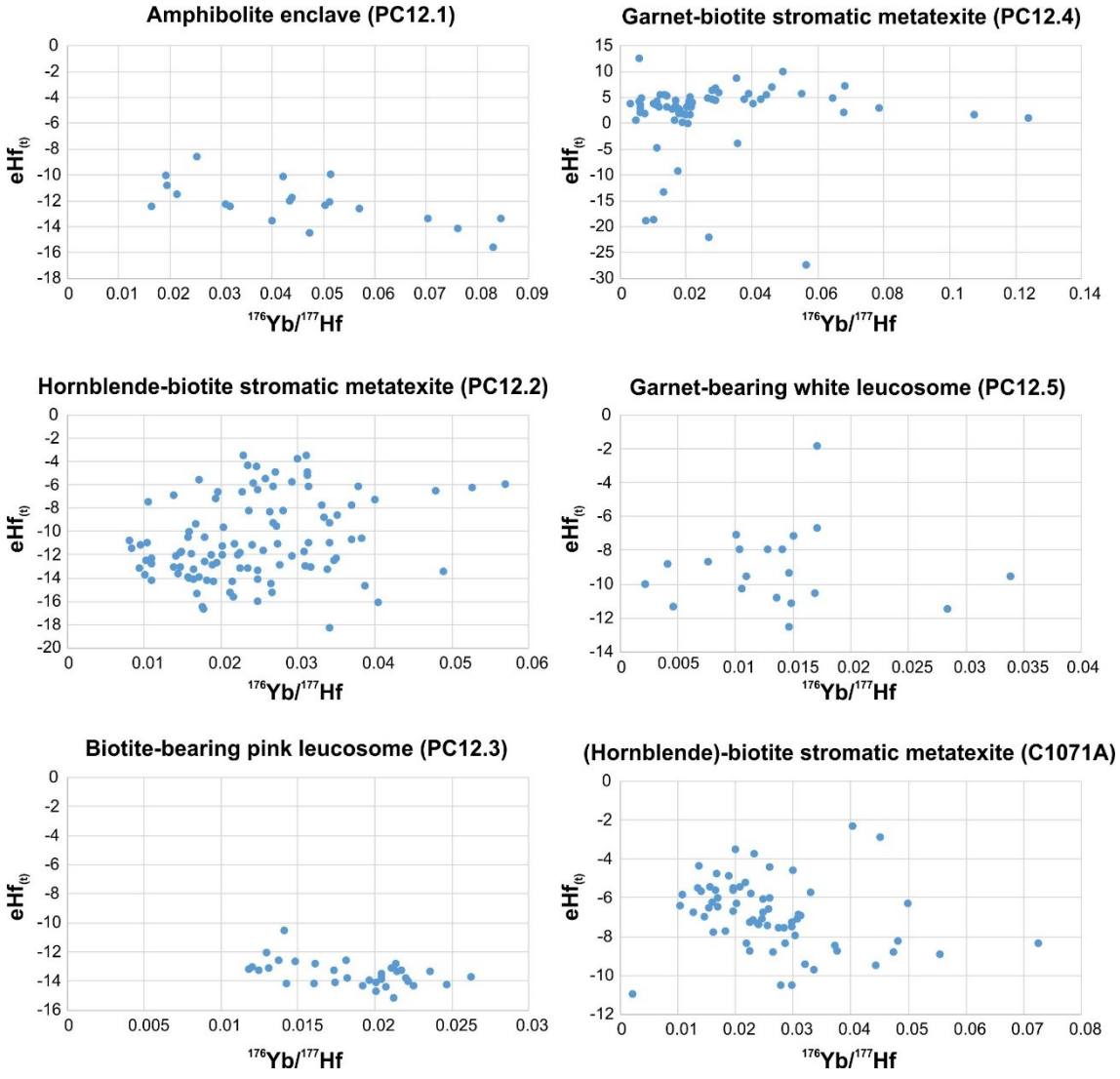

9.13 APPENDIX M – Supplementary data 3 (Chapter 5): Petrography

9.13.1 Amphibolite enclave (PC12.1)

Sample PC12.1 is a fine- to coarse-grained amphibolite enclave in the biotite-bearing pink leucosome (sample PC12.3), with centimeter-sized hornblende crystals (up to 1 cm) and a discrete foliation. It is composed of plagioclase (30–50%), hornblende (22 – 40%), biotite (10 – 15%), quartz (5 – 12%) and ilmenite (3 – 5%), with minor apatite, zircon, titanite, ilmenite and rare pyrite and chalcopyrite. A nematogranoblastic texture is observed, with oriented hornblende and biotite defining the foliation (Figure 4A). Rare ortho- and clinopyroxene are locally found between clusters of non-oriented hornblende crystals (Figure 4B), and it is not clear whether they consist of igneous relicts or relicts of a granulite-facies assemblage. Polygonal contacts between plagioclase and quartz crystals are commonly observed.

9.13.2 Hornblende-biotite stromatic metatexite (PC12.2)

The hornblende-biotite stromatic metatexite consists of mm- to cm-thick layered migmatite with melanocratic (dark gray) to mesocratic (gray) bands interleaved with leucocratic (pink) bands, which exhibit diffuse transitions between them (Figure 4C). Leucocratic bands are lepidogranoblastic, exhibiting a foliation marked mainly by biotite crystals, with variable amounts of plagioclase (23 – 70%), orthoclase (6 – 42%) and quartz (5 – 23%) in straight to sinuous contacts, with biotite (8 – 16%), hornblende (3 – 11%) and opaque minerals (ilmenite and magnetite, 1 – 2%) accounting for 10 – 20 vol%. Antiperthitic plagioclase and microperthitic orthoclase are often observed. Mafic bands (Figure 4C) are nematogranoblastic and lepidogranoblastic, with strongly oriented hornblende (15 – 25%) and biotite (25 – 35%) in the main foliation. Opaque minerals (ilmenite, magnetite, pyrite and chalcopyrite, 2 – 7%), plagioclase (35 – 40%), orthoclase (5 – 15%), quartz (5 – 10%) and accessory apatite, monazite, zircon and titanite are also present. Late muscovite is often observed at the contacts between biotite and feldspars. Quartz often exhibits chessboard extinction patterns.

9.13.3 Biotite-bearing pink leucosome (PC12.3)

The biotite-bearing pink leucosome is medium- to coarse-grained in the hornblende-biotite-stromatic gneiss. Metric-sized leucosome discordant to the main foliation that crosscut other lithotypes in the outcrop are coarse- to very coarse-grained (microcline phenocrysts up to 2 cm, Figure 4E-F), commonly microperthitic, and a matrix composed of fine- to coarse-grained microcline (35-45%), plagioclase (30 – 35%) and quartz (20 – 30%), with fine- to coarse-grained biotite (5 – 15%), minor

opaque minerals, apatite and zircon. Quartz often exhibits chessboard extinction patterns. Myrmekite occurs at the contacts between microcline and plagioclase. Late carbonate and clinozoisite are observed after plagioclase, as well as late muscovite after microcline.

9.13.4 Garnet-biotite stromatic metatexite (PC12.4)

The garnet-biotite stromatic metatexite consists of mm- to cm-thick sharp-layered migmatite. Mesocratic bands (Figure 5A) are fine- to medium-grained, composed of garnet (5 – 15%), biotite (15 – 25%), plagioclase (25 – 35%), K-feldspar (predominantly orthoclase, locally microcline; 10 – 20%) and quartz (10 – 20%). Mesocratic bands exhibit a main foliation (Sn) marked by oriented biotite crystals. Leucocratic bands (Figure 5B) are fine- to coarse- grained, composed of garnet (0 – 5%), biotite (green and brown, 0 – 5%), plagioclase (40 – 45%), K-feldspar (orthoclase and microcline, often perthitic; 30 – 35%) and quartz (25 – 30%). Medium-grained garnet crystals are mostly rounded and usually contain inclusions of quartz, plagioclase or minor biotite, either exhibiting circular patterns or oriented according to Sn, and probably corresponds to a peritectic phase. Fine-grained garnet crystals are usually euhedral and free of inclusions and might belong to a later generation (crystallized from the melt?). Green biotite is usually found at the borders or along fractures in garnet. Rare late muscovite is associated with partial replacement of feldspars. Quartz from both types of bands may exhibit chessboard extinction patterns. Minor amounts of apatite and zircon are observed. Disequilibrium textures marked by biotite-plagioclase-quartz skeletal intergrowths (Figure 5A) are often observed in mesocratic bands.

9.13.5 Garnet-bearing white leucosome (PC12.5)

The garnet-bearing white leucosome is medium- to coarse-grained and is observed both as millimetric bands in the garnet-biotite stromatic metatexite and as decimeter- to metric-sized pockets and bodies parallel to the banding. It is isotropic (Figure 5C-D) and is composed of garnet (5 – 10%), K-feldspar (microcline>perthitic orthoclase; 35 – 45%), plagioclase (rare antiperthite; 28 – 35%) and quartz (15 – 30%). Garnet crystals are euhedral to subhedral and might contain inclusions of quartz, plagioclase or opaque minerals without internal orientation. Minor biotite, muscovite, zircon, apatite and opaque minerals are observed. Myrmekite is often observed at the contacts between plagioclase and K-feldspars. Quartz often exhibits chessboard extinction patterns.

9.13.6 (Hornblende-)biotite-stromatic metatexite (C1071A)

The (hornblende)-biotite stromatic metatexite consists of mm- to cm-thick layered migmatite with a diffuse contact between mesocratic (gray) and medium- to coarse grained leucocratic (pink to gray) bands (Figure 5E-F). Mesocratic bands exhibit hornblende (0 – 5%), biotite (15 – 25%), perthitic microcline (15 – 20%), plagioclase (30 – 40%) and quartz (15 – 20%). Leucocratic bands exhibit biotite (5 – 10%), perthitic microcline (20 – 40%), plagioclase (15 – 30%) and quartz (20 – 30%). Minor apatite, opaque minerals and zircon are observed on both bands. Hornblende, when observed, is partially replaced by biotite-plagioclase-quartz (+opaque minerals) symplectites. Quartz often exhibits chessboard extinction patterns. A foliation, parallel to the banding, is marked by biotite crystals, defining a granolepidoblastic texture.

9.14 APPENDIX N – Supplementary data 4 (Chapter 5): U-Pb and Lu-Hf compilation from the Brasília and Ribeira orogens

(a) $^{176}Yb/^{177}Hf = (^{176}Yb/^{173}Yb)_{true}$ x $(^{173}Yb/^{177}Hf)_{meassured}$ x $(M_{173(Yb)}/M_{177(Hf)})^{b(Hf)}$, b(Hf) = ln($^{179}Hf/^{177}Hf_{true}$ / $^{179}Hf/^{177}Hf_{measured}$)/ ln ($M_{179(Hf)}/M_{177(Hf)}$)
M=mass of respective isotope. The $^{176}Lu/^{177}Hf$ were calculated in a similar way by using the $^{175}Lu/^{177}Hf$ and b(Yb)

(b) Mean Hf signal in volt

(c) Uncertainties are quadratic additions of the within-run precision and the daily reproducibility of the zircon standards. Uncertainties for the standard quoted at 2SD (2 standard deviation)

(d) Initial $^{176}Hf/^{177}Hf$ and ƐHf calculated using the apparent Pb-Pb ages of respective zircon domains, and the CHUR parameters: $^{176}Lu/^{177}Hf$ = 0.0336, and $^{176}Hf/^{177}Hf$ = 0.282785 (Bouvier et al., 2008)
(e) Two stage model age in billion years using the measured $^{176}Lu/^{177}Lu$ of each spot (first stage = age of zircon), a value of 0.0113 for the average continental crust (second stage), and a average MORB (DM) $^{176}Lu/^{177}Hf$ and $^{176}Hf/^{177}Hf$ of 0.0384 and 0.283164

Bouvier, A., Vervoort, J.D., Patchett, P.J., 2008. The Lu-Hf and Sm-Nd isotopic composition of CHUR: constraints from unequilibrated chondrites and implications for the bulk composition of terrestrial planets. Earth and Planetary Science Letters 273, 48-57.
(f) $^{206}Pb/^{238}U$ age

Matteini et al. 2010

Grain#	$^{176}Lu/^{177}Hf$ [a]	±2s	$^{176}Hf/^{177}Hf$	±2s [c]	age [f] (Ma)	$^{176}Hf/^{177}Hf_{(t)}$ [d]	eHf(t) [d]	±2s [c]
Goiás Magmatic Arc (metasedimentary rock, Sample MR 214)								
MR214_Z3	0.001410	34	0.282625	46	799	0.282601	13.57	0.88
MR214_Z13	0.001716	14	0.282603	46	918	0.282574	12.61	0.88
MR214_Z14	0.001844	14	0.282643	46	867	0.282611	13.93	0.88
MR214_Z23	0.001780	9	0.282547	42	908	0.282516	10.56	0.74
MR214_Z24	0.001868	22	0.282632	44	914	0.2826	13.54	0.81
MR214_Z32	0.001948	18	0.282606	42	921	0.282572	12.56	0.74
Goiás Magmatic Arc (banded mylonitic granite, Sample MR164)								
MR164_Z2	0.000581	10	0.281875	20	1307	0.28186	-3.36	0.38
MR164_Z3	0.000663	16	0.28194	22	817	0.28193	-11.82	0.10
MR164_Z4	0.000977	3	0.281604	25	2050	0.281564	2.94	0.88
MR164_Z5	0.000966	26	0.281141	39	2570	0.281092	-1.94	0.83
MR164_Z6	0.001791	9	0.282012	32	839	0.281983	-9.47	0.44
MR164_Z7	0.001749	28	0.282026	51	860	0.281997	-8.5	1.10
MR164_Z8	0.001262	75	0.281705	34	1887	0.281658	2.56	0.42
MR164_Z9	0.001197	28	0.281668	25	1353	0.281636	-10.27	0.26
MR164_Z13	0.000486	35	0.282039	19	1119	0.282028	-1.61	0.27
MR164_Z15	0.000376	3	0.281506	22	2108	0.281491	1.65	1.05
MR164_Z16	0.000399	1	0.280802	21	2605	0.280781	-12.19	1.52
MR164_Z18	0.000544	2	0.281393	22	1877	0.281373	-7.81	0.84
MR164_Z24	0.001808	84	0.282034	29	1167	0.281993	-1.8	0.06
MR164_Z25	0.000999	11	0.281909	22	1572	0.281878	3.24	0.54
MR164_Z12	0.001037	5	0.281979	25	1160	0.281956	-3.26	0.09
Goiás Magmatic Arc (monzogranitic gneiss, Sample PM III 95)								
PM III 95_Z1	0.000864	7	0.282056	25	747	0.282044	-9.35	0.26

PM III 95_Z6	0.000696	4	0.282219	27	1206	0.282203	6.52	0.06
PM III 95_Z7	0.000829	7	0.282021	25	776	0.282008	-9.95	0.23
PM III 95_Z8	0.000923	3	0.282053	25	777	0.282039	-8.85	0.24
PM III 95_Z9	0.001221	8	0.282003	26	805	0.281984	-10.16	0.23
PM III 95_Z10	0.001002	9	0.281807	28	1876	0.28177	6.28	0.62
PM III 95_Z11	0.001379	8	0.282133	22	1166	0.282133	2.03	0.22
PM III 95_Z12	0.001298	11	0.281639	33	2125	0.281585	5.37	0.67
PM III 95_Z14	0.000535	8	0.28135	26	2172	0.281327	-2.7	0.94
PM III 95_Z15	0.000868	20	0.281825	31	824	0.281811	-15.88	0.42
PM III 95_Z16	0.000889	11	0.281794	21	1128	0.281774	-10.43	0.20
PM III 95_Z17	0.001157	10	0.2821	22	863	0.282081	-5.45	0.06
PM III 95_Z18	0.000673	7	0.282069	28	878	0.282057	-5.96	0.27
PM III 95_Z19	0.000372	2	0.281254	26	2021	0.281239	-9.27	0.80
PM III 95_Z20	0.001416	26	0.282127	26	827	0.282104	-5.44	0.22
PM III 95_Z21	0.001163	26	0.282085	25	792	0.282067	-7.52	0.24
PM III 95_Z22	0.000962	5	0.281888	27	1328	0.281863	-2.81	0.16
PM III 95_Z24	0.000783	9	0.28186	19	750	0.281849	-16.18	0.06
Goiás Magmatic Arc (metadiorite, Sample MR 157)								
MR157_Z4	0.001550	17	0.282592	33	620	0.282574	6.2	0.67
MR157_Z6	0.001039	10	0.28257	43	643	0.282558	5.6	1.02
MR157_Z7	0.001412	28	0.282652	32	634	0.282636	8.37	0.63
MR157_Z8	0.000758	2	0.282523	39	637	0.282514	4.05	0.88
MR157_Z9	0.001030	1	0.282499	39	630	0.282487	3.11	0.88

Matteini, M., Junges, S.L., Dantas, E.L., Pimentel, M.M., Bühn, B., 2010. In situ zircon U-Pb and Lu-Hf isotope systematic on magmatic rocks: insights on the crustal evolution of the Neoproterozoic Goiás Magmatic Arc, Brasília belt, Central Brazil. Gondwana Research, 17(1), 1 – 12

Mora et al. 2014

Grain#	**$^{176}Lu/^{177}Hf$ [a]**	**±2s**	**$^{176}Hf/^{177}Hf$**	**±2s [c]**	**age [f] (Ma)**	**$^{176}Hf/^{177}Hf_{(t)}$ [d]**	**eHf(t) [d]**	**±2s [c]**
Metatexitic Unit - Leucosome (Sample Gx-77A2)								
1.1p	0.000225	1.00E-06	0.281895	2.40E-05	593	0.281893	-18.05	
9.1sb	0.000528	1.00E-06	0.282007	2.90E-05	590	0.282001	-14.26	
8.1p	0.001100	4.40E-05	0.281626	4.90E-05	670	0.281612	-26.27	
5.1sb	0.000914	2.00E-05	0.281838	3.80E-05	611	0.281827	-19.97	
7.1p	0.000800	1.10E-05	0.281867	2.70E-05	592	0.281858	-19.3	
20.1p	0.000431	1.10E-05	0.281841	2.60E-05	608	0.281836	-19.73	
32.1sb	0.000856	1.30E-05	0.281792	3.00E-05	604	0.281783	-21.7	
11.1p	0.000549	1.60E-05	0.281871	2.70E-05	597	0.281865	-18.95	
31.1sb	0.000456	4.00E-06	0.282024	2.60E-05	620	0.282019	-12.99	
29.1sb	0.000626	2.00E-06	0.281941	2.90E-05	613	0.281934	-16.13	
19.1p	0.000187	1.00E-06	0.28204	2.40E-05	610	0.282038	-12.53	
16.2p	0.000185	3.00E-06	0.282006	2.20E-05	613	0.282004	-13.66	

Metatexitic Unit - Paleosome (Sample Gx-77B1)								
4.1pn	0.000275	1.00E-06	0.28207	2.50E-05	617	0.282066	-11.36	
3.1pb	0.000270	4.00E-06	0.282242	2.40E-05	626	0.282239	-5.06	
2.1pn	0.000298	2.00E-06	0.282106	2.10E-05	618	0.282103	-10.06	
1.1pn	1.460738	4.60E-05	0.282022	2.50E-05	612	0.282012	-13.53	
8.1pb	0.000324	7.00E-06	0.282177	2.50E-05	626	0.282173	-7.38	
22.1pb	0.000423	6.00E-06	0.282017	3.70E-05	606	0.282012	-13.53	
23.1pn	0.000231	1.00E-06	0.282179	2.40E-05	608	0.282176	-7.67	
14.2pn	1.460620	7.00E-05	0.282053	2.40E-05	634	0.282076	-10.65	
10.1pb	0.000194	2.00E-06	0.282144	2.40E-05	616	0.282142	-8.72	
15.1pn	0.000451	1.00E-06	0.282199	2.40E-05	619	0.282194	-6.8	
16.1pn	0.000438	1.30E-05	0.282129	2.60E-05	630	0.282124	-9.05	
17.2pn	0.000502	6.00E-06	0.281909	2.40E-05	615	0.281903	-17.2	

Mora, C.A.S., Campos Neto, M.C., Basei, M.A.S., 2014. Syn-collisional lower continental crust anataxis in the Neoproterozoic Socorro-Guaxupé Nappe System, southern Brasília Orogen, Brazil: constraints from zircon U-Pb dating, Sr-Nd-Hf signatures and whole-rock geochemistry. Precambrian Research, 255, 847–864.

Cioffi et al. 2016a

Grain#	**$^{176}Lu/^{177}Hf$ [a]**	**±2s**	**$^{176}Hf/^{177}Hf$**	**±2s [c]**	**age [f] (Ma)**	**$^{176}Hf/^{177}Hf_{(t)}$ [d]**	**eHf(t) [d]**	**±2s [c]**
Tonalitic orthogneiss (Sample 1E)								
16.1	0.001391	2.20E-05	0.281581	4.30E-05	2126	0.281525	3.44	
3.1	0.003938	8.80E-05	0.281668	4.50E-05	2124	0.281508	2.82	
4.1	0.00069	1.40E-05	0.281605	2.40E-05	2122	0.281577	5.23	
5.1	0.001109	2.90E-05	0.281679	3.50E-05	2135	0.281634	7.54	
8.1	0.001306	3.60E-05	0.281571	3.30E-05	2140	0.281518	3.52	
9.1	0.000752	1.00E-05	0.281638	3.10E-05	2123	0.281608	6.32	
11.1	0.001785	2.60E-05	0.281633	3.90E-05	2137	0.281561	4.97	
12.1	0.000653	8.00E-06	0.281599	3.10E-05	2137	0.281572	5.4	
21.1	0.001082	3.50E-05	0.281708	3.70E-05	2129	0.281666	8.47	
Porphyroclastic granite (Sample 6)								
1.1	0.000732	1.50E-05	0.281608	2.50E-05	2086	0.281579	4.47	
24.1	0.000567	2.00E-06	0.281644	3.00E-05	2072	0.281622	5.65	
12.1	0.000704	1.10E-05	0.281665	3.60E-05	2060	0.281637	5.94	
15.1	0.000767	7.00E-06	0.281627	2.70E-05	2114	0.281596	5.71	
16.1	0.000879	2.10E-05	0.281625	2.80E-05	2090	0.28159	4.94	
19.1	0.001197	1.90E-05	0.281684	2.30E-05	2064	0.281637	6.02	
22.1	0.001187	1.20E-05	0.281591	3.10E-05	2102	0.281544	3.58	
21.1	0.000885	2.20E-05	0.281588	2.30E-05	2067	0.281554	3.12	
13.1	0.000728	1.90E-05	0.281637	3.00E-05	2083	0.281608	5.42	
5.1	0.000674	1.80E-05	0.281539	2.10E-05	2076	0.281513	1.87	
7.1	0.000528	6.00E-06	0.281553	2.70E-05	2059	0.281532	2.17	

Tonalitic orthogneiss (Sample 7A)

4.1	0.000465	3.00E-06	0.281622	2.80E-05	2118	0.281603	6.06	
5.1	0.001509	6.70E-05	0.281654	3.20E-05	2100	0.281594	5.3	
1.1	0.000661	9.00E-06	0.281553	2.50E-05	2151	0.281526	4.06	
15.1	0.000815	2.60E-05	0.281656	3.10E-05	2151	0.281623	7.5	
17.1	0.000693	8.00E-06	0.28163	2.90E-05	2148	0.281602	6.68	
19.1	0.000436	2.40E-05	0.281692	3.90E-05	2121	0.281675	8.66	
22.1	0.000532	5.00E-06	0.281604	3.20E-05	2174	0.281582	6.58	
21.1	0.000379	3.00E-06	0.28155	2.80E-05	2142	0.281535	4.18	
24.1	0.000497	6.00E-06	0.281563	3.50E-05	2119	0.281543	3.95	
16.1	0.000673	4.00E-06	0.281552	2.80E-05	2141	0.281525	3.8	
14.1	0.00085	2.00E-05	0.28162	3.50E-05	2154	0.281586	6.25	

Cioffi, C.R., Campos Neto, M.C., Möller, A., Rocha, B.C., 2016a. Paleoproterozoic continental crust generation events at 2.15 and 2.08 Ga in the basement of the southern Brasília Orogen, SE Brazil. Precambrian Research, 275, 176–196.

Westin et al. 2016

Grain#	$^{176}Lu/^{177}Hf$ [a]	±2s	$^{176}Hf/^{177}Hf$	±2s [c]	age [f] (Ma)	$^{176}Hf/^{177}Hf_{(t)}$ [d]	eHf(t) [d]	±2s [c]
Sâo Vicente Complex								
Plagioclase-quartz-biotite-epidote gneiss with K-feldspar and hornblende (Sample C-502)								
C-502 Plagioclase-quartz-biotite-epidote gneiss with K-feldspar and hornblende	0.000565		0.281576	2.09E-05	2110	0.281553	4.2	0.7
	0.000650		0.281589	2.41E-05	2120	0.281563	4.8	0.9
	0.000591		0.281561	3.36E-05	2132	0.281537	4.1	1.2
	0.000570		0.281568	2.14E-05	2141	0.281545	4.6	0.8
	0.000612		0.281562	2.12E-05	2148	0.281537	4.5	0.8
	0.000766		0.281569	2.71E-05	2186	0.281537	5.4	1.0
Epidote-plagioclase-biotite-quartz gneiss with carbonate (Sample C-505)								
C-505 Epidote-plagioclase-biotite-quartz gneiss with carbonate	0.000393		0.281482	2.30E-05	2112	0.281466	1.2	0.8
	0.000630		0.281500	2.34E-05	2120	0.281475	1.6	0.8
	0.000538		0.281465	2.00E-05	2127	0.281443	0.7	0.7
	0.000421		0.281441	1.76E-05	2132	0.281424	0.1	0.6
	0.000856		0.281468	3.89E-05	2141	0.281433	0.7	1.4
	0.000599		0.281496	2.14E-05	2142	0.281471	2.0	0.8
	0.000466		0.281464	2.17E-05	2178	0.281444	1.9	0.8
Biotite-plagioclase-quartz schist (Sample C-506C)								
C-506C Biotite-plagioclase-quartz schist	0.001227		0.281521	1.69E-05	2104	0.281472	1.2	0.6
	0.001117		0.281514	2.10E-05	2122	0.281469	1.5	0.7
	0.001231		0.281508	2.44E-05	2135	0.281458	1.4	0.9
	0.001420		0.281467	3.13E-05	2136	0.281409	-0.3	1.1
Muscovite quartzite (Sample C-510)								
C-510 Muscovite quartzite	0.000674		0.281578	1.74E-05	2099	0.281551	3.9	0.6
	0.000517		0.281563	1.97E-05	2115	0.281542	3.9	0.7

	0.000276		0.281549	1.55E-05	2126	0.281538	4.0	0.6
	0.000477		0.281523	1.68E-05	2133	0.281504	3.0	0.6
	0.000740		0.281506	1.99E-05	2140	0.281476	2.2	0.7
	0.002096		0.281630	1.84E-05	2145	0.281544	4.7	0.7
	0.000452		0.281516	1.89E-05	2156	0.281498	3.3	0.7
	0.000391		0.281464	1.85E-05	2167	0.281448	1.8	0.7
	0.000672		0.281478	2.20E-05	2173	0.281451	2.0	0.8
	0.001072		0.281587	2.00E-05	2185	0.281543	5.6	0.7
	0.000757		0.281519	1.81E-05	2199	0.281487	3.9	0.6
	0.001827		0.281606	2.34E-05	2224	0.281529	6.0	0.8
	0.000927		0.281527	1.71E-05	2248	0.281487	5.0	0.6
	0.000133		0.280805	1.53E-05	2695	0.280798	-9.0	0.5
	0.000620		0.280778	1.90E-05	2814	0.280745	-8.1	0.7
	0.000884		0.280848	2.23E-05	2895	0.280799	-4.3	0.8
Muscovite quartzite (Sample C-559)								
C-559 Muscovite quartzite	0.000937		0.281355	3.16E-05	2113	0.281317	-4.1	1.1
	0.000750		0.281519	1.70E-05	2134	0.281488	2.5	0.6
	0.000447		0.281564	2.00E-05	2145	0.281546	4.8	0.7
	0.000733		0.281423	1.80E-05	2159	0.281393	-0.4	0.6
	0.000675		0.281527	2.99E-05	2175	0.281499	3.8	1.1
Hornblende amphibolite (boudin) (Sample C-509)								
C-509 Hornblende amphibolite (*boudin*)	0.000635		0.281613	2.41E-05	2041	0.281589	3.9	0.9
	0.000352		0.281620	3.04E-05	2071	0.281606	5.2	1.1
	0.000711		0.281615	1.75E-05	2085	0.281587	4.8	0.6
	0.000729		0.281612	1.44E-05	2094	0.281583	4.9	0.5
	0.000438		0.281641	4.05E-05	2111	0.281623	6.7	1.4
	0.000450		0.281666	2.06E-05	2137	0.281648	8.2	0.7

Westin, A., Campos Neto, M.C., Hawkesworth, C.J., Cawood, P.A., Dhuime, B., Delavault, H., 2016. A Paleoproterozoic intra-arc basin associated with a juvenile source in the Southern Brasilia Orogen: Application of U-Pb and Hf–Nd isotopic analyses to provenance studies of complex areas. Precambrian Research, 276, 178–193.

Tedeschi et al. 2016

Grain#	$^{176}Lu/^{177}Hf$ [a]	±2s	$^{176}Hf/^{177}Hf$	±2s [c]	age [f] (Ma)	±2s	$^{176}Hf/^{177}Hf_{(t)}$ [d]	eHf(t) [d]	±2s [c]
Elói Mendes Unit (Banded Mafic Granulite, Sample C-833-A)									
28	0.000527	3.93E-06	0.281327	2.24E-04	2428	40	0.281303	2.72	0.66
51	0.000212	1.27E-06	0.281730	1.95E-05	1987	24	0.281722	7.34	0.64
49	0.000131	7.89E-07	0.281397	1.95E-05	1682	63	0.281393	-11.36	0.64
48	0.000203	1.22E-06	0.281574	1.78E-05	618	20	0.281572	-29.16	0.64
72	0.000341	2.18E-06	0.281872	2.03E-05	627	21	0.281868	-18.45	0.65
74	0.000281	1.94E-06	0.281338	1.43E-05	2468	18	0.281325	4.41	0.64
79	0.000134	8.07E-07	0.281296	1.93E-05	2462	68	0.281290	3.03	0.64
78	0.000531	3.19E-06	0.281454	2.27E-05	2480	45	0.281428	8.39	0.65

82	0.000116	6.98E-07	0.281413	2.33E-05	2227	65	0.281408	1.75	0.64
81	0.000208	1.25E-06	0.281632	2.02E-05	654	12	0.281630	-26.29	0.64
80	0.000320	1.92E-06	0.281797	2.81E-05	638	15	0.281793	-20.86	0.65
83	0.000267	1.61E-06	0.281587	2.19E-05	2504	69	0.281574	14.12	0.64
89	0.000225	1.35E-06	0.281335	1.77E-05	2559	65	0.281324	6.52	0.64
87	0.000212	1.28E-06	0.281591	2.30E-05	607	27	0.281588	-28.81	0.64
90	0.000633	3.84E-06	0.281706	1.91E-05	617	28	0.281699	-24.67	0.65
91	0.000226	1.36E-06	0.281306	1.92E-05	2124	76	0.281297	-4.60	0.64
54	0.000227	1.36E-06	0.281323	1.79E-05	627	12	0.281321	-37.85	0.64
98	0.000347	2.44E-06	0.281358	2.31E-05	2546	91	0.281341	6.83	0.65
97	0.000228	1.38E-06	0.281344	2.16E-05	2479	37	0.281333	4.98	0.64
102	0.000165	1.00E-06	0.281384	1.89E-05	1876	22	0.281378	-7.42	0.64
104	0.000036	2.19E-07	0.281321	2.32E-05	1956	61	0.281320	-7.64	0.64
105	0.000349	2.13E-06	0.281407	1.98E-05	637	17	0.281403	-34.70	0.64
106	0.000436	2.64E-06	0.281244	2.01E-05	1765	43	0.281229	-15.28	0.65
101.1	0.000188	1.23E-06	0.281313	1.83E-05	1876	22	0.281306	-9.98	0.64
102.1(101.2)	0.000191	1.67E-06	0.281312	1.96E-05	654	38	0.281309	-37.64	0.64
107	0.000041	2.50E-07	0.281325	2.01E-05	2011	73	0.281324	-6.25	0.64
Elói Mendes Unit (Hbl-Bt-bearing granitic Leucosome, Sample C-838-B)									
27	0.000372	3.44E-06	0.281552	1.78E-05	683	5	0.281547	-28.6	0.8
29	0.000259	1.58E-06	0.281220	1.35E-05	630	6	0.281217	-41.4	0.7
28	0.000582	3.58E-06	0.281187	1.95E-05	1365	59	0.281172	-26.5	0.8
25	0.000219	1.70E-06	0.281216	1.95E-05	659	5	0.281213	-40.9	0.7
24	0.000459	2.80E-06	0.281039	2.67E-05	1926	12	0.281023	-18.9	0.8
20	0.000419	2.53E-06	0.281780	2.13E-05	666	6	0.281775	-20.9	0.8
10	0.000644	4.19E-06	0.281332	1.49E-05	647	5	0.281324	-37.3	0.8
9	0.000340	3.41E-06	0.281216	1.97E-05	666	5	0.281212	-40.8	0.8
8	0.000660	8.81E-06	0.280972	1.89E-04	2075	43	0.280946	-18.2	0.8
47	0.000276	1.65E-06	0.281203	1.77E-05	630	6	0.281200	-42.0	0.7
79	0.000184	1.10E-06	0.281244	1.98E-05	571	3	0.281242	-41.9	0.7
78	0.000642	3.86E-06	0.281123	2.19E-05	1479	36	0.281105	-26.2	0.8
77	0.000476	2.86E-06	0.281322	1.75E-05	612	3	0.281317	-38.3	0.8
99	0.000038	2.29E-07	0.280987	2.03E-05	518	5	0.280987	-52.1	0.7
61	0.000580	4.09E-06	0.281124	1.53E-05	601	4	0.281118	-45.6	0.8
84	0.000731	4.63E-06	0.280966	1.60E-05	2725	19	0.280928	-3.7	0.8
Elói Mendes Unit (Banded Granulite, Sample C-838-A)									
14	0.000317	2.09E-06	0.282038	1.20E-05	613	5	0.282033892	-12.9	0.6
15	0.000535	4.26E-06	0.282063	1.17E-05	691	3	0.282055619	-10.4	0.7
19	0.001227	7.36E-06	0.282068	1.61E-05	660	4	0.28205249	-11.2	0.7
17	0.000930	5.58E-06	0.282029	1.89E-05	610	4	0.282018507	-13.5	0.7
18	0.001062	6.37E-06	0.282042	2.35E-05	633	5	0.282029626	-12.6	0.7
30	0.000266	1.60E-06	0.282006	1.75E-05	607	4	0.282003326	-14.1	0.6
48	0.001050	6.30E-06	0.282079	1.88E-05	687	9	0.282065126	-10.1	0.7
56	0.000254	1.54E-06	0.282038	1.49E-05	610	4	0.282035106	-12.9	0.6
55	0.000687	4.14E-06	0.282072	1.83E-05	601	7	0.282063867	-12.1	0.7

54	0.000299	1.80E-06	0.282051	1.54E-05	589	12	0.282047817	-13.0	0.6
52	0.000498	3.01E-06	0.282089	1.56E-05	683	5	0.282082713	-9.6	0.6
49	0.000497	3.19E-06	0.282126	1.48E-05	650	7	0.282119555	-9.0	0.6
50	0.000541	3.47E-06	0.281998	1.52E-05	607	7	0.28199225	-14.5	0.6
96	0.000769	4.62E-06	0.282001	1.41E-05	601	4	0.281992567	-14.6	0.7
94	0.001357	8.14E-06	0.282066	2.08E-05	616	3	0.282050587	-12.2	0.7
89	0.000173	1.04E-06	0.282027	1.50E-05	607	4	0.28202539	-13.3	0.6
88	0.000372	2.23E-06	0.282055	1.72E-05	626	3	0.282050847	-12.0	0.6
87	0.000378	2.27E-06	0.282000	1.39E-05	602	5	0.281995771	-14.5	0.6
75	0.000479	2.94E-06	0.282045	1.39E-05	661	6	0.282038885	-11.6	0.6
73	0.000575	3.46E-06	0.282083	1.38E-05	659	3	0.282075517	-10.4	0.7
113	0.000338	2.04E-06	0.282025	1.77E-05	706	16	0.282020292	-11.3	0.6
111	0.000473	2.86E-06	0.282065	1.41E-05	624	3	0.282059163	-11.8	0.6
114	0.000560	3.80E-06	0.282033	1.20E-05	613	5	0.282026901	-13.1	0.7
127	0.000647	3.91E-06	0.282053	1.52E-05	604	2	0.282045849	-12.7	0.7
126	0.000586	3.64E-06	0.282011	1.98E-05	630	4	0.282003645	-13.6	0.7
130	0.000842	5.05E-06	0.282004	1.50E-05	675	5	0.281993434	-12.9	0.7
145	0.000389	2.33E-06	0.281998	1.81E-05	1393	48	0.281987671	3.1	0.6
146	0.000223	1.34E-06	0.281326	1.47E-05	622	7	0.28132339	-37.9	0.6
150	0.000507	3.07E-06	0.282037	1.51E-05	603	8	0.28203079	-13.2	0.6
163	0.000368	2.25E-06	0.282028	1.37E-05	609	3	0.282023404	-13.4	0.6
165	0.000275	1.67E-06	0.282058	1.55E-05	628	5	0.282055248	-11.8	0.6
166	0.001300	7.81E-06	0.282034	2.12E-05	591	6	0.282019974	-13.9	0.7
19	0.000261	1.57E-06	0.282010	1.67E-05	621	5	0.282006966	-13.7	0.6
13	0.000243	1.46E-06	0.282024	1.65E-05	600	4	0.282021218	-13.6	0.6
12	0.000192	1.26E-06	0.282038	1.49E-05	613	4	0.282035475	-12.8	0.6
10	0.001017	6.11E-06	0.282002	1.51E-05	641	7	0.281989907	-13.8	0.7
Elói Mendes Unit (Opdalite, Sample C-832)									
12	0.000522	3.19E-06	0.282109	1.59E-05	720	6	0.282102	-8.1	0.7
14	0.000885	5.47E-06	0.281953	1.37E-05	770	6	0.281940	-12.7	0.7
17	0.000485	2.91E-06	0.281968	1.79E-05	659	6	0.281962	-14.4	0.6
18	0.000676	4.06E-06	0.281994	1.87E-05	681	5	0.281986	-13.1	0.7
19	0.000265	1.59E-06	0.281979	2.14E-05	674	5	0.281975	-13.6	0.6
20	0.000329	1.99E-06	0.281974	1.53E-05	715	7	0.281970	-12.9	0.6
30	0.000703	6.82E-06	0.281943	2.24E-05	761	6	0.281933	-13.1	0.7
31	0.000707	4.31E-06	0.281971	1.28E-05	748	6	0.281961	-12.5	0.7
32	0.000180	1.08E-06	0.281994	1.46E-05	730	5	0.281991	-11.8	0.6
33	0.001567	9.41E-06	0.281961	1.39E-05	715	5	0.281940	-13.9	0.7
34	0.001326	1.05E-05	0.281938	1.41E-05	743	5	0.281920	-14.0	0.7
36	0.000256	3.07E-06	0.281990	1.82E-05	713	6	0.281987	-12.3	0.6
38	0.001094	6.72E-06	0.281956	1.31E-05	725	5	0.281941	-13.7	0.7
39	0.000761	4.63E-06	0.281971	1.45E-05	721	5	0.281960	-13.1	0.7
50	0.000579	3.92E-06	0.281964	1.31E-05	707	10	0.281956	-13.5	0.7
51	0.000253	2.77E-06	0.281941	1.83E-05	679	6	0.281938	-14.8	0.6
54	0.000489	3.12E-06	0.281982	1.80E-05	637	5	0.281976	-14.4	0.6

55	0.000432	3.44E-06	0.281916	1.93E-05	678	5	0.281911	-15.8	0.6
57	0.001118	1.06E-05	0.281986	2.45E-05	776	7	0.281970	-11.5	0.7
59	0.000194	2.53E-06	0.281988	2.03E-05	650	9	0.281986	-13.8	0.6
70	0.000501	3.02E-06	0.281931	1.38E-05	654	6	0.281925	-15.8	0.6
71	0.000381	2.65E-06	0.281974	1.45E-05	691	23	0.281969	-13.5	0.6
72	0.000512	3.11E-06	0.281966	1.28E-05	683	5	0.281959	-14.0	0.6
76	0.000929	5.58E-06	0.281943	2.08E-05	786	10	0.281930	-12.7	0.7
90	0.000973	5.85E-06	0.281983	1.18E-05	727	6	0.281970	-12.6	0.7
96	0.000847	5.09E-06	0.281966	1.12E-05	669	7	0.281955	-14.4	0.7
97	0.000541	3.25E-06	0.281977	1.77E-05	676	10	0.281970	-13.8	0.6
98	0.001277	7.66E-06	0.281955	1.79E-05	711	5	0.281938	-14.1	0.7
110	0.000403	2.43E-06	0.281922	1.35E-05	665	4	0.281917	-15.8	0.6
113	0.000831	8.73E-06	0.281959	1.66E-05	695	5	0.281948	-14.1	0.7
115	0.000541	3.26E-06	0.281941	1.69E-05	636	5	0.281935	-15.9	0.6
Elói Mendes Unit (Mafic Enclave, Sample C716B)									
4	0.000794	4.77E-06	0.282178	1.62E-05	664	5	0.282168	-7.03	0.68
1	0.000203	1.22E-06	0.282201	1.67E-05	655	14	0.282199	-6.13	0.64
8	0.001272	7.64E-06	0.282144	1.45E-05	638	15	0.282129	-8.96	0.72
7	0.001005	6.08E-06	0.282157	1.66E-05	637	13	0.282145	-8.44	0.70
6	0.000533	3.21E-06	0.282098	1.77E-05	635	9	0.282092	-10.36	0.66
5	0.000619	4.15E-06	0.281931	2.41E-05	642	4	0.281923	-16.17	0.66
13	0.000513	3.85E-06	0.282157	1.37E-05	636	24	0.282151	-8.24	0.66
12	0.000830	1.08E-05	0.282174	1.57E-05	630	19	0.282164	-7.91	0.75
17	0.000438	2.66E-06	0.282189	1.43E-05	656	12	0.282184	-6.63	0.65
20	0.000310	1.87E-06	0.282195	1.97E-05	625	11	0.282191	-7.07	0.65
27	0.001003	6.03E-06	0.282166	1.54E-05	610	22	0.282155	-8.69	0.70
32	0.001029	6.27E-06	0.282166	1.55E-05	612	16	0.282154	-8.67	0.70
36	0.000459	3.37E-06	0.282192	1.22E-05	617	28	0.282186	-7.42	0.66
35	0.000468	3.15E-06	0.282181	1.65E-05	631	15	0.282175	-7.50	0.65
39	0.000964	6.30E-06	0.282215	1.83E-05	627	23	0.282203	-6.59	0.70
43	0.000723	4.34E-06	0.282166	2.10E-05	626	14	0.282158	-8.23	0.67
46	0.000299	1.80E-06	0.282165	2.14E-05	633	13	0.282161	-7.94	0.65
49	0.000448	2.69E-06	0.282175	2.04E-05	636	20	0.282169	-7.58	0.65
62	0.000539	3.23E-06	0.282052	1.81E-05	642	20	0.282046	-11.84	0.66
63	0.000740	4.44E-06	0.282150	2.15E-05	612	20	0.282141	-9.12	0.67
61	0.000766	4.71E-06	0.282148	1.98E-05	628	35	0.282139	-8.85	0.67
60	0.000769	4.78E-06	0.282177	1.71E-05	641	12	0.282168	-7.52	0.68
58	0.000831	5.00E-06	0.282153	1.63E-05	633	14	0.282143	-8.57	0.67
55	0.001068	1.07E-05	0.282146	2.25E-05	631	16	0.282134	-8.97	0.78

Tedeschi, M., Pedrosa-Soares, A.; Dussin, I., Lanari, P., Novo, T., Pinheiro, M. A. P., Lana, C., Peters, D. 2018. Protracted zircon geochronological record of UHT garnet-free granulites in the Southern Brasília orogen (SE Brazil): Petrochronological constraints on magmatism and metamorphism. Precambrian Research 316: 103-126.

Motta, 2018

Grain#	$^{176}Lu/^{177}Hf$ [a]	±2s [c]	$^{176}Hf/^{177}Hf$	±2s [c]	age [f] (Ma)	$^{176}Hf/^{177}Hf_{(t)}$ [d]	eHf(t) [d]	±2s [c]
Granulite Unit (Felsic Grt granulite, Sample VAB01)								
VAB01 - 1	0.000010	3.00E-07			599	0.282288	-4.22	
VAB01 - 2	0.000025	3.00E-07			599	0.282314	-3.31	
VAB01 - 3	0.000023	3.00E-07			622	0.282297	-3.39	
VAB01 - 4	0.000009	3.00E-07			586	0.282268	-5.22	
VAB01 - 6	0.000028	1.00E-06			578	0.282311	-3.89	
VAB01 - 7	0.000054	2.70E-06			628	0.282245	-5.08	
VAB01 - 8	0.000026	1.30E-06			561	0.282277	-5.47	
VAB01 - 9	0.000065	3.00E-05			626	0.282286	-3.67	
VAB01 - 10	0.000023	3.00E-07			592	0.282272	-4.95	
VAB01 - 11	0.000090	3.00E-07			628	0.282274	-4.07	
VAB01 - 13	0.000041	4.30E-06			628	0.282272	-4.15	
VAB01 - 14	0.000595	5.00E-06			611	0.282227	-6.10	
VAB01 - 18	0.000322	1.70E-05			578	0.282251	-6.02	
VAB01 - 5	0.000242	4.00E-05			592	0.282256	-5.50	
VAB01 - 19	0.000080	2.90E-06			624	0.282261	-4.61	
VAB01 - 16	0.000594	2.30E-05			689	0.282325	-0.87	
VAB01 - 15	0.001002	5.10E-05			663	0.282251	-4.11	
VAB01 - 17	0.001908	9.20E-05			649	0.282242	-4.73	
VAB01 - 12	0.000916	1.80E-05			702	0.282223	-4.21	
Granulite Unit (Felsic Grt granulite, Sample VAB19)								
VAB01 - 1	0.000010	3.00E-07			599	0.282288	-4.22	
VAB19 - 1	0.000406	2.90E-05			600	0.282271	-4.78	
VAB19 - 2	0.000006	4.00E-07			607	0.282255	-5.21	
VAB19 - 4	0.000020	7.00E-07			596	0.282293	-4.12	
VAB19 - 8	0.000004	3.00E-07			577	0.282254	-5.92	
VAB19 - 10	0.000515	4.50E-05			601	0.282255	-5.34	
VAB19 - 9	0.000359	1.50E-06			594	0.281962	-15.87	
VAB19 - 5	0.000774	2.50E-05			685	0.282239	-4.02	
VAB19 - 3	0.000860	1.70E-05			697	0.282231	-4.04	
RGM55 - 1	0.000700	5.10E-06			624	0.282181	-7.45	
RGM55 - 4	0.000683	3.70E-06			625	0.282166	-7.96	
RGM55 - 12	0.000706	7.30E-06			631	0.282154	-8.26	
RGM55 - 15	0.000641	2.70E-06			628	0.282181	-7.34	
RGM55 - 17	0.001049	6.40E-05			624	0.28215	-8.55	
RGM55 - 5	0.000629	5.60E-06			604	0.282189	-7.62	
RGM55 - 6	0.000880	1.60E-05			615	0.282191	-7.30	
RGM55 - 2	0.000905	1.60E-05			614	0.282181	-7.69	
RGM55 - 7	0.000758	1.70E-05			618	0.282181	-7.57	
RGM55 - 8	0.006460	1.50E-05			611	0.282201	-7.04	
RGM55 - 10	0.000636	6.20E-06			612	0.282157	-8.58	

RGM55 - 11	0.000604	6.70E-06			615	0.282144	-8.96	
RGM55 - 14	0.000613	1.00E-06			594	0.28218	-8.15	
RGM55 - 18	0.000829	4.70E-05			597	0.282164	-8.66	
RGM55 - 20	0.000080	6.20E-05			599	0.282133	-9.71	
RGM55 - 3	0.000930	4.60E-05			654	0.282148	-7.96	
RGM55 - 16	0.000944	2.80E-05			661	0.282157	-7.45	
RGM55 - 13	0.000895	1.90E-05			652	0.282134	-8.48	
RGM55 - 9	0.000689	1.60E-05			640	0.282175	-7.31	
RGM55 - 19	0.001157	4.40E-05			631	0.282207	-6.36	
Granulite Unit (Diatexite, Sample RGM55)								
RGM55 - 1	0.000700	5.10E-06			624	0.282181	-7.45	
RGM55 - 4	0.000683	3.70E-06			625	0.282166	-7.96	
RGM55 - 12	0.000706	7.30E-06			631	0.282154	-8.26	
RGM55 - 15	0.000641	2.70E-06			628	0.282181	-7.34	
RGM55 - 17	0.001049	6.40E-05			624	0.28215	-8.55	
RGM55 - 5	0.000629	5.60E-06			604	0.282189	-7.62	
RGM55 - 6	0.000880	1.60E-05			615	0.282191	-7.30	
RGM55 - 2	0.000905	1.60E-05			614	0.282181	-7.69	
RGM55 - 7	0.000758	1.70E-05			618	0.282181	-7.57	
RGM55 - 8	0.006460	1.50E-05			611	0.282201	-7.04	
RGM55 - 10	0.000636	6.20E-06			612	0.282157	-8.58	
RGM55 - 11	0.000604	6.70E-06			615	0.282144	-8.96	
RGM55 - 14	0.000613	1.00E-06			594	0.28218	-8.15	
RGM55 - 18	0.000829	4.70E-05			597	0.282164	-8.66	
RGM55 - 20	0.000080	6.20E-05			599	0.282133	-9.71	
RGM55 - 3	0.000930	4.60E-05			654	0.282148	-7.96	
RGM55 - 16	0.000944	2.80E-05			661	0.282157	-7.45	
RGM55 - 13	0.000895	1.90E-05			652	0.282134	-8.48	
RGM55 - 9	0.000689	1.60E-05			640	0.282175	-7.31	
RGM55 - 19	0.001157	4.40E-05			631	0.282207	-6.36	
Granulite Unit/Paraguassu Suite (Charnockite, Sample RGM57)								
RGM57 - 1	0.000391	5.30E-06			599	0.282126	-9.97	
RGM57 - 2	0.002291	2.70E-05			619	0.282096	-10.56	
RGM57 - 3	0.000335	2.40E-05			604	0.282127	-9.80	
RGM57 - 4	0.001370	2.50E-05			611	0.282156	-8.61	
RGM57 - 5	0.001859	5.90E-05			613	0.282105	-10.40	
RGM57 - 6	0.000316	2.30E-06			605	0.282127	-9.77	
RGM57 - 7	0.000379	5.60E-06			588	0.282168	-8.72	
RGM57 - 8	0.000793	1.90E-05			614	0.282171	-8.03	
RGM57 - 9	0.001244	1.40E-05			605	0.282164	-8.48	
Granulite Unit/Paraguassu Suite (Charnockite, Sample RGM02)								
RGM02 - 1	0.000534	2.70E-05			629	0.28201	-13.40	
RGM02 - 2	0.000382	2.00E-05			616	0.281984	-14.62	
RGM02 - 3	0.000608	3.40E-05			599	0.282012	-13.99	
RGM02 - 4	0.000790	1.60E-04			620	0.28196	-15.37	

RGM02 - 5	0.000757	5.50E-05			626	0.281989	-14.20	
RGM02 - 6	0.001290	1.00E-04			627	0.281969	-14.89	
RGM02 - 7	0.001510	6.10E-05			642	0.282007	-13.21	
RGM02 - 8	0.001080	1.20E-04			620	0.281982	-14.57	
RGM02 - 9	0.000575	4.60E-05			611	0.281992	-14.42	
RGM02 - 10	0.001049	9.80E-05			639	0.281962	-14.85	
RGM02 - 11	0.000555	1.60E-05			605	0.281998	-14.36	
Granulite Unit/Paraguassu Suite (Charnockite, Sample RGM04)								
RGM04 - 1	0.001818	6.50E-05			624	0.281965	-15.11	
RGM04 - 2	0.001094	2.40E-05			598	0.282042	-12.96	
RGM04 - 3	0.001044	7.10E-05			640	0.282023	-12.67	
RGM04 - 4	0.001673	3.50E-05			644	0.281995	-13.59	
RGM04 - 5	0.001495	7.90E-05			624	0.281949	-15.64	
RGM04 - 6	0.002270	1.20E-04			636	0.281948	-15.43	
RGM04 - 7	0.000763	2.60E-05			611	0.28202	-13.43	
RGM04 - 8	0.001395	7.60E-05			634	0.281976	-14.47	
RGM04 - 9	0.000975	4.20E-05			633	0.282001	-13.60	
RGM04 - 10	0.000718	2.10E-05			630	0.282014	-13.24	
Granulite Unit/Paraguassu Suite (Charnockite, Sample RGM53)								
RGM53 - 1	0.000436	5.40E-06			624	0.281968	-14.99	
RGM53 - 2	0.000516	9.50E-05			626	0.282035	-12.57	
RGM53 - 3	0.000787	2.70E-05			611	0.282028	-13.16	
RGM53 - 4	0.000896	7.40E-06			610	0.281987	-14.64	
RGM53 - 5	0.000758	2.50E-05			628	0.281977	-14.58	
RGM53 - 6	0.000415	1.30E-04			612	0.282021	-13.37	
RGM53 - 7	0.002000	6.80E-06			623	0.281985	-14.42	
RGM53 - 8	0.000538	3.60E-06			623	0.282006	-13.68	
RGM53 - 9	0.000920	7.30E-05			612	0.282001	-14.07	
RGM53 - 10	0.000749	1.80E-05			605	0.282009	-13.95	
RGM53 - 11	0.000806	7.90E-06			610	0.281946	-16.09	

Motta, R. G. 2018. Formação, transformação e evolução da crosta continental inferior: investigando o Orógeno Brasília Meridional. Tese de Doutorado. Instituto de Geociências, Universidade de São Paulo. 210 pp

Frugis et al., 2018

Grain#	**$^{176}Lu/^{177}Hf$ [a]**	**±2s**	**$^{176}Hf/^{177}Hf$**	**±2s [c]**	**age [f] (Ma)**	**$^{176}Hf/^{177}Hf_{(t)}$ [d]**	**eHf(t) [d]**	**±2s [c]**
Serra da Boa Vista Unit (metapelite, Sample SNA-228)								
64.1	0.001301	3.25E-05			1452	0.281623	-9.72	2.96
54.1	0.001057	1.33E-05			987	0.281820	-12.75	2.72
53.1	0.001099	3.37E-05			976	0.281871	-11.22	1.54
58.1	0.000987	7.37E-05			1249	0.281968	-1.7	1.27
40.1	0.001946	4.79E-05			1266	0.281925	-3.64	1.31
45.1	0.000786	2.23E-05			1969	0.280911	-22.92	1.71

47.1	0.002387	9.28E-05			1215	0.281985	-2.97	1.39
49.1	0.000600	1.61E-05			1816	0.281632	-0.54	1.17
32.1	0.001558	2.07E-05			1342	0.281998	0.92	1.4
52.1	0.001221	3.84E-05			1760	0.281588	-4.09	2.82
62.1	0.000399	8.94E-05			1222	0.281813	-7.31	1.74
1.1	0.001491	5.08E-05			1489	0.281843	-1.3	2.27
8.1	0.000519	6.39E-06			1012	0.282024	-4.61	1.6
13.1	0.000740	3.86E-05			1244	0.282044	1.12	1.45
11.1	0.001288	4.15E-05			968	0.282029	-5.91	1.93
14.1	0.001167	1.51E-05			1962	0.282075	17.75	3.54
7.1	0.001167	1.51E-05			1289	0.282066	2.51	1.6
6.1	0.001260	4.08E-05			961	0.282085	-4.07	1.35
16.1	0.001147	3.26E-05			980	0.281913	-9.66	1.55
15.1	0.000653	5.72E-05			1233	0.282099	2.87	1.47
21.1	0.001880	1.01E-04			1220	0.282144	3.19	1.39
22.1	0.001678	6.38E-05			1009	0.282060	-4.18	1.43
Serra da Boa Vista Unit (metapsammite, Sample SNA-213)								
4.1	0.000824	4.17E-05			1269	0.282030	1.11	1.15
1.1	0.000490	1.22E-05			1323	0.282053	3.4	1.6
8.1	0.002366	6.55E-05			1219	0.281979	-3.09	1.53
7.1	0.000827	5.44E-05			982	0.282209	1.08	1.25
6.1	0.000966	4.83E-05			1834	0.281520	-4.55	1.86
19.1	0.001531	3.04E-05			977	0.282165	-1.07	2.27
12.1	0.000619	4.02E-05			1220	0.282043	0.65	1.32
11.1	0.000658	8.90E-06			1340	0.281968	0.62	1.53
21.1	0.001113	1.25E-05			1908	0.281387	-7.8	2.01
18.1	0.000918	5.07E-05			1082	0.282057	-2.18	1.68
17.1	0.001657	5.35E-05			1306	0.282102	3.75	2.19
13.1	0.000855	4.67E-06			1302	0.282139	5.67	1.43
32.1	0.001192	4.79E-05			1407	0.282042	4.23	1.29
30.1	0.001848	2.74E-04			1974	0.281742	5.29	2.2
27.1	0.000964	3.37E-05			1224	0.282184	5.45	1.89
33.1	0.001598	1.25E-04			1332	0.282167	6.66	2.16
22.1	0.001382	6.50E-05			1105	0.282208	3.34	1.52
26.1	0.001008	9.72E-06			1834	0.281644	-0.22	1.72
24.1	0.000847	2.51E-05			1421	0.282005	3.55	1.76
39.1	0.001010	1.08E-04			1263	0.282208	7.11	3
44.1	0.001647	7.45E-05			1300	0.282125	4.42	2.32
65.1	0.000853	8.46E-06			1448	0.282062	6.2	1.77
Serra da Boa Vista Unit (metapelite, Sample SNA-125)								
4.1	0.000682	5.36E-05			1215	0.281944	-3.04	1.6
3.1	0.000805	3.09E-05			1297	0.281651	-11.71	2.07
11.1	0.000411	2.02E-05			1399	0.281868	-1.38	1.63
12.1	0.001301	3.06E-05			1870	0.281224	-14.69	2.04
16.2	0.000602	1.12E-05			1491	0.281610	-8.65	2.71

17.1	0.001853	1.00E-05			1771	0.281385	-11.83	3.01
20.1	0.000672	1.66E-05			1504	0.281542	-10.82	2.43
22.1	0.001153	5.20E-05			1208	0.281408	-22.59	3.31
23.1	0.000462	4.56E-06			1307	0.281850	-4.12	4.49
36.1	0.001641	4.34E-05			912	0.281512	-25.66	4.98
33.1	0.000808	2.03E-05			1033	0.281998	-5.24	2.48
34.1	0.001279	4.74E-05			1286	0.281255	-26.41	4.55
37.1	0.000843	8.09E-06			903	0.281587	-22.73	10.29
44.1	0.001430	5.48E-05			1351	0.281765	-7.02	2.23
43.1	0.001302	4.81E-05			1718	0.281799	2.36	2.42
46.1	0.001183	4.72E-05			1772	0.281623	-2.53	1.84
51.1	0.000833	8.10E-05			1186	0.281841	-7.48	2.46
52.1	0.001110	2.68E-05			1095	0.281803	-11.01	2.23
50.1	0.001865	1.32E-04			1576	0.281685	-5.4	1.95
56.1	0.001917	7.74E-05			1866	0.281317	-12.24	1.42
58.1	0.001251	2.37E-05			1177	0.281970	-3.4	1.85
59.1	0.000759	2.57E-05			1224	0.281840	-6.58	1.64
55.1	0.001143	1.08E-04			1380	0.281894	-1.56	1.26
Serra da Boa Vista Unit (metapelite, Sample NESG-1446)								
1.1	0.000286	2.80E-05			675	0.282066	-10.51	2.49
12.1	0.000109	7.37E-06			810	0.282125	-5.3	2.19
11.1	0.000244	1.16E-05			663	0.282040	-11.67	2.13
9.1	0.000109	3.46E-06			615	0.282044	-12.55	1.31
7.1	0.001303	1.46E-05			592	0.281742	-24.24	1.82
Serra da Boa Vista Unit (metapelite, Sample NESG-1434)								
8.1	0.001268	6.83E-05			1722	0.281804	2.66	1.88
4.1	0.001346	1.13E-04			1250	0.281968	-1.97	1.41
3.1	0.000779	3.32E-05			1581	0.281699	-3.65	2.04
2.1	0.000576	2.56E-05			1869	0.281211	-14.25	1.51
15.1	0.001051	8.39E-05			2034	0.281634	3.85	1.37
21.1	0.000782	4.70E-05			1063	0.281973	-5.46	2.3
Santo Antônio Unit (metagraywacke, Sample SNA-201)								
23.1	0.001221	1.41E-04			743	0.282625	10.34	2.08
1.1	0.001003	1.03E-04			679	0.282745	13.32	0.92
40.1	0.001367	1.04E-04			602	0.280501	-67.99	72.6
28.1	0.001992	2.49E-05			659	0.282553	5.65	1.74
16.1	0.001092	3.02E-05			676	0.282349	-0.8	1.95
14.1	0.001354	3.06E-05			679	0.282437	2.23	1.87
38.1	0.001345	1.63E-04			711	0.282310	-1.54	2.42
43.1	0.001599	9.36E-05			720	0.282380	0.99	2.46
37.1	0.000957	2.72E-05			823	0.282377	3.44	2.18
34.1	0.000971	2.63E-05			884	0.282407	5.86	2.05
2.1	0.000900	6.98E-05			886	0.282096	-5.09	1.2
11.1	0.000756	1.20E-05			778	0.282279	-0.9	1.96
56.1	0.001293	2.60E-05			746	0.282251	-2.88	1.56

54.1	0.000965	9.65E-05			759	0.282511	6.79	2.2
49.1	0.001028	3.39E-05			811	0.282584	10.5	1.61
55.1	0.001415	9.32E-05			863	0.282064	-7.03	1.91
24.1	0.000593	2.47E-05			818	0.282189	-3.1	1.16
22.1	0.000934	1.08E-05			832	0.282435	5.71	1.33
25.1	0.001393	1.49E-05			988	0.281803	-13.55	2
Santo Antônio Unit (amphibolite, Sample NESG-1552)								
4.1	0.000907	1.24E-05			672	0.282447	2.63	1.22
1.1	0.001594	7.61E-05			692	0.282503	4.76	0.92
11.1	0.000650	2.29E-05			767	0.282023	-10.16	1.38
12.1	0.001669	9.80E-05			787	0.282008	-10.78	1.36
10.1	0.001429	7.96E-05			821	0.282022	-9.44	0.94
2.2	0.001353	7.63E-05			833	0.282162	-4.16	1.34
6.1	0.000944	3.24E-05			795	0.282055	-8.57	1.26
5.1	0.002417	1.69E-05			964	0.282367	5.26	1.56
3.1	0.001767	7.04E-05			792	0.282050	-9.25	1.72
25.1	0.001104	8.03E-06			957	0.282334	4.77	1.17
27.1	0.001137	3.00E-05			1171	0.282105	1.34	1.18
34.1	0.001465	4.46E-05			954	0.282529	11.39	0.77
33.1	0.001465	4.46E-05			793	0.282529	7.91	0.77
29.1	0.001403	6.35E-05			793	0.282001	-10.78	0.92
31.1	0.002170	3.88E-05			779	0.282100	-7.95	1.46
9.1	0.001389	1.76E-05			1267	0.281993	-0.75	2.37
22.1	0.001100	1.62E-05			807	0.282024	-9.48	1.1
21.2	0.001107	5.55E-05			801	0.282026	-9.54	1.57
18.1	0.001616	1.27E-04			2118	0.281389	-3.77	1.81
24.1	0.001319	2.28E-05			2,195	0.281483	-46.01	2.09
32.1	0.000967	5.47E-05			1975	0.281327	-8.26	1.62
39.1	0.001229	4.88E-05			752	0.282537	7.44	1.07
26.2	0.001577	4.60E-05			720	0.282026	-11.54	0.86
37.2	0.000408	1.39E-05			1262	0.282026	1.15	1.71
20.1	0.001540	3.91E-05			778	0.282042	-9.69	1.2
16.1	0.000482	1.32E-05			788	0.281770	-18.58	1.21
13.1	0.001772	3.76E-05			790	0.281978	-11.82	1.61
14.1	0.001183	1.04E-04			801	0.282043	-8.99	1.26
Santo Antônio Unit (Grt-Bt-Pl schist, Sample NESG-1010)								
22.1	0.000580	8.78E-06			680	0.282127	-8.37	1.84
38.1	0.000734	1.54E-05			685	0.282097	-9.39	2.29
28.1	0.000733	7.72E-06			689	0.282170	-6.72	2.12
54.1	0.000592	9.36E-06			728	0.282478	5.13	3.51
79.1	0.001069	1.00E-05			677	0.282560	6.67	2.81
36.1	0.000685	2.85E-05			730	0.281701	-22.38	2.05
26.3	0.000463	9.93E-06			766	0.282253	-1.95	1.67
57.1	0.001125	9.91E-06			700	0.282305	-1.87	2.51
17.1	0.001622	1.80E-04			749	0.282293	-1.49	2.49

27.1	0.000953	1.39E-05			798	0.282422	4.51	3.19
18.1	0.000955	3.74E-05			692	0.282474	4.03	2.86
34.2	0.000786	6.64E-06			729	0.282379	1.56	3.38
48.1	0.000762	1.92E-05			784	0.281892	-14.5	3.07
88.1	0.001234	3.39E-05			802	0.282103	-6.87	2.86
65.2	0.000805	1.43E-05			820	0.282171	-3.85	1.76
10.2	0.001326	4.21E-05			2464	0.281987	25.65	1.62
1.1	0.000958	9.60E-06			812	0.281708	-20.47	1.99
29.2	0.000441	2.50E-05			808	0.282369	3.12	3.09
45.1	0.000946	8.61E-06			801	0.281733	-19.86	3.1
56.1	0.000560	3.70E-06			799	0.282055	-8.26	2.13
2.1	0.000473	3.27E-06			921	0.281455	-26.79	3.28
20.1	0.000768	1.78E-05			823	0.281975	-10.7	2.54
66.1	0.001487	2.70E-05			986	0.281829	-12.75	2.17
78.1	0.000577	3.07E-06			994	0.281873	-10.4	2.51
63.1	0.000572	8.92E-06			1011	0.281909	-8.76	3.26
19.1	0.001106	6.10E-06			1010	0.282046	-4.26	2.13
3.2	0.003126	5.54E-05			1045	0.282029	-5.52	2.28
5.3	0.000765	5.16E-05			1204	0.282064	0.91	1.85
12.2	0.000290	1.72E-06			1241	0.281937	-2.39	2.01
73.1	0.002130	1.03E-04			1242	0.281757	-10.26	2.9
77.1	0.000922	1.20E-05			1250	0.281872	-5.03	3.25
74.1	0.000884	9.19E-06			1793	0.281364	-10.9	2.58
4.1	0.000745	5.51E-05			1555	0.281731	-3.06	1.9
15.2	0.000496	2.27E-03			1934	0.281181	-13.75	1.78
30.1	0.000556	5.94E-03			1447	0.281651	-8.13	2.38
69.1	0.000596	1.31E-02			1542	0.281695	-4.48	2.16
53.1	0.000629	2.46E-02			2014	0.281061	-16.35	2.89
70.1	0.000286	8.91E-03			2091	0.281058	-14.24	2.38
64.1	0.000311	4.71E-02			1786	0.281553	-3.65	2.25
87.1	0.001403	3.73E-02			1868	0.281379	-9.35	2.04
86.1	0.001701	6.38E-02			1956	0.281522	-2.72	2.15
31.1	0.000621	4.39E-03			1976	0.281197	-12.37	3.17
3.3	0.000895	1.63E-02			2027	0.281328	-6.95	3.12
24.1	0.000569	2.32E-02			2039	0.281242	-9.3	1.92

Liberdade Nappe (Grt quartzite, Sample SNA-180A)

3.1	0.000216	2.96E-06			1476	0.281516	-11.94	5.61
4.3	0.001213	9.55E-05			1114	0.281756	-12.35	2.39
5.1	0.000704	2.00E-05			1213	0.281671	-12.78	2.11
9.1	0.000614	3.19E-05			1041	0.281654	-17.16	2.16
14	0.000614	3.19E-05			2849	0.281654	23.87	2.16
24	0.001028	2.61E-05			1530	0.281365	-16.91	1.77
18	0.000862	1.50E-05			1217	0.281508	-18.61	2.28
30	0.001108	6.74E-05			1274	0.281555	-15.89	3.24
61	0.001802	8.02E-05			1110	0.281751	-13.05	2.11

62	0.001274	8.09E-05			1003	0.281720	-16.1	2.34
Liberdade Nappe (metamafic lens, Sample SNA-172E)								
1.1	0.000650	2.38E-05			835	0.281892	-13.31	0.76
3.1	0.001477	5.44E-05			866	0.282126	-4.81	0.8
8.1	0.001549	2.82E-05			1125	0.282278	6.14	1.07
9.1	0.001284	1.10E-04			715	0.282133	-7.7	0.75
10.1	0.001425	7.28E-05			734	0.282084	-9.11	0.87
18.1	0.001232	5.24E-05			641	0.282004	-13.87	0.88
35.1	0.002210	6.75E-05			984	0.281964	-8.47	1.82
43.1	0.000964	9.66E-05			790	0.281904	-14.04	2.64
45.1	0.001521	2.74E-05			1124	0.281734	-13.14	2.12
2.1	0.001944	5.14E-05			760	0.281745	-20.8	1.71
14.1	0.000527	3.87E-05			1866	0.281197	-14.76	2.12
16.1	0.000868	1.05E-04			698	0.281773	-20.64	1.56
Liberdade Nappe (Retroeclogitic amphibolite, Sample SNA-205B)								
28.1	0.005078	2.44E-04			1480	0.282220	8.31	1.92
27.1	0.002665	7.80E-05			1481	0.282227	10.96	1.53
29.1	0.002154	1.77E-04			1419	0.282198	10.42	1.47
33.1	0.003298	2.66E-04			1491	0.282266	11.71	1.54
30.1	0.002441	1.17E-04			1468	0.282242	11.71	1.24
31.1	0.004068	1.67E-04			1445	0.282297	12.04	1.74
38.1	0.004219	1.93E-04			1468	0.282367	14.37	1.75
39.1	0.000474	1.83E-06			2072	0.281699	7.43	1.16
35.1	0.002832	1.78E-04			1516	0.282241	11.28	1.9
34.1	0.001005	1.29E-05			2061	0.281713	7.22	1.15
32.1	0.002386	1.62E-04			1479	0.282260	12.39	1.45
Liberdade Nappe (metavolcanoclastic, Sample SNA-168)								
27.1	0.003086	1.06E-04			1460	0.281998	1.99	1.67
35.1	0.003699	1.39E-04			1460	0.282106	5.24	1.66
4.1	0.002513	1.03E-04			1487	0.282042	4.12	1.63
32.1	0.002877	7.15E-05			1490	0.282086	5.34	1.66
33.1	0.003199	1.65E-04			1483	0.282034	3.16	1.44
17.1	0.002950	1.07E-04			1481	0.282064	4.46	1.72
16.1	0.002113	2.34E-04			1492	0.281974	2.09	1.46
38.1	0.003613	5.30E-05			1463	0.282023	2.37	1.71
36.1	0.002465	8.11E-05			1423	0.281985	2.16	1.43
37.1	0.004057	1.34E-04			1474	0.282098	4.6	1.86
8.1	0.005332	1.51E-04			1446	0.281989	-0.54	2.37
2.1	0.002565	9.25E-05			1463	0.281764	-5.75	1.93
3.1	0.004477	1.66E-04			1472	0.281964	-0.5	1.79
1.1	0.000911	2.07E-05			2052	0.281318	-7.03	1.82
5.1	0.001854	1.24E-04			1477	0.281829	-2.72	1.38
6.1	0.003289	1.05E-04			1469	0.281891	-1.93	1.78
7.1	0.003774	6.08E-05			1453	0.281944	-0.54	1.88
12.1	0.003435	1.33E-04			1488	0.281884	-2.32	1.71

9.1	0.000511	3.10E-06			2055	0.281409	-3.25	1.08
21.1	0.003292	1.79E-04			1461	0.281866	-2.84	1.61
24.1	0.000468	2.46E-06			1997	0.281449	-1.77	1.19
23.1	0.003179	1.66E-04			1469	0.281849	-3.33	1.57

Frugis, G.L., Campos Neto, M.C., Lima, R.B., 2018. Eastern Paranapanema and southern São Francisco orogenic margins: records of enduring Neoproterozoic oceanic convergence and collision in southern Brasília Orogen. Precambrian Research, 308, 35 – 57.

Westin et al., 2019

Grain#	$^{176}Lu/^{177}Hf$ [a]	±2s	$^{176}Hf/^{177}Hf$	±2s [c]	age [f] (Ma)	$^{176}Hf/^{177}Hf_{(t)}$ [d]	eHf(t) [d]	±2s [c]
Carrancas Group - Westin et al. 2019								
UPPER UNIT Muscovite quartzite with K-feldspar (Sample C-547)								
1.1	0.001333		0.281552	2.46E-05	1906	0.281503	-2.3	0.9
4.1	0.000934		0.282112	1.79E-05	1128	0.282092	0.8	0.6
20.1	0.001010		0.282197	2.00E-05	1212	0.282174	5.6	0.7
22.1	0.001990		0.282042	2.38E-05	1539	0.281984	6.3	0.8
23.1	0.000807		0.281688	1.45E-05	1735	0.281662	-0.6	0.5
28.1	0.001084		0.281511	1.90E-05	1884	0.281473	-3.9	0.7
29.1	0.000583		0.282112	1.44E-05	1293	0.282098	4.7	0.5
31.1	0.000668		0.281366	1.89E-05	2047	0.281339	-4.9	0.7
36.1	0.000969		0.282061	1.87E-05	1452	0.282034	6.1	0.7
37.1	0.000823		0.281859	1.67E-05	1379	0.281837	-2.5	0.6
39.1	0.000837		0.281567	1.56E-05	1847	0.281538	-2.4	0.6
42.1	0.001643		0.282075	2.19E-05	1271	0.282035	2.0	0.8
43.1	0.001061		0.282075	2.94E-05	1189	0.282051	0.7	1.0
44.1	0.000592		0.281874	1.68E-05	1516	0.281857	1.3	0.6
45.1	0.000631		0.280741	1.32E-05	2771	0.280707	-10.4	0.5
49.1	0.001625		0.282128	1.70E-05	1161	0.282093	1.6	0.6
50.1	0.000840		0.281581	1.50E-05	1779	0.281552	-3.5	0.5
58.1	0.001501		0.282111	2.09E-05	1361	0.282072	5.4	0.7
59.1	0.000785		0.282058	1.45E-05	1403	0.282037	5.1	0.5
66.1	0.001153		0.281952	1.87E-05	975	0.281931	-8.4	0.7
INTERMEDIATE UNIT Kyanite-staurolite-garnet-plagioclase gneiss (Sample C-552A)								
1.1	0.000457		0.281471	1.91E-05	2165	0.281452	1.9	0.7
5.1	0.000578		0.281887	1.49E-05	1463	0.281871	0.6	0.5
6.1	0.000739		0.281402	1.47E-05	2036	0.281374	-3.9	0.5
7.1	0.001029		0.281459	1.84E-05	1961	0.281421	-3.9	0.7
8.1	0.000893		0.280947	1.85E-05	2785	0.280899	-3.3	0.7
9.1	0.000522		0.281460	1.66E-05	2208	0.281438	2.4	0.6
11.1	0.001458		0.281707	2.05E-05	1637	0.281662	-2.9	0.7
12.1	0.000902		0.281556	2.46E-05	2108	0.281520	3.0	0.9
14.1	0.001044		0.282131	1.88E-05	1233	0.282107	3.7	0.7
25.1	0.000687		0.282136	1.56E-05	1262	0.282120	4.8	0.6

43.1	0.001344	0.281686	2.41E-05	1870	0.281639	1.7	0.9
44.1	0.000621	0.280942	1.90E-05	2728	0.280910	-4.3	0.7
51.1	0.001173	0.281071	2.51E-05	2705	0.281010	-1.2	0.9
55.1	0.001405	0.282095	3.52E-05	943	0.282070	-4.2	1.2
63.1	0.002184	0.282027	2.06E-05	1487	0.281965	4.5	0.7
LOWER UNIT Muscovite quartzite with plagioclase (Sample C-543)							
20.1	0.001472	0.281536	1.81E-05	2189	0.281474	3.2	0.6
30.1	0.001450	0.281513	1.90E-05	2152	0.281454	1.6	0.7
31.1	0.000711	0.281452	2.25E-05	2123	0.281423	-0.1	0.8
33.1	0.001369	0.281495	1.27E-05	2138	0.281440	0.8	0.5
36.1	0.000510	0.281494	2.02E-05	2171	0.281472	2.7	0.7
40.1	0.001426	0.281476	2.10E-05	2147	0.281418	0.3	0.7
42.1	0.000989	0.280944	2.14E-05	2837	0.280891	-2.4	0.8
52.1	0.000482	0.281095	2.57E-05	2682	0.281070	0.4	0.9
60.1	0.001223	0.281501	1.80E-05	2242	0.281449	3.6	0.6
63.1	0.000763	0.281450	2.52E-05	2475	0.281414	7.8	0.9

Westin, A., Campos Neto, M.C., Cawood, P.A., Hawkesworth, C.J., Dhuime, B., Delavault, H., 2019. The Neoproterozoic southern passive margin of the São Francisco craton: Insights on the pre-amalgamation of West Gondwana from U-Pb and Hf-Nd isotopes. Precambrian Research, 320, 454–471. https://doi.org/10.1016/j.precamres.2018.11.018.

Kuster et al., 2020

Grain#	$^{176}Lu/^{177}Hf$ [a]	±2s	$^{176}Hf/^{177}Hf$	±2s [c]	age [f] (Ma)	±2s	$^{176}Hf/^{177}Hf_{(t)}$ [d]	eHf(t) [d]	±2s [c]
Andrelândia Nappe (quartzite, Sample MAR367)									
ZR-39	0.000667	1.94E-05			961	36	0.282122	-1.93	0.13
ZR-19	0.001029	3.01E-05			973	43	0.282011	-5.60	0.41
ZR-28	0.000827	2.80E-05			978	32	0.282018	-5.23	0.35
ZR-36	0.000825	5.13E-06			984	24	0.282011	-5.36	0.16
ZR-32	0.001370	5.41E-05			1005	57	0.282057	-3.23	0.31
ZR-29	0.000698	2.59E-06			1099	30	0.282195	3.79	0.12
ZR-44	0.000742	5.33E-06			1128	30	0.282142	2.54	0.09
ZR-62	0.000354	1.59E-05			1155	29	0.282000	-1.85	0.13
ZR-78	0.000501	3.22E-05			1326	22	0.281838	-3.71	0.30
ZR-60	0.000730	4.66E-05			1357	31	0.281766	-5.58	0.48
ZR-22	0.001074	2.76E-05			1433	19	0.281980	3.76	0.15
ZR-8	0.002524	1.31E-05			1443	18	0.282082	7.61	0.14
ZR-23	0.000857	3.02E-05			1519	21	0.281857	1.36	0.07
ZR-30	0.000941	3.43E-05			1551	32	0.281801	0.10	0.01
ZR-59	0.000895	2.22E-05			1641	23	0.281484	-9.06	0.35
ZR-73	0.000497	8.68E-06			1643	54	0.281592	-5.19	0.26
ZR-40	0.001246	7.69E-06			1795	22	0.281727	3.08	0.06
ZR-18	0.001654	2.76E-05			1795	29	0.281701	2.17	0.07
ZR-20	0.001766	4.05E-05			1807	19	0.281610	-0.80	0.03

ZR-27	0.001011	5.88E-05			1886	24	0.281564	-0.59	0.04
ZR-16	0.001359	1.21E-05			1965	19	0.281634	3.71	0.07
ZR-31	0.000609	3.77E-06			1969	46	0.281324	-7.20	0.21
ZR-76	0.001395	2.20E-05			2007	17	0.281475	-0.95	0.02
ZR-7	0.000236	9.88E-06			2058	16	0.281281	-6.68	0.33
ZR-61	0.003248	2.10E-04			2099	21	0.281572	4.60	0.34
ZR-102	0.000811	4.38E-05			2099	15	0.281489	1.67	0.10
ZR-71	0.000981	3.52E-05			2121	22	0.281330	-3.47	0.16
Lima Duarte Nappe (quartzite, Sample BJM8)									
ZR-4	0.000497	2.20E-06			1776	26	0.281579	-2.59	0.05
ZR-1	0.000559	7.70E-07			2194	21	0.281057	-11.49	0.13
ZR-6	0.000496	9.64E-07			2071	31	0.281495	1.23	0.02
ZR-8	0.000518	1.10E-05			2059	25	0.281099	-13.13	0.44
ZR-14	0.000519	3.99E-06			2012	25	0.281674	6.22	0.12
ZR-18	0.000340	8.75E-07			2093	22	0.281384	-2.19	0.03
ZR-40	0.001008	5.24E-06			2181	30	0.281528	4.96	0.09
ZR-43	0.000803	1.45E-05			2122	30	0.281537	3.90	0.13
ZR-45	0.000443	5.99E-06			2177	40	0.281399	0.28	0.01
ZR-46	0.000432	2.87E-07			2047	30	0.281405	-2.51	0.04
ZR-74	0.000909	8.18E-06			2644	16	0.281016	-2.45	0.04
ZR-47	0.000383	2.69E-06			2062	28	0.281403	-2.27	0.05
ZR-78	0.001223	1.72E-05			2125	25	0.281635	7.46	0.20
ZR-71	0.001052	6.61E-05			2176	31	0.281390	-0.06	0.00
ZR-80	0.001049	9.20E-06			2271	21	0.281429	3.53	0.06
ZR-57	0.000738	5.42E-06			2632	16	0.280996	-3.46	0.05
ZR-31	0.000253	3.65E-07			2377	30	0.281306	1.64	0.02
ZR-61	0.000492	5.65E-07			2478	16	0.281326	4.69	0.04
Liberdade Nappe (quartzite, Sample KA109)									
ZR-01	0.000369	9.12E-07			1198	25	0.282150	4.43	0.11
ZR-26	0.000740	2.71E-06			1237	22	0.282117	4.14	0.09
ZR-23	0.000880	2.24E-05			1534	20	0.281743	-2.33	0.09
ZR-33	0.000693	8.70E-06			1526	31	0.281762	-1.82	0.06
ZR-21	0.000751	1.09E-05			1538	16	0.281883	2.74	0.07
ZR-6	0.000650	5.12E-06			1852	24	0.281561	-1.48	0.03
ZR-3	0.000664	2.16E-05			1779	20	0.281592	-2.06	0.09
ZR-8	0.001212	7.69E-06			2021	23	0.281385	-3.83	0.07
ZR-9	0.001262	1.87E-05			2307	22	0.281430	4.42	0.11
ZR-10	0.000708	1.56E-05			1148	24	0.282092	1.24	0.05
ZR-12	0.001998	1.59E-05			1059	34	0.282167	1.88	0.08
ZR-17	0.000708	7.44E-06			1369	18	0.281934	0.69	0.02
ZR-38	0.001141	1.22E-05			1241	18	0.282053	1.95	0.05
ZR-37	0.001327	1.91E-05			1960	18	0.281309	-7.95	0.19
ZR-36	0.000556	4.89E-06			1739	29	0.281835	5.64	0.14
ZR-44	0.000672	1.55E-05			1151	21	0.282096	1.46	0.06
ZR-45	0.000723	1.33E-05			973	44	0.282088	-2.86	0.18

ZR-46	0.000591	3.52E-06			1725	27	0.281637	-1.73	0.04
ZR-48	0.001768	3.75E-05			1213	33	0.282179	5.79	0.28
ZR-34	0.000453	1.42E-06			1227	26	0.282049	1.50	0.04
ZR-56	0.000731	9.98E-06			2765	31	0.280929	-2.70	0.07
ZR-57	0.000681	1.26E-05			2023	44	0.281519	0.97	0.04
ZR-83	0.000531	6.73E-06			1965	28	0.281084	-15.83	0.43
ZR-86	0.000359	3.62E-07			1769	29	0.281727	2.49	0.04
ZR-75	0.001104	5.92E-05			1365	21	0.281967	1.74	0.12

Kuster, K., Ribeiro, A., Trouw, R. A. J., Dussin, I., Marimon, R. S. 2020. The Neoproterozoic Andrelândia group: Evolution from an intraplate continental margin to an early collisional basin south of the São Francisco craton, Brazil. Journal of South American Earth Sciences, 102, 102666.

Balis et al. 2020

Grain#	$^{176}Lu/^{177}Hf$ [a]	±2s [c]	$^{176}Hf/^{177}Hf$	±2s [c]	age [f] (Ma)	$^{176}Hf/^{177}Hf_{(t)}$ [d]	eHf(t) [d]	±2s [c]
São Roque Domain								
Barro Branco orthogneiss (Sample BB-04C)								
4.1	0.00128	9.0E-05	0.282239	5.5E-05	705	0.282222	-4.19	1.94
6.1	0.00095	4.0E-05	0.282244	4.5E-05	687	0.282231	-4.25	1.59
8.1	0.00065	2.1E-05	0.282153	2.9E-05	680	0.282145	-7.47	1.03
9.1	0.00108	4.1E-05	0.282322	3.6E-05	668	0.282308	-1.95	1.28
11.1	0.00110	5.6E-05	0.282143	5.3E-05	680	0.282129	-8.04	1.88
13.1	0.00097	6.2E-05	0.282275	4.0E-05	680	0.282263	-3.30	1.41
15.1	0.00190	2.1E-04	0.282406	2.1E-05	680	0.282382	0.93	0.73
16.1	0.00036	2.5E-05	0.282179	3.9E-05	645	0.282174	-7.21	1.39
18.1	0.00044	8.4E-06	0.282223	3.5E-05	697	0.282218	-4.51	1.23
22.1	0.00051	8.4E-05	0.282207	3.8E-05	678	0.282201	-5.53	1.35
Inequigranular orthogneiss (Sample BB-09)								
2.1	0.00041	6.4E-06	0.281777	5.3E-05	625	0.281772	-21.89	1.88
3.1	0.00015	1.1E-05	0.282052	2.7E-05	625	0.282050	-12.07	0.95
10.1	0.00035	6.4E-06	0.282109	3.0E-05	625	0.282104	-10.13	1.06
14.1	0.00027	1.0E-05	0.282143	4.3E-05	625	0.282140	-8.87	1.53
16.1	0.00015	6.5E-06	0.282046	5.0E-05	647	0.282044	-11.77	1.76
17.1	0.00031	9.2E-06	0.282081	4.2E-05	646	0.282077	-10.62	1.50
19.1	0.00013	1.2E-05	0.282107	4.9E-05	625	0.282105	-10.10	1.75
20.1	0.00021	8.7E-06	0.282093	5.0E-05	625	0.282090	-10.64	1.77
23.1	0.00008	6.3E-06	0.282025	6.1E-05	625	0.282024	-12.98	2.15
25.1	0.00048	4.0E-06	0.282130	5.0E-05	694	0.282124	-7.90	1.76
Biotite schist (Sample BB-06)								
1.1	0.00058	1.0E-05	0.281588	3.8E-05	2188	0.281564	6.40	1.34
7.1	0.00092	2.4E-05	0.281367	3.8E-05	2308	0.281327	0.75	1.36
13.1	0.00074	4.2E-05	0.281360	3.7E-05	2378	0.281327	2.39	1.32
14.1	0.00039	2.5E-06	0.281585	5.0E-05	2111	0.281570	4.81	1.79
17.1	0.00066	6.7E-06	0.280669	4.3E-05	3288	0.280627	-1.09	1.53

20.1	0.00143	3.8E-05	0.281167	4.1E-05	2925	0.281087	6.68	1.45
22.1	0.00136	5.9E-06	0.281577	3.4E-05	2227	0.281519	5.71	1.22
26.1	0.00048	8.8E-06	0.281476	3.0E-05	2222	0.281455	3.33	1.07
27.1	0.00075	3.1E-05	0.281054	3.3E-05	2681	0.281015	-1.62	1.19
28.1	0.00072	4.1E-06	0.280915	4.2E-05	2703	0.280878	-5.99	1.50
29.1	0.00107	1.6E-05	0.281449	4.1E-05	2203	0.281403	1.04	1.47
32.1	0.00129	1.9E-05	0.281623	5.1E-05	2185	0.281569	6.51	1.82
33.1	0.00066	4.9E-05	0.281624	4.5E-05	2175	0.281596	7.23	1.59
34.1	0.00076	3.7E-05	0.281452	4.0E-05	2124	0.281421	-0.16	1.41
36.1	0.00089	2.0E-05	0.281617	4.1E-05	2142	0.281581	5.93	1.46
39.1	0.00072	4.1E-06	0.281581	4.4E-05	2159	0.281551	5.26	1.55
43.1	0.00107	3.9E-05	0.281373	6.7E-05	2121	0.281329	-3.50	2.39
50.1	0.00090	7.8E-06	0.281385	4.2E-05	2204	0.281347	-0.93	1.48
56.1	0.00028	5.0E-06	0.281355	4.6E-05	2088	0.281344	-3.73	1.63
59.1	0.00032	5.0E-06	0.281383	4.2E-05	2073	0.281371	-3.15	1.48

Balis, M., Campos Neto, M. C., Alves, A. 2020. Serra do Barro Branco orthogneiss: An untimely record of West Gondwana amalgamation in the São Roque Domain. Precambrian Research, 350, 105913.

Marimon et al., 2020

Grain#	$^{176}Lu/^{177}Hf$ [a]	±2s	$^{176}Hf/^{177}Hf$	±2s [c]	age [f] (Ma)	$^{176}Hf/^{177}Hf_{(t)}$ [d]	eHf(t) [d]	±2s [c]
Lower São Tomé das Letras Fm. (metaconglomerate, Sample RSM145)								
ZR-78	0.000705	4.58E-06	0.281329	3.52E-05	2116	0.281301	-4.63	0.29
ZR-20	0.000515	4.90E-06	0.281373	2.87E-05	2124	0.281352	-2.61	0.41
ZR-15	0.000595	1.42E-05	0.281269	3.73E-05	2129	0.281244	-6.33	0.26
ZR-12	0.000429	5.80E-06	0.281267	3.02E-05	2131	0.281250	-6.10	0.39
ZR-41	0.000537	3.59E-06	0.281127	3.01E-05	2133	0.281105	-11.19	0.39
ZR-76	0.000567	1.20E-05	0.281287	4.03E-05	2141	0.281264	-5.37	0.21
ZR-62	0.000464	1.11E-05	0.281316	3.27E-05	2143	0.281298	-4.13	0.35
ZR-2B	0.000207	1.08E-06	0.281194	3.82E-05	2659	0.281184	3.87	0.49
ZR-77	0.001091	3.67E-05	0.281203	3.25E-05	2672	0.281148	2.90	0.60
ZR-4	0.000233	4.14E-06	0.281108	2.41E-05	2687	0.281096	1.39	0.76
ZR-11	0.000354	1.10E-06	0.281064	3.66E-05	2697	0.281046	-0.15	0.54
ZR-7	0.000302	1.80E-06	0.281233	3.09E-05	2703	0.281217	6.10	0.64
ZR-32	0.000615	3.42E-06	0.281109	3.50E-05	2720	0.281077	1.50	0.58
ZR-6	0.000332	9.10E-07	0.280728	3.32E-05	3007	0.280709	-4.85	0.74
ZR-39	0.000247	3.92E-06	0.280726	2.84E-05	3235	0.280711	0.64	0.94
ZR-30	0.000194	2.29E-06	0.280710	3.05E-05	3241	0.280698	0.31	0.90
ZR-3	0.000942	1.58E-05	0.280780	4.32E-05	3244	0.280721	1.20	0.68
Chapada das Perdizes Fm. (Ms quartzite Sample RSM167)								
ZR-68	0.000691	1.28E-06	0.281863	3.06E-05	1537	0.281843	1.28	0.24
ZR-12	0.001094	3.92E-06	0.281531	3.30E-05	1602	0.281498	-9.48	0.21
ZR-73	0.001534	1.99E-05	0.281836	3.40E-05	1757	0.281785	4.27	0.31

ZR-74	0.000761	3.31E-06	0.281732	3.72E-05	1766	0.281706	1.68	0.20
ZR-46	0.000909	1.33E-05	0.281561	3.23E-05	1871	0.281529	-2.19	0.47
ZR-55	0.000294	3.47E-06	0.281558	3.18E-05	1896	0.281548	-0.94	0.51
ZR-33	0.000973	2.53E-05	0.281607	3.73E-05	1930	0.281572	0.69	0.35
ZR-39	0.000798	6.24E-05	0.281663	4.71E-05	1991	0.281632	4.26	0.06
ZR-6	0.000346	1.92E-06	0.281552	3.69E-05	1999	0.281539	1.12	0.43
ZR-27	0.000250	1.49E-06	0.281476	2.84E-05	2122	0.281466	1.39	0.84
ZR-9	0.000388	6.14E-07	0.281461	3.73E-05	2123	0.281445	0.65	0.52
ZR-10	0.000391	2.87E-06	0.281551	3.42E-05	2127	0.281535	3.94	0.64
ZR-53	0.000543	1.00E-05	0.281503	4.41E-05	2132	0.281481	2.14	0.29
ZR-77	0.000489	3.45E-06	0.281390	4.55E-05	2462	0.281367	5.79	0.54
ZR-4	0.000158	3.83E-07	0.280861	3.37E-05	2709	0.280852	-6.74	1.19
ZR-30	0.000290	1.06E-05	0.281003	3.66E-05	2709	0.280988	-1.93	1.08
ZR-41	0.000428	1.96E-06	0.280895	2.89E-05	2781	0.280872	-4.34	1.42
ZR-25	0.000532	1.80E-06	0.280909	3.53E-05	2786	0.280880	-3.94	1.20
ZR-45	0.000728	6.29E-06	0.280916	2.36E-05	2790	0.280877	-3.97	1.62
ZR-43	0.000622	1.24E-06	0.281000	3.95E-05	2821	0.280967	-0.05	1.09
ZR-65	0.000591	6.34E-07	0.280983	3.12E-05	2828	0.280951	-0.45	1.39
ZR-66	0.000141	1.22E-05	0.280908	3.52E-05	2867	0.280901	-1.31	1.28
ZR-75	0.000559	4.74E-06	0.281035	3.50E-05	2870	0.281005	2.46	1.29
ZR-20	0.000311	4.61E-06	0.280840	3.73E-05	2915	0.280822	-2.97	1.25
ZR-14	0.000530	1.19E-06	0.280768	3.48E-05	3018	0.280737	-3.57	1.44
Campestre Fm. (Schist Sample RSM132)								
ZR-63	0.002349	1.53E-05	0.282292	5.04E-05	1126	0.282242	6.06	0.83
ZR-18	0.000998	3.81E-05	0.281845	8.11E-05	1284	0.281820	-5.30	0.89
ZR-29	0.002394	1.00E-04	0.282127	4.98E-05	1529	0.282058	8.71	0.45
ZR-14	0.000737	9.45E-06	0.281908	2.45E-05	1556	0.281886	3.26	0.47
ZR-41	0.000858	2.00E-05	0.281364	4.86E-05	2125	0.281329	-3.42	0.12
ZR-3	0.000374	2.84E-05	0.281234	4.43E-05	2132	0.281219	-7.17	0.14
ZR-53	0.000872	1.74E-05	0.281502	4.06E-05	2206	0.281465	3.31	0.48
ZR-54	0.000515	1.06E-05	0.281497	3.05E-05	2208	0.281475	3.69	0.84
ZR-09	0.001287	1.04E-05	0.281500	5.19E-05	2230	0.281445	3.15	0.10
ZR-58	0.000941	2.60E-05	0.281479	4.00E-05	2309	0.281438	4.73	0.60
ZR-21	0.000365	2.05E-05	0.280857	4.58E-05	3114	0.280836	2.20	0.57
Lower São Tomé das Letras Fm. (Ms quartzite Sample LVR25)								
ZR-36	0.001511	1.55E-05	0.282184	3.82E-05	1026	0.282155	0.70	0.48
ZR-80	0.000410	6.35E-06	0.281839	3.27E-05	1074	0.281831	-9.69	0.25
ZR-79	0.000707	2.35E-05	0.282020	3.30E-05	1094	0.282006	-3.04	0.24
ZR-4	0.000395	8.07E-06	0.282187	2.87E-05	1230	0.282178	6.16	0.03
ZR-9	0.000499	3.41E-05	0.282162	2.76E-05	1213	0.282151	4.80	0.06
ZR-85	0.000433	9.62E-06	0.281678	2.06E-05	1305	0.281667	-10.25	0.38
ZR-19	0.000612	9.25E-06	0.281820	2.93E-05	1312	0.281805	-5.22	0.08
ZR-28	0.001702	1.06E-04	0.282181	2.93E-05	1373	0.282136	7.94	0.14
ZR-30	0.001152	1.75E-05	0.282162	2.66E-05	1433	0.282131	9.10	0.29
ZR-41	0.000917	1.59E-05	0.281960	2.61E-05	1494	0.281934	3.54	0.36

ZR-7	0.000531	8.46E-07	0.281864	2.50E-05	1540	0.281849	1.56	0.43
ZR-5	0.000877	8.28E-06	0.282069	3.04E-05	1545	0.282043	8.57	0.25
ZR-20	0.000876	1.07E-05	0.281932	2.53E-05	1581	0.281906	4.51	0.46
ZR-67	0.000711	3.92E-05	0.281790	3.80E-05	1746	0.281767	3.37	0.16
ZR-34	0.001100	6.49E-05	0.281905	3.97E-05	1785	0.281868	7.86	0.13
ZR-24	0.000486	6.44E-06	0.281546	3.31E-05	1796	0.281530	-3.89	0.38
ZR-16	0.001437	4.70E-05	0.281779	3.49E-05	1813	0.281730	3.61	0.33
ZR-54	0.000678	2.16E-05	0.281556	2.99E-05	1877	0.281531	-1.96	0.56
ZR-37	0.000948	9.35E-06	0.281815	3.04E-05	1887	0.281781	7.14	0.56
ZR-3	0.001074	2.18E-05	0.281706	4.03E-05	1907	0.281667	3.55	0.22
ZR-15	0.000669	7.63E-06	0.281447	3.21E-05	2045	0.281420	-2.02	0.63
ZR-12	0.000643	1.05E-05	0.281266	2.60E-05	2624	0.281234	4.83	1.38
ZR-6	0.000542	9.17E-06	0.280908	2.39E-05	3134	0.280875	4.09	1.94
Lower São Tomé das Letras Fm. (Sample RSM 168)								
ZR-55	0.001821	7.42E-06	0.282169	4.42E-05	1004	0.282134	-0.52	0.71
ZR-62	0.000970	2.50E-05	0.282268	3.35E-05	1096	0.282247	5.57	0.25
ZR-23	0.000380	9.65E-06	0.282227	3.49E-05	1155	0.282219	5.91	0.25
ZR-34	0.000520	4.72E-06	0.282144	4.03E-05	1157	0.282133	2.87	0.44
ZR-3	0.000589	9.00E-06	0.282236	2.87E-05	1220	0.282222	7.51	0.03
ZR-43	0.000860	2.97E-05	0.282255	2.80E-05	1221	0.282235	8.00	0.05
ZR-24	0.002048	2.15E-05	0.282355	5.42E-05	1227	0.282307	10.68	0.87
ZR-83	0.002023	1.13E-04	0.282315	4.47E-05	1331	0.282264	11.52	0.44
ZR-13	0.001821	8.15E-06	0.282302	5.30E-05	1424	0.282253	13.24	0.66
ZR-18	0.000317	2.29E-06	0.282162	4.85E-05	1429	0.282153	9.82	0.49
ZR-38	0.000381	4.34E-06	0.281810	3.70E-05	1498	0.281799	-1.18	0.03
ZR-9	0.000740	4.30E-05	0.282035	5.29E-05	1535	0.282013	7.27	0.56
ZR-16	0.000351	3.84E-06	0.281685	3.79E-05	1578	0.281674	-3.76	0.01
ZR-20	0.001076	5.74E-06	0.281896	3.86E-05	1689	0.281862	5.43	0.09
ZR-57	0.000545	1.80E-05	0.281852	4.30E-05	1747	0.281834	5.80	0.02
ZR-11	0.001075	2.24E-05	0.281851	3.02E-05	1757	0.281815	5.35	0.45
ZR-17	0.000413	2.94E-06	0.281720	4.11E-05	1795	0.281706	2.34	0.09
ZR-56	0.001151	3.65E-05	0.281718	4.26E-05	1853	0.281677	2.66	0.09
ZR-26	0.001004	3.14E-05	0.281702	3.61E-05	1863	0.281667	2.53	0.33
ZR-29	0.000553	3.56E-06	0.281810	3.66E-05	1966	0.281790	9.26	0.41
ZR-65	0.000707	5.98E-06	0.281625	3.81E-05	1352	0.281607	-11.30	0.20
Chapada das Perdizes Fm. (Ms quartzite Sample RSM6)								
ZR-58	0.001770	7.16E-06	0.282401	5.50E-05	997	0.282368	7.57	1.10
ZR-28	0.001127	3.98E-05	0.282324	3.61E-05	1020	0.282303	5.80	0.41
ZR-102	0.000696	2.12E-05	0.282046	4.41E-05	1041	0.282032	-3.32	0.68
ZR-103	0.000632	1.24E-05	0.282150	2.82E-05	1051	0.282137	0.65	0.10
ZR-118	0.000655	7.80E-06	0.282124	3.79E-05	1165	0.282109	2.24	0.35
ZR-76	0.000370	5.75E-06	0.282075	2.72E-05	1197	0.282067	1.48	0.06
ZR-2	0.000460	1.97E-06	0.282140	3.01E-05	1225	0.282129	4.30	0.02
ZR-10	0.000463	2.02E-06	0.282112	2.62E-05	1245	0.282101	3.77	0.13
ZR-18	0.001313	1.36E-05	0.282083	3.01E-05	1251	0.282052	2.15	0.00

ZR-7	0.001320	5.14E-05	0.282124	3.00E-05	1315	0.282091	5.02	0.06
ZR-93	0.000493	1.55E-05	0.281987	3.44E-05	1317	0.281975	0.93	0.09
ZR-8	0.001183	8.61E-06	0.282020	3.93E-05	1388	0.281989	3.06	0.21
ZR-49	0.000208	1.79E-05	0.282104	3.35E-05	1434	0.282098	7.98	0.04
ZR-60	0.000703	1.38E-05	0.282019	2.86E-05	1454	0.281999	4.92	0.23
ZR-5	0.000428	6.63E-05	0.281993	4.33E-05	1517	0.281980	5.70	0.23
ZR-24	0.000669	8.46E-06	0.281898	2.89E-05	1542	0.281878	2.65	0.30
ZR-34	0.000842	4.25E-05	0.281924	3.08E-05	1548	0.281899	3.53	0.24
ZR-61	0.000804	5.73E-05	0.281785	3.83E-05	1727	0.281758	2.63	0.13
ZR-77	0.000560	9.66E-07	0.281692	3.68E-05	1734	0.281673	-0.22	0.19
ZR-53	0.001295	2.25E-05	0.281579	3.15E-05	1831	0.281534	-2.91	0.46
ZR-4	0.001115	3.10E-05	0.281652	3.74E-05	1843	0.281613	0.14	0.27
ZR-66	0.000568	8.21E-06	0.281617	3.33E-05	1861	0.281597	-0.02	0.43
ZR-42	0.000501	2.69E-06	0.281425	3.15E-05	1948	0.281406	-4.77	0.57
ZR-59	0.000870	1.97E-05	0.281370	2.71E-05	1953	0.281338	-7.09	0.73
ZR-47	0.000785	1.18E-05	0.281209	3.36E-05	1986	0.281179	-11.97	0.53
ZR-43	0.001001	7.88E-05	0.281192	5.20E-05	1991	0.281154	-12.74	0.12
ZR-86	0.001340	2.68E-05	0.281367	4.54E-05	2554	0.281302	5.61	0.63
ZR-48	0.000556	7.67E-06	0.281158	3.38E-05	2733	0.281129	3.66	1.21
ZR-115	0.000558	3.42E-06	0.281087	3.01E-05	2785	0.281057	2.32	1.39
Lower São Tomé das Letras Fm. (Ms quartzite Sample RSM151)								
ZR-19	0.000677	2.07E-05	0.281270	3.40E-05	1991	0.281245	-9.52	0.52
ZR-25	0.000452	8.51E-06	0.281351	3.70E-05	2071	0.281334	-4.50	0.48
ZR-86	0.001383	2.04E-05	0.281564	3.87E-05	2073	0.281509	1.79	0.43
ZR-88	0.000607	4.34E-06	0.281241	3.67E-05	2110	0.281217	-7.74	0.53
ZR-47	0.000832	9.02E-06	0.281389	4.40E-05	2113	0.281356	-2.76	0.27
ZR-21	0.000854	2.10E-05	0.281439	3.60E-05	2123	0.281405	-0.77	0.57
ZR-67	0.001353	2.78E-05	0.281616	4.23E-05	2126	0.281561	4.87	0.35
ZR-54	0.000666	1.16E-05	0.281080	3.23E-05	2130	0.281053	-13.10	0.70
ZR-28	0.000438	3.57E-06	0.281299	3.31E-05	2131	0.281282	-4.96	0.68
ZR-23	0.000712	6.49E-06	0.281288	3.84E-05	2134	0.281259	-5.72	0.49
ZR-26	0.000644	1.79E-05	0.281349	4.00E-05	2137	0.281323	-3.37	0.44
ZR-51	0.001045	1.44E-05	0.281339	3.04E-05	2138	0.281296	-4.28	0.78
ZR-29	0.000627	1.61E-05	0.281225	3.99E-05	2593	0.281194	2.68	0.86
ZR-71	0.000381	1.67E-05	0.281171	2.79E-05	2604	0.281152	1.47	1.30
ZR-68	0.000508	8.51E-06	0.281011	3.29E-05	2680	0.280985	-2.71	1.19
ZR-4N	0.000902	3.57E-05	0.281146	4.00E-05	2708	0.281099	2.01	0.96
ZR-81	0.000708	3.34E-05	0.280849	3.73E-05	2770	0.280811	-6.79	1.11
ZR-11	0.000886	2.25E-05	0.280955	4.25E-05	2783	0.280908	-3.04	0.94
ZR-48	0.001338	8.87E-06	0.280856	4.30E-05	3131	0.280775	0.47	1.25
ZR-15	0.000703	1.22E-05	0.280746	3.44E-05	3263	0.280702	0.99	1.68
Chapada das Perdizes Fm. (Quartzite Sample RSM56)								
ZR-108	0.002197	5.56E-05	0.282205	4.50E-05	1177	0.282156	4.19	0.59
ZR-113	0.000719	4.81E-06	0.281968	2.88E-05	1200	0.281951	-2.57	0.00
ZR-8	0.001030	1.38E-05	0.281914	2.26E-05	1205	0.281890	-4.61	0.23

ZR-104	0.000683	1.22E-05	0.281888	3.19E-05	1218	0.281872	-4.95	0.09
ZR-102	0.000866	1.35E-05	0.281903	4.11E-05	1223	0.281883	-4.46	0.41
ZR-16	0.000679	7.04E-06	0.281945	3.19E-05	1236	0.281929	-2.55	0.08
ZR-114	0.000901	1.01E-05	0.281796	3.44E-05	1494	0.281770	-2.28	0.06
ZR-19	0.000934	3.42E-05	0.281652	2.66E-05	1691	0.281622	-3.02	0.51
ZR-21	0.000852	1.39E-06	0.281746	3.80E-05	1797	0.281717	2.78	0.20
ZR-49	0.001086	2.13E-05	0.281724	3.11E-05	1940	0.281684	4.92	0.58
ZR-25	0.000739	5.94E-06	0.281707	2.83E-05	1943	0.281680	4.83	0.68
ZR-111	0.000982	2.60E-06	0.281701	2.92E-05	1964	0.281664	4.77	0.67
ZR-117	0.001232	6.25E-06	0.281623	2.52E-05	1975	0.281577	1.91	0.82
ZR-97	0.000782	9.87E-06	0.281602	2.76E-05	1978	0.281573	1.84	0.74
ZR-98	0.000334	2.55E-06	0.281371	3.75E-05	2015	0.281358	-4.95	0.42
ZR-122	0.000534	1.53E-06	0.281679	3.27E-05	2022	0.281659	5.92	0.60
ZR-46	0.000455	3.91E-06	0.281554	2.84E-05	2024	0.281536	1.62	0.75
ZR-29	0.000624	7.33E-06	0.281491	3.25E-05	2043	0.281467	-0.42	0.62
ZR-50	0.000602	7.06E-06	0.281442	2.28E-05	2066	0.281419	-1.61	0.99
ZR-119	0.000268	1.36E-06	0.281542	2.32E-05	2106	0.281532	3.34	1.01
ZR-118	0.000533	2.28E-06	0.281673	2.96E-05	2116	0.281652	7.85	0.79
ZR-99	0.000494	3.55E-06	0.281549	2.85E-05	2156	0.281529	4.41	0.86
ZR-125	0.000801	9.59E-06	0.281572	3.56E-05	2175	0.281539	5.21	0.63
ZR-55	0.000601	9.02E-06	0.281636	3.22E-05	2177	0.281611	7.83	0.75
ZR-100	0.000743	6.09E-06	0.281091	2.81E-05	2767	0.281052	1.71	1.45
Chapada das Perdizes Fm. (Ms quartzite Sample LVR43)								
ZR-23	0.000396	3.24E-06	0.282165	3.34E-05	985	0.282158	-0.13	0.35
ZR-6	0.000117	2.18E-05	0.282207	2.84E-05	993	0.282205	1.74	0.16
ZR-18	0.000673	1.54E-05	0.282148	4.63E-05	1166	0.282133	3.12	0.65
ZR-55	0.000548	6.85E-05	0.282081	3.12E-05	1225	0.282068	2.14	0.06
ZR-75	0.000845	7.70E-06	0.282139	3.54E-05	1237	0.282119	4.23	0.20
ZR-13	0.000937	4.18E-06	0.281875	3.06E-05	1358	0.281851	-2.55	0.07
ZR-57	0.000324	1.84E-06	0.282050	2.84E-05	1429	0.282041	5.85	0.22
ZR-30	0.000378	2.18E-05	0.281889	4.43E-05	1448	0.281879	0.53	0.33
ZR-47	0.001396	1.05E-04	0.281995	3.90E-05	1517	0.281955	4.81	0.08
ZR-5	0.001012	1.39E-05	0.282153	2.60E-05	1567	0.282123	11.91	0.42
ZR-59	0.000526	9.44E-06	0.281871	2.92E-05	1573	0.281855	2.53	0.32
ZR-40	0.000874	8.40E-07	0.281966	3.79E-05	1613	0.281939	6.45	0.05
ZR-33	0.001338	5.80E-05	0.281772	4.06E-05	1734	0.281728	1.73	0.06
ZR-46	0.000759	1.60E-05	0.281802	2.60E-05	1767	0.281776	4.20	0.60
ZR-58	0.001196	4.20E-05	0.281703	3.88E-05	1773	0.281663	0.32	0.15
ZR-42	0.001833	9.54E-06	0.281798	3.16E-05	1806	0.281735	3.63	0.44
ZR-21	0.000928	4.21E-06	0.281730	3.53E-05	1814	0.281698	2.51	0.31
ZR-51	0.000980	1.66E-05	0.281653	3.25E-05	1816	0.281619	-0.26	0.42
ZR-10	0.000439	1.29E-05	0.281585	2.49E-05	1892	0.281569	-0.26	0.75
ZR-14	0.000925	3.20E-05	0.281896	3.24E-05	1897	0.281863	10.27	0.50
ZR-31	0.000561	2.32E-06	0.281323	3.09E-05	1953	0.281303	-8.33	0.59
ZR-49	0.000969	1.74E-05	0.281650	2.82E-05	1969	0.281614	3.08	0.71

ZR-36	0.000662	4.74E-06	0.281413	2.82E-05	1975	0.281388	-4.80	0.71
ZR-15	0.000479	3.67E-06	0.281318	2.86E-05	1996	0.281300	-7.43	0.71
ZR-20	0.000708	3.90E-05	0.281388	3.84E-05	2025	0.281361	-4.60	0.39
ZR-45	0.001495	7.62E-05	0.281693	3.81E-05	2171	0.281631	8.39	0.54
ZR-96	0.000336	3.43E-07	0.280960	2.35E-05	2617	0.280943	-5.68	1.47
ZR-98	0.000223	3.34E-06	0.281048	2.60E-05	2710	0.281037	-0.16	1.46
ZR-88	0.000312	8.19E-06	0.281000	3.09E-05	2750	0.280984	-1.12	1.33
ZR-41	0.000450	8.99E-06	0.281057	2.34E-05	2838	0.281032	2.69	1.68
ZR-95	0.001405	4.38E-05	0.281083	3.02E-05	2936	0.281004	3.98	1.53
ZR-48	0.000523	4.28E-06	0.280596	2.90E-05	3468	0.280561	0.84	2.07
Lower São Tomé das Letras Fm. (Sample RSM72)								
ZR-20A	0.001700	6.83E-05	0.282308	8.93E-05	1206	0.282269	8.84	0.46
ZR-7	0.001271	1.82E-05	0.281968	3.07E-05	1231	0.281939	-2.29	0.10
ZR-29A	0.000887	2.15E-05	0.282026	4.63E-05	1247	0.282005	0.40	0.02
ZR-61	0.001300	1.50E-04	0.282301	4.21E-05	1279	0.282269	10.49	1.55
ZR-85	0.001762	7.48E-05	0.282181	5.16E-05	1508	0.282131	10.84	0.63
ZR-03A	0.000747	1.33E-06	0.281871	2.46E-05	1509	0.281849	0.87	0.01
ZR-44	0.000864	1.54E-05	0.281927	3.82E-05	1537	0.281902	3.37	0.12
ZR-54	0.001499	1.75E-04	0.282043	4.60E-05	1572	0.281998	7.59	1.02
ZR-52	0.001118	4.04E-05	0.282110	3.59E-05	1606	0.282076	11.14	0.61
ZR-9A	0.000942	3.95E-05	0.281906	3.05E-05	1651	0.281877	5.10	0.25
ZR-57A	0.001152	2.94E-05	0.281664	3.14E-05	1863	0.281623	0.99	0.03
ZR-50A	0.001790	3.92E-05	0.281908	3.49E-05	1881	0.281844	9.24	0.26
ZR-11A	0.001002	1.65E-04	0.281552	3.87E-05	2103	0.281511	2.55	0.43

Marimon, R. S., Trouw, R. A. J., Dantas, E. L., Ribeiro, A. 2020. U-Pb and Lu-Hf isotope systematics on detrital zircon from the southern São Francisco Craton's Neoproterozoic passive margin: Tectonic implications. Journal of South American Earth Sciences, 100, 102539.

Santiago et al., 2020

Grain#	**$^{176}Lu/^{177}Hf$ [a]**	**±2s**	**$^{176}Hf/^{177}Hf$**	**±2s [c]**	**age [f] (Ma)**	**$^{176}Hf/^{177}Hf_{(t)}$ [d]**	**eHf(t) [d]**	**±2s [c]**
Caixixe Batolith (Ribeira Belt)								
Felsic Orthogneiss (Sample 06)								
ZR-15	0.001001	6.00E-05	0.282655	5.70E-05	853	0.282639	13.93	1.1
ZR-14	0.000817	1.90E-05	0.28259	4.90E-05	832	0.282577	11.27	0.4
ZR-12	0.000653	2.30E-05	0.282523	4.10E-05	846	0.282512	9.29	0.6
ZR-3	0.001016	1.90E-05	0.282596	3.50E-05	846	0.28258	11.7	0.4
Felsic Orthogneiss (Sample 25)								
5.1	0.00069	4.00E-06	0.28257	2.60E-05	844	0.282559	10.9	0.2
9.1	0.00094	7.00E-06	0.282559	2.40E-05	838	0.282544	10.24	0.3
14.1	0.00069	6.00E-06	0.282569	2.10E-05	839	0.282558	10.76	0.3
13.1	0.00087	1.10E-05	0.282528	1.80E-05	853	0.282514	9.51	0.3
11.1	0.00081	6.00E-06	0.282548	2.70E-05	842	0.282535	10.01	0.3
10.1	0.00091	6.00E-06	0.28258	2.70E-05	842	0.282566	11.09	0.3

Mafic Enclave (Sample 38)

13.1	0.00135	1.60E-05	0.282532	1.40E-05	862	0.28251	9.58	0.4
14.1	0.00148	1.30E-05	0.282542	2.90E-05	856	0.282518	9.72	0.2
11.1	0.00151	1.00E-05	0.282541	2.20E-05	859	0.282517	9.74	0.2
15.1	0.00198	1.40E-05	0.282512	1.90E-05	864	0.28248	8.55	0.2
2.1	0.00094	6.00E-06	0.282515	2.00E-05	826	0.2825	8.41	0.2
3.1	0.00097	8.00E-06	0.282533	1.80E-05	884	0.282517	10.31	0.3
3.2	0.0014	1.90E-05	0.282509	1.30E-05	812	0.282488	7.65	0.2
4.2	0.00133	2.50E-05	0.282485	1.60E-05	827	0.282464	7.16	0.2
6.1	0.00128	9.00E-06	0.282513	1.90E-05	853	0.282492	8.75	0.3
7.1	0.00153	1.00E-05	0.282533	1.80E-05	860	0.282508	9.46	0.2

Santiago, R., Caxito, F. A., Pedrosa-Soares, A., Neves, M. A., Dantas, E. L. 2020. Tonian island arc remnants in the northern Ribeira orogen of Western Gondwana: The Caxixe batholith (Espírito Santo, SE Brazil). Precambrian Research, 351, 105944.

Marimon et al., 2021

Grain#	**$^{176}Lu/^{177}Hf$ [a]**	**±2s**	**$^{176}Hf/^{177}Hf$**	**±2s [c]**	**age [f] (Ma)**	**$^{176}Hf/^{177}Hf_{(t)}$ [d]**	**eHf(t) [d]**	**±2s [c]**
Santo Antônio Unit (Syn-Collisional - meta-graywacke, Sample RSM146)								
ZR-57	0.000545	6.00E-06	0.281814	3.4E-05	930	0.281804	-14.03	0.41
ZR-55	0.002225	3.00E-06	0.2825	4.6E-05	1007	0.282456	10.83	0.77
ZR-43	0.000024	1.00E-06	0.282255	3.6E-05	1185	0.282255	7.71	0.28
ZR-103	0.000453	2.00E-06	0.281981	3.2E-05	1206	0.281971	-1.89	0.12
ZR-70	0.000362	3.00E-06	0.282115	2.3E-05	1216	0.282106	3.14	0.23
ZR-58	0.000348	5.00E-06	0.282209	3.4E-05	1230	0.282201	6.83	0.16
ZR-62	0.000626	7.00E-06	0.281005	2.8E-05	1232	0.28099	-36.07	0.05
ZR-61	0.00053	6.00E-06	0.282085	4.2E-05	1236	0.282073	2.42	0.44
ZR-86	0.000542	3.00E-06	0.281959	3.2E-05	1331	0.281945	0.06	0.01
ZR-6	0.000772	2.50E-05	0.28208	4.3E-05	1391	0.282059	5.44	0.32
ZR-3	0.000688	6.00E-06	0.281941	3.2E-05	1414	0.281922	1.1	0.09
ZR-9	0.000582	7.00E-06	0.2819	3.7E-05	1511	0.281882	1.91	0.03
ZR-36	0.000533	5.00E-06	0.281945	2.6E-05	1522	0.281929	3.82	0.38
ZR-71	0.000636	3.00E-06	0.281545	3.3E-05	1786	0.281523	-4.56	0.38
ZR-12	0.000592	2.00E-06	0.281756	3.5E-05	1796	0.281735	3.21	0.31
ZR-83	0.000012	1.00E-06	0.281434	3.0E-05	1882	0.281434	-5.52	0.56

ZR-87	0.000652	8.00E-06	0.281706	3.3E-05	1882	0.281682	3.3	0.44
ZR-85	0.000343	1.40E-05	0.281525	2.8E-05	1887	0.281513	-2.6	0.64
ZR-23	0.000639	1.40E-05	0.281508	4.5E-05	1998	0.281483	-1.08	0.13
ZR-67	0.000497	9.00E-06	0.281648	3.2E-05	2113	0.281627	6.67	0.69
ZR-65	0.000404	4.00E-06	0.281338	3.8E-05	2126	0.281321	-3.91	0.5
ZR-4	0.000654	1.10E-05	0.281107	3.8E-05	2683	0.281072	0.17	1
ZR-102	0.001328	1.23E-04	0.281083	5.2E-05	2685	0.281012	-1.89	0.51
ZR-31	0.00106	4.00E-06	0.281117	3.2E-05	2701	0.28106	0.19	1.23
ZR-47	0.00055	1.50E-05	0.281001	3.7E-05	2704	0.280972	-2.89	1.06
ZR-77	0.000552	4.00E-06	0.281084	4.1E-05	2704	0.281055	0.06	0.94
ZR-44	0.000525	4.00E-06	0.281039	3.4E-05	2712	0.28101	-1.32	1.2
ZR-26	0.000564	1.50E-05	0.281104	3.4E-05	2771	0.281073	2.29	1.24
ZR-91	0.000168	1.00E-05	0.280776	2.9E-05	2794	0.280767	-8.07	1.43
ZR-40	0.000645	1.10E-05	0.28091	3.4E-05	2832	0.280874	-3.37	1.29
ZR-68	0.000908	3.00E-06	0.28109	3.6E-05	2834	0.281039	2.55	1.24
ZR-107	0.00065	3.10E-05	0.280875	3.4E-05	2908	0.280838	-2.87	1.35
ZR-25	0.001457	4.80E-05	0.280749	3.0E-05	3359	0.280651	1.12	1.93
Santo Antônio Unit (Syn-Collisional - meta-graywacke, Sample RSM76)								
ZR-28	0.000753	2.80E-05	0.281375	4.5E-05	2110	0.281344	-3.47	0.22
ZR-36	0.000307	5.00E-06	0.281376	3.9E-05	2127	0.281363	-2.39	0.45
ZR-63	0.000841	4.70E-05	0.281475	3.5E-05	2143	0.281439	0.7	0.61
ZR-35	0.000755	1.40E-05	0.281499	3.5E-05	2219	0.281466	3.4	0.7
ZR-55	0.001475	3.50E-05	0.281666	4.6E-05	2228	0.281602	8.43	0.3
ZR-48	0.000788	2.90E-05	0.281439	3.8E-05	2329	0.281403	3.7	0.69
ZR-42	0.00137	5.20E-05	0.28168	3.5E-05	2342	0.281616	11.61	0.81
ZR-26	0.000423	1.70E-05	0.281181	3.6E-05	2450	0.28116	-2.1	0.87
ZR-4	0.00053	1.50E-05	0.281012	4.8E-05	2706	0.280984	-2.4	0.35
ZR-30	0.000397	4.00E-06	0.280914	3.3E-05	2712	0.280893	-5.5	1.2
ZR-37	0.000577	5.00E-06	0.281047	3.0E-05	2720	0.281016	-0.95	1.32
ZR-69	0.00051	5.00E-06	0.280863	4.3E-05	2723	0.280836	-7.27	0.86

ZR-62	0.000754	1.40E-05	0.280982	4.0E-05	2736	0.280941	-3.24	0.98
Santo Antônio Unit (Syn-Collisional - meta-graywacke, RSM138)								
ZR-22	0.000425	4.00E-06	0.280958	2.9E-05	2618	0.280936	-6.17	1.29
ZR-40	0.001158	4.70E-05	0.281183	3.5E-05	2691	0.281122	2.15	1.11
ZR-99	0.001571	6.00E-06	0.281142	2.3E-05	2830	0.281054	2.97	1.67
ZR-90	0.001712	4.10E-05	0.280855	3.4E-05	3019	0.280753	-3.29	1.47
ZR-106	0.001302	3.80E-05	0.280767	3.0E-05	3360	0.28068	2.17	1.93

Marimon, R. S., Trouw, R. A. J., Dantas, E. L., Ribeiro, A., Santos. P., Kuster, K., Vinagre, R. 2021. Provenance of passive-margin and syn-collisional units: Implications for the geodynamic evolution of the Southern Brasília Orogen, West Gondwana. Sedimentary Geology, 413, 105823

Costa et al., 2022

Grain#	**$^{176}Lu/^{177}Hf$ [a]**	**±2s [c]**	**$^{176}Hf/^{177}Hf$**	**±2s [c]**	**age [f] (Ma)**	**$^{176}Hf/^{177}Hf_{(t)}$ [d]**	**eHf(t) [d]**	**±2s [c]**
Biotite-bearing granitic leucosome (Sample EX-92-L)								
10	0.001385	8.32E-05	0.282404	2.19E-05	723	0.282385	2.01	1.10
11	0.001265	7.60E-05	0.282354	2.39E-05	682	0.282337	-0.60	1.19
12	0.000118	1.23E-05	0.282088	2.00E-05	662	0.282087	-9.92	1.00
13	0.001199	7.29E-05	0.282217	2.50E-05	645	0.282202	-6.24	1.25
14	0.001289	7.75E-05	0.282402	2.81E-05	785	0.282383	3.32	1.41
15	0.001144	6.88E-05	0.282323	2.28E-05	699	0.282308	-1.26	1.14
16	0.001495	1.02E-04	0.282377	2.17E-05	769	0.282355	1.98	1.09
17	0.001756	1.05E-04	0.282395	2.01E-05	686	0.282372	0.70	1.01
18	0.002262	1.96E-04	0.282498	1.95E-05	746	0.282466	5.39	0.97
19	0.001656	1.00E-04	0.282432	2.31E-05	797	0.282407	4.47	1.15
20	0.001182	7.30E-05	0.282398	2.53E-05	762	0.282381	2.74	1.27
21	0.002371	1.96E-04	0.282428	1.82E-05	762	0.282394	3.19	0.91
22	0.001603	9.86E-05	0.282440	2.30E-05	570	0.282422	-0.10	1.15
23	0.001217	8.74E-05	0.282361	1.95E-05	665	0.282345	-0.70	0.98
24	0.001451	9.14E-05	0.282399	1.44E-05	701	0.282380	1.34	0.72
25	0.001644	9.96E-05	0.282418	2.09E-05	727	0.282396	2.47	1.05
26	0.001271	8.00E-05	0.282414	2.31E-05	666	0.282398	1.17	1.16
27	0.001792	1.15E-04	0.282466	2.48E-05	657	0.282444	2.62	1.24
28	0.001391	8.74E-05	0.282408	2.02E-05	790	0.282388	3.60	1.01
29	0.001655	9.98E-05	0.282260	1.82E-05	717	0.282238	-3.35	0.91
30	0.002262	1.37E-04	0.282462	1.63E-05	624	0.282435	1.54	0.81
31	0.002224	1.48E-04	0.282469	2.34E-05	756	0.282438	4.60	1.17
32	0.000867	5.21E-05	0.282212	1.98E-05	733	0.282200	-4.31	0.99
33	0.001315	8.99E-05	0.282393	1.97E-05	741	0.282375	2.06	0.99
35	0.002095	1.26E-04	0.282443	1.82E-05	539	0.282422	-0.84	0.91
36	0.001195	1.26E-04	0.282419	2.43E-05	781	0.282402	3.90	1.21

37	0.000947	6.09E-05	0.282397	1.83E-05	684	0.282384	1.10	0.92
39	0.002511	1.37E-04	0.282475	1.58E-05	601	0.282446	1.43	0.79
40	0.001803	1.37E-04	0.282450	2.38E-05	593	0.282430	0.67	1.19
41	0.001134	7.63E-05	0.282396	1.90E-05	623	0.282382	-0.32	0.95
42	0.001570	9.86E-05	0.282373	1.81E-05	613	0.282355	-1.55	0.91
43	0.001526	9.86E-05	0.282430	2.20E-05	783	0.282408	4.16	1.10
44	0.001072	7.87E-05	0.282453	1.99E-05	749	0.282437	4.45	1.00
45	0.001499	9.26E-05	0.282413	1.98E-05	722	0.282393	2.27	0.99
46	0.001718	1.03E-04	0.282428	2.38E-05	682	0.282406	1.85	1.19
47	0.001078	6.61E-05	0.282393	2.22E-05	791	0.282377	3.23	1.11
48	0.001322	8.00E-05	0.282413	2.86E-05	676	0.282396	1.34	1.43
49	0.001490	9.12E-05	0.282397	1.82E-05	725	0.282377	1.77	0.91
50	0.001814	1.29E-04	0.282424	1.96E-05	704	0.282400	2.12	0.98
51	0.001666	1.02E-04	0.282425	2.03E-05	706	0.282403	2.27	1.01
52	0.001824	1.18E-04	0.282421	2.00E-05	767	0.282395	3.34	1.00
53	0.001302	7.83E-05	0.282404	2.12E-05	639	0.282388	0.24	1.06
54	0.003384	2.04E-04	0.282616	2.61E-05	752	0.282568	9.12	1.31
55	0.002381	1.44E-04	0.282507	1.93E-05	776	0.282472	6.28	0.96
56	0.002001	1.29E-04	0.282469	2.73E-05	889	0.282435	7.54	1.37
57	0.000985	7.05E-05	0.282385	2.14E-05	711	0.282372	1.28	1.07
58	0.001670	4.78E-04	0.282475	2.35E-05	667	0.282454	3.20	1.17
59	0.002427	1.53E-04	0.282388	1.57E-05	701	0.282356	0.49	0.79
60	0.000722	6.40E-05	0.282377	1.58E-05	729	0.282367	1.51	0.79
61	0.000699	4.99E-05	0.282380	1.83E-05	682	0.282371	0.61	0.92
62	0.000643	4.43E-05	0.282153	2.01E-05	677	0.282145	-7.53	1.01
63	0.000774	7.26E-05	0.282212	1.70E-05	637	0.282203	-6.37	0.85
64	0.001208	1.98E-04	0.282392	2.48E-05	739	0.282375	2.00	1.24
65	0.001521	1.22E-04	0.282419	2.53E-05	783	0.282397	3.77	1.27

Costa, F. M., Penna, J. L. A., Martins, L. C. D., Tedeschi, M., Novo, T. A., Araujo, C. S., Vieira Rossi, P. L., Lana, C., Pedrosa-Soares, A. C. 2022. Zircon petrochronology reveals the moderately juvenile signature of a diatexite from the boundary zone between the Brasília and Ribeira orogens (SE Brazil): Relict of a Tonian arc? Journal of South American Earth Sciences 116, 103767. https://doi.org/10.1016/j.jsames.2022.103767

Santiago et al., 2022

Grain#	$^{176}Lu/^{177}Hf$ [a]	±2s	$^{176}Hf/^{177}Hf$	±2s [c]	age [f] (Ma)	$^{176}Hf/^{177}Hf_{(t)}$ [d]	eHf(t) [d]	±2s [c]
Arc-related metassedimentary successions (Grt-Sil-Bt gneiss, Sample 7)								
1.sSMPABC107	0.000612	6.00E-05	0.282078	5.70E-05	708	0.282070	-9.50	1.00
1.sSMPABC109	0.001112	6.00E-05	0.282045	5.70E-05	714	0.282030	-10.80	1.00
1.sSMPABC110	0.001078	6.00E-05	0.281983	5.70E-05	716	0.281968	-12.90	1.00
1.sSMPABC112	0.000593	6.00E-05	0.281621	5.70E-05	1021	0.281610	-18.70	2.00
1.sSMPABC113	0.00131	6.00E-05	0.282066	5.70E-05	746	0.282048	-9.40	1.00
1.sSMPABC116	0.000733	6.00E-05	0.282084	5.70E-05	651	0.282075	-10.60	1.00

1.sSMPABC117	0.001358	6.00E-05	0.282069	5.70E-05	642	0.282052	-11.60	1.00
1.sSMPABC118	0.001361	6.00E-05	0.282053	5.70E-05	817	0.282032	-8.40	1.00
1.sSMPABC119	0.001293	6.00E-05	0.282019	5.70E-05	742	0.282001	-11.20	1.00
1.sSMPABC120	0.001004	6.00E-05	0.282043	5.70E-05	758	0.282029	-9.80	1.00
1.sSMPABC097	0.000913	6.00E-05	0.28203	5.70E-05	716	0.282018	-11.20	1.00
1.sSMPABC097	0.000948	6.00E-05	0.282061	5.70E-05	716	0.282048	-10.10	1.00
1.sSMPABC115	0.000558	6.00E-05	0.282003	5.70E-05	723	0.281996	-11.80	2.00
1.sSMPABC114	0.002272	6.00E-05	0.281942	5.70E-05	1143	0.281893	-5.90	0.00
1.sSMPABC99	0.000994	6.00E-05	0.282025	5.70E-05	745	0.282011	-10.70	1.00
Arc-related metassedimentary successions (Hbl-bearing gneiss, Sample 13)								
1.sSMPABC187	0.001249	2.10E-05	0.282133	7.50E-05	629	0.282118	-9.50	0.00
1.sSMPABC180	0.001298	1.50E-05	0.282168	7.80E-05	639	0.282152	-8.10	0.00
1.sSMPABC217	0.001566	6.00E-05	0.282427	5.70E-05	630	0.282408	0.80	0.00
1.sSMPABC216	0.001165	6.00E-05	0.282444	5.70E-05	602	0.282431	0.90	0.00
1.sSMPABC219	0.002174	6.00E-05	0.282422	5.70E-05	640	0.282396	0.50	0.00
1.sSMPABC220	0.000967	6.00E-05	0.282268	5.70E-05	594	0.282257	-5.40	0.00
1.sSMPABC215	0.001753	6.00E-05	0.281982	5.70E-05	571	0.281963	-16.40	1.00
1.sSMPABC227	0.00138	6.00E-05	0.282183	5.70E-05	611	0.282167	-8.20	1.00
1.sSMPABC228	0.001521	6.00E-05	0.282407	5.70E-05	623	0.282389	-0.10	0.00
1.sSMPABC231	0.001438	6.00E-05	0.282173	5.70E-05	622	0.282157	-8.40	1.00
1.sSMPABC179	0.00093	6.00E-05	0.282516	5.70E-05	698	0.282504	5.70	0.00
1.sSMPABC178	0.001791	6.00E-05	0.282448	5.70E-05	632	0.282427	1.40	0.00
1.sSMPABC168	0.001141	6.00E-05	0.282135	5.70E-05	553	0.282123	-11.10	1.00
1.sSMPABC167	0.001332	6.00E-05	0.282403	5.70E-05	618	0.282388	-0.30	0.00
1.sSMPABC169/170	0.000812	6.00E-05	0.282111	5.70E-05	624	0.282102	-10.30	1.00
1.sSMPABC173	0.001062	6.00E-05	0.28249	5.70E-05	649	0.282477	3.60	0.00
1.sSMPABC171	0.000966	6.00E-05	0.282045	5.70E-05	624	0.282033	-12.70	1.00
1.sSMPABC174	0.001374	6.00E-05	0.282096	5.70E-05	601	0.282081	-11.50	1.00
1.sSMPABC175	0.000736	6.00E-05	0.282491	5.70E-05	633	0.282482	3.40	0.00
1.sSMPABC176	0.001316	6.00E-05	0.282165	5.70E-05	608	0.282150	-8.90	1.00
1.sSMPABC177	0.00116	6.00E-05	0.282161	5.70E-05	613	0.282147	-8.90	1.00
1.sSMPABC218	0.001078	6.00E-05	0.282515	5.70E-05	643	0.282502	4.30	0.00
1.sSMPABC230	0.001158	6.00E-05	0.282129	5.70E-05	634	0.282115	-9.60	1.00
1.sSMPABC214	0.001432	6.00E-05	0.282401	5.70E-05	598	0.282385	-0.80	0.00
1.sSMPABC193	0.001333	6.00E-05	0.282364	5.70E-05	629	0.282348	-1.40	0.00
1.sSMPABC189	0.000926	6.00E-05	0.282473	5.70E-05	627	0.282462	2.60	0.00
1.sSMPABC190	0.001768	6.00E-05	0.282073	5.70E-05	602	0.282053	-12.50	1.00
1.sSMPABC160	0.001141	6.00E-05	0.28241	5.70E-05	605	0.282397	-0.20	0.00
1.sSMPABC150	0.000733	6.00E-05	0.282331	5.70E-05	597	0.282323	-3.00	0.00
1.sSMPABC192	0.000921	6.00E-05	0.282487	5.70E-05	621	0.282476	2.90	0.00
1.sSMPABC211	0.000966	6.00E-05	0.282454	5.70E-05	619	0.282443	1.70	0.00
1.sSMPABC232	0.001147	6.00E-05	0.282192	5.70E-05	600	0.282179	-8.10	1.00
1.sSMPABC235	0.001387	6.00E-05	0.282376	5.70E-05	606	0.282360	-1.50	0.00
1.sSMPABC234	0.000822	6.00E-05	0.282498	5.70E-05	606	0.282489	3.10	0.00
1.sSMPABC233	0.001259	6.00E-05	0.28203	5.70E-05	607	0.282016	-13.70	1.00

1.sSMPABC209	0.001326	6.00E-05	0.281999	5.70E-05	602	0.281984	-14.90	1.00
1.sSMPABC210	0.00133	6.00E-05	0.282178	5.70E-05	610	0.282163	-8.40	1.00
1.sSMPABC157	0.000625	6.00E-05	0.282472	5.70E-05	598	0.282465	2.00	0.00
1.sSMPABC158	0.001587	6.00E-05	0.282451	5.70E-05	675	0.282431	2.60	0.00
1.sSMPABC195	0.001141	6.00E-05	0.282117	5.70E-05	591	0.282104	-10.90	1.00
1.sSMPABC152	0.001582	6.00E-05	0.282244	5.70E-05	592	0.282226	-6.60	0.00
1.sSMPABC151	0.001061	6.00E-05	0.282512	5.70E-05	609	0.282500	3.50	0.00
1.sSMPABC148	0.001685	6.00E-05	0.28225	5.70E-05	600	0.282231	-6.20	0.00
1.sSMPABC198	0.000821	6.00E-05	0.281864	5.70E-05	623	0.281854	-19.00	2.00
1.sSMPABC197	0.000873	6.00E-05	0.282505	5.70E-05	612	0.282495	3.40	0.00
1.sSMPABC207	0.003219	6.00E-05	0.282468	5.70E-05	758	0.282422	4.10	0.00
1.sSMPABC149	0.000819	6.00E-05	0.282481	5.70E-05	623	0.282472	2.80	0.00
1.sSMPABC140	0.001921	6.00E-05	0.282419	5.70E-05	594	0.282398	-0.50	0.00
1.sSMPABC139	0.001501	6.00E-05	0.282121	5.70E-05	629	0.282104	-10.10	1.00
1.sSMPABC147	0.001096	6.00E-05	0.282102	5.70E-05	601	0.282089	-11.20	1.00
1.sSMPABC163	0.000751	6.00E-05	0.282493	5.70E-05	646	0.282484	3.80	0.00
1.sSMPABC137	0.000988	6.00E-05	0.282033	5.70E-05	605	0.282021	-13.50	1.00
1.sSMPABC271	0.00112	6.00E-05	0.282482	5.70E-05	631	0.282469	2.90	0.00
1.sSMPABC247	0.000786	6.00E-05	0.282076	5.70E-05	593	0.282067	-12.20	1.00
1.sSMPABC208	0.001122	6.00E-05	0.282113	5.70E-05	617	0.282100	-10.50	1.00
1.sSMPABC236	0.001308	6.00E-05	0.282494	5.70E-05	713	0.282477	5.00	0.00
1.sSMPABC230	0.001499	6.00E-05	0.282145	5.70E-05	616	0.282128	-9.50	1.00
1.sSMPABC237	0.000754	6.00E-05	0.281858	5.70E-05	646	0.281849	-18.70	2.00
1.sSMPABC252	0.001616	6.00E-05	0.282258	5.70E-05	595	0.282240	-6.00	0.00
1.sSMPABC255	0.002667	6.00E-05	0.282299	5.70E-05	623	0.282267	-4.40	0.00

Santiago, R., Caxito, F. A., Pedrosa-Soares, A., Neves, M. A., Calegari, S. S., Lana, C. 2022. Detrital zircon U – Pb and Lu – Hf constraints on the age, provenance and tectonic setting of arc-related high-grade units of the transition zone of the Araçuaí and Ribeira orogens (SE Brazil). Journal of South American Earth Sciences, 116, 103861.

9.15 APPENDIX O – Lu-Hf and U-Pb data from sample P013 (Chapter 6)

Zircon LA-MC-ICP-MS U-Pb results - Layered orthopyroxene-garnet diatexite (P013)

					Isotope ratios[c]							Ages (Ma)						
Spot number	CL-domain	Th ppm	U ppm	Th/U[b]	$^{207}Pb/^{206}Pb$[e]	2 s [%]	$^{207}Pb/^{235}U$	2 s [%]	$^{206}Pb/^{238}U$	2 s [%]	Rho[d]	$^{206}Pb/^{238}U$	2 s abs	$^{207}Pb/^{235}U$	2 s abs	$^{207}Pb/^{206}Pb$	2 s abs	% Disc.[e]
P013_009	**c**	436	185	0.42	0.06356	1.01	1.04519	1.90	0.11926	1.61	0.85	726	11	726	10	727	21	0.1
P013_010	**r**	192	49	0.26	0.06350	1.24	1.00822	2.07	0.11516	1.65	0.80	703	11	708	11	725	26	0.8
P013_011	**r**	292	94	0.32	0.06096	1.28	0.88813	2.04	0.10567	1.59	0.78	648	10	645	10	638	28	-0.3
P013_012	**c**	71	263	3.68	0.06063	1.67	0.83126	2.39	0.09944	1.71	0.72	611	10	614	11	626	36	0.5
P013_014	**c**	205	112	0.55	0.06014	1.10	0.81458	1.95	0.09824	1.61	0.83	604	9	605	9	609	24	0.2
P013_015	**c**	133	80	0.60	0.06711	1.27	1.28119	2.04	0.13846	1.61	0.79	836	13	837	12	841	26	0.2
P013_016	**r**	74	20	0.27	0.06036	1.38	0.82881	2.16	0.09959	1.67	0.77	612	10	613	10	617	30	0.2
P013_032	**r**	510	419	0.82	0.06000	1.05	0.81268	1.91	0.09824	1.59	0.83	604	9	604	9	604	23	0.0
P013_033	**c**	581	765	1.32	0.05949	1.06	0.81733	1.91	0.09964	1.59	0.83	612	9	607	9	585	23	-0.9
P013_035	**c**	413	214	0.52	0.06080	1.18	0.85247	2.03	0.10169	1.65	0.81	624	10	626	10	632	26	0.3
P013_036	**r**	128	233	1.82	0.06047	1.35	0.83205	2.13	0.09979	1.65	0.77	613	10	615	10	621	29	0.3
P013_047	**c**	16	11	0.69	0.06358	4.04	1.07087	4.75	0.12216	2.50	0.53	743	18	739	25	728	86	-0.5
P013_048	**c**	82	310	3.76	0.06042	1.41	0.80302	2.21	0.09639	1.70	0.77	593	10	599	10	619	30	0.9
P013_050	**c**	387	322	0.83	0.07180	1.32	1.61578	2.09	0.16322	1.62	0.77	975	15	976	13	980	27	0.2
P013_051	**c**	695	357	0.51	0.06227	1.00	0.94969	1.89	0.11061	1.61	0.85	676	10	678	9	683	21	0.3
P013_052	**r**	661	178	0.27	0.06120	1.01	0.88969	1.91	0.10543	1.61	0.85	646	10	646	9	646	22	0.0
P013_053	**c**	806	233	0.29	0.06276	1.07	1.10040	1.90	0.12716	1.57	0.83	772	11	754	10	700	23	-2.4
P013_054	**r**	158	103	0.65	0.06370	1.27	1.04265	2.06	0.11871	1.62	0.79	723	11	725	11	732	27	0.3
P013_056	**c**	439	45	0.10	0.05939	1.06	0.84238	1.92	0.10287	1.60	0.83	631	10	620	9	581	23	-1.7
P013_057	**c**	670	274	0.41	0.06433	0.99	1.08858	1.88	0.12273	1.60	0.85	746	11	748	10	752	21	0.2
P013_059	**c**	426	91	0.21	0.06154	1.12	0.90992	1.94	0.10724	1.59	0.82	657	10	657	9	658	24	0.1
P013_060	**c**	209	96	0.46	0.06521	1.35	1.16074	2.13	0.12910	1.64	0.77	783	12	782	12	781	28	0.0
P013_067	**r**	627	69	0.11	0.06302	3.33	1.00936	4.08	0.11617	2.37	0.58	708	16	709	21	709	71	0.0
P013_068	**c**	51	68	1.35	0.06729	1.50	1.29838	2.30	0.13994	1.75	0.76	844	14	845	13	847	31	0.1
P013_069	**c**	511	29	0.06	0.06435	1.03	1.08688	1.92	0.12250	1.62	0.84	745	11	747	10	753	22	0.3

P013_072	**c**	50	71	1.41	0.05998	2.07	0.80247	2.78	0.09703	1.86	0.67	597	11	598	13	603	45	0.2
P013_073	**c**	1117	1315	1.18	0.06341	1.06	1.04391	1.97	0.11939	1.66	0.84	727	11	726	10	722	22	-0.1
P013_074	**c**	223	187	0.84	0.06083	1.12	0.86256	1.98	0.10284	1.64	0.83	631	10	632	9	633	24	0.1
P013_075	**c**	87	759	8.70	0.05975	1.44	0.85227	2.20	0.10345	1.66	0.76	635	10	626	10	595	31	-1.4
P013_077	**c**	377	134	0.35	0.06098	1.07	0.88624	1.94	0.10540	1.62	0.83	646	10	644	9	639	23	-0.2
P013_078	**c**	363	315	0.87	0.06414	1.06	1.08634	1.94	0.12284	1.63	0.84	747	11	747	10	746	22	0.0
P013_079	**r**	36	140	3.93	0.06235	2.15	0.94540	2.84	0.10997	1.86	0.65	673	12	676	14	686	46	0.5
P013_088	**c**	162	401	2.47	0.06100	1.25	0.85579	2.05	0.10175	1.63	0.80	625	10	628	10	639	27	0.5
P013_089	**r**	245	213	0.87	0.06064	1.41	0.85274	2.23	0.10199	1.73	0.78	626	10	626	10	626	30	0.0
P013_090	**c**	163	206	1.26	0.05989	1.39	0.80143	2.22	0.09705	1.73	0.78	597	10	598	10	600	30	0.1
P013_091	**c**	844	321	0.38	0.06559	1.14	1.18848	2.00	0.13142	1.65	0.82	796	12	795	11	793	24	-0.1
P013_092	**r**	564	174	0.31	0.06296	1.24	1.00767	2.03	0.11607	1.60	0.79	708	11	708	10	707	26	0.0
P013_093	**c**	126	216	1.71	0.06125	1.34	0.85304	2.14	0.10101	1.67	0.78	620	10	626	10	648	29	1.0
P013_094	**c**	214	327	1.53	0.05946	1.39	0.80022	2.18	0.09761	1.69	0.77	600	10	597	10	584	30	-0.6
P013_095	**c**	378	78	0.21	0.06221	1.13	0.95522	2.02	0.11136	1.67	0.83	681	11	681	10	681	24	0.1
P013_096	**c**	200	399	2.00	0.06048	1.24	0.84746	2.08	0.10162	1.67	0.80	624	10	623	10	621	27	-0.1
P013_097	**c**	423	243	0.58	0.06504	1.03	1.13706	1.93	0.12679	1.63	0.84	770	12	771	10	776	22	0.2
P013_098	**r**	38	45	1.19	0.06020	2.57	0.80217	3.23	0.09664	1.95	0.60	595	11	598	15	611	56	0.6
P013_099	**c**	409	205	0.50	0.07736	1.14	2.05276	2.01	0.19245	1.66	0.82	1135	17	1133	14	1130	23	-0.1
P013_100	**r**	71	93	1.30	0.06004	1.81	0.81458	2.53	0.09841	1.77	0.70	605	10	605	12	605	39	0.0
P013_107	**c**	1056	189	0.18	0.06179	1.06	0.92003	1.96	0.10799	1.65	0.84	661	10	662	10	667	23	0.2
P013_108	**r**	177	166	0.94	0.06030	1.50	0.82653	2.25	0.09941	1.68	0.74	611	10	612	10	614	32	0.2
P013_109	**c**	879	65	0.07	0.06182	1.07	0.91720	1.94	0.10761	1.62	0.83	659	10	661	9	668	23	0.3
P013_110	**c**	358	202	0.57	0.06284	1.03	0.98900	1.93	0.11415	1.63	0.84	697	11	698	10	703	22	0.2
P013_111	**r**	136	169	1.24	0.05950	1.57	0.79220	2.36	0.09656	1.77	0.75	594	10	592	11	585	34	-0.3
P013_113	**c**	774	562	0.73	0.06213	3.38	1.02029	4.13	0.11910	2.37	0.57	725	16	714	21	679	72	-1.6
P013_114	**r**	430	502	1.17	0.06344	1.31	1.02839	2.16	0.11756	1.72	0.80	717	12	718	11	723	28	0.3
P013_118	**r**	152	236	1.55	0.06304	1.25	1.01209	2.06	0.11644	1.63	0.79	710	11	710	11	710	27	0.0
P013_120	**c**	737	268	0.36	0.06711	1.03	1.28564	1.96	0.13894	1.67	0.85	839	13	839	11	841	21	0.1
P013_127	**c**	180	559	3.10	0.05936	3.30	0.79903	4.12	0.09762	2.47	0.60	600	14	596	19	580	72	-0.7
P013_128	**r**	60	139	2.33	0.06082	1.53	0.85679	2.28	0.10217	1.69	0.74	627	10	628	11	633	33	0.2
P013_130	**r**	189	93	0.49	0.06066	3.53	0.85057	4.37	0.10169	2.57	0.59	624	15	625	21	627	76	0.1
P013_135	**c**	435	110	0.25	0.06509	1.29	1.14366	2.10	0.12743	1.66	0.79	773	12	774	11	777	27	0.2

P013_136	**c**	244	152	0.62	0.06511	3.28	1.15731	3.97	0.12892	2.24	0.56	782	17	781	22	778	69	-0.1
P013_137	**c**	117	465	3.98	0.06035	1.28	0.83600	2.12	0.10047	1.69	0.80	617	10	617	10	616	28	0.0
P013_138	**c**	64	222	3.49	0.06071	2.24	0.81509	2.95	0.09737	1.91	0.65	599	11	605	14	629	48	1.1
P013_140	**c**	446	337	0.76	0.06359	3.32	1.13013	4.01	0.12889	2.25	0.56	782	17	768	22	728	70	-1.8
P013_147	**r**	329	121	0.37	0.06050	1.06	0.93481	1.96	0.11206	1.64	0.84	685	11	670	10	622	23	-2.1
P013_148	**c**	280	198	0.71	0.06352	1.13	1.04067	1.98	0.11882	1.62	0.82	724	11	724	10	726	24	0.1
P013_149	**r**	155	135	0.87	0.06303	1.25	1.00923	2.08	0.11613	1.66	0.80	708	11	708	11	709	27	0.1
P013_150	**c**	97	278	2.87	0.06024	1.66	0.80337	2.45	0.09672	1.80	0.74	595	10	599	11	612	36	0.6
P013_151	**c**	800	412	0.51	0.06325	1.08	1.02236	1.99	0.11723	1.67	0.84	715	11	715	10	717	23	0.1
P013_152	**c**	134	194	1.44	0.06025	1.23	0.81299	2.06	0.09786	1.66	0.80	602	10	604	9	613	27	0.4
P013_153	**c**	246	177	0.72	0.06625	1.18	1.22416	2.02	0.13401	1.64	0.81	811	13	812	11	814	25	0.2
P013_154	**c**	1039	323	0.31	0.06172	1.10	0.92298	1.96	0.10846	1.62	0.83	664	10	664	10	664	24	0.1
P013_155	**r**	537	233	0.43	0.06303	1.03	0.93196	1.94	0.10724	1.64	0.85	657	10	669	10	709	22	1.8
P013_157	**r**	169	398	2.36	0.06022	3.55	0.81814	4.42	0.09854	2.63	0.59	606	15	607	20	611	77	0.2
P013_158	**c**	420	169	0.40	0.07184	1.07	1.63377	2.00	0.16495	1.69	0.84	984	15	983	13	981	22	-0.1
P013_159	**c**	165	193	1.17	0.10454	1.04	4.36233	1.98	0.30265	1.69	0.85	1704	25	1705	17	1706	19	0.1
P013_160	**c**	1801	164	0.09	0.06523	3.23	1.16263	3.93	0.12928	2.25	0.57	784	17	783	22	782	68	0.0
P013_167	**r**	892	194	0.22	0.06458	1.03	1.17526	1.94	0.13199	1.64	0.85	799	12	789	11	761	22	-1.2
P013_168	**c**	306	247	0.81	0.06084	1.13	0.86991	2.00	0.10369	1.65	0.83	636	10	636	9	634	24	0.0
P013_171	**c**	110	303	2.77	0.05976	1.34	0.80410	2.16	0.09759	1.70	0.79	600	10	599	10	595	29	-0.2
P013_172	**r**	355	116	0.33	0.06571	1.14	1.20593	2.06	0.13310	1.72	0.83	806	13	803	11	797	24	-0.2
P013_173	**c**	977	733	0.75	0.06229	3.40	0.95266	4.20	0.11092	2.48	0.59	678	16	679	21	684	73	0.2
P013_174	**r**	127	320	2.52	0.05988	1.39	0.80055	2.24	0.09696	1.76	0.78	597	10	597	10	599	30	0.1
P013_175	**c**	188	132	0.70	0.06449	1.29	1.10491	2.10	0.12425	1.66	0.79	755	12	756	11	758	27	0.1
P013_177	**c**	240	65	0.27	0.07217	1.07	1.65680	1.97	0.16650	1.66	0.84	993	15	992	13	991	22	0.0
P013_178	**r**	442	145	0.33	0.06067	1.07	0.85322	1.97	0.10200	1.65	0.84	626	10	626	9	627	23	0.1
P013_180	**r**	175	82	0.47	0.06098	1.18	0.85138	2.07	0.10126	1.70	0.82	622	10	625	10	639	25	0.6
P013_181	**c**	149	53	0.36	0.06188	2.29	0.89032	2.50	0.10435	1.00	0.40	640	6	647	12	670	49	1.0
~~**P013_182**~~	~~**c**~~	~~88~~	~~25~~	~~0.29~~	~~0.07061~~	~~2.18~~	~~1.20445~~	~~2.40~~	~~0.12371~~	~~1.01~~	~~0.42~~	~~752~~	~~7~~	~~803~~	~~13~~	~~946~~	~~45~~	~~6.8~~
P013_183	**c**	204	29	0.14	0.06723	2.62	1.27838	2.86	0.13791	1.16	0.41	833	9	836	16	845	54	0.4
P013_184	**c**	128	17	0.13	0.06237	2.33	0.92833	2.57	0.10795	1.09	0.42	661	7	667	13	687	50	0.9
P013_185	**c**	723	22	0.03	0.06276	2.02	0.98927	2.22	0.11432	0.92	0.41	698	6	698	11	700	43	0.1
P013_186	**c**	278	40	0.14	0.06104	2.23	0.86581	2.45	0.10288	1.01	0.41	631	6	633	12	641	48	0.3

P013_187	**c**	331	48	0.14	0.06014	2.13	0.83427	2.33	0.10061	0.95	0.41	618	6	616	11	609	46	-0.3
P013_188	**c**	91	19	0.21	0.06843	2.43	1.37564	2.65	0.14580	1.07	0.40	877	9	879	16	882	50	0.1
P013_189	**c**	515	9	0.02	0.06042	2.31	0.82003	2.53	0.09843	1.03	0.41	605	6	608	12	619	50	0.5
P013_190	**c**	313	38	0.12	0.05966	3.96	0.79639	4.57	0.09682	2.27	0.50	596	13	595	21	591	86	-0.2
P013_191	**c**	107	58	0.54	0.06028	2.29	0.84303	2.50	0.10143	1.01	0.40	623	6	621	12	614	49	-0.3
P013_192	**c**	1793	33	0.02	0.05991	3.96	0.79078	4.58	0.09573	2.30	0.50	589	13	592	21	600	86	0.4
P013_193	**c**	645	28	0.04	0.06174	2.04	0.91618	2.24	0.10762	0.93	0.41	659	6	660	11	665	44	0.2
P013_194	**c**	694	93	0.13	0.07927	3.23	2.19360	3.50	0.20069	1.35	0.39	1179	15	1179	25	1179	64	0.0
P013_195	**c**	894	18	0.02	0.06585	2.04	1.17533	2.28	0.12945	1.02	0.45	785	8	789	13	802	43	0.6
P013_196	**c**	170	100	0.59	0.05999	2.17	0.80084	2.37	0.09682	0.97	0.41	596	6	597	11	603	47	0.3
P013_197	**c**	837	152	0.18	0.06293	3.77	0.97220	4.28	0.11204	2.01	0.47	685	13	690	22	706	80	0.7
P013_198	**c**	2221	37	0.02	0.06185	2.23	0.91794	2.45	0.10764	1.02	0.42	659	6	661	12	669	48	0.3
P013_199	**c**	673	106	0.16	0.06304	2.03	1.02174	2.23	0.11755	0.92	0.41	716	6	715	12	710	43	-0.2
P013_200	**c**	93	128	1.37	0.05948	2.71	0.79988	3.02	0.09753	1.33	0.44	600	8	597	14	585	59	-0.5
P013_201	**c**	825	46	0.06	0.06376	2.35	1.02392	2.61	0.11647	1.13	0.43	710	8	716	14	734	50	0.8
P013_202	**c**	207	22	0.10	0.06122	2.19	0.87677	2.42	0.10387	1.02	0.42	637	6	639	12	647	47	0.3
P013_203	**c**	429	38	0.09	0.06651	2.23	1.21313	2.48	0.13228	1.08	0.43	801	8	807	14	823	47	0.7
P013_204	**c**	1119	67	0.06	0.06082	2.47	0.85682	2.72	0.10218	1.12	0.41	627	7	628	13	633	53	0.2
P013_205	**c**	206	43	0.21	0.07859	3.60	2.10716	3.91	0.19446	1.53	0.39	1145	16	1151	27	1162	71	0.5
P013_206	**r**	307	19	0.06	0.07855	4.14	2.10709	4.52	0.19454	1.84	0.41	1146	19	1151	32	1161	82	0.5
P013_207	**c**	534	88	0.17	0.07337	2.07	1.73858	2.31	0.17186	1.01	0.44	1022	10	1023	15	1024	42	0.1
P013_208	**c**	661	20	0.03	0.07257	3.50	1.65507	3.84	0.16541	1.59	0.42	987	15	991	25	1002	71	0.5
P013_211	**c**	38	31	0.82	0.06010	5.12	0.81438	5.83	0.09828	2.78	0.48	604	16	605	27	607	111	0.1
P013_212	**c**	444	40	0.09	0.06045	3.93	0.87079	4.47	0.10447	2.14	0.48	641	13	636	21	620	85	-0.7
P013_213	**c**	345	32	0.09	0.06261	3.81	0.93163	4.34	0.10792	2.08	0.48	661	13	668	21	695	81	1.2
~~**P013_214**~~	~~**c**~~	~~532~~	~~50~~	~~0.09~~	~~0.15764~~	~~2.08~~	~~4.37055~~	~~2.30~~	~~0.20108~~	~~0.98~~	~~0.43~~	~~1181~~	~~11~~	~~1707~~	~~19~~	~~2431~~	~~35~~	~~44.5~~
P013_215	**c**	383	73	0.19	0.05996	2.13	0.83946	2.36	0.10154	1.00	0.43	623	6	619	11	602	46	-0.7
~~**P013_216**~~	~~**c**~~	~~233~~	~~46~~	~~0.20~~	~~0.11127~~	~~2.12~~	~~2.74620~~	~~2.35~~	~~0.17900~~	~~1.01~~	~~0.43~~	~~1062~~	~~10~~	~~1341~~	~~18~~	~~1820~~	~~38~~	~~26.3~~
P013_217	**c**	507	157	0.31	0.06533	2.17	1.14749	2.40	0.12739	1.02	0.42	773	7	776	13	785	46	0.4
P013_218	**c**	158	21	0.13	0.06817	2.08	1.36694	2.31	0.14543	1.00	0.43	875	8	875	14	874	43	-0.1
P013_219	**c**	553	94	0.17	0.06502	2.61	1.12026	2.87	0.12496	1.18	0.41	759	8	763	16	775	55	0.5
P013_220	**c**	623	26	0.04	0.05994	2.15	0.83566	2.37	0.10112	1.00	0.42	621	6	617	11	601	47	-0.7
P013_221	**r**	457	26	0.06	0.05996	2.23	0.82009	2.46	0.09919	1.03	0.42	610	6	608	11	602	48	-0.3

~~**P013_222**~~	~~**c**~~	~~580~~	~~30~~	~~0.05~~	~~0.08910~~	~~2.04~~	~~2.46901~~	~~2.25~~	~~0.20098~~	~~0.94~~	~~0.42~~	~~1181~~	~~10~~	~~1263~~	~~16~~	~~1406~~	~~39~~	~~7.0~~
P013_223	**c**	637	60	0.09	0.06487	2.10	1.10220	2.29	0.12323	0.93	0.40	749	7	754	12	770	44	0.7
P013_224	**r**	563	32	0.06	0.06490	2.07	1.12919	2.27	0.12618	0.92	0.41	766	7	767	12	771	44	0.2
P013_225	**c**	59	61	1.03	0.06022	2.66	0.82890	2.91	0.09983	1.18	0.41	613	7	613	13	611	57	-0.1
P013_226	**c**	268	13	0.05	0.06634	2.23	1.23786	2.47	0.13533	1.06	0.43	818	8	818	14	817	47	0.0
~~**P013_227**~~	~~**c**~~	~~316~~	~~35~~	~~0.11~~	~~0.08053~~	~~2.12~~	~~1.69815~~	~~2.35~~	~~0.15294~~	~~1.01~~	~~0.43~~	~~917~~	~~9~~	~~1008~~	~~15~~	~~1210~~	~~42~~	~~9.9~~
P013_228	**c**	366	103	0.28	0.06251	2.27	0.94937	2.52	0.11015	1.09	0.43	674	7	678	13	692	48	0.6
P013_229	**c**	1161	69	0.06	0.06228	2.09	0.94513	2.30	0.11007	0.97	0.42	673	6	676	11	684	45	0.4
P013_230	**c**	148	83	0.56	0.05972	2.31	0.80753	2.54	0.09807	1.04	0.41	603	6	601	12	593	50	-0.3
P013_231	**r**	120	64	0.53	0.05992	2.37	0.79875	2.59	0.09668	1.06	0.41	595	6	596	12	601	51	0.2
~~**P013_232**~~	~~**c**~~	~~384~~	~~30~~	~~0.08~~	~~0.06586~~	~~9.11~~	~~0.85567~~	~~9.95~~	~~0.09423~~	~~4.00~~	~~0.40~~	~~581~~	~~22~~	~~628~~	~~48~~	~~802~~	~~191~~	~~38.1~~
P013_233	**c**	374	77	0.20	0.06462	2.09	1.08180	2.27	0.12142	0.89	0.39	739	6	745	12	762	44	3.1
P013_234	**c**	138	26	0.19	0.06058	2.45	0.80760	2.65	0.09668	1.02	0.38	595	6	601	12	625	53	5.0
~~**P013_235**~~	~~**c**~~	~~424~~	~~51~~	~~0.12~~	~~0.07267~~	~~9.44~~	~~1.33854~~	~~10.32~~	~~0.13359~~	~~4.18~~	~~0.40~~	~~808~~	~~32~~	~~863~~	~~62~~	~~1005~~	~~192~~	~~24.3~~
~~**P013_236**~~	~~**c**~~	~~725~~	~~85~~	~~0.12~~	~~0.07761~~	~~2.04~~	~~1.88485~~	~~2.24~~	~~0.17614~~	~~0.91~~	~~0.41~~	~~1046~~	~~9~~	~~1076~~	~~15~~	~~1137~~	~~41~~	~~8.7~~
P013_237	**c**	524	228	0.44	0.06402	2.12	1.04367	2.28	0.11823	0.83	0.36	720	6	726	12	742	45	3.1
~~**P013_238**~~	~~**c**~~	~~945~~	~~312~~	~~0.33~~	~~0.07590~~	~~2.03~~	~~1.65134~~	~~2.19~~	~~0.15779~~	~~0.83~~	~~0.38~~	~~944~~	~~7~~	~~990~~	~~14~~	~~1093~~	~~41~~	~~15.7~~
~~**P013_239**~~	~~**c**~~	~~640~~	~~72~~	~~0.11~~	~~0.06097~~	~~2.33~~	~~0.81543~~	~~2.51~~	~~0.09700~~	~~0.95~~	~~0.38~~	~~597~~	~~5~~	~~605~~	~~12~~	~~638~~	~~50~~	~~6.9~~
P013_240	**c**	374	31	0.08	0.06153	3.91	0.86743	4.46	0.10224	2.15	0.48	628	13	634	21	658	84	4.8
P013_241	**c**	425	88	0.21	0.06326	2.26	0.99929	2.45	0.11456	0.93	0.38	699	6	703	12	717	48	2.6
P013_242	**c**	163	107	0.66	0.05986	2.14	0.80650	2.31	0.09772	0.86	0.37	601	5	600	11	598	46	-0.4
~~**P013_244**~~	~~**c**~~	~~288~~	~~52~~	~~0.18~~	~~0.07762~~	~~2.11~~	~~1.89697~~	~~2.29~~	~~0.17725~~	~~0.88~~	~~0.38~~	~~1052~~	~~9~~	~~1080~~	~~15~~	~~1137~~	~~42~~	~~8.1~~
~~**P013_245**~~	~~**c**~~	~~430~~	~~60~~	~~0.14~~	~~0.09183~~	~~2.05~~	~~2.29223~~	~~2.21~~	~~0.18104~~	~~0.84~~	~~0.38~~	~~1073~~	~~8~~	~~1210~~	~~16~~	~~1464~~	~~39~~	~~36.5~~
P013_246	**c**	255	71	0.28	0.06354	2.08	1.03146	2.27	0.11774	0.89	0.39	718	6	720	12	726	44	1.2
P013_247	**c**	182	51	0.28	0.06333	3.91	1.01368	4.38	0.11609	1.97	0.45	708	13	711	23	719	83	1.6
P013_248	**c**	54	46	0.84	0.06010	3.68	0.82148	4.16	0.09914	1.94	0.47	609	11	609	19	607	80	-0.4
P013_249	**c**	518	88	0.17	0.06460	3.73	1.12654	4.14	0.12648	1.80	0.44	768	13	766	23	761	79	-0.8
P013_250	**c**	538	90	0.17	0.06197	2.10	0.93100	2.28	0.10896	0.88	0.39	667	6	668	11	673	45	1.0
P013_251	**c**	111	36	0.33	0.06255	3.45	0.95542	3.80	0.11078	1.60	0.42	677	10	681	19	693	74	2.3
P013_252	**c**	410	120	0.29	0.06377	2.19	1.06121	2.40	0.12070	0.99	0.41	735	7	734	13	734	46	0.0
~~**P013_253**~~	~~**c**~~	~~197~~	~~22~~	~~0.11~~	~~0.07388~~	~~2.48~~	~~1.33878~~	~~2.72~~	~~0.13143~~	~~1.12~~	~~0.41~~	~~796~~	~~8~~	~~863~~	~~16~~	~~1038~~	~~50~~	~~8.4~~
P013_254	**c**	483	51	0.11	0.05957	2.12	0.77716	2.33	0.09462	0.97	0.42	583	5	584	10	588	46	0.2
P013_255	**r**	538	28	0.05	0.05949	2.05	0.78917	2.27	0.09621	0.96	0.42	592	5	591	10	585	45	-0.2

P013_256	**c**	199	31	0.15	0.06305	2.70	0.97757	2.96	0.11245	1.21	0.41	687	8	692	15	710	57	0.8
P013_257	**r**	189	41	0.22	0.06300	2.41	0.98921	2.66	0.11388	1.13	0.42	695	7	698	14	708	51	0.4
P013_258	**c**	52	66	1.26	0.06010	3.31	0.79824	3.59	0.09633	1.40	0.39	593	8	596	16	607	71	0.5
P013_259	**c**	113	92	0.82	0.06043	2.35	0.81436	2.58	0.09773	1.05	0.41	601	6	605	12	619	51	3.0
P013_260	**c**	220	51	0.23	0.06469	2.34	1.10149	2.54	0.12349	1.00	0.39	751	7	754	14	764	49	1.8
~~**P013_261**~~	~~**c**~~	~~121~~	~~33~~	~~0.27~~	~~0.07181~~	~~3.19~~	~~1.29585~~	~~3.51~~	~~0.13088~~	~~1.45~~	~~0.41~~	~~793~~	~~11~~	~~844~~	~~20~~	~~981~~	~~65~~	~~23.7~~
P013_262	**c**	242	49	0.20	0.06156	2.10	0.86994	2.30	0.10250	0.93	0.41	629	6	636	11	659	45	4.7
P013_263	**c**	442	198	0.45	0.06117	2.09	0.87231	2.28	0.10342	0.89	0.39	634	5	637	11	645	45	1.7
~~**P013_264**~~	~~**c**~~	~~665~~	~~52~~	~~0.08~~	~~0.07282~~	~~2.06~~	~~1.35454~~	~~2.25~~	~~0.13491~~	~~0.89~~	~~0.40~~	~~816~~	~~7~~	~~870~~	~~13~~	~~1009~~	~~42~~	~~23.7~~
P013_265	**c**	698	61	0.09	0.06043	2.12	0.80455	2.32	0.09656	0.93	0.40	594	5	599	11	619	46	4.2
P013_266	**r**	1550	82	0.05	0.06147	3.90	0.86515	4.47	0.10207	2.19	0.49	627	13	633	21	656	84	4.7
P013_267	**c**	449	242	0.54	0.06496	2.16	1.13445	2.37	0.12666	0.98	0.41	769	7	770	13	773	45	0.6
P013_268	**c**	281	24	0.09	0.06243	2.31	0.93808	2.54	0.10898	1.06	0.42	667	7	672	13	689	49	3.3
P013_269	**c**	370	50	0.14	0.06146	2.15	0.88910	2.36	0.10492	0.97	0.41	643	6	646	11	655	46	1.9
P013_270	**c**	415	26	0.06	0.06217	4.90	0.95399	5.49	0.11129	2.47	0.45	680	16	680	28	680	105	0.0

aFraction of the non-radiogenic ^{206}Pb in the analyzed zircon spot, where f_{206}=[$^{206}Pb/^{204}Pb$]c/[$^{206}Pb/^{204}Pb$]s (c=common; s=sample)

bTh/U ratios and amount of Pb, Th and U (in pmm) are calculated relative to 91500 reference zircon

cCorrected for background and within-run Pb/U fractionation and normalised to reference zircon GJ-1 (ID-TIMS values/measured value); $^{207}Pb/^{235}U$ calculated using ($^{207}Pb/^{206}Pb$)/($^{238}U/^{206}Pb$ * 1/137.88)

dRho is the error correlation defined as the quotient of the propagated errors of the $^{206}Pb/^{238}U$ and the $^{207}/^{235}U$ ratio

eDegree of discordance = 100 - ($^{206}Pb/^{238}U$ age * 100/$^{207}Pb/^{206}U$ age)

c-core

r-rim

s-single phase

Hf isotopes results determined by LA-ICP-MS - Layered orthopyroxene-garnet diatexite (P013)

Grain#	CL-Domain	$^{176}Yb/^{177}Hf$ [a]	±2s	$^{176}Lu/^{177}Hf$ [a]	±2s	$^{178}Hf/^{177}Hf$	$^{180}Hf/^{177}Hf$	Sig_{Hf} [b] (V)	$^{176}Hf/^{177}Hf$	±2s [c]	age [f] (Ma)	±2s	$^{176}Hf/^{177}Hf_{(t)}$ [d]	eHf(t) [d]	±2s [c]	age [f] (Ma)	±2s	eHf(t) [d]	±2s [c]
											(measured)					(pref./min.)			
P013-181	**c**	0.011191	9	0.000395	2	1.467476	1.883893	11.750590	0.282085	24	640	6	0.282080	-10.7	1.20	640	6	-7.7	1.20
P013-183	**c**	0.016838	15	0.000649	4	1.467490	1.883988	12.037887	0.282034	22	833	9	0.282024	-8.3	1.11	773	7	-9.6	1.10
P013-185	**c**	0.022825	19	0.000860	5	1.467498	1.883877	14.728391	0.282054	15	698	6	0.282043	-10.7	0.75	773	7	-9.0	0.75
P013-187	**c**	0.006803	13	0.000272	5	1.467468	1.884143	12.795977	0.281955	19	618	6	0.281952	-15.7	0.95	773	7	-12.2	0.95
P013-189	**c**	0.002019	2	0.000063	0	1.467528	1.883932	10.241921	0.281996	23	605	6	0.281995	-14.4	1.13	773	7	-10.7	1.13
P013-190	**c**	0.003427	4	0.000124	1	1.467450	1.884133	17.169892	0.282058	18	596	13	0.282057	-12.5	0.87	596	13	-8.5	0.88
P013-191	**c**	0.013837	11	0.000503	3	1.467497	1.884111	10.440633	0.281899	19	623	6	0.281893	-17.7	0.97	739	6	-15.1	0.97
P013-193	**c**	0.006836	9	0.000285	3	1.467436	1.884073	16.638642	0.282004	17	659	6	0.282001	-13.0	0.83	773	7	-10.5	0.83
P013-194	**c**	0.017793	15	0.000683	4	1.467509	1.883990	14.848326	0.282052	17	1179	15	0.282036	0.0	0.85	1179	15	0.0	0.85
P013-196	**c**	0.000150	0	0.000004	0	1.467470	1.883911	13.601358	0.281983	14	596	6	0.281983	-15.1	0.71	773	7	-11.1	0.71
P013-199	**c**	0.009174	14	0.000351	6	1.467507	1.883895	13.754582	0.282005	19	716	6	0.282000	-11.8	0.96	773	7	-10.5	0.96
P013-200	**c**	0.000894	1	0.000033	0	1.467451	1.883932	12.184334	0.282002	17	600	8	0.282002	-14.3	0.84	773	7	-10.5	0.84
P013-206	**r**	0.005631	5	0.000228	1	1.467521	1.883825	10.130603	0.282052	20	1146	19	0.282047	-0.4	1.02	1146	19	-0.4	1.02
P013-207	**c**	0.010089	8	0.000368	2	1.467518	1.884029	11.738739	0.281999	17	1022	10	0.281992	-5.2	0.87	1022	10	-5.2	0.87
P013-212	**c**	0.008365	7	0.000315	2	1.467522	1.884053	11.593179	0.282020	18	641	13	0.282016	-12.9	0.91	773	7	-10.0	0.91
P013-215	**c**	0.001683	1	0.000062	0	1.467567	1.884012	13.446545	0.282018	16	623	6	0.282018	-13.2	0.80	773	7	-9.9	0.80
P013-217	**c**	0.010061	8	0.000389	2	1.467537	1.883960	12.426262	0.281976	18	773	7	0.281971	-11.5	0.89	773	7	-11.5	0.89
P013-218	**c**	0.011341	9	0.000447	3	1.467490	1.883719	13.816548	0.282057	13	875	8	0.282050	-6.4	0.66	875	8	-6.4	0.66
P013-223	**c**	0.014871	24	0.000559	9	1.467483	1.883956	12.696289	0.282017	16	749	7	0.282009	-10.7	0.80	773	7	-10.2	0.80
P013-233	**c**	0.008276	8	0.000322	2	1.467433	1.884326	12.027320	0.281916	16	739	6	0.281912	-14.4	0.82	739	6	-14.4	0.82
P013-234	**c**	0.002249	2	0.000073	0	1.467440	1.884366	14.191305	0.281861	20	595	6	0.281860	-19.5	1.00	739	6	-16.2	1.00
P013-237	**c**	0.014818	12	0.000552	4	1.467412	1.884299	11.824181	0.282003	17	720	6	0.281996	-11.8	0.83	773	7	-10.7	0.83
P013-240	**c**	0.010723	14	0.000446	5	1.467536	1.883793	11.637281	0.281882	26	628	13	0.281876	-18.2	1.27	739	6	-15.7	1.27
P013-241	**c**	0.002300	3	0.000086	1	1.467507	1.883943	12.207429	0.281921	18	699	6	0.281920	-15.0	0.91	739	6	-14.1	0.91
P013-242	**c**	0.000248	0	0.000008	0	1.467494	1.884252	12.307611	0.282010	17	601	5	0.282010	-14.0	0.85	773	7	-10.2	0.85
P013-246	**c**	0.002942	2	0.000103	1	1.467507	1.884000	9.909977	0.281954	18	718	6	0.281952	-13.4	0.88	773	7	-12.2	0.88
P013-249	**c**	0.019570	16	0.000734	4	1.467545	1.884046	10.077913	0.281992	20	768	13	0.281981	-11.3	1.00	773	7	-11.2	1.00

P013-250	**c**	0.012012	10	0.000449	3	1.467501	1.884337	12.594932	0.282014	20	667	6	0.282008	-12.6	1.00	773	7	-10.2	1.00
P013-256	**c**	0.020188	16	0.000851	5	1.467506	1.883984	12.754392	0.281896	19	687	8	0.281885	-16.5	0.95	739	6	-15.4	0.95
P013-260	**c**	0.019137	15	0.000719	4	1.467454	1.884180	12.610851	0.282073	17	751	7	0.282063	-8.8	0.87	751	7	-8.3	0.87
P013-262	**c**	0.000618	1	0.000020	0	1.467445	1.884071	12.774665	0.281999	14	629	6	0.281999	-13.8	0.71	773	7	-10.6	0.71
P013-263	**c**	0.012860	10	0.000478	3	1.467533	1.883933	11.178598	0.281991	25	634	5	0.281986	-14.1	1.25	773	7	-11.1	1.25
P013-266	**r**	0.016820	14	0.000650	4	1.467496	1.884013	13.283638	0.282022	17	627	13	0.282014	-13.3	0.86	773	7	-10.1	0.86
P013-267	**c**	0.008691	7	0.000306	2	1.467575	1.884076	8.050685	0.281971	28	769	7	0.281966	-11.8	1.39	773	7	-11.7	1.39
P013-268	**c**	0.003286	3	0.000111	1	1.467470	1.883950	12.125760	0.281940	14	667	7	0.281938	-15.1	0.72	739	6	-13.5	0.72
P013-269	**c**	0.005083		0.000192		1.467501	1.883955	11.926402	0.281976	22	643	6	0.281973	-14.4	1.11	773	7	-11.5	1.11
P013-270	**c**	0.006336		0.000236		1.467509	1.883782	11.238314	0.281945	20	680	16	0.281942	-14.7	0.99	739	6	-13.4	0.99

(a) $^{176}Yb/^{177}Hf = (^{176}Yb/^{173}Yb)_{true} \times (^{173}Yb/^{177}Hf)_{meassured} \times (M_{173(Yb)}/M_{177(Hf)})^{b(Hf)}$, $b(Hf) = \ln(^{179}Hf/^{177}Hf_{true} / {}^{179}Hf/^{177}Hf_{measured}) / \ln (M_{179(Hf)}/M_{177(Hf)})$

M=mass of respective isotope. The $^{176}Lu/^{177}Hf$ were calculated in a similar way by using the $^{175}Lu/^{177}Hf$ and b(Yb)

(b) Mean Hf signal in volt

(c) Uncertainties are quadratic additions of the within-run precision and the daily reproducibility of the zircon standards. Uncertainties for the standard quoted at 2SD (2 standard deviation)

(d) Initial $^{176}Hf/^{177}Hf$ and ƐHf calculated using the apparent Pb-Pb ages of respective zircon domains, and the CHUR parameters: $^{176}Lu/^{177}Hf = 0.0336$, and $^{176}Hf/^{177}Hf = 0.282785$ (Bouvier et al., 2008)

(e) Two stage model age in billion years using the measured $^{176}Lu/^{177}Lu$ of each spot (first stage = age of zircon), a value of 0.0113 for the average continental crust (second stage), and a average MORB (DM) $^{176}Lu/^{177}Hf$ and $^{176}Hf/^{177}Hf$ of 0.0384 and 0.283164

Bouvier, A., Vervoort, J.D., Patchett, P.J., 2008. The Lu-Hf and Sm-Nd isotopic composition of CHUR: constraints from unequilibrated chondrites and implications for the bulk composition of terrestrial planets. Earth and Planetary Science Letters 273, 48-57.

(f) $^{206}Pb/^{238}U$ age

c-core

r-rim

s-single phase

Zircon LA-MC-ICP-MS U-Pb results - Standards - GJ-1, Plesovice, BB

				Isotope ratios[c]							Ages (Ma)						
Spot number	Th ppm	U ppm	Th/U[b]	$^{207}Pb/^{206}Pb$[e]	2 s [%]	$^{207}Pb/^{235}U$	2 s [%]	$^{206}Pb/^{238}U$	2 s [%]	Rho[d]	$^{206}Pb/^{238}U$	2 s abs	$^{207}Pb/^{235}U$	2 s abs	$^{207}Pb/^{206}Pb$	2 s abs	% Disc.[e]
Analysis P013_009 to P013_180																	
BB Ref. Mat.																	
1.sSMPABC002	183	408	0.45	0.05914	1.07	0.73771	1.93	0.09	1.61	0.83	558	9	561	8	572	23	0
1.sSMPABC021	189	408	0.46	0.05852	3.57	0.73591	4.49	0.09	2.72	0.61	563	15	560	20	549	78	0
1.sSMPABC022	190	422	0.45	0.05903	1.10	0.73838	1.95	0.09	1.61	0.83	560	9	561	8	568	24	0
1.sSMPABC042	199	443	0.45	0.05779	3.62	0.73930	4.51	0.09	2.69	0.60	572	15	562	20	522	79	-2
1.sSMPABC081	183	403	0.45	0.05888	1.14	0.74851	2.00	0.09	1.65	0.82	569	9	567	9	563	25	0
1.sSMPABC101	198	422	0.47	0.05934	1.18	0.75952	2.02	0.09	1.64	0.81	572	9	574	9	580	26	0
1.sSMPABC121	175	405	0.43	0.05840	3.60	0.73519	4.52	0.09	2.74	0.61	563	15	560	20	545	79	-1
1.sSMPABC141	194	421	0.46	0.05873	1.12	0.72774	1.98	0.09	1.62	0.82	555	9	555	8	557	25	0
1.sSMPABC142	191	416	0.46	0.05898	1.58	0.74636	2.41	0.09	1.82	0.76	566	10	566	10	566	34	0
1.sSMPABC161	164	391	0.42	0.05849	1.09	0.74073	1.98	0.09	1.65	0.83	566	9	563	9	548	24	-1
GJ-1 Ref. Mat.																	
1.sSMPABC003	15	471	0.03	0.06001	1.07	0.80403	1.91	0.10	1.59	0.83	598	9	599	9	604	23	0
1.sSMPABC004	14	446	0.03	0.06005	1.05	0.80498	1.90	0.10	1.59	0.83	598	9	600	9	605	23	0
1.sSMPABC023	15	460	0.03	0.05985	1.09	0.81085	1.94	0.10	1.60	0.83	604	9	603	9	598	24	0
1.sSMPABC024	15	477	0.03	0.05971	1.11	0.81172	1.98	0.10	1.65	0.83	606	10	603	9	593	24	0
1.sSMPABC043	15	481	0.03	0.06007	1.05	0.81305	1.92	0.10	1.61	0.84	604	9	604	9	606	23	0
1.sSMPABC044	15	480	0.03	0.06008	1.09	0.81066	1.93	0.10	1.60	0.83	602	9	603	9	606	24	0
1.sSMPABC064	15	458	0.03	0.06005	1.08	0.81261	1.98	0.10	1.65	0.84	604	10	604	9	605	23	0
1.sSMPABC083	15	470	0.03	0.06031	3.51	0.81532	4.39	0.10	2.64	0.60	603	15	605	20	615	76	0
1.sSMPABC084	15	477	0.03	0.05926	1.08	0.80716	1.93	0.10	1.60	0.83	607	9	601	9	577	23	-1

1.sSMPABC103	15	466	0.03	0.05953	1.06	0.80229	1.93	0.10	1.62	0.84	601	9	598	9	587	23	-1
1.sSMPABC104	15	465	0.03	0.05996	1.12	0.81686	2.00	0.10	1.66	0.83	607	10	606	9	602	24	0
1.sSMPABC123	14	472	0.03	0.05905	1.20	0.79629	2.02	0.10	1.62	0.80	601	9	595	9	569	26	-1
1.sSMPABC124	14	448	0.03	0.05997	1.08	0.80871	1.95	0.10	1.62	0.83	602	9	602	9	602	23	0
1.sSMPABC143	14	432	0.03	0.05973	1.08	0.80503	1.97	0.10	1.64	0.84	601	9	600	9	594	23	0
1.sSMPABC144	14	453	0.03	0.06012	1.10	0.80932	1.97	0.10	1.64	0.83	601	9	602	9	608	24	0
1.sSMPABC163	15	457	0.03	0.05974	1.12	0.81452	2.00	0.10	1.66	0.83	608	10	605	9	594	24	0
1.sSMPABC164	13	415	0.03	0.05802	3.65	0.78174	4.49	0.10	2.61	0.58	601	15	586	20	531	80	-2
1.sSMPABC183	14	426	0.03	0.06010	1.15	0.81308	2.03	0.10	1.67	0.82	603	10	604	9	607	25	0
1.sSMPABC184	14	422	0.03	0.05877	1.45	0.78992	2.26	0.10	1.74	0.77	600	10	591	10	559	32	-1
Plesovice Ref. Mat.																	
1.sSMPABC005	175	783	0.22	0.05337	1.45	0.39508	2.36	0.05	1.86	0.79	337	6	338	7	344	33	0
1.sSMPABC006	183	770	0.24	0.05337	1.05	0.39349	1.92	0.05	1.61	0.84	336	5	337	6	345	24	0
1.sSMPABC025	196	850	0.23	0.05341	1.09	0.39644	1.90	0.05	1.56	0.82	338	5	339	5	346	25	0
1.sSMPABC045	196	846	0.23	0.05310	1.44	0.39256	2.36	0.05	1.87	0.79	337	6	336	7	333	33	0
1.sSMPABC065	217	946	0.23	0.05333	1.09	0.39467	1.94	0.05	1.60	0.83	337	5	338	6	343	25	0
1.sSMPABC066	203	886	0.23	0.05235	1.28	0.38879	2.05	0.05	1.60	0.78	338	5	333	6	301	29	-1
1.sSMPABC086	208	891	0.23	0.05373	3.92	0.40388	5.63	0.05	4.04	0.72	342	13	344	17	360	88	1
1.sSMPABC105	206	906	0.23	0.05321	1.44	0.39966	2.37	0.05	1.88	0.79	342	6	341	7	338	33	0
1.sSMPABC106	203	899	0.23	0.05321	1.41	0.39676	2.26	0.05	1.76	0.78	339	6	339	7	338	32	0
1.sSMPABC125	194	850	0.23	0.05358	3.92	0.40269	5.62	0.05	4.03	0.72	342	13	344	17	354	89	0
1.sSMPABC126	201	878	0.23	0.05329	3.90	0.39611	5.63	0.05	4.06	0.72	339	13	339	16	341	88	0
1.sSMPABC145	63	457	0.14	0.05325	1.45	0.39371	2.36	0.05	1.86	0.79	337	6	337	7	340	33	0
1.sSMPABC146	113	797	0.14	0.05321	2.35	0.39980	3.46	0.05	2.55	0.74	342	8	341	10	338	53	0
1.sSMPABC166	110	765	0.14	0.05315	1.11	0.39485	1.97	0.05	1.63	0.83	338	5	338	6	335	25	0
1.sSMPABC185	194	836	0.23	0.05347	1.25	0.39872	2.09	0.05	1.68	0.80	340	6	341	6	349	28	0
1.sSMPABC186	204	905	0.23	0.05336	1.23	0.39307	2.10	0.05	1.71	0.81	336	6	337	6	344	28	0

Analysis P013_181 to P013_270

BB Ref. Mat.

1.sSMPABC003	82	659	0.12	0.05849	2.05	0.73065	2.19	0.09	0.77	0.35	559	4	557	9	548	45	0
1.sSMPABC004	84	672	0.12	0.05825	2.03	0.73826	2.17	0.09	0.78	0.36	567	4	561	9	539	44	-1
1.sSMPABC023	74	558	0.13	0.05835	4.00	0.73471	4.64	0.09	2.35	0.51	563	13	559	20	543	87	-1
1.sSMPABC024	75	563	0.13	0.05841	2.06	0.73008	2.23	0.09	0.87	0.39	559	5	557	10	545	45	-1
1.sSMPABC043	71	516	0.14	0.05862	2.12	0.73987	2.31	0.09	0.94	0.41	565	5	562	10	553	46	0
1.sSMPABC044	70	501	0.14	0.05796	4.04	0.73196	4.69	0.09	2.38	0.51	565	13	558	20	528	89	-1
1.sSMPABC043	78	587	0.13	0.05816	2.03	0.74377	2.22	0.09	0.91	0.41	572	5	565	10	536	44	-1
1.sSMPABC044	79	592	0.13	0.05844	2.02	0.74353	2.21	0.09	0.89	0.40	569	5	564	10	546	44	-1
1.sSMPABC063	78	581	0.13	0.05860	3.98	0.73289	4.64	0.09	2.38	0.51	560	13	558	20	552	87	0
1.sSMPABC064	76	563	0.14	0.05814	3.99	0.73042	4.65	0.09	2.38	0.51	562	13	557	20	535	87	-1
1.sSMPABC083	76	559	0.14	0.05849	3.97	0.72931	4.64	0.09	2.40	0.52	558	13	556	20	548	87	0
1.sSMPABC084	74	551	0.13	0.05900	2.04	0.73649	2.24	0.09	0.93	0.42	559	5	560	10	567	44	0
1.sSMPABC103	73	539	0.14	0.05823	2.06	0.73311	2.28	0.09	0.96	0.42	563	5	558	10	538	45	-1
1.sSMPABC104	76	544	0.14	0.05822	2.06	0.73442	2.27	0.09	0.96	0.42	564	5	559	10	538	45	-1
1.sSMPABC123	74	530	0.14	0.05814	2.12	0.72930	2.34	0.09	1.00	0.43	561	5	556	10	535	46	-1
1.sSMPABC124	72	522	0.14	0.05848	2.09	0.72843	2.31	0.09	1.00	0.43	558	5	556	10	548	46	0

GJ-1 Ref. Mat.

1.sSMPABC001	5	342	0.01	0.05960	2.19	0.80442	2.37	0.10	0.90	0.38	602	5	599	11	589	47	0
1.sSMPABC002	5	341	0.01	0.05997	2.14	0.81143	2.31	0.10	0.86	0.37	603	5	603	11	603	46	0
1.sSMPABC021	4	291	0.01	0.06013	2.03	0.80445	2.20	0.10	0.85	0.38	597	5	599	10	608	44	0
1.sSMPABC022	4	289	0.01	0.05964	2.08	0.79798	2.25	0.10	0.87	0.38	597	5	596	10	591	45	0
1.sSMPABC041	4	270	0.02	0.05970	2.15	0.80444	2.35	0.10	0.95	0.40	601	5	599	11	593	47	0
1.sSMPABC042	4	267	0.02	0.05993	2.10	0.80764	2.30	0.10	0.94	0.41	601	5	601	11	601	46	0
1.sSMPABC041	5	313	0.02	0.05983	2.06	0.81160	2.26	0.10	0.93	0.41	605	5	603	10	597	45	0

1.sSMPABC042	5	316	0.01	0.06013	2.03	0.81340	2.23	0.10	0.92	0.41	603	5	604	10	608	44	0
1.sSMPABC061	5	305	0.02	0.05989	2.07	0.79896	2.28	0.10	0.96	0.42	595	5	596	10	600	45	0
1.sSMPABC062	5	302	0.02	0.05980	2.04	0.80465	2.24	0.10	0.92	0.41	600	5	599	10	596	44	0
1.sSMPABC081	5	305	0.02	0.05977	2.04	0.79166	2.25	0.10	0.94	0.42	591	5	592	10	595	44	0
1.sSMPABC082	5	298	0.02	0.05930	2.06	0.79426	2.27	0.10	0.95	0.42	598	5	594	10	578	45	-1
1.sSMPABC101	5	294	0.02	0.06007	2.11	0.80930	2.32	0.10	0.97	0.42	601	6	602	11	606	46	0
1.sSMPABC102	5	293	0.02	0.05952	2.12	0.81131	2.33	0.10	0.97	0.42	608	6	603	11	586	46	-1
1.sSMPABC121	5	290	0.02	0.05986	2.21	0.80975	2.46	0.10	1.08	0.44	603	6	602	11	599	48	0
1.sSMPABC122	4	284	0.02	0.05992	3.94	0.80047	4.56	0.10	2.29	0.50	596	13	597	21	601	85	0
Plesovice Ref. Mat.																	
1.sSMPABC005	15	453	0.03	0.05320	2.14	0.39059	2.28	0.05	0.79	0.35	334	3	335	7	337	49	0
1.sSMPABC006	38	920	0.04	0.05296	2.08	0.39147	2.22	0.05	0.78	0.35	337	3	335	6	327	47	0
1.sSMPABC025	32	754	0.04	0.05292	2.08	0.38738	2.25	0.05	0.87	0.38	333	3	332	6	325	47	0
1.sSMPABC026	33	759	0.04	0.05300	4.31	0.39067	5.77	0.05	3.84	0.67	336	13	335	17	329	98	0
1.sSMPABC045	32	696	0.05	0.05285	2.12	0.39794	2.32	0.05	0.95	0.41	343	3	340	7	322	48	-1
1.sSMPABC046	30	739	0.04	0.05273	2.16	0.39871	2.36	0.05	0.95	0.40	344	3	341	7	317	49	-1
1.sSMPABC045	35	806	0.04	0.05266	2.01	0.40029	2.21	0.06	0.91	0.41	346	3	342	6	314	46	-1
1.sSMPABC046	33	836	0.04	0.05300	2.00	0.40316	2.20	0.06	0.91	0.41	346	3	344	6	329	45	-1
1.sSMPABC065	32	739	0.04	0.05263	2.04	0.39018	2.26	0.05	0.98	0.43	338	3	334	6	313	46	-1
1.sSMPABC066	32	737	0.04	0.05251	2.06	0.39357	2.25	0.05	0.92	0.41	341	3	337	6	308	47	-1
1.sSMPABC085	22	567	0.04	0.05269	4.33	0.39119	5.79	0.05	3.84	0.66	338	13	335	17	315	99	-1
1.sSMPABC086	14	392	0.04	0.05257	2.34	0.39016	2.68	0.05	1.30	0.48	338	4	334	8	310	53	-1
1.sSMPABC105	28	583	0.05	0.05275	4.35	0.39266	5.79	0.05	3.83	0.66	339	13	336	17	318	99	-1
1.sSMPABC106	28	624	0.05	0.05258	2.10	0.39259	2.31	0.05	0.97	0.42	340	3	336	7	311	48	-1
1.sSMPABC125	30	641	0.05	0.05312	2.15	0.38921	2.37	0.05	1.02	0.43	334	3	334	7	334	49	0
1.sSMPABC126	32	640	0.05	0.05257	2.13	0.38895	2.36	0.05	1.01	0.43	337	3	334	7	310	48	-1

aFraction of the non-radiogenic ^{206}Pb in the analyzed zircon spot, where f_{206}=[$^{206}Pb/^{204}Pb$]c/[$^{206}Pb/^{204}Pb$]s (c=common; s=sample)

bTh/U ratios and amount of Pb, Th and U (in pmm) are calculated relative to 91500 reference zircon

cCorrected for background and within-run Pb/U fractionation and normalised to reference zircon GJ-1 (ID-TIMS values/measured value); $^{207}Pb/^{235}U$ calculated using ($^{207}Pb/^{206}Pb$)/($^{238}U/^{206}Pb$ * 1/137.88)

dRho is the error correlation defined as the quotient of the propagated errors of the $^{206}Pb/^{238}U$ and the $^{207}/^{235}U$ ratio

eDegree of discordance = 100 - ($^{206}Pb/^{238}U$ age * 100/$^{207}Pb/^{206}U$ age)

c-core
r-rim
s-single phase

Hf isotopes results determined by LA-ICP-MS - Standards - BB, GJ-1, TEMORA

Grain#	$^{176}Yb/^{177}Hf$ [a]	±2s	$^{176}Lu/^{177}Hf$ [a]	±2s	$^{178}Hf/^{177}Hf$	$^{180}Hf/^{177}Hf$	Sig_{Hf} [b] (V)	$^{176}Hf/^{177}Hf$	±2s [c]	age [f] (Ma)	±2 s	$^{176}Hf/^{177}Hf_{(t)}$ [d]	eHf(t) [d]	±2s [c]
										(measured)				
GJ-1_001.dat	0.006008	6	0.000248	2	1.467186	1.886783	4.956039	0.282000	28	603	1	0.281997	-14.4	1.39
GJ-1_002.dat	0.006051	5	0.000249	2	1.467260	1.886811	5.040085	0.282008	32	603	1	0.282006	-14.1	1.59
GJ-1_003.dat	0.006081	5	0.000249	2	1.467263	1.886984	5.104119	0.282027	29	603	1	0.282024	-13.5	1.45
GJ-1_160.dat	0.006048	6	0.000248	2	1.467141	1.886862	5.140041	0.282016	23	603	1	0.282013	-13.9	1.14
GJ-1_161.dat	0.006014	5	0.000246	2	1.467251	1.886790	5.125451	0.282012	29	603	1	0.282009	-14.0	1.47
GJ-1_162.dat	0.006072	5	0.000248	2	1.467223	1.886977	5.121263	0.281996	31	603	1	0.281993	-14.6	1.54
GJ-1_238.dat	0.006017	6	0.000248	2	1.467257	1.886804	4.471310	0.282022	29	603	1	0.282020	-13.6	1.45
GJ-1_239.dat	0.006007	5	0.000247	1	1.467239	1.887050	4.554080	0.281969	34	603	1	0.281966	-15.5	1.69
GJ-1_240.dat	0.006024	5	0.000247	2	1.467257	1.886970	4.618339	0.282039	31	603	1	0.282036	-13.1	1.54

GJ-1 (608Ma): $^{176}Hf/^{177}Hf$=0.282000±0.000005 **Average: 0.282007**

BB_004.dat	0.004311	6	0.000153	2	1.467260	1.886838	6.846729	0.281672	22	560	1	0.281670	-27.0	1.08
BB_005.dat	0.004302	5	0.000153	1	1.467290	1.886891	6.863237	0.281672	24	560	1	0.281671	-27.0	1.19
BB_006.dat	0.004350	3	0.000155	1	1.467197	1.886823	6.856792	0.281677	22	560	1	0.281676	-26.8	1.12
BB_163.dat	0.004391	4	0.000155	1	1.467299	1.886881	6.845445	0.281675	23	603	1	0.281674	-25.9	1.12
BB_164.dat	0.004246	3	0.000150	1	1.467186	1.886955	6.878093	0.281664	23	603	1	0.281662	-26.3	1.16
BB_165.dat	0.004193	5	0.000149	1	1.467255	1.886846	6.990812	0.281661	25	603	1	0.281659	-26.4	1.24
BB_241.dat	0.004232	3	0.000151	1	1.467252	1.887051	6.152638	0.281673	35	560	1	0.281672	-26.9	1.72
BB_242.dat	0.004177	4	0.000149	1	1.467251	1.886861	6.134279	0.281677	28	560	1	0.281676	-26.8	1.40
BB_243.dat	0.004241	3	0.000150	1	1.467256	1.887065	6.191014	0.281608	23	560	1	0.281606	-29.2	1.13
BB (560Ma): $^{176}Hf/^{177}Hf$=0.2816713±0.0000028							**Average:**	**0.281663**						
TEM_007.dat	0.027296	22	0.001043	6	1.467232	1.886945	8.649990	0.282684	20	417	1	0.282676	5.4	1.02
TEM_008.dat	0.041422	33	0.001651	10	1.467243	1.886808	10.339454	0.282683	23	417	1	0.282670	5.2	1.15
TEM_009.dat	0.027370	22	0.001153	7	1.467250	1.886834	7.721384	0.282682	24	417	1	0.282673	5.3	1.21
TEM_166.dat	0.021759	19	0.000926	6	1.467236	1.886915	7.509353	0.282698	17	417	1	0.282690	5.9	0.88
TEM_167.dat	0.055998	58	0.002060	17	1.467281	1.886897	6.824099	0.282676	30	417	1	0.282660	4.9	1.51
TEM_168.dat	0.035200	30	0.001311	9	1.467246	1.886877	7.084646	0.282734	24	417	1	0.282723	7.1	1.22
TEM_244.dat	0.029519	24	0.001165	7	1.467259	1.886923	8.685108	0.282721	23	417	1	0.282712	6.7	1.16
TEM_245.dat	0.020728	17	0.000796	5	1.467216	1.886968	7.497426	0.282651	28	417	1	0.282645	4.3	1.42
TEM_246.dat	0.027352	30	0.001071	11	1.467190	1.886805	7.405677	0.282708	30	417	1	0.282700	6.3	1.49
Temora (417Ma): $^{176}Hf/^{177}Hf$=0.282686±0.000007							**Average:**	**0.282683**						

[a] $^{176}Yb/^{177}Hf = (^{176}Yb/^{173}Yb)_{true} \times (^{173}Yb/^{177}Hf)_{meassured} \times (M_{173(Yb)}/M_{177(Hf)})^{b(Hf)}$, $b(Hf) = \ln(^{179}Hf/^{177}Hf_{true} / {}^{179}Hf/^{177}Hf_{measured}) / \ln (M_{179(Hf)}/M_{177(Hf)})$

M=mass of respective isotope. The $^{176}Lu/^{177}Hf$ were calculated in a similar way by using the $^{175}Lu/^{177}Hf$ and b(Yb)

[b] Mean Hf signal in volt

[c] Uncertainties are quadratic additions of the within-run precision and the daily reproducibility of the zircon standards. Uncertainties for the standard quoted at 2SD (2 standard deviation)

(d) Initial $^{176}Hf/^{177}Hf$ and ƐHf calculated using the apparent Pb-Pb ages of respective zircon domains, and the CHUR parameters: $^{176}Lu/^{177}Hf = 0.0336$, and $^{176}Hf/^{177}Hf = 0.282785$ (Bouvier et al., 2008)
(e) Two stage model age in billion years using the measured $^{176}Lu/^{177}Lu$ of each spot (first stage = age of zircon), a value of 0.0113 for the average continental crust (second stage), and a average MORB (DM) $^{176}Lu/^{177}Hf$ and $^{176}Hf/^{177}Hf$ of 0.0384 and 0.283164

Bouvier, A., Vervoort, J.D., Patchett, P.J., 2008. The Lu-Hf and Sm-Nd isotopic composition of CHUR: constraints from unequilibrated chondrites and implications for the bulk composition of terrestrial planets. Earth and Planetary Science Letters 273, 48-57.
(f) $^{206}Pb/^{238}U$ age

9.16 APPENDIX P – Compilation of UHT metamorphism occurrences in Brazil (Chapter 6)

Reference	Tectonic Domain	Occurrence	Region	Protolith	Lithotype	Mineral assemblage	Geochemical Signature	U-Pb Age	eHf	Peak T (°C)	Peak P (kbar)	Retro T (°C)	Retro P (kbar)	Anatexis conditions	Interpreted tectonic setting
Baldwin and Brown, 2008	Brasília orogen (Northern)	Anápolis-Itauçu Complex	Goiânia (GO)	Impure arenite	Impure quartzite	Spr+Grt+Opx+Sil +Qz ±Rt		ca. 649 - 634 Myr		980		870			Back arc/Collision
Baldwin et al., 2005	Brasília orogen (Northern)	Anápolis-Itauçu Complex	Goiânia (GO)	Impure arenite	Impure quartzite	Spr+Grt+Opx+Sil +Qz ±Rt				1025	8.8				Collision + Delamination/Slab break off
Baldwin et al., 2007	Brasília orogen (Northern)	Anápolis-Itauçu Complex	Goiânia (GO)	Impure arenite	Impure quartzite	Spr+Grt+Opx+Sil +Qz ±Rt		ca. 640 Ma		965		780			
Barbosa et al., 2006	São Francisco Craton	Jequié block	Brejões-Santa Inês (BA)	Pelites	Aluminous - magnesian granulites	Hc+Sil+Grt+Crd+ Pl+Qz		ca. 2.1 - 2.0 Gyr		1051	7.5	887	7.1		Collision + Magma underplating
Barbosa et al., 2006	São Francisco Craton	Jequié block	Brejões-Santa Inês (BA)	Pelites	Aluminous - magnesian granulites	Hc+Sil+Grt+Crd+ Pl+Qz		ca. 2.1 - 2.0 Gyr		985	8.2	850	7.3		Collision + Magma underplating
Belém, 2006	Araçuaí orogen (Northern)	Jequitinhonha Complex	Itamaraju - BA	Black shale	Gr-Sil-Crd-Grt-Bt gneiss					917	7.4			~630 °C	
Campos-Neto and Caby, 1999	Brasília orogen (Southern)	Socorro-Guaxupé Nappe (Basal Granulite Unit)	Varginha Shear Zone		Granulites					900	12				Subduction/Collision Magma underplating
Campos-Neto and Caby, 2000	Brasília orogen (Southern)	Socorro-Guaxupé Nappe (Basal Granulite Unit)	Varginha Shear Zone	Basic plutonic rock	Opx-Grt granulites		Calc-alkaline (Continental arc)	ca. 630 - 625 Myr		920	11.7	720	10.5		Subduction/Collision
Campos-Neto and Caby, 2000	Brasília orogen (Southern)	Socorro-Guaxupé Nappe (Basal Granulite Unit)	Varginha Shear Zone	Basic plutonic rock	Opx-Grt granulites		Calc-alkaline (Continental arc)	ca. 630 - 625 Myr		850	13.8	720	9		Subduction/Collision
Del Lama et al., 2000	Brasília orogen (Southern)	Socorro-Guaxupé Nappe (Basal Granulite Unit)	Varginha Shear Zone		Grt granulites			ca. 660 - 630 Myr		950	14	700	10		Subduction/Collision
Gradim, 2013 Gradim et al., 2014	Araçuaí orogen (Northern)	Nova Venécia Complex	Nova Venécia - ES	Paragneiss (pelite)	Sp-Crd-Grt-Sil-Bt gneiss		Active continental margin	590 ± 10 Ma ?		930	6.1				Back-arc/Slab window

Leite et al., 2009	Itabuna-Salvador-Curaçá Belt	Tanque Novo-Ipirá Complex	Capim Grosso (BA)		Sapphirine-bearing granulites	Opx+Spr+Bt Sil+Opx+Spr+Bt+Kfs+Pl Grt+Ops+Bt+Kfs+Pl		ca. 2.1 - 2.0 Gyr		950	8				
Moraes and Fuck, 2000	Brasília orogen (Northern)	Barro Alto Complex	Goianésia - GO		Aluminous granulites			ca. 820 - 770 Myr		980	7.9	750	7.9		Collision + Extension
Moraes et al., 2002	Brasília orogen (Northern)	Anápolis-Itauçu Complex	Damolândia (GO)		Qz-rich Granulite	Rt+Sp+Opx+Grt+Sil+Crd+Bt+Pl+Qtz ±Spr				960	8.1	600	6		Collision + Delamination/Slab break off
Moraes et al., 2002	Brasília orogen (Northern)	Anápolis-Itauçu Complex	Damolândia (GO)		Qz-poor Granulite	Spr+Sp+Opx+Grt+Sil+Crd+Pl±Crn±Qz				975	8.5	600	6		Collision + Delamination/Slab break off
Moraes et al., 2002	Brasília orogen (Northern)	Anápolis-Itauçu Complex	Goiânia (GO)	Impure arenite	Impure quartzite	Spr+Grt+Opx+Sil+Qz ±Rt				1012	9.4	850	9		Collision + Delamination/Slab break off
Moraes et al., 2002	Brasília orogen (Northern)	Anápolis-Itauçu Complex	Damolândia (GO)	Pelite	Metapelitic gneiss	Ilm+Rt+Sp+Opx+Grt+Sil+Crd+Pl+Qz				975	9.7	600	6		Collision + Delamination/Slab break off
Moreira, 1997 Costa, 1998	Araçuaí orogen (Southern)	Juiz de Fora Complex	Manhuaçu - MG	Basic volcanic rock	Opx-Cpx granulites	Opx+Cpx+Pl+Qz± Kfs	Calc-alkaline (Island arc)			990	10				Back-arc(?)
Motta et al., 2021	Brasília orogen (Southern)	Socorro-Guaxupé Nappe (Basal Granulite Unit)	Varginha (MG)		Grt mafic granulite	Grt+Ilm+Mag+Qz+Opx+Cpx+Pl				919	11				
Motta et al., 2021	Brasília orogen (Southern)	Socorro-Guaxupé Nappe (Basal Granulite Unit)	Varginha (MG)		Grt felsic granulite	Cpx+Opx+Grt+Kfs+Pl+Qz±Ilm		ca. 625 - 595 Myr	-6.02 - -3.31	1009	11.5	870	8.5	~625 °C	
Reno et al., 2009	Brasília orogen (Southern)	Socorro-Guaxupé Nappe	Varginha (MG)		Opx-Cpx granulite	Cpx+Opx+Kfs+Pl+Qz				900	15				
Reno et al., 2009	Brasília orogen (Southern)	Socorro-Guaxupé Nappe	Varginha (MG)		Grt-Opx granulite	Grt+Opx+Qz+Pl+Hbl		622 ± 28		900	15				
Reno et al., 2009	Brasília orogen (Southern)	Três Pontas-Varginha Nappe	Varginha (MG)		Ky-Grt granulite	Qz+Grt+Kfs+Ky+Ilm+Pl		647 ± 11		900	16				
Rocha et al., 2017	Brasília orogen (Southern)	Socorro-Guaxupé Nappe (Metatexite Unit)	Alfenas (MG)		Opx-Grt-bearing leucosome	Opx+Grt+Pl+Kfs+Qtz		ca. 630 - 625 Myr		1030	11.7	865	8.9		Collision + Extension

Rocha et al., 2018	Brasília orogen (Southern)	Socorro-Guaxupé Nappe (Basal Granulite Unit)	Alfenas (MG)		Grt-rich granulite	Opx+Grt+Pl+Kfs+Qtz		ca. 630 - 625 Myr		900	12				Collision + Extension
Rossi-Vieira et al. (submitted)	Araçuaí orogen (Southern)	Caparaó Suite	Serra do Caparaó (MG/ES)	Paragneisses (pelite)	Hc-Sil-Grt diatexite	Ilm+Hc+Sil+Grt+Pl+Or+Qz		ca. 635 - 610 Myr (UHT peak) ca. 610 - 590 Myr (melt crystallization)		1035	7.1	745	5.3		Subduction/Slab window
Rossi-Vieira et al. (submitted)	Araçuaí orogen (Southern)	Caparaó Suite	Serra do Caparaó (MG/ES)	Paragneisses (greywacke)	Opx-Grt diatexite	Ilm+Opx+Grt+Pl+Or+Qz ±Rt		ca. 635 - 610 Myr (UHT peak) ca. 610 - 590 Myr (melt crystallization)	-19.5 - -8.77	978	9.6	670	5		Subduction/Slab window
Tedeschi et al., 2018	Brasília orogen (Southern)	Socorro-Guaxupé Nappe (Basal Granulite Unit)	Bandeira do Sul / Botelhos (MG)		Banded granulite	Hbl+Opx+Cpx+Pl+Kfs +Bt+Qtz		ca. 660 - 630 Myr	-14.1 - 8.2	998		740	5.7		Subduction/Collision Magma underplating
Tesser et al., 2021	Borborema Province	Arapiaca Complex	Arapiaca (AL)		Spr-bearing diatexite	Crd+Grt+Sill+Mag+Sp+Opx+Spr+Crn+Rt+Ilm+Hem+Kfs+Pl+Qz		ca. 2.08 - 2.03 Gyr		970	8.5	910	7.7		Collision + Magma underplating
Wisniowski et al., 2021	Araçuaí orogen	Nova Venécia Complex	São Gabriel da Baunilha - ES	Paragneiss (pelite)	Pl-Grt-Qz-Crd-Sil-Hc-Kfs Hornfels			520 ± 19 Ma		970	5.6				Orogenic collapse
Wisniowski et al., 2021	Araçuaí orogen	Nova Venécia Complex	São Gabriel da Baunilha - ES	Paragneiss (pelite)	Pl-Grt-Qz-Crd-Sil-Hc-Kfs Hornfels			520 ± 19 Ma		1010	6				Orogenic collapse